# MILD COMBUSTION: MODELLING CHALLENGES, EXPERIMENTAL CONFIGURATIONS AND DIAGNOSTIC TOOLS

EDITED BY: Alessandro Parente and Mara de Joannon
PUBLISHED IN: Frontiers in Mechanical Engineering

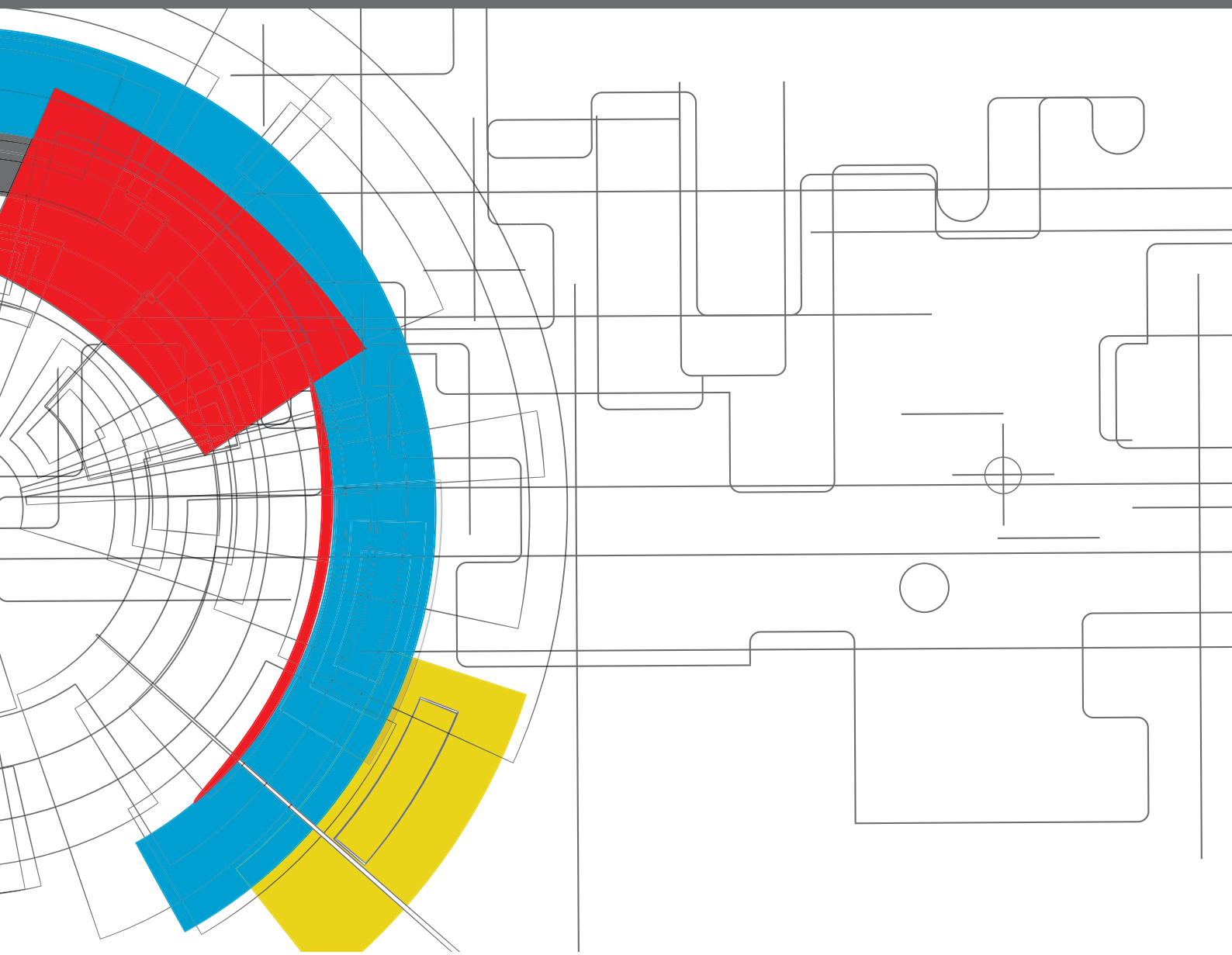

frontiers Research Topics

ISSN 1664-8714
ISBN 978-2-88971-700-2
DOI 10.3389/978-2-88971-700-2

## About Frontiers

Frontiers is more than just an open-access publisher of scholarly articles: it is a pioneering approach to the world of academia, radically improving the way scholarly research is managed. The grand vision of Frontiers is a world where all people have an equal opportunity to seek, share and generate knowledge. Frontiers provides immediate and permanent online open access to all its publications, but this alone is not enough to realize our grand goals.

## Frontiers Journal Series

The Frontiers Journal Series is a multi-tier and interdisciplinary set of open-access, online journals, promising a paradigm shift from the current review, selection and dissemination processes in academic publishing. All Frontiers journals are driven by researchers for researchers; therefore, they constitute a service to the scholarly community. At the same time, the Frontiers Journal Series operates on a revolutionary invention, the tiered publishing system, initially addressing specific communities of scholars, and gradually climbing up to broader public understanding, thus serving the interests of the lay society, too.

## Dedication to Quality

Each Frontiers article is a landmark of the highest quality, thanks to genuinely collaborative interactions between authors and review editors, who include some of the world's best academicians. Research must be certified by peers before entering a stream of knowledge that may eventually reach the public - and shape society; therefore, Frontiers only applies the most rigorous and unbiased reviews.
Frontiers revolutionizes research publishing by freely delivering the most outstanding research, evaluated with no bias from both the academic and social point of view. By applying the most advanced information technologies, Frontiers is catapulting scholarly publishing into a new generation.

## What are Frontiers Research Topics?

Frontiers Research Topics are very popular trademarks of the Frontiers Journals Series: they are collections of at least ten articles, all centered on a particular subject. With their unique mix of varied contributions from Original Research to Review Articles, Frontiers Research Topics unify the most influential researchers, the latest key findings and historical advances in a hot research area! Find out more on how to host your own Frontiers Research Topic or contribute to one as an author by contacting the Frontiers Editorial Office: frontiersin.org/about/contact

# MILD COMBUSTION: MODELLING CHALLENGES, EXPERIMENTAL CONFIGURATIONS AND DIAGNOSTIC TOOLS

Topic Editors:
**Alessandro Parente,** Université libre de Bruxelles, Belgium
**Mara de Joannon,** Istituto di ricerche sulla combustione (IRC), Italy

**Citation:** Parente, A., de Joannon, M., eds. (2021). MILD Combustion: Modelling Challenges, Experimental Configurations and Diagnostic Tools. Lausanne: Frontiers Media SA. doi: 10.3389/978-2-88971-700-2

# Table of Contents

frontiers in Mechanical Engineering

EDITORIAL
published: 04 October 2021
doi: 10.3389/fmech.2021.726633

# Editorial: MILD Combustion: Modelling Challenges, Experimental Configurations, and Diagnostic Tools

*Alessandro Parente*[1]* *and Mara de Joannon*[2]*

[1]Aero-Thermo-Mechanics Laboratory, Ecole Polytechnique de Bruxelles, Université Libre de Bruxelles, Brussels, Belgium, [2]Istituto di Scienze e Tecnologie per l'Energia e la Mobilità Sostenibili (STEMS), Consiglio Nazionale delle Ricerche (CNR), Naples, Italy

**Keywords: computational fluid dynamics, chemical kinetics, colorless combustion, distributed combustion, flameless combustion, MILD combustion, laser diagnostics, turbulence–chemistry-radiation interactions**

**Editorial on the Research Topic**

**MILD Combustion: Modelling Challenges, Experimental Configurations, and Diagnostic Tools**

Over the last years, particular attention has been paid to combustion regimes that are able to ensure stable, complete, and efficient combustion, together with a strong reduction of pollutants, such as CO, $NO_x$, and soot. Moderate or Intense Low oxygen Dilution (MILD) combustion (Cavaliere and de Joannon, 2004) has gathered increasing attention in recent years, as it ensures very high combustion efficiencies with very low pollutant emissions, compared to conventional combustion regimes, due to the reduced temperature peaks and macroscale homogeneity, achieved by means of high recirculation of exhausts in the reaction volume. Such a combustion regime shares similarities with other combustion concepts, such as flameless combustion (Wünning and Wünning, 1997), high temperature air combustion (HiTAC) (Katsuki and Hasegawa, 1998), and colorless distributed combustion (CDC) (Arghode and Gupta, 2010). The acronym MILD will be retained for the rest of the present editorial.

MILD combustion has been implemented in several furnace-based power generation and manufacturing applications; however, its extensive application is still partially hindered by the limited understanding of many facets of underpinning elementary processes and their peculiar interplay in this combustion mode.

One of the major peculiarities derived from the change of the elementary processes is related to the very strong interactions between turbulence and chemistry occurring in this regime. In MILD combustion, two contrasting effects emerge: Damköhler number is of the order of unity or less, whereas the turbulence level is very high, to ensure effective gas recirculation and mixing at the microscale. These two characteristics lead to a new paradigm of the combustion process where no flame fronts are visible and the combustion process covers an extensive part of the combustion chamber. It is evident that some principles, well consolidated for a standard combustion process, are no longer applicable in MILD combustion. For example, many common combustion model assumptions, such as the infinitely thin reaction zone, cannot be made in MILD conditions. Analogously, consolidated kinetic models are not able to accurately reproduce experimental data at least in some relevant working conditions.

To overcome these issues, many effective tools for studying and designing MILD combustion processes and systems with novel conceptual approaches have been developed over the years. However, consolidated combustion models and a consistent experimental database are still required to identify MILD combustion regimes and to effectively represent chemical kinetics, heat transfer, turbulence–chemistry interactions, and other processes in this peculiar regime.

OPEN ACCESS

***Edited and reviewed by:***
*Timothy S. Fisher, University of California, Los Angeles, United States*

***Correspondence:**
*Mara de Joannon*
*mara.dejoannon@stems.cnr.it*
*Alessandro Parente*
*alessandro.parente@ulb.be*

***Specialty section:***
*This article was submitted to Thermal and Mass Transport, a section of the journal Frontiers in Mechanical Engineering*

***Received:*** *17 June 2021*
***Accepted:*** *13 August 2021*
***Published:*** *04 October 2021*

***Citation:***
*Parente A and de Joannon M (2021) Editorial: MILD Combustion: Modelling Challenges, Experimental Configurations, and Diagnostic Tools. Front. Mech. Eng 7:726633. doi: 10.3389/fmech.2021.726633*

The objective of this research topic is to highlight and discuss open issues, opportunities, and new findings in MILD combustion, with a focus on modelling approaches, experimental configurations (available and under development), and the critical assessment of existing diagnostic tools.

The research topic has two main cores. The first is represented by reviews on key issues faced over the years since the formal definition of MILD combustion in the early 2000s. This part represents an excellent reference summary for an exhaustive overview of this process, with the accent on the open questions.

Indeed, the review by Sabia and de Joannon highlights the critical effects of the high dilution level on the chemical kinetics of fuel oxidation, focusing on the role of diluent species. Based on the literature data, they show how the overall reduction of reaction rates due to dilution stresses the competition among different kinetic paths and brings out very peculiar behaviors, previously undetected, that help better understand chemical kinetics and the role of third body effect in MILD and standard combustion conditions.

Li and Parente thoroughly review the application of reactor-based models to the simulation of a canonical MILD combustion system, the jet in hot co-flow (JHC). The effectiveness of the partially stirred reactor and eddy dissipation concept combustion models in the context of Reynolds Average Navier–Stokes (RANS) and large eddy simulation (LES) is assessed. The importance of taking into account finite rate chemistry effects and of providing a reliable estimation of the characteristic time scales is underlined.

Reduced reaction rates and the mixing between diluted and/or preheated reactants in MILD combustion locally induce the formation of peculiar reaction structures which are reviewed by Sorrentino et al. They focus on the igni-diffusive structures and their "distributed ignition" nature. The authors analyze the main characteristics of such structures in the mixture fraction space, namely, the thickness of the oxidation structures, the presence/absence of a pyrolysis region, and the loss of correlation between the maximum heat release rate and the stoichiometric mixture fraction.

The peculiar characteristics of such a process also impact the formation of nitrogen oxides (NOx). Iavarone and Parente provide an evaluation of the possible kinetic pathways active in MILD conditions and outline suitable modelling approaches to predict $NO_x$ emissions in CFD simulations. An assessment of the performances of selected models in estimating $NO_x$ formation for lab-scale MILD combustion burners is then presented, followed by a discussion about relevant modelling issues, perspectives, and opportunities for future research.

Heat transfer plays a particular role in MILD combustion. Sorrentino et al. highlight the role of heat transfer in the combustion peculiarities of MILD reactors. In particular, the thermal behavior of these systems is analyzed to stress the distinctive role of heat losses, the relative contributions of both the convective and radiative terms, and their influence on MILD macroscopic features.

The experimental study of MILD combustion requires the establishment of new experimental configurations and diagnostic methodologies. Medwell and Evans review a number of optical diagnostic techniques (Rayleigh and Raman scattering, planar laser-induced fluorescence, coherent anti-Stokes Raman scattering ( CARS), and spectroscopy) for the characterization of the MILD combustion of gas and liquid fuels in the JHC.

Chinnici et al. discuss the hybridization of MILD combustion with renewable sources, reviewing the numerical work on a hybrid solar receiver combustor (HSRC), coupling a MILD combustion burner with a concentrated solar radiation receiver. The authors analyze the efficiency of the system as a function of the solar radiation contribution, indicating the requirements in terms of the reactor dimension to reach an appropriate coupling efficiency.

The second core of the research topic is represented by articles focused on original research on different topics under discussion in MILD combustion, covering the fundamental understanding of the process, its numerical modelling, and the identification of optimal reactive scalars to assist experimental diagnostics.

Swaminathan relies on recent direct numerical simulation (DNS) data to show that a revised theory involving at least two chemical timescales is required to describe the inception of MILD combustion and describe the strong interactions between autoignition and flame propagation. Moreover, the relevance of MILD combustion to supersonic combustion is explored theoretically, providing qualitative support using experimental and numerical Schlieren images.

Sidey-Gibbons and Mastorakos analyze the critical phenomena in MILD combustion using an asymptotic theory for extinction conditions of non-premixed flames and well-stirred reactors. Results of the analysis suggest that MILD combustion systems do not show sudden ignition and extinction behavior, and therefore exhibit a smooth, stretched S-shaped curve rather than a folded one with inflection points, thus providing a potential alternative definition of MILD combustion.

Ferrarotti et al. investigate the correlation between the heat releaser rate (HRR) and species mole fractions and net reaction rates in the JHC, suggesting that typical markers (O, OH, and OH*) correlate fairly well with HRR, but improved correlations can be achieved with appropriate species mole fraction combinations, particularly for the MILD region of the flame.

Goktolga et al. present direct numerical simulations of igniting mixing layers, considered representative of the JHC configuration, using both detailed chemistry and the multistage flamelet-generated manifold (MuSt-FGM) approach. Results indicate that the MuSt-FGM approach can predict the ignition delay time fairly well, while it overpredicts the average heat release rate.

Amaduzzi et al. benchmark the flamelet-generated manifold (FGM) approach with a reactor-based model, the partially stirred reactor (PaSR), for a MILD system with internal recirculation. The results show that the FGM model strongly overpredicts temperature profiles in the reactive region while yielding better results along the central thermocouple. The PaSR closure with a dynamic estimation

of the mixing constant is found to provide improved results for both lateral and central thermocouple measurements. A flame index analysis indicates how the FGM model predicts a typical non-premixed region after the injection zone, contrary to the experimental observation.

Perpignan et al. present a novel approach for the automatic generation of chemical reactor networks (CRNs) from simplified CFD simulations, for the subsequent evaluation of pollutant emissions. Data from a non-premixed burner fuelled with $CH_4$ at various equivalence ratios are used for this purpose. The CRN results are capable of reproducing the non-monotonic behavior with an equivalence ratio, which cannot be captured by simplified CFD simulations. However, the agreement between experimental and predicted $NO_x$ emissions is not fully satisfactory, indicating a need for improving the clustering step in the CRN generation process.

In conclusion, the research topic provides a comprehensive overview on the key features and existing challenges in MILD combustion, highlighting the current research efforts and the opportunities ahead. The unique combination of review and original research articles makes it a key collection for researchers and practitioners starting or already in the field.

## AUTHOR CONTRIBUTIONS

All authors listed have made a substantial, direct, and intellectual contribution to the work and approved it for publication.

## ACKNOWLEDGMENTS

This Research Topic originated from the first international workshop on MILD combustion that took place in Naples on January 25–26, 2019, with the support of the European Research Council (ERC) under the European Union's Horizon 2020 research and innovation programme under grant agreement no. 714605 (VADEMECOM project, www.vademecom.eu), and the SMARTCATs COST Action CM1404 "Chemistry of Smart Energy Carriers and Technologies" (www.smartcats.eu).

## REFERENCES

Arghode, V. K., and Gupta, A. (2010). Effect of Flow Field for Colorless Distributed Combustion (CDC) for Gas Turbine Combustion. *Appl. Energy* 87 (5), 1631–1640.

Cavaliere, A., and De Joannon, M. (2004). Mild Combustion. *Prog. Energy Combust. Sci.* 30 (4).

Katsuki, M., and Hasegawa, T. (1998). The Science and Technology of Combustion in Highly Preheated Air. *Symp. Combust. Proc.* 27 (2), 3135–3146.

Wünning, J. A., and Wünning, J. G. (1997). Flameless Oxidation to Reduce Thermal No-Formation. *Prog. Energy Combust. Sci.* 23 (1), 81–94.

**Conflict of Interest:** The authors declare that the research was conducted in the absence of any commercial or financial relationships that could be construed as a potential conflict of interest.

frontiers in Mechanical Engineering

ORIGINAL RESEARCH
published: 02 October 2019
doi: 10.3389/fmech.2019.00059

# Physical Insights on MILD Combustion From DNS

*N. Swaminathan**

*Department of Engineering, Cambridge University, Cambridge, United Kingdom*

MILD combustion is gaining interest in recent times because it is attractive for green combustion technology. However, its fundamental aspects are not well-understood. Recent progresses made on this topic using direct numerical simulation data are presented and discussed in a broader perspective. It is shown that a revised theory involving at least two chemical timescales is required to describe the inception of this combustion not only showing both autoignition and flame characteristics but also a strong interaction between these two phenomena. The reaction zones have complex morphological and topological features and the most probable shape is pancake-like structure implying micro-volume combustion under MILD conditions unlike the sheet-combustion in conventional cases. Relevance of the MILD (micro-volume) combustion to supersonic combustion is explored theoretically and qualitative support is shown and discussed using experimental and numerical Schlieren images.

**Keywords: MILD combustion, Scramjet, DNS, morphology, inception, S-curve**



***Edited by:***
*Mara de Joannon,*
*Istituto di Ricerche sulla Combustione (IRC), Italy*

***Reviewed by:***
*Shiyou Yang,*
*Ford Motor Company, United States*
*Khanh Duc Cung,*
*Southwest Research Institute, United States*

***Correspondence:**
*N. Swaminathan*
*ns341@cam.ac.uk*

***Specialty section:***
*This article was submitted to Thermal and Mass Transport, a section of the journal Frontiers in Mechanical Engineering*

***Received:*** *28 May 2019*
***Accepted:*** *19 September 2019*
***Published:*** *02 October 2019*

***Citation:***
*Swaminathan N (2019) Physical Insights on MILD Combustion From DNS. Front. Mech. Eng. 5:59. doi: 10.3389/fmech.2019.00059*

## 1. INTRODUCTION

The world total primary energy supply (TPES) has increased from 6.2Btoe (Billion ton of oil equivalent) in 1973 to about 13.8Btoe in 2016 (International Energy Agency, 2019)[1]. This 220% increase over a period of 43 years will continue further and more than 90% of this supply comes from combustion of coal, oil, gas, or renewable biomasses. **Figure 1** shows the future projections of potential combustion share of TPES under three different scenarios. The inset is the actual data from International Energy Agency (2019) showing a gradual drop of the combustion share and a small rise in 2012 is because of the increase in coal combustion in some of the countries around the world. If one naively projects this data by assuming that the progress in technology to replace combustion for meeting the energy demand is steady and organic following the current trends then the combustion share is likely to be more than 80% even by the year 2070 (the curve with open triangle). The slope of this curve is related to the progress and advancement of alternative energy technologies. If one keeps an optimistic view for the non-combustion technologies progressing at 50% faster pace compared to the current trend then the combustion share falls just below 80% by 2070. This share decreases to 77% by the year 2070 even if one assumes that the alternative technologies progress at 70% faster pace, which is a highly optimistic view. It seems that a radical paradigm shift is required for a significant reduction of the combustion share and whether this is practical or not is an open question. A pragmatic approach to mitigate combustion impact on the environment is to seek for alternative combustion concepts and technologies which can significantly reduce $CO_2$ and other pollutants emission and can also be employed as retrofits into the existing systems. Fuel-lean and MILD (moderate, intense, or low dilution) combustion concepts emerge as potential solutions.

[1] 1 ton of oil equivalent is 41.89 BJ or 11.64 MWh of energy.

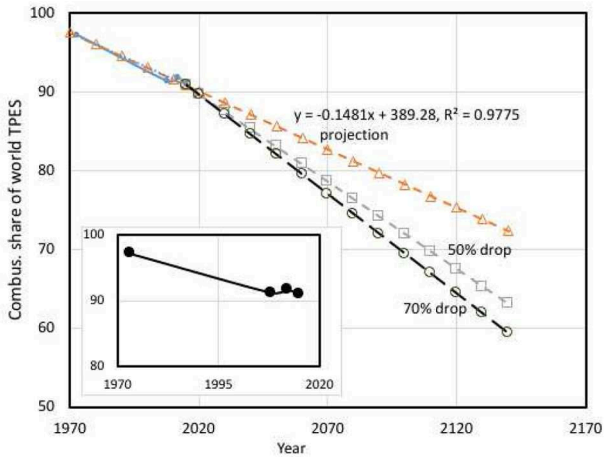


**FIGURE 1 |** The contribution of combustion to world TPES and its future projection.

The interest here is on MILD combustion because of its ability to simultaneously reduce pollutants emission and increase overall thermal efficiency (Wünning and Wünning, 1997; Cavaliere and de Joannon, 2004). The efficiency gain comes from the energy recovered by recirculating hot gases and the emission reduction is because of reduced oxygen level in and temperature rise across combustion zones under MILD conditions. This mode of combustion is said to occur when the fuel-air mixture temperature, $T_r$, is higher than the reference auto-ignition temperature, $T_{ign}$, for a given mixture and the temperature rise, $\Delta T = (T_b - T_r)$, is smaller than $T_{ign}$ (Cavaliere and de Joannon, 2004), where $T_b$ is the burnt gas temperature. These two conditions are typically achieved by diluting the fuel-air mixture with exhaust gases and the dilution level is controlled carefully to keep the oxygen level typically below 5% by volume. If one uses $(T_r - T_{ign})$ and $\Delta T - T_{ign}$ as two axes as suggested by Cavaliere and de Joannon (2004) then the MILD combustion locates in the fourth quadrant and this is sketched in **Figure 2** with pictures representing typical combustion types identified (Doan, 2018). The temperature raise, $\Delta T$ is larger than $T_{ign}$ for HiTAC and conventional (Feedback) combustion whereas it is smaller than $T_{ign}$ for the MILD and pilot-assisted combustion. The MILD combustion has $T_r - T_{ign} > 0$ since the reactant temperature is larger than $T_{ign}$. Typically, one expects the autoignition process to be dominant under this condition but direct numerical simulation (DNS) studies showed the presence of autoignition fronts with premixed and non-premixed flames and also their interactions (Minamoto, 2013; Doan, 2018). This challenges the use of conventional flame theories and models for MILD combustion.

The heat release rate in this combustion is distributed spatially yielding a homogeneous temperature field with no visible flame (Katsuki and Hasegawa, 1998; de Joannon et al., 2000; Ozdemir and Peters, 2001; Minamoto and Swaminathan, 2014b; Sidey and Mastorakos, 2015; Sorrentino et al., 2016) and thus the MILD combustion is also called as "flameless" combustion. These features are atypical of conventional combustion having strong heat release in thin regions leading to inhomogeneous temperature or density field. DNS studies showed that some features of conventional combustion are also present under MILD conditions (Minamoto and Swaminathan, 2014b; Doan and Swaminathan, 2019b). Furthermore, the chemical kinetics plays a strong role in the inception of MILD combustion which can lead to some unconventional behaviors of reaction zones in response to scalar dissipation (or fluid dynamic strain) rate (Doan and Swaminathan, 2019c). Hence, the objective here is to survey the past DNS studies on MILD combustion and provide a broader perspective on MILD combustion physics by answering the following questions

1. What is the inception mechanism for MILD combustion?
2. What is the main combustion mode, autoignition or flames, under MILD conditions or is it a mixed mode combustion?
3. What are the typical morphological and topological features of reaction zones in MILD conditions?
4. What is the simplest way to model MILD combustion?

Since these questions are of fundamental nature, analysing DNS data is the best possible way to answer them. Also, it is worth to note that the modern combustion concepts such as Homogeneous Charge Compression Ignition (HCCI), Reactivity Controlled Compression Ignition (RCCI), and Gasoline Compression Ignition (GCI) for automotive engines may share some common features with MILD combustion. The next section reviews the DNS data briefly. The insights gained in many past studies are reviewed and discussed in section 3 to answer the above questions. The tentative modeling ideas arising from the physical insights are presented in section 4 and the relevance of MILD combustion to supersonic combustion, which is a topic of long-standing interest for high-speed air transport, is discussed in section 5. The conclusions are summarized in the final section.

## 2. DNS OF MILD COMBUSTION

Direct numerical simulation of turbulent combustion under MILD conditions is not common and only two research groups have attempted this in the past using two different flow configurations. van Oijen (2013) and his co-workers (Göktolga et al., 2015) considered ignition in a temporally evolving turbulent mixing layer between counter-flowing fuel and hot oxidant streams to mimic the flow and reacting features of jet-in-hot-coflow burner of Adelaide (Dally et al., 2002) operating under MILD conditions. The results of these studies suggested that autoignition occurred at the most reactive mixture fraction, $Z_{MR}$, with different ignition delays depending on temperature and scalar dissipation rate experienced locally by the most reactive mixture. Also, the molecular diffusion of heat and mass were shown to be important and thus 3D simulations are inevitable to understand MILD combustion physics.

The DNS studies at Cambridge considered a cubic domain with carefully constructed flow and mixture conditions mimicking MILD combustion with recirculated hot exhaust gases. These simulations were conducted in two stages for

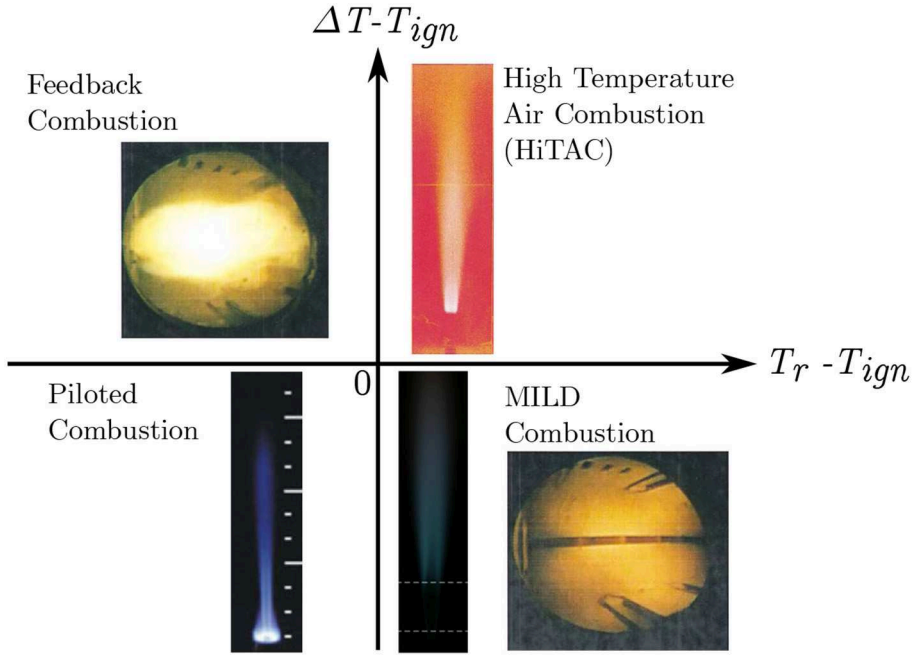


**FIGURE 2 |** A diagram showing various combustion types: HiTAC (Fujimori et al., 1998), feedback or conventional (de Joannon et al., 2000), piloted (Dunn et al., 2010), and MILD (de Joannon et al., 2000; Medwell et al., 2007) combustion. This diagram is adapted from Doan (2018) under a Creative Commons license.

computational economy. The first stage considered the mixing of reactants/fuel-air mixture with hot exhaust gases while the second stage involved combustion as shown in **Figure 3**. Both premixed (Minamoto, 2013) and non-premixed (Doan, 2018) MILD combustion were studied. For non-premixed MILD combustion, typically oxidant stream is diluted using the hot exhaust gases as shown schematically in **Figure 3** and this is called as hot-oxidant and diluted-oxidant by de Joannon et al. (2012). The DNS procedures are described in detail by Minamoto and Swaminathan (2014b) for premixed and by Doan et al. (2018) for non-premixed cases, and a brief summary is given below.

The initial and inflowing fields of mixture fraction, $Z$, reaction progress variable, $c$, scalar mass fractions, $Y_\alpha$, and velocity fields, $u_i$, were generated in 5 preprocessing steps marked in **Figure 3** without step 5. Bilger mixture fraction was used to define $Z$ (Bilger et al., 1990) and the reaction progress variable was based on fuel mass fraction. A decaying homogeneous isotropic turbulence was simulated in step 1 to obtain the turbulence field inside the computational domain. Laminar MILD premixed flames for various $Z$ values were computed and the scalar mass fractions were tabulated as a function of $Z$ and $c$ in step 2. Initial turbulent mixture fraction and reaction progress variable fields were constructed with prescribed means, $\langle Z \rangle$ and $\langle c \rangle$, and lengthscales, $\ell_Z$ and $\ell_c$ in step 3. Only the progress variable field was considered for the premixed cases. The step 4 mapped the species mass fractions $Y_\alpha(c, Z)$ obtained in step 2 onto the initial mixture fraction and progress variable fields. The turbulence and scalar fields obtained respectively in steps 1 and 4 were allowed to interact in step 5 for about one large eddy turnover time, 40 $\mu$s, of the initial turbulence field. This step is not shown in **Figure 3**. This time is much shorter than the time, 140 $\mu$s, required for the normalized temperature $c_T = (T - T_r)/(T_b - T_r)$ to increase by about 10% in a perfectly stirred reactor having a mixture representative of volume-averaged DNS condition. The scalar fields obtained at the end of step 5 included unburnt, $c = 0$, burnt, $c = 1$ and also partially burnt, intermediate values of $c$, mixtures with equivalence ratio, $\phi$, varying from 0 to 10 inside the computational domain for non-premixed cases and it was fixed to be 0.8 for the premixed cases. These preprocessed fields were then used as the initial and inflowing conditions for the MILD combustion DNS in the second stage shown in **Figure 3**. Elaborate details are discussed by Minamoto and Swaminathan (2014b) and Doan et al. (2018).

The combustion kinetics was described using MS-58 mechanism involving 19 species and 58 reactions (Doan et al., 2018), which was a modified version of Smooke and Giovangigli mechanism (Smooke and Giovangigli, 1991) with OH* chemistry from Kathrotia et al. (2012). The elementary reactions with OH* precursors were taken from KEE-58 mechanism (Bilger et al., 1990). This combined mechanism is validated in detail by Doan et al. (2018). The premixed MILD combustion DNS used Smooke and Giovangigli mechanism without OH*.

The thermochemical conditions of the MILD mixture used for the DNS are listed in **Table 1**. Since methane is used as fuel for these mixtures the reference ignition temperature is about $T_{ign} =$ 900 K. The mixtures NP-M1 and NP-M3 are for non-premixed cases whereas the other two mixtures are for premixed cases. The air is diluted for the non-premixed MILD combustion (see **Figure 3**) whereas the fuel-air mixture is diluted for the premixed

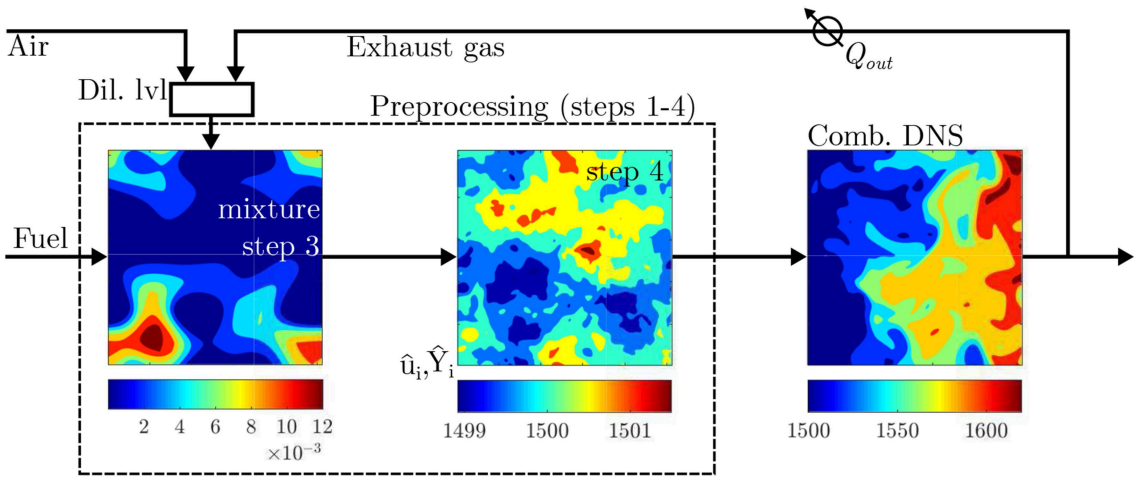


**FIGURE 3 |** A schematic of DNS steps followed for non-premixed MILD combustion with internal recirculation of exhaust gases, adapted from Doan et al. (2018) under a Creative Commons license.

**TABLE 1 |** Thermochemical condition of the oxidizer for MILD mixture.

| Mixture | $X_{CH_4}$ | $X_{O_2,r}$ | $X_{H_2O,r}$ | $X_{CO_2,r}$ | $X_{N_2,r}$ | $T_r$(K) |
|---|---|---|---|---|---|---|
| NP-M1 | | 0.035 | 0.134 | 0.067 | 0.764 | 1,500 |
| NP-M3 | | 0.020 | 0.146 | 0.073 | 0.761 | 1,500 |
| P-M1 | 0.019 | 0.048 | 0.121 | 0.061 | 0.751 | 1,500 |
| P-M3 | 0.014 | 0.035 | 0.132 | 0.066 | 0.753 | 1,500 |

cases. The diluted mixture temperature is kept to be $T_r = 1,500$ K, which is comparable to that used in the experiments of Suzukawa et al. (1997). These conditions suggest that the combustion is strictly in the MILD regime of **Figure 2**. The conditions of three non-premixed and three premixed turbulent MILD cases are listed in **Table 2**. The non-premixed cases are simulated by Doan et al. (2018) and premixed cases are from the study of Minamoto and Swaminathan (2014b). The cases NP1 and NP2 used the mixture NP-M1, which has the same $O_2$ level as for P-M3 and these two turbulent cases differed by the lengthscale ratio, $\ell_Z/\ell_c$. The case of $\ell_Z/\ell_c < 1$ was not considered because the mixing length scale for mixture fraction field is generally larger than the chemical length scales such as the flame thickness or ignition kernel size at $T_r$ as large as 1,500 K. The mixture NP-M3 with 2% of $O_2$ was used for the turbulent case NP3. The premixed cases P1 and P2 had the same dilution level as in the mixture P-M1 but different turbulence conditions – P1 had $(u'/S_L, \Lambda_0/\delta_f) = (6.26, 10.8)$ which gave the Damköhler and Karlovitz numbers to be 1.72 and 4.78, respectively, whereas the case P2 had (3.8, 12.3) yielding 3.25 and 2.11 for the Damköhler, $\mathrm{Da} = (\Lambda_0/\delta_f)/(u'/S_L)$, and Karlovitz, $\mathrm{Ka} = (u'/S_L)^{3/2}(\Lambda_0/\delta_f)^{-1/2}$, numbers. The case P3 had the same turbulence as for P1 at the inlet but used more diluted mixture P-M3 and hence the combustion characteristics are Da = 0.69 and Ka = 11.9. The burning velocity and Zeldovich flame thickness of the freely propagating laminar premixed flame used in the step 2 of the preprocessing step for the premixed MILD cases are $S_L$ and $\delta_f$, respectively. The RMS of velocity fluctuations in the initial turbulence field with an integral length scale $\Lambda_0$ is $u'$. **Table 2** lists the characteristics of the initial scalar fields relevant for the discussion in this paper. Further detail can be found in the studies of Minamoto and Swaminathan (2014b) and Doan et al. (2018).

The cubic domain of size $L_x \times L_y \times L_z = 10 \times 10 \times 10$ mm$^3$ with inflow and non-reflecting outflow boundary conditions in the $x$-direction and periodic conditions in the transverse, $y$ and $z$, directions was used. The domain was discretized using $512 \times 512 \times 512$ uniformly distributed grid points which ensured that all chemical and turbulence lengthscales were resolved for the three non-premixed and, P1 and P2 premixed cases. For the case P3, 384 grid points were used in all three directions. The DNS code SENGA2 solving fully compressible conservation equations for mass, momentum, internal energy, and species mass fractions, $Y_i$, was used. These simulations were made on HECToR and ARCHER, the UK national high performance computing facility. Other detail such as numerical scheme, computational time, etc., can be found in the studies of Minamoto (2013) and Doan (2018).

## 3. INSIGHTS

**Figure 4** shows the normalized heat release rate, $\dot{Q}^+ = \dot{Q}\delta_{th}/\rho_r S_L c_p \Delta T$, iso-surface having a value of 2. For the premixed case, the normalizing quantities are taken from a MILD flame element (laminar MILD flame) having an equivalence ratio of 0.8 whereas for the non-premixed case the local equivalence ratio is used to get the normalizing thermo-chemical quantities. This result is shown at about $1.5\tau_f$, where $\tau_f$ is the flow through time defined as the ratio of computational domain length $L_x$ to the mean velocity, $U_{in}$, at the inlet boundary. The figure on the left is for the premixed MILD case P3 and on the right is for the non-premixed case NP1 and these two cases have almost the same

**TABLE 2 |** DNS initial conditions.

| Case | $\Lambda_0/\ell_Z$ | $\langle X_{O_2} \rangle$ | $X_{O_2}^{max}$ | $ell_Z/\ell_c$ | $\langle Z \rangle$ | $Z_{st}$ | $\sigma_Z$ | $\langle c \rangle$ | $\sigma_c$ |
|---|---|---|---|---|---|---|---|---|---|
| NP1 | 0.60 | 0.027 | 0.035 | 1.30 | 0.008 | 0.010 | 0.008 | 0.56 | 0.26 |
| NP2 | 0.79 | 0.029 | 0.035 | 1.01 | 0.008 | 0.010 | 0.011 | 0.56 | 0.28 |
| NP3 | 0.60 | 0.016 | 0.020 | 1.30 | 0.005 | 0.006 | 0.006 | 0.56 | 0.26 |
| P1 | | 0.035 | 0.048 | | 0.011 | 0.014 | 0.001 | 0.5 | 0.01 |
| P2 | | 0.035 | 0.048 | | 0.011 | 0.014 | 0.001 | 0.5 | 0.01 |
| P3 | | 0.025 | 0.035 | | 0.008 | 0.010 | 0.001 | 0.5 | 0.01 |

dilution level and overall equivalence ratio. Thus, the overall temperature rise, which is about 200 K, is the same for these two cases and hence the temperature variation across the domain is shown only for the non-premixed case NP1. Typical thickness of local zones with strong heat release can be seen to be thin in some parts of domain and thick zones can also be seen in other parts visible in **Figure 4**. It is also observed that heat release (chemical reactions) occur in extremely convoluted zones distributed over a very large portion of the computational domain in both cases. This increases the possibility for interactions of reaction zones and clearly differentiates MILD combustion from conventional combustion having a clear flame front with localized heat release. Furthermore, reactions occur near the entrance of the computational domain, shown by the presence of the iso-surfaces there (see **Figure 4**), which is due to the elevated temperature of incoming stream with radicals initiating reactions.

Although there are some minor differences in the spatial distribution of the heat release, the overall pattern is more or less the same in these two cases. Hence, there is no difference whether the MILD combustion occurs in premixed or non-premixed mode as long as the turbulence and mixture thermo-chemical conditions are kept to be similar. This is not so for conventional combustion in premixed and non-premixed modes as it is well-known that the combustion is concentrated around the stoichiometric mixture fraction in non-premixed conventional combustion. The striking similarity is interesting and advantageous for developing MILD combustion models. However, there are complexities such as frequent and abundant interaction of reaction zones which are not easy to deal with in the classical turbulent combustion modeling such as flamelets, flame surface density approaches. Further insights on these points are discussed in section 4.

## 3.1. MILD Combustion Inception

The conventional non-premixed combustion aspects such as ignition (inception) and extinction are studied typically using S-curves which are constructed by solving steady flamelet equation in the mixture fraction space (Pitsch and Fedotov, 2001). This equation is

$$\frac{N_{Z,st}}{N_{Z,st}^0}\theta_{st} = \dot{\omega}\left(\theta_{st}\right), \tag{1}$$

with $N_{Z,st}$ as the mixture fraction scalar dissipation rate (SDR) at stoichiometry and its reference value is $N_{Z,st}^0$. The normalized temperature is $\theta_{st} = \left(T_{st} - T_{st,r}\right)/\left(T_{st,p} - T_{st,r}\right) = \left(T_{st} - T_{st,r}\right)/\Delta T_{st}$. The normalized reaction is written for a one-step reaction and it involves a Damköhler number, $\widehat{Da}$, normalized activation temperature, $\beta = T_{a,eff}/T_{st,p}$, and heat release factor $\alpha$. The exact form of this expression is not required here but can be found in earlier studies (Pitsch and Fedotov, 2001; Doan and Swaminathan, 2019c). A root which satisfies the above equation is obtained for given values of $N_{Z,st}/N_{Z,st}^0$, $\beta$ and various other parameters. The variation of $\theta_{st}$ with $N_{Z,st}/N_{Z,st}^0$ obtained thus for $\widehat{Da} = 100$, $\alpha = 0.679$ $\beta_{ref} = 8.03$ and 5 different values of $\beta$ is shown in **Figure 5A**. The ignition and extinction points are also marked in this figure. There is no stable combustion between these two critical points and they move toward each other as $\beta$ decreases leading to a monotonic increase of $\theta_{st}$ as $N_{Z,st}$ decreases, which can be seen for $\beta = 2$ and 4 in the figure. The inception region is highlighted using an ellipse in **Figure 5A**, showing a drop in the normalized temperature as the SDR (mixing rate) increases. This behavior is contrary to what is observed for the inception of MILD combustion in the DNS results shown in **Figure 5B** for the three non-premixed cases. The symbols represent the variation of doubly conditioned SDR obtained as $\langle N_Z|\theta_{st}, Z_{st}\rangle = \int N_Z \; P\left(N_Z|\theta_{st}, Z_{st}\right) \; dN_Z$ with $\theta_{st}$, where $P$ is the probability density function (PDF) of SDR conditioned appropriately. One can also consider $\langle N_Z|\theta\rangle$ vs $\theta$ which is also shown in the figure. These results are constructed using samples collected over the entire sampling period of $1.5\tau_f$. It is clear that the normalized temperature increases with mixing rate or SDR in the inception stage. This is because of the presence of radicals such as OH promoting chemical reactions in the incoming mixture which is absent for one-step reaction used for the S-curve analysis.

The importance of OH becomes more apparent if one plots $\Delta Y_{OH} = \left(Y_{OH} - Y_{OH}^c\right)$ with $\theta$. The symbol $Y_{OH}^c$ is the local value of the incoming OH mass fraction when there is no combustion, alternatively this is the local value due to convective-diffusive transport of the incoming OH mass fraction. This was obtained by performing a DNS with the same initial and inflowing fields as the MILD combustion cases but with no chemical reaction (Doan and Swaminathan, 2019a,c). Thus, $\Delta Y_{OH} < 0$ means that OH coming from the inlet is consumed and $\Delta Y_{OH} > 0$ implies that OH is produced locally. Since the interest is in the inception stage of MILD combustion, the variation of $\Delta Y_{OH}$ with corresponding $\theta$ is shown in **Figure 6** for the samples collected from the first 5% of the computational domain in regions with large heat release rate, which are marked using $\widehat{N}_Z = N_Z/\max(N_Z) > 0.2$. The normalized temperature

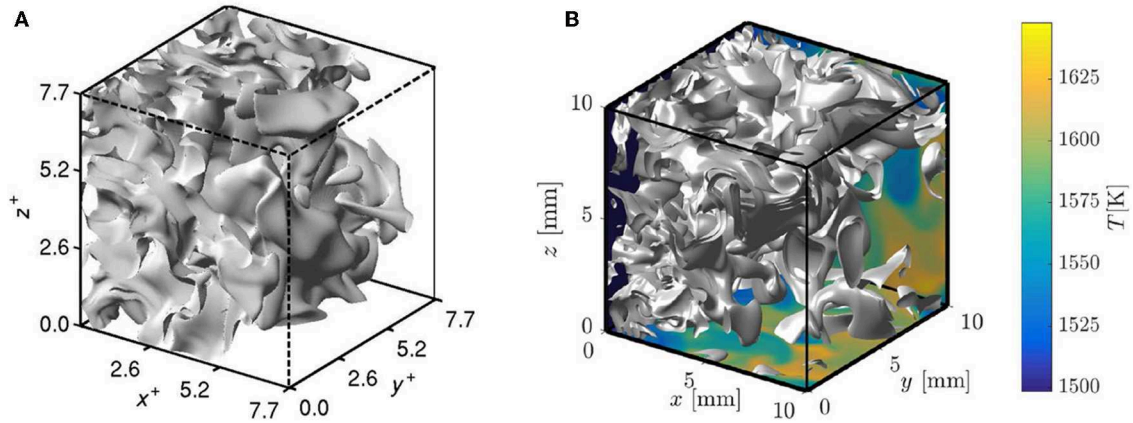


**FIGURE 4 |** Iso-surface of normalized heat release rate of 2 from **(A)** P3 and **(B)** NP1 MILD combustion cases. The temperature field is shown in the bottom and side surfaces in **(B)**. The axes are normalized using the laminar flame thermal thickness for the premixed case P3. These figures are adapted from Minamoto (2013) for P3 and Doan (2018) for NP1 cases under a Creative Commons license.

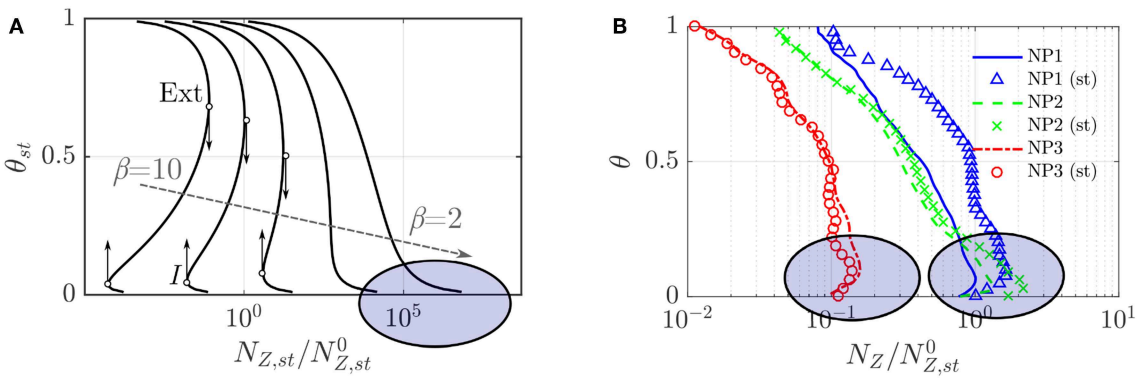


**FIGURE 5 |** Variation of normalized temperature at stoichiometry location with the corresponding mixture fraction dissipation rate in **(A)** conventional non-premixed and **(B)** turbulent MILD non-premixed combustion. The variation of $\langle N_Z|\theta\rangle$ with $\theta$ constructed using the entire DNS sample is also shown in **(B)** using lines. These figures are adapted from Doan and Swaminathan (2019c) under a Creative Commons license.

increase is seen only in the regions with negative $\Delta Y_{OH}$ implying the key role played by the incoming OH in the inception of MILD combustion. This leads to the increase of $\theta$ with $N_Z$ seen in **Figure 5**, which is different from the S-curve behavior. Hence, an alternative theory giving due importance for the role of chemical kinetics in the formation and consumption of radicals such as OH is required for MILD combustion. Such a theory is yet to be developed and it seems that at least two chemical time scales may be required to investigate the physics of MILD combustion inception.

The PDF of $\Delta Y_{OH}$ conditioned on the heat release rate is depicted in **Figure 6B** for the case NP1 at an arbitrarily chosen time. The nine curves shown are for $(\dot{Q}/\dot{Q}_{max})$ ranging from 0.1 to 0.9, where $\dot{Q}_{max}$ is the maximum heat release rate observed in the data. The PDF shows a bimodal behavior for low heat release rate; the peak at negative $\Delta Y_{OH}$ is because of the OH in the incoming stream and thus they signify the unreacted mixtures whereas the peak at positive $\Delta Y_{OH}$ is for the product mixtures. The bimodal PDF shifts gradually into a monomodal PDF for locations with large heat release rate. The OH-PLIF (planar laser-induced fluorescence) commonly used for the combustion diagnostics will pick the signals, coming from mixtures with low heat release, corresponding to the right peak and is likely to miss the signals from regions with large heat release rate since $Y_{OH}$ is almost the same as the background value, $Y^c_{OH}$. Thus, one needs extra care for studying MILD combustion using PLIF techniques (Doan and Swaminathan, 2019a).

## 3.2. Flame or Ignition?

From the fundamental perspective, the flame is established where there is convective-diffusive-reactive balance for the local scalar flux. When this balance is compensated by the temporal derivative (unsteady) term then the flame propagates. If there is ignition then typically the mixture is homogeneous locally and thus the convective and diffusive fluxes are small compared to the contributions from reactive and unsteady terms of

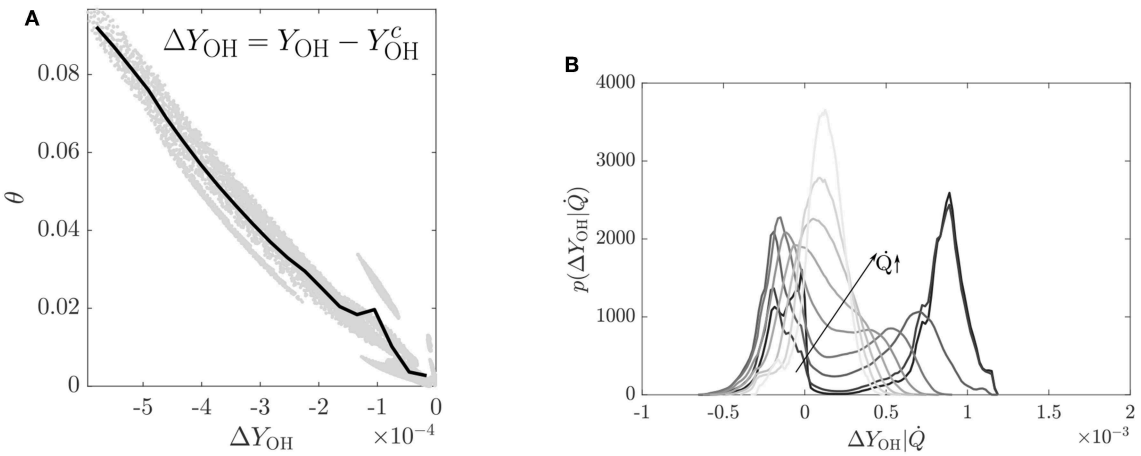


**FIGURE 6 | (A)** Variation of $\Delta Y_{OH}$ with $\theta$ for sample collected in the initial 5% of the computation domain and with $\widehat{N}_Z > 0.2$ at an arbitrarily chosen time for the case NP1. The line denotes $\langle\theta|\Delta Y_{OH}\rangle$, adapted from Doan and Swaminathan (2019c) with permission. **(B)** PDF of $\Delta Y_{OH}$ conditioned on $\dot{Q}$ for the case NP1 at an arbitrarily chosen time, adapted from Doan and Swaminathan (2019a) under a Creative Commons license.

the species balance equation. All of these can be seen quite clearly if one writes the balance equation for species $i$ using standard notations:

$$\frac{\partial \rho Y_i}{\partial t} + \underbrace{\frac{\partial \rho u_j Y_i}{\partial x_j}}_{\mathcal{C}:\ \text{conv.}} - \underbrace{\frac{\partial}{\partial x_j}\left(\rho D_i \frac{\partial Y_i}{\partial x_j}\right)}_{\mathcal{D}:\ \text{diff.}} - \underbrace{\dot{\omega}_i}_{\mathcal{R}:\ \text{react.}} = 0,$$
$$\implies \frac{\partial \rho Y_i}{\partial t} + \mathcal{B}_i = 0, \tag{2}$$

where $\mathcal{B}_i \equiv (\mathcal{C} - \mathcal{D}) - (\mathcal{R})$. For a closer understanding of local flux-balance, one may write $\mathcal{B} = |\mathcal{C} - \mathcal{D}| - |\mathcal{R}|$ and hence $\mathcal{B} = 0$ implies a steady flame-like structure locally while $\mathcal{B} < 0$ suggests an ignition-like structure and a positive value of $\mathcal{B}$ signifies propagating flame. The ambiguity may arise for $\mathcal{B} \geq 0$ if there exists purely convective-diffusive type balance, which can be eliminated by conditioning $\mathcal{B}$ on the normalized heat release rate, $\dot{Q}^+$. This analysis has been done in the past and some of those results are shown in **Figures 7**, **8** to aid the discussion here. Minamoto et al. (2014) showed that ignition fronts and flames are present and also there are regions with entangled flame and ignition. This is depicted in **Figure 7**, where $\mathcal{B}^+$ represents $\mathcal{B}$ value normalized using $\rho_r$, $S_L$ and $\delta_{th}$ for the mixture used for the turbulent premixed case P3. It is apparent that the MILD combustion involves conventional features like flames and autoignition in some regions and also these two features can coexist in some other regions of the flow. This is a unique aspect of MILD combustion and which attribute is favored locally depends on the scalar gradient driving the various fluxes. Minamoto and Swaminathan (2014b) showed that the scalar gradient in the direction normal to the reaction zone is as strong as the tangential gradients in MILD combustion which is contrary to the conventional combustion showing stronger normal gradient compared to the tangential components [see Figure 11 of Minamoto and Swaminathan (2014b) and Figure 5.5 of Minamoto (2013)] for the premixed MILD combustion cases, P1 to P3 in **Table 2**. Similar behaviors were observed for the non-premixed cases NP1 to NP3. The time evolution of these attributes and their structures are studied by Doan et al. (2018) and Doan and Swaminathan (2019b). An example of this complex evolution is shown in **Figure 8** depicting the Lagrangian tracks of few fluid parcels colored using $\mathcal{B}$ values. It is quite normal to see an ignition fronts evolving into steady or propagating flames in conventional combustion which is also seen in **Figure 8**. The intriguing and also quite unusual behavior observed in the figure is the evolution of a flame-like structure into ignition-like behavior as one moves along a particular track, which is indicated by the $\mathcal{B}$ changing from its positive to negative value. This is because of mixing and burning of unburnt mixtures of varied equivalence ratio in non-premixed cases and a close interaction between scalar mixing and chemical reactions. Overall, the MILD combustion is observed to display both autoignition and flame characteristics and a strong interaction between them.

Takeno index, which is related to the gradients of fuel and oxidizer, can be used to delineate non-premixed and premixed reaction zones present in non-premixed MILD combustion. This analysis showed that the contributions to the overall heat release from premixed and non-premixed modes are comparable and the contribution of rich premixed mode decreased for the highly diluted case, NP3, compared to the case NP1 (Doan et al., 2018). The contribution of lean premixed mode did not change much between these two cases but the non-premixed mode contribution nearly doubled for NP3 compared to the NP1 case. Doan et al. (2018) also reported that the ignition front-like structures contributed about 25%, which is not small, to the overall heat release. The physical picture emerging from these insights is that the non-premixed MILD combustion involves rich and lean premixed zones, non-premixed zones and ignition front-like structures. A similar picture was also observed for premixed MILD combustion but without non-premixed zones (Minamoto et al., 2014).

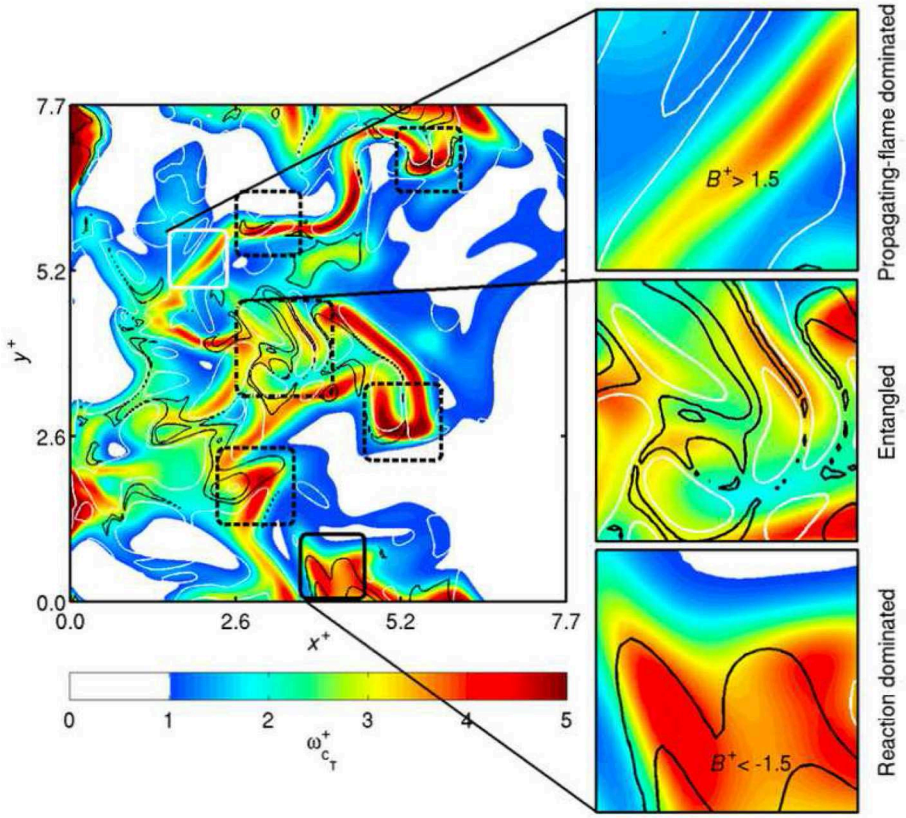


**FIGURE 7 |** Typical contours of $\dot{Q}^+$ (color map) are shown along with flame dominated ($\mathcal{B}^+ = 1.5$, white contours) and reaction dominated ($\mathcal{B}^+ = -1.5$, black contours) regions from the case P3. The results are shown for the mid *x*-*y* plane at an arbitrarily chosen time. Typical reaction and flame dominated regions are marked respectively using a black box and a white box with solid lines, which are enlarged at bottom right and top right respectively. Several regions showing entangled reaction and flame characteristics are marked using black boxes with dashed lines and one of such region is enlarged on the side, adapted from Minamoto (2013) under a Creative Commons license.

## 3.3. Typical Morphological and Topological Features of Reaction Zones

Reaction zones can be identified using a threshold for $\dot{Q}^+$ but Minamoto (2013) suggested that the conditional average of the heat release rate weighted by the scalar dissipation rate of reaction progress variable, $N_c$, and surface area, $\mathcal{S}$, and conditioned on $\dot{Q}$, i.e., $\mathcal{Z}(\xi) = \langle \Delta S N_c \dot{Q} | \dot{Q} = \xi \rangle$, is more suited to identify heat releasing zones in MILD combustion. The surface area, $\Delta S$, is identified using $\dot{Q} = \xi$ and the value of $\xi^+$ corresponding to $(\mathcal{Z}/\mathcal{Z}_{max}) = 1$ served as a suitable threshold to identify heat releasing zone iso-surfaces in various cases investigated. A typical reaction zone identified using this method is shown in **Figure 9A** for the premixed case P1 and this is not a simply connected surface which is commonly seen in conventional turbulent premixed combustion. Also, this iso-surface is observed to enclose a volume and there are holes, indicated by the arrows, and this volume is extending over a good portion of the computational domain. It is not easy to characterize this reaction zone using the common shapes such as sheet, ribbon, tube, and blob. However, one can unambiguously define three length scales for any 3D objects using Minkowski functionals and there are 4 functionals for a 3D object (Minkowski, 1903), which are given by Sahni et al. (1998)

$$\mathcal{F}_0 = \mathcal{V}, \quad \mathcal{F}_1 = \frac{\mathcal{S}}{6}, \quad \mathcal{F}_2 = \frac{1}{3\pi}\int_S \frac{\kappa_1 + \kappa_2}{2}\, dS, \quad \text{and}$$
$$\mathcal{F}_3 = \frac{1}{2\pi}\int_S \kappa_1 \kappa_2 \, dS, \tag{3}$$

where $\mathcal{V}$ is the volume enclosed by the iso-surface $S$ identified as above having a surface area of $\mathcal{S}$. The two principal curvatures at a given point on $S$ are $\kappa_1$ and $\kappa_2$ ($\kappa_1 \geq \kappa_2$). These four functionals are Galilean invariant morphological properties of the object, the reaction zone identified as above. The fourth functional is the Euler characteristics of the object and thus it is related to the genus of the object $G = 1 - 0.5\,\mathcal{F}_3$ (Leung et al., 2012; Minamoto et al., 2014). Now, the three length scales ordered as $T < W < L$ are defined using these four functionals as (Sahni et al., 1998)

$$\text{Thickness, } T \equiv \frac{\mathcal{F}_0}{2\,\mathcal{F}_1}; \quad \text{Width, } W \equiv \frac{2\,\mathcal{F}_1}{\pi\,\mathcal{F}_2};$$
$$\text{Length, } L \equiv \frac{3\,\mathcal{F}_3}{4(G+1)}. \tag{4}$$

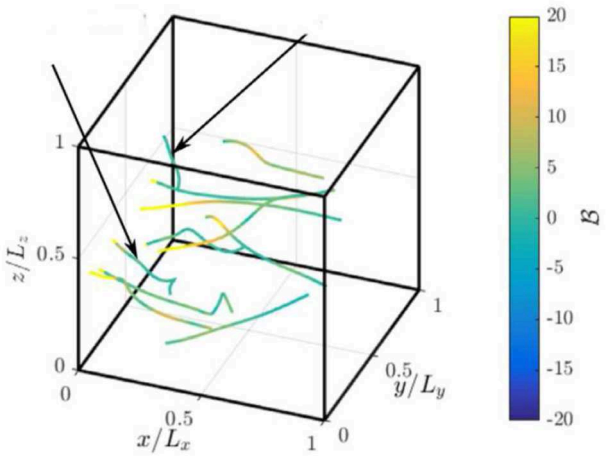


**FIGURE 8 |** Evolution of $\mathcal{B}$ along Lagrangian tracks of chosen fluid parcels and the tracks are drawn for a duration from 1 to $1.5\tau_f$. This results is shown for the case NP3 in **Table 2**, adapted from Doan (2018) under a Creative Commons license.

These scales are representative and do not give the exact dimensions in the three directions except for a sphere of radius $r$ for which $T = W = L = r$. Two *shape finders*, known as planarity $P$ and filamentarity $F$ can be defined using these three length scales and are given by Sahni et al. (1998)

$$P = \frac{W - T}{W + T} \quad \text{and} \quad F = \frac{L - W}{L + W}. \tag{5}$$

**Figure 9B** shows the typical values of $P$ and $F$ for the reaction zones extracted from the cases P1 to P3 at an arbitrarily chosen time. For the sake of comparison, the values for the reaction zones of a conventional premixed flame are also shown in the figure. The premixed flame reaction zones have large $P$ and relatively lower $F$ values implying that these zones have sheet-like morphology, which is well-known. A wide range of $P$ and $F$ values is observed for the MILD reaction zones with the most probable values of $P \simeq 0.4$ to 0.5 and $F \simeq 0.15$ to 0.25. These most probable values suggest that the MILD reaction zones are like pancakes although there are reaction zones which are blob-like (very small values of $P$ and $F$). Also, the topology, which refers to the connection, of MILD reaction zones are complex, see **Figure 7**. The non-premixed cases NP1 to NP3 showed similar variations for $P$ and $F$. Hence, the MILD reaction zones are not simply-connected surfaces as in the conventional combustion and they have complex morphological and topological features, which are quite challenging for modeling.

## 4. MODELING

Minamoto and Swaminathan (2014a) showed that these complex features, specifically interaction of reaction zones, pose challenges for flamelet-based modeling approaches. However, if one treats the local reaction zones as a collection of perfectly or well-stirred reactors (PSR or WSR) then the statistical variations of major and minor species mass fractions and mean reaction rates can be captured quite well. This was demonstrated by Minamoto and Swaminathan (2014a) for RANS approach and by Minamoto and Swaminathan (2015) for filtered reaction required for large eddy simulations (LESs). The filtered or mean reaction rate of progress variable required for LES or RANS is written as

$$\overline{\dot{\omega}_c} = \int_0^1 \int_0^1 \dot{\omega}_c(\xi, \zeta)\ P(\xi, \zeta)\ \ d\xi\ d\zeta, \tag{6}$$

where $\xi$ and $\zeta$ are the sample space variables for mixture fraction and progress variable respectively and $P(\xi, \zeta)$ is the joint PDF which is to be modeled using either presumed or transported PDF approaches. The reaction rate, $\dot{\omega}(\xi, \zeta)$, can be found from the results of PSR/WSR operating over a range of mixture fraction values for the presumed PDF approach. This is the tabulated chemistry approach used in many past turbulent combustion studies employing flamelets-based models. For the transported PDF approach, the reaction rate function can be computed using the Arrhenius rate expression for the elementary reactions involved in the kinetic modeling. The performance of these two PDF approaches for MILD combustion is investigated by Chen et al. (2017) using jet in hot coflow (JHC) burner of Dally et al. (2002) as a validation case and reported that the results of tabulated chemistry approach compared well, except for CO, with the results of multi-environment PDF calculation by Lee et al. (2015). The various turbulence combustion models available are tested for MILD combustion by De and Dongre (2015) and they observed that Lagrangian (transported) PDF models compared well with measured mean temperature and major species mass fractions. The use of EDC, eddy dissipation concept, model for MILD combustion has also been explored in the past (Christo and Dally, 2005; Aminian et al., 2012; Parente et al., 2016; Li et al., 2017). Also, partially stirred reactor (PaSR) based models have been used in past studies of MILD combustion (Li et al., 2017). Many of these numerical investigations of MILD combustion used the JHC involving relatively simple flows as the validation case. The cyclonic MILD combustor of Sorrentino et al. (2017) was investigated numerically using the tabulated chemistry approach with both adiabatic and non-adiabatic PSR models by Chen et al. (2018) and it was observed that the numerical results compared well with measurements when non-adiabatic effects are included at the PSR and CFD levels. A careful survey of these past studies suggests that the PSR-based model can work well if the CFD model and reactors are built to be physically consistent with the experiments. *A priori* study using DNS data showed that this approach works well for sub-grid modeling also when the LES filter width is larger than the thermal thickness for the given thermo-chemical and mixture conditions (Minamoto and Swaminathan, 2015) and *a posteriori* validation of this SGS model is yet to be performed.

## 5. RELEVANCE TO SUPERSONIC COMBUSTION

Supersonic combustion is a longstanding technological area of interest for aerospace applications. Fuel, either hydrocarbon or hydrogen, is injected into a supersonic stream and the shockwave pattern emerging from the interaction of the cross-stream fuel jet with the supersonic air stream increases the static temperature and pressure. The combustion mode and the mechanism for flame stabilization under this condition is not well-understood and there are still many outstanding issues (Cain and Walton, 2002). The objective of this discussion is not to review and discuss these issues but it is rather to highlight that the combustion conditions and characteristics are akin to MILD combustion using simple theoretical arguments and by inspecting experimental and numerical Schlieren results.

**Figure 10** shows a simple schematic of a supersonic ramjet combustor tube. The stagnation temperature and Mach number of the air stream entering the tube are $T_{0,2}$ and $M_2$. These quantities change to $T_{0,3}$ and $M_3$ after the fuel is injected and $f$ is the fuel-air ratio. The stagnation temperature and Mach number just after the combustion zone are $T_{0,4}$ and $M_4$, respectively. The stagnation temperature is related to the static temperature at a given location through $T_0/T = 1 + 0.5(\gamma - 1)M^2$, where $\gamma$ is the ratio of specific heat capacities. A simple energy balance across the combustion zone gives $\mathcal{Q} = f\,\Delta H_c \simeq c_p\left(T_{0,4} - T_{0,3}\right)$, where $\mathcal{Q}$ is the rate of heat release per unit air flow rate and the factor $(1 + f)$ is neglected for the last part of the above energy balance expression since $f \ll 1$. A simple rearrangement of this equation after making use of the relationship between the stagnation and static temperatures given above yields

$$\frac{\Delta T}{T_3}\left(1 + \frac{\gamma - 1}{2}M_4^2\right) = \left(\frac{f\,\Delta H_c}{c_p\,T_3}\right) + \frac{\gamma - 1}{2}\left(M_3^2 - M_4^2\right), \quad (7)$$

where $\Delta T = (T_4 - T_3)$ is the static temperature raise across the combustion zone. In the view of **Figure 2**, $T_3$ is the reactant temperature and from a practical perspective $T_3$ must be larger than the ignition temperature, $T_{ign}$, say, by a small $\delta T$ so that $\delta T/T_3 \ll 1$. It is quite easy to verify that $\left(T_3 - T_{ign}\right)/T_3$ is larger than zero. For a typical supersonic combustor operation, $f = 0.01$, $\gamma = 1.3$, $c_p = 1.2$ kJ/kg-K, $M_3 = 3.3$, and $M_4 = 2.7$ (Prisell, 2006) and substituting these values into Equation (7) one gets $\Delta T/T_3 \simeq 0.4$ for typical hydrocarbons with $\Delta H_c = 40$ MJ/kg and 0.6 for hydrogen with $\Delta H_c = 120$ MJ/kg. Thus, $\left(\Delta T - T_{ign}\right)/T_3$ is negative which implies that the combustion conditions in a typical scramjet combustor lies in the fourth quadrant of **Figure 2** corresponding to MILD combustion. Further evidence to this deduction is given in the comparison of Schlieren images in **Figure 11**. The image shown on the left is from the experimental studies of Scherrer et al. (2016) and the one on the right is from the DNS case NP3. The numerical Schlieren, obtained as explained by Doan and Swaminathan (2019a), should be compared qualitatively to region marked as "Combustion" in the experimental image and the later image also shows shock waves. The similarities between these two images are quite interesting and offer support to the above deduction. Thus, one must be cautious in using classical turbulence combustion models to study supersonic combustion which is likely to be MILD combustion showing quite complex and unique attributes as discussed in earlier sections. These deductions and observations are similar to and consistent with

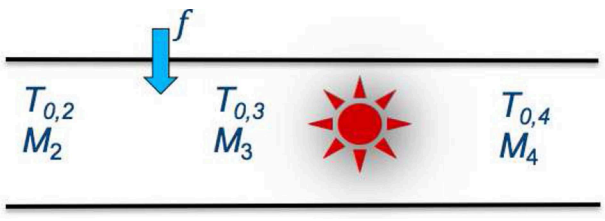


**FIGURE 10 |** A schematic of a scramjet combustor tube.

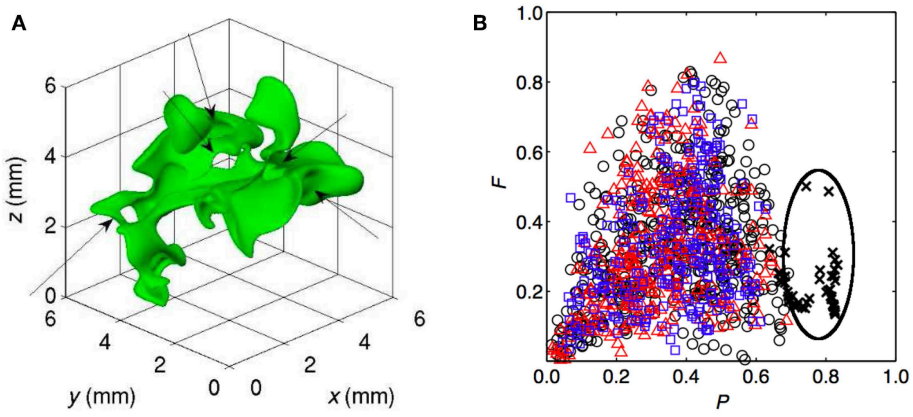


**FIGURE 9 | (A)** Morphology of a typical heat releasing zone in the MILD combustion case, P1. **(B)** Values of *shape finder*, *P* and *F*, in the cases P1 ○, P2 △, P3 □, and conventional premixed combustion ×, adapted from Minamoto (2013) under a Creative Commons license.

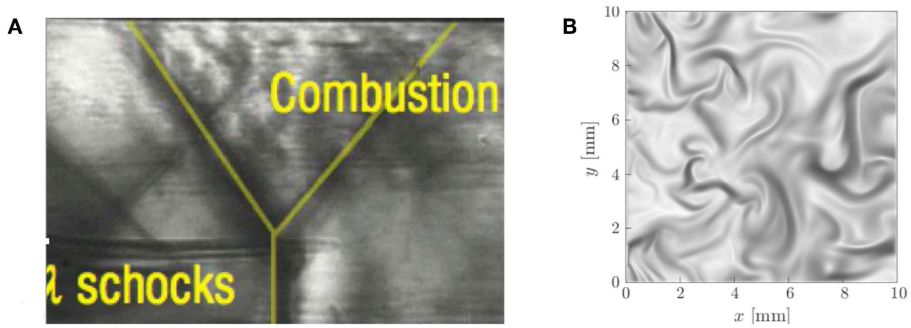


**FIGURE 11 | (A)** Schlieren picture from a scramjet combustor experiment (adapted from Scherrer et al., 2016 with permission from them) and **(B)** numerical Schlieren from the case NP3, adapted from Doan and Swaminathan (2019a) under a Creative Commons license.

the views on micro-volume combustion expressed by Shentinkov (1958) and Summerfield et al. (1955).

## 6. SUMMARY AND CONCLUSION

Turbulent combustion under MILD conditions has potentials to achieve ultra-low emissions, including $CO_2$, and high thermal efficiency. Although this topic has been explored using modern experimental techniques since 1990s, a good understanding on their complexities and intricacies has evolved only in the last decade. Direct numerical simulations (DNS) have provided some detailed insights into this problem and it seems that the inception of MILD combustion cannot be described using the classical S-curve and alternative theories involving at least two chemical timescales is required. Such a theory is yet to be developed. The reaction zones under MILD conditions are observed to show the characteristics of autoignition and both premixed and non-premixed flames. The local scalar gradients controlling the various fluxes dictate the local combustion behavior. These gradients can be tailored by designing appropriate flow and scalar mixing patterns. The thermochemical and mixture conditions also play a role here. Despite the complexities of MILD reaction zones, they can be seen as homogeneous reactors locally and thus modeling approaches such as tabulated chemistry using PSR/WSR can work quite well if the CFD model and the reactor conditions are designed to be physically consistent with combustor conditions of interest. Overall, the MILD combustion could be seen as micro-volume combustion proposed in 1950s by Summerfield et al. (1955) and Shentinkov (1958). The relevance of this micro-volume combustion to supersonic combustion is shown and discussed. Further investigations using different fuels, dilution level and turbulence conditions would be useful to assess further the insights presented in this paper. Also, targeted and carefully conducted laser diagnostics of combustion under MILD condition is required.

## DATA AVAILABILITY STATEMENT

The datasets analyzed in this manuscript are not publicly available. Requests to access the datasets should be directed to ns341@cam.ac.uk.

## AUTHOR CONTRIBUTIONS

This paper was fully conceived and written by NS.

## FUNDING

These works were supported by EPSRC, Cambridge Trust, Nihon Keidanren, Qualcomm European Research Studentship Fund in Technology and UKCTRF. Many of the DNS calculations were performed on the HECToR and ARCHER, UK National Supercomputing Service (http://www.archer.ac.uk) using computing time provided by EPSRC under the RAP project numbered e419 and the UKCTRF (e305). The relevance of MILD combustion to supersonic combustion was realized during my sabbatical stay at Indian Institute of Science (IISc), Bangalore, in 2018 summer, which was supported by the Centre of Excellence in Hypersonics, IISc.

## ACKNOWLEDGMENTS

The broader perspectives presented here are based on Ph.D. theses of Yuki Minamoto and Nguyen Anh Khoa Doan. Their curiosities and inquisitive nature helped me to understand the MILD combustion better and their comments on a draft of this paper are acknowledged.

## REFERENCES

Aminian, J., Galletti, C., Shahhosseini, S., and Tognotti, L. (2012). Numerical investigation of a MILD combustion burner: analysis of mixing field, chemical kinetics and turbulence-chemistry interaction. *Flow Turbul. Combust.* 88, 597–623. doi: 10.1007/s10494-012-9386-z

Bilger, R. W., Starner, S. H., and Kee, R. J. (1990). On reduced mechanisms for methane-air combustion in nonpremixed flames. *Combust. Flame* 80, 135–149.

Cain, T., and Walton, C. (2002). "Review of experiments on ignition and flameholidng in supersonic flow," in *38th AIAA/ASME/SAE/ASEE Joint Propulsion Conference & Exhibit* AIAA-2002-3877 (Indianapolis, IN). doi: 10.2514/6.2002-3877

Cavaliere, A., and de Joannon, M. (2004). Mild combustion. *Prog. Energy Combust. Sci.* 30, 329–366. doi: 10.1016/j.pecs.2004.02.003

Chen, Z., Reddy, V. M., Ruan, S., Doan, N. A. K., Roberts, W. L., and Swaminathan, N. (2017). Simulation of MILD combustion using perfectly stirred reactor model. *Proc. Combust. Inst.* 36, 4279–4286. doi: 10.1016/j.proci.2016.06.007

Chen, Z. X., Doan, N. A. K., Lv, X. J., Swaminathan, N., Ceriello, G., Sorrentino, G., et al. (2018). Numerical study of a cyclonic combustor under moderate or intense low-oxygen dilution conditions using non-adiabatic tabulated chemistry. *Energy Fuels* 32, 10256–10265. doi: 10.1021/acs.energyfuels.8b01103

Christo, F. C., and Dally, B. B. (2005). Modeling turbulent reacting jets issuing into a hot and diluted coflow. *Combust. Flame* 142, 117–129. doi: 10.1016/j.combustflame.2005.03.002

Dally, B. B., Karpetis, A. N., and Barlow, R. S. (2002). Structure of turbulent non-premixed jet flames in a diluted hot coflow. *Proc. Combust. Inst.* 29, 1147–1154. doi: 10.1016/S1540-7489(02)80145-6

de Joannon, M., Sabia, P., Cozzolino, G., Sorrentino, G., and Cavaliere, A. (2012). Pyrolitic and oxidative structures in hot oxidant diluted oxidant (HODO) MILD combustion. *Combust. Sci. Technol.* 184, 1207–1218. doi: 10.1080/00102202.2012.664012

de Joannon, M., Saponaro, A., and Cavaliere, A. (2000). Zero-dimensional analysis of diluted oxidation of methane in rich conditions. *Proc. Combust. Inst.* 28, 1639–1646. doi: 10.1016/S0082-0784(00)80562-7

De, A., and Dongre, A. (2015). Assessment of turbulence-chemistry interaction models in MILD combustion regime. *Flow Turbul. Combust.* 94, 439–478. doi: 10.1007/s10494-014-9587-8

Doan, N. A. K. (2018). *Physical Insights of Non-Premixed MILD Combustion using DNS* (Ph.D. thesis). University of Cambridge, Cambridge, United Kingdom. doi: 10.17863/CAM.32380

Doan, N. A. K., and Swaminathan, N. (2019c). Role of radicals on MILD combustion inception. *Proc. Combust. Inst.* 37, 4539–4546. doi: 10.1016/j.proci.2018.07.038

Doan, N. A. K., and Swaminathan, N. (2019a). Analysis of markers for combustion mode and heat release in MILD combustion using DNS data. *Combust. Sci. Technol.* 191, 1059–1078. doi: 10.1080/00102202.2019.1610746

Doan, N. A. K., and Swaminathan, N. (2019b). Autoignition and flame propagation in non-premixed mild combustion. *Combust. Flame* 201, 234–243. doi: 10.1016/j.combustflame.2018.12.025

Doan, N. A. K., Swaminathan, N., and Minamoto, Y. (2018). DNS of MILD combustion with mixture fraction variations. *Combust. Flame* 189, 173–189. doi: 10.1016/j.combustflame.2017.10.030

Dunn, M. J., Masri, A. R., Bilger, R. W., and Barlow, R. S. (2010). Finite rate chemistry effects in highly sheared turbulent premixed flames. *Flow Turbul. Combust.* 85, 621–648. doi: 10.1007/s10494-010-9280-5

Fujimori, T., Riechelmann, D., and Sato, J. (1998). "Effect of liftoff on $NO_x$ emission of turbulent jet flame in high-temperature coflowing air," in *27th Symposium Combustion* (Boulder, CO), 1149–1155. doi: 10.1016/S0082-0784(98)80517-1

Göktolga, M. U., van Oijen, J. A., and de Goey, L. P. H. (2015). 3D DNS of MILD combustion: a detailed analysis of heat loss effects, preferential diffusion, and flame formation mechanisms. *Fuel* 159, 784–795. doi: 10.1016/j.fuel.2015.07.049

International Energy Agency (2019). *Key World Energy Statistics*. Report by IEA. Available online at: www.iea.org/statistics (accessed May 13, 2019).

Kathrotia, T., Riedel, U., Seipel, A., Moshammer, K., and Brockhinke, A. (2012). Experimental and numerical study of chemiluminescent species in low-pressure flames. *Appl. Phys. B Lasers Opt.* 107, 571–584. doi: 10.1007/s00340-012-5002-0

Katsuki, M., and Hasegawa, T. (1998). "The science and technology of combustion in highly preheated air," in *27th Symposium Combustion, Vol. 27* (Boulder, CO), 3135–3146.

Lee, J., Jeon, S., and Kim, Y. (2015). Multi-environment probability density function approach for turbulent CH4/H2 flames under the MILD combustion condition. *Combust. Flame* 162, 1464–1476. doi: 10.1016/j.combustflame.2014.11.014

Leung, T., Swaminathan, N., and Davidson, P. A. (2012). Geometry and interaction of structures in homogeneous isotropic turbulence. *J. Fluid Mech.* 710, 453–481. doi: 10.1017/jfm.2012.373

Li, Z., Cuoci, A., Sadiki, A., and Parente, A. (2017). Comprehensive numerical study of the adelaide jet in hot-coflow burner by means of rans and detailed chemistry. *Energy* 139, 555–570. doi: 10.1016/j.energy.2017.07.132

Medwell, P. R., Kalt, P. A. M., and Dally, B. B. (2007). Simultaneous imaging of oh, formaldehyde, and temperature of turbulent nonpremixed jet flames in a heated and diluted coflow. *Combust. Flame* 148, 48–61. doi: 10.1016/j.combustflame.2006.10.002

Minamoto, Y. (2013). *Physical Aspects and Modelling of Turbulent MILD Combustion* (Ph.D. thesis). University of Cambridge, Cambridge, United Kingdom.

Minamoto, Y., and Swaminathan, N. (2014a). Modelling paradigms for MILD combustion. *Int. J. Adv. Eng. Sci. Appl. Math.* 6, 65–75. doi: 10.1007/s12572-014-0106-x

Minamoto, Y., and Swaminathan, N. (2014b). Scalar gradient behaviour in MILD combustion. *Combust. Flame* 161, 1063–1075. doi: 10.1016/j.combustflame.2013.10.005

Minamoto, Y., and Swaminathan, N. (2015). Subgrid scale modelling for MILD combustion. *Proc. Combust. Inst.* 35, 3529–3536. doi: 10.1016/j.proci.2014.07.025

Minamoto, Y., Swaminathan, N., Cant, R. S., and Leung, T. (2014). Reaction zones and their structure in MILD combustion. *Combust. Sci. Technol.* 186, 1075–1096. doi: 10.1080/00102202.2014.902814

Minkowski, H. (1903). Volumen und oberfläche. *Math. Ann.* 57, 447–495.

Ozdemir, I. B., and Peters, N. (2001). Characteristics of the reaction zone in a combustor operating at MILD combustion. *Exp. Fluids* 30, 683–695. doi: 10.1007/s003480000248

Parente, A., Malik, M. R., Contino, F., Cuoci, A., and Dally, B. B. (2016). Extension of the eddy dissipation concept for turbulence/chemistry interactions to MILD combustion. *Fuel* 163, 98–111. doi: 10.1016/j.fuel.2015.09.020

Pitsch, H., and Fedotov, S. (2001). Investigation of scalar dissipation rate fluctuations in non-premixed turbulent combustion using a stochastic approach. *Combust. Theor. Model.* 5, 41–57. doi: 10.1088/1364-7830/5/1/303

Prisell, E. G. (2006). *The Feasibility of the Scramjet; An Analysis Based on First Principles*. Available online at: https://www.icas.org/ICAS_ARCHIVE/ICAS2006/ABSTRACTS/530.HTM

Sahni, V., Sathyaprakash, B. S., and Shandarin, S. F. (1998). Shapefinders: a new shape diagnostic for large-scale structure. *Astrophys. J.* 495, L5–L8. doi: 10.1086/311214

Scherrer, D., Dessornes, O., Ferrier, M., Vincent-Randonnier, A., Moule, Y., and Sabelnikov, V. (2016). Research on supersonic combustion and scramjet combustors at ONERA. *Aerospacelab J.* 11, 1–20. doi: 10.12762/2016.AL11-04

Shentinkov, E. S. (1958). "Calculation of flame velocity in turbulent stream," in *Symposium (International) on Combustion, Vol. 7* (Oxford, UK), 583–589.

Sidey, J. A. M., and Mastorakos, E. (2015). Visualization of mild combustion from jets in cross-flow. *Proc. Combust. Inst.* 35, 3537–3545. doi: 10.1016/j.proci.2014.07.028

Smooke, M. D., and Giovangigli, V. (1991). "Formulation of the premixed and nonpremixed test problems," in *Reduced Kinetic Mechanisms and Asymptotic Approximations for Methane-Air Flames; Vol. 384 of Lecture Notes in Physics*,

ed M. D. Smooke (Berlin; Heidelberg: Springer), 1–28. doi: 10.1007/BFb0035362

Sorrentino, G., Sabia, P., Bozza, P., Ragucci, R., and de Joannon, M. (2017). Impact of external operating parameters on the performance of a cyclonic burner with high level of internal recirculation under MILD combustion conditions. *Energy* 137, 1167–1174. doi: 10.1016/j.energy.2017.05.135

Sorrentino, G., Sabia, P., de Joannon, M., Cavaliere, A., and Ragucci, R. (2016). The effect of diluent on the sustainability of MILD combustion in a cyclonic burner. *Flow Turbul. Combust.* 96, 449–468. doi: 10.1007/s10494-015-9668-3

Summerfield, M., Reiter, S. H., Kebely, V., and Mascolo, R. W. (1955). The structure and propagation mechanism of turbulent flames in high speed flow. *J. Jet Propulsion* 25, 377–384.

Suzukawa, Y., Sugiyama, S., Hino, Y., Ishioka, M., and Mori, I. (1997). Heat transfer improvement and $NO_x$ reduction by highly preheated air combustion. *Energy Convers. Manage.* 38, 1061–1071.

van Oijen, J. A. (2013). Direct numerical simulation of autoigniting mixing layers in MILD combustion. *Proc. Combust. Inst.* 34, 1163–1171. doi: 10.1016/j.proci.2012.05.070

Wünning, J. A., and Wünning, J. G. (1997). Flameless oxidation to reduce thermal no-formation. *Prog. Energy Combust. Sci.* 23, 81–94. doi: 10.1016/S0360-1285(97)00006-3

**Conflict of Interest:** The author declares that the research was conducted in the absence of any commercial or financial relationships that could be construed as a potential conflict of interest.

frontiers in Mechanical Engineering

REVIEW
published: 22 October 2019
doi: 10.3389/fmech.2019.00061

# Hybrid Solar-MILD Combustion for Renewable Energy Generation

*Alfonso Chinnici*, Graham J. Nathan and Bassam B. Dally*

*Centre for Energy Technology, School of Mechanical Engineering, The University of Adelaide, Adelaide, SA, Australia*

The intermittent nature of solar energy limits its further deployment to applications where firm supply and constant output is required. While energy storage is a viable option to increase solar share, in itself is not sufficient without an additional dispatchable energy source. Combustion of both fossil-based and renewable fuels can provide the demand ready energy source required and lends itself to hybridization with tower based Concentrated Solar Thermal, CST, energy. The Hybrid Solar Receiver Combustor, HSRC, is a novel technology that integrates both sources of energy in one device and offers tangible benefits in increased solar share, thermal efficiency and reduced capital and operation costs. This paper reports a brief review of the different findings from experimental and computational research carried out at the Center for Energy Technology of the University of Adelaide into optimizing the HSRC design, developing the first-of-a-kind laboratory-scale HSRC unit and evaluating its performance under different fuels, operating conditions and modes of operation. It highlights the benefits and need for utilizing MILD combustion in the HSRC to match the heat transfer characteristics and stability required to achieve similar operational range and efficiency from both sources of energy. A 5-$kW_{el}$ xenon-arc solar simulator and the combustion of a wide variety of fuels are used as the energy sources. This paper reports on the effectiveness of MILD combustion under these conditions and in particular it discusses flame stability envelop and its relation to heat extraction, temperature and pollutant emissions. It also reports on thermal efficiency, heat losses and heat flux distribution within the cavity for all fuels and operating conditions. It is found that the HSRC thermal performance is similar under the three operation modes (solar, combustion, and combined) and that operating under MILD combustion mode allowed fuel flexibility, homogeneous heat distribution and very low emission of $NO_x$ and CO. Also found that H/C ratio plays a minor role in the radiated energy to the heat exchanger within the cavity. Future research and further technology development need is also discussed in this paper.

**Keywords: hybrid systems, MILD combustion, concentrated solar energy, hydrogen, heat transfer**

OPEN ACCESS

***Edited by:***
*Alessandro Parente,*
*Université Libre de Bruxelles, Belgium*

***Reviewed by:***
*Mário Costa,*
*Instituto Superior Técnico,*
*Universidade de Lisboa, Portugal*
*Sudarshan Kumar,*
*Indian Institute of Technology*
*Bombay, India*

****Correspondence:***
*Alfonso Chinnici*
*alfonso.chinnici@adelaide.edu.au*

***Specialty section:***
*This article was submitted to Thermal and Mass Transport, a section of the journal Frontiers in Mechanical Engineering*

***Received:*** *29 April 2019*
***Accepted:*** *03 October 2019*
***Published:*** *22 October 2019*

***Citation:***
*Chinnici A, Nathan GJ and Dally BB (2019) Hybrid Solar-MILD Combustion for Renewable Energy Generation. Front. Mech. Eng. 5:61. doi: 10.3389/fmech.2019.00061*

## INTRODUCTION

Concerted effort has been spent on carbon abatement from the energy generation sector over the last two decades. The majority of the investment has targeted the power generation sector as it accounts for more than third of carbon emission (IEA, 2018). Renewable power from wind, solar PV, and hydro have made a tangible impact on carbon emission worldwide. Multiple agencies have predicted that almost all of electricity generation will be carbon neutral by the year 2050,

consistent with meeting current commitments to COP21 (http://www.cop21paris.org). However, decarbonizing the power sector alone will not be enough to keep the $CO_2$ level in the atmosphere below 350 ppm to prevent the atmosphere temperature from rising above 2 degrees (https://unfccc.int/process-and-meetings/the-paris-agreement/the-paris-agreement). Hence, beyond electrical energy, the two major energy sectors that should be targeted are the industry and transport sectors (Philibert, 2017). Philibert (2017) notes that electricity makes up to 26% of industry needs and the rest is in the form of thermal energy, almost half of it is at temperatures above 400°C. Similarly, transport is a major contributor to carbon emission, and while electric vehicles are likely to play a role in the light duty transport market, alternative fuels that can utilize existing internal combustion technologies will also be needed. The above highlights the need for generating renewable thermal energy at temperatures above 400°C and the production of alternative renewable fuels to replace fossil fuels.

Concentrating Solar Thermal (CST) technologies are promising avenues to generate high temperature thermal energy as well as alternative fuels, termed solar fuels (Kodama, 2003; Romero and Steinfeld, 2012; Agrafiotis et al., 2014). CST inherent intermittency is incompatible with industry needs of firm dispatchable supply and processes that require constant operating conditions (Jafarian et al., 2013, 2014). Thermal energy storage is one avenue to store heat using molten salts, phase change material or sensible energy storage. Thermal storage in locations of excellent solar resource can double the solar share from 20 to 40% (Nathan et al., 2017, 2018). Nonetheless, storage alone will never be sufficient to guarantee firm supply from a CST system, without solar multiples of more than 50 times, even at the best solar locations (Kueh et al., 2015). This finding highlights the need for the coupling of CST systems with other dispatchable source of energy to guarantee firm supply and constant output. Nathan et al. (2014) proposed the concept of combining CST and combustion as a means to solve this problem. The "hybrid" system capitalizes on CST low $CO_2$ emissions feature and harnesses stored chemical energy in fuels via combustion. This allows to use CST when needed while also encompassing the utilization of a wide range of fuels (including alternative, renewables low-carbon, and/or carbon-free fuels) and technologies able to offer a trade-off between the net cost and the net level of $CO_2$ mitigation.

The Hybrid Solar-Receiver-Combustor (HSRC) concept is a cost-effective and efficient method to utilize combustion to compensate for the variability and intermittency of the solar resource for applications in high-temperature processes (Nathan et al., 2014). Of the possible CST technologies available, the tower system with a large heliostat field and a cavity receiver are the most suitable to achieve the required high temperature and to contain the combustion products and achieve exhaust heat recovery. Cavity receivers trap the radiation via the aperture and reduces re-radiation inherent in tubular and bill-board style receivers (Goswami and Kreith, 2007). This single device concept allows three modes of operation namely; solar-only, combustion-only and a mixed-mode. A sketch of the HSRC concept is shown in **Figure 1**.

Lim et al. (2016a,b,c, 2017a,b) have identified an HSRC configuration that achieves similar thermal performance in the combustion-only mode to that of a stand-alone combustor through an efficient use of the sensible heat from the combustion products. They showed that such a system has the potential to lower the capital cost by up to 21%. They also estimated that the HSRC can achieve up to a 19% reduction (depending on the natural gas price) in the levelized cost of electricity relatively to an equivalent cavity receiver with a back-up, stand-alone combustor. This estimate could be low as it only considers, as stated by Nathan et al. (2017), "the first three of the following five potential benefits that were identified by Nathan et al. (2014), as being: (1) reduced heat losses by reducing the total area heat exchange surfaces; (2) avoided start-up and shut-down losses associated with the need to warm-up the combustion system prior to its use; (3) reduced total infrastructure by the need to construct only one device instead of two; (4) increased capacity to manage thermal shock associated with short-term fluctuations in solar resource by using combustion to compensate for any reduction in Concentrating Solar Radiation (CSR); and (5) potential to harvest the solar resource at a lower total flux, owing to the possibility of supplementing the solar resource with combustion". While a movable shutter can be used to seal the aperture during combustion-only operations, the simultaneous use of both the solar resource and the fuel is needed to harness the potential benefits (4) and (5). This, in turn, results in a combustion process directly-irradiated by CSR. As highlighted by Nathan et al. (2017), "this is a unique combustion regime, given that CSR can readily achieve fluxes some three to five times higher than is found in conventional systems (2–4 $MW/m^2$ compared with the 800 $kW/m^2$ of a gas turbine). The radiation also extends right through the visible spectrum, while irradiation from combustion systems is typically dominated by the infra-red spectrum". Therefore, new fundamental understandings of these interactions are needed to progress the technology development.

Dong et al. (2016) and Medwell et al. (2011) investigated the influence of CSR on the structure of laminar jet flames and in particular soot propensity. They found that most of the radiation is absorbed by the fuels, ethylene in this case, that peak soot volume fraction increased by up to 250% and that the overall soot volume fraction increased by 55%.

Based on the techno-economics work of Lim et al. (2016a,b,c, 2017a,b), Chinnici et al. conducted multiple studies (Chinnici et al., 2017a,b, 2018a,b,c, 2019a,b) to investigate design concepts of an experimental HSRC system that can work under a variety of fuels, is suitable to hybridization with CSR and achieves equivalent high thermal efficiency for all three modes of operation. Chinnici et al. (2018a) proposed the use of MILD combustion (de Joannon et al., 2012; Evans et al., 2017, 2019) in the cavity due to its stability, fuel flexibility, efficient use of low-carbon and carbon-free, renewable fuels (Derudi et al., 2007; Parente et al., 2008; Ayoub et al., 2012), low emission and enhanced and semi-homogenous heat transfer. This paper provides a review of the different findings from the experimental and computational research into optimizing the

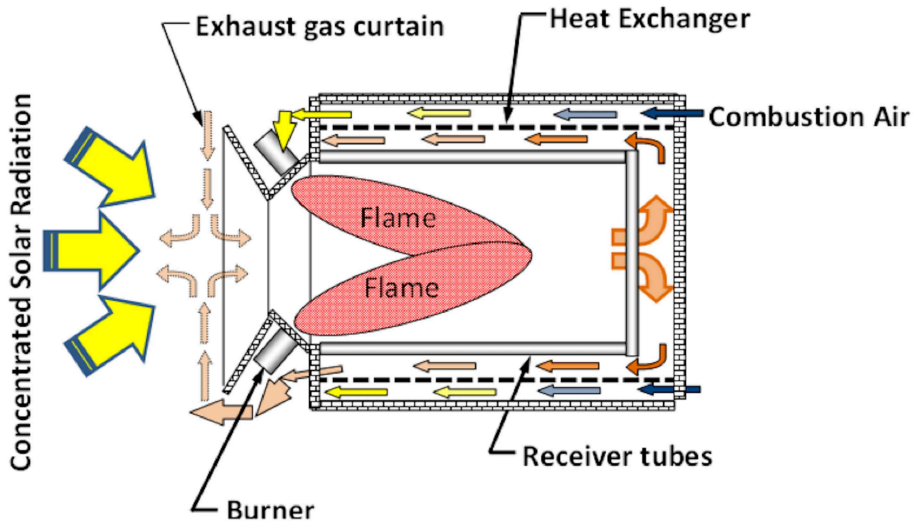


**FIGURE 1 |** Schematic diagram of the conceptual design of the Hybrid Solar Receiver Combustor, HSRC. Adapted from Lim et al. (2016a).

HSRC design and evaluating its performance under different fuels and operating conditions.

## METHODS

This section describes in brief the methods employed by Chinnici et al. (2017a,b, 2018a,b,c, 2019a,b) in the design, development and testing of the first-of-a-kind HSRC unit. A combination of numerical and experimental analyses was performed with the aim to achieve a proof-of-concept of the HSRC technology while also advancing current fundamental understanding of MILD and mixed processes.

Computational Fluid-Dynamic (CFD) was employed both in the initial design optimization of the device (geometry, selection of the most appropriate combustion technology) and to better understand the influence of the two main modes of operation (combustion-only and solar-only) and fuel type on heat transfer, thermal performance and combustion characteristics within the HSRC. To this aim, a 3-D CFD RANS model of a HSRC unit was developed using commercial codes to identify an optimized configuration and to complement the experimental investigation. A Monte-Carlo ray tracing method was used to describe the heat transfer from CSR. The MILD process was modeled using the Eddy Dissipation Concept (EDC) for turbulence-chemistry interactions, simplified and detailed mechanism for the chemistry, and the Discrete Ordinate (DO) approach for the radiation. Additional details of the model set-up and mesh can be found in Chinnici et al. (2017a,b, 2018b). In the design stage, the influence of several geometrical and operating parameters on the performance of the device was assessed to identify an optimized HSRC configuration for further experimental tests. In particular, the influence of the length-to-diameter (*L/D*) cavity ratio, the shape of the outlet section of the cavity, the annular jet arrangement, the heat exchanger (HX) design, and the type of combustion mode (conventional vs. MILD) were investigated. In a second stage, the CFD model of the optimized HSRC configuration was validated against experimental data and further numerical analysis was carried out to better understand the heat transfer mechanisms within the device.

Based on the initial design optimization, a 20 kW laboratory scale MILD HSRC (**Figure 2**) was developed, built and tested. All the details of the experimental set-up and rig can be found in Chinnici et al. (2018a), so that only the key features are summarized here. The device retains all the characteristics of conventional tubular solar receivers, i.e., an insulated cavity (with a length-to-diameter cavity ratio, $L/D = 3$) with an opening to allow CSR into it, and a heat exchanger (HX) carrying out the heat transfer fluid, HTF (air). In addition, the device features a combustor with a unique annular jet arrangement (Long et al., 2017, 2018a,b), which generates an intense recirculation of hot products needed for the establishment of the MILD regime, and a conical outlet section for the exhaust. For solar-only operations, the aperture was open while it was sealed by a conventional swirl burner (used to pre-heat the cavity prior to switch to MILD combustion) for combustion-only and combined modes (Chinnici et al., 2018a). A 5 $kW_{el}$ xenon-arc solar simulator and the combustion of a wide variety of fuels, namely natural gas (NG), liquefied petroleum gas (LPG), hydrogen ($H_2$), and their blends ($H_2$/NG, $H_2$/LPG with different $H_2$%) were used as the energy sources for the three modes. The total power input, $P_{in}$, the equivalence ratio, $\phi$, and the total HTF flow rate ($Q_{HTF}$) were varied in the range 10–20 $kW_{th}$, 0.8–1, and 150–1,000 *slpm*, respectively. **Table 1** summarizes all the key operating conditions investigated by Chinnici et al. (2017a,b, 2018a,b,c, 2019a,b).

The device features a series of N-thermocouples to continuously measure the inner wall cavity temperature, the total heat transfer rate through each section of the HX, the total heat extracted from the HX as well as the total

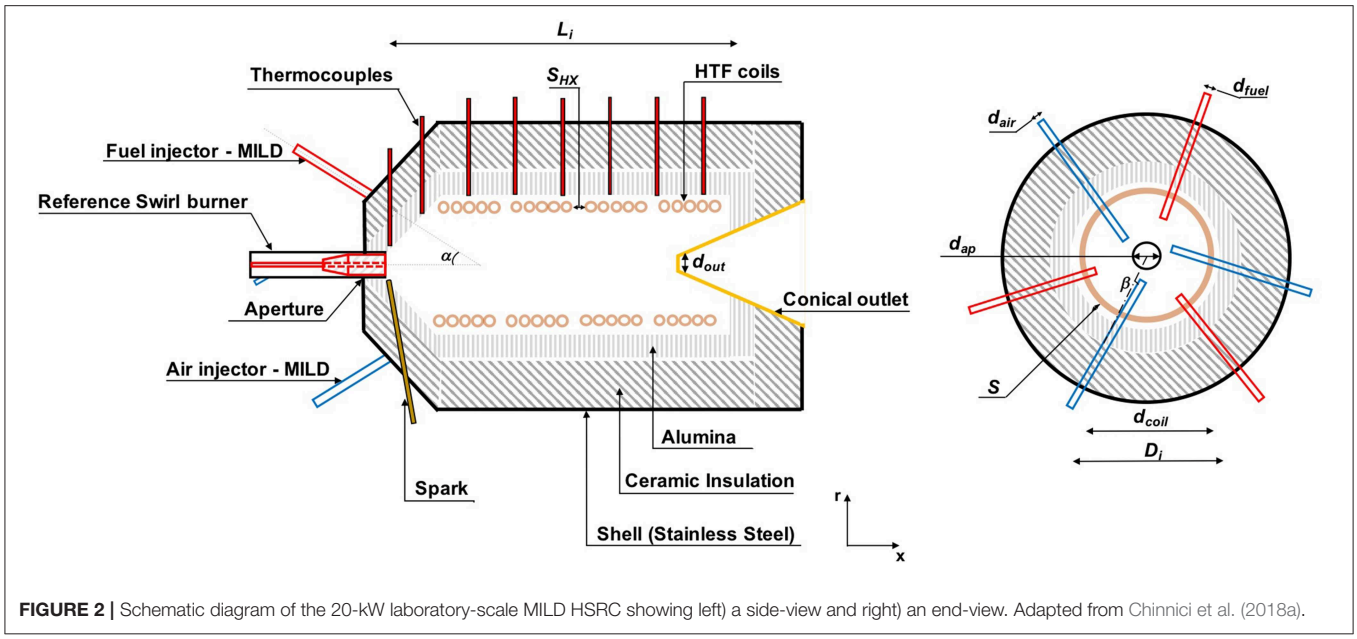


**FIGURE 2 |** Schematic diagram of the 20-kW laboratory-scale MILD HSRC showing left) a side-view and right) an end-view. Adapted from Chinnici et al. (2018a).

**TABLE 1 |** Experimental operating conditions for all the modes of operation investigated by Chinnici et al.

| Mode | Fuel | Fuel/$H_2$, *mol/mol* | $P_{in}$, kW | $\phi$ | *S/F*, % | HTF flow rate, *slpm* |
|---|---|---|---|---|---|---|
| Solar-only | / | / | 0.8 | / | $\infty$ | 150–1,000 |
| Combustion-only (MILD, conventional) | NG/$H_2$ | 0 | 10–20 | 0.9 | / | 150–1,000 |
| Mixed | | 25 | | | 4–8 | |
| | | 50 | | | | |
| | | 75 | | | | |
| | | $\infty$* | | | | |
| Combustion-only (MILD, conventional) | LPG/$H_2$ | 0 | 10–20 | 0.9 | / | 150–1,000 |
| Mixed | | 25 | | | 4–8 | |
| | | 50 | | | | |
| | | 75 | | | | |
| | | $\infty$* | | | | |

*Only pure NG and LPG cases were considered for conventional combustion cases (*).*

and specific (radiative, convective, conductive) heat losses. A portable gas analyser was also employed to continuously monitor the composition of the exhaust stream. Details of these measurements together with their accuracies and definition of warm-up and steady-state conditions can be found in (Chinnici et al., 2018a).

To assess the performance of the device for each case investigated, Chinnici et al. defined an "*absorption efficiency*" ($\eta_{abs}$), i.e., the ratio of the heat absorbed by the HX to the total thermal input. To assess the effects of heat recovery on the performance of the device, they also defined a "*potential thermal efficiency*" ($\eta_{th}$), assuming that 80% of the sensible heat in the exhaust stream is recovered. The energy balance of the system for each mode, together with the details regarding the measurements and calculations of each efficiency and heat loss terms can be found in Chinnici et al. (2018a, 2019b).

# KEY RESEARCH FINDINGS

As discussed in section Methods, the research into the HSRC and its operation involved initial design optimization and experimental testing. This section presents the key findings from the experimental and computational research into optimizing the design and evaluating the HSRC performance under different fuels and operating conditions at laboratory-scale. The experimental rig described in section Methods was used to investigate the effect of mode of operation, fuel type and heat extraction on the stability and thermal performance characteristics of the device.

## Computational Analysis

### Influence of Geometry and Modes of Operation on Performance

The geometrical parameters are essential for achieving the desired thermal efficiency and operation flexibility of the device. The reasons for this dependency relates to the importance of high rate of recirculation and reactants injection separation to achieve MILD combustion conditions. It also relates to the different heat transfer modes between the solar resource (radiation) and combustion (mostly convection). Ensuring the capture and distribution of solar radiation as well as the enhanced recirculation rate for MILD combustion requires careful selection of the aspect ratio of the diameter and the length of the device.

**Figure 3** presents the combined effects of varying the length-to-diameter cavity ratio (*L/D*, for a fixed *D*), outlet shape (with and without cone), and mode of operation (MILD, conventional combustion, and solar-only mode) on the calculated thermal performance of the device, employing NG as fuel. Here, $P_{in}$

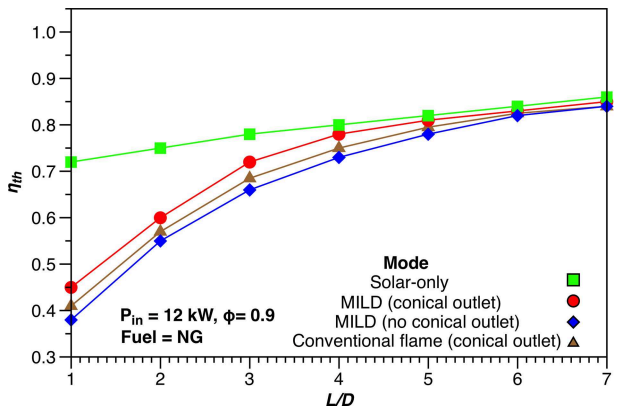


**FIGURE 3 |** Calculated values of the thermal efficiency, $\eta_{th}$, as a function of the length-to-diameter cavity ratio, *L/D*, by varying the shape of the outlet section, mode of operation and combustion type (MILD vs. conventional).

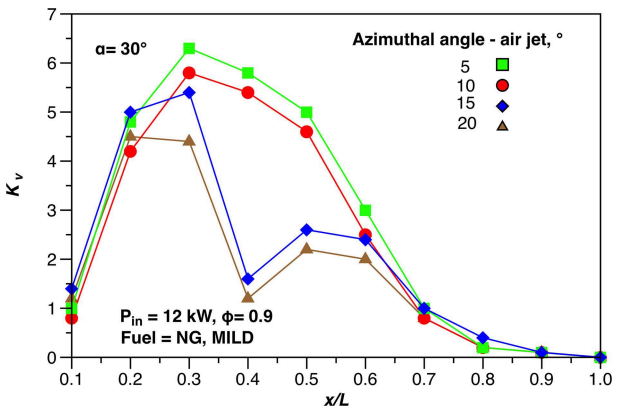


**FIGURE 4 |** Calculated values of the recirculation rate factor, Kv, along the x-axis of the device, by varying the azimuthal angle ($\beta$) of the air jets, and for a fixed value of the air jet inclination angle ($\alpha$). The case refers to MILD operations (fuel = NG) with L/D = 3 and a conical outlet.

was fixed to 12 kW for all cases (with $\phi = 0.9$ for combustion operations) and a fixed temperature ($T_{coil}$ = 1,000 K) was applied as boundary conditions to the HX. It can be seen that the cavity length strongly influences the performance of the device. In particular, it was found that, for a conical outlet section, relatively long cavities ($L/D \geq 3$) are required to achieve similar performance under the different modes while for all the other configurations the values of $\eta_{th}$ were predicted to be lower for combustion operations than for the solar-only modes. This because, for combustion-only and mixed operations, the predicted values of the heat losses due to the unrecovered heat from the exhaust are greater than the convective heat losses under solar-only mode. Also, it can be seen that the shape of the outlet section is a key design parameter. In particular, for HSRC geometries with a circular outlet section, a cavity of sufficiently length ($L/D > 5$) is needed to achieve similar performance under the different modes. This because the use of a conical outlet enhances the recirculation of hot products into the device, which leads to an increase in the convective heat transfer rate. **Figure 3** also shows that, for a fixed HSRC geometry, the MILD regime provides a better match with the solar-only mode in terms of performance in comparison with conventional combustion processes.

**Figure 4** presents the influence of the air jets arrangement on the calculated value of the recirculation rate factor, $K_v$ (Chinnici et al., 2017b), for MILD operations and for a fixed value of L/D (L/D = 3) and shape of the outlet section (conical). Here, the azimuthal angle of the air jet, $\beta$, was varied while fixing its inclination angle ($\alpha = 30^{\circ}$). It can be seen that the design of the annular burner arrangement significantly influences $K_v$, and hence the recirculation of hot products within the device and the rate of convective heat transfer. In particular, it was found that the maximum peak value of $K_v$ (6.3, which is a value higher than that of conventional MILD burners) was generated for a value of $\beta = 5^{\circ}$. This configuration also features a value of $K_v > 3$ for more than 35% of the device length. Therefore, this burner configuration was selected for further experimental investigation.

Overall, the numerical analysis of the device indicates that the geometry design and the selection of the combustion regime are critical parameters that need to be taken into account to identify suitable, optimized HSRC configurations for which similar performance can be achieved in the different modes of operation.

## Heat Transfer Analysis of MILD and Solar-Only Modes

To further assess how the mode of operation and composition of the fuel influence the dominant heat transfer mechanisms within the device, **Table 2** reports the calculated values of the radiative ($\dot{Q}_{abs,rad}$), convective ($\dot{Q}_{abs,conv}$), and the total rate of energy absorbed by the HTF pipes, for solar-only operations ($P_{in}$ = 12 kW, inlet peak flux = 1 MW/m$^2$), and for five fuels (NG, LPG, $H_2$, NG/$H_2$ = 1/1 v/v, and LPG/$H_2$ = 1/1 v/v) under MILD operations ($P_{in} = 12$ kW, $\phi = 0.9$), for the optimized laboratory-scale HSRC configuration. The calculated values of $\eta_{th}$, mean absorption coefficient, $\alpha_g$, and normalized emissive source term, $R_e = \frac{a_g}{a_{g,r}}\left(\frac{T_g}{T_r}\right)^4$, are also reported. Here, $T_g$ is the mean gas temperature within the cavity and the subscript $r$ represents reference values ($T_r = 298$ K and $a_{g,r} = 1$ m$^{-1}$). It can be seen that the majority of the energy input is transferred by radiation under solar mode and by a combination of radiation and convection under MILD combustion. For combustion operations, the ratio $\dot{Q}_{abs,rad}/\dot{Q}_{abs,conv}$ was found to be >1 for all the cases investigated. For the $H_2$ case, the calculated values of $\dot{Q}_{abs,rad}$ and $R_e$ were greater than those of LPG, NG, and fuel blends cases. This because of a higher flame temperature, despite a lower value of $\alpha_g$ (Chinnici et al., 2018b). In addition, the NG case features the smallest value of $R_e$ (despite $\alpha_g$being the lowest) due to the lower adiabatic flame temperature (the emissive power is a function of ${T_g}^4$). For the NG case, a higher value of $\dot{Q}_{abs,conv}$ was calculated in comparison with the other cases, "owing to a greater inlet air jet momentum, which, in turn, leads to an increase in the recirculation rate" (Chinnici et al., 2018b). Overall, the analysis highlights that, for the geometry and operating conditions

**TABLE 2 |** Calculated values of the average absorption coefficient, $a_g$, normalized emissive source term, $R_e$, convective and radiative heat transfer rates, and thermal efficiency for all the cases analyzed here ($P_{in}$ = 12 kW, $\phi$ = 0.9, boundary conditions HTF coils: $T_{coil}$ = 1,000 K).

| Mode | Fuel type | $\eta_{th}$ | $\dot{Q}_{abs,rad}$ kW | $\frac{\dot{Q}_{abs,rad}}{\dot{Q}_{abs,conv}}$ | $a_g$, $m^{-1}$ | $R_e$ |
|---|---|---|---|---|---|---|
| Solar-only | / | 0.78 | | | / | / |
| Combustion-only | NG | 0.72 | 1.655 | 1.79 | 0.7 | 180 |
| Combustion-only | LPG | 0.73 | 1.74 | 1.91 | 0.68 | 184 |
| Combustion-only | $H_2$ | 0.75 | 1.95 | 2.13 | 0.62 | 192 |
| Combustion-only | NG/$H_2$ 1/1 | 0.73 | 1.76 | 1.95 | 0.66 | 186 |
| Combustion-only | LPG/$H_2$ 1/1 | 0.735 | 1.82 | 2 | 0.64 | 189 |

*Data from Chinnici et al. (2018b).*

investigated, the H/C ratio of the fuel stream plays a minor role in the radiated energy to the heat exchanger within the cavity under MILD operations. This is mainly because the calculated mean equivalent optical length is relatively small (∼0.2 m).

## Experimental Analysis

### Influence of Mode of Operation and Fuel Type on Wall Temperature, Heat Flux Distribution, and Pollutants Emissions

**Figure 5** presents the axial distribution of the normalized wall temperature (inner layer), $T_c/T_{c,max}$, and normalized heat flux through the HTF coils, $Q/Q_{max}$, for combustion-only (MILD and conventional combustion), solar-only and mixed mode (MILD and solar simultaneously), for a fixed value of $P_{in}$ (12 kW for combustion operations), $\phi$ (0.9) and $Q_{HTF}$ (150 slpm), and for the NG case. Here, $Q_{max}$ and $T_{c,max}$ are the maximum peak of the heat flux and wall temperature, respectively. It can be seen that the combustion-only and solar-only modes feature two different heat flux distributions, indicating that there is a need to manage the challenges associated with it (e.g., thermal stresses on HTF pipes). Nevertheless, it can also be seen that the MILD regime features a relatively uniform flux, and that this characteristic is also preserved under mixed conditions. That is, the use of a MILD process reduces the risk associated with hot spots within the HSRC for both combustion and combined operations in comparison with conventional combustion processes.

**Figure 6** presents the measured values of $T_c$, $Q$ under stable MILD and mixed operations, for a fixed HTF flow rate ($Q_{HTF}$ = 150 slpm) and by varying the fuel type ($P_{in}$ = 12 kW and $\phi$ = 0.9). It can be seen that, regardless of the composition of the fuel and mode of operation, the cavity features uniform heat flux and temperature distribution. The substitution of NG with LPG or $H_2$ leads to a relatively small increase in the measured values of $T_c$ and $Q$ (of up to 1.5 and 3.5%, respectively). In addition, the simultaneous addition of CSR and MILD combustion into the cavity does not alter the shape of the heat flux and wall cavity temperature. This indicates that the MILD regime of NG, LPG, $H_2$, and their blends can be successfully established and sustained in a cavity collecting heat from multiple energy sources and in fluid/heat communication with the ambient through the aperture. It is worth noting that only a small fraction of ambient air (<10% of the inlet combustion air) was entrained into the device under mixed operations, for all the cases investigated.

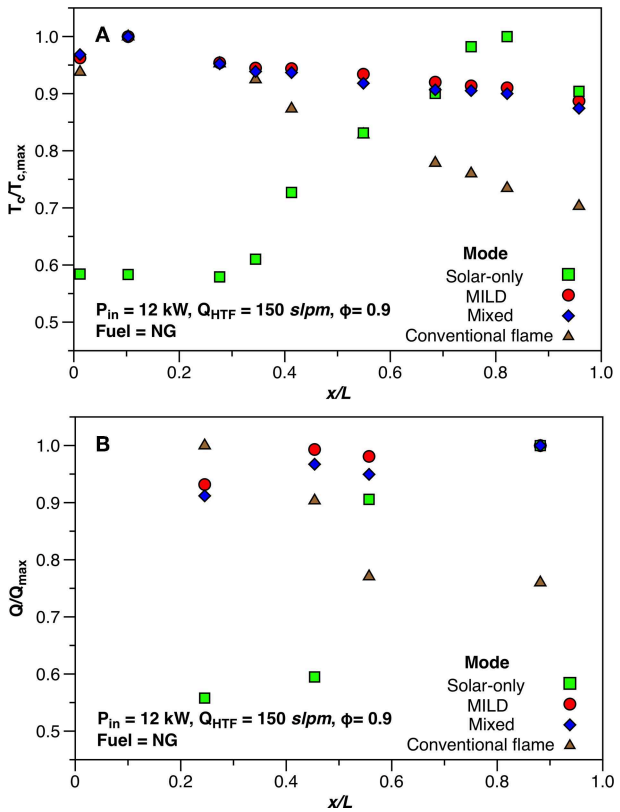


**FIGURE 5 |** Axial distribution for all modes of operation of **(A)** the wall cavity temperature normalized by its maximum value, $T_c/T_{c,max}$, and **(B)** heat flux through HTF coils normalized by its maximum value, $Q/Q_{max}$. Conditions for combustion operations: $P_{in}$ = 12 kW, $\phi$ = 0.9, $Q_{HTF}$ = 150 slpm, fuel = NG. Data from Chinnici et al. (2018a,b, 2019b).

**Figure 7** shows the influence of the mode of operation (MILD and mixed) and fuel composition on the $NO_x$ emissions, for a fixed value of $P_{in}$, $\phi$, and $Q_{HTF}$ ($P_{in}$ = 12 kW, $\phi$ = 0.9, $Q_{HTF}$ = 150 slpm). It can be seen that for stable MILD operations, ultra-low NOx emissions (<20 ppmv @ 3%$O_2$) were measured for all the cases investigated. It can be seen that a variation in the fuel type only leads to a relatively minor change in the $NO_x$ emissions (the maximum $NO_x$ variation was ∼6 ppmv, obtained by replacing NG with $H_2$). Also, it was found that the $NO_x$ emissions exhibit almost a linear dependence on the percentage of $H_2$ in the fuel stream. This trend is consistent with previous works in different MILD burner configurations. In addition, it can be seen that the presence of CSR does not alter the $NO_x$ emissions of the MILD process significantly. This further indicates that the fundamental characteristics of the MILD regime are preserved in the mixed mode. It is also

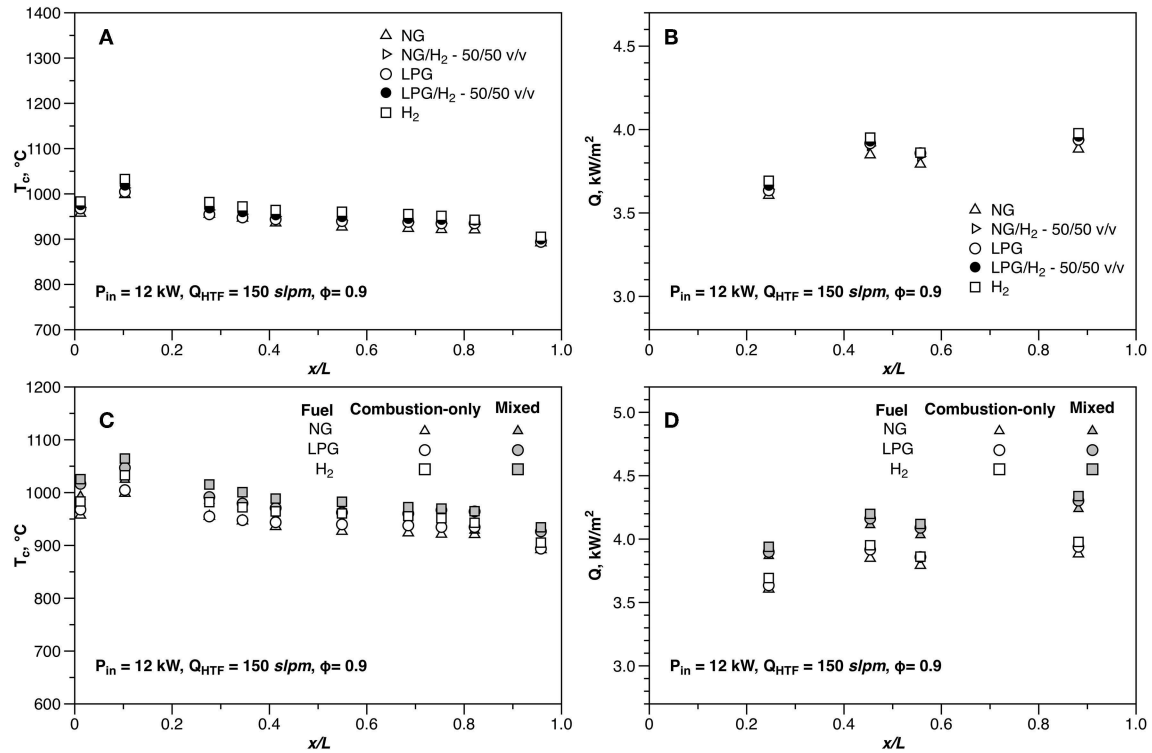


**FIGURE 6 | (A,C)** Measured axial distribution of the wall cavity temperature, $T_c$, and **(B,D)** heat flux through the HTF coils, $Q$, for the MILD **(A,B)** and mixed **(C,D)** modes of operation, as a function of the fuel type, and for a fixed HTF flow rate (150 slpm), thermal input ($P_{in}$ = 12 kW) and equivalence ratio ($\phi$ = 0.9). Data from Chinnici et al. (2018a,b); Chinnici et al. (2019a).

worth noting that the CO emissions were <10 ppmv for all cases investigated, indicating that the residence time within the cavity is sufficient to enable complete conversion, and that the maximum recorded $NO_x$ value under MILD conditions was ∼85% lower than that of conventional combustion (not shown).

## Influence of Mode of Operation, Fuel Type, and Heat Extraction on Thermal Performance and Heat Losses

**Figure 8** presents the measured values of $\eta_{abs}$ and $\eta_{th}$ for the different fuels considered here, under MILD and mixed operations ($P_{in}$ = 12 and 15 kW, $\phi$ = 0.9), and by varying $Q_{HTF}$. The measured performance for conventional combustion and solar-only operations are also reported for comparison. A comparison of $\eta_{th}$ under the different modes highlights that the device can achieve similar performance (up to ∼90%) in all modes, with a maximum outlet HTF temperature ($T_{max,HTF}$) >750°C. This despite the energy sources (CSR, chemical energy stored in fuels) collected into the device being different in nature and featuring different heat transfer mechanisms. Also, the values of $\eta_{abs}$ are higher for the MILD regime than those of conventional combustion (up to ∼5%), and similar to those of the solar-only mode. For mixed operations, a net thermal gain was found in comparison with combustion operations. In particular, despite a slight decrease in $\eta_{th}$ (∼2%), the specific fuel consumption, i.e., the fuel consumption per unit of useful thermal output to the HTF (Chinnici et al., 2018a), was reduced by up to 20%. It can also be seen that, for MILD operations, the replacement of NG or LPG with $H_2$ leads to an increase in $\eta_{abs}$, of up to ∼9%. This difference is attributed to a higher radiative heat transfer rate (due to a higher cavity temperature) rather than the convection term. In fact, for the $H_2$ case, the inlet jet air momentum is ∼45% lower than that of LPG and NG, which, in turn, leads to a lower recirculation rate within the cavity (and hence, a lower rate of convective heat transfer).

To further assess the influence of the mode of operation on thermal performance, **Table 3** reports the values of the total and specific heat losses for the MILD and mixed operations, for the different fuels investigated here ($P_{in}$ = 12 kW, $\phi$ = 0.9, $Q_{HTF}$ = 150 slpm). The values for the solar-only mode are also reported for comparison. For solar-operations, the convective heat losses represent the main loss, ∼45% of the total losses due to the relatively low cavity temperature. For MILD operations, the sensible heat in the exhaust represents the main loss, ∼70% of the total losses. For mixed operations, the additional convective and radiative losses are relatively low (∼5% of the total losses), which further explains the thermal net gain in comparison with combustion-only operations. Also, the convective term is similar for both MILD and mixed operations, which indicates that only a small amount of ambient air is entrained into the cavity through the aperture under mixed mode (∼2.5% of the combustion air), for the geometry analyzed here.

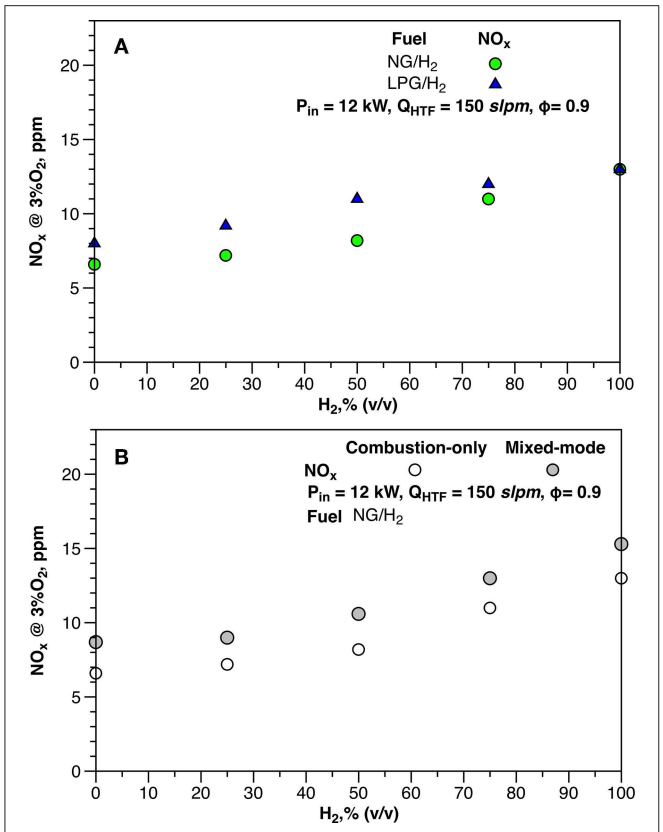


**FIGURE 7 |** Measured NOx emissions for the MILD **(A,B)** and mixed **(B)** modes of operation, as a function of the fuel type, and for a fixed HTF flow rate (150 slpm), thermal input ($P_{in}$ = 12 kW) and equivalence ratio ($\phi$ = 0.9). Data from Chinnici et al. (2018a,b); Chinnici et al. (2019a).

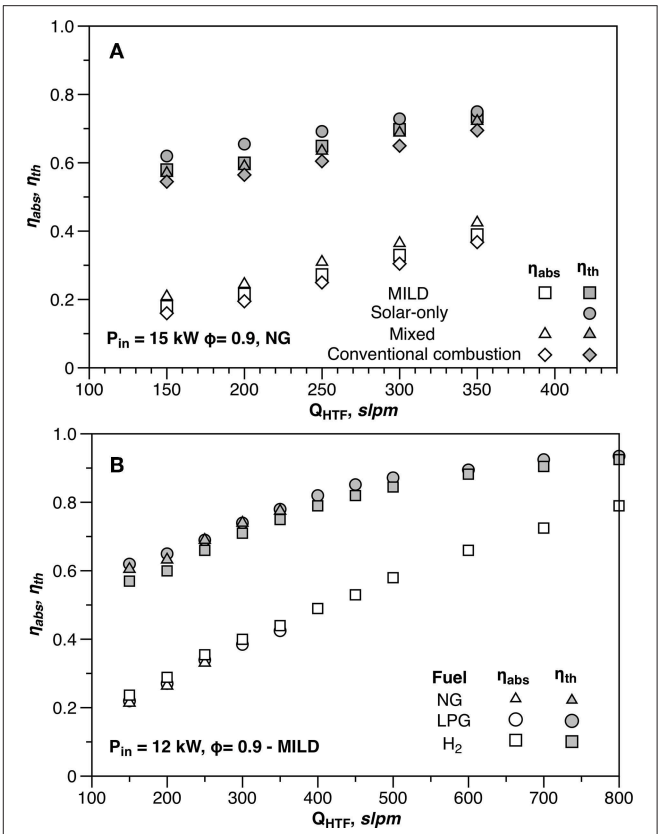


**FIGURE 8 |** Measured values of absorption ($\eta_{abs}$) and thermal ($\eta_{th}$) efficiencies for **(A)** the different modes of operation, and **(B)** the different fuel analyzed under MILD conditions. Data from Chinnici et al. (2018b).

**TABLE 3 |** Measured values of the heat losses for the different modes of operation and fuel analyzed, conditions for combustion operations: $P_{in}$ = 12 kW, $\phi$ = 0.9, $Q_{HTF}$ = 150 slpm.

| Fuel | Mode | $\dot{Q}_{ex}$ | $\dot{Q}_{conv}$ | $\dot{Q}_{rad}$ | $\dot{Q}_{cond}$ |
|---|---|---|---|---|---|
| / | Solar mode | / | 0.18 | 0.0033 | 0.12 |
| NG | Combustion-only | 5.8 | N/A | 0.15 | 3.2 |
| NG | Mixed | 5.65 | 0.22 | 0.45 | 3.25 |
| LPG | Combustion-only | 5.5 | N/A | 0.18 | 3.3 |
| LPG | Mixed | 5.2 | 0.25 | 0.5 | 3.32 |
| $H_2$ | Combustion-only | 4.8 | N/A | 0.28 | 3.75 |
| $H_2$ | Mixed | 4.62 | 0.29 | 0.62 | 3.8 |

*Data from Chinnici et al. (2018b).*

## Influence of Mode of Operation, Fuel Type, and Heat Extraction on Stability Characteristics

**Figure 9** presents the stability maps ($\eta_{abs}$-$H_2$% domain) for both MILD and MILD-solar processes for all the fuels investigated here, and for different values of the heat extraction (for a fixed value of $P_{in}$ and $\phi$). It can be seen that, regardless of the fuel composition and mode of operation, the stability maps feature three distinctive regions. For low to moderate values of the heat extraction, the MILD process can be successfully stabilized within the HSRC, which features no visible flame, ultra-low $NO_x$ (<20 ppmv) and a uniform temperature field. An increase in the heat extracted leads to the occurrence of a dynamic behavior, which features temporal oscillations of species and temperature, appearance of a reddish-colored flame and high CO emissions (up to ∼1,000 ppmv). This well-known behavior is attributed to an insufficient amount of enthalpy needed to stabilize the MILD process. A further increase in the heat extracted leads to the conditions $T_{out} < T_{self-ign}$ (being $T_{out}$ and $T_{self-ign}$ the exhaust temperature and the self-ignition temperature of the mixture, respectively) or $\tau_{ign} > \tau_{res}$ (being $\tau_{ign}$ and $\tau_{res}$ the ignition delay time of the mixture and the mean gas residence time within the cavity, respectively), so that the combustion process can no longer be sustained.

For both MILD and combined operations, it can be seen that the combustion process can be stabilized in a wider range of conditions by substituting NG with $H_2$ or LPG (the extension of the dynamic region reduces of ∼60 and ∼20%, respectively, in comparison with the NG case). This is attributed to thermo-kinetic effects rather than thermal only (Chinnici et al., 2018b) since the cavity temperature varied of only ∼2% by varying the fuel composition. In addition, it can be seen that either the

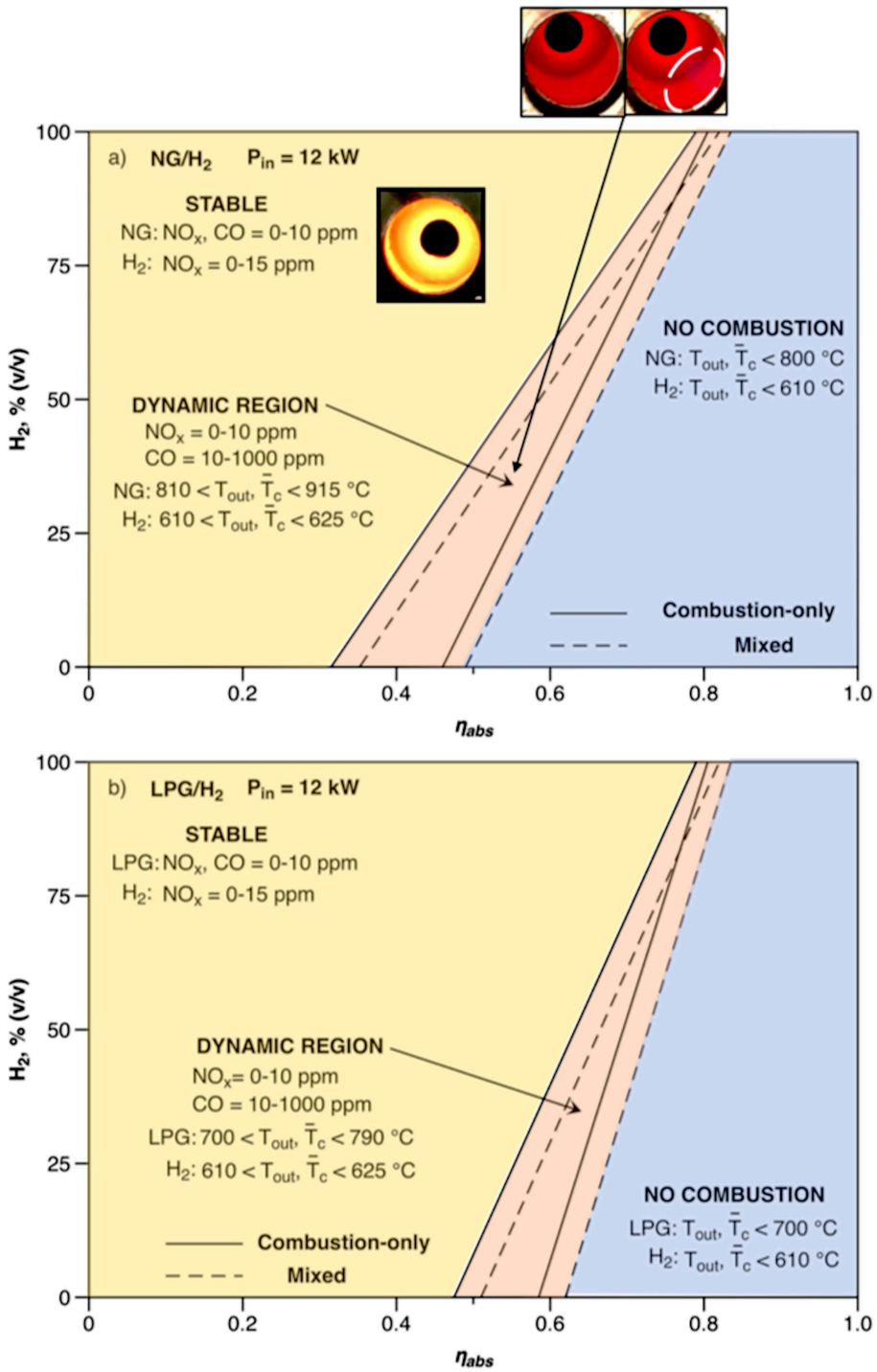


**FIGURE 9 |** Experimental stability maps for combustion-only and mixed operations, and for **(a)** NG/$H_2$ and **(b)** LPG/$H_2$ mixtures ($P_{in}$ = 12 kW, $\phi$ = 0.9). The deduced boundaries for each system behavior are based on ~100 data points for each fuel. Typical in-furnace images for stable MILD and dynamic behavior are also reported (photos taken during combustion-only modes with the aperture open prior to switch to mixed operations). Data from Chinnici et al. (2018b).

addition of $H_2$ or CSR to the MILD regime enhances the stability of the combustion process, shifting the instability limits toward lower operating temperatures and reducing the extension of the dynamic region.

## CONCLUSIONS

The current paper provided a review of the design, development, and testing of the first-of-a-kind Hybrid Solar Receiver

Combustor technology, carried out at the Center for Energy Technology of the University of Adelaide. The key findings from the research into the HSRC and its operation are as follows:

- *Technology Development*: Despite the different nature of the energy sources and their different heat transfer contributions (radiation-dominated for CSR, combination of radiation, and convection for the combustion process), similar thermal performance can be achieved under the different modes of operation, for a wide range of operating conditions and fuel type. The experimental investigation showed that a net thermal gain can be achieved for very low solar fluxes (∼6%) under combined mode, with a maximization of solar harness relatively to conventional tubular receiver and ∼20% reduction in the specific fuel consumption in comparison with combustion-only operations. This confirms that the economic benefits estimated by previous techno-economic analyses are realistic in terms of LCOE and fuel consumption reduction. The use of MILD combustion for combustion-only and combined operations allows fuel flexibility/switchability, homogeneous heat distribution, very low emission of $NO_x$ and CO, and a better heat transfer match with CSR in comparison with conventional combustion processes. Nevertheless, the heat flux distributions for the solar and combustion-only modes of operation are significantly different for the present configuration, indicating that an appropriate design of the combustor and solar concentrating optics is required to minimize these differences and develop suitable control strategies for large-scale applications.
- *Fundamental understanding*: The main features of the MILD regime (ultra-low $NO_x$, uniform temperature) are preserved in the combined mode (regardless of the fuel composition), despite the addition of CSR to the process and the heat/mass transport into and from the cavity through the aperture. The stability analysis revealed that both MILD and MILD-solar processes can be successfully stabilized in a wide range of heat extraction values. Also, the combustion process can be stabilized in a broader range of operating conditions by either adding CSR or $H_2$ to the MILD regime. Furthermore, it was found that H/C ratio of the fuel stream only play a minor role in the radiated energy to the heat exchanger within the cavity and pollutant emissions.

## FUTURE DIRECTIONS

A review of the key findings and current understanding of the influence of CSR on a combustion process also highlighted the need for further research to support the technology development. Particularly, the available experimental data are limited to a very low value of the solar-to-fuel, *S/F*, ratio (<10%) so that new data are required to assess the performance of the mixed mode at medium to high *S/F* values (10–50%). Also, all the data were collected under no wind conditions, so that the effects of wind speed and direction on the performance and stability characteristics of the device are presently not available. This is critical as the wind significantly influences the convective heat losses within a solar receiver. Data under well-controlled conditions (wind tunnel) are required to fill in this gap and for model validation. The use of active controls (e.g., sealing gas systems) to mitigate the effects arising from wind should be also investigated prior to scale-up. Measurements under transients loading are also needed to assess the system response in terms of performance and mechanical/thermal stresses. The use of different alternative fuels (e.g., syngas, ammonia) under MILD and mixed operations needs to be investigated to further the understanding of the influence of the fuel composition on performance.

The analysis also showed that a cavity of sufficient length (L/D $\geq$ 3) is needed to achieve similar performance under the different modes of operation. The calculated difference in the heat transfer rate between MILD and concentrated solar radiation implies that a different combustion technology, featuring higher radiative heat transfer rates, and heat fluxes similar to those of CSR (e.g., infrared radiant burners), may be required for direct hybridization of very short cavities or for solar receiver design different from tubular receivers (e.g., billboard receivers).

## AUTHOR CONTRIBUTIONS

All the authors contributed to the conception and design of the work. In addition, AC performed the experimental and numerical analyses, collected and interpreted the data, and drafted the majority of the paper. BD drafted the introduction of the manuscript and revised the paper. GN provided a critical review of the paper.

## FUNDING

The support of the Australian Research Council and of FCT Combustion and Vast Solar through the ARC Linkage scheme LP110200060 was gratefully acknowledged.

## ACKNOWLEDGMENTS

This work was supported with supercomputing resources provided by the Phoenix HPC service at the University of Adelaide. The authors also acknowledge the use of the Thebarton facilities of the University of Adelaide.

## REFERENCES

Agrafiotis, C., von Storch, H., Roeb, M., and Sattler, C. (2014). Solar thermal reforming of methane feedstocks for hydrogen and syngas production - a review. *Renew. Sustain. Energy Rev.* 29, 656–682. doi: 10.1016/j.rser.2013.08.050

Ayoub, M., Rottier, C., Carpentier, S., Villermaux, C., Boukhalfa, A. M., and Honore, D. (2012). An experimental study of mild flameless combustion of methane/hydrogen mixtures. *Int. J. Hydrogen Energy* 37, 6912–6921. doi: 10.1016/j.ijhydene.2012.01.018

Chinnici, A., Nathan, G. J., and Dally, B. B. (2018a). Experimental demonstration of the hybrid solar receiver combustor. *Appl. Energy* 224, 426–437. doi: 10.1016/j.apenergy.2018.05.021

Chinnici, A., Nathan, G. J., and Dally, B. B. (2018b). Combined solar energy and combustion of hydrogen-based fuels under MILD conditions. *Int. J. Hydrogen Energy* 43, 20086–20100. doi: 10.1016/j.ijhydene.2018.09.027

Chinnici, A., Nathan, G. J., and Dally, B. B. (2018c). Performance of a hybrid solar receiver combustor. *AIP Conf. Proc*. 2033:180004. doi: 10.1063/1.5067176

Chinnici, A., Nathan, G. J., and Dally, B. B. (2019a). An experimental study of the stability and performance characteristics of a Hybrid Solar Receiver Combustor operated in the MILD combustion regime. *Proc. Combust. Inst.* 37, 5687–5695. doi: 10.1016/j.proci.2018.05.099

Chinnici, A., Tian, Z. F., Lim, J. H., Nathan, G. J., and Dally, B. B. (2017a). Comparison of system performance in a hybrid solar receiver combustor operating with MILD and conventional combustion. Part I: Solar-only and combustion-only employing conventional combustion. *Solar Energy* 147, 489–503. doi: 10.1016/j.solener.2017.02.055

Chinnici, A., Tian, Z. F., Lim, J. H., Nathan, G. J., and Dally, B. B. (2017b). Comparison of system performance in a hybrid solar receiver combustor operating with MILD and conventional combustion. Part II: Effect of the combustion mode. *Solar Energy* 147, 479–488. doi: 10.1016/j.solener.2017.02.054

Chinnici, A., Tian, Z. F., Lim, J. H., Nathan, G. J., and Dally, B. B. (2019b). Thermal performance analysis of a syngas-fuelled hybrid solar receiver combustor operated in the MILD combustion regime. *Combust. Sci. Technol.* 191, 2–17. doi: 10.1080/00102202.2018.1452381

de Joannon, M., Chinnici, A., Sabia, P., and Ragucci, R. (2012). Optimal post-combustion conditions for the purification of $CO_2$-rich exhaust streams from non-condensable reactive species. *Chem. Eng. J.* 211–212, 318–326. doi: 10.1016/j.cej.2012.09.053

Derudi, M., Villani, A., and Rota, R. (2007). Sustainability of mild combustion of hydrogen-containing hybrid fuels. *Proc. Combust. Inst.* 31, 3393–3400. doi: 10.1016/j.proci.2006.08.107

Dong, X., Sun, Z., Gu, D., Ashman, P. J., Alwahabi, Z. T., Dally, B. B., et al. (2016). The influence of high flux broadband irradiation on soot concentration and temperature of a sooty flame. *Combust. Flame* 171, 103–111. doi: 10.1016/j.combustflame.2016.05.026

Evans, M. J., Chinnici, A., Medwell, P. R., and Ye, J. (2017). Ignition features of methane and ethylene fuel-blends in hot and diluted coflows. *Fuel* 203, 279–289. doi: 10.1016/j.fuel.2017.04.113

Evans, M. J., Medwell, P. R., Sun, Z., Chinnici, A., Ye, J., Chan, Q. N., et al. (2019). Downstream evolution of n-heptane/toluene flames in hot and vitiated coflows. *Combust. Flame* 202, 78–89. doi: 10.1016/j.combustflame.2019.01.008

Goswami, D. Y., and Kreith, F. (2007). *Handbook of Energy Efficiency and Renewable Energy*. Boca Raton, FL: CRC Press.

IEA (2018). *Global Energy & $CO_2$ Status Report. The Latest Trends in Energy and Emissions 2018*. IEA Report.

Jafarian, M., Arjomandi, M., and Nathan, G. J. (2013). A hybrid solar and chemical looping combustion system for solar thermal energy storage. *Appl. Energy* 103, 671–678. doi: 10.1016/j.apenergy.2012.10.033

Jafarian, M., Arjomandi, M., and Nathan, G. J. (2014). The energetic performance of a novel hybrid solar thermal & chemical looping combustion plant. *Appl. Energy* 132, 74–85. doi: 10.1016/j.apenergy.2014.06.052

Kodama, T. (2003). High-temperature solar chemistry for converting solar heat to chemical fuels. *Prog. Energy Combus. Sci.* 29, 567–597. doi: 10.1016/S0360-1285(03)00059-5

Kueh, K., Nathan, G. J., and Saw, W. (2015). Storage capacities required for a solar thermal plant to avoid unscheduled reductions in output. *Solar Energy* 118, 209–221. doi: 10.1016/j.solener.2015.04.040

Lim, J. H., Chinnici, A., Dally, B., and Nathan, G. (2017a). Assessing the techno-economics of modular hybrid solar thermal systems. *AIP Conf. Proc*. 1850:110007. doi: 10.1063/1.4984481

Lim, J. H., Chinnici, A., Dally, B. B., and Nathan, G. J. (2016a). Assessment of the potential benefits and constraints of a hybrid solar receiver and combustor operated in the MILD combustion regime. *Energy* 116, 735–745. doi: 10.1016/j.energy.2016.10.017

Lim, J. H., Dally, B. B., Chinnici, A., and Nathan, G. J. (2017b). Techno-economic evaluation of modular hybrid concentrating solar power systems. *Energy* 129, 158–170. doi: 10.1016/j.energy.2017.04.067

Lim, J. H., Nathan, G., Dally, B., and Chinnici, A. (2016c). Techno-economic assessment of a hybrid solar receiver and combustor. *AIP Conf. Proc*. 1734:070020. doi: 10.1063/1.4949167

Lim, J. H., Nathan, G. J., Hu, E., and Dally, B. B. (2016b). Analytical assessment of a novel hybrid solar tubular receiver and combustor. *Appl. Energy* 162, 298–307. doi: 10.1016/j.apenergy.2015.10.048

Long, S., Lau, T. C. W., Chinnici, A., Tian, Z. F., Dally, B. B., and Nathan, G. J. (2017). Experimental and numerical investigation of the iso-thermal flow characteristics within a cylindrical chamber with multiple planar-symmetric impinging jets. *Phys Fluids* 29:105111. doi: 10.1063/1.4986132

Long, S., Lau, T. C. W., Chinnici, A., Tian, Z. F., Dally, B. B., and Nathan, G. J. (2018a). Iso-thermal flow characteristics of rotationally symmetric jets generating a swirl within a cylindrical chamber. *Phys Fluids* 30:055110. doi: 10.1063/1.5026719

Long, S., Lau, T. C. W., Chinnici, A., Tian, Z. F., Dally, B. B., and Nathan, G. J. (2018b). The influence of aspect ratio on the iso-thermal flow characteristics of multiple confined jets. *Phys Fluids* 30:125108. doi: 10.1063/1.5063500

Medwell, P. R., Nathan, G. J., Chan, Q. N., Alwahabi, Z. T., and Dally, B. B. (2011). The influence on the soot distribution within a laminar flame of radiation at fluxes of relevance to concentrated solar radiation. *Combust. Flame* 158, 1814–1821. doi: 10.1016/j.combustflame.2011.01.006

Nathan, G. J., Battye, D. L., and Ashman, P. J. (2014). Economic evaluation of a novel fuel-saver hybrid combining a solar receiver with a combustor for a solar power tower. *Appl. Energy* 113, 1235–1243. doi: 10.1016/j.apenergy.2013.08.079

Nathan, G. J., Dally, B. B., Alwahabi, Z. T., Van Eyk, P. J., Jafarian, M., and Ashman, P. J. (2017). Research challenges in combustion and gasification arising from emerging technologies employing directly irradiated concentrating solar thermal radiation. *Proc. Combus. Inst.* 36, 2055–2074. doi: 10.1016/j.proci.2016.07.044

Nathan, G. J., Jafarian, M., Dally, B. B., Saw, W. L., Ashman, P. J., Hu, E., et al. (2018). Solar thermal hybrids for combustion power plant: a growing opportunity. *Prog. Energy Combust. Sci.* 64, 4–28. doi: 10.1016/j.pecs.2017.08.002

Parente, A., Galletti, C., and Tognotti, L. (2008). Effect of the combustion model and kinetic mechanism on the MILD combustion in an industrial burner fed with hydrogen enriched fuels. *Int. J. Hydrogen Energy* 33, 7553–7564. doi: 10.1016/j.ijhydene.2008.09.058

Philibert, C. (2017). *Renewable Energy for Industry: From Green Energy to Green Materials and Fuels*. IEA Report.

Romero, M., and Steinfeld, A. (2012). Concentrating solar thermal power and thermochemical fuels. *Energy Environ. Sci.* 5, 9234–9245. doi: 10.1039/c2ee21275g

**Conflict of Interest:** The authors declare that the research was conducted in the absence of any commercial or financial relationships that could be construed as a potential conflict of interest.

frontiers in Mechanical Engineering

ORIGINAL RESEARCH
published: 26 November 2019
doi: 10.3389/fmech.2019.00063

# Modeling Pollutant Emissions of Flameless Combustion With a Joint CFD and Chemical Reactor Network Approach

*André A. V. Perpignan, Rishikesh Sampat and Arvind Gangoli Rao**

*Faculty of Aerospace Engineering, Delft University of Technology, Delft, Netherlands*

OPEN ACCESS

***Edited by:***
*Alessandro Parente,*
*Université Libre de Bruxelles, Belgium*

***Reviewed by:***
*Sudarshan Kumar,*
*Indian Institute of Technology Bombay, India*
*Seyed Ehsan Hosseini,*
*Arkansas Tech University, United States*

****Correspondence:***
*Arvind Gangoli Rao*
*A.GangoliRao@tudelft.nl*

***Specialty section:***
*This article was submitted to Thermal and Mass Transport, a section of the journal Frontiers in Mechanical Engineering*

***Received:*** *30 April 2019*
***Accepted:*** *04 November 2019*
***Published:*** *26 November 2019*

***Citation:***
*Perpignan AAV, Sampat R and Gangoli Rao A (2019) Modeling Pollutant Emissions of Flameless Combustion With a Joint CFD and Chemical Reactor Network Approach. Front. Mech. Eng. 5:63. doi: 10.3389/fmech.2019.00063*

The Flameless Combustion (FC) regime has been pointed out as a promising combustion technique to lower the emissions of nitrogen oxides ($NO_x$) while maintaining low CO and soot emissions, as well as high efficiencies. However, its accurate modeling remains a challenge. The prediction of pollutant species, especially $NO_x$, is affected by the usually low total values that require higher precision from computational tools, as well as the incorporation of relevant formation pathways within the overall reaction mechanism that are usually neglected. The present work explores a multiple step modeling approach to tackle these issues. Initially, a CFD solution with simplified chemistry is generated [both the Eddy Dissipation Model (EDM) as well as the Flamelet Generated Manifolds (FGM) approach are employed]. Subsequently, its computational cells are clustered to form ideal reactors by user-defined criteria, and the resulting Chemical Reactor Network (CRN) is subsequently solved with a detailed chemical reaction mechanism. The capabilities of the clustering and CRN solving computational tool (AGNES—Automatic Generation of Networks for Emission Simulation) are explored with a test case related to FC. The test case is non-premixed burner based on jet mixing and fueled with $CH_4$ tested for various equivalence ratios. Results show that the prediction of CO emissions was improved significantly with respect to the CFD solution and are in good agreement with the experimental data. As for the $NO_x$ emissions, the CRN results were capable of reproducing the non-monotonic behavior with equivalence ratio, which the CFD simulations could not capture. However, the agreement between experimental values and those predicted by CRN for $NO_x$ is not fully satisfactory. The clustering criteria employed to generate the CRNs from the CFD solutions were shown to affect the results to a great extent, pointing to future opportunities in improving the multi-step procedure and its application.

**Keywords: automatic chemical reactor networks, flamelet-generated manifolds, flameless combustion, MILD combustion, $NO_x$ emissions**

# INTRODUCTION

Combustion of fossil fuels and industrial processes were estimated to contribute with around 65% of all anthropogenic greenhouse gases emissions in 2010, while being responsible for ∼85% of anthropogenic $CO_2$ emissions (IPCC, 2014). While there have been efforts to reduce emissions, the global $CO_2$ emissions have been increasing every year (International Energy Agency, 2018). Most scenarios developed for the future energy supply largely involve the combustion of biofuels, biomass, synthetic fuels, or hydrogen (Ellabban et al., 2014; Scarlat et al., 2015; Nastasi and Basso, 2016). Therefore, progress in combustion technology is necessary for the energy transition and also for the long term solutions that are being considered (Paltsev et al., 2018).

## Motivation

Even though the major species of combustion are primarily dictated by the fuel that is being used, the emission of minor pollutant species is dictated by the combustion process. The emission of minor pollutants (CO, $NO_x$, soot, and unburnt hydrocarbons) have a significant influence on local as well as the global environment. Carbon monoxide (CO) is a harmful substance usually present in flue gases when hydrocarbon or alcohol fuels are employed. Other typical pollutants are nitrogen oxides ($NO_x$). When air is used as an oxidizer, the formation of $NO_x$ tends to occur during combustion as the $N_2$ contained in air dissociates in the combustion reactions (Glarborg et al., 2018). The $NO_x$ emission from aircraft cruising in the upper layers of the troposphere or in the lower layers of the stratosphere is responsible for the formation of ozone (Grewe et al., 2012). At lower altitudes, the $NO_x$ emission is directly linked to respiratory diseases (World Health Organization, 2013), and is responsible for the acidification of water and rain that harms vegetation and wildlife (Camargo and Alonso, 2006). Therefore, there are tight regulations for the emission of CO and $NO_x$ and future restrictions on these emissions are being tightened, thereby posing challenges to designers of combustion systems.

One of the promising combustion technologies to lower pollutant emissions is the Flameless Combustion (FC) regime. Despite the fact that the FC regime does not have a clear and universally accepted definition, or that its physics are not yet fully understood (Perpignan et al., 2018a), it is clear that the regime has potential to substantially decrease emissions. Usually characterized by distributed reaction zones with lower temperature and species gradients, FC was shown to yield low $NO_x$ emissions while maintaining low CO (Kruse et al., 2015).

The modeling of FC is still challenging. Particularly, modeling tools able to predict pollutant emissions are required in order to assess, design and improve devices reliant on the regime. The use of Computational Fluid Dynamics (CFD) for modeling combustion largely relies on the use of simplified chemistry, as detailed chemical reaction mechanisms composed of hundreds of species and reactions cannot be accommodated at reasonable computational costs. Apart from the sheer number of reaction, solving detailed chemistry also adds the complexity of dealing with the wide range time-scales of the various chemical reactions, which causes the systems of equations to be stiff. Usually, the focus and strength of CFD has been on predicting reaction zone structures, temperatures and velocities, and not pollutant emissions.

## CRNs for Emission Prediction

The lack of detailed chemical schemes has been pointed out as the main cause of discrepancy often seen between CFD and experimental results in emissions (Lyra and Cant, 2013). Because of that, the use of Chemical Reactor Networks (CRNs) to predict pollutant emissions has gained attention. A CRN is a set of ideal chemical reactors, in which detailed chemical reaction mechanisms can be applied at relatively low computational costs. On the other hand, most approaches developed for CRNs neglect turbulence-chemistry interaction and complex flow structures.

The design of CRNs manually has provided valuable results. The designs are usually based on experimental results or CFD simulations. The work of Lebedev et al. (2009) presented a CRN composed of six reactors to model a gas turbine combustor. The authors defined the CRN based on the mixture fraction field predicted via CFD. Likewise, utilizing velocity, temperature and species fields coming from CFD simulations, Park et al. (2013) developed a CRN to model a lean-premixed gas turbine combustor and obtained good matches with respect to experimental data.

More recently, Prakash et al. (2018) studied the effect of exhaust gas recirculation (EGR) on the emissions of a lean premixed gas turbine combustor using a manually designed CRN. The adoption of EGR might cause the required conditions for FC to occur, as $O_2$ concentrations drop and initial temperatures rise. Studying FC, the work of Perpignan et al. (2018b) showed the results of a CRN manually built based on CFD made with the Flamelet Generated Manifolds (FGM) approach, which is also employed in the present work. The authors achieved better agreement with CO and $NO_x$ experimental data using the CRN than with the reacting CFD. The focus was on a gas turbine combustor designed to operate under the FC regime. The detailed chemistry enabled the analysis of the $NO_x$ formation pathways, showing that the thermal pathway is not as important as the prompt, NNH and $N_2O$ pathways. This showcases the capability of in-depth chemistry analysis when utilizing CRNs.

The application of CRNs to predict emissions from FC systems has, in principle, advantages when compared to conventional combustion systems (Perpignan et al., 2018a). The highly distributed reaction zones, as well as lower gradients of species and temperatures, are better represented by ideal reactors (Cavaliere and de Joannon, 2004). However, this observation is valid for the largest scales, as there is evidence FC might be composed highly interactive flamelets at the smaller scales (Minamoto et al., 2013, 2014; Minamoto and Swaminathan, 2014).

The manual generation of CRNs is, nonetheless, particularly reliant on the experience of the designer and suffers from the lack of repeatability as a significant amount of trial and error approach is involved. Additionally, creating networks manually impedes the reproducibility of results and hampers systematic studies.

As an attempt to avoid these issues, strategies to generate CRNs automatically based on CFD solutions have been developed.

Early applications of automatic CRN generation were employed in simulations for analyzing furnaces (Benedetto et al., 2000; Faravelli et al., 2001; Falcitelli et al., 2002). Promising results were achieved as 3D CFD simulations were post-processed. The works utilized temperature and stoichiometry to define the ideal reactors, which could be PSRs or PFRs, based on the angle of the velocity vector. The underlying assumption was that the simplified chemistry models employed in the CFD were enough to predict temperature, velocity and major species. Moreover, these works provided insights into important variables to be taken into account when clustering CFD cells: temperature, a variable capturing the flow direction, and at least one measure of composition.

The same computational tool (with the same clustering criteria) was employed by Frassoldati et al. (2005) in the case of the swirling flame of the TECFLAM burner test case. The authors showed the effect of varying the number of reactors on the result of $NO_x$ emissions. For that specific case, having 300 reactors proved to be enough to guarantee no significant variation with a further increase in the number of reactors. Good agreement with the outlet value of $NO_x$ was shown, as only one operating condition was simulated.

Fichet et al. (2010) presented another strategy to use a CFD solution as an input to build a CRN. The authors utilized a gas turbine combustor to showcase the capabilities of the approach. They opted for discarding the temperatures calculated with CFD and recalculated the temperatures based on the heat release of the chemical reactions predicted by the CRN. There was no systematic study on the advantages and disadvantages of this approach. The authors reported good agreement between measured and simulated $NO_x$ emissions. However, only one operating condition was available.

Similarly, Monaghan et al. (2012) utilized the Sandia Flame D as a test case and post-processed a CFD solution to build CRNs. The authors reported improved results for minor species (OH and NO) with respect to the initial CFD solution. The strategy to cluster CFD computational cells into reactors involved using mixture fraction, temperature and the axial coordinate.

In yet another example, Cuoci et al. (2013) utilized a few test cases to explore their computational tool, including the one utilized in the present work, presented in section The Test Case. The authors analyzed one of the operating conditions to which they reported improved $NO_x$ predictions, while CO was overpredicted to some extent. According to the authors, the source of deviation in NO was the incorrect temperatures predicted by the CFD simulations.

Despite the valuable developments, the full potential and limitations of using both CFD and CRN are not fully known. For example, the effect of different clustering criteria on the final solution is not clear, and that is one of the objectives of the present work. Additionally, there are other unknowns in the approach, as the effect of neglecting turbulence chemistry-interaction or taking it into account (via a PaSR—Partially Stirred Reactor approach, for example), or the pros and cons of solving the energy equation in the CRN step.

For these reasons, Automatic Generation of Networks for Emission Simulation (AGNES) (Sampat, 2018) was developed at the Delft University of Technology. The computational tool uses Cantera (Goodwin et al., 2018), an open-source software dedicated to chemical kinetics as a framework. Yousefian et al. (2017) reviewed the available hybrid computational tools based on CRNs for emissions predictions. In their evaluation of the different available solvers for CRNs, the authors highlighted two of the characteristics of Cantera that made it attractive for the development of AGNES: the capability of solving the energy equation and the fact that it is a free and open source solver, as further discussed in section Chemical Reactor Networks. Being able to modify and control the code was essential for the development of AGNES.

In the present paper, AGNES is utilized to simulate a test case related to the FC regime, in order to showcase its capabilities, limitations, and improvement opportunities. Additionally, the analysis of the results aims to clarify the reasons for the emission behavior in the chosen test case. The unique contribution of the present research is the assessment of different clustering criteria on the outlet emissions of an FC system that has a complex $NO_x$ behavior with varying equivalence ratio, as shown in section The Test Case.

## THE TEST CASE

In order to evaluate the performance of AGNES, a test case was chosen based on the available information and the relevance to FC. Data availability on emission characteristics of the combustor for various operating conditions was a stringent requirement in making the selection. The test case described by Veríssimo et al. (2011) was chosen as a test case. The combustor was developed to study FC in a non-premixed combustion mode. The combustor consists of a cylindrical combustion chamber with a central air jet surrounded by 16 fuel jets in the burner head. This configuration is a variation of the most common jet-induced recirculation geometry in which a central fuel jet is surrounded by air jets (Hosseini and Wahid, 2013). The inlet air was preheated to 673.15 K, while the fuel (pure methane) was at room temperature.

The equivalence ratio was varied by maintaining the fuel mass flow (heat input of 10 kW) and altering the air mass flow. Data on OH* chemiluminescence, flue-gas temperatures and, more importantly, emissions of CO and $NO_x$ were acquired for all operating conditions. The equivalence ratio was varied from $\phi = 0.455–0.909$ and the behavior of CO and $NO_x$ emissions was found to be non-monotonic. The authors reported a peak in $NO_x$ around $\phi = 0.53$, while CO was practically undetectable for the runs at $\sim\phi = 0.53$ and 0.59 (see **Figure 1**).

This behavior was explained by the authors based on a combined effect of the global equivalence ratio and the mixing characteristics of the combustor. Starting from condition *a* in **Figure 1** and going toward leaner conditions, more air flow was added. The higher central air jet momentum was responsible, according to the authors, for quicker and stronger entrainment of the fuel, which had weaker jets. The stronger mixing of fresh reactants caused more intense reaction zones (as shown

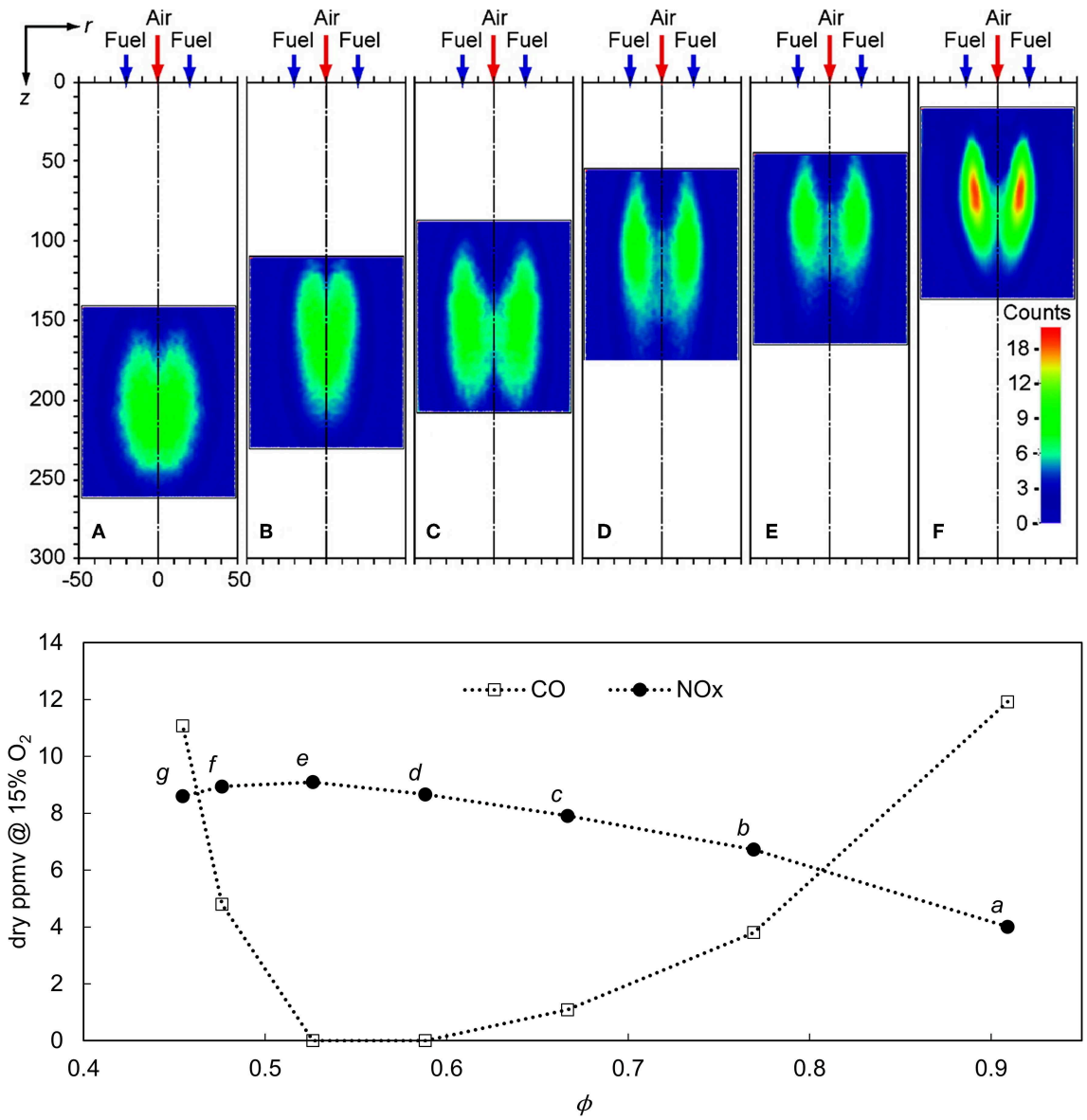


**FIGURE 1 |** Mean OH* images for diverse global equivalence ratio values. From left to right, $\phi \cong 0.91, 0.77, 0.67, 0.59, 0.53, 0.48$ (**Above**). Emissions of $NO_x$ and CO in dry volumetric ppm adapted from Veríssimo et al. (2011) (**Below**).

in **Figure 1**), while not allowing as much mixing of combustion products prior to the reactions. The result was then higher $NO_x$ and lower CO. This trend was dominant up to conditions *e* or *f*, in which the usual pattern of having lower $NO_x$ and higher CO as going leaner becomes dominant over the mixing characteristics.

In a more recent study, Zhou et al. (2017) performed OH and $CH_2O$ PLIF on the same setup, and referred to operating conditions *a*, *c,* and *e* as flameless, transition and conventional modes, respectively. They support that conditions *e* and *f* behave like conventional diffusion flames, as mixing with combustion products is apparently minimal and combustion is dictated by the mixing between fuel and air. As mixing with combustion products is allowed by the weaker entrainment of fuel by the air jet, the combustion regime transitions to FC. A summary of the operating conditions with $\phi$, air mass flow rate and outlet $O_2$ concentration is shown in **Table 1**.

For conditions *b* and *d*, Veríssimo et al. (2011) provided point-measurements at various radial stations. Temperatures, major species ($CO_2$ and $O_2$) and pollutants (CO, UHC, and $NO_x$) were measured at 10 radial positions at each of the 10 stations.

The test case was simulated before, by Cuoci et al. (2013) and Lamouroux et al. (2014), for example. However, the focus of these previous works was on local values and a single operating condition for the former, and on the effect of including heat losses on local values for the latter. The focus of the present work is

**TABLE 1 |** Operating conditions investigated by Veríssimo et al. (2011).

| Run | $\phi$ | $\dot{m}_{air}$ [kg/s ·$10^{-3}$] | Outlet $O_2$ [% vol.] |
|---|---|---|---|
| *a* | 0.909 | 3.950 | 1.959 |
| *b* | 0.769 | 4.594 | 4.356 |
| *c* | 0.667 | 5.138 | 6.506 |
| *d* | 0.588 | 5.804 | 8.035 |
| *e* | 0.526 | 6.634 | 9.425 |
| *f* | 0.476 | 7.279 | 10.440 |
| *g* | 0.455 | 7.522 | 10.882 |

instead on the outlet emissions of CO and $NO_x$ across different operating conditions.

## COMPUTATIONAL MODELING

In an attempt to overcome the challenges in predicting emissions at affordable computational costs, a three-step approach is adopted in the current research: (1) solution of the flow-field with CFD using simplified chemistry and a turbulence-chemistry interaction model, (2) clustering of computational cells into ideal reactors based on criteria imposed to the CFD solution, and (3) solution of the generated CRN with detailed chemical reaction mechanisms. In the following subsections, the details of these steps are presented.

The specific objectives of the performed modeling are:

i. Evaluating the performance of the chosen CFD modeling
ii. Evaluating the performance of the developed computational tool
iii. Comparing the results obtained with CFD and CRNs
iv. Obtaining minor species concentration more accurately than those obtained with the CFD simulations used as input to the CRN simulations
v. Analyzing the $NO_x$ formation pathways for different operating conditions of the combustor

### Computational Fluid Dynamics

The simulations were performed in order to assess the performance of CFD in predicting pollutant emissions and, more importantly, to generate the inputs for the subsequent modeling steps. The RANS (Reynolds Averaged Navier-Stokes) approach was adopted along two different turbulence-chemistry interaction models: EDM (Eddy Dissipation Model) (Magnussen and Hjertager, 1976) and FGM (van Oijen and De Goey, 2000). All simulations were performed in ANSYS Fluent®. The EDM was chosen to perform a comparison with FGM. The assumption behind the model is that reactions are chemically fast and are controlled by turbulent mixing. Therefore, it was not expected that the EDM would perform accurately, at least not for all the operating conditions of the chosen test case. The EDM is possibly the simplest turbulence-chemistry interaction model and the objective of utilizing it was to assess how the quality of the CFD simulation utilized as input affects the results obtained solving the resulting CRNs.

A two-step reaction mechanism was adopted for $CH_4$ combustion, as shown by Equations (1) and (2). The EDM determines the reaction rates based on large turbulence time scales ($k/\varepsilon$), as shown in Equation (3) (Magnussen and Hjertager, 1976).

$$CH_4 + 1.5\,O_2 \leftrightarrow CO + 2\,H_2O \tag{1}$$

$$CO + 0.5\,O_2 \leftrightarrow CO_2 \tag{2}$$

$$R_{i,r} = \left(4C_{i,r}M_i\rho\frac{\varepsilon}{k}\right)\min\left[\min_{reac.}\left(\frac{Y_{reac.}}{C_{reac.,r}M_{reac}}\right), 0.5\frac{\sum_{prod.} Y_{prod.}}{\sum_{prod.}^{N} C_{prod.,r}M_{prod.}}\right] \tag{3}$$

The choice for FGM was based on its relatively low computational cost with respect to other models (Eddy Dissipation Concept, Conditional Source-term Estimation or transported-PDF, for example), and on its performance for various combustion systems (Verhoeven et al., 2012; van Oijen, 2018). This approach has shown to be promising for the modeling of FC, provided the progress and control variables are adequately chosen (Perpignan et al., 2018a). The approach allows the use of detailed chemistry in the pre-calculation generation of flamelets. Non-premixed flamelets were chosen due to the nature of the analyzed burner, and were solved using the GRI 3.0 chemical reaction mechanism (Smith et al.). Tests were performed utilizing the GRI 2.11 (Bowman et al.) and the POLIMI C1-C3 (Ranzi et al., 2012) mechanisms, but no significant differences were observed.

The underlying assumption of the FGM model, or any flamelet-based approach for turbulent combustion, is that a turbulent flame can be represented as an ensemble of laminar flames. The flamelets were calculated in the mixture fraction space according to Equation (4), for species, and Equation (5), for temperature, according to the formulation of van Oijen and De Goey (2000). The pre-calculated flamelet quantities were then tabulated based on mixture fraction, a predefined progress variable and enthalpy, which are the variables that require transport equations. A presumed $\beta$ shape PDF was employed to account for the turbulence-chemistry interaction, which was a function of the mean and variance of the mixture fraction.

$$\rho\frac{\partial Y_i}{\partial t} = \frac{\rho\chi}{2}\frac{\partial^2 Y_i}{\partial f^2} + S_i \tag{4}$$

$$\rho\frac{\partial T}{\partial t} = \frac{\rho\chi}{2}\frac{\partial^2 T}{\partial f^2} - \frac{1}{c_p}\sum_i S_i H_i + \frac{\rho\chi}{2c_p}\left[\frac{\partial c_p}{\partial f} + \sum_i c_{p,i}\frac{\partial Y_i}{\partial f}\right]\frac{\partial T}{\partial f} \tag{5}$$

The adopted progress variable as assumed to be dependent on the mass fraction of CO and $CO_2$. Tests performed including $H_2O$ and $H_2$ in the definition of the progress variable, species adopted by previous works, did not provide better results for this case. In order to calculate $NO_x$ species from the CFD simulations to perform a comparison with the results of AGNES, additional transport equations for NO, HCN, $N_2O$, and $NH_3$ were included. Reactions representing the thermal, prompt, and $N_2O$ pathways

were considered. Reaction rates of $NO_x$ species accounted for the temperature fluctuations by means of a $\beta$-PDF.

The closure for the RANS equations was achieved using the $k$-$\varepsilon$ turbulence model. Since the burner has round air and fuel jets, the $C_{\varepsilon 1}$ constant was adjusted to 1.6 to correct for the well-known round jet anomaly (Pope, 1978; Shih et al., 1995). Tests using a Reynolds Stress model did not provide superior results.

The modeling of heat loss is extremely important for the prediction of the temperature and the resulting emissions. The modeling of radiation was performed with the Discrete Ordinates model along with the weighted-sum-of-gray-gases approach to determine the required fluid properties. Heat conduction through the walls was imposed via wall temperature profiles. The profiles were determined partially based on the reported temperature values 5 mm from the walls for conditions *b* and *d*, as well as the outlet temperature. The profiles were first estimated by extrapolating the available data at the radial locations to the wall location. Subsequently, the resulting profile at the wall was multiplied by a factor to meet the outlet temperatures obtained in the experiments, thereby resulting in the same overall heat loss. For conditions in which local measurements were not available, linear interpolations and extrapolations of the profiles were performed, based on the equivalence ratio.

The computational mesh used was fully hexahedral and a 45° sector was simulated, which included two fuel ports, as shown in **Figure 2**. The angle was adopted to guarantee a good mesh quality in terms of skewness. The mesh refinement was defined based on monitoring the outlet values of chemical species, as well as mid-plane averaged quantities, to guarantee no significant changes were attained with further refinement. The initial mesh size was ∼1 million elements and other four mesh sizes were tested until the difference in outlet species and averaged quantities was negligible. The final mesh was composed of ∼2.5 million elements.

Periodicity was imposed on the lateral boundaries. The first set of simulations was performed with mass flow inlets of air and fuel with uniform profiles. As the effect of having a developed flow velocity profile imposed as the boundary was shown to influence the results, this was adopted for the simulations herein reported. The developed flow velocity profile was assumed to follow Equation (6), a power-law velocity profile. The turbulence intensity was assumed to be 5% of the mean velocity. Tests with increased intensity did not significantly affect the results. Turbulence length scale at the boundaries was estimated based on the pipe diameters for both air and fuel, as it was imposed to be 7% of these dimensions. The outlet boundary condition was imposed to have zero static gauge pressure.

$$\frac{u}{u_{\max}} = \left(1 - \frac{r}{(D/2)}\right)^{\frac{1}{7}} \tag{6}$$

## Chemical Reactor Networks

In order to simulate combustion with detailed chemistry at affordable computational costs, AGNES was employed. Having the results from the CFD simulations, the tool first clusters computational cells into reactors based on user-defined criteria. Clustering is executed with a Breadth First Search (BFS) algorithm used to traverse the computational domain. Such a domain traversal algorithm was chosen to ensure that the clustered cells are indeed connected to each other in the mesh, forming a continuous domain, and preventing the clustering of discontinuous pockets of cells satisfying the criteria. The clustering process proceeds until the total number of reactors (clusters) reaches the set-point imposed by the user, or until the specified maximum tolerance is attained. The quantity range value $\alpha$ is defined as shown in Equation (7), and it is dependent on a certain tolerance $\delta$. The new local value, calculated by averaging the clustered cells, is allowed to deviate from the original local value as expressed by Equation (8). Several variables can be used simultaneously as criteria and every criterion must be satisfied for a cell to be included in a cluster.

$$\alpha = \delta\,(c_{\max} - c_{\min}) \tag{7}$$

$$\alpha \geq |c_{cluster} - c_{cell}| \tag{8}$$

The resulting reactors have their properties assigned based on the properties of the CFD cells that compose the reactors. When maintaining temperatures as obtained from the CFD solution, which is the case for the present paper, averaged static temperatures are assigned, although total values are used during clustering to guarantee total enthalpy conservation.

The mass flow exchanged between reactors is calculated based on the mass flow between cells in the CFD solution. There is an inherent mass imbalance due to the precision of the CFD solution which needs to be corrected to ensure consistent mass conservation. This is done by accounting for the mass flow between any two reactors as a fraction of the total outflow from the source reactor and assembling a system of equations. The boundary conditions of total inflow and outflow are accounted for in the system. The system of equations (mass, species, and energy conservation) is solved for, giving a vector of total outflow from each reactor and the "corrected" mass flow between reactors is recalculated using this vector and the matrix of outflow fractions. The mass exchange between reactors is also stored and maintained when solving the CRN simulation.

The system of ODEs is characterized by non-linearity and stiffness. The stiffness of the system is attributed to the wide range of time scales encountered for the reactions involved. Some reactions, such as those responsible for heat release, are much faster than those responsible for the formation of minor species such as that of $NO_x$. This makes it difficult to integrate as the fast reactions require a small time step to be captured whereas the slow reactions need to be integrated over a larger time scale. Therefore, two levels of solvers are implemented, a local and a global. The local solver treats each reactor individually, whereas the global solver treats all the reactors simultaneously as a system. Cantera is used in the following ways:

i. As a chemistry book keeping tool, in which Cantera ensures a consistent physical and chemical state of the reactors in the form of their temperature, density, and species mass fraction and storing the chemical reaction mechanism with all its thermodynamic properties.

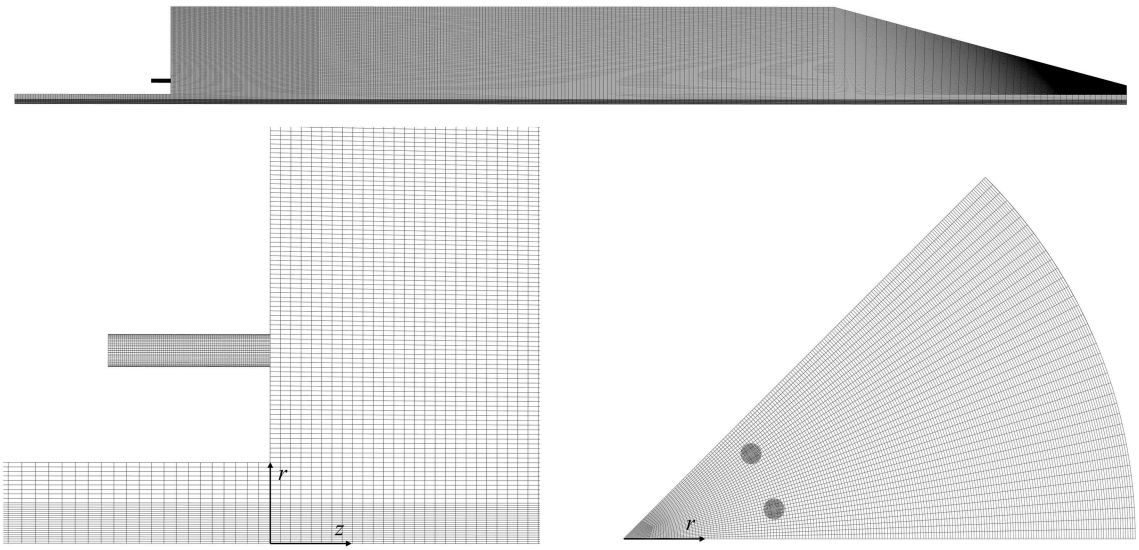


**FIGURE 2 |** Hexahedral mesh employed for CFD simulations.

ii. It can also be used to solve a reactor network, in which Cantera calls SUNDIALS to perform ODE integration of a stiff system of equations, while treating it as a dense matrix.

At the local solver level, both features are used, whereas at the global solver level Cantera is used only as a chemistry book keeping tool, as shown in **Figure 3**. This is due to Cantera's solver limitations of being unable to simultaneously handle large number of reactors, hence the governing equations are written explicitly and solved using SciPy, a Python-based ecosystem for mathematics, science, and engineering, to solve a sparse matrix equation for the entire network of reactors.

As previously mentioned, both a local and a global solver are employed. Locally, the solver available in Cantera is used to advance each reactor individually, changing its state and that of its connected reservoirs. This solver employs a different time-step to each reactor, based on its residence time. The global solver employs Cantera only to maintain the consistency of the chemical states, while all reactors are solved simultaneously with the sparse solver.

All reactors were considered to be PSRs. No turbulence fluctuation was taken into account in the CRNs. They were neglected because approaches with and without the inclusion of fluctuations are still being successfully employed (Yousefian et al., 2017) and a logical first step in the development of AGNES was to start without them. Moreover, this first application of AGNES is aimed at investigating the effect of clustering criteria on the solution. The inclusion of fluctuations may be important in some cases, as shown by Cuoci et al. (2013). For this reason AGNES will be modified to be capable of including fluctuations in the future.

The results herein presented were obtained by imposing a 3% tolerance. This resulted in different numbers of reactors for each test condition and imposed clustering criteria. Simulations were performed with both GRI 3.0 and GRI 2.11 mechanisms,

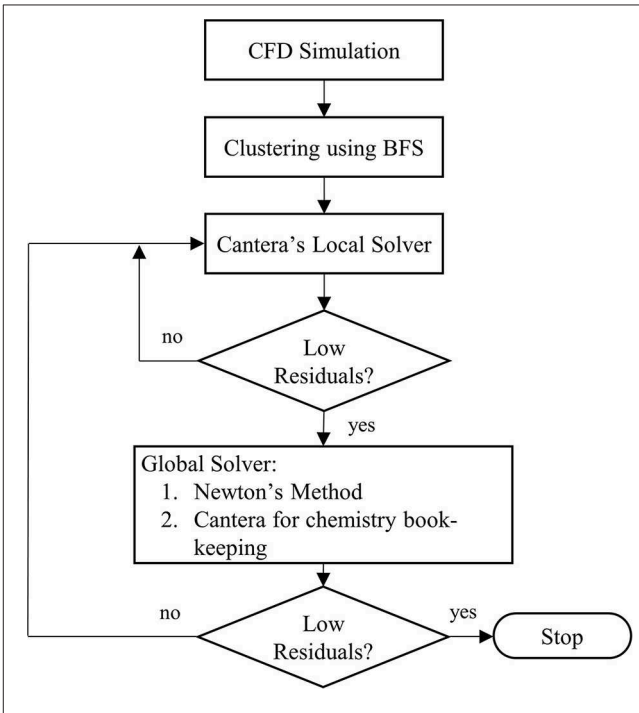


**FIGURE 3 |** Flowchart of AGNES.

to investigate the effect on $NO_x$ formation, as it has been shown that there are relevant differences in the $NO_x$ formation pathways under FC conditions (Perpignan et al., 2018b).

Several tests with various clustering criteria were performed in order to evaluate their efficacy to the present test case (Sampat, 2018). Apart from the obvious choice of temperature as a criterion, it was observed that the inclusion of velocity direction

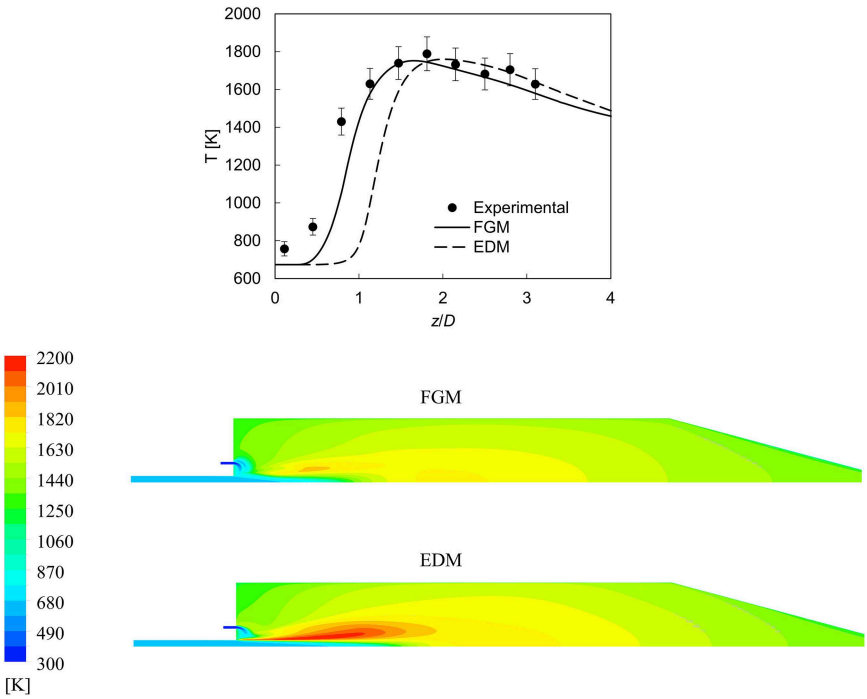


**FIGURE 4 |** Experimental and CFD temperature results along the centerline of the combustor (**Above**) and temperature contour plots (**Below**) for condition *b* ($\phi \cong 0.77$) using FGM and EDM.

as a criterion was fundamental to capture the recirculation within the combustor, a key for capturing the chemistry within FC. Additionally, a variable acting as a tracer of the fuel, as well as a variable indicating the progress of reactions were required. In the present work, these are the $Y_{CH4}$ and $Y_{H2O}$, respectively. Two sets of criteria are explored, one with the aforementioned variables, and one with the inclusion of $Y_{O2}$.

## RESULTS

In this section, the results obtained from CFD simulations are presented and discussed. The extent to which the CFD modeling was able to replicate the experimental data is shown, in terms of temperatures, major species and pollutant emissions. Subsequently, the results obtained with AGNES are thoroughly analyzed.

### CFD Results

As expected, the FGM simulations showed better results when compared to the EDM, as shown in **Figure 4**. The temperature rise occurs earlier in FGM, better representing the experimental data points. It is worth noting the discrepancy between experimental and simulation values in the data point ($z/D = 0.11$). This difference might be attributed to the heating of the burner head and its piping, which might have caused the pre-heating of air to a temperature higher than that reported by the authors. Another hypothesis would be the effect of radiation on the thermocouple, although the authors assessed this effect. The error in temperature measurements was estimated by Veríssimo et al. (2011) to be around 5% (as is shown by the error bars in **Figure 4**).

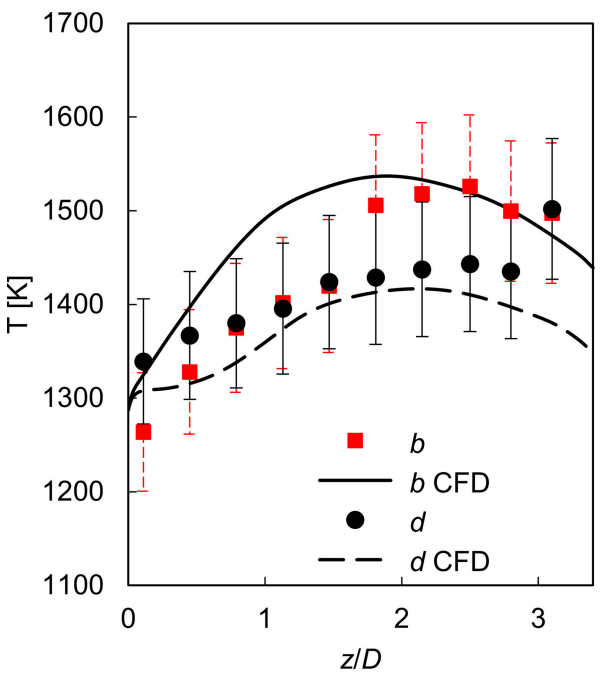


**FIGURE 5 |** Experimental and CFD temperature results along the axial line where $r = 45$ mm for conditions *b* ($\phi \cong 0.77$) and *d* ($\phi \cong 0.59$).

Although the centerline values of temperature shown in **Figure 4** depict that FGM was superior, the extent of that is not well-represented. The peak temperatures attained in the combustor are not located at the centerline, but at the region where fuel and air mix. In this region, EDM peak temperatures are much higher than those predicted by FGM, as seen in the contours of **Figure 4**. Additionally, looking only at the centerline values shown in **Figure 4** it may seem that reactions with FGM occur faster than with EDM, but that is not the case.

A major difficulty in simulating the case at hand is the uncertainties related to heat losses. Radiative heat losses play a role in the combustor, as well as conduction through the walls. The total heat loss can be derived by the reported values of outlet temperatures, although the exact location where the temperatures were measured is not fully clear. Therefore, a wall temperature profile was imposed based on the results available at 5 mm from the wall ($r/D = 0.45$), attempting to maintain them as close as possible. Temperature at this position is, however, not only dependent on the wall temperatures, but also on the reaction rates, recirculation, and radiation. The extent to which the simulations are able to reproduce these values is shown in **Figure 5**.

The centerline values of $O_2$ and $CO_2$ shown in **Figure 6** indicate that predictions for condition *d* were more accurate than for the condition *b*. The reasons for this may be related to the fact that condition *d* is, according to Veríssimo et al. (2011) and Zhou et al. (2017), closer to a conventional diffusion flame, while condition *b* would be more representative of FC, making it more difficult to model, as a control variable representing vitiated recirculated gases may be required for the representation of FC with FGM (Huang et al., 2017). However, the values of $CO_2$ and $O_2$ close to the outlet should not be dependent on the combustion regime or the type of modeling. As also shown in **Figure 7**, simulations for condition *b* have higher $CO_2$ and lower $O_2$ values at the outlet. The discrepancy between simulations and experimental values on the $O_2$ values close to the outlet for condition *b* has been shown before in the results of Cuoci et al. (2013). The experimental uncertainty of 10% in the composition data does not justify the difference alone. Therefore, the uncertainty of the reported mass flows is probably causing the discrepancies.

The overall agreement between experimental data and the FGM simulations is good (**Figures 7**, **8**). The largest deviations for temperatures occur closer to the burner head ($z/D = 0.11$), especially for condition *b*. Further downstream in the combustion chamber, the agreement is better. Simulations presented the overall characteristic of retaining lower temperatures near the centerline for longer axial distances, while combustion was more progressed (i.e., lower $O_2$ and higher $CO_2$ concentrations). This can be explained by a possible imperfect prediction of the mixing between burnt gases and reactants, as well as the effect that burnt gases have on the incoming reactants. Moreover, the aforementioned apparent inconsistency in temperature modeling (or measurements) close to the burner head, as well as the uncertainty related to mass flows might also have contributed.

The radial profiles (**Figures 7**, **8**) show that the effects of the central jet spreading rate seem to be overpredicted in the simulations. This can be noticed by the fact that the gradients of the profiles tend to be lower than those obtained in the experiments for intermediate axial positions ($z/D = 1.13$ and $1.81$). This was also the case in the reported previous computational works on the same test case (Cuoci et al., 2013; Lamouroux et al., 2014). However, the discrepancies could also be a result of poor prediction of reaction rates or heat transfer, instead of an artifact of the jet spreading prediction.

The predictions of pollutant emissions from the CFD modeling is poor, both in terms of the absolute values as well as in the trends (**Figure 9**). The emission of CO is highly overpredicted, in some conditions up to two orders of magnitude. The NO prediction is, on the other hand, underpredicted. The trend of NO is also not captured, as values

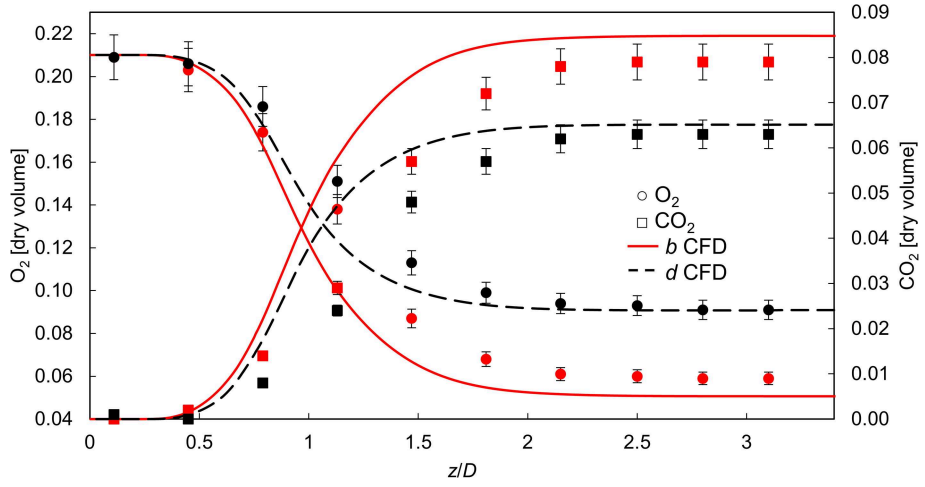


**FIGURE 6 |** Experimental and CFD results along the centerline of the combustor for $O_2$ and $CO_2$ concentrations for conditions *b* ($\phi \cong 0.77$) and *d* ($\phi \cong 0.59$).

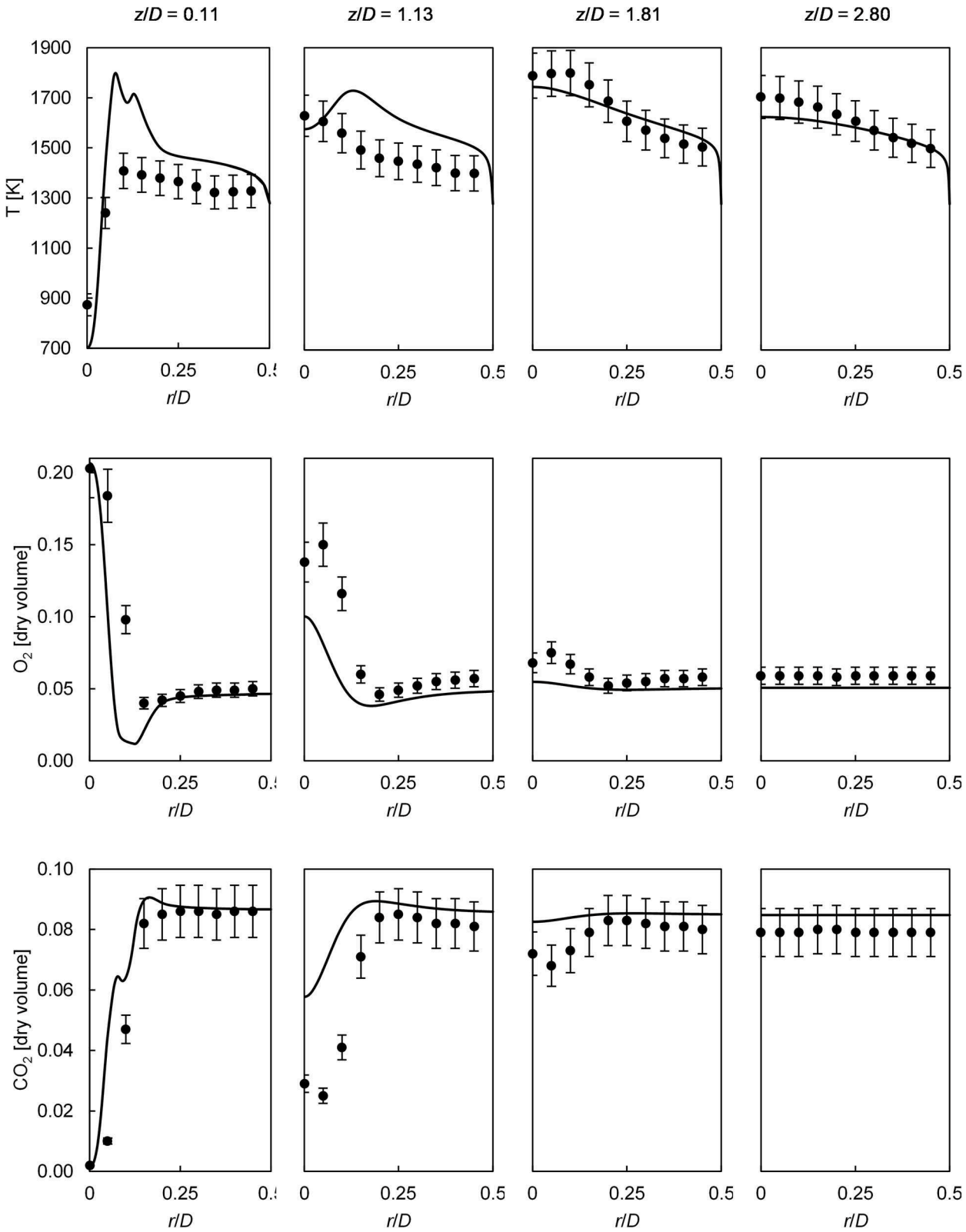


**FIGURE 7 |** Comparisons of experimental and CFD (FGM) parameters: temperature, $O_2$ concentration, and $CO_2$ concentration results along radial lines for condition *b* ($\phi \cong 0.77$).

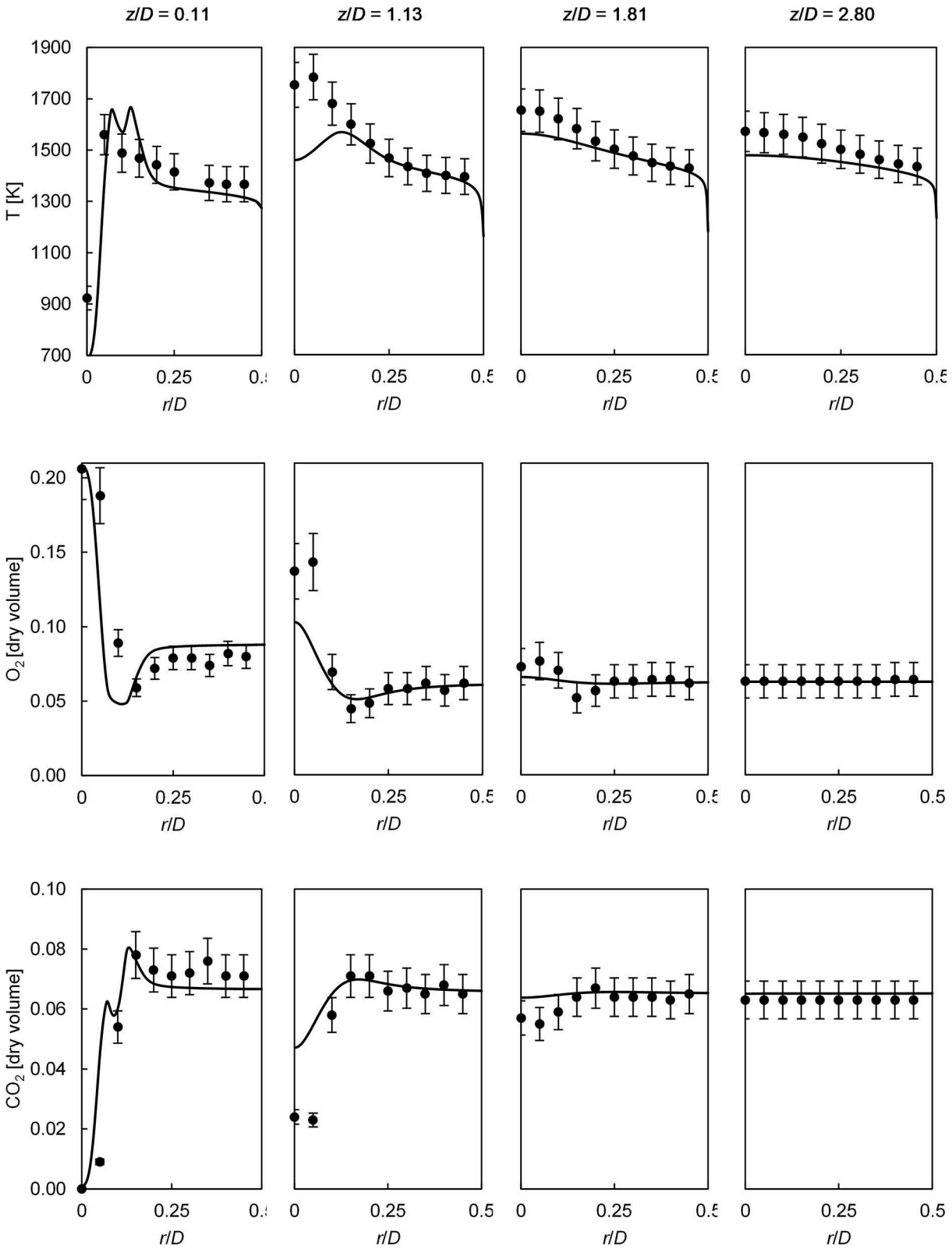


**FIGURE 8 |** Comparisons of experimental and CFD (FGM) parameters: temperature, $O_2$ concentration, and $CO_2$ concentration results along radial lines for condition *d* ($\phi \cong 0.59$).

increase monotonically with increasing $\phi$. These results were to a certain extent expected, as the accurate prediction of CO with FGM is challenging (Ramaekers et al., 2010) and the $NO_x$ species modeling was not based on a detailed chemical reaction mechanism.

Finally, the CFD results based on FGM performed reasonably well in order to be used as an input to the CRN simulations. Most of the variables have a good level of agreement (apart from pollutants). Better results could be expected by utilizing an FGM approach that is more suitable for modeling FC, such as the diluted-FGM, developed by Huang et al. (2017). Perhaps the mixing in the combustor has unsteady characteristics which can be captured adequately only by LES. However, previous attempts of simulating the test case with LES along with tabulated chemistry did not provide improved results (Lamouroux et al., 2014).

## AGNES Results

The results obtained from the CRN simulations performed with AGNES are discussed herein with respect to the combustion model obtained from the CFD input (FGM or EDM), to the clustering criteria, and chemical reaction mechanism.

The CO predictions are improved significantly with respect to the CFD simulations performed with FGM, regardless of the clustering criteria (**Figure 10**). The same is valid for simulations based on the EDM, in which the main difference with respect to FGM is in the predictions of CO for conditions closer to stoichiometry. All results predict the trend of CO and have fairly similar values. Additionally, no significant difference between GRI 3.0 and GRI 2.11 can be noticed.

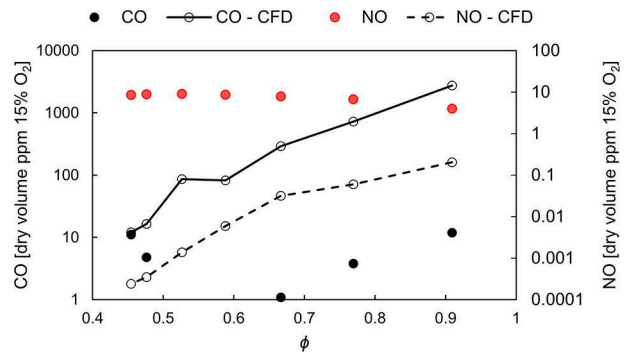


**FIGURE 9 |** Outlet CO and NO results from CFD performed with FGM compared with experimental values.

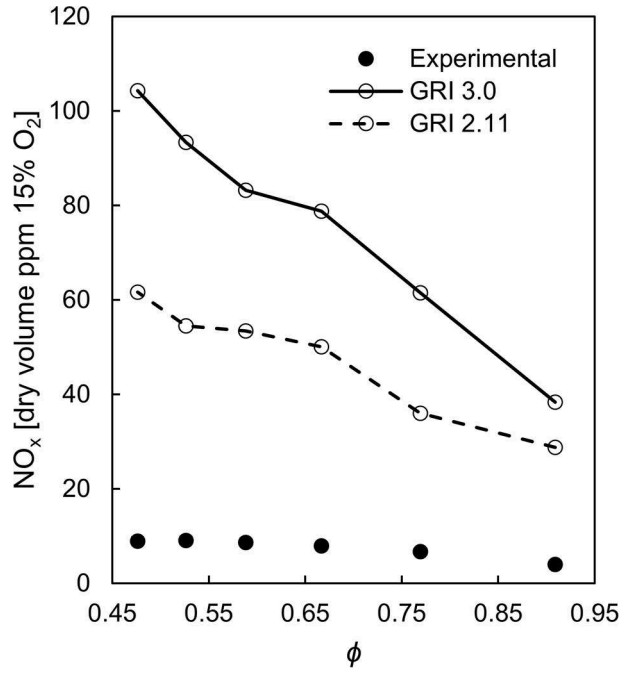


**FIGURE 11 |** Outlet $NO_x$ results from AGNES having CFD simulations performed with EDM as input compared with experimental results.

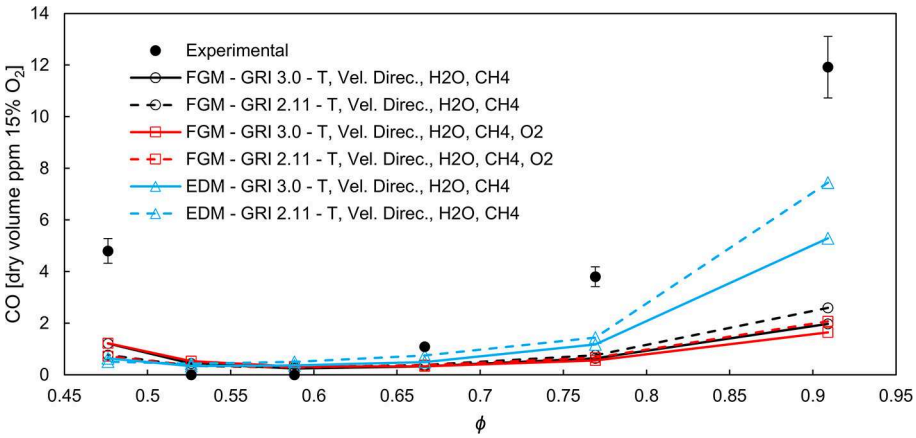


**FIGURE 10 |** Outlet CO results from AGNES compared with experimental results. Different input simulations for AGNES (FGM or EDM) and post-processing options (GRI 3.0 or GRI 2.11, as well as clustering criteria).

The calculated $NO_x$ values based on the EDM simulations are overpredicted, as expected (**Figure 11**). The high peak temperatures attained with the modeling are responsible for the results being up to one order of magnitude higher. The results obtained from FGM are more complex to analyze (**Figure 12**). When temperature, velocity direction, $Y_{CH4}$ and $Y_{H2O}$ are employed as clustering criteria, the $NO_x$ trend obtained with GRI 2.11 reaction mechanism is monotonic and its slope is the opposite of the experimental data: condition *a* had the highest $NO_x$ value. For GRI 3.0, overall values are higher than those of GRI 2.11 (a behavior previously reported by Perpignan et al., 2018b), but condition *a* has a lower value than condition *b*, making the overall trend non-monotonic. The values, however, are not in good agreement with experiments for both chemical reaction mechanism.

The inclusion of $Y_{O2}$ as a clustering criterion is fundamental to attain a trend closer to experimental data with respect to the non-monotonic behavior of the emissions. The results using GRI 2.11 have values in the same order of magnitude as the experimental values (below 10 ppm). Such difference highlights that the choice of clustering criteria has an effect on the accuracy of the solution. The computational time can also be affected by the choice of criteria, as the required number of reactors changes. Additionally, the variables available from the CFD input can potentially influence the choice for a given CFD modeling approach, provided it has advantageous variables to be employed as clustering criteria.

One should bear in mind that all experimental values were below 10 ppm, and such low values pose a significant challenge for computational simulations. The improvement with respect to the values predicted directly via CFD is remarkable, and that enables the use of AGNES to aid the design of FC combustors. The peak of $NO_x$ emissions is, however, not predicted by any simulation. While experiments reported the highest values of $NO_x$ for the condition *e*, simulations had maximum values for the condition *b*, which are also closer to experimental values for the case of GRI 2.11 that included $Y_{O2}$ as a clustering criterion.

The analysis of local $NO_x$ values for condition *b* presented in **Figure 13** shows that there are significant discrepancies. Similarly to the results from CFD (**Figure 7**), the radial profiles have larger differences between central ($r/D \sim 0$) and peripheral ($r/D \sim 0.5$) locations than the experimental profiles for locations close to the burner head. Further downstream ($z/D = 1.81$ and 2.80), the opposite is true, as computations have flatter profiles than experiments. On the other hand, the centerline profile shows that the results are satisfactory and certainly represent an improvement with respect to the original CFD calculations. The overprediction of temperatures in locations close to the burner head (as shown in **Figure 7**) also play a role, as $NO_x$ values are increased at $z/D = 0.11$. The fact that $NO_x$ formation takes place in a relatively short axial region (around $z/D = 1.13$) and then stays relatively constant is remarkable, as seen in both simulations and experiments.

Additionally, some features should be further investigated. The fact that the GRI 2.11 can be more accurate raises doubts regarding the prompt $NO_x$ formation, as discussed by Perpignan and Rao (2019). The GRI 2.11 is supposedly inferior to its successor, GRI 3.0, but the apparent better representation of the prompt $NO_x$ pathway might be related to different reaction rates in vitiated environments. The chemistry of $NO_x$ formation was shown to be different in previous literature, not only because of thermal $NO_x$ abatement (Nicolle and Dagaut, 2006; Fortunato et al., 2018).

In order to understand what causes the non-monotonic behavior of $NO_x$, the rates of formation by each pathway were estimated. The rates of the reactions responsible for NO formation at the end of each pathway were taken into account. It is important to highlight that the pathways are not independent and interact with each other. Therefore, isolating their respective contributions is not entirely possible. Nonetheless, the analysis herein performed serves as an indication. The largest source of uncertainty is concerning the thermal and prompt pathways. The N atoms that are products along the prompt pathway tend to react via the second reaction of the Zeldovich pathway (Lefebvre

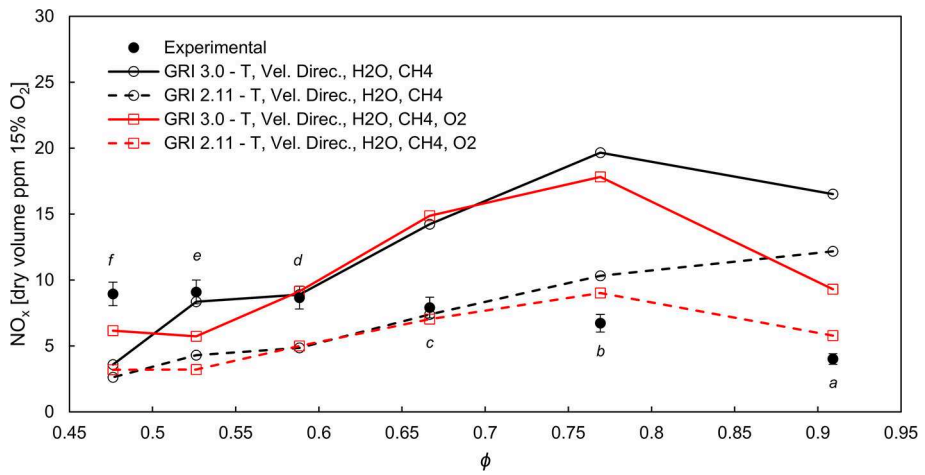


**FIGURE 12 |** Outlet $NO_x$ results from AGNES having CFD simulations performed with FGM as input compared with experimental results. Two different clustering criteria sets.

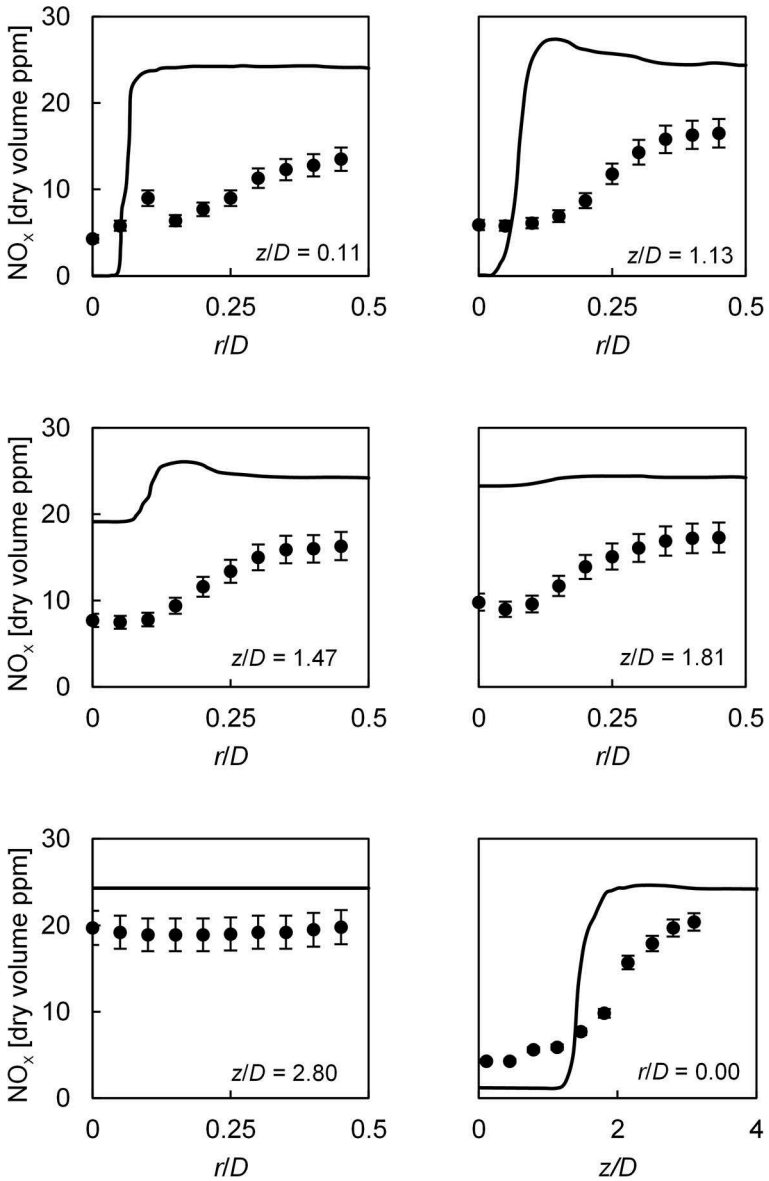


**FIGURE 13 |** $NO_x$ values at selected local profiles. Comparison between experimental data and AGNES results obtained using an FGM simulation as input, GRI 2.11 and T, velocity direction, $Y_{H2O}$, $Y_{CH4}$, and $Y_{O2}$ as clustering criteria for condition *b* ($\phi \cong 0.77$).

and Ballal, 2010). Therefore, the NO formation coming from the second and third reactions of the Zeldovich pathway was neglected. The thermal NO contribution is considered to be that of the first equation ($O + N_2 \leftrightarrow NO + N$), which is the rate limiting step of the pathway (Glarborg et al., 2018).

As far as the prompt pathway is concerned, the GRI 2.11 mechanism considers the route to follow the HCN → CN → NCO → NO pathway, which was for long believed to be pathway through which the reactions progressed (Lefebvre and Ballal, 2010). Currently, it is known that the NCN route is active instead (Glarborg et al., 2018). In the present analysis, the prompt pathway is considered as it was in the development of GRI 2.11. Therefore, the NO forming reactions shown in Equations (9)–(13) were taken into account to calculate the NO formation rate.

$$NCO + O \leftrightarrow NO + CO \quad (9)$$

$$NCO + OH \leftrightarrow NO + H + CO \quad (10)$$

$$NCO + O_2 \leftrightarrow NO + CO_2 \quad (11)$$

$$CH + NO \leftrightarrow HCN + O \quad (12)$$

$$CH + NO \leftrightarrow H + NCO \quad (13)$$

The contribution of the $N_2O$ pathway was calculated by the NO formation rates of Equations (14)–(16). On Equation (15), it is clear that the $N_2O$ pathway interacts with the prompt pathway

via the formation of NCO. That interaction, however, does not directly interfere with the calculation of the NO formation rate, as $N_2O$ and NCO are on opposite sides of the reaction.

$$N_2O + O \leftrightarrow 2NO \quad (14)$$

$$NCO + NO \leftrightarrow N_2O + CO \quad (15)$$

$$NH + NO \leftrightarrow N_2O + H \quad (16)$$

Finally, the NNH pathway was taken into account with the only reaction forming NO in the pathway present in GRI 2.11 (Equation 17).

$$NNH + O \leftrightarrow NH + NO \quad (17)$$

In **Figure 14**, a comparison between the NO formation rates for conditions *a*, *b,* and *e* is displayed for the case with GRI 2.11 and $Y_{O2}$ included as a clustering criterion. The figure displays the results along an axial line at the radial position $r = 15$ mm. This position was found to have the highest rates of formation and, therefore, it was selected. Several conclusions can be drawn from this analysis. The first important fact is that thermal NO decreases as $\phi$ is reduced (going from condition *a–f*). In fact, the rates of thermal NO reduces as much as 3 orders of magnitude from condition *a* to *f*, showing that the contribution of thermal NO cannot explain the overall trend.

Secondly, the role of the prompt pathway is shown to be important. The rates of NO production by prompt peak for condition *b*, which explains why this condition has the highest total value of $NO_x$. Possibly, this peak was predicted for condition *b* in the simulations while it occurs for condition *e* according to the experimental data. The prompt pathway was previously shown to be responsible for the peak in NO at lean values for systems operating under FC or with high recirculation (Perpignan et al., 2018b; Perpignan and Rao, 2019).

Thirdly, the role of the NNH pathway is also prominent. Its peak NO formation value is higher at condition *b* than at condition *a*. It should be noted that reactions tend to occur further downstream for condition *b* if compared to the other two conditions. This is an indication of how important the predictions of jet development, recirculation and entrainment

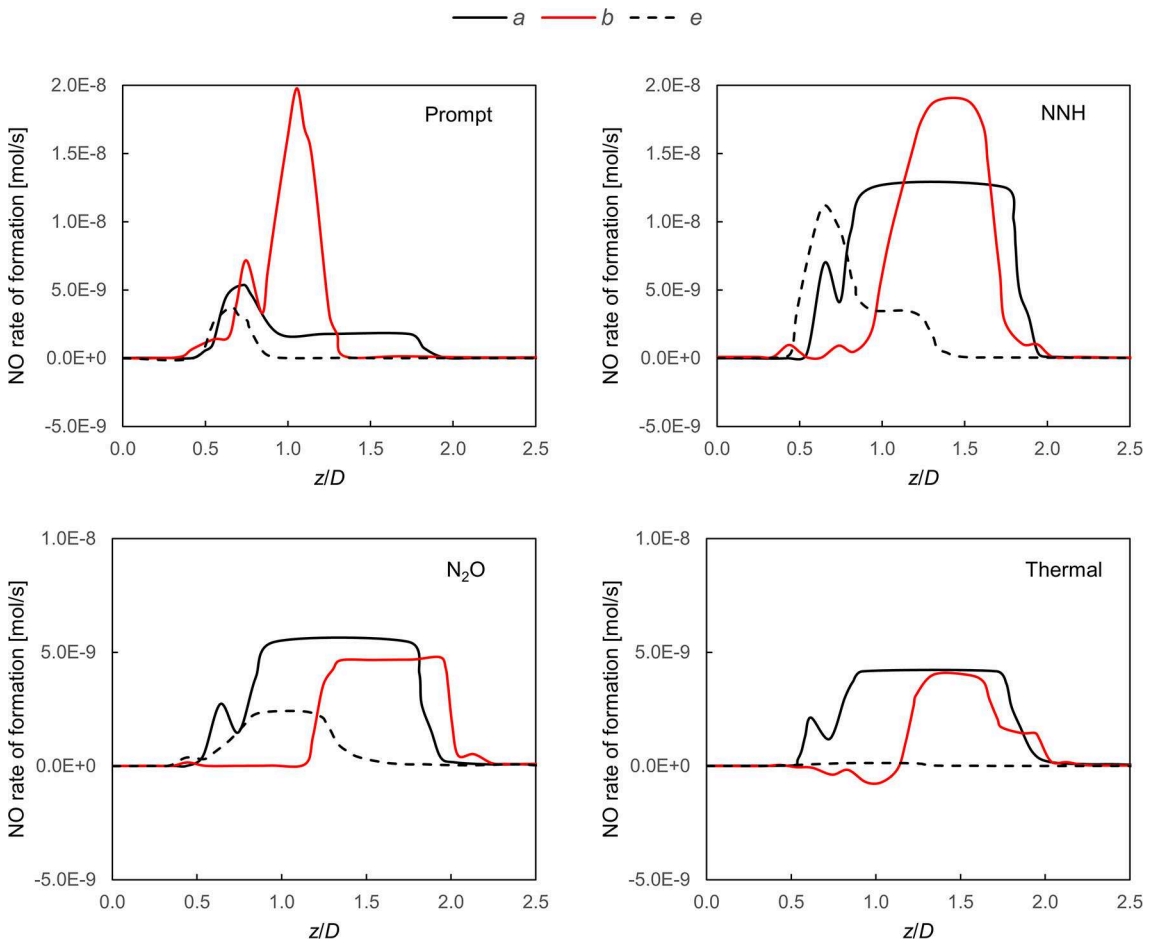


**FIGURE 14 |** NO formation rates at $r = 15$ mm along the axial direction for the different formation pathways. Values presented for conditions *a* ($\phi \cong 0.91$), *b* ($\phi \cong 0.77$), and *e* ($\phi \cong 0.53$).

coming from the CFD solutions are, since NO formation via pathways other than thermal is dependent on slight variations in composition.

## CONCLUSIONS AND RECOMMENDATIONS

The current work presented CFD and CRN simulations of a combustor developed to investigate FC. The FGM model and the EDM were employed in RANS simulations for simulating several operating conditions of the combustor. The CFD results were post-processed and CRNs were built via clustering of the mesh cells and solved with AGNES.

The following conclusions can be drawn from the study:

- The RANS CFD simulations performed with FGM are able to replicate experimental data to a good extent. The main discrepancies were found near the burner head region.
- CFD simulations performed slightly better for the condition in which a conventional combustion regime was attained (*d*) if compared to the condition with FC (*b*).
- The CO emission predictions of all simulations performed with AGNES had a fairly good agreement. The proposed approach can achieve good predictions of CO even with computationally cheap and robust CFD modeling as the EDM.
- The use of AGNES significantly improved the $NO_x$ predictions with respect to CFD, and a reasonable agreement with experiments was achieved.
- Simulations showed that, remarkably, the $NO_x$ is formed in a relatively narrow region (from $z/D = 1.5$–$2.0$, approximately).
- The variables chosen as clustering criteria proved to have a significant influence on the obtained results. For a given case, a certain set of criteria could prove to be necessary or optimal with respect to the number of reactors. To the best of our knowledge, this finding has not been previously presented in the literature.
- NO formation in the combustor seems to be dictated by the prompt and NNH pathways. The variation of prompt $NO_x$ is responsible for the non-monotonic behavior of $NO_x$ with $\phi$.

Further investigations should be carried out to improve or clarify the following issues:

- The proposed method should be explored further in order to optimize clustering criteria.
- The reproduction of outlet emissions for the employed case may require the use of a CFD model able to perform both in the FC regime as well as in conventional combustion, as different operating conditions result in different combustion regimes.
- The validation and subsequent use of chemical reaction mechanisms for highly vitiated conditions would probably aid the performance of AGNES.
- The assessment on the effect of including turbulent fluctuations on the CRN is recommendable. This can be done by clustering the computational cells based on fluctuation values and/or by employing a Partially Stirred Reactor approach.
- The prompt pathway should be investigated under FC and highly vitiated environments due its key role.

## DATA AVAILABILITY STATEMENT

All datasets generated for this study are included in the article.

## AUTHOR CONTRIBUTIONS

AP conceived the idea behind the paper, performed CFD simulations, and took the lead in the writing of the paper. RS wrote the code for AGNES, performed CRN simulations, and actively contributed with the writing. AG supervised the performed worked, was fundamental in discussions about the methods and results, and actively contributed with the writing.

## FUNDING

AP had his PhD research funded by CNPq (National Counsel of Technological and Scientific Development—Brazil) via the Science without Borders program.

## ACKNOWLEDGMENTS

The authors would like to thank CNPq (National Counsel of Technological and Scientific Development—Brazil) support via the Science without Borders program. RS would like to thank Mitsubishi Turbocharger and Engine Europe B.V. (MTEE) for the opportunity of a MSc thesis during which AGNES was developed and Ir. Eline ter Hofstede, R&D Engineer at MTEE, for providing guidance during the project.

## REFERENCES

Benedetto, D., Pasini, S., Falcitelli, M., La Marca, C., and Tognotti, L. (2000). Emission prediction from 3-D completemodelling to reactor network analysis. *Combust. Sci. Technol.* 153, 279–294. doi: 10.1080/00102200008947265

Bowman, C. T., Hanson, R. K., Davidson, D. F., Gardiner W.C. Jr., Lissianski, V., Smith, G. P., et al. Available online at: http://www.me.berkeley.edu/gri_mech/ (accessed February 01, 2019).

Camargo, J. A., and Alonso, Á. (2006). Ecological and toxicological effects of inorganic nitrogen pollution in aquatic ecosystems: a global assessment. *Environ. Int.* 32, 831–849. doi: 10.1016/j.envint.2006.05.002

Cavaliere, A., and de Joannon, M. (2004). Mild combustion. *Prog. Energy Combust. Sci.* 30, 329–366. doi: 10.1016/j.pecs.2004.02.003

Cuoci, A., Frassoldati, A., Stagni, A., Faravelli, T., Ranzi, E., and Buzzi-Ferraris, G. (2013). Numerical modeling of $NO_x$ formation in turbulent flames using a kinetic post-processing technique. *Energy Fuels* 27, 1104–1122. doi: 10.1021/ef3016987

Ellabban, O., Abu-Rub, H., and Blaabjerg, F. (2014). Renewable energy resources: current status, future prospects and their enabling technology. *Renew. Sustain. Energy Rev.* 39, 748–764. doi: 10.1016/j.rser.2014.07.113

Falcitelli, M., Tognotti, L., and Pasini, S. (2002). An algorithm for extracting chemical reactor network models from CFD simulation of industrial combustion systems. *Combust. Sci. Technol.* 174, 27–42. doi: 10.1080/713712951

Faravelli, T., Bua, L., Frassoldati, A., Antifora, A., Tognotti, L., and Ranzi, E. (2001). A new procedure for predicting $NO_x$ emissions from furnaces. *Comput. Chem. Eng.* 25, 613–618. doi: 10.1016/S0098-1354(01)00641-X

Fichet, V., Kanniche, M., Plion, P., and Gicquel, O. (2010). A reactor network model for predicting $NO_x$ emissions in gas turbines. *Fuel* 89, 2202–2210. doi: 10.1016/j.fuel.2010.02.010

Fortunato, V., Mosca, G., Lupant, D., and Parente, A. (2018). Validation of a reduced NO formation mechanism on a flameless furnace fed with $H_2$-enriched low calorific value fuels. *Appl. Therm. Eng.*, 144, 877–889. doi: 10.1016/j.applthermaleng.2018.08.091

Frassoldati, A., Frigerio, S., Colombo, E., Inzoli, F., and Faravelli, T. (2005). Determination of $NO_x$ emissions from strong swirling confined flames with an integrated CFD-based procedure. *Chem. Eng. Sci.* 60, 2851–2869. doi: 10.1016/j.ces.2004.12.038

Glarborg, P., Miller, J. A., Ruscic, B., and Klippenstein, S. J. (2018). Modeling nitrogen chemistry in combustion. *Prog. Energy Combust. Sci.* 67, 31–68. doi: 10.1016/j.pecs.2018.01.002

Goodwin, D. G., Speth, R. L., Moffat, H. K., and Weber, B. W. (2018). *Cantera: An Object-Oriented Software Toolkit for Chemical Kinetics, Thermodynamics, and Transport Processes*. Version 2.4.0. Available online at: https://www.cantera.org

Grewe, V., Dahlmann, K., Matthes, S., and Steinbrecht, W. (2012). Attributing ozone to $NO_x$ emissions: implications for climate mitigation measures. *Atmos. Environ.* 59, 102–107. doi: 10.1016/j.atmosenv.2012.05.002

Hosseini, S. E., and Wahid, M. A. (2013). Biogas utilization: experimental investigation on biogas flameless combustion in lab-scale furnace. *Energy Convers. Manag.* 74, 426–432. doi: 10.1016/j.enconman.2013.06.026

Huang, X., Tummers, M. J., and Roekaerts, D. J. E. M. (2017). Experimental and numerical study of MILD combustion in a lab-scale furnace. *Energy Procedia* 120, 395–402. doi: 10.1016/j.egypro.2017.07.231

International Energy Agency. (2018). *World Energy Outlook 2018*.

IPCC (2014). *Climate Change 2014: Synthesis Report. Contribution of Working Groups I, II and III to the Fifth Assessment Report of the Intergovernmental Panel on Climate Change,* eds Core Writing Team, R. K. Pachauri, and L. A. Meyer. (Geneva: IPCC), 151.

Kruse, S., Kerschgens, B., Berger, L., Varea, E., and Pitsch, H. (2015). Experimental and numerical study of MILD combustion for gas turbine applications. *Appl. Energy* 148, 456–465. doi: 10.1016/j.apenergy.2015.03.054

Lamouroux, J., Ihme, M., Fiorina, B., and Gicquel, O. (2014). Tabulated chemistry approach for diluted combustion regimes with internal recirculation and heat losses. *Combust. Flame* 161, 2120–2136. doi: 10.1016/j.combustflame.2014.01.015

Lebedev, A. B., Secundov, A. N., Starik, A. M., Titova, N. S., and Schepin, A. M. (2009). Modeling study of gas-turbine combustor emission. *Proc. Combust. Inst.* 32, 2941–2947. doi: 10.1016/j.proci.2008.05.015

Lefebvre, A. H., and Ballal, D. R. (2010). *Gas Turbine Combustion: Alternative Fuels and Emissions.* Boca Raton, FL: CRC press. doi: 10.1201/9781420086058

Lyra, S., and Cant, R. S. (2013). Analysis of high pressure premixed flames using Equivalent Reactor Networks for predicting $NO_x$ emissions. *Fuel* 107, 261–268. doi: 10.1016/j.fuel.2012.12.066

Magnussen, B. F., Hjertager, B. H. (1976). On mathematical modeling of turbulent combustion with special emphasis on soot formation and combustion. *Symp. Int. Combust.* 16, 719–729. doi: 10.1016/S0082-0784(77)80366-4

Minamoto, Y., Dunstan, T. D., Swaminathan, N., and Cant, R. S. (2013). DNS of EGR-type turbulent flame in MILD condition. *Proc. Combust. Inst.* 34, 3231–3238. doi: 10.1016/j.proci.2012.06.041

Minamoto, Y., and Swaminathan, N. (2014). Scalar gradient behaviour in MILD combustion. *Combust. Flame* 161, 1063–1075. doi: 10.1016/j.combustflame.2013.10.005

Minamoto, Y., Swaminathan, N., Cant, R. S., and Leung, T. (2014). Reaction zones and their structure in MILD combustion. *Combust. Sci. Technol.* 186, 1075–1096. doi: 10.1080/00102202.2014.902814

Monaghan, R. F., Tahir, R., Cuoci, A., Bourque, G., Füri, M., Gordon, R. L., et al. (2012). Detailed multi-dimensional study of pollutant formation in a methane diffusion flame. *Energy Fuels* 26, 1598–1611. doi: 10.1021/ef201853k

Nastasi, B., and Basso, G. L. (2016). Hydrogen to link heat and electricity in the transition towards future Smart Energy Systems. *Energy* 110, 5–22. doi: 10.1016/j.energy.2016.03.097

Nicolle, A., and Dagaut, P. (2006). Occurrence of NO-reburning in MILD combustion evidenced via chemical kinetic modeling. *Fuel* 85, 2469–2478. doi: 10.1016/j.fuel.2006.05.021

Paltsev, S., Sokolov, A., Gao, X., and Haigh, M. (2018) *Meeting the Goals of the Paris Agreement: Temperature Implications of the Shell Sky Scenario*. Joint Program Report Series Report 330, 10p. Available online at: http://globalchange.mit.edu/publication/16995

Park, J., Nguyen, T. H., Joung, D., Huh, K. Y., and Lee, M. C. (2013). Prediction of NO x and CO emissions from an industrial lean-premixed gas turbine combustor using a chemical reactor network model. *Energy Fuels* 27, 1643–1651. doi: 10.1021/ef301741t

Perpignan, A. A. V., and Rao, A. G. (2019). Effects of chemical reaction mechanism and $NO_x$ formation pathways on an inter-turbine burner. *Aeronaut. J.* doi: 10.1017/aer.2019.12. [Epub ahead of print].

Perpignan, A. A. V., Rao, A. G., and Roekaerts, D. J. (2018a). Flameless combustion and its potential towards gas turbines. *Prog. Energy Combust. Sci.* 69, 28–62. doi: 10.1016/j.pecs.2018.06.002

Perpignan, A. A. V., Talboom, M. G., Levy, Y., and Rao, A. G. (2018b). Emission modeling of an interturbine burner based on Flameless Combustion. *Energy Fuels* 32, 822–838. doi: 10.1021/acs.energyfuels.7b02473

Pope, S. B. (1978). An explanation of the turbulent round-jet/plane-jet anomaly. *AIAA J.* 16, 279–281. doi: 10.2514/3.7521

Prakash, V., Steimes, J., Roekaerts, D. J. E. M., Klein, S. A. (2018). "In modelling the effect of external flue gas recirculation on $NO_x$ and CO emissions in a premixed gas turbine combustor with chemical reactor networks," in *Proceedings of ASME Turbo Expo* (Oslo). doi: 10.1115/GT2018-76548

Ramaekers, W. J. S., Van Oijen, J. A., and De Goey, L. P. H. (2010). A priori testing of flamelet generated manifolds for turbulent partially premixed methane/air flames. *Flow Turbul. Combust.* 84, 439–458. doi: 10.1007/s10494-009-9223-1

Ranzi, E., Frassoldati, A., Grana, R., Cuoci, A., Faravelli, T., Kelley, A. P., et al. (2012). Hierarchical and comparative kinetic modeling of laminar flame speeds of hydrocarbon and oxygenated fuels. *Prog. Energy Combust. Sci.* 38, 468–501. doi: 10.1016/j.pecs.2012.03.004

Sampat, R. P. (2018). *Automatic generation of chemical reactor networks for combustion simulations* (Master of Sciences Thesis). Delft: Delft University of Technology.

Scarlat, N., Dallemand, J. F., Monforti-Ferrario, F., and Nita, V. (2015). The role of biomass and bioenergy in a future bioeconomy: policies and facts. *Environ. Dev.* 15, 3–34. doi: 10.1016/j.envdev.2015.03.006

Shih, T. H., Liou, W. W., Shabbir, A., Yang, Z., and Zhu, J. (1995). A new k-$\epsilon$ eddy viscosity model for high reynolds number turbulent flows. *Comp. Fluids* 24, 227–238. doi: 10.1016/0045-7930(94)00032-T

Smith, G. P., Golden, D. M., Frenklach, M., Moriarty, N. W., Eiteneer, B., Goldenberg, M., et al. Available online at: http://www.me.berkeley.edu/gri_mech/ (accessed February 01, 2019).

van Oijen, J. A. (2018). "Modeling of turbulent premixed flames using flamelet generated manifolds," in *Modeling and Simulation of Turbulent Combustion*, eds S. De, A. K. Agarwal, S. Chaudhuri, and S. Sen (Singapore: Springer), 241–265. doi: 10.1007/978-981-10-710-3_7

van Oijen, J. A., and De Goey, L. P. H. (2000). Modelling of premixed laminar flames using flamelet-generated manifolds. *Combust. Sci. Technol.* 161, 113–137. doi: 10.1080/00102200008935814

Verhoeven, L. M., Ramaekers, W. J. S., Van Oijen, J. A., and De Goey, L. P. H. (2012). Modeling non-premixed laminar co-flow flames using flamelet-generated manifolds. *Combust. Flame* 159, 230–241. doi: 10.1016/j.combustflame.2011.07.011

Veríssimo, A. S., Rocha, A. M. A., and Costa, M. (2011). Operational, combustion, and emission characteristics of a small-scale combustor. *Energy Fuels* 25, 2469–2480. doi: 10.1021/ef200258t

World Health Organization. (2013). *Review of Evidence on Health Aspects of Air Pollution–REVIHAAP Project*. Copenhagen: World Health Organization.

Yousefian, S., Bourque, G., and Monaghan, R. F. (2017). "Review of hybrid emissions prediction tools and uncertainty quantification methods for gas turbine combustion systems," in *Proceedings of ASME Turbo Expo* (Charlotte, NC).

Zhou, B., Costa, M., Li, Z., Aldén, M., and Bai, X. S. (2017). Characterization of the reaction zone structures in a laboratory combustor using optical diagnostics: from flame to flameless combustion. *Proc. Combust. Inst.* 36, 4305–4312. doi: 10.1016/j.proci.2016.06.182

**Conflict of Interest:** The authors declare that the research was conducted in the absence of any commercial or financial relationships that could be construed as a potential conflict of interest.

# NOMENCLATURE

**Acronyms**

| | |
|---|---|
| AGNES | Automatic Generation of Networks for Emission Simulation |
| BFS | Breadth First Search |
| CRN | Chemical Reactor Network |
| CFD | Computational Fluid Dynamics |
| EDM | Eddy Dissipation Model |
| FC | Flameless Combustion |
| FGM | Flamelet Generated Manifolds |
| PDF | Probability Density Function |

**Symbols**

| | |
|---|---|
| $c_p$ | Specific heat capacity at constant pressure [J/gK] |
| $D$ | Diameter [m] |
| $H$ | Enthalpy [J/kg] |
| $M$ | Molar mass [kg/mol] |
| $R$ | Reaction rate [kg/m$^3$s] |
| $S$ | Source-term [kg/m$^3$s] |
| $T$ | Temperature [K] |
| $Y$ | Mass fraction [-] |
| $c$ | Generic variable from CFD solution |
| $f$ | Mixture fraction [-] |
| $k$ | Turbulent kinetic energy [m$^2$/s$^2$] |
| $r$ | Radial coordinate [m] |
| $u$ | Velocity [m/s] |
| $z$ | Axial coordinate [m] |
| $\alpha$ | Range of a given quantity for AGNES clustering [-] |
| $\delta$ | Tolerance for AGNES clustering [-] |
| $\varepsilon$ | Turbulent dissipation rate [m$^2$/s$^3$] |
| $\rho$ | Density [kg/m$^3$] |
| $\chi$ | Scalar dissipation rate [1/s] |
| $\phi$ | Equivalence Ratio [-] |

**Subscripts**

| | |
|---|---|
| *reac*. | Reactants |
| *prod*. | Products |
| $i$ | Chemical species |
| $r$ | Reaction |

frontiers in Mechanical Engineering

REVIEW
published: 29 November 2019
doi: 10.3389/fmech.2019.00065

# Understanding and Interpreting Laser Diagnostics in Flames: A Review of Experimental Measurement Techniques

*Michael J. Evans* and Paul R. Medwell*

*School of Mechanical Engineering, The University of Adelaide, Adelaide, SA, Australia*

There is a wealth of existing experimental data of flames collected using laser diagnostics. The primary objective of this review is to provide context and guidance in interpreting these laser diagnostic data. This educational piece is intended to benefit those new to laser diagnostics or with specialization in other facets of combustion science, such as computational modeling. This review focuses on laser-diagnostics in the context of the commonly used canonical jet-in-hot-coflow (JHC) burner, although the content is applicable to a wide variety of configurations including, but not restricted to, simple jet, bluff body, swirling and stratified flames. The JHC burner configuration has been used for fundamental studies of moderate or intense low oxygen dilution (MILD) combustion, autoignition and flame stabilization in hot environments. These environments emulate sequential combustion or exhaust gas recirculation. The JHC configuration has been applied in several burners for parametric studies of MILD combustion, flame reaction zone structure, behavior of fuels covering a significant range of chemical complexity, and the collection of data for numerical model validation. Studies of unconfined JHC burners using gaseous fuels have employed point-based Rayleigh-Raman or two-dimensional Rayleigh scattering measurements for the temperature field. While the former also provides simultaneous measurements of major species concentrations, the latter has often been used in conjunction with planar laser-induced fluorescence (PLIF) to simultaneously provide quantitative or qualitative measurements of radical and intermediary species. These established scattering-based thermography techniques are not, however, effective in droplet or particle laden flows, or in confined burners with significant background scattering. Techniques including coherent anti-Stokes Raman scattering (CARS) and non-linear excitation regime two-line atomic fluorescence (NTLAF) have, however, been successfully demonstrated in both sooting and spray flames. This review gives an overview of diagnostics techniques undertaken in canonical burners, with the intention of providing an introduction to laser-based measurements in combustion. The efficacy, applicability and accuracy of the experimental techniques are also discussed, with examples from studies of flames in JHC burners. Finally, current and future directions for studies of flames using the JHC configuration including spray flames and studies and elevated pressures are summarized.

**Keywords: laser diagnostics, jet in hot coflow (JHC), vitiated coflow burner (VCB), autoignition, planar thermography, moderate or intense low oxygen dilution (MILD) combustion, laser-induced fluorescence (LIF)**

OPEN ACCESS

***Edited by:***
*Alessandro Parente, Université libre de Bruxelles, Belgium*

***Reviewed by:***
*Dirk J. E. M. Roekaerts, Delft University of Technology, Netherlands*
*Giancarlo Sorrentino, University of Naples Federico II, Italy*

****Correspondence:***
*Michael J. Evans*
*m.evans@adelaide.edu.au*

***Specialty section:***
*This article was submitted to Thermal and Mass Transport, a section of the journal Frontiers in Mechanical Engineering*

***Received:*** *30 April 2019*
***Accepted:*** *15 November 2019*
***Published:*** *29 November 2019*

***Citation:***
*Evans MJ and Medwell PR (2019) Understanding and Interpreting Laser Diagnostics in Flames: A Review of Experimental Measurement Techniques. Front. Mech. Eng. 5:65. doi: 10.3389/fmech.2019.00065*

# 1. INTRODUCTION

Laser diagnostics are a well-established cornerstone of experimental combustion research. Laser diagnostics facilitate the measurement of temperature, velocity and a variety of chemical species in flames. Accurate experimental measurements are a unique source of invaluable real data to bolster the fundamental understanding of combustion. Laser-based measurements can provide data encompassing a broad range of length and temporal scales of flames. Furthermore, experiments are an essential tool for further advances in computational modeling, both by providing data for validation as well as identifying realistic boundary conditions for numerical studies.

Laser-based diagnostics enable measurements of flames without the need for intrusive sampling probes or thermocouples which disturb the flow-field of a flame and may have additional catalytic effects (Eckbreth, 1996). Not only can physical probes affect the flames they are measuring, they have limited spatial and temporal resolutions which limits their efficacy in turbulent flames. Lasers, however, can provide virtually instantaneous measurements at spatial resolutions of similar order of magnitude to Kolmogorov length-scales.

Flames in hot and diluted coflows are analogous to practical implementations of fuel issuing into preheated and oxygen-vitiated environments such as found in furnaces with exhaust gas recirculation (EGR) (Dally et al., 2004), modern diesel engines (Yao et al., 2009), and sequential or inter-turbine burners (ITBs) for gas turbines (Sturgess et al., 2005; Döbbeling et al., 2007; Perpignan et al., 2018). Fundamental studies of these flames have not only provided significant insight into autoignition processes, but have been used to generate extensive datasets in simplified configurations for validating turbulence-chemistry interaction models for numerical modeling of combustion systems. Fundamental studies of laminar and turbulent jet flames issuing into high temperature, low oxygen environments have been undertaken in jet in hot coflow (JHC) burners (Dally et al., 2002; Medwell et al., 2007, 2008; Oldenhof et al., 2010, 2011; Oldenhof et al., 2012; Medwell and Dally, 2012a; Sepman et al., 2013; Ye et al., 2016, 2017, 2018; Evans et al., 2017b, 2019a,b; Kruse et al., 2019), hot cross-flow burners (Sidey and Mastorakos, 2017), vitiated coflow burners (VCBs) (Cabra et al., 2002, 2005; Gordon et al., 2008, 2009; Macfarlane et al., 2018, 2019; Ramachandran et al., 2019), and partially premixed jet burners (PPJBs) (Dunn et al., 2007a; Dunn et al., 2009), as have spray flames in hot coflow burners (Correia Rodrigues et al., 2015a,b; Wang et al., 2019b). In each case, fresh fuel issues from a jet into a stream of hot gas generated by lean premixed flames, resulting in $\lesssim$15% $O_2$ (by vol.). The remainder of the oxidant streams are typically composed of $H_2O$, $CO_2$, $N_2$, and minor species. As each of these burners share this common jet-and-annular-coflow-burner configuration, they will all be referred to herein as JHC burners for ease of readability. Research undertaken in JHC burners has focussed on ignition processes in hot and diluted environments, particularly toward understanding high temperature autoignition (Mastorakos, 2009), and ignition processes in the moderate or intense low oxygen dilution (MILD) combustion regime (Cavaliere and de Joannon, 2004). Combustion in the MILD regime features homogeneous temperature distributions, low peak temperatures and temperature fluctuations, and offers reduced formation of soot and $NO_x$. Furthermore, fundamental studies of the MILD combustion regime in JHC burners often feature order unity Damköhler with reduced chemical timescales approaching those of the turbulent jet. These characteristics of low temperature increases, and subsequently low radical species concentrations, lead to the requirement of highly sensitive temperature and species measurements in studying MILD combustion. Fortuitously, the often soot-free flames allow a variety of different laser diagnostics.

Experimental studies of diffusion flames in hot and vitiated conditions similar to those encountered in MILD combustion have revealed the existence of "weak-to-strong" transition points (Medwell et al., 2008; Medwell and Dally, 2012a; Evans et al., 2015a, 2019c). This occurs when a weakly reacting, attached diffusion undergoes a rapid increase in temperature and reaction zone thickness (Medwell et al., 2008; Medwell and Dally, 2012a). These transition points, which will be addressed at length in section 7, are critical to the stabilization and structure of flames emanating into hot and vitiated environments, and the capacity to predict this phenomenon is essential for practical, novel implementations of MILD combustion and similar low-emissions combustion technologies. Such improved understanding these transitions—and the structure of the upstream flames leading to their formation—may be achieved through targeted laser-diagnostics studies and subsequently validated, complementary numerical modeling. The high fidelity data that laser diagnostics can provide allows for the detailed study of reactive structures across the broad range of spatial and temporal scales in different optically-accessible JHC burners and reactors (Plessing et al., 1998; Cabra et al., 2002, 2005; Dally et al., 2002; Medwell et al., 2007, 2008; Gordon et al., 2008, 2009; Oldenhof et al., 2010, 2011; Oldenhof et al., 2012; Medwell and Dally, 2012a; Sepman et al., 2013; Sorrentino et al., 2015, 2016; Ye et al., 2016, 2017, 2018; Evans et al., 2017b, 2019a,b; Sidey and Mastorakos, 2017; Macfarlane et al., 2018, 2019; Kruse et al., 2019; Ramachandran et al., 2019). Laser diagnostics a provide means to investigate the small-scale and distributed reaction zones in macroscopically-near-homogeneous MILD combustion conditions. Such research not only improves the understanding of the behavior of these regimes, but provide reference cases and motivation for complementary numerical studies (Ihme and See, 2011; de Joannon et al., 2012; Ihme et al., 2012; Minamoto and Swaminathan, 2014; Minamoto et al., 2014; Sabia et al., 2015; Sidey and Mastorakos, 2015; Medwell et al., 2016; Evans et al., 2017a,b, 2019c; Sorrentino et al., 2017; Doan and Swaminathan, 2019; Wang et al., 2019a) which could otherwise be performed in isolation or target conditions with either limited practical applicability or data for model validation.

This paper presents a review of laser diagnostics applicable to studies of flames in canonical burners—particularly focusing on the JHC configuration—for the benefit of readers new to, or outside of, this field. Despite this particular focus on JHC burners, the techniques and discussions are also relevant to simple jet, bluff body, swirling and stratified flames. The paper will initially

provide a brief background on laser-based experimentation, before discussing challenges of data quantification in laser-diagnostics. Having provided the requisite background, the paper then discusses the techniques used for velocity, species and temperature measurements of flames stabilized in JHC burners, the technical challenges they present and the findings from these studies. Finally, future diagnostics needed for better understanding flames in JHC burners will be discussed.

## 2. PRINCIPLES OF LASER DIAGNOSTICS

### 2.1. Principles of Light-Matter Interactions

Light can interact with matter in a range of different ways. Light can scatter off of atoms, molecules and particles in predictable ways, or—on a quantum scale—a photon can be absorbed and a new photon emitted. These new photons may have the same energy as the original (and thus be at the same wavelength), may have less energy or, in some cases, more energy. Detecting these emitted photons produces a quantifiable "signal." The total number of these detected photons and their energies correspond to the intensity of the signal and its spectral response, respectively. The relationship between photon energy ($E$) and its wavelength ($\lambda$) or frequency ($f$) is given by Equation (1), where $h$ is Planck's constant and $c$ is the speed of light:

$$E = \frac{h \cdot c}{\lambda} = h \cdot f \tag{1}$$

Equation (1) highlights that shorter wavelength photons have more energy than longer wavelength photons, i.e., ultraviolet (UV) photons have more energy than visible photons. Similarly, photon energy decreases from UV to blue to green to red to infrared light. Relevant UV wavelengths for combustion diagnostics lie between ~190 and 400 nm and visible light is considered as 400 and 700 nm.

Scattering of light from a dielectric particle (with effective diameter $d_p$) is dependent on the wavelength of the incident light. Large particles (e.g., droplets or solid particles) scatter light according to the complex Mie theory (Eckbreth, 1996). Mie scattering is a far-field solution of Maxwell's equations in spherical coordinates, with light emanating from the surface of the particle of size $d_p$. This results in direction-dependent scattering described by an infinite series of Legendre polynomials. Mie scattering is typically several orders of magnitude greater than the related phenomenon of Rayleigh scattering and is the underlying principle for techniques such as particle image velocimetry. Because of this disparate intensity, excessive Mie scattering may also prohibit other scattering measurements with lower signal levels, such as Rayleigh scattering.

Small, polarizable particles (e.g., atoms or molecules) may scatter light according to Rayleigh scattering. This follows a first-order approximation for particles much smaller than the wavelength of incident light. Scattering in any given direction scales as $d_p^6 \cdot \lambda^{-4}$ and is a function of the effective refractive index of the particle. At molecular level, Rayleigh scattering occurs when a molecule absorbs a photon, increasing its internal energy, and then emits a photon at the same wavelength. This is shown using a simplified three-level energy diagram in **Figure 1**, where "0" is the "ground state." The same simplified model of excitation may also be applied to individual atoms. The amount of Rayleigh scattering due to individual molecular species can be quantified and characterized by its Rayleigh cross-section ($\sigma$). Values of $\sigma$ are tabulated for common gases in various sources (Namer and Schefer, 1985; Eckbreth, 1996; Masri et al., 1996; Kohse-Höinghaus and Jeffries, 2002; Sutton and Driscoll, 2004). The intensity of scattered light from a stationary molecule is a function of the direction compared to the incoming light. Following calibration and estimation of the gas composition, this can provide the local number of molecules per unit volume (number density, $n$) and, hence, local temperature based on the ideal gas law. In non-reacting flows, results from this method can be accurate to within 1% (Arndt et al., 2019).

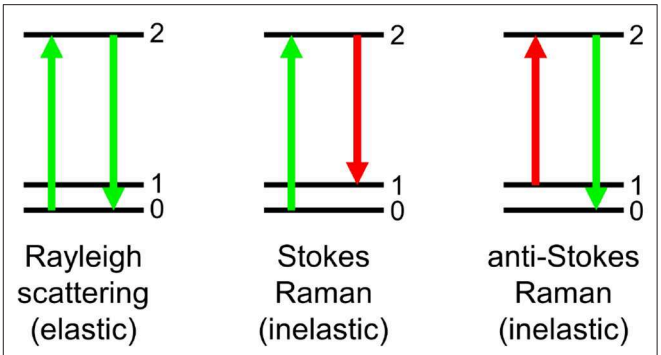


**FIGURE 1 |** Three-level model of excitation levels, showing Rayleigh **(left)** and Raman (Stokes, **center**, and anti-Stokes, **right**) processes. Note that the highest energy levels in these models need not necessarily correspond to stable atomic or molecular vibrational states.

Spontaneous Raman scattering is a non-linear analog of Rayleigh scattering, but produces signals approximately three orders of magnitude weaker. Whereas Rayleigh scattering emits only at the incident wavelength, Raman scattering from an atom or molecule in its ground state emits a lower energy photon corresponding to relaxation to an excited energy state (see **Figure 1**). This emitted photon is at a longer wavelength and the process is referred to as Stokes Raman scattering. Referring again to **Figure 1**, the opposite of this process—where a higher energy photon is emitted—is termed anti-Stokes Raman scattering. This requires atoms or molecules to already be in an excited state. Although this occurs in flames, only a small fraction of molecules are excited at flame temperatures, resulting in significantly weaker signals than Stokes Raman. Optical pumping prior to anti-Stokes Raman scattering excites a larger fraction of atoms or molecules than from thermal energy alone, and forms the conceptual basis of techniques such as coherent anti-Stokes Raman scattering (CARS) thermography (see section 6). Raman, Rayleigh and Mie scattering are all effectively instantaneous processes and measurement signals are dependent on the pulse energy, rather than the pulse duration although this may affect the background signal from secondary scattering or optical breakdown (plasma formation) (Eckbreth, 1996; Kojima and

Nguyen, 2002). This is more prevalent at higher pressures where species number densities are higher (Eckbreth, 1996; Jiang et al., 2017).

Energy levels of atoms/molecules probed in optical diagnostics may be "virtual" (as is the case for Rayleigh and Raman scattering), or allowable energy levels (also termed "resonant," as is the case in fluorescence techniques). Atomic and molecular energy levels are conceptually similar, with atomic energy levels corresponding to quasi-stable electron orbital shells and the latter being allowable states for combinations of molecular rotations and vibrations. Molecular levels correspond to allowable rotational energies of the molecules about each of its axes and the vibrational energies of the intramolecular bonds. Molecular excitation states are often closely grouped, with the discrete energies being a function of both the rotational and vibrational state. Probing these states by exciting molecules to a given energy level results in the emission of a lower energy, longer wavelength photon as the molecule cascades to its ground states. This process is known as laser-induced fluorescence (LIF) and is one of the most widely used approaches for detecting certain species within flames (see section 4). A similar process of exciting atoms, albeit from both the ground and thermally excited states (analogous to Stokes and anti-Stokes Raman scattering), is two-line atomic fluorescence (TLAF) which may be used for thermography (see section 6).

## 2.2. Laser Operation

Lasers supply "coherent" light centered about a given wavelength ($\sim$180–10,000 nm), with a precision of $\lesssim$0.1 nm, and often much less. This distribution in wavelength is described as the laser "linewidth." Emitted photons from lasers are generated from atoms or molecules in a "gain medium" excited through "optical pumping." High energy photons are absorbed and lower energy (longer wavelength) photons are emitted as the atom or molecule returns to its ground state. The output wavelength of a laser is subsequently a property of the gain medium and, additionally, properties of the optical components used in the construction of the laser.

Lasers used for diagnostics of flames stabilized in JHC burners are often flashlamp-pumped solid-state lasers or high energy dye lasers. Lasers for diagnostics are often "pulsed" such that the laser energy is delivered as short ($\lesssim$10 ns), high energy pulses (or "shots") at repetition rates between 10 Hz and 10 kHz. These brief periods of illumination enables the image to effectively "freeze the flow" and capture an image at one very specific instant in time. Similarly, multiple laser diagnostic techniques used "simultaneously" often employ pulsed lasers separated by $\sim$100 ns, which is much slower than the flow or chemical timescales.

Many diagnostic techniques require specific unique wavelength light required to excite energy transitions in atoms and molecules of interest. These techniques necessitate the use of lasers which can be tuned to preselected specific wavelengths. Dye lasers are used to provide a tunable source of high energy laser pulses, spanning from deep UV to mid-IR ($\sim$190 nm to $\sim$4.5 $\mu$m, respectively). Dye lasers use specific dyes to fluoresce at a desired wavelength when pumped with shorter wavelength light. Dyes themselves are often organic solids which are dissolved in solvents, such as ethanol, for use. Individual dyes have different effective lifetimes and, as a general rule-of-thumb, dyes pumped by UV lasers must be replaced significantly more often than those pumped with visible wavelengths. Not all wavelengths may be efficiently obtained by direct dye pumping and, in these cases, non-linear frequency doubling or two-mixing wave processes are employed. For example, the former is often used to generate the wavelengths near 283 nm for OH-LIF (discussed in sections 2.4 and 4), the latter used to generate the 410 nm laser for indium TLAF (section 6) and both are used in series to generate the 226 nm beam for NO-LIF studies.

An important consideration beyond laser wavelength and pulse energy is the intensity profile emanating from the laser. These profiles may be approximated as Gaussian, triangular, or "top-hats" (Gordon et al., 2008; Dunn and Masri, 2010), but are often significantly more complex due to imperfections in mirrors and sheet-forming-optics, and vary between individual laser pulses (i.e., shot-to-shot). Variations in beam profile may also be caused by variations in refractive index, inherent in flames, which result in refraction of the beam termed "beam-steering" (Kruse et al., 2018). As such, beam profiles may also be measured for each individual shot. This may be performed using a dedicated beam profiling camera, imaging fluorescence or scattering from a cuvette or glass sheet, or with a reference burner either in-plane or using a portion of the incident light sheet.

## 2.3. Data Collection and Processing

Due to the relatively low signal level, often only over very brief periods of time, scientific cameras used in combustion diagnostics are often intensified CCD (ICCD) cameras, although intensified scientific CMOS (sCMOS) cameras are becoming more prevalent as this technology matures. For simplicity, only CCD cameras will be referred to, though the operating principle is the same. Optical intensifiers operate by focusing photons onto a light-sensitive photocathode (e.g., through a camera lens), which in-turn releases electrons. Photocathode materials have specific sensitivities to different wavelengths of light and so must be appropriately selected as part of experimental design. A microchannel plate (MCP) behind the photocathode acts as an amplifier when a voltage is applied, accelerating electrons onto a phosphor screen. The phosphor screen is either imaged onto the CCD or coupled with fiber-optics. Modern CCD and sCMOS imaging systems have resolutions ranging of several megapixels and bit-depths between 12 and 16, meaning that each pixel can return a value between 0 and $2^{12}$ (4,096) to $2^{16}$ (65,536).

Scientific camera assemblies are often Peltier cooled to reduce thermal noise with the intensifier and detector. Cooling is often required as thermal interactions result in a non-zero baseline reading called "dark-charge." This, along with the uniformity of the detection system (the CCD, intensifier and imaging optics), must be corrected for, particularly in quantitative measurements. Intensified scientific cameras are also prone to noise, which may be quantified using the signal-to-noise (SNR) ratio for a particular experiment or dataset. Signal may be effectively increased through the use of on-chip binning where a square number of pixels (usually four) act as a "superpixel" at a cost of

in-plane resolution. This in-plane resolution is often less than the light sheet thickness which is typically ∼0.1–0.2 mm (Gordon et al., 2008; Medwell et al., 2008; Kaiser and Frank, 2011; Ye et al., 2016) and limits the actual resolution of the imaging system. Smoothing is a means of improving SNR in raw data prior to post-processing. Smoothing may commonly be applied as square median or Gaussian filters, however "contour-aligned smoothing," an anisotropic median filter which obtains filter sizes from a reference image, has shown significant success in improving SNR by up to a factor of ten (Starner et al., 1995).

Measurements made using pulsed lasers provide instantaneous data which may be analyzed in isolation to study transient processes such as ignition or instabilities or as part of an ensemble of repeated measurements. It is critical to ensure that a sufficient number of measurements are used in calculating mean and root-mean-squared deviation from the mean (often simply referred to as the RMS) to ensure convergence. In laminar or statistically-stationary turbulent flames, this number is not a function of the measurement rate (e.g., in Hz) on the condition that measurements are not biased by individual, transient processes. For example, high-repetition rate (∼kHz) diagnostics may require more measurements to provide mean data, because processes such as the formation and evolution of an ignition kernel may be captured over several measurements and would not be independent from one-another. Despite this, the actual time required to record a sufficient number of independent data points to be statistically converged is still likely to be faster at 1 kHz than at 10 Hz.

Quantitatively, the convergence of mean data may be assessed using the standard-error-of-the-mean. It is important to highlight that this uncertainty is not the same as the RMS of the data. The standard-error-of-the-mean captures the statistical uncertainty of the mean data and is evaluated as the standard deviation of the measured data, divided by the square-root of the number of independent samples. This metric provides a range within which the mean data should lie and a range of uncertainty for comparison with modeling studies. As the standard-error-of-the-mean decreases with larger sample sizes, this statistical uncertainty may be readily reduced to within a few percent of the measured mean value using several hundred measurements.

Convergence of the RMS data requires more independent images than mean data. These RMS data represent the physical variations in the measurements, rather than the statistical uncertainty of mean data. The RMS consequently represents the statistical variation due to factors such as turbulence and may be further used to validate the choice of probabilistic distributions in numerical models.

## 2.4. Quantitative Laser Diagnostics

Laser diagnostics can provide experimental single-point (0-D), line (1-D), and image (2-D) data produced by the interaction of coherent light and the constituents of a flame. Laser light can interact with individual atoms, molecules, solid particles or liquids droplets, and the resultant signal can provide qualitative or quantitative data. Laser diagnostics techniques can be qualitative, quantitative using underlying and measurable physical properties, or semi-quantitative—requiring simplified modeling to produce absolute values. Each of these broad categories require varying complexity and produce different levels of diagnostic information. It is important, however, that they be clearly distinguished to avoid confusion to the readers of experimental studies.

Qualitative experimental measurements are the simplest form of laser-based diagnostics techniques. Measurements, such as qualitative LIF or Raman scattering, are often used to indicate the presence of certain chemical species in flames, such as the OH, CH, or NO radicals (Arndt et al., 2013; Foo et al., 2017; Macfarlane et al., 2017; Sidey and Mastorakos, 2017; Evans et al., 2019d), polycyclic aromatic hydrocarbons (PAH) species (Bartos et al., 2017; Sirignano et al., 2017; Makwana et al., 2018; Wang et al., 2018), $N_2$ or fuel gases (Starner et al., 1995; Jiang et al., 2017). The signals emitted from LIF and Raman processes are dependent on the incident laser-pulse energies, laser wavelengths, the corresponding detection wavelengths, and the proportion of light that is captured. Therefore, the intensity of the detected signal cannot be directly interpreted as estimates of absolute values. This may be due to unknown incident beam profiles, or a lack of calibration data or reference-images. Even accounting for corrections to the laser energy distribution, detector uniformity and dark-charge, the collected signals do not necessarily represent normalized species distributions. Similarly, it is often required to calculate or estimate local collisional quenching (a function of the gas composition) and/or the Boltzmann distribution of the probed species—as described below.

The discrete energy states occupied by atoms and molecules, in the absence of reactions or irradiation, are governed by the Boltzmann distribution. According to this distribution, the ratio of atoms or particles in two energy levels, separated by an energy difference ($\Delta E_{ij}$) at some temperature ($T$) is given by:

$$\frac{N_j}{N_i} = e^{-\Delta E_{ij}/(kT)} \tag{2}$$

where $k$ is the Boltzmann constant, $N$ the population fraction in each energy state and $j$ is the higher energy state. This relationship becomes important when selecting excitation transitions for LIF experiments, and may be used to determine temperatures from comparative measurements of atomic, such as indium (Medwell et al., 2009a) or gallium (Borggren et al., 2017), and simple-molecular species, such as NO or OH (McMillin et al., 1994; Richardson et al., 2016). Similarly, the change in temperature across the reaction zone can introduce additional uncertainties in qualitative measurements (Sidey and Mastorakos, 2015; Kruse et al., 2019), or semi-quantitative measurements which do not include corrections to temperature (Medwell et al., 2007, 2008, 2009b; Ye et al., 2018). The latter approach may be considered valid following careful selection of excitation wavelength, to ensure little variation (e.g., $\lesssim$10% Medwell et al., 2007) in the Boltzmann fraction across the reaction zone.

Collisions between molecules are fundamental to reacting flows. While many collisions may cause, or enhance, chemical reactions, collisions between vibrationally-excited species and large particles may also result in de-excitation, without the

emission of a photon. This process is known as collisional quenching and directly affects LIF measurements. Collisional quenching of an excited species may be evaluated using the local temperature, known collisional quenching coefficients between two-given species (e.g., OH and $N_2$) and their number densities. This dependence on number density allows the effects of collisional quenching to be estimated using only the most populous species in a flame, such as $O_2$, $N_2$, CO, $CO_2$, and fuel gases. Furthermore, although these coefficients are well-known for a number of diatomic species, such as OH and NO, their calculation is significantly more challenging for more complex intermediary combustion species, such as $CH_2O$, preventing their quantification.

Temperature-dependent population distributions result in temperature-dependent absorption and Raman spectra. These spectra may be theoretically computed and subsequently used to determine flame temperatures and compositions by scanning excitation wavelengths in laminar flames or, with more application to turbulent flames in hot and diluted coflows, collecting single-shot spectra at a point or line from Rayleigh-Raman (Carter and Barlow, 1994; Masri et al., 1996; Barlow et al., 2000, 2015; Barlow, 2007; Dunn et al., 2009; Magnotti and Barlow, 2017) or CARS (van Veen and Roekaerts, 2005; Oldenhof et al., 2010; Correia Rodrigues et al., 2015a). These techniques are both capable of high accuracy temperature measurements to within 1.5% (Magnotti and Barlow, 2017) and 2% (Roy et al., 2010), although Rayleigh-Raman simultaneously provides quantified measurements of mixture fraction and major species to within 10% (Magnotti and Barlow, 2017). Specifically, in turbulent flames, accuracies of 2% are possible in measurements of CH4 (Magnotti and Barlow, 2017), 3% of $N_2$ concentration, whilst $CO_2$ and $H_2O$ concentrations can be measured to within 6% and equivalence ratio ($\Phi$) measured to within 10% (Fuest et al., 2012). Similarly, concentrations of $O_2$ may be measured to within 2% in laminar flames (Fuest et al., 2012). Both techniques have been extensively described in previous literature (Eckbreth, 1996; Kohse-Höinghaus and Jeffries, 2002), and are not discussed in-depth here.

Laser energy profiles in pulsed laser systems vary shot-to-shot. Whilst energy-profiles can be reasonably approximated as Gaussian for qualitative measurements (Cavaliere et al., 2013), and have been assumed as constant between shots in studies of non-linear and saturated LIF (Dunn et al., 2007a), linear LIF and Rayleigh techniques—where signal is proportional to laser fluence (energy divided by beam area)—are sensitive to inhomogeneities in the energy profile, as is the single-shot NTLAF thermography technique (Medwell et al., 2009a). Calibration data or simultaneous imaging of reference burners can be used to provide ensemble-averaged or instantaneous profiles, respectively, and additionally provide values for other system-calibration constants, such as image solid-angle and collection efficiency (Medwell et al., 2007, 2009b; Dunn and Masri, 2010).

For fluorescence measurements of individual species, the collected signal is a function of both the concentration of the species and the local temperature. The measured signal depends on the number density ($n$, see section 2.1) of the species of interest as each pixel or detector images a specified spatial volume, rather than a predetermined number of moles of gas. The number density for species $i$ is given by:

$$n_i = X_i \cdot \frac{P \cdot N_A}{R \cdot T} \tag{3}$$

where $X$ is the mole fraction of species $i$, $P$ is the pressure, $N_A$ is Avogadro's number, $R$ the universal gas constant and $T$ is the temperature. It is therefore possible to estimate mole fractions from simultaneous species and temperature measurements, however, this introduces a dependency on accurate temperature measurements. Accordingly, species measurements may be reported in units of number density (Medwell et al., 2007, 2008; Ye et al., 2018). This coupling has promoted the use of iterative solution processes for calculating the mole fraction of species such as OH simultaneously with temperature (Gordon et al., 2008, 2009).

## 3. VELOCITY-FIELD MEASUREMENTS

Velocity and turbulence measurements in flames stabilized in JHC burners are critical for understanding turbulence-chemistry interactions and providing accurate boundary conditions for numerical model validation. Optical velocity measurements in gaseous flames are either performed using particle image velocimetry (PIV) or laser Doppler anemometry (LDA, also known as laser Doppler velocimetry). Both of these techniques require seeded particles which are capable of enduring flame temperatures, such as alumina, and faithfully following the flow. This latter condition requires a Stokes number less than unity and typically demands micron or sub-micron diameter particles (Honoré et al., 2000; Oldenhof et al., 2010; Oldenhof et al., 2012; Barlow et al., 2012). The condition that particles be spherical is particularly critical for LDA measurements, which may also be used to measure the velocity of fuel droplets in dilute spray flames (Kawazoe et al., 1990; Yuan, 2015). The reliance on particles in these techniques makes them susceptible to thermophoresis effects, where gas expansion due to strong thermal gradients results in local pressure differential biasing the flow away from the high temperature region. This effect scales with $\Delta T$ (Mungal et al., 1995; Frank et al., 1999), and is hence less of a concern in the near-field region of jet flames in hot and diluted coflows, where peak flame temperatures and thermal gradients are reduced (Plessing et al., 1998; Dally et al., 2002; Cavaliere and de Joannon, 2004). Particle seeding must be ensured in the both the jet and hot coflow streams to ensure even and unbiased measurements in the mixing region. This requirement to seed particles into the coflow has restricted velocity measurements in JHC burners which generate hot and diluted coflows on porous bed burners (Dally et al., 2002; Medwell et al., 2007, 2008; Ye et al., 2017, 2018; Evans et al., 2019b; Kruse et al., 2019).

Particle image velocimetry is a planar technique using Mie scattering from particles illuminated by a pair of pulsed lasers separated by a known time interval. Image pairs are most often captured using two identical lasers and a double-pulsed camera, although other configurations (such as two

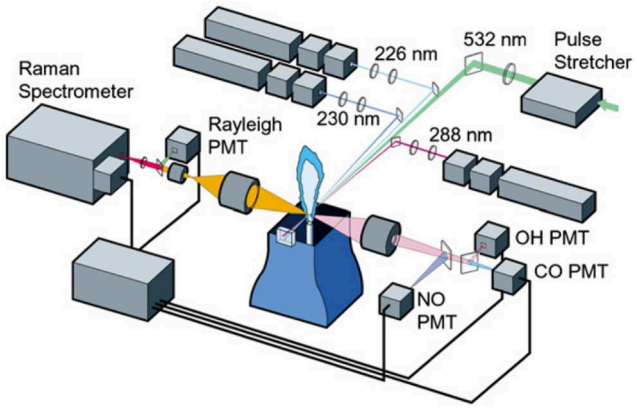


**FIGURE 2 |** Layout of a single-point Rayleigh-Raman-LIF experiment, including measurements of CO-, OH-, and NO-LIF (Barlow, 2007). Reprinted from *Proceedings of the Combustion Institute*, vol. 31, R.S. Barlow, "Laser diagnostics and their interplay with computations to understand turbulent combustion," pp. 49–75, Copyright 2007, with permission from Elsevier.

cameras or lasers of different colors) have been demonstrated. The displacement of groups of particles are subsequently calculated using cross-correlation between the image pairs, using interrogation windows of between 8 and 64 pixels. The size of interrogation windows and timing between pulses is dictated by the requirement that sufficient particles must be present in the corresponding interrogation windows in each image. As such different timings or multiple cameras may be required to measure velocities at different locations in a flame. The use of interrogation windows results in less velocity vectors than imaging pixels, although cameras used for PIV are typically of higher resolution than ICCD cameras, used for species and temperature measurements. Spurious velocity vectors may be generated by particles entering or leaving the light sheet and the need to avoid this has led to the development and refinement of stereo and tomographic PIV, employing thicker light sheets and multiple cameras. Scattering from soot and highly luminous flames may also provide interference.

Particle image velocimetry is able to provide planar information of the velocity field, and may be used to estimate the local strain-rate, vorticity and the RMS fluctuations in velocity. Velocities calculated by PIV inherently overestimate true values in regions of high gradients due to the need for interrogation windows (Kähler et al., 2012), but can be as accurate as 2% of the maximum flow speed (Kamal et al., 2015). Despite this, alternative image post-processing approaches have been proposed. When used in conjunction with scalar imaging techniques such as PLIF, PIV can provide information about fluid entrainment, local turbulence intensity and the behavior of the local flow-field during events such as ignition or extinction.

Laser Doppler anemometry measures the Doppler shift from a modulated, continuous wave laser to calculated particle velocity at a single point in a single direction. This may be extended to two or three lasers to measure multiple velocity components simultaneously. Unlike PIV, LDA is not limited by the repetition rate of a laser or camera and data are collected at sufficiently high frequencies to calculate first and second temporal derivatives at a single point. This technique is often used for measuring velocities at the jet and coflow exits in canonical burners with an accuracy within 0.5% for mean velocity and 2% for RMS (Wu et al., 2006; Kamal et al., 2015).

## 4. SPECIES MEASUREMENTS

Concentrations and images of major, intermediary and radical combustion species in jet flames in hot and diluted coflows have been obtained through single-point Rayleigh-Raman-LIF (Cabra et al., 2002, 2005; Dally et al., 2002; Dunn et al., 2009; Sepman et al., 2013) and planar LIF (Medwell et al., 2007, 2008, 2009b; Gordon et al., 2008, 2009; Dunn et al., 2009; Oldenhof et al., 2011; Oldenhof et al., 2012; O'Loughlin and Masri, 2011, 2012; Arndt et al., 2012, 2013; Sidey and Mastorakos, 2015; Ye et al., 2016, 2017, 2018; Kruse et al., 2019) measurements.

Single-point Rayleigh-Raman-LIF experiments performed in JHC burners have provided quantitative ensemble data of simultaneously measured temperature, major species and mixture fraction via Rayleigh-Raman, with CO- and OH-LIF (Cabra et al., 2002, 2005; Dally et al., 2002; Dunn et al., 2009; Sepman et al., 2013), often using an experimental configuration similar to that shown in **Figure 2**. The configuration in **Figure 2** shows a 532 nm beam for Rayleigh-Raman measurements and three UV beams for CO-, OH- and NO-LIF, as well as lenses and photomultiplier tubes (PMTs) for signal detection. These experiments have investigated ignition processes and finite-rate chemistry in premixed (Dunn et al., 2009) and non-premixed flames in hot and diluted coflows (Dally et al., 2002; Sepman et al., 2013), including partial-premixing leading to autoignition (Cabra et al., 2002, 2005) and the structure of flames stabilized in hot coflows with as little as 3% $O_2$. These high fidelity measurements have provided mean and RMS data, across a range of discrete radial and axial locations, which may be represented in scatter-plots, such as those presented in **Figure 3** for an autoignitive, lifted $CH_4$/air flame (Cabra et al., 2005). The data produced by these studies may be compared against strained opposed-flow or equilibrium chemistry, as done in **Figure 3**, or directly used for validation of combustion models within computational fluid dynamics frameworks (Hochgreb, 2019). The comparisons of scatter data against laminar opposed-flow simulations allow for the identification of regions where the time-averaged flames may or may not be treated as steady, laminar flamelets (Sepman et al., 2013). It is important to note from **Figure 3** that the majority of measured points in diluted $H_2$ flames lie on either the pure mixing or strained-flamelet lines after the $z/d_{jet}$ of 11, with the remainder of points indicating transient ignition processes (Cabra et al., 2005). Here $z$ is the downstream location and $d_{jet}$ is the inner diameter of the pipe from which the central fuel jet issues. These transient processes were less prevalent for $CH_4$/air in a hotter coflow with less $O_2$, with the flame transitioning from almost pure mixing to completely burnt between $40 \lesssim z/d_{jet} \lesssim 50$ (Cabra et al., 2005). Similarly, mean temperature and species measurements in a JHC burner with both preheated fuel and a hot coflow with ∼4% $O_2$

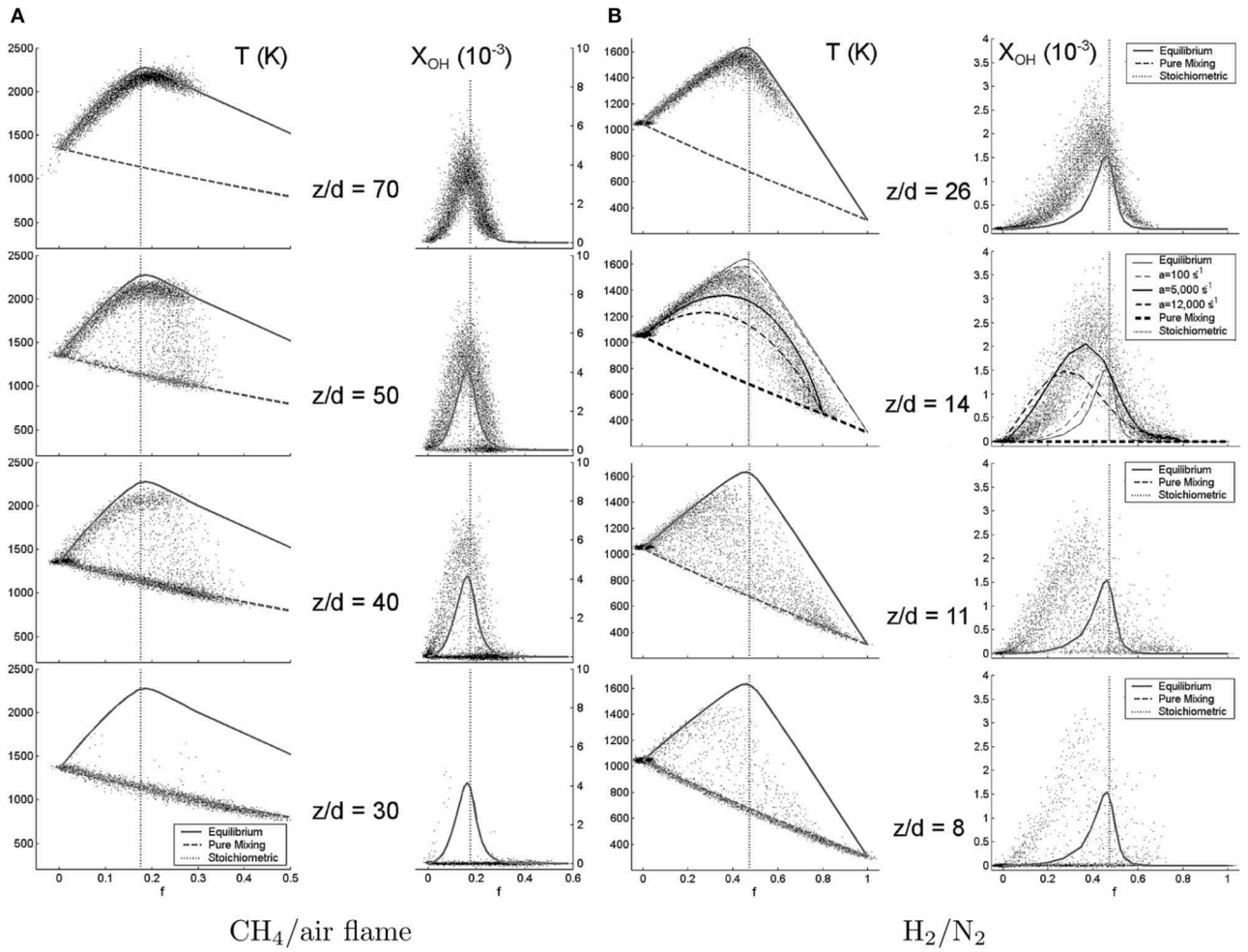


**FIGURE 3 |** Scatter-plot of instantaneous temperature and OH mole fraction at four axial stations in two different flames [with **(A)** $CH_4$/air and **(B)** $H_2/N_2$ fuels] measured using Rayleigh-Raman-LIF. Curves represent calculated distributions (Cabra et al., 2005). Reprinted from *Combustion and Flame*, vol. 143, R. Cabra, J.Y. Chen, R.W. Dibble, A.N. Karpetis, R.S. Barlow, "Lifted methane-air jet flames in a vitiated coflow," pp. 491–506, Copyright 2005, with permission from Elsevier.

in the coflow demonstrated evidence of incomplete combustion, although the results did not offer any indication of whether the flames were dominated by transient processes (e.g., $z/d_{jet} = 40$ in at **Figure 3**) or if there was a bimodal distribution between burning and pure mixing states (Sepman et al., 2013).

Simultaneous planar LIF (PLIF) imaging provides increased spatial information about species distributions and may allow for direct, two-dimensional comparison of the spatial distributions and, in some cases, concentrations of intermediary and radical species (as well as the flow- and temperature-fields). Simultaneous planar imaging of OH and $CH_2O$ has been undertaken as part of numerous experimental campaigns in the JHC configurations (Medwell et al., 2007, 2008; Gordon et al., 2008, 2009; Duwig et al., 2012; Macfarlane et al., 2017, 2018; Ye et al., 2018). One such experimental configuration is represented in **Figure 4**, providing an overview of the optical layout required for simultaneous imaging of OH, $CH_2O$ and Rayleigh scattering for temperature (discussed in more detail in section 5), presented in **Figure 5**. The experimental arrangement shown in **Figure 4** includes two dye-lasers for PLIF imaging and a third Nd:YAG laser for Rayleigh scattering thermometry. The laser sheets are co-planar in the imaging region. Overlap is achieved through the use of long-wave-pass (LWP) dichroic mirrors (also referred to as dichroic beamsplitters) which transmit light with wavelengths greater than some design value, and reflect light with shorter wavelengths. Short-wave-pass (SWP) dichroic mirrors—not used in the configuration shown in **Figure 4**—transmit shorter wavelengths and reflect longer wavelengths. Dedicated ICCD cameras are used to separately image the OH-PLIF, $CH_2O$-PLIF and Rayleigh scattering signals, normal to the laser beam path (Medwell et al., 2007, 2008).

The image "triplets" presented in **Figure 5** show OH, $CH_2O$ and temperature from two separate studies. The figure shows images taken from a study of turbulent $C_2H_4$ flames in different coflows issuing into 1100 K coflows with 3% and 9% $O_2$, by volume and ignition kernel formation for a turbulent natural

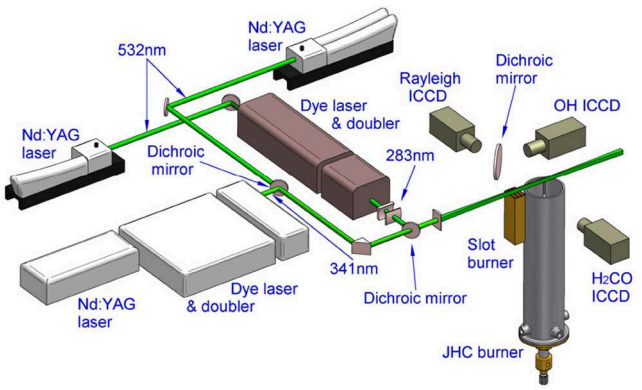


**FIGURE 4 |** Layout of a planar Rayleigh-LIF experiment, including measurements of OH- and $CH_2O$-LIF (Medwell et al., 2007). Reprinted from *Combustion and Flame*, vol. 148, P.R. Medwell, P.A.M. Kalt, B.B. Dally, "Simultaneous imaging of OH, formaldehyde, and temperature of turbulent nonpremixed jet flames in a heated and diluted coflow," pp. 48–61, Copyright 2007, with permission from Elsevier.

gas (NG)/Helium (∼53% He by volume) flame issuing into a 1475 K coflow with 11% $O_2$, by volume. Image triplets in **Figure 5** show different flame-fronts and ignition structures. These include "weak-to-strong" transition points (**Figure 5A**) labeled 9% $O_2$—$C_2H_4$, 9% $O_2$—$C_2H_4$/Air and 9% $O_2$—$C_2H_4$/$N_2$ which are further discussed in section 7), as well as lifted triple-flames and ignition kernels (**Figure 5B**). It should be noted, that although a fluorescence signal may appear to be present on the centerline in the measured OH-LIF profiles of the $C_2H_4$ flames in Medwell et al. (2008) (not reproduced here), this is due to Raman scattering from the fuel and is not indicative of OH.

Imaging of $CH_2O$ is most commonly performed using the Nd:YAG third-harmonic wavelength of 355 nm (Gordon et al., 2007, 2008; Duwig et al., 2012; Macfarlane et al., 2017, 2018; Ye et al., 2018) or—less often—near 341 nm using a frequency-doubled tunable-dye laser (Medwell et al., 2007, 2008). The latter approach targets a specific energy transition, which allows for amelioration of the effect of Boltzmann fraction on the $CH_2O$ signal (Medwell et al., 2007). Significant work has been undertaken to estimate Boltzmann corrections for excitation by 355 nm photons (Gordon et al., 2008; Macfarlane et al., 2018). The increased number of assumptions in using 355 nm for excitation is, practically, outweighed by the experimental simplicity of using a frequency-tripled Nd:YAG laser with 30–300 mJ/pulse (Macfarlane et al., 2018; Ye et al., 2018) compared to a frequency-doubled tunable-dye laser outputting ∼10 mJ/pulse (Medwell et al., 2007, 2008). In addition to this, temperature-dependent quenching corrections have been estimated for 355 nm $CH_2O$-[P]LIF based on calibration (Paul and Najm, 1998; Kyritsis et al., 2004; Gordon et al., 2008) or estimated $O_2$ and $N_2$ concentrations (Yamasaki and Tezaki, 2005; Macfarlane et al., 2018) with temperatures dependencies between $T^{-1} - T^{-0.5}$. The choice of temperature exponent is most significant in the preheat zone, and has little effect on the estimated normalized concentrations in the reaction zone, near the peak LIF signals (Kyritsis et al., 2004; Gabet and Sutton, 2014). Despite this, calculations of constant quenching cross-sections have shown only minor differences from a $T^{-0.5}$ dependence model in premixed flames (Ayoola et al., 2006).

## 5. THERMOGRAPHY IN GASEOUS, SOOT-FREE FLAMES

Temperature measurements in flames in JHC burners have been undertaken using semi-quantitative Rayleigh scattering (Dunn et al., 2007a; Medwell et al., 2007, 2008; Gordon et al., 2008; Ye et al., 2018), Rayleigh-Raman (Cabra et al., 2002, 2005; Dally et al., 2002; Dunn et al., 2009), CARS (Oldenhof et al., 2010, 2011; Correia Rodrigues et al., 2015a,b), and NTLAF (Evans et al., 2019b; Kruse et al., 2019). Of these techniques, Rayleigh-based techniques may only be used in gaseous, soot-and-droplet-free "clean" flames, in cases without significant background scattering: fluorescence or non-linear techniques are required in sooty or particle-or-droplet-laden flames.

The hot and diluted coflows of JHC flames suppress the formation of soot (Medwell et al., 2008; de Joannon et al., 2012; Ye et al., 2016, 2017; Evans et al., 2017b, 2019b). Soot may be suppressed for typically sooty fuels such as ethylene under MILD combustion conditions (Medwell et al., 2008; Evans et al., 2017b). In clean flames, thermometry may be performed using Rayleigh scattering. This method has been used to estimate temperature-fields in JHC-stabilized flames (Dunn et al., 2007a; Medwell et al., 2007, 2008; Gordon et al., 2008; Ye et al., 2018) by extracting number density from a location with a known effective Rayleigh cross-section ($\sigma_{eff}$). Local values of $\sigma_{eff}$ are a function of the local composition, and is evaluated using the species with significant mole fractions. This includes $N_2$, $O_2$, $H_2$, $H_2O$, $CO_2$, CO and all constituents of the fuel stream (Gordon et al., 2008). The calculation of the cross section may also require intermediary species such as $C_2H_2$ and $C_2H_4$ which are formed in significant concentrations during the combustion of larger hydrocarbons (Ye et al., 2015).

The determination of temperature from Rayleigh scattering measurements depends on both the accuracy of the estimated composition and scattering cross-section. As it is not feasible to measure the concentrations of all species, the composition of the flames is estimated using opposed-flow flamelet calculations in conjunction with estimations determined from Raman scattering and/or PLIF measurements. The former approach was discussed at length in section 2.4 and may probe multiple species to provide quantitative measurements after extensive calibration, although this has currently been restricted to point and line measurements only due to the high laser energies and complex optical layouts required. Spontaneous planar Raman has, however, been performed in a non-reacting $H_2/N_2$ system using a 10 kHz 532 nm laser delivering 750 mJ over a pulse duration of 70 ns at pressures ranging between atmospheric and 20 bar (Jiang et al., 2017).

Species estimates for Rayleigh thermometry may be calculated using opposed-flow flame calculations. This approach requires knowledge of the reaction zone and hence must include a simultaneous measurement of a reaction-zone-indicator, such as OH or CH. This approach is valid for line or planar images, where

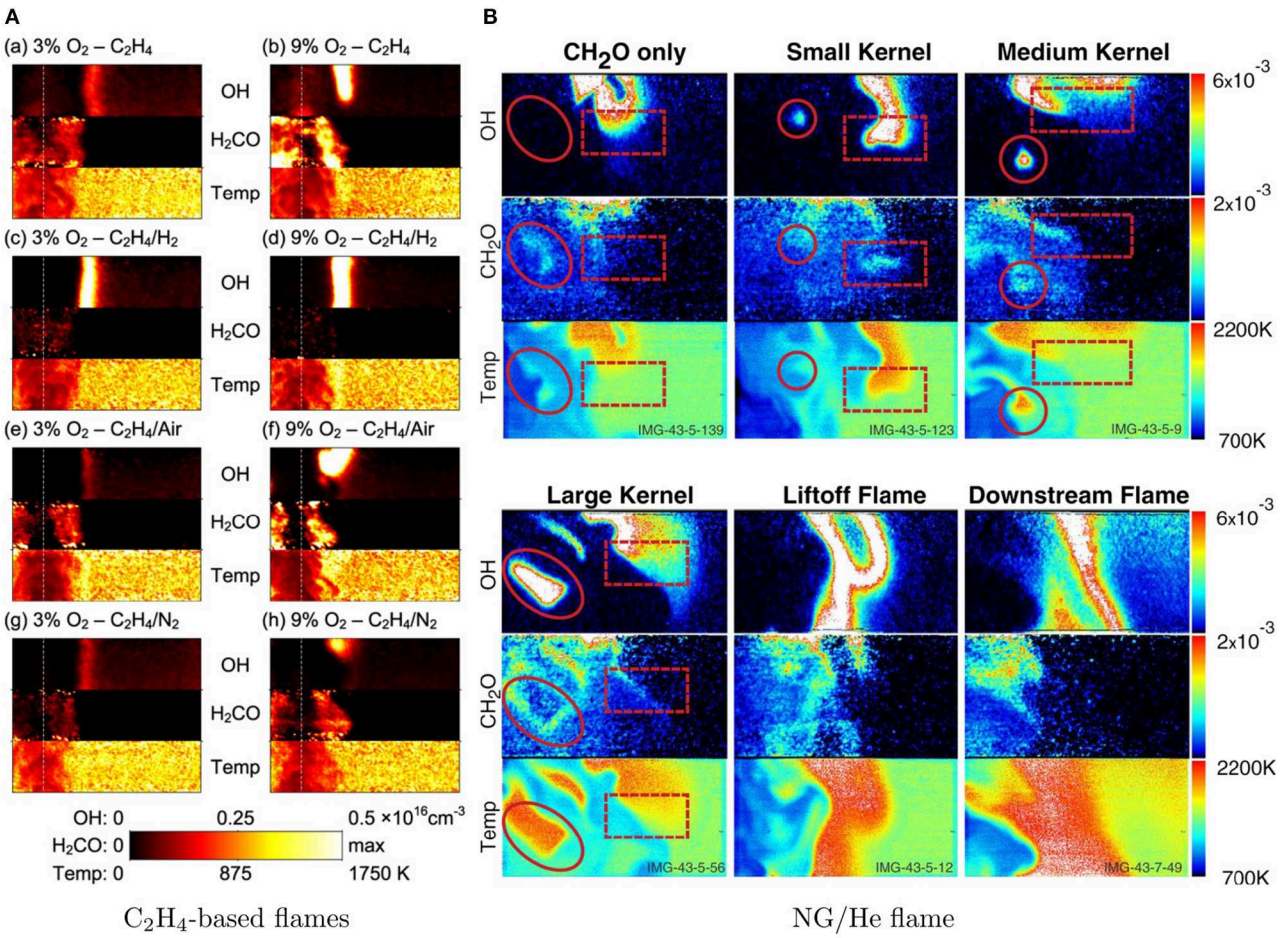


**FIGURE 5 |** Sets of OH, $CH_2O$ and temperature image "triplets" of $C_2H_4$-based (Medwell et al., 2008) and NG/He flames (Gordon et al., 2008) issuing into hot and diluted coflows. Left **(A)**: reprinted from *Combustion and Flame*, vol. 152, P.R. Medwell, P.A.M. Kalt, B.B. Dally, "Imaging of diluted turbulent ethylene flames stabilized on a Jet in Hot Coflow (JHC) burner," pp. 100–113, Copyright 2008, with permission from Elsevier. Right **(B)**: reprinted from *Combustion and Flame*, vol. 155, R.L. Gordon, A.R. Masri, E. Mastorakos, "Simultaneous Rayleigh temperature, OH- and $CH_2O$-LIF imaging of methane jets in a vitiated coflow," pp. 181–195, Copyright 2008, with permission from Elsevier.

only one reaction zone is evident. Instances with "branched" reaction zones prohibit the assignment of "fuel" and "oxidant" sides of the reaction zone, and the validity of the opposed-flow flame approximation. The reacting or mixing-only opposed-flow calculations, allow for row-by-row matching of the calculated $\sigma_{eff}$ from which an absolute temperature may be calculated. Typical uncertainties in this technique are approximately 10%, predominantly due to uncertainties in $\sigma_{eff}$ and calibration assumptions (Gordon et al., 2008).

Rayleigh scattering may be performed using precalibrated beam profiles or a reference burner. The latter serves as a beam profile, species and temperature reference, which also lends itself to semi-quantified species measurements. Furthermore, polarization filters may be incorporated into the imaging system to reduce the influence of background scatter. The use of polarization filters, however, necessitates an additional term in the scattering equation to account for depolarization along the line-of-sight between the burner. This term is called the "King correction factor" and is a result of depolarization due to non-spherical molecules. This may affect the resulting measurements by up to 5% (Dunn et al., 2009). Depolarization may also be leveraged for species measurement, however, by measuring both the polarized and depolarized components of the Rayleigh signal and has been successfully demonstrated in simple jet flames (Fielding et al., 2002; Frank et al., 2002; Schießl et al., 2009). The depolarized signal is approximately two orders of magnitude weaker than the polarized signal, although still an order of magnitude greater than spontaneous Raman scattering (Fielding et al., 2002). Although the effective signal-to-noise ratio (SNR) could further be reduced through the application of contour-aligned smoothing (Starner et al., 1995). The ratio of the two signals, with *a priori* knowledge of the depolarization of each species, subsequently allows for the estimation of the local mixture and, hence, temperature (Fielding et al., 2002; Frank et al., 2002; Schießl et al., 2009).

Simultaneous measurements of species and temperature may be performed in "clean" flames using the previously described Rayleigh-Raman technique. Although this is a very

well established technique (Masri et al., 1996; Nguyen et al., 1996; Frank and Barlow, 1998; Cabra et al., 2002; Dally et al., 2002; Barlow et al., 2005, 2015; Dunn et al., 2010; Magnotti and Barlow, 2017), it suffers from the low signal provided by spontaneous Raman scattering, which is ∼1,000 times less than the corresponding, linear Rayleigh signal (Eckbreth, 1996; Frank et al., 2002). This promotes the use of high energy lasers, although short, high power laser pulses may result in "optical breakdown" (plasma formation). This is often overcome using a combination of multiple lasers (Dunn, 2008), laser pulse-stretching, combining beam-splitters and optical delay lines to extend the effective duration of a single laser pulse by up to an order of magnitude (Dunn, 2008). This is common practice to reduce the SNR of the Raman measurements, and a similar intracavity optical layout has previously been successfully demonstrated in simple jet and bluff-body flames (Starner et al., 1995; Kelman et al., 1998; Masri et al., 1998). In addition to pulse stretching, contour-aligned smoothing has been used to improve SNR of planar measurements by an order of magnitude (Starner et al., 1995). Improved SNR in point measurements has also been demonstrated by using a ∼10 mJ/pulse, 350 ns pulse, 527 nm laser in preference to a ∼50 mJ/pulse, 10 ns pulse, 532 nm laser (Mokhov et al., 2005). Notably, this shorter wavelength serves to increase the Raman scattering signal (which approximately goes as $\lambda^{-4}$, Masri et al., 1996), although UV wavelengths may increase interference due to resulting LIF signals from species such as $CH_2O$ and PAH (Masri et al., 1996).

The instantaneous mixture fraction field provided by line and planar imaging of species may be spatially differentiated to provide estimates of scalar dissipation. Mixture fraction can be calculated directly in Rayleigh-Raman measurements, with the assumption that the measured major species are the major contributors the mixture fraction. Mixture fraction has also been parameterized using relative Raman and Rayleigh stokes signals directly, which also maps to temperature through a one-step chemical reaction (Starner et al., 1995). Irrespective of whether they use measured or predicted species concentrations, these evaluations of mixture fraction, however, all employ a simple two-stream formula for mixture fraction used in studies of $CH_4$ and $H_2$ flames with air as the only oxidant stream (Bilger et al., 1990). This does not, in general, hold in regions downstream of a JHC burner where an arbitrary fuel, hot coflow and surrounding air mix. The JHC configuration therefore requires a three-stream mixture fraction to characterize the whole flow-field (Ihme and See, 2011; Ihme et al., 2012; Evans et al., 2019c).

## 6. THERMOGRAPHY IN SOOTING AND SPRAY FLAMES

Fuel particles, droplets and soot restrict the use of spontaneous scattering thermography techniques in flames. Diagnostics for particle or droplet laden flames are therefore required to investigate the behavior of complex fuels in JHC burners. Similarly, although the coflow in JHC burners suppresses soot formation, soot has still been observed in flames fuelled by aromatic hydrocarbons such as toluene (Evans et al., 2019b; Kruse et al., 2019). The techniques which can be applied in sooting and particle or droplet laden flames may also be applicable to flames in confined chambers, although this is still restricted by optical access and the validity of underlying assumptions in the technique.

Coherent anti-Stokes Raman spectroscopy (CARS) is a non-linear thermometry technique whereby the spectrum of a given species in the flame (often $N_2$) is measured. This three-photon technique requires two crossed lasers to excite a molecule to a "virtual" energy level, with a fourth photon emitted in a predetermined direction and measured by a spectrometer (Eckbreth, 1996; Barlow, 2007). Extending this, the use of a broad linewidth "probe beam" allows for a significant portion of the emission spectrum to be measured in a single pulse. The efficacy and accuracy of this technique has been the subject of numerous reviews (Eckbreth, 1996; Kohse-Höinghaus and Jeffries, 2002; Roy et al., 2010) and, as such, the theory is not addressed in-depth here. Temperatures measured with this technique can be accurate to within 2% following the appropriate selection of pump and probe wavelengths (van Veen and Roekaerts, 2005), although may be biased in regions of high thermal gradients in systems with large measurement volumes (Roy et al., 2010). This spatial limitation may be overcome using one-dimensional line measurements achievable with lasers capable of producing broad-linewidth pulses in femtosecond-scale pulses (Roy et al., 2010).

Coherent anti-Stokes Raman spectroscopy has been used in both gaseous and droplet-laden flames stabilized in JHC burners (Oldenhof et al., 2010, 2011; Correia Rodrigues et al., 2015a,b). This diagnostic has provided instantaneous, point-wise measurements of temperature to better understand flame structure and to provide accurate validation data and boundary conditions for numerical studies. Despite the high accuracy and robustness of CARS, it is widely limited to single-point measurements, although line and planar measurements have been demonstrated (Roy et al., 2010; Bohlin and Kliewer, 2014).

Two-color laser-imaging techniques may be used to provide planar imaging of flame reaction-zones. Such techniques use the Boltzmann distribution to calculate temperature from signals of the same species excited using different wavelengths. Well-characterized species such as OH may be used for two-color LIF by exciting two known energy transitions. This may be used to measure temperatures with an accuracy of 15% for mean measurements, or 30% for single-shot (Palmer and Hanson, 1996; Richardson et al., 2016), although local accuracies of 4–7% are possible (Giezendanner-Thoben et al., 2005). Measurements are often made in the linear regime and, like other two-color techniques, inherently include the assumption that quenching is not energy level dependent. This technique is only effective, however, in regions where these species are generated and are consequently limited to the reaction unless seeded into the flame.

An alternative to probing flame radical species is to seed selected atomic species into the flame. Useful species must have appropriate energy level distributions which allow for thermal excitation of the species in flame temperatures. One such species is indium, which has an excited energy level 0.24 eV above its ground level (Medwell et al., 2009a; Borggren et al., 2017).

This corresponds to approximately 3% of the population existing in the excited level at a temperature of 800 K, making it an appropriate element for temperature measurement. Indium at concentrations ∼100 ppm may be introduced by several means: as sublimated $In(CH_3)_3$ vapor (Borggren et al., 2017), dissolved in water or ethanol as $InCl_3$ (Medwell et al., 2009a, 2014; Chan et al., 2010; Evans et al., 2019d), or introduced directly into the gas-phase as nanoparticles through ablation (Chan et al., 2012; Medwell et al., 2012; Gu et al., 2015). All three seeding methods, however, require atomic indium to be liberated from salt or nanoparticles for TLAF measurements.

Indium TLAF measurements are performed using two-line atomic fluorescence (TLAF) by optically pumping to an excited state and measuring the emitted photons. Using the diagram in **Figure 1**, this technique uses two lasers corresponding to the atomic transitions 0→2 and 1→2 in indium (Medwell et al., 2009a, 2010; Chan et al., 2010; Borggren et al., 2017) and hence have been termed as the "Stokes" and "anti-Stokes" processes (Medwell et al., 2009a). Although photons may be measured at the same wavelength as the excitation wavelength, this results in interference from Rayleigh and Mie scattering. Subsequently, the signal from exciting the ground energy level (Stokes, 0→2) is measured at the photons corresponding to the transition to the thermally excited state (2→1) and probing the thermally excited state (anti-Stokes, 1→2) is measured using the transition to the ground state (2→0). This technique only provides weak signal in the linear regime and is often extended to the non-linear regime for single-shot imaging.

Non-linear excitation regime two-line atomic fluorescence (NTLAF) thermography extends TLAF from a ratio technique, providing higher measurable signal at the cost of increased complexity. A typical NTLAF arrangement is shown in **Figure 6**, also showing simultaneous time-resolved laser-induced incandescence (TiRe-LII) and OH-PLIF (Kruse et al., 2019). This arrangement shows the two dye lasers and three cameras required to perform NTLAF measurements, and the system required to produce conditional distributions of temperature, OH-LIF signal, soot volume fraction and soot primary particle diameter and has been applied to laminar and turbulent jet flames, as well as flames stabilized in a JHC burner (Foo et al., 2017, 2018, 2019; Gu et al., 2017; Evans et al., 2019b; Kruse et al., 2019). Specifically, simultaneous measurements of sooting toluene and toluene/*n*-heptane flames in a JHC burner have shown both the formation of soot in the hot-coflow-controlled region (Evans et al., 2019b; Kruse et al., 2019) and the strong influence of the coflow $O_2$ concentration on the evolution of soot, and associated radiative heat release, downstream (Evans et al., 2019b).

The NTLAF equation and its derivation were provided by Medwell et al. (2009a). It is important to note that this technique requires the calibration of three constants and that spectral overlap is ensured by using relatively broad laser linewidths ∼0.5 $cm^{-1}$. The NTLAF technique has been shown to provide temperatures with an accuracy within 100–150 K (∼5–10% of mean values); however, are only valid where sufficient signal exists. This conditioning roughly corresponds to flame temperatures greater than 800 K (due to the small population of thermally excited indium below this temperature) and $\Phi \geq 0.8$ (below which the atomic indium is oxidized). Planar NTLAF thermography has been demonstrated in sooting and spray flames, although cannot capture the lean ignition processes which occur in flames in hot coflows (Cabra et al., 2005; Evans et al., 2016a). A further complication of the NTLAF technique is the large non-linear excitation regime between linear and saturated TLAF, which imposes the requirement of shot-to-shot measurements of laser energy profiles.

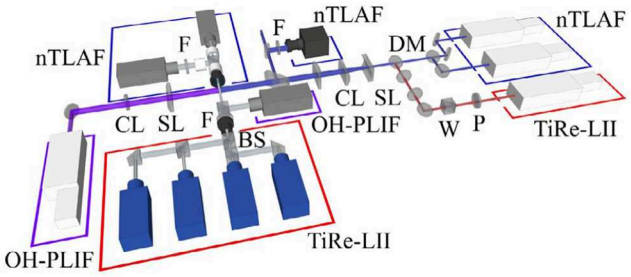


**FIGURE 6 |** Layout of a planar NTLAF and OH-PLIF experiment, also showing measurements for sooting volume fraction and size with time-resolved laser-induced incandescence (not discussed here) (Kruse et al., 2019). Bandpass filters are denoted by F, cylindrical and spherical lenses are CL and SL respectively, DM is a dichroic mirror, BS are 50/50 beam-splitters, W is a waveplate and P is a polarizer. Reprinted from *Proceedings of the Combustion Institute*, vol. 37, S. Kruse, J. Ye, Z. Sun, A. Attilli, B.B. Dally, P.R. Medwell, H. Pitsch, "Experimental investigation of soot evolution in a turbulent non-premixed prevaporized toluene flame," pp. 849–857, Copyright 2019, with permission from Elsevier.

## 7. CONTRIBUTION OF LASER DIAGNOSTICS TOWARD UNDERSTANDING FLAMES IN JHC BURNERS

### 7.1. Measurements of Temperature and Species

Qualitative and quantitative PLIF has been used to measure and visualize structures, species distributions and infer relative magnitudes of selected reaction rates in flames stabilized in JHC burners. Comparisons between single-point measurements and equilibrium calculations (recall **Figure 3**) provide indications of the flame progress at different downstream locations (Dally et al., 2002; Cabra et al., 2005). With the addition of simultaneous multi-species (and hence mixture fraction) point data provided by Rayleigh-Raman measurements, LIF of radical species has been used to identify ignition at most-reactive mixture fractions and flame evolution in mixture fraction-space (Cabra et al., 2005; Mastorakos, 2009). This can be seen in the experimental data shown in **Figure 3**, where elevated temperatures and non-zero OH concentrations begin to appear in the leanest mixtures before extending to richer regions of the flame (Cabra et al., 2005). This conclusion has been further supported by direct numerical simulations (DNS) and transient flamelet modeling (Mastorakos, 2009). This technique has not, however, been performed under

MILD combustion conditions in flames which appear visibly lifted or exhibit a "weak-to-strong transition" in a continuous flame-front (Medwell et al., 2008, 2016; Medwell and Dally, 2012a; Evans et al., 2016b; Ye et al., 2017).

The Rayleigh-Raman diagnostic technique has been extended to one-dimensional data measurements, and extensive measurements of piloted jet flames have been performed to quantify scalar dissipation, length scales and flame-sheet orientation (Karpetis and Barlow, 2002; Barlow et al., 2005; Magnotti and Barlow, 2017), these have not been performed on flames in hot and diluted coflows. This is despite strong coupling between the burning state and heat release profiles of such flames to scalar dissipation rate (Oberlack et al., 2000; Özdemir and Peters, 2001; Ihme et al., 2012; Evans et al., 2016b; Ye et al., 2016, 2017).

Planar imaging of radical species and intermediary species provides instantaneous of images in, and near, the flame-front. The imaging of specific species in the flame can be used as a surrogate for the reaction-zone, such as OH or CH, or to identify fuel decomposition using species such as $CH_2O$. Aromatic hydrocarbons, such as toluene or polycyclic aromatic hydrocarbons (PAH) may also be targeted in PLIF studies as soot precursors (Sirignano et al., 2017), but often provide interference due to their broad, molecular-size-dependent absorption and emission spectra (Sirignano et al., 2017). This interference is particularly evident with high pulse powers ($\sim$10 mJ/pulse over $\sim$10 ns), such as 355 nm beams used for imaging $CH_2O$ (Gordon et al., 2009; Ye et al., 2018). Despite this, PAH—and consequently soot—formation is suppressed with hot and diluted oxidants, reducing the potential for interference (Medwell et al., 2008; de Joannon et al., 2012; Evans et al., 2017b; Ye et al., 2017). Interference from Raman scattering can also be evident depending on the combination of LIF species and fuel-structure, and was used to explain the on-axis signal in OH-PLIF measurements of $C_2H_4$ flames in a JHC burner (Medwell et al., 2008).

## 7.2. Reaction-Zone Imaging in Understanding Flame Stabilization

Images of the OH radical may be interpreted as representing the lean side of the reaction-zone. Consequently, OH-PLIF can provide indications of flame stabilization mechanisms, such as the formation and growth of isolated ignition kernels (Gordon et al., 2008; Oldenhof et al., 2011), triple flame bases (Gordon et al., 2008) or a "weak-to-strong transition" in a continuous flame-front (Medwell et al., 2008, 2016; Medwell and Dally, 2012a; Evans et al., 2016b; Ye et al., 2017), which may each be seen in **Figure 5**. The occurrence of these structures is largely dependent on the combination of fuel/oxidant composition and temperatures (Medwell et al., 2008, 2016; Medwell and Dally, 2012a; Evans et al., 2016a,b), which dictates both the stoichiometric and most-reactive mixture fractions, and the underlying flow-field, which governs the local strain-field between the fuel and oxidant streams (Ye et al., 2016). Of these mechanisms, ignition kernel formation and autoignitive triple flames have been examined at significant length, and a full discussion is not provided here (Gordon et al., 2008; Mastorakos, 2009; Yoo et al., 2011; Arndt et al., 2012, 2019; Sidey and Mastorakos, 2015; Macfarlane et al., 2017, 2018, 2019; Ramachandran et al., 2019). Observations from OH-PLIF (Medwell et al., 2008), and resulting numerical studies (Medwell et al., 2009b; Evans et al., 2016b, 2017a,b) suggest that the least studied of these mechanisms—the "weak-to-strong transition"—anchors as a weakly reacting diffusion flame close to the jet exit, in $\Phi \approx 0.2$ (Evans et al., 2016a) under temperature and flow-field conditions almost identical to the laminar coflow stream. These weak diffusion flames allow for the diffusion of $O_2$ in the fuel stream (in a process which has been termed, "reaction-zone weakening" Medwell et al., 2009b) and provide enhanced formation of precursors, such as $CH_2O$ (Medwell et al., 2009b; Medwell and Dally, 2012b), before a critical "transition point" where thermal run-away occurs (Medwell et al., 2008; Evans et al., 2016b). It has been hypothesized that these weak reaction zones are confined between the extinction strain-rate on the fuel-side, and the lean flammability-limit on the oxidant-side (Evans et al., 2016b). This hypothesis has been supported by Reynolds-averaged Navier-Stokes (RANS) modeling (Evans et al., 2017a), although there has not been any experimental confirmation of this through quantitative mixture fraction measurements.

It has been shown that flame stabilization under MILD combustion conditions is highly sensitive to the radical pool in the hot oxidant stream (Medwell et al., 2013, 2016; Evans et al., 2017b; Doan and Swaminathan, 2019). These radical and intermediary species significantly reduce ignition delay times in low oxygen conditions (Medwell et al., 2013, 2016; Evans et al., 2017b; Doan and Swaminathan, 2019), but have less of an effect in conventional autoignition processes with $\gtrsim$6% $O_2$ (by vol.) (Medwell et al., 2016; Evans et al., 2017b). Measurable radical species such as OH have been reported in hot coflows with $\lesssim$9% $O_2$, with concentrations of equilibrium OH in the coflow increasing with dilution level (Medwell et al., 2007, 2008). Coflow OH concentrations may, however, be up to an order of magnitude less than OH in the flame reaction zone, particularly with the addition of $H_2$ to the central fuel jet (Medwell et al., 2007, 2008; Evans et al., 2015b). Subsequently, coflow OH concentrations are not often visible in images used in the description of flame stabilization, such as **Figure 7** (Evans et al., 2015b).

## 7.3. Effects of Coflow Composition on Flame Lift-Off and Structure

The combination of reaction-zone weakening and weak-to-strong transition points results in the appearance of a non-monotonic trend in lift-off height with changing oxidant dilution (Medwell and Dally, 2012a), as shown in **Figure 7**. This figure shows an ensemble of OH-PLIF images from $C_2H_4$ flames issuing into 1250-K coflows with $O_2$ concentrations of 3–11% (by volume) (Evans et al., 2015b). The scale is kept constant in all images and the figures are normalized by the instantaneous beam-profile (Evans et al., 2015b). The figure shows that the transition/lift-off height decreases with increasing coflow $O_2$ concentrations between 6–11% (**Figures 7J,O,P**), although a distinguishable OH front exists in the coflow with 3% $O_2$

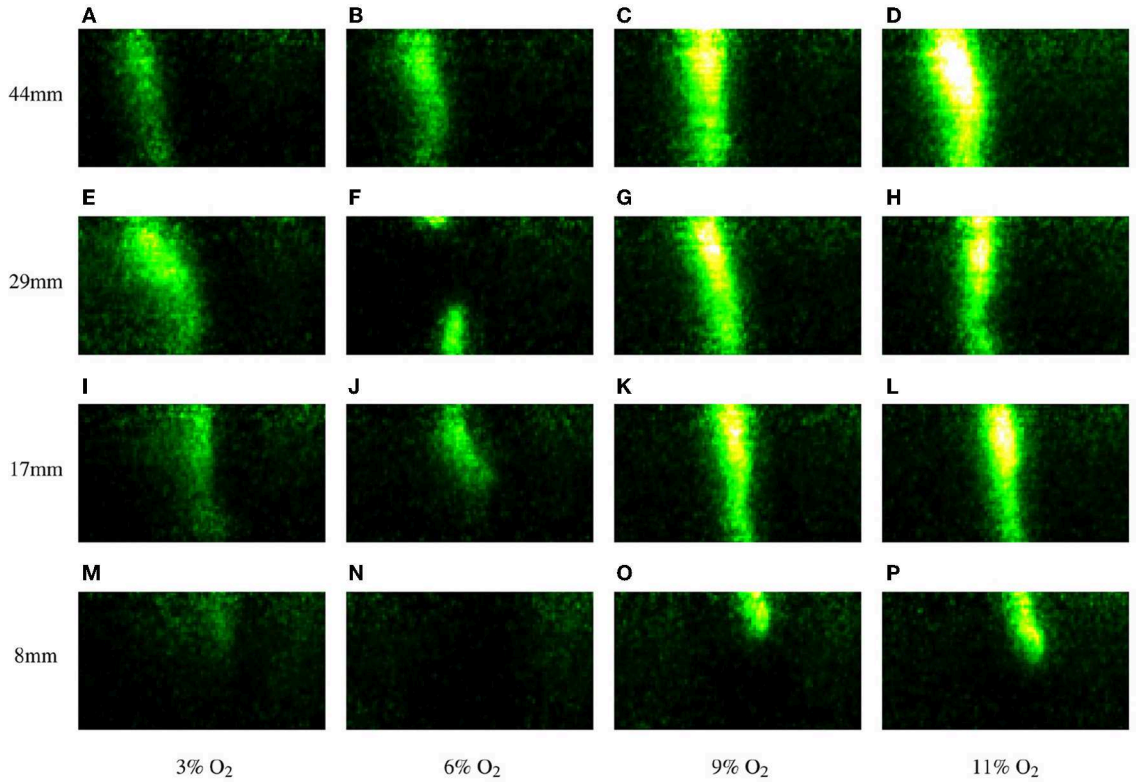


**FIGURE 7 |** Instantaneous OH-PLIF images of ethylene jet flames centered at different heights above the jet exit plane in 1250 K coflows with different $O_2$ concentrations (given in % volume) and labeled **(A–P)** for discussion. The right-hand edges of the images correspond to the fuel jet centerline (Evans et al., 2015b).

(**Figure 7M**) at a similar height to that in the 9% $O_2$ coflow. An absence of isolated ignition kernels was reported in this study (Evans et al., 2015b). These observations are consistent with similar studies of $C_2H_4$ (Medwell et al., 2008) and *n*-heptane (Ye et al., 2017) in JHC burners. This unbroken weak-to-strong transition is, however, in contrast to the isolated autoignition kernels seen in experimental investigations of $CH_4$/NG (Gordon et al., 2008, 2009; Oldenhof et al., 2010, 2011) and $C_2H_4$ (Yoo et al., 2011; Luo et al., 2012) flames in hotter coflows (1395–1550 K) with 7.6–23% $O_2$ (by mass). It is important to note that kernel formation in cases with less than 14% $O_2$ (by volume) initializes 60–80 mm above the jet exit plane (Oldenhof et al., 2010, 2011) and may be subject to entrainment of quiescent air (Evans et al., 2019b). Despite this potential influence of the surrounding air, this phenomenon has also been observed in subsequent chemiluminescence imaging of $CH_4$ flames in confined coflows with 6.9% $O_2$ (by volume) and coflows of 1170–1475 K (Ramachandran et al., 2019), where ignition kernels were more significantly prevalent for fuel jets with Re $<$ 10k, than for faster jets. The burner used in this study, however, used a thick-walled central jet with an I.D. of 5.3 mm and O.D. of 9.5 mm (Ramachandran et al., 2019), which is significantly greater than the 0.2 mm (Oldenhof et al., 2011), 0.6 mm (Evans et al., 2019b; Kruse et al., 2019) or 0.9 mm (Cabra et al., 2002, 2005; Medwell et al., 2007, 2008, 2009b; Evans et al., 2015b; Ye et al., 2017) used in other experimental studies or continuous boundary conditions used in DNS investigations (Yoo et al., 2011; Luo et al., 2012). The differences between the observed stabilization mechanisms of jet flames with similar Reynolds number, in coflows with similar temperature and oxygen concentration but significantly different jet wall thickness (Medwell and Dally, 2012a; Ramachandran et al., 2019) demonstrates the influence of the flow-field on flame stabilization mechanisms, and differences which must be considered before directly comparing results.

Planar images of the OH radical in flames stabilized in hot coflows can be used to provide insight into the flame-front (Medwell et al., 2007, 2008; Gordon et al., 2008, 2009; Ye et al., 2016, 2017, 2018; Macfarlane et al., 2017, 2018, 2019) and, in combination with simultaneous PIV, its interaction with the underlying flow-field (Lyons et al., 2005; Oldenhof et al., 2011; Oldenhof et al., 2012). This latter approach is not available simultaneously with Rayleigh scattering measurements of temperature, due to the overwhelming Mie scattering signal from PIV seed particles. Images of OH-PLIF indicate the continuity of the flame-front, and may be used to identify "holes" or "ruptures" in the flame (Lyons et al., 2005). An example of this may be seen in **Figure 7F**. It was reported that only this case at this height exhibited any "holes" and that discontinuities were present in 35% of images (Evans et al., 2015b). No discontinuities were observed in the other cases at any of the

different measurement heights (Evans et al., 2015b). Although these holes may be indicative of local extinction, such features must be interpreted with caution, as they may be indicative of several different mechanisms (Watson et al., 2000; Watson et al., 2002; Lyons et al., 2005). Further information about the local mixture fraction or flow-field would, however, be required to draw definitive conclusions.

## 7.4. Further Analyses of Transitional Flames and Ignition Processes

Flame stabilization of lifted and "transitional" turbulent flames in JHC burners has been studied experimentally using laser-based diagnostics (Medwell et al., 2007, 2008; Gordon et al., 2008; Ye et al., 2016, 2017, 2018), photographs and chemiluminescence imaging (Medwell and Dally, 2012a; Evans et al., 2016b, 2017b; Ramachandran et al., 2019), analytical analyses (Evans et al., 2016b), and numerical modeling (Shabanian et al., 2013; Evans et al., 2015a, 2017a; Medwell et al., 2016). The culmination of these studies have revealed the strong influence of the oxidant radical pool (Medwell and Dally, 2012a; Evans et al., 2017b) and the effects of the underlying flow-field (Evans et al., 2016b; Ye et al., 2016) on flames in hot coflows with $\lesssim$6% $O_2$.

Analytical analyses of $CH_4$, $C_2H_4$, and $CH_4/H_2$ diffusion flames in these coflows have suggested that MILD combustion may be reasonably approximated by a monotonic flamelet, with ignition or extinction points (Evans et al., 2016b). It is imperative to note that this analogy was proposed as a phenomenological description of the global process, rather than as a substitute for high-accuracy measurements or detailed chemical analyses (Evans et al., 2016b). The same study proposed that the weak-to-strong transition may be indicative of a weak diffusion flame preceding a "conventional ignition" point (Evans et al., 2016b), as was shown in **Figure 5A**). Numerical modeling of transitional flames has been met with varied success (Shabanian et al., 2013; Evans et al., 2015a). Although experimentally observed weak-to-strong transitions have been reproduced in RANS modeling (Evans et al., 2015a), this modeling study required significant adjustment of model parameters to replicate experimental results. This "parameter-tuning" was required due to the low turbulence Reynolds number of the jet flame (De et al., 2011; Parente et al., 2016), Damköhler number of order unity (Galletti et al., 2007; Mardani et al., 2011) and strong preferential diffusion effects (Medwell et al., 2009b). The combination of these effects has additionally, in the authors' experience, resulted in significant sensitivity to inlet conditions and subgrid models in large-eddy simulations (LES) with flamelet tabulation. Although, partially-stirred reactor and transported PDF models have demonstrated good agreement (Li et al., 2019; Wang et al., 2019a). The modeling challenges posed by this configuration highlight the need for more experimental insight and validation data for the generation of comprehensive turbulence-chemistry interaction models. Laser-based measurements are thus essential in this configuration, with this dataset still beyond replication by DNS due to the substantial computational resources required and the subsequent need for simplifications in geometry, chemistry, inlet conditions and/or species transport.

## 7.5. Heat Release Rate Imaging

Analyses of simultaneous PLIF images can provide insight into the structure of flames, such as the effect of weakening reaction zones (Medwell et al., 2009b) or estimations of normalized heat release rate (Paul and Najm, 1998; Gordon et al., 2009). Distributions of heat release rate are based on the assumption that the formation of HCO from OH and $CH_2O$ is the dominant exothermic reaction in the flame (Paul and Najm, 1998; Gordon et al., 2009). It follows that the overlap between OH and $CH_2O$ distributions (or $n_{OH} \times n_{CH_2O}$) may be used to provide an estimation of the relative, local heat release rate. In practice, this analysis further assumes that the true concentration of $CH_2O$ scales linearly with the normalized $CH_2O$ after quenching and Boltzmann fraction approximations described previously. This analysis was initially performed in $CH_4$/NG flames (Paul and Najm, 1998; Gordon et al., 2009), and has been supported by numerical simulations (Gordon et al., 2009; Sidey et al., 2016). The interpretation of $n_{OH} \times n_{CH_2O}$ being representative of heat release rate has also been used in the analysis of dimethyl ether (DME) (Macfarlane et al., 2017, 2018), which is shown with chemiluminescence imaging in **Figure 8**. Although both OH and $CH_2O$ are routinely imaged using PLIF, their overlap may not always provide a suitable combination for estimating heat release rate, particularly in the MILD combustion regime (Sidey and Mastorakos, 2016). This has been confirmed numerically for flames with *n*-heptane (Ye et al., 2017), as well as both $C_2H_4$ and 1:1 $CH_4/H_2$ (by volume), with the product of OH and $HO_2$ proposed as a heat release rate marker for the latter two fuels (Evans et al., 2017b).

## 7.6. Current Directions

Laser-based studies of gaseous fuelled-flames in the JHC configuration have included hydrogen, methane, ethylene, propane, acetone, ethanol and its isomer dimethyl-ether, n-heptane, toluene, octan-1-ol and its isomer di-*n*-butyl-ether and larger hydrocarbons (Cabra et al., 2002, 2005; Dally et al., 2002; Medwell et al., 2007, 2008, 2009b; Oldenhof et al., 2010, 2011; Arndt et al., 2012, 2013, 2016; Medwell and Dally, 2012a; Papageorge et al., 2014; Walters, 2016; Ye et al., 2016, 2017, 2018; Evans et al., 2017b; Kruse et al., 2019), whilst only methanol (Wang et al., 2019b), and ethanol (Correia Rodrigues et al., 2015a,b) have been investigated in liquid spray flames due to the added complexity of diagnostics in two-phase flows. It is also noteworthy that there has been little research of either gaseous or spray flames at elevated pressures (Evans et al., 2019a), although it has been noted that there are both very few high quality datasets under these conditions, and a particular need for measurements pertaining to soot formation in liquid spray flames (Hochgreb, 2019). This is due to the technical challenges involved in the development of both appropriate facilities and diagnostic tools.

Laser diagnostics have proven to be a valuable tool in understanding flames in JHC burners. Laser diagnostics have identified phenomena which have not yet been replicated by numerical modeling which promotes the need for further, high quality measurements in canonical and poorly understood configurations.

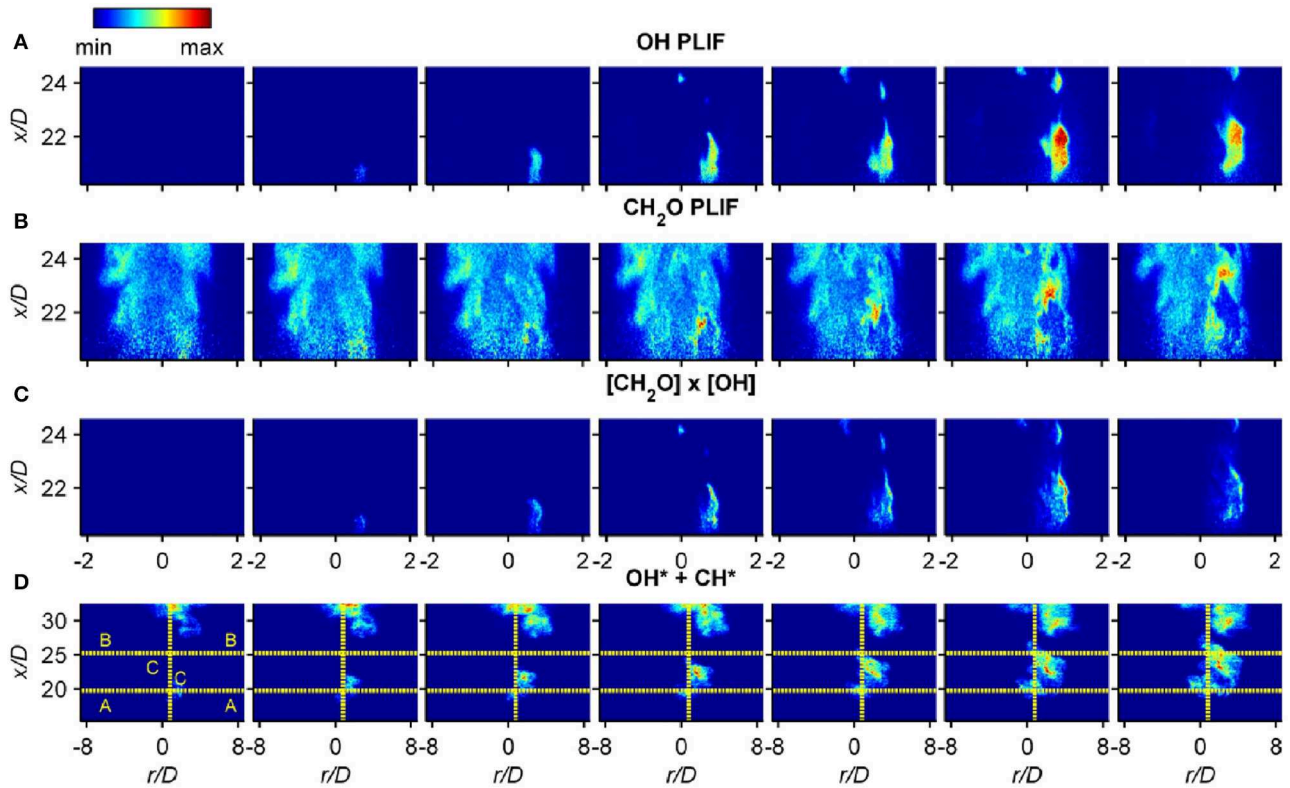


**FIGURE 8 |** Images of **(A)** OH-PLIF, **(B)** $CH_2O$-PLIF, **(C)** the overlap of $CH_2O$-PLIF and OH-PLIF (used as a heat release rate surrogate) and **(D)** the sum of CH* and OH* chemiluminescence (Macfarlane et al., 2017). Reprinted from *Proceedings of the Combustion Institute*, vol. 36, A.R.W. Macfarlane, M.J. Dunn, M. Juddoo, A.R. Masri, "Stabilization of turbulent auto-igniting dimethyl ether jet flames issuing into a hot vitiated coflow," pp. 1661–1668, Copyright 2017, with permission from Elsevier.

## 8. ONGOING AND FUTURE CHALLENGES

Optical diagnostics of flames in JHC burners have revealed a wealth of information about the ignition and structure of flames in hot and diluted environments. There are, however, ongoing challenges particularly for measurements in confined burners. These include:

- Measurements of mixture fraction have not been undertaken in transitional flames stabilized in JHC burners, despite such data having been taken in similar MILD (Dally et al., 2002) and autoignitive (Cabra et al., 2002, 2005; Dunn et al., 2009; Dunn et al., 2010) flames. Quantitative Rayleigh-Raman or polarized/depolarized Rayleigh scattering (Fielding et al., 2002; Frank et al., 2002; Schießl et al., 2009) measurements extending from the jet exit plane of a JHC burner to beyond the weak-to-strong transition would provide further insight into the ignition processes in MILD combustion and transitional flames and the downstream evolution of the reaction zone.
- Planar imaging of scalar dissipation has been performed in a variety of lifted and partially premixed flames using Rayleigh-Raman (Masri et al., 1996; Barlow et al., 2005) and polarized/depolarized Rayleigh scattering (Fielding et al., 2002; Frank et al., 2002; Schießl et al., 2009). Although gradients of temperature have been imaged in partially premixed flames stabilized on JHC burners (Dunn et al., 2007b; Gordon et al., 2009), semi-quantified or normalized measurements of scalar dissipation in non-premixed flames stabilized in hot and diluted coflows with $O_2$ concentrations $\leq$6% would provide insight into the structure of the reaction zone in MILD combustion conditions and the non-monotonic trends in flame stabilization evident from OH-PLIF.
- Practical implementation of MILD combustion in inter-turbine burners (ITBs) requires an improved understanding and modeling capability of turbulence-chemistry interactions at elevated pressures. These both require high quality, quantified experimental data. The acquisition of these data presents a number of challenges, not least the requirement of optical diagnostics suitable for confined, high-pressure JHC burners. Flames in such pressurized burners are implicitly confined—increasing background scatter and beam-steering effects—and are more susceptible to PAH and soot formation and soot growth (Karataş and Ömer L. Gülder, 2012), which may limit the efficacy and validity of simultaneous quantitative diagnostics. Additional quantification challenges in these conditions include the evaluation of quenching of different fluorescent and seeded species at elevated pressures and the need to resolve smaller Kolmogorov length-scales resulting from increased gas densities.

- The vast majority of studies performed in JHC burners have focussed on gaseous fuels. This is despite most transport fuels being carried and injected in the liquids phase. Although several studies of complex prevaporized liquid fuels have been undertaken in coflows with 3–9% $O_2$ (by vol.), only simple liquid spray flames have been the focus of laser-based diagnostic studies. Extension of laser-based studies to liquid, and additionally solid, fuels using techniques established for sooting (Chan Q. et al., 2011; Chan Q. N. et al., 2011) and swirling (Evans et al., 2019d) or piloted spray (Medwell et al., 2013) flames.
- Rayleigh scattering has been central to the success of optical diagnostics of flames stabilized in JHC burners. This is currently the only diagnostic approach which can provide planar measurements of temperature without limitations of selected species formation or the requirement of particle seeding. Without modification this technique cannot be applied to confined or particle or droplet laden flames. Two modifications to the Rayleigh scattering technique include filtered Rayleigh scattering (Hofmann and Leipert, 1996; Kearney et al., 2005) and the use of structured laser illumination planar imaging (SLIPI) (Aldén et al., 2011; Kempema and Long, 2014; Kristensson et al., 2015) which offer the potential solutions to the removal of Mie and unstructured background scattering, respectively. These or other techniques to measure the temperature field—such as the extension of CARS to line and planar measurements or combinations of two-color diagnostics suitable to low temperatures and a broad range of mixture fractions—will facilitate the collection of quantitative experimental data for absolute measurements and the further development of conditional statistics.
- Many current numerical combustion models cannot reliably predict the structure of flames stabilized in JHC burners without tuning of turbulence-chemistry interaction model constants or physical parameters (De et al., 2011; Evans et al., 2015a, 2019c; Parente et al., 2016; Ferrarotti et al., 2019), although recent LES have (Li et al., 2019) demonstrated less sensitivity than has been observed in equivalent RANS models (Wang et al., 2019a). Furthermore, these models are often calibrated using one or more of a limited set of high quality Rayleigh-Raman-LIF (Dally et al., 2002; Cabra et al., 2005), CARS-LIF-LDA (Oldenhof et al., 2010, 2011), or Rayleigh-LIF (Medwell et al., 2008) data. Although these measurements have all targeted flames in JHC burners, they do not form a consistent dataset. This reinforces the ongoing need for high quality measurements in validation configurations, with an emphasis on the systematic variation of boundary conditions, to provide individual cases and trends which challenge current numerical modeling approaches.

## 9. CONCLUSIONS

The interactions between light and matter form the basis of laser diagnostics in flames. This review provides fundamental background and guidance to aid in the interpretation of laser-based measurements, whilst highlighting findings from experimental studies of flames in jet in hot coflow burners. This review has discussed the importance of laser-induced fluorescence, velocimetry, Rayleigh and Raman scattering measurements in studies of JHC burners, and highlighted potential techniques needed to meet future challenges in diagnostics.

The findings presented in this review reinforce the advantages of, and ongoing need for, laser-based diagnostics of flames to fill knowledge gaps which cannot be addressed by modeling or theory alone. Laser-based diagnostics have been used to identify different flame stabilization mechanisms in JHC burners, including ignition kernels and weak-to-strong transitions. These measurements have been supplemented with numerical analyses, however measurements of instantaneous mixture fraction, strain-rate and scalar dissipation would still be required to answer outstanding questions about flame structure and discontinuities in the flame sheet under a narrow range of conditions.

There is still a need to better understand flame stabilization and structure in JHC burners in environments better representing practical systems. The challenges these environments present to current modeling approaches and the lack of appropriate validation data cements the importance of laser-based measurements, and the ongoing need to continue to develop the capabilities of laser diagnostics.

## AUTHOR CONTRIBUTIONS

Both authors jointly drafted the outline of the work and discussed the content and contribution. ME produced the initial draft and revisions (scientific, grammatical, and stylistic) were made by both authors.

## FUNDING

Financial salary support provided to ME by the Australian Research Council through the Discovery Projects Programme.

## ACKNOWLEDGMENTS

The authors thank Prof. Bassam Dally and Dr. Alfonso Chinnici of the University of Adelaide for their helpful discussions. The authors also acknowledge support from The University of Adelaide and financial support from the Australian Research Council.

## REFERENCES

Aldén, M., Bood, J., Li, Z., and Richter, M. (2011). Visualization and understanding of combustion processes using spatially and temporally resolved laser diagnostic techniques. *Proc. Combust. Inst.* 33, 69–97. doi: 10.1016/j.proci.2010.09.004

Arndt, C., Gounder, J., Meier, W., and Aigner, M. (2012). Auto-ignition and flame stabilization of pulsed methane jets in a hot vitiated coflow studied with high-speed laser and imaging techniques. *Appl. Phys. B* 108, 407–417. doi: 10.1007/s00340-012-4945-5

Arndt, C. M., Papageorge, M. J., Fuest, F., Sutton, J. A., and Meier, W. (2019). Experimental investigation of the auto-ignition of a

transient propane jet-in-hot-coflow. *Proc. Combust. Inst.* 37, 2117–2124. doi: 10.1016/j.proci.2018.06.195

Arndt, C. M., Papageorge, M. J., Fuest, F., Sutton, J. A., Meier, W., and Aigner, M. (2016). The role of temperature, mixture fraction, and scalar dissipation rate on transient methane injection and auto-ignition in a jet in hot coflow burner. *Combust. Flame* 167, 60–71. doi: 10.1016/j.combustflame.2016.02.027

Arndt, C. M., Schießl, R., Gounder, J. D., Meier, W., and Aigner, M. (2013). Flame stabilization and auto-ignition of pulsed methane jets in a hot coflow: influence of temperature. *Proc. Combust. Inst.* 34, 1483–1490. doi: 10.1016/j.proci.2012.05.082

Ayoola, B., Balachandran, R., Frank, J., Mastorakos, E., and Kaminski, C. (2006). Spatially resolved heat release rate measurements in turbulent premixed flames. *Combust. Flame* 144, 1–16. doi: 10.1016/j.combustflame.2005.06.005

Barlow, R., Fiechtner, G., Carter, C., and Chen, J.-Y. (2000). Experiments on the scalar structure of turbulent $CO/H_2/N_2$ jet flames. *Combust. Flame* 120, 549–569. doi: 10.1016/S0010-2180(99)00126-1

Barlow, R., Frank, J., Karpetis, A., and Chen, J.-Y. (2005). Piloted methane/air jet flames: transport effects and aspects of scalar structure. *Combust. Flame* 143, 433–449. doi: 10.1016/j.combustflame.2005.08.017

Barlow, R., Meares, S., Magnotti, G., Cutcher, H., and Masri, A. (2015). Local extinction and near-field structure in piloted turbulent $CH_4$/air jet flames with inhomogeneous inlets. *Combust. Flame* 162, 3516–3540. doi: 10.1016/j.combustflame.2015.06.009

Barlow, R. S. (2007). Laser diagnostics and their interplay with computations to understand turbulent combustion. *Proc. Combust. Inst.* 31, 49–75. doi: 10.1016/j.proci.2006.08.122

Barlow, R. S., Dunn, M. J., Sweeney, M. S., and Hochgreb, S. (2012). Effects of preferential transport in turbulent bluff-body-stabilized lean premixed $CH_4$/air flames. *Combust. Flame* 159, 2563–2575. doi: 10.1016/j.combustflame.2011.11.013

Bartos, D., Dunn, M., Sirignano, M., D'Anna, A., and Masri, A. R. (2017). Tracking the evolution of soot particles and precursors in turbulent flames using laser-induced emission. *Proc. Combust. Inst.* 36, 1869–1876. doi: 10.1016/j.proci.2016.07.092

Bilger, R., Stårner, S., and Kee, R. (1990). On reduced mechanisms for methane · air combustion in nonpremixed flames. *Combust. Flame* 80, 135–149. doi: 10.1016/0010-2180(90)90122-8

Bohlin, A., and Kliewer, C. J. (2014). Diagnostic imaging in flames with instantaneous planar coherent Raman spectroscopy. *J. Phys. Chem. Lett.* 5, 1243–1248. doi: 10.1021/jz500384y

Borggren, J., Weng, W., Hosseinnia, A., Bengtsson, P.-E., Aldén, M., and Li, Z. (2017). Diode laser-based thermometry using two-line atomic fluorescence of indium and gallium. *Appl. Phys. B* 123:278. doi: 10.1007/s00340-017-6855-z

Cabra, R., Chen, J.-Y., Dibble, R., Karpetis, A., and Barlow, R. (2005). Lifted methane-air jet flames in a vitiated coflow. *Combust. Flame* 143, 491–506. doi: 10.1016/j.combustflame.2005.08.019

Cabra, R., Myhrvold, T., Chen, J., Dibble, R., Karpetis, A., and Barlow, R. (2002). Simultaneous laser Raman-Rayleigh-LIF measurements and numerical modeling results of a lifted turbulent $H_2/N_2$ jet flame in a vitiated coflow. *Proc. Combust. Inst.* 29, 1881–1888. doi: 10.1016/S1540-7489(02)80228-0

Carter, C. D., and Barlow, R. S. (1994). Simultaneous measurements of NO, OH, and the major species in turbulent flames. *Opt. Lett.* 19, 299–301. doi: 10.1364/OL.19.000299

Cavaliere, A., and de Joannon, M. (2004). Mild combustion. *Prog. Energ. Combust.* 30, 329–366. doi: 10.1016/j.pecs.2004.02.003

Cavaliere, D. E., Kariuki, J., and Mastorakos, E. (2013). A comparison of the blow-off behaviour of swirl-stabilized premixed, non-premixed and spray flames. *Flow Turbul. Combust.* 91, 347–372. doi: 10.1007/s10494-013-9470-z

Chan, Q., Medwell, P., Alwahabi, Z., Dally, B., and Nathan, G. (2011). Assessment of interferences to nonlinear two-line atomic fluorescence (NTLAF) in sooty flames. *Appl. Phys. B* 104, 189–198. doi: 10.1007/s00340-011-4497-0

Chan, Q. N., Medwell, P. R., Dally, B. B., Alwahabi, Z. T., and Nathan, G. J. (2012). New seeding methodology for gas concentration measurements. *Appl. Spectrosc.* 66, 803–809. doi: 10.1366/11-06553

Chan, Q. N., Medwell, P. R., Kalt, P. A., Alwahabi, Z. T., Dally, B. B., and Nathan, G. J. (2011). Simultaneous imaging of temperature and soot volume fraction. *Proc. Combust. Inst.* 33, 791–798. doi: 10.1016/j.proci.2010.06.031

Chan, Q. N., Medwell, P. R., Kalt, P. A. M., Alwahabi, Z. T., Dally, B. B., and Nathan, G. J. (2010). Solvent effects on two-line atomic fluorescence of indium. *Appl. Opt.* 49, 1257–1266. doi: 10.1364/AO.49.001257

Correia Rodrigues, H., Tummers, M., van Veen, E., and Roekaerts, D. (2015a). Effects of coflow temperature and composition on ethanol spray flames in hot-diluted coflow. *Int. J. Heat Fluid Flow* 51, 309–323. doi: 10.1016/j.ijheatfluidflow.2014.10.006

Correia Rodrigues, H., Tummers, M. J., van Veen, E. H., and Roekaerts, D. J. (2015b). Spray flame structure in conventional and hot-diluted combustion regime. *Combust. Flame* 162, 759–773. doi: 10.1016/j.combustflame.2014.07.033

Dally, B., Karpetis, A., and Barlow, R. (2002). Structure of turbulent non-premixed jet flames in a diluted hot coflow. *Proc. Combust. Inst.* 29, 1147–1154. doi: 10.1016/S1540-7489(02)80145-6

Dally, B., Riesmeier, E., and Peters, N. (2004). Effect of fuel mixture on moderate and intense low oxygen dilution combustion. *Combust. Flame* 137, 418–431. doi: 10.1016/j.combustflame.2004.02.011

de Joannon, M., Sabia, P., Cozzolino, G., Sorrentino, G., and Cavaliere, A. (2012). Pyrolitic and oxidative structures in hot oxidant diluted oxidant (HODO) MILD combustion. *Combust. Sci. Technol.* 184, 1207–1218. doi: 10.1080/00102202.2012.664012

De, A., Oldenhof, E., Sathiah, P., and Roekaerts, D. (2011). Numerical simulation of delft-jet-in-hot-coflow (DJHC) flames using the eddy dissipation concept model for turbulence-chemistry interaction. *Flow Turbul. Combust.* 87, 537–567. doi: 10.1007/s10494-011-9337-0

Doan, N., and Swaminathan, N. (2019). Role of radicals on MILD combustion inception. *Proc. Comb. Inst.* 37, 4539–4546. doi: 10.1016/j.proci.2018.07.038

Döbbeling, K., Hellat, J., and Koch, H. (2007). 25 years of BBC/ABB/Alstom lean premix combustion technologies. *J. Eng. Gas Turb. Power* 1, 2–12. doi: 10.1115/1.2181183

Dunn, M., and Masri, A. (2010). A comprehensive model for the quantification of linear and nonlinear regime laser-induced fluorescence of OH under $A^2\Sigma^+ \leftarrow X^2\Pi$ (1, 0) excitation. *Appl. Phys. B* 101, 445–463. doi: 10.1007/s00340-010-4129-0

Dunn, M., Masri, A., Bilger, R., Barlow, R., and Wang, G.-H. (2009). The compositional structure of highly turbulent piloted premixed flames issuing into a hot coflow. *Proc. Combust. Inst.* 32, 1779–1786. doi: 10.1016/j.proci.2008.08.007

Dunn, M. J. (2008). *Finite-rate chemistry effects in turbulent premixed combustion*. (Ph.D. Thesis). School of Aeronautical, Mechanical and Mechatronic Engineering, The University of Sydney, Sydney, NSW, Australia.

Dunn, M. J., Masri, A. R., and Bilger, R. W. (2007a). A new piloted premixed jet burner to study strong finite-rate chemistry effects. *Combust. Flame* 151, 46–60. doi: 10.1016/j.combustflame.2007.05.010

Dunn, M. J., Masri, A. R., and Bilger, R. W. (2007b). "Lifted turbulent premixed flames issuing into a hot coflow, imaging of temperature and OH," in *16th Australasian Fluid Mechanics Conference (AFMC)* (Gold Coast, QLD: School of Engineering, The University of Queensland), 1344–1349.

Dunn, M. J., Masri, A. R., Bilger, R. W., and Barlow, R. S. (2010). Finite rate chemistry effects in highly sheared turbulent premixed flames. *Flow Turbul. Combust.* 85, 621–648. doi: 10.1007/s10494-010-9280-5

Duwig, C., Li, B., Li, Z., and Aldén, M. (2012). High resolution imaging of flameless and distributed turbulent combustion. *Combust. Flame* 159, 306–316. doi: 10.1016/j.combustflame.2011.06.018

Eckbreth, A. C. (1996). *Laser Diagnostics for Combustion Temperature and Species, Volume 3 of Combustion Science and Technology, 2nd Edn*. Amsterdam: CRC Press.

Evans, M. J., Chinnici, A., Medwell, P. R., and Ye, J. (2017a). Ignition features of methane and ethylene fuel-blends in hot and diluted coflows. *Fuel* 203, 279–289. doi: 10.1016/j.fuel.2017.04.113

Evans, M. J., Medwell, P. R., and Chan, Q. N. (2019a). "Commissioning a confined and pressurised jet in hot and vitiated coflow burner," in *11th Mediterranean Combustion Symposium* (Tenerife).

Evans, M. J., Medwell, P. R., Sun, Z., Chinnici, A., Ye, J., Chan, Q. N., et al. (2019b). Downstream evolution of *n*-heptane/toluene flames in hot and vitiated coflows. *Combust. Flame* 202, 78–89. doi: 10.1016/j.combustflame.2019.01.008

Evans, M. J., Medwell, P. R., and Tian, Z. F. (2015a). Modeling lifted jet flames in a heated coflow using an optimized eddy dissipation concept model. *Combust. Sci. Technol.* 187, 1093–1109. doi: 10.1080/00102202.2014.1002836

Evans, M. J., Medwell, P. R., Tian, Z. F., Frassoldati, A., Cuoci, A., and Stagni, A. (2016a). Ignition characteristics in spatially zero-, one- and two-dimensional laminar ethylene flames. *AIAA J.* 54, 3255–3264. doi: 10.2514/1.J054958

Evans, M. J., Medwell, P. R., Tian, Z. F., Ye, J., Frassoldati, A., and Cuoci, A. (2017b). Effects of oxidant stream composition on non-premixed laminar flames with heated and diluted coflows. *Combust. Flame* 178, 297–310. doi: 10.1016/j.combustflame.2016.12.023

Evans, M. J., Medwell, P. R., Wu, H., Stagni, A., and Ihme, M. (2016b). Classification and lift-off height prediction of non-Premixed MILD and autoignitive flames. *Proc. Combust. Inst.* 36, 4297–4304. doi: 10.1016/j.proci.2016.06.013

Evans, M. J., Medwell, P. R., and Ye, J. (2015b). "Laser-induced fluorescence of hydroxyl in ethylene jet flames in hot and diluted coflows," in *7th Australian Conference on Laser Diagnostics in Fluid Mechanics and Combustion* (Melbourne, VIC).

Evans, M. J., Petre, C., Medwell, P. R., and Parente, A. (2019c). Generalisation of the eddy-dissipation concept for jet flames with low turbulence and low Damköhler number. *Proc. Combust. Inst.* 37, 4497–4505. doi: 10.1016/j.proci.2018.06.017

Evans, M. J., Sidey, J. A., Ye, J., Medwell, P. R., Dally, B. B., and Mastorakos, E. (2019d). Temperature and reaction zone imaging in turbulent swirling dual-fuel flames. *Proc. Combust. Inst.* 37, 2159–2166. doi: 10.1016/j.proci.2018.07.076

Ferrarotti, M., Li, Z., and Parente, A. (2019). On the role of mixing models in the simulation of mild combustion using finite-rate chemistry combustion models. *Proc. Combust. Inst.* 37, 4531–4538. doi: 10.1016/j.proci.2018.07.043

Fielding, J., Frank, J. H., Kaiser, S. A., Smooke, M. D., and Long, M. B. (2002). Polarized/depolarized Rayleigh scattering for determining fuel concentrations in flames. *Proc. Combust. Inst.* 29, 2703–2709. doi: 10.1016/S1540-7489(02)80329-7

Foo, K. K., Evans, M. J., Sun, Z., Medwell, P. R., Alwahabi, Z. T., Nathan, G. J., et al. (2019). Calculated concentration distributions and time histories of key species in an acoustically forced laminar flame. *Combust. Flame* 204, 189–203. doi: 10.1016/j.combustflame.2019.03.019

Foo, K. K., Sun, Z., Medwell, P. R., Alwahabi, Z. T., Dally, B. B., and Nathan, G. J. (2017). Experimental investigation of acoustic forcing on temperature, soot volume fraction and primary particle diameter in non-premixed laminar flames. *Combust. Flame* 181, 270–282. doi: 10.1016/j.combustflame.2017.04.002

Foo, K. K., Sun, Z., Medwell, P. R., Alwahabi, Z. T., Nathan, G. J., and Dally, B. B. (2018). Influence of nozzle diameter on soot evolution in acoustically forced laminar non-premixed flames. *Combust. Flame* 194, 376–386. doi: 10.1016/j.combustflame.2018.05.026

Frank, J., and Barlow, R. (1998). Simultaneous Rayleigh, Raman, and LIF measurements in turbulent premixed methane-air flames. *Proc. Combust. Inst.* 27, 759–766. doi: 10.1016/S0082-0784(98)80470-0

Frank, J. H., Kaiser, S. A., and Long, M. B. (2002). Reaction-rate, mixture-fraction, and temperature imaging in turbulent methane/air jet flames. *Proc. Combust. Inst.* 29, 2687–2694. doi: 10.1016/S1540-7489(02)80327-3

Frank, J. H., Kalt, P. A., and Bilger, R. W. (1999). Measurements of conditional velocities in turbulent premixed flames by simultaneous OH PLIF and PIV. *Combust. Flame* 116, 220–232. doi: 10.1016/S0010-2180(98)00041-8

Fuest, F., Barlow, R. S., Chen, J.-Y., and Dreizler, A. (2012). Raman/Rayleigh scattering and CO-LIF measurements in laminar and turbulent jet flames of dimethyl ether. *Combust. Flame* 159, 2533–2562. doi: 10.1016/j.combustflame.2011.11.001

Gabet, K. N., and Sutton, J. A. (2014). Narrowband versus broadband excitation for $CH_2O$ PLIF imaging in flames using a frequency-tripled nd:yag laser. *Exp. Fluids* 55:1774. doi: 10.1007/s00348-014-1774-9

Galletti, C., Parente, A., and Tognotti, L. (2007). Numerical and experimental investigation of a mild combustion burner. *Combust. Flame* 151, 649–664. doi: 10.1016/j.combustflame.2007.07.016

Giezendanner-Thoben, R., Meier, U., Meier, W., Heinze, J., and Aigner, M. (2005). Phase-locked two-line OH planar laser-induced fluorescence thermometry in a pulsating gas turbine model combustor at atmospheric pressure. *Appl. Opt.* 44, 6565–6577. doi: 10.1364/AO.44.006565

Gordon, R. L., Masri, A. R., and Mastorakos, E. (2008). Simultaneous Rayleigh temperature, OH- and $CH_2O$-LIF imaging of methane jets in a vitiated coflow. *Combust. Flame* 155, 181–195. doi: 10.1016/j.combustflame.2008.07.001

Gordon, R. L., Masri, A. R., and Mastorakos, E. (2009). Heat release rate as represented by [OH] × [CH2O] and its role in autoignition. *Combust. Theor. Model.* 13, 645–670. doi: 10.1080/13647830902957200

Gordon, R. L., Masri, A. R., Pope, S. B., and Goldin, G. M. (2007). A numerical study of auto-ignition in turbulent lifted flames issuing into a vitiated co-flow. *Combust. Theor. Model.* 11, 351–376. doi: 10.1080/13647830600903472

Gu, D., Sun, Z., Dally, B. B., Medwell, P. R., Alwahabi, Z. T., and Nathan, G. J. (2017). Simultaneous measurements of gas temperature, soot volume fraction and primary particle diameter in a sooting lifted turbulent ethylene/air non-premixed flame. *Combust. Flame* 179, 33–50. doi: 10.1016/j.combustflame.2017.01.017

Gu, D. H., Sun, Z. W., Medwell, P. R., Alwahabi, Z. T., Dally, B. B., and Nathan, G. J. (2015). Mechanism for laser-induced fluorescence signal generation in a nanoparticle-seeded flow for planar flame thermometry. *Appl. Phys. B* 118, 209–218. doi: 10.1007/s00340-014-5972-1

Hochgreb, S. (2019). Mind the gap: turbulent combustion model validation and future needs. *Proc. Combust. Inst.* 37, 2091–2107. doi: 10.1016/j.proci.2018.05.003

Hofmann, D., and Leipert, A. (1996). Temperature field measurements in a sooting flame by filtered Rayleigh scattering (FRS). *Proc. Combust. Inst.* 26, 945–950. doi: 10.1016/S0082-0784(96)80306-7

Honoré, D., Lecordier, B., Susset, A., Jaffré, D., Perrin, M., Most, J., and Trinite, M. (2000). Time-resolved particle image velocimetry in confined bluff-body burner flames. *Exp. Fluids* 29, S248–S254. doi: 10.1007/s003480070027

Ihme, M., and See, Y. C. (2011). LES flamelet modeling of a three-stream MILD combustor： Analysis of flame sensitivity to scalar inflow conditions. *Proc. Combust. Inst.* 33, 1309–1217. doi: 10.1016/j.proci.2010.05.019

Ihme, M., Zhang, J., He, G., and Dally, B. B. (2012). Large-eddy simulation of a jet-in-hot-coflow burner operating in the oxygen-diluted combustion regime. *Flow Turbul. Combust.* 89, 449–464. doi: 10.1007/s10494-012-9399-7

Jiang, N., Hsu, P. S., Mance, J. G., Wu, Y., Gragston, M., Zhang, Z., et al. (2017). High-speed 2D Raman imaging at elevated pressures. *Opt. Lett.* 42, 3678–3681. doi: 10.1364/OL.42.003678

Kähler, C. J., Scharnowski, S., and Cierpka, C. (2012). On the resolution limit of digital particle image velocimetry. *Exp. Fluids* 52, 1629–1639. doi: 10.1007/s00348-012-1280-x

Kaiser, S. A., and Frank, J. H. (2011). The effects of laser-sheet thickness on dissipation measurements in turbulent non-reacting jets and jet flames. *Meas. Sci. Technol.* 22:045403. doi: 10.1088/0957-0233/22/4/045403

Kamal, M. M., Zhou, R., Balusamy, S., and Hochgreb, S. (2015). Favre- and reynolds-averaged velocity measurements: interpreting PIV and LDA measurements in combustion. *Proc. Combust. Inst.* 35, 3803–3811. doi: 10.1016/j.proci.2014.06.061

Karataş, A. E., and Ömer L. Gülder (2012). Soot formation in high pressure laminar diffusion flames. *Prog. Energ. Combust. Sci.* 38, 818–845. doi: 10.1016/j.pecs.2012.04.003

Karpetis, A., and Barlow, R. (2002). Measurements of scalar dissipation in a turbulent piloted methane/air jet flame. *Proc. Combust. Inst.* 29, 1929–1936. doi: 10.1016/S1540-7489(02)80234-6

Kawazoe, H., Ohsawa, K., and Fujikake, K. (1990). LDA measurement of fuel droplet sizes and velocities in a combustion field. *Combust. Flame* 82, 151–162. doi: 10.1016/0010-2180(90)90094-8

Kearney, S. P., Schefer, R. W., Beresh, S. J., and Grasser, T. W. (2005). Temperature imaging in nonpremixed flames by joint filtered Rayleigh and Raman scattering. *Appl. Opt.* 44, 1548–1558. doi: 10.1364/AO.44.001548

Kelman, J. B., Eltobaji, A. J., and Masri, A. R. (1998). Laser imaging in the stabilisation region of turbulent lifted flames. *Combust. Sci. Technol.* 135, 117–134. doi: 10.1080/00102209808924153

Kempema, N. J., and Long, M. B. (2014). Quantitative Rayleigh thermometry for high background scattering applications with structured laser illumination planar imaging. *Appl. Opt.* 53, 6688–6697. doi: 10.1364/AO.53.006688

Kohse-Höinghaus, K. and Jeffries, J. B., editors (2002). *Applied Combustion Diagnostics*. New York, NY: Taylor & Francis.

Kojima, J., and Nguyen, Q.-V. (2002). Laser pulse-stretching with multiple optical ring cavities. *Appl. Opt.* 41, 6360–6370. doi: 10.1364/AO.41.006360

Kristensson, E., Ehn, A., Bood, J., and Aldén, M. (2015). Advancements in Rayleigh scattering thermometry by means of structured illumination. *Proc. Combust. Inst.* 35, 3689–3696. doi: 10.1016/j.proci.2014.06.056

Kruse, S., Medwell, P., Beeckmann, J., and Pitsch, H. (2018). The significance of beam steering on laser-induced incandescence measurements in laminar counterflow flames. *Appl. Phys. B* 124:212. doi: 10.1007/s00340-018-7072-0

Kruse, S., Ye, J., Sun, Z., Attili, A., Dally, B., Medwell, P., and Pitsch, H. (2019). Experimental investigation of soot evolution in a turbulent non-premixed prevaporized toluene flame. *Proc. Combust. Inst.* 37, 849–857. doi: 10.1016/j.proci.2018.05.075

Kyritsis, D. C., Santoro, V. S., and Gomez, A. (2004). The effect of temperature correction on the measured thickness of formaldehyde zones in diffusion flames for 355 nm excitation. *Exp. Fluids* 37, 769–772. doi: 10.1007/s00348-004-0860-9

Li, Z., Cuoci, A., and Parente, A. (2019). Large eddy Simulation of MILD combustion using finite rate chemistry: Effect of combustion sub-grid closure. *Proc. Combust. Inst.* 37, 4519–4529. doi: 10.1016/j.proci.2018.09.033

Luo, Z., Yoo, C. S., Richardson, E. S., Chen, J. H., Law, C. K., and Lu, T. (2012). Chemical explosive mode analysis for a turbulent lifted ethylene jet flame in highly-heated coflow. *Combust. Flame* 159, 265–274. doi: 10.1016/j.combustflame.2011.05.023

Lyons, K., Watson, K., Carter, C., and Donbar, J. (2005). On flame holes and local extinction in lifted-jet diffusion flames. *Combust. Flame* 142, 308–313. doi: 10.1016/j.combustflame.2005.04.006

Macfarlane, A., Dunn, M., Juddoo, M., and Masri, A. (2017). Stabilisation of turbulent auto-igniting dimethyl ether jet flames issuing into a hot vitiated coflow. *Proc. Combust. Inst.* 36, 1661–1668. doi: 10.1016/j.proci.2016.08.028

Macfarlane, A., Dunn, M., and Masri, A. (2019). The influence of fuel type and partial premixing on the structure and behaviour of turbulent autoigniting flames. *Proc. Combust. Inst.* 37, 2277–2285. doi: 10.1016/j.proci.2018.09.006

Macfarlane, A. R., Dunn, M., Juddoo, M., and Masri, A. (2018). The evolution of autoignition kernels in turbulent flames of dimethyl ether. *Combust. Flame* 197, 182–196. doi: 10.1016/j.combustflame.2018.07.022

Magnotti, G., and Barlow, R. (2017). Dual-resolution Raman spectroscopy for measurements of temperature and twelve species in hydrocarbon–air flames. *Proc. Combust. Inst.* 36, 4477–4485. doi: 10.1016/j.proci.2016.06.128

Makwana, A., Wang, Y., Iyer, S., Linevsky, M., Santoro, R. J., Litzinger, T. A., et al. (2018). Effect of fuel composition on soot and aromatic species distributions in laminar, co-flow flames. part 2. partially-premixed fuel. *Combust. Flame* 189, 456–471. doi: 10.1016/j.combustflame.2017.08.015

Mardani, A., Tabejamaat, S., and Mohammadi, M. B. (2011). Numerical study of the effect of turbulence on rate of reactions in the MILD combustion regime. *Combust. Theor. Model.* 15, 753–772. doi: 10.1080/13647830.2011.561368

Masri, A., Dibble, R., and Barlow, R. (1996). The structure of turbulent nonpremixed flames revealed by Raman-Rayleigh-LIF measurements. *Prog. Energy Combust. Sci.* 22, 307–362. doi: 10.1016/S0360-1285(96)00009-3

Masri, A., Kelman, J., and Dally, B. (1998). The instantaneous spatial structure of the recirculation zone in bluff-body stabilized flames. *Proc. Combust. Inst.* 27, 1031–1038. doi: 10.1016/S0082-0784(98)80503-1

Mastorakos, E. (2009). Ignition of turbulent non-premixed flames. *Prog. Energy Combust. Sci.* 35, 57–97. doi: 10.1016/j.pecs.2008.07.002

McMillin, B. K., Seitzman, J. M., and Hanson, R. K. (1994). Comparison of NO and OH planar fluorescence temperature measurements in scramjet model flowfield. *AIAA J.* 32, 1945–1952. doi: 10.2514/3.12237

Medwell, P. R., Chan, Q. N., Dally, B. B., Alwahabi, Z. T., Mahmoud, S., Metha, G. F., et al. (2012). Flow seeding with elemental metal species via an optical method. *Appl. Phys. B* 107, 665–668. doi: 10.1007/s00340-012-5065-y

Medwell, P. R., Chan, Q. N., Dally, B. B., Mahmoud, S., Alwahabi, Z. T., and Nathan, G. J. (2013). Temperature measurements in turbulent non-premixed flames by two-line atomic fluorescence. *Proc. Combust. Inst.* 34, 3619–3627. doi: 10.1016/j.proci.2012.06.027

Medwell, P. R., Chan, Q. N., Kalt, P. A. M., Alwahabi, Z. T., Dally, B. B., and Nathan, G. J. (2009a). Development of temperature imaging using two-line atomic fluorescence. *Appl. Opt.* 48, 1237–1248. doi: 10.1364/AO.48.001237

Medwell, P. R., Chan, Q. N., Kalt, P. A. M., Alwahabi, Z. T., Dally, B. B., and Nathan, G. J. (2010). Instantaneous temperature imaging of diffusion flames using two-line atomic fluorescence. *Appl. Spectrosc.* 64, 173–176. doi: 10.1366/000370210790619573

Medwell, P. R., and Dally, B. B. (2012a). Effect of fuel composition on jet flames in a heated and diluted oxidant stream. *Combust. Flame* 159, 3138–3145. doi: 10.1016/j.combustflame.2012.04.012

Medwell, P. R., and Dally, B. B. (2012b). Experimental observation of lifted flames in a heated and diluted coflow. *Energy Fuels* 26, 5519–5527. doi: 10.1021/ef301029u

Medwell, P. R., Evans, M. J., Chan, Q. N., and Katta, V. R. (2016). Laminar flame calculations for analysing trends in autoignitive jet flames in a hot and vitiated coflow. *Energy Fuels* 30, 8680–8690. doi: 10.1021/acs.energyfuels.6b01264

Medwell, P. R., Kalt, P. A. M., and Dally, B. B. (2007). Simultaneous imaging of OH, formaldehyde, and temperature of turbulent nonpremixed jet flames in a heated and diluted coflow. *Combust. Flame* 148, 48–61. doi: 10.1016/j.combustflame.2006.10.002

Medwell, P. R., Kalt, P. A. M., and Dally, B. B. (2008). Imaging of diluted turbulent ethylene flames stabilized on a Jet in Hot Coflow (JHC) burner. *Combust. Flame* 152, 100–113. doi: 10.1016/j.combustflame.2007.09.003

Medwell, P. R., Kalt, P. A. M., and Dally, B. B. (2009b). Reaction zone weakening effects under hot and diluted oxidant stream conditions. *Combust. Sci. Technol.* 181, 937–953. doi: 10.1080/00102200902904138

Medwell, P. R., Masri, A. R., Pham, P. X., Dally, B. B., and Nathan, G. J. (2014). Temperature imaging of turbulent dilute spray flames using two-line atomic fluorescence. *Exp. Fluids* 55:1840. doi: 10.1007/s00348-014-1840-3

Minamoto, Y., and Swaminathan, N. (2014). Scalar gradient behaviour in MILD combustion. *Combust. Flame* 161, 1063–1075. doi: 10.1016/j.combustflame.2013.10.005

Minamoto, Y., Swaminathan, N., Cant, R. S., and Leung, T. (2014). Reaction zones and their structure in MILD combustion. *Combust. Sci. Technol.* 186, 1075–1096. doi: 10.1080/00102202.2014.902814

Mokhov, A., Gersen, S., and Levinsky, H. (2005). Spontaneous Raman measurements of acetylene in atmospheric-pressure methane/air flames. *Chem. Phys. Lett.* 403, 233–237. doi: 10.1016/j.cplett.2005.01.021

Mungal, M. G., Lourenco, L. M., and Krothapalli, A. (1995). Instantaneous velocity measurements in laminar and turbulent premixed flames using on-line PIV. *Combust. Sci. Technol.* 106, 239–265. doi: 10.1080/00102209508907781

Namer, I., and Schefer, R. (1985). Error estimates for Rayleigh scattering density and temperature measurements in premixed flames. *Exp. Fluids* 3, 1–9. doi: 10.1007/BF00285264

Nguyen, Q., Dibble, R., Carter, C., Fiechtner, G., and Barlow, R. (1996). Raman-LIF measurements of temperature, major species, OH, and NO in a methane-air bunsen flame. *Combust. Flame* 105, 499–510. doi: 10.1016/0010-2180(96)00226-X

Oberlack, M., Arlitt, R., and Peters, N. (2000). On stochastic Damköhler number variations in a homogeneous flow reactor. *Combust. Theor. Model.* 4, 495–510. doi: 10.1088/1364-7830/4/4/307

Oldenhof, E., Tummers, M. J., van Veen, E. H., and Roekaerts, D. J. E. M. (2010). Ignition kernel formation and lift-off behaviour of jet-in-hot-coflow flames. *Combust. Flame* 157, 1167–1178. doi: 10.1016/j.combustflame.2010.01.002

Oldenhof, E., Tummers, M. J., van Veen, E. H., and Roekaerts, D. J. E. M. (2011). Role of entrainment in the stabilisation of jet-in-hot-coflow flames. *Combust. Flame* 158, 1553–1563. doi: 10.1016/j.combustflame.2010.12.018

Oldenhof, E., Tummers, M. J., van Veen, E. H., and Roekaerts, D. J. E. M. (2012). Transient response of the Delft jet-in-hot coflow flames. *Combust. Flame* 159, 697–706. doi: 10.1016/j.combustflame.2011.08.001

O'Loughlin, W., and Masri, A. (2011). A new burner for studying auto-ignition in turbulent dilute sprays. *Combust. Flame* 158, 1577–1590. doi: 10.1016/j.combustflame.2010.12.021

O'Loughlin, W., and Masri, A. R. (2012). The structure of the auto-ignition region of turbulent dilute methanol sprays issuing in a vitiated co-flow. *Flow Turbul. Combust.* 89, 13–35. doi: 10.1007/s10494-012-9388-x

Özdemir, İ. B., and Peters, N. (2001). Characteristics of the reaction zone in a combustor operating at mild combustion. *Exp. Fluids* 30, 683–695. doi: 10.1007/s003480000248

Palmer, J. L., and Hanson, R. K. (1996). Temperature imaging in a supersonic free jet of combustion gases with two-line OH fluorescence. *Appl. Opt.* 35, 485–499. doi: 10.1364/AO.35.000485

Papageorge, M., Arndt, C., Fuest, F., Meier, W., and Sutton, J. (2014). High-speed mixture fraction and temperature imaging of pulsed, turbulent fuel jets auto-igniting in high-temperature, vitiated co-flows. *Exp. Fluids* 55:1763. doi: 10.1007/s00348-014-1763-z

Parente, A., Malik, M. R., Contino, F., Cuoci, A., and Dally, B. B. (2016). Extension of the eddy dissipation concept for turbulence/chemistry interactions to MILD combustion. *Fuel* 163, 98–111. doi: 10.1016/j.fuel.2015.09.020

Paul, P. H., and Najm, H. N. (1998). Planar laser-induced fluorescence imaging of flame heat release rate. *Proc. Combust. Inst.* 27, 43–50. doi: 10.1016/S0082-0784(98)80388-3

Perpignan, A. A., Rao, A. G., and Roekaerts, D. J. (2018). Flameless combustion and its potential towards gas turbines. *Prog. Energy Combust. Sci.* 69, 28–62. doi: 10.1016/j.pecs.2018.06.002

Plessing, T., Peters, N., and Wünning, J. G. (1998). Laseroptical investigation of highly preheated combustion with strong exhaust gas recirculation. *Proc. Combust. Inst.* 27, 3197–3204. doi: 10.1016/S0082-0784(98)80183-5

Ramachandran, A., Narayanaswamy, V., and Lyons, K. M. (2019). Observations on the role of auto-ignition in flame stabilization in turbulent non-premixed jet flames in vitiated coflow. *J. Eng. Gas Turb. Power* 141:061018. doi: 10.1115/1.4042807

Richardson, D. R., Jiang, N., Blunck, D. L., Gord, J. R., and Roy, S. (2016). Characterization of inverse diffusion flames in vitiated cross flows via two-photon planar laser-induced fluorescence of CO and 2-D thermometry. *Combust. Flame* 168, 270–285. doi: 10.1016/j.combustflame.2016.03.005

Roy, S., Gord, J. R., and Patnaik, A. K. (2010). Recent advances in coherent anti-Stokes Raman scattering spectroscopy: fundamental developments and applications in reacting flows. *Prog. Energy Combust. Sci.* 36, 280–306. doi: 10.1016/j.pecs.2009.11.001

Sabia, P., de Joannon, M., Sorrentino, G., Giudicianni, P., and Ragucci, R. (2015). Effects of mixture composition, dilution level and pressure on auto-ignition delay times of propane mixtures. *Chem. Eng. J.* 277, 324–333. doi: 10.1016/j.cej.2015.04.143

Schießl, R., Kaiser, S., Long, M., and Maas, U. (2009). Application of reduced state spaces to laser-based measurements in combustion. *Proc. Combust. Inst.* 32, 887–894. doi: 10.1016/j.proci.2008.05.063

Sepman, A., Mokhov, A., and Levinsky, H. (2013). Spatial structure and NO formation of a laminar methane–nitrogen jet in hot coflow under MILD conditions: a spontaneous Raman and LIF study. *Fuel* 103, 705–710. doi: 10.1016/j.fuel.2012.10.010

Shabanian, S. R., Medwell, P. R., Rahimi, M., Frassoldati, A., and Cuoci, A. (2013). Kinetic and fluid dynamic modeling of ethylene jet flames in diluted and heated oxidant stream combustion conditions. *Appl. Therm. Eng.* 52, 538–554. doi: 10.1016/j.applthermaleng.2012.12.024

Sidey, J., and Mastorakos, E. (2015). Visualization of MILD combustion from jets in cross-flow. *Proc. Combust. Inst.* 35, 3537–3545. doi: 10.1016/j.proci.2014.07.028

Sidey, J., and Mastorakos, E. (2017). Visualisation of turbulent swirling dual-fuel flames. *Proc. Combust. Inst.* 36, 1721–1727. doi: 10.1016/j.proci.2016.08.045

Sidey, J. A., Giusti, A., and Mastorakos, E. (2016). Simulations of laminar non-premixed flames of kerosene with hot combustion products as oxidiser. *Combust. Theor. Model.* 20, 958–973. doi: 10.1080/13647830.2016.1201146

Sidey, J. A., and Mastorakos, E. (2016). Simulations of laminar non-premixed flames of methane with hot combustion products as oxidiser. *Combust. Flame* 163, 1–11. doi: 10.1016/j.combustflame.2015.07.034

Sirignano, M., Bartos, D., Conturso, M., Dunn, M., D'Anna, A., and Masri, A. R. (2017). Detection of nanostructures and soot in laminar premixed flames. *Combust. Flame* 176, 299–308. doi: 10.1016/j.combustflame.2016.10.009

Sorrentino, G., de Joannon, M., Sabia, P., Ragucci, R., and Cavaliere, A. (2017). Numerical investigation of the ignition and annihilation of $CH_4/N_2/O_2$ mixtures under MILD operative conditions with detailed chemistry. *Combust. Theor. Model.* 21, 120–136. doi: 10.1080/13647830.2016.1220624

Sorrentino, G., Sabia, P., de Joannon, M., Cavaliere, A., and Ragucci, R. (2016). The effect of diluent on the sustainability of MILD combustion in a cyclonic burner. *Flow Turbul. Combust.* 96, 449–468. doi: 10.1007/s10494-015-9668-3

Sorrentino, G., Sabia, P., de Joannon, M., Ragucci, R., Cavaliere, A., Göktolga, U., et al. (2015). Development of a novel cyclonic flow combustion chamber for achieving MILD/flameless combustion. *Energy Proc.* 66, 141–144. doi: 10.1016/j.egypro.2015.02.079

Starner, S., Bilger, R., and Long, M. (1995). A method for contour-aligned smoothing of joint 2d scalar images in turbulent flames. *Combust Sci. Technol.* 107, 195–203. doi: 10.1080/00102209508907802

Sturgess, G., Zelina, J., Shouse, D. T., and Roquemore, W. (2005). Emissions reduction technologies for military gas turbine engines. *J. Propul. Power* 21, 193–217. doi: 10.2514/1.6528

Sutton, J. A., and Driscoll, J. F. (2004). Rayleigh scattering cross sections of combustion species at 266, 355, and 532 nm for thermometry applications. *Opt. Lett.* 29, 2620–2622. doi: 10.1364/OL.29.002620

van Veen, E. H., and Roekaerts, D. (2005). Thermometry for turbulent flames by coherent anti-Stokes Raman spectroscopy with simultaneous referencing to the modeless excitation profile. *Appl. Opt.* 44, 6995–7004. doi: 10.1364/AO.44.006995

Walters, E. M. (2016). *Stability and liftoff of non-premixed large hydrocarbon flames in MILD conditions*. (Masters thesis). College of Engineering, Oregon State University, Corvallis, OR, United States.

Wang, H., Zhou, H., Ren, Z., and Law, C. K. (2019a). Transported pdf simulation of turbulent $CH_4/H_2$ flames under MILD conditions with particle-level sensitivity analysis. *Proc. Combust. Inst.* 37, 4487–4495. doi: 10.1016/j.proci.2018.05.167

Wang, Y., Jain, A., and Kulatilaka, W. (2019b). CO imaging in piloted liquid-spray flames using femtosecond two-photon LIF. *Proc. Combust. Inst.* 37, 1305–1312. doi: 10.1016/j.proci.2018.05.016

Wang, Y., Makwana, A., Iyer, S., Linevsky, M., Santoro, R. J., Litzinger, T. A., et al. (2018). Effect of fuel composition on soot and aromatic species distributions in laminar, co-flow flames. part 1. non-premixed fuel. *Combust. Flame* 189, 443–455. doi: 10.1016/j.combustflame.2017.08.011

Watson, K., Lyons, K., Carter, C., and Donbar, J. (2002). Simultaneous two-shot CH planar laser-induced fluorescence and particle image velocimetry measurements in lifted $CH_4$/air diffusion flames. *Proc. Combust. Inst.* 29, 1905–1912. doi: 10.1016/S1540-7489(02)80231-0

Watson, K., Lyons, K., Donbar, J., and Carter, C. (2000). Simultaneous Rayleigh imaging and CH-PLIF measurements in a lifted jet diffusion flame. *Combust. Flame* 123, 252–265. doi: 10.1016/S0010-2180(00)00133-4

Wu, Z., Masri, A. R., and Bilger, R. W. (2006). An experimental investigation of the turbulence structure of a lifted $H_2/N_2$ jet flame in a vitiated co-flow. *Flow Turb. Combust.* 76, 61–81. doi: 10.1007/s10494-005-9006-2

Yamasaki, Y., and Tezaki, A. (2005). Non-linear pressure dependence of a-state fluorescence lifetime of formaldehyde. *Appl. Phys. B* 80, 791–795. doi: 10.1007/s00340-005-1798-1

Yao, M., Zheng, Z., and Liu, H. (2009). Progress and recent trends in homogeneous charge compression ignition (HCCI) engines. *Prog. Energy Combust. Sci.* 35, 398–437. doi: 10.1016/j.pecs.2009.05.001

Ye, J., Medwell, P. R., Dally, B. B., and Evans, M. J. (2016). The transition of ethanol flames from conventional to MILD combustion. *Combust. Flame* 171, 173–184. doi: 10.1016/j.combustflame.2016.05.020

Ye, J., Medwell, P. R., Evans, M. J., and Dally, B. B. (2015). "Quantitative Rayleigh temperature imaging in turbulent flameames of prevaporised n-heptane," in *7th Australian Conference on Laser Diagnostics in Fluid Mechanics and Combustion* (Melbourne, VIC).

Ye, J., Medwell, P. R., Evans, M. J., and Dally, B. B. (2017). Characteristics of turbulent n-heptane jet flames in a hot and diluted coflow. *Combust. Flame* 183, 330–342. doi: 10.1016/j.combustflame.2017.05.027

Ye, J., Medwell, P. R., Kleinheinz, K., Evans, M. J., Dally, B. B., and Pitsch, H. G. (2018). Structural differences of ethanol and DME jet flames in a hot diluted coflow. *Combust. Flame* 192, 473–494. doi: 10.1016/j.combustflame.2018.02.025

Yoo, C. S., Richardson, E. S., Sankaran, R., and Chen, J. H. (2011). A DNS study on the stabilization mechanism of a turbulent lifted ethylene jet flame in highly-heated coflow. *Proc. Combust. Inst.* 33, 1619–1627. doi: 10.1016/j.proci.2010.06.147

Yuan, R. (2015). *Measurements in swirl-stabilised spray flames at blow-off*. (Ph.D. thesis). University of Cambridge, Cambridge, United Kingdom.

**Conflict of Interest:** The authors declare that the research was conducted in the absence of any commercial or financial relationships that could be construed as a potential conflict of interest.

frontiers in Mechanical Engineering

HYPOTHESIS AND THEORY
published: 21 January 2020
doi: 10.3389/fmech.2019.00072

# MILD Combustion Limit Phenomena

*Jenni A. M. Sidey-Gibbons*[*†] *and Epaminondas Mastorakos*[†]

*Hopkinson Lab, Department of Engineering, University of Cambridge, Cambridge, United Kingdom*

This work contains an analysis of the existence of critical phenomena in MILD combustion systems through an exploration of classical results from high-energy asymptotics theory for extinction conditions of non-premixed flames and well-stirred reactors. Through the derivation of an expression linking burning rate to Damköhler number, the criteria for a folded S-Shaped Curve, representative of a combustion system with sudden extinction and ignition behavior, was derived. This theory is discussed in detail, with particular focus on the limitations of the global chemistry it presents. The conditions reported by various previously-published numerical and experimental investigations are then discussed in the context of this theory. Of these investigations, those with the highest level of preheat and dilution had monotonic rather than folded S-Shaped Curves, indicating a lack of sudden extinction phenomena. It suggests that MILD combustion systems are those which lack sudden ignition and extinction behavior, therefore exhibiting a smooth, stretched S-Shaped Curve rather than a folded one with inflection points. The results suggest that the delineation between folded versus monotonic S-Shaped Curves may provide a useful alternative definition of MILD combustion.

**Keywords: MILD combustion, extinction, limit phenomena, S-shaped curve, hot product dilution**

OPEN ACCESS

***Edited by:***
*Mara de Joannon,*
*Istituto di ricerche sulla combustione (IRC), Italy*

***Reviewed by:***
*Amir Mardani,*
*Sharif University of Technology, Iran*
*Giancarlo Sorrentino,*
*University of Naples Federico II, Italy*

***Correspondence:**
*Jenni A. M. Sidey-Gibbons*
*jams4@cam.ac.uk*

*†These authors have contributed equally to this work*

***Specialty section:***
*This article was submitted to Thermal and Mass Transport, a section of the journal Frontiers in Mechanical Engineering*

***Received:*** *01 May 2019*
***Accepted:*** *24 December 2019*
***Published:*** *21 January 2020*

***Citation:***
*Sidey-Gibbons JAM and Mastorakos E (2020) MILD Combustion Limit Phenomena. Front. Mech. Eng. 5:72. doi: 10.3389/fmech.2019.00072*

## 1. INTRODUCTION

Analyses mapping the transition between fully burning, partially burning, and chemically frozen states are crucial to the understanding of ignition and extinction behavior in general combustion systems. The examination of these critical phenomena is essential considering the practical applications relying on the successful occurrence or avoidance of ignition and extinction events. Detailing these behaviors in complex systems, such as those involving preheat and dilution as in the MILD regime, is of particular importance. Ignition may be achieved through a supply of heat or fuel-attacking radicals to a combustible mixture; in the case of hot product dilution, both are relevant and, from the results in Sidey et al. (2014), have a significant effect on a systems autoignition and propagation behavior. In conventional systems, with the supply of heat and/or oxidation initiation radicals, if the rate of heat addition or chain-branching radical production dominates, thermal runaway will occur, and the system mixture will ignite. Conversely, if the rate of cooling or deactivating and quenching reactions dominate, the mixture will not successfully combust. From this, it follows that extinction must then occur through the removal of heat or chain-branching radicals. This may be achieved in numerous ways, including the mixing with a cold or inert gas or reduction in mixture equivalence ratio or pressure, as discussed in Law (2006).

Observable from the results of the jet in cross-flow experiment presented in Sidey and Mastorakos (2015) and autoignition and propagation results presented in Sidey et al. (2014), the high temperature and reactive species concentration in burned product oxidiser dictates that MILD combustion systems may be dominated by autoignition behavior. MILD system reactants are preheated and, in the cases discussed throughout this work, in the presence of chain-branching

radicals through mixing with hot combustion products. Mixing with hot products dilutes the reactants such that, in the absence of the heat or radicals supplied through this mixing, the reactants would be unable to initiate thermal runaway. Any ignition attempt with a similar concentration of fresh reactants diluted with a cold, inert gas (say, $CO_2$) would be unsuccessful because the system would lack the ability for sufficient heat and radical production to reach feedback combustion conditions. Once reactant mixtures diluted with hot combustion products autoignite, they continue to burn in an autoignition regime continually supplied with hot combustion products either through an external or internal recirculation system. The ability of a flame to propagate, as opposed to autoignite, in a premixed system heavily diluted with hot, reactive gas is discussed in Sidey et al. (2014). Due to this constant supply of heat and, in some cases, combustion radical species, required as parameters of the MILD combustion systems presented in this work, all of which are adiabatic and well-mixed, it follows that conventional extinction conditions cannot occur.

The lack of conventional extinction behavior in MILD combustion systems was addressed theoretically by Cavaliere and de Joannon (2004) through the examination of a well-stirred reactor (WSR). The working temperature of a WSR, $T_{WSR}$, and the initial temperature of its reactants, $T_\circ$ are reported in **Figure 1**, from Cavaliere and de Joannon (2004), as a function of reactant $O_2$ mole fraction, $X_{O2}$. The system, designated as atmospheric $CH_4$-air in stoichiometric quantities with a residence time, $\tau_{res}$, of 1 s, ignites from a weakly burning state at $T_{si}$, the system self-ignition temperature. This self-ignition, or autoignition, temperature is not a fundamental system parameter and is instead dependent on reactor and mixture characteristics, but is well defined for a WSR with a known $\tau_{res}$ and reactants of known composition. The behavior of the system working temperature, $T_{WSR}$, is heavily dependent on $X_{O2}$. Specifically, as dilution increases, and thus $X_{O2}$ decreases, $T_{WSR}$ is reduced. Cavaliere and de Joannon take $T_\circ = 1100K$ as a specific example in **Figure 1**; for the most highly diluted case, the temperature rise during combustion, $\Delta T$, is very low. This case, adhering to the conditions very high reactant preheat temperature and very low combustion temperature rise, exemplifies the Cavaliere and de Joannon definition of MILD combustion. The relationship between $T_{WSR}$ and $T_\circ$ in **Figure 1** provides a comparison between the peak temperature of the system and its reaction timescale, linked to $T_\circ$. Through this graphical analysis, known as an S-Shaped Curve analysis, the criticality characteristics of a system may be assessed. Conventional S-Shaped Curves are characterized by a weakly burning lower branch, intensely burning high temperature branch, and an unstable region connecting the two; these curves are referred to as "folded" (**Figure 1**, $X_{O2} = 0.1, 0.2$). As the peak temperature, or burning rate, of an intensely burning system on a folded S-Shaped Curve is decreased, extinction will occur when conditions of the unstable region are reached. Alternatively, systems which do not exhibit this sudden extinction behavior are described by smooth or monotonic S-Shaped Curves in which intensely and weakly burning branches are connected and no unstable region exists. In **Figure 1**, Cavaliere and de Joannon demonstrate that MILD combustion systems, defined by a high preheat temperature and low temperature rise during combustion, may approach fully-stable, monotonic S-Shaped Curve behavior and therefore may not extinguish as conventional systems do.

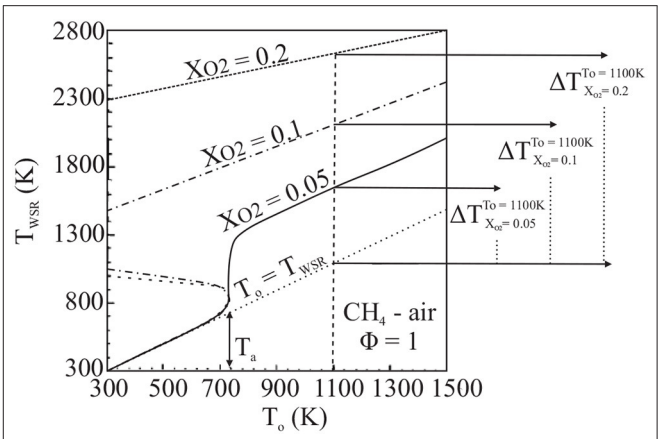


**FIGURE 1 |** WSR behavior as a function of dilution ($X_{O2}$) demonstrating conventional folded ($X_{O2} = 0.1, 0.2$) and smooth (MILD condition, $X_{O2} = 0.05$) S-Shaped Curves, from Cavaliere and de Joannon (2004).

The absence of sudden extinction behavior in combustion systems with reactants mixed extensively with preheated diluent, either inert or reacting, has been observed experimentally and theoretically. Libby and Williams (1983) reported on the smooth transition between thin and diffuse reaction zones of premixed laminar flames resulting from counterflowing reactants and combustion products at high rates of strain. Smooke et al. (1991), in a study investigating fresh premixed $CH_4$-air reactants counterflowing against hot combustion products, observed that cases in which the burned product temperature was above 1480 K, no extinction strain rate could be reached experimentally or numerically. Similarly, Darabiha et al. (1988), Darabiha and Candel (1992) reported similar behavior in both $C_3H_8$-air and $H_2$-air systems and suggested that the dissolution of conventional extinction and ignition behavior occurs when the hot stream temperature nears the adiabatic flame temperature of the cold reactants. This is in agreement with (Libby and Williams, 1983), who suggested that reaction zone and extinction behavior transitions occur when the hot product streams in such systems are cooled from their adiabatic flame temperature. Mastorakos et al. (1995) studied the effect of simultaneous preheat and dilution on turbulent counterflow flames experimentally by flowing either pure fuel or premixed fuel and air against hot combustion products from a second premixed flame. They reported that, even at very high strain rates, preheated and diluted flames would not extinguish, a finding consistent with theoretical work by Bray et al. (1996). Bray et al. investigated the extinction behavior of counterflow flames in which the opposing streams had unequal enthalpies. They found that, if an opposing stream was heated extensively, the mean reaction rate of the system in question was always above zero at its stagnation point. In practice, this means that sudden extinction

phenomenon disappeared if one opposing stream, even if inert, was heated above a critical temperature within the range of hot combustion products. Choi and Katsuki (2002) also commented on the unusual extinction characteristics arising from extensive preheat and dilution, reporting that combustion reactions occur even with air excessively diluted with a preheated inert gas. Medwell et al. (2007) investigated flames produced with a heated and diluted co-flow apparatus with OH, formaldehyde, and temperature monitoring. Their work reported areas of distributed combustion zones with increased co-flow hot product concentration. As in the case of dilution with an inert gas in the Bray et al. and Mastorakos et al. studies, the presence of radical species in the initial reactant concentration was not necessary for the dissolution of conventionally observed extinction behavior. The high preheat temperature of the inert diluent initiates chain-branching reactions and the production of autoignition radicals upon mixing with the oxidiser and fuel.

With a focus primarily on the temperature of the hot overflowing stream rather than composition, many of these studies have not extensively investigated the critical phenomenon physics linked to reactive diluent, such as in the counterflow cases discussed in Sidey and Mastorakos (2016). Considering the lack of sudden extinction behavior due to preheat alone, the addition of radical species in the reactant composition at the system's boundary condition would exacerbate the ability of the system to react even at very high rates of strain. Coriton et al. (2010) and Coriton et al. (2013) investigated the effect of hot product stoichiometry and flame heat loss on laminar counterflow flames and observed that a regime without sudden extinction behavior occurs when sufficient oxidizing species are present in the hot combustion product stream. They identified the role of key radical pools in extinction behavior and concluded that the thickening of the heat release rate profile under MILD conditions was due to a shift in OH and O production rates. In this study, the absence of an abrupt extinction event in the highly diluted cases was attributed to sustained concentrations of OH and O in counterflow reaction zone in contrast to the depleted H, OH, and O concentrations leading to abrupt extinction in conventional flames. While the depletion of key $CH_4$ attacking radicals such as H, OH, and O would lead to extinction, this effect must be coupled with temperature; the production of both heat and chain-branching intermediate species are intrinsically linked in systems diluted with preheated gas. In the presence of high temperatures, these radicals are produced immediately and, through further oxidation reactions, the radicals themselves lead to increased temperatures through a positive feedback process. The absence of these radicals may be due to quenching, competing weakly- or non-exothermic reactions, or simply a reduction in system temperature.

Despite the observation of the lack of extinction behavior in systems involving extensive dilution, the fundamental nature of this behavior is not strongly linked with the conditions of the MILD regime. This work aims to extend conventional extinction and ignition analysis specifically to MILD combustion processes to assess the existence of sudden limit phenomena in heavily diluted and preheated combustion systems with a simplified analysis.

Not only do we believe this work provides a link between the work of Cavaliere and de Joannon (2004) and the combustion analyses presented in Law (2006), but also presents the ideal that the presence of a classical extinction point may be used as a tool to delineate MILD combustion regimes. A mathematical analysis for investigating the presence of critical phenomena in simplified combustion systems from Law (2006) will be presented.

The capability of heavily diluted combustible mixtures, both from the non-premixed and premixed studies in Sidey and Mastorakos (2016) and Sidey et al. (2014) respectively, to exhibit sudden limit phenomena based on the presented analysis will be assessed. Finally, the conditions for critical phenomena will be discussed in comparison with previous studies and generalized for the MILD regime.

## 2. CRITICAL PHENOMENA IN CONVENTIONAL COMBUSTION SYSTEMS

The ignitability of a combustion system is often evaluated through the comparison of burning rate and a metric indicative of the residence time available for reaction, usually Damköhler number, *Da*:

$$Da = \frac{\text{characteristic diffusion time}}{\text{characteristic reaction time}} = \frac{\tau_m}{\tau_c} \tag{1}$$

Damköhler number is a non-dimensionalized number indicative of time available for a reaction to proceed at a specified rate. As Damköhler number tends to $\infty$, $\tau_m$ must be very large and/or $\tau_c$ very small, indicating that the system must have reached an equilibrium state with a very fast reaction occurring in a long flow timespan. Conversely, a null Damköhler number describes a system with a very short residence time and comparatively long reaction time; the system is chemically frozen. In counterflow non-premixed systems, the flow may be characterized by the strain rate, $A$, a parameter describing the velocity gradient between the counterflowing streams. Systems with high rates of strain have very low associated reaction zone residence times, making them analogous to low Damköhler number systems. Low rates of strain allow for relatively long residence times allowing reactions to proceed, often to completion. Low strain rate counterflowing systems have a high Damköhler number.

A comparison of system burning rate or maximum temperature (indicative of burning rate) with Damköhler number results in an S-Shaped Curve, similar to that discussed with (Cavaliere and de Joannon, 2004) shown in **Figure 2**. As discussed briefly with **Figure 1**, S-Shaped Curves typically appear folded (**Figure 2**, left): a low Damköhler number and low temperature branch associated with frozen or weakly-reacting cases, a high temperature and high Damköhler number branch associated with fully burning cases, and an unstable region connecting the two branches. The inflection points on the S-Shaped Curve, or the points at which the upper and lower branches connect to the unstable transition region, are critical Damköhler numbers at which system ignition and extinction occur ($Da_I$ and $Da_E$, respectively). A

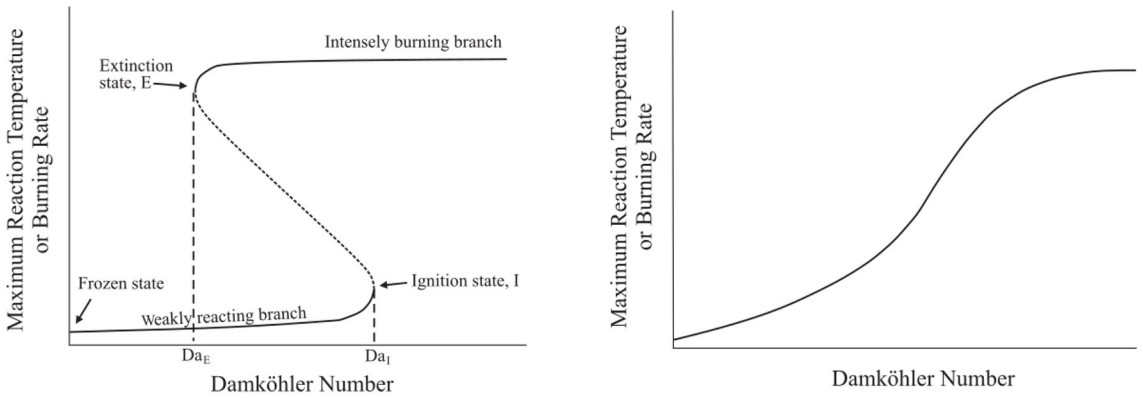


**FIGURE 2 |** Folded (left) vs. smooth S-Shaped Curves detailing the transitions between weakly reacting, unstable, and fully burning branches in a combustion system. Adapted from Law (2006).

system's behavior may, under certain conditions, be appear as a smooth S-Shaped Curve on the burning rate–Damköhler number plot (**Figure 2**, right). These system lack critical points and, rather, transition smoothly from a frozen to burning state. As mentioned, these systems do not have a defined extinction Damköhler number or strain rate, but instead transition smoothly to a frozen, non-reacting state as residence time in comparison with reaction time becomes relatively small.

Through the analysis of simplified combustion systems, one may derive the criteria for the existence of critical points on the S-Shaped Curve in terms of system parameters such as preheat temperature. Furthermore, considering the unconventional extinction behavior of MILD combustion systems, reported in the work discussed in Sidey et al. (2014), and the regime definition involving preheat temperature (Cavaliere and de Joannon, 2004), it is important to investigate the applicability of this analysis to the MILD regime.

## 2.1. Condition for a Folded S-Shaped Curve

In order to investigate the existence of critical points, an assessment of the operation limits of two simplified combustion systems must be performed, beginning with an adiabatic thermal explosion. The energy and species governing equations for such a system, a lean, homogeneous body of gas at $T_\circ$ which ignites adiabatically after time $t$, with one-step global Arrhenius kinetics, are as follows, from Law (2006):

$$\rho_\circ c_v \frac{dT}{dt} = -Q\dot{\omega}_F = -QBc_F e^{-T_a/T} \tag{2}$$

$$\frac{dc_F}{dt} = \dot{\omega}_F = Bc_F e^{-T_a/T} \tag{3}$$

The fuel reaction rate, $\dot{\omega}_F$, of Equations (2) and (3) is assumed to be of the Arrhenius form with the pre-exponential factor composed of $B$, the collision frequency factor, and $c_F$, the fuel concentration. By stoichiometrically weighting both temperature and fuel concentration ($\tilde{T} = (c_v/qY_F)T$ and $\tilde{c}_F = c_F/c_{F,\circ}$) to apply a coupling function, Equations (2) and (3) can be expressed as follows:

$$\frac{d\tilde{T}}{dt} = B\tilde{c}_F e^{-T_a/T} \tag{4}$$

$$\frac{d\tilde{c}_F}{dt} = -B\tilde{c}_F e^{-T_a/T} \tag{5}$$

with the coupling function, $\Xi$ stemming from the following linear combination:

$$(4) + (5): \qquad \Xi = \tilde{T} + \tilde{c}_F \tag{6}$$

The resulting conserved scalar balance equation is:

$$\frac{d\Xi}{dt} = \frac{d}{dt}\left(\tilde{T} + \tilde{c}_F\right) = 0 \tag{7}$$

Integrating Equation (7), recalling that $\tilde{c}_{F,\circ} = c_{F,\circ}/c_{F,\circ} = 1$, gives:

$$\tilde{T} - \tilde{T}_\circ = 1 - \tilde{c}_F \tag{8}$$

This result, linking the stoichiometrically weighted temperature with fuel concentration is useful when considering the energy balance in the second simplified combustion system: a well-stirred reactor (WSR) or Longwell bomb (Longwell and Weiss, 1955). Recall that through the analysis of a WSR system, an S-Shaped Curve was derived in Cavaliere and de Joannon (2004). The WSR energy balance, which relates the initial system and flame or reaction zone temperature, $T_f$, on the LHS to the reaction characteristics, assumed to be one-step Arrhenius, on the RHS. Note that because the WSR involves a changing flow, constant pressure system, Equation (9) differs from Equation (2) in that it requires $c_p$ rather than $c_v$.

$$\dot{V}\rho_\circ c_p(\tilde{T}_f - \tilde{T}_\circ) = VQBc_F e^{\tilde{T}_a/\tilde{T}_\circ} \tag{9}$$

With the substitution of non-dimensional stoichiometrically weighted temperature ($\tilde{T} = \left(c_p/qY_F\right) T$) and fuel concentration ($\tilde{c}_F = \tilde{T}_{ad} - \tilde{T}_f$[1]), Equation (9) becomes:

$$\frac{1}{B}\frac{\dot{V}}{V}\left(\tilde{T}_f - \tilde{T}_\circ\right) = \left(\tilde{T}_{ad} - \tilde{T}_f\right) e^{(-\tilde{T}_a/\tilde{T}_f)} \tag{10}$$

The term $B\frac{V}{\dot{V}}$, presented in reciprocal form on the LHS of Equation 10, is a form of Damköhler number, characterizing the residence time in relation to the reaction time. Equation 10 expresses the convective transport (LHS, controlled by *Da*) and chemical release (RHS, controlled by the Arrhenius one-step reaction term or burning rate) in the WSR. As discussed by Law (2006), this analysis may be extended to general reaction zones treated as a WSR - an assumption applicable the cases presented in this work considering the rigorous mixing and WSR-like behavior of the MILD regime. It is important to note that the precise definition of Damköhler number, whether it be strain rate, initial temperature, or collisional Damköhler number, is immaterial as long as it describes the ratio of transport or residence time to reaction time of the system.

After the derivation of the relationship between the chemical (burning rate) and diffusion terms of a generalized reaction zone, the existence of critical points of ignition and extinction may be determined. Graphically, critical points on S-Shaped Curve are points where the slope on the $Da - T_f$ curve are vertical, or infinite. Mathematically, this condition may be expressed as:

$$\left.\frac{dlnDa}{dT_f}\right|_{cr} = 0 \tag{11}$$

Taking the natural logarithm of Equation (10) gives:

$$ln(\tilde{T}_f - \tilde{T}_\circ) = ln(Da) + ln(\tilde{T}_{ad} - \tilde{T}_f) + \left(\frac{-\tilde{T}_a}{\tilde{T}_f}\right) \tag{12}$$

Followed by the derivative:

$$\frac{1}{\tilde{T}_f - \tilde{T}_\circ} = \frac{dlnDa}{dT_f} - \frac{1}{\tilde{T}_{ad} - \tilde{T}_f} + \frac{-1}{\tilde{T}_f} + \frac{\tilde{T}_a}{\tilde{T}_f^2} \tag{13}$$

Applying the above to the critical points and substituting in Equation (11) gives:

$$\frac{1}{\tilde{T}_{f,cr} - \tilde{T}_\circ} + \frac{1}{\tilde{T}_{ad} - \tilde{T}_{f,cr}} = \frac{\tilde{T}_a}{\tilde{T}_{f,cr}^2} \tag{14}$$

In Equation (14), the first term in the LHS describes effects due to system preheat whereas the second term in the LHS describes the effects due to composition reflected in $\tilde{T}_{ad}$. If the critical point is the system ignition point ($\tilde{T}_{f,cr} = \tilde{T}_I$), the system preheat temperature term dominates as $\tilde{T}_I$ is likely to be close to $\tilde{T}_\circ$. For extinction ($\tilde{T}_{f,cr} = \tilde{T}_E$), $\tilde{T}_E$ is likely close to $\tilde{T}_{ad}$ and the composition term will heavily influence Equation (14) as opposed to the smaller preheat temperature term. This implies that reaching the ignition state is directly affected by the heat loss of the system whereas the extinction state is affected by the composition of the system or, rather, the ability of the system to sustain chain-branching and propagating reactions.

Equation (14) may be rearranged to give a general expression for the critical temperature (both ignition and extinction) in quadratic form:

$$\frac{\tilde{T}_{ad} - \tilde{T}_{f,cr} + \tilde{T}_{f,cr} - \tilde{T}_\circ}{\tilde{T}_{ad}\tilde{T}_{f,cr} - \tilde{T}_{f,cr}^2 - \tilde{T}_\circ\tilde{T}_{ad} + \tilde{T}_\circ\tilde{T}_{f,cr}} = \tilde{T}_a\frac{1}{\tilde{T}_{f,cr}^2} \tag{15}$$

$$\frac{\tilde{T}_{f,cr}^2}{\tilde{T}_a} = \frac{-\tilde{T}_{f,cr}^2 + (\tilde{T}_\circ + \tilde{T}_{ad})\tilde{T}_{f,cr} - \tilde{T}_\circ\tilde{T}_{ad}}{\tilde{T}_{ad} - \tilde{T}_\circ} \tag{16}$$

Solving Equation 16 for the root $\tilde{T}_{f,cr}$ gives:

$$\left(\frac{1}{\tilde{T}_a} + \frac{1}{\tilde{T}_{ad} - \tilde{T}_\circ}\right)\tilde{T}_{f,cr}^2 - \frac{\tilde{T}_\circ + \tilde{T}_{ad}}{\tilde{T}_{ad} - \tilde{T}_\circ}\tilde{T}_{f,cr} + \frac{\tilde{T}_\circ\tilde{T}_{ad}}{\tilde{T}_{ad} - \tilde{T}_\circ} = 0 \tag{17}$$

which, through the substitution of $\tilde{T}_{ad} = \tilde{T}_\circ + 1$, leads to the following quadratic equation and the determination of $\tilde{T}_{f,cr}$ as a root:

$$\left(1 + \frac{1}{\tilde{T}_a}\right)\tilde{T}_{f,cr}^2 - \left(\tilde{T}_\circ + \tilde{T}_{ad}\right)\tilde{T}_{f,cr} + \tilde{T}_\circ\left(1 + \tilde{T}_\circ\right) = 0 \tag{18}$$

$$\tilde{T}_{f,cr} = \frac{(\tilde{T}_{ad} + \tilde{T}_\circ) \pm \sqrt{1 - 4(\tilde{T}_\circ\tilde{T}_{ad}/\tilde{T}_a)}}{2(1 + 1/\tilde{T}_a)} \tag{19}$$

$\tilde{T}_{f,cr}$ only exists, from Equation (19), if the term under the square root is positive. This means that, in order for a combustion system to behave with critical extinction or ignition phenomena, the system must meet the condition:

$$\tilde{T}_a \geq 4\tilde{T}_\circ(1 + \tilde{T}_\circ) \tag{20}$$

This condition is useful when considering the definition of the MILD combustion regime. It links the system preheat temperature, $T_\circ$, and composition, the non-dimensionalizing terms of $\tilde{T}_\circ$ ($c_p$ and $Y_F$), to the activation energy of the system, $\tilde{T}_a$, as criteria for critical phenomena manifested as inflection points on a folded S-Shaped Curve. This means that the limit phenomena of a system may be estimated solely by its composition and preheat characteristics, two already well-defined MILD parameters. If the condition outlined by Equation (20) is not fulfilled, the S-Shaped Curve cannot contain any inflection points and the system will not exhibit any sudden extinction behavior.

[1]Recall that, from Equation (8), $\tilde{T} - \tilde{T}_\circ = 1 - \tilde{c}_F$. Further, through the application of conservation of energy across a flame with no heat loss and constant $c_p$, $c_p(T_{ad} - T_\circ) = qY_F$ and, non-dimensionalized, $\tilde{T}_\circ + 1 = \tilde{T}_{ad}$).

## 3. CRITICAL PHENOMENA IN THE MILD REGIME

### 3.1. Laminar Counterflow $CH_4$-Hot Product Flames

This result may be easily applied to combustion systems meeting MILD criteria by considering counterflow flames with hot combustion product as an oxidiser presented in Sidey and Mastorakos (2016) and mixtures of varying dilution in Sidey et al. (2014). This analysis may begin with the assumption that a reduced global one-step methane reaction, given below with a corresponding activation temperature, $T_a$, is suitable to approximate MILD system chemistry.

$$CH_4 + 2O_2 \rightarrow CO_2 + 2H_2O \qquad T_a = 24356\ K$$
Westbrook and Dryer (1981) (21)

This assumption carries implications for the present analysis. Obviously considering the results of Sidey and Mastorakos (2016) and Sidey et al. (2014), the presence of hot combustion products in MILD systems affects the activation temperature. In particular, the presence of radical species in the oxidiser may significantly encourage ignition. The effects of radical species are not included in the global, one-step reaction considered here. This analysis is therefore limited in its application, and may only be used as an exercise to understand the behavior of some MILD systems rather than a rigorous chemical tool.

Note that the use of this chemistry in this work is not a statement that complex chemistry is not required for MILD combustion. However, many complex combustion phenomena may be adequately understood through a 1-step chemistry description, including the well-known bending behavior of turbulent flame speed vs. turbulent intensity in Nivarti and Cant (2017). This does not mean that complex chemistry is not needed to understand the details of such phenomenon, but that the high activation energy concept still has usefulness in characterizing combustion from a theoretical perspective. While performing a series of calculations with complex chemistry we would locate the transition from sudden extinction to no sudden extinction more accurately in parameter space in this work, the transition distance is not substantially large. Further, considering the development of 1-step models tune activation energy in order to describe global combustion parameters like flame speed or extinction strain rate, a global chemistry framework is appropriate within the context of this work.

Recalling the definitions of the stoichiometrically weighted non-dimensionalized temperature terms, Equation (20) may be written as:

$$\frac{c_p T_a}{qY_F} \geq 4\frac{c_p T_\circ}{qY_F}\left(1 + \frac{c_p T_\circ}{qY_F}\right) \tag{22}$$

First considering the $CH_4$-hot product flames, $q = 50100\ KJ/kg$ and values for $c_p$, $T_\circ$, and $Y_F$, given in **Table 1**, are obtained from the composition of the MILD counterflow systems presented in Sidey and Mastorakos (2016). Note that the value for $Y_F$ is taken to be $Y_{F,stoic}$ from the reaction of $CH_4$ and hot products, assumed to be $H_2O$, $CO_2$, $N_2$, and $O_2$. $T_\circ$ is taken to be the equilibrium mixing, or frozen, temperature of $CH_4$ and hot combustion products mixed in stoichiometric quantities. As the conditions in **Table 1** and $T_a$ the one-step reaction of methane (Reaction 21) are substituted into (Equation 20), it becomes clear that, for extensively preheated and diluted systems, the condition in Equation (20) is not satisfied. This result is presented graphically in **Figure 3**. The equality in Equation (20) is plotted as a solid line in **Figure 3**: any system operating above this line will have a folded S-Shaped Curve while anything below it does not meet the aforementioned condition and will have a monotonic S-Shaped Curve.

Note that each of the cases examined in this analysis will have a $\tilde{T}_a = 4\tilde{T}_\circ(1 + \tilde{T}_\circ)$ curve, although they do not differ from each other significantly. The conventional, non-preheated, stoichiometric, $CH_4$-air system, marked "Conv.," and a preheated, stoichiometric, $CH_4$-air system, marked "Preheat," both lie within the folded S-Shaped Curve region on **Figure 3**. The $CH_4$ heavily diluted MILD combustion systems, or cases

**TABLE 1 |** Quantities relating to the counterflow systems in Sidey and Mastorakos (2016) relevant to the critical phenomena condition (Equation 20).

| Case | $c_p$ $kJ/kgK$ | $Y_{F,stoic}$ | $c_p/qY_{F,stoic}$ $K^{-1}$ | $T_\circ$ $K$ |
|---|---|---|---|---|
| Conventional | 1.075 | 0.05500 | 0.0004 | 298 |
| 0.6 | 1.593 | 0.02187 | 0.0015 | 1408 |
| 0.7 | 1.479 | 0.01621 | 0.0018 | 1731 |
| 0.8 | 1.493 | 0.01060 | 0.0028 | 1920 |
| 0.9 | 1.503 | 0.00534 | 0.0056 | 2097 |

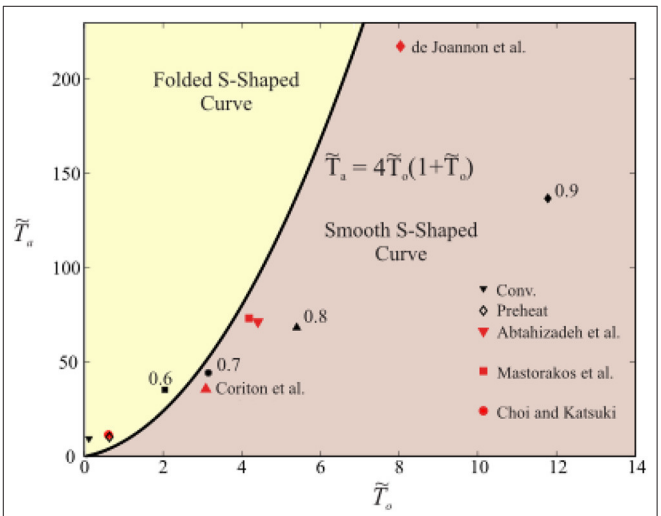


**FIGURE 3 |** A plot of the function defining the requirement for the existence of critical points or a folded S-Shaped Curve in a $CH_4$ combustion system, Equation (20), and points from $CH_4$/hot product simulations presented in Sidey et al. (2014) and highly diluted cases from Coriton et al. (2010), Abtahizadeh et al. (2012), Mastorakos et al. (1995), Choi and Katsuki (2002), and de Joannon et al. (2012).

with $\Phi = 0.7, 0.8$, and 0.9 hot combustion products as an oxidiser, approximated through this analysis do not have folded S-Shaped Curves. This analysis is extended to similar counterflow non-premixed and premixed studies in the literature, with each symbol marked with its respective reference. The most heavily diluted cases presented by de Joannon et al. (2012) (preheated and diluted $CH_4/N_2$ and air), Mastorakos et al. (1995) ($CH_4$-vitiated air at 1,750 K), Coriton et al. (2010) ($CH_4$/air and 2,200 K hot products), and Abtahizadeh (Abtahizadeh et al., 2012) ($CH_4$-vitiated air at 1415 K) all lie within the region of monotonic S-Shaped Curves in agreement with the findings reported in their associated references. The Choi and Katsuki (2002) case ($CH_4$-vitiated air, diluted 20–50% by mole fraction) lies in the folded S-Shaped Curve region. This is due to the relatively low initial temperature of the oxidiser, $T_o$, and low level of dilution in comparison with the other studies presented here. However, Choi and Katsuki (2002) still reported on the absence of typical extinction behavior at these conditions. This discrepancy may be associated with the approximations made in this analysis, particularly the estimation of $Y_{F,stoic}$ from values reported in the literature.

These results suggest that systems with extensive hot product recirculation do not extinguish suddenly even under heavily strained conditions. Instead, they would exhibit smooth transition behavior between intensely burning and near-frozen states. This behavior is dependent on both preheat temperature and dilution, evidenced by the typical extinction behavior of the case with preheated, undiluted air as an oxidiser ("Preheat"). This is approximately consistent with estimations made by Smooke et al. (1991) and Mastorakos et al. (1995) that no extinction behavior occurs when a hot product stream is heated above 1,480 K or 1,550 K, respectively.

The above quantification of the boundary separating the folded vs. monotonic behavior is sensitive mostly to the value used for activation energy, $T_a$. An increase or decrease of $T_a$ by 10% does not change the results presented here. In other words, each study presented in **Figure 3** remains in either the folded or smooth s-shaped curve area of the figure if the $T_a$ were altered by 10%. Sensitivity analysis shows that a 20-25% variation in $T_a$ may result in substantial enough changes to make a particular estimate of an experimental condition to jump from a non-folded to a folded regime. But such large uncertainties in the activation energy in the fuels used here are not expected, given the usual accuracy in the empirical 1-step models concerning flame speed or extinction strain rate.

This is in agreement with the numerical result discussed in Sidey and Mastorakos (2016); heavily diluted and preheated counterflow flames do not exhibit critical extinction behavior even at very high strain rates. The results may be viewed in the context of this analysis by plotting the inverse of strain rate, $1/A$, a metric indicative of residence versus reaction time, or Damköhler number, and maximum temperature. In **Figure 4**, the S-Shaped Curves of $CH_4$ (left) and kerosene (right) conventional and MILD counterflow flames are plotted. For the $CH_4$-oxidant systems where an extinction strain rate does exist ($CH_4$ burning with air, $\Phi$ = 0.6, 0.7 hot products), the S-Shaped Curve is folded with multiple solutions on distinct burning and weakly reaction branches. The unsteady region connecting the two branches is not plotted as it does not exert a physical presence within the system, and the intensely burning branch simply jumps to a frozen solution when sudden extinction occurs. These results are in partial agreement with those arising from the analysis based on Equation (20), with error in the prediction of $\Phi = 0.7$ case behavior likely due to the assumption of a global one-step reaction and estimation of $T_a$. The highly diluted ($\Phi$ = 0.8, 0.9 hot product oxidiser) cases do not show any sudden extinction behavior and, as predicted by **Figure 3**, exhibit monotonic S-Shaped Curves devoid of unsteady regions.

Similarly to $CH_4$ conventional flames, kerosene flames with air as an oxidiser suddenly extinguish at a specified strain rate, and therefore have a folded S-Shaped Curve. S-Shaped Curves for MILD kerosene counterflow flames at above atmospheric pressures are all smooth, indicating that there is an absence of extinction behavior in MILD kerosene systems and that this behavior is not pressure dependent. Based on results for $CH_4$ systems, it is reasonable to expect that, with estimates of kerosene $T_a$ and $T_\circ$, $c_p$, and $Y_{F,stoic}$ for kerosene-0.6 hot products counterflow flames, these systems would not meet the conditions for a folded S-Shaped Curve and therefore lie below the function plotted on **Figure 3**.

## 3.2. Premixed $CH_4$-Air-Hot Product Reactants of Varying Dilution, $\zeta$

This analysis may also be applied to the mixtures of $CH_4$, air, and hot combustion products, the composition of which is designated by a dilution variable, defined in Sidey and Mastorakos (2016). Although the autoignition and premixed flame systems presented in Sidey et al. (2014) are fundamentally inapplicable to a discussion on extinction considering they are unstrained, the mixtures of varying dilution studied in these systems is. If in a strained system, these mixtures are representative of cases in which fresh reactants are mixed hot combustion products in varying degrees, similar to those discussed in Mastorakos et al. (1995), Smooke et al. (1991), Darabiha et al. (1988), and Darabiha and Candel (1992).

As explained in detail in Sidey et al. (2014), these mixtures are obtained by mixing cold, fresh reactants of a specified equivalence ratio ($\Phi = 0.6, 1.0$, and 1.3 from Sidey et al. (2014), with the addition of $\Phi = 0.7, 0.8$, and 0.9 allowing for a comparison with the lean counterflow flame cases discussed here) adiabatically with hot combustion products from a premixed flame of the same equivalence ratio. The result is a series of $CH_4$-air-hot product mixtures of varying dilution, $\zeta$. A low $\zeta$ defines a mixture of mostly fresh reactants while high $\zeta$ indicates a high fraction of hot combustion products: $\zeta = 0.2$ is defined as a mixture of 20% hot combustion products and 80% cold reactants.

The mixture preheat temperature, $T_\circ$, is plotted against $X_{O2}$ in **Figure 5** for each dilution case. The two are linked such that as the fraction of hot combustion products in the mixture, or $\zeta$, increases, $X_{O2}$ is reduced and the bulk temperature of the mixture increases. For low levels of dilution, each case satisfies the condition for critical points on the S-Shaped Curve (Equation 20). However, as $T_\circ$ increases and $O_2$ available for

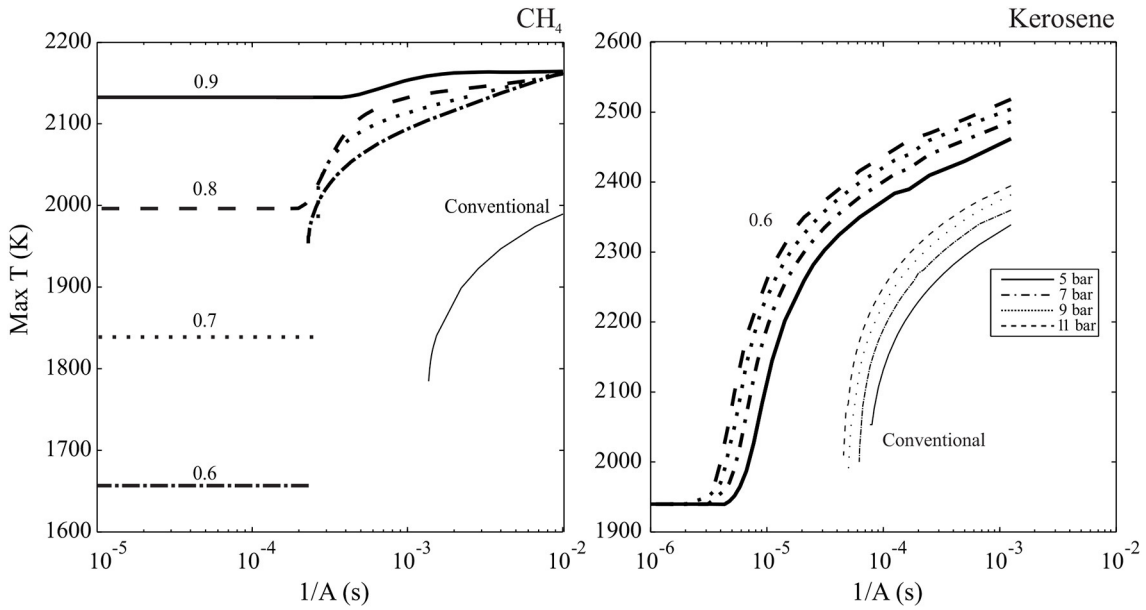


**FIGURE 4 |** Maximum temperature of methane **(Left)** and kerosene **(Right)** counterflow MILD (bold, marked with equivalence ratio of hot combustion product oxidiser) and conventional flames varying with strain rate, $A$, from Sidey et al. (2016) and Sidey and Mastorakos (2015).

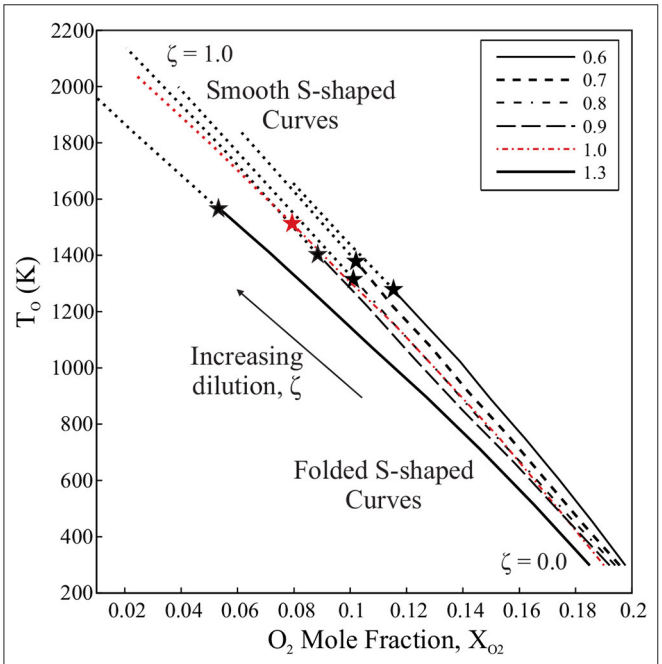


**FIGURE 5 |** S-Shaped Curve behavior for mixtures of increasing hot product dilution, $\zeta$ based on the mixing procedure of Sidey et al. (2014). Patterned, bold lines mark regions where mixtures satisfy the condition for a folded S-Shaped Curve, while dotted lines regions where mixtures fail to satisfy Equation 20, suggesting smooth S-Shaped Curve behavior. The "⋆" symbols mark the point of transition from folded to smooth S-Shaped Curves.

reaction is reduced, the critical points on each mixture's S-Shaped Curve disappear, marked with a transition from a bold, patterned to dotted line in **Figure 5**. The point of this transition is marked with a "⋆" symbol for each case. The conditions at which the loss of critical points is estimated by this analysis are summarized in **Table 2**. Note that both $T_\circ$ and composition ($Y_F$ and $X_{O2}$) affect the existence of sudden extinction behavior for each dilution case. Despite this, each equivalence ratio case seems to transition into a region characterized by smooth S-Shaped Curves at a dilution ratio of $\zeta = 0.7$ or 0.8, or, rather, a hot product fraction of 70–80% by mass. If considering the suggestion by Darabiha et al. (1988) and Darabiha and Candel (1992) that sudden extinction events cease to occur when preheat temperature approaches adiabatic flame temperature, it is worthwhile to note that the S-Shaped Curves of the mixtures in **Figure 5** become smooth within 550 K of each case's adiabatic flame temperature or around 1,400 K.

It is also worthwhile to note that, in Sidey et al. (2014), premixed flame simulations failed to converge due to a tendency of the diluted mixture to autoignite at the cold boundary at a dilution ratio varying from $\zeta = 0.6$ to 0.7. This limit coincides with the emergence of elongated ignition events visible in the

**TABLE 2 |** Dilution characteristics for which the condition in Equation (20) is not met and diluted mixtures are described by smooth S-Shaped Curves (see **Figure 5**).

| Case | $Y_F$ | $T_\circ$ K | $X_{O2}$ | $\zeta$ |
|---|---|---|---|---|
| 0.6 | 0.0067 | 1410 | 0.1030 | 0.8 |
| 0.7 | 0.0082 | 1530 | 0.0886 | 0.8 |
| 0.8 | 0.0125 | 1490 | 0.0853 | 0.7 |
| 0.9 | 0.0124 | 1580 | 0.0716 | 0.7 |
| 1.0 | 0.0165 | 1700 | 0.0603 | 0.7 |
| 1.3 | 0.0141 | 1730 | 0.0352 | 0.8 |

PFR results, also in Sidey et al. (2014). From these comparisons, it is clear that a shift in autoignition, propagation, and limit phenomena behavior all seem to occur in agreement with the non-existence of critical points on a diluted and preheated system's S-Shaped Curve as predicted by the condition in Equation (20).

## 4. DISCUSSION

In this work, the existence of sudden limit behavior in highly preheated and diluted systems is investigated. The lack of sudden extinction phenomena of combustion systems involving significant dilution and subsequent mixing with hot combustion products has been reported in numerical and experimental investigations, including Libby and Williams (1983), Smooke et al. (1991), Darabiha et al. (1988), Darabiha and Candel (1992), Bray et al. (1996), and Mastorakos et al. (1995). Its understanding and prediction is not only useful for the application of such concepts in practical devices, but for further definition of the MILD combustion regime and is perhaps most accessible through S-Shaped Curve theory. Through the derivation of an expression linking burning rate to Damköhler number in a WSR, the criteria for a folded S-Shaped Curve, representative of a combustion system with sudden extinction and ignition behavior, was developed in Law (2006). This condition, $\tilde{T}_a \geq 4\tilde{T}_\circ(1+\tilde{T}_\circ)$, was used to assess the existence of a folded vs. monotonic S-Shaped Curve in the non-premixed counterflow $CH_4$-air cases in Sidey et al. (2014). The simulation results agreed well with predicted S-Shaped Curve behavior, with the exception of the case in which fuel was burned in $\Phi = 0.7$ hot combustion product oxidiser, although this is likely due to the estimation of $CH_4$ activation temperature, $T_a$, through a global one-step oxidation reaction. The limits of the existence of critical points on the S-Shaped Curve agreed well with estimations made by Smooke et al. (1991) and Mastorakos et al. (1995). Although these results are of interest, they should not be taken as a rigorous explanation of the MILD regime as the chemical complexity of systems involving hot combustion products has been significantly simplified with the assumption of a one-step, global reaction. Despite this, within strict limitations, this analysis provides interesting insight into the limit behavior of MILD systems.

Mixtures of varying dilution based on those examined in unstrained premixed systems in Sidey et al. (2014) were also investigated in this analysis. Although no specific mixture temperature, $T_\circ$, or $O_2$ content, $X_{O2}$, was found to be transition point from folded to smooth S-Shaped Curve behavior, the S-Shaped Curve behavior of all the cases investigated here became monotonic at a once diluted with 70-80% hot combustion products ($\zeta = 0.7, 0.8$). Although this result is not directly applicable to unstrained premixed configurations which do not allow for extinction behavior, it is worthwhile to note that this limit of folded S-Shaped Curve behavior coincides well with the limit of the mixture's ability to support a freely propagating laminar flame. Furthermore, the emergence of monotonic S-Shaped Curve behavior coincides with the elongation of a mixture's primary autoignition event in a premixed system.

Supported by results from Sidey and Mastorakos (2016) and Sidey et al. (2014), it may be assumed that, as acknowledged by Cavaliere and de Joannon (2004), the MILD regime is characterized by a monotonic S-Shaped Curve. This result is accurately predicted by the (Liñán, 1974) analysis assessing the existence of turning points in a system's S-Shaped Curve. This theoretical result validates the numerical and experimental observation that MILD systems do not undergo sudden extinction behavior, even at very high rates of strain.

## 5. CONCLUSIONS

The lack of sudden extinction behavior and the ignition tendencies in heavily preheated and diluted strained non-premixed systems and unstrained premixed systems raises questions about critical phenomena in the MILD combustion regime. This work presents an analysis based on the existence of critical phenomena in conventional combustion systems, manifested as a folded S-Shaped Curve on a burning rate vs. Damköhler number plot. This analysis is limited in its application as it is unable to capture the effect of complex chemistry introduced by the presence of radical species in MILD systems. However, it provides a useful context as a first step for considering such systems and, although it over simplifies the definition of activation temperature, provides interesting insight into preheated and diluted combustion. It shows that, for heavily diluted and preheated $CH_4$ combustion systems, sudden extinction phenomena cannot occur and the system behavior is described by a monotonic S-Shaped Curve.

The choice of employing simple chemistry should be thought of as a choice to use high-activation energy concepts as a useful tool for as characterizing combustion from a theoretical perspective. This adds an important perspective for understanding MILD combustion; if one employs this high-activation energy theory to various experimental configurations reported in the literature as MILD, one sees that these studies fall in a different part of the catastrophe surface. Within this analysis, critical phenomena of the mixtures investigated here ceased to exist at a level of dilution which corresponded to the point at which the mixtures were deemed to become MILD according to the autoignition and premixed flame analysis in Sidey et al. (2014). It follows that the extinction vs. no extinction behavior presented here may be used as a tool to delineate MILD combustion regimes from conventional ones.

## DATA AVAILABILITY STATEMENT

The datasets generated for this study are available on request to the corresponding author.

## AUTHOR CONTRIBUTIONS

JS-G contributed to the theoretical development and writing of this work. EM contributed to the theoretical development and background of this work.

## FUNDING

JS-G would like to acknowledge funding by Rolls-Royce Canada, the Cambridge Overseas Trust, Jesus College Cambridge, and the National Research Council of Canada. The funders were not involved in the study design, collection, analysis, interpretation of data, the writing of this article or the decision to submit it for publication.

## REFERENCES

Abtahizadeh, E., van Oijen, J., and de Goey, P. (2012). Numerical study of MILD combustion with entrainment of burned gas into oxidizer and/or fuel streams. *Combust. Flame* 159, 2155–2165. doi: 10.1016/j.combustflame.2012.02.004

Bray, K. N. C., Champion, M., and Libby, P. A. (1996). Extinction of premixed flames in turbulent counterflowing streams with unequal enthalpies. *Combust. Flame* 107, 53–64.

Cavaliere, A., and de Joannon, M. (2004). MILD combustion. *Prog. Energy Combust. Sci.* 30, 329–366. doi: 10.1016/j.pecs.2004.02.003

Choi, G., and Katsuki, M. (2002). Chemical kinetic study on the reduction of nitric oxide in highly preheated air combustion. *Proc. Combust. Inst.* 29, 1165–1171. doi: 10.1016/S1540-7489(02)80147-X

Coriton, B., Frank, J. H., and Gomez, A. (2013). Effects of strain rate, turbulence, reactant stoichiometry and heat losses on the interaction of turbulent premixed flames with stoichiometric counterflowing combustion products. *Combust. Flame* 160, 2442–2456. doi: 10.1016/j.combustflame.2013.05.009

Coriton, B., Smooke, M. D., and Gomez, A. (2010). Effect of the composition of the hot product stream in the quasi-steady extinction of strained premixed flames. *Combust. Flame* 157, 2155–2164. doi: 10.1016/j.combustflame.2010.05.002

Darabiha, N., and Candel, S. (1992). The influence of the temperature on extinction and ignition limits of strained hydrogen-air diffusion flames. *Combust. Sci. Technol.* 86, 67–85.

Darabiha, N., Candel, S., Giovangigli, V., and Smooke, M. D. (1988). Extinction of strained premixed propane-air flames with complex chemistry. *Combust. Sci. Technol.* 60, 267–285.

de Joannon, M., Sorrentino, G., and Cavaliere, A. (2012). MILD combustion in diffusion-controlled regimes of hot diluted fuel. *Combust. Flame* 159, 1832–1839. doi: 10.1016/j.combustflame.2012.01.013

Law, C. K. (2006). *Combustion Physics*. New York, NY: Cambridge University Press.

Libby, P. A., and Williams, F. A. (1983). Strained premixed laminar flames under nonadiabatic conditions. *Combust. Sci. Technol.* 31, 1–42.

Liñán, A. (1974). The asymptotic structure of counterflow diffusion flames for large activation energies. *Acta Astronaut.* 1, 1007–1039.

Longwell, J. P., and Weiss, M. A. (1955). High temperature reaction rates in hydrocarbon combustion. *J. Ind. Eng. Chem.* 47, 1634–1643.

Mastorakos, E., Taylor, A. M. K. P., and Whitelaw, J. H. (1995). Extinction of turbulent counterflow flames with reactants diluted by hot products. *Combust. Flame* 102, 101–114.

Medwell, P. R., Kalt, P. A. M., and Dally, B. B. (2007). Simultaneous imaging of OH, formaldehyde, and temperature of turbulent nonpremixed jet flames in a heated and diluted coflow. *Combust. Flame* 148, 48–61. doi: 10.1016/j.combustflame.2006.10.002

Nivarti, G., and Cant, S. (2017). Direct numerical simulation of the bending effect in turbulent premixed flames. *Proc. Combust. Inst.* 36, 1903–1910. doi: 10.1016/j.proci.2016.07.076

Sidey, J., Gordon, R., and Mastorakos, E. (2014). Simulations of autoignition and laminar premixed flames in methane/air mixutres diulted with hot products. *Combust. Sci. Technol.* 186, 453–465. doi: 10.1080/00102202.2014.883217

Sidey, J., and Mastorakos, E. (2015). Visualization of MILD combustion from jets in cross-flow. *Proc. Combust. Inst.* 35, 3537–3545. doi: 10.1016/j.proci.2014.07.028

Sidey, J. A., Giusti, A., and Mastorakos, E. (2016). Simulations of laminar non-premixed flames of kerosene with hot combustion products as oxidiser. *Combust. Theory Model.* 20, 958–973. doi: 10.1080/13647830.2016.1201146

Sidey, J. A., and Mastorakos, E. (2016). Simulations of laminar non-premixed flames of methane with hot combustion products as oxidiser. *Combust. Flame* 163, 1–11. doi: 10.1016/j.combustflame.2015.07.034

Smooke, M., Crump, J., Seshadri, K., and Giovangigli, V. (1991). Comparison between experimental measurements and numerical calculations of the structure of counterflow, diluted, methane-air, premixed flames. *Proc. Combust. Inst.* 23, 463–470. doi: 10.1016/S0082-0784(06)80292-4

Westbrook, C. K., and Dryer, F. L. (1981). Simplified reaction mechanisms for the oxidation of hydrocarbon fuels in flames. *Combust. Sci. Technol.* 27, 31–43.

**Conflict of Interest:** The authors declare that the research was conducted in the absence of any commercial or financial relationships that could be construed as a potential conflict of interest.

## NOMENCLATURE

| | |
|---|---|
| $B$ | Constant |
| $c$ | Molar concentration |
| $D_a$ | Damköhler number |
| $Q$ | Heat release |
| $T$ | Temperature |
| $T_a$ | Activation temperature |
| $T_f$ | Flame or reaction zone temperature |
| $T_\circ$ | Initial temperature |
| $V$ | Reactor volume |
| $\rho$ | Density |
| $\tau_c$ | Characteristic reaction time |
| $\tau_m$ | Characteristic diffusion or flow time |
| $cr$ | Critical point |
| $E, I$ | Extinction and Ignition, respectively |
| $f$ | Flame or reaction zone |
| $\circ$ | Initial |
| $LHS$ | left hand side |
| $RHS$ | right hand side |

frontiers in Mechanical Engineering

ORIGINAL RESEARCH
published: 13 February 2020
doi: 10.3389/fmech.2020.00006

# Modeling Temperature Variations in MILD Combustion Using MuSt-FGM

*M. Ugur Göktolga*, Philip de Goey and Jeroen van Oijen*

*Power and Flow, Mechanical Engineering, Eindhoven University of Technology, Eindhoven, Netherlands*

The energy demand in the world is ever increasing, and for some applications combustion is still the only reliable source, and will remain as such in the foreseeable future. To be able to mitigate the environmental effects of combustion, we need to move to cleaner technologies. Moderate or intense low oxygen dilution (MILD) combustion is one of these technologies, which offer less harmful emissions, especially nitric oxide and nitrogen dioxide (NOx). It is achieved by the recirculation of the flue gases into the fresh reactants, reducing the oxygen content, and thereby causing the oxidation reactions to occur at a milder pace, as the acronym suggests. This results in a flameless combustion process and reduces the harmful emissions to negligible amounts. To assist in the design and development of combustors that work in the MILD regime, reliable and efficient models are required. In this study, modeling of the effects of temperature variation in the oxidizer of a MILD combustion case is tackled. The turbulent scales are fully resolved by performing direct numerical simulations (DNS), and chemistry is modeled using multistage flamelet generated manifolds (MuSt-FGM). In order to model the temperature variations, a passive scalar which is created by normalizing the initial temperature in the oxidizer is defined as a new control variable. During flamelet creation, it was observed that not all the compositions are autoigniting. Several approaches are proposed to solve this issue. The results from these cases are compared against the ones performed using detailed chemistry. With the best performing approach, the ignition delay is predicted fairly well, but the average heat release rate is over-predicted. Some possible causes of this mismatch are also given in the discussion.

**Keywords: multistage FGM, MILD combustion, temperature variations, DNS, jet in hot coflow**

OPEN ACCESS

***Edited by:***
*Mara de Joannon,*
*Istituto di Ricerche sulla Combustione (IRC), Italy*

***Reviewed by:***
*Shiyou Yang,*
*Ford Motor Company, United States*
*Kan Zha,*
*Sandia National Laboratories (SNL), United States*

****Correspondence:***
*M. Ugur Göktolga*
*m.u.goktolga@tue.nl*

***Specialty section:***
*This article was submitted to Thermal and Mass Transport, a section of the journal Frontiers in Mechanical Engineering*

***Received:*** *07 October 2020*
***Accepted:*** *24 January 2020*
***Published:*** *13 February 2020*

***Citation:***
*Göktolga MU, de Goey P and van Oijen J (2020) Modeling Temperature Variations in MILD Combustion Using MuSt-FGM. Front. Mech. Eng. 6:6. doi: 10.3389/fmech.2020.00006*

## 1. INTRODUCTION

Moderate or intense low oxygen dilution (MILD) combustion is a relatively new technology that provides low emissions and high efficiency. The basic idea in MILD combustion is to recirculate the burned flue gases back, mix them with the reactants so that the combustion occurs at a milder rate (as the acronym suggests), and the temperature increase is much lower than in a conventional flame. It provides high efficiency, and reduces the emissions of CO, $SO_x$, soot, and especially $NO_x$ (Cavaliere and de Joannon, 2004; Derudi and Rota, 2011; De Joannon et al., 2012), owing to lower flame temperatures. There are different definitions of MILD combustion in the literature. Cavaliere and de Joannon (2004) define MILD combustion as the combustion mode where the temperature of the reactants are high enough to autoignite, and the temperature increase in the combustor is less than the autoignition temperature in Kelvin.

Wünning and Wünning (1997) make the distinction based on the furnace temperature and exhaust recirculation rate. More recently, Evans et al. (2017) came up with a new definition based on the unique S-curve of MILD combustion: there are no jumps between ignition and extinction events but a continuous ignition curve. They analyzed different premixed and non-premixed MILD cases and have shown that their definition agreed well with the experimental observations of gradual ignition in MILD conditions. Even though there are some discussions on which definition suits MILD combustion the best, overall characteristics are nevertheless well agreed on.

The beneficial characteristics of MILD combustion attracted attention from the combustion research and development communities. It has been applied to the steel and metallurgy industries starting from the 1990s (Li et al., 2011). More recently, opportunities of applying MILD combustion to gas turbines (Duwig et al., 2007; Albin et al., 2015; Kruse et al., 2015; Perpignan et al., 2018) and gasification processes (Tang et al., 2010) have been investigated. However, potential of MILD combustion is beyond these applications, as mentioned in Li et al. (2011). Therefore, additional efforts need to be made to fully understand the physical mechanisms in MILD combustion, and thereby expand its application areas and fulfill its potential.

To explore the physical mechanisms of MILD combustion, numerous experimental studies have been performed, with lab scale burners of different complexities. One of the most used configurations is the jet in hot coflow (JHC) configuration, where a hot and diluted oxidizer is created using a secondary burner, and a fuel jet is issued into this diluted oxidizer. Fuel and oxidizer mix via diffusion and entrainment, and the flame is stabilized by autoignition at a certain distance from the fuel nozzle. This way, the diluted nature of MILD combustion is imitated, without the need for real exhaust gas recirculation. The JHC configuration was utilized in both laminar (Sepman et al., 2013a,b) and turbulent conditions (Dally et al., 2002; Oldenhof et al., 2011; Duwig et al., 2012; Ma and Roekaerts, 2016) to achieve MILD combustion.

MILD combustion has been studied extensively using computational fluid dynamics (CFD) as well. Abtahizadeh et al. and Sepman et al. investigated the laminar JHC burner from University of Groningen using detailed chemistry (Abtahizadeh et al., 2013; Sepman et al., 2013b). In the former study, the effects of preheating and dilution were investigated, and it was found that in the presence of both preheating and dilution, the flame transitions into the MILD regime, and stabilizes via autoignition. In the latter study, it was demonstrated that the MILD case emits much less NO compared to the conventional flame. A reasonable agreement between experimental and numerical results was obtained in both cases. De et al. (2011) employed the eddy dissipation concept (EDC) with a Reynolds averaged Navier-Stokes (RANS) model to simulate the JHC experiments from Delft University of Technology (Oldenhof et al., 2011). They predicted the radial profiles of temperature and velocity reasonably well, but failed to match the lift-off heights found in the experiments. Another RANS study to investigate the JHC burner from The University of Adelaide was conducted by Christo and Dally (2005). They employed different turbulence and chemistry models, and concluded that the EDC with the standard k-$\epsilon$ turbulence model produces the best agreement with the experimental results. In addition, they stressed that preferential diffusion effects should be taken into account due to the high hydrogen content in the fuel. There have been several large eddy simulations (LES) of JHC burners as well. Kulkarni and Polifke applied a flamelet/progress variable (FPV) approach and found that the heat losses in the coflow are crucial in determining the lift-off height (Kulkarni and Polifke, 2013). Ihme et al. (2012) employed an FPV formulation with a three stream approach to account for the outermost cold air stream in the experiments from Adelaide. They also tried to fit the controlling variables to accurately represent the species profile of the coflow. In their computations, addition of the third stream yielded satisfactory results in terms of temperature and species profiles. In all the turbulent JHC simulations; turbulence, chemistry, and their interactions were modeled simultaneously. Therefore, it is difficult to judge which part of the modeling effort is failing when the results are not matching well with the experiments.

In order to understand the complex physical and chemical phenomena and their interactions in MILD combustion, detailed calculations need to be performed before any modeling effort. Minamoto et al. carried out the first 3D DNSs of MILD combustion (Minamoto et al., 2013, 2014). They simulated a premixed MILD system whose composition is obtained via 1D laminar flames, and compared the results with a conventional premixed case to examine differences in flame structures. They concluded that there are strong chemically reacting zones in the MILD regime, but unlike traditional premixed flames, the reaction layers are not sheet like and they interact with each other. Although their studies shed light on MILD combustion flame structures for premixed cases, they do not provide any interpretation for spontaneous mixing and chemistry, which is the case in many MILD systems including JHC experiments. van Oijen (2013) performed 2D DNS of autoigniting mixing layers representative of the JHC burner in Dally et al. (2002) and compared the results with 1D diffusive layer simulation results. His results show that the ignition delay times for the diffusive layer simulations and the 2D DNS are almost the same, and they are strongly dependent on preferential diffusion effects. Nevertheless, real turbulence effects could not be reproduced in his study since 2D turbulence lacks vortex stretching phenomena and has an inverse energy cascade. In addition, heat loss and the resulting non-uniform temperature profile of the coflow found in the experiments were not taken into account. In their 3D DNS study, Göktolga et al. (2015) demonstrated that the heat loss effects have a large influence on the ignition delay, and even in 3D turbulence the effects of preferential diffusion are still of utmost importance. Furthermore, they showed that due to flame curvature-preferential diffusion interactions, the species scatter differently in the composition space. More recently, Doan et al. (2018) investigated a MILD combustion case with 3D DNS, including mixture fraction and chemical progress variations in the inflow boundary conditions. They found out that ignition front, premixed flames, and non-premixed flames all coexist, without the presence of triple flame structures. Swaminathan (2019) has recently compiled the DNS works on

MILD combustion. He concludes that the reactions zones in MILD combustion display autoignition characteristics of both non-premixed and premixed flames. He further deduces that reaction regions can be seen as homogeneous reactors and thus can be modeled accurately with tabulated chemistry using perfectly stirred reactors as canonical flames.

In combustion modeling, it is often the case that the total enthalpy at each mixture fraction does not deviate from the value corresponding to adiabatic mixing. For many cases this is a valid assumption (Cabra et al., 2002; Barlow et al., 2005). However, if there is heat loss through the combustor walls (Lammel et al., 2012), or the flame is considerably radiating (Dally et al., 1998), or there are heat losses even before the mixture enters the combustor (Dally et al., 2002; Mendez et al., 2015); then this assumption is no longer valid and the effects of the enthalpy change need to be modeled. In the context of flamelet based chemistry tabulation methods such as flamelet/progress variable (FPV) (Pierce and Moin, 2004), flame prolongation of ILDM (FPI) (Gicquel et al., 2000), and FGM; the most often used approach is to utilize the enthalpy as an additional control variable (Fiorina et al., 2003; Ihme and Pitsch, 2008; Donini et al., 2013).

In this study, the conditions to simulate are selected as the HM1 case of the Adelaide JHC case (Dally et al., 2002), because it is shown to operate in MILD combustion. In those experiments, there is a large variation in the oxidizer temperature when the oxidizer enters the primary combustor, because of the cooling jacket around the fuel (Dally et al., 2002). In some studies, this effect was completely ignored (Afarin and Tabejamaat, 2013; Chen et al., 2017). However, it was shown in Göktolga et al. (2015) that this temperature variation is of utmost importance for the ignition delay and related chemistry. Therefore, to have an accurate description of this case, taking the species and especially temperature variations in the oxidizer into account is a must, as has been addressed by several studies before (Ihme and See, 2011; Ihme et al., 2012; Sarras et al., 2014; Ma and Roekaerts, 2016). Ihme and See (2011) have utilized a three stream FPV approach to include the effects of the air shroud present in the Adelaide JHC experiments. They have introduced an extra control variable called oxidizer split, which was set to 0 and 1 for the diluted coflow and air shroud regions, respectively. By varying the progress variable and the oxidizer split in the coflow region, they included the temperature and species variations in the coflow. They applied this approach to simulate the HM3 ($Y_{O_2} = 9\%$) case of the Adelaide JHC case, and later their work was extended by Ihme et al. (2012) to model the HM1 and HM2 ($Y_{O_2} = 3\%$ and $Y_{O_2} = 6\%$, respectively) cases as well. Sarras et al. (2014) also introduced an extra mixture fraction to take the oxygen variations in the coflow, and further utilized enthalpy deficit to model the temperature variation, to model the Delft JHC burner (Oldenhof et al., 2011). Ma and Roekaerts (2016) used enthalpy directly as a control variable to model the enthalpy deficit due to intense droplet evaporation, to simulate spray combustion operating under MILD conditions.

With ever growing chemical reaction mechanisms, the use of detailed chemistry in 3D computations become more prohibitive despite the advances in computational hardware. Not only are there many species for which the transport equations are solved, but also the time step needed are quite small because of the stiffness of the chemical reactions. There are many chemistry reduction models proposed to decrease the computational requirements. One of them is flamelet generated manifolds (FGM) (van Oijen and de Goey, 2000). In FGM, it is assumed that a 3D flame is composed of 1D flamelets (Peters, 1984); and the composition space can be represented with lower dimensional manifold. To model a flame with FGM; 1D flames are solved, necessary thermo-chemical variables are stored in FGM tables as functions of a few control variables, and then transport equations for only those control variables are solved and required thermo-chemical are retrieved from the FGM tables. Göktolga et al. showed that for MILD combustion, standard FGM cannot model both the pre-ignition and oxidation regions accurately, and proposed a multistage (MuSt) FGM (Göktolga et al., 2017). In this method, different progress variables are used for each combustion stage to capture those stages properly. Because in FGM the diffusion processes are modeled as well, effects like flame propagation can be captured adequately. In Göktolga et al. (2017), it was shown that another very crucial flame stabilization mechanism in MILD combustion, namely the autoignition, can be captured with MuSt-FGM.

The aim of this study to model the effects of temperature variation in the oxidizer of the Adelaide JHC case using MuSt-FGM. In the remaining following sections the numerical methods and simulation setup are detailed, results are presented, and some conclusions are drawn.

## 2. NUMERICAL METHODS AND SIMULATION SETUP

As mentioned earlier, in an FGM study, firstly 1D flamelet calculations are performed. In this study, counter-flow flames with a strain rate of 200 $s^{-1}$ are used as the flamelet type. The details of the counter-flow canonical configuration can be found in Vasavan et al. (2018). The calculations are performed using the 1D flame code called Chem1D (Somers, 1994). As the control variable representing the mixing between the fuel and the oxidizer, transported mixture fraction $Z_t$ is used. Since this is a MuSt-FGM study, the chemical progress for the pre-ignition and oxidation stage are represented by two different progress variables. In this study they are selected as $\mathcal{Y}_1 = Y_{HO_2}$ and $\mathcal{Y}_2 = Y_{H_2O}$, because the fuel in this case contains 50% hydrogen by volume, and thus the reactions are dominated by hydrogen chemistry. Two different tables for the pre-ignition and oxidation region are created with $\mathcal{Y}_1 = Y_{HO_2}$ and $\mathcal{Y}_2 = Y_{H_2O}$, transport equations for both $\mathcal{Y}_1$ and $\mathcal{Y}_2$ are solved simultaneously, and the table lookup is performed depending on which stage the combustion is. Further details of the MuSt-FGM method can be found in Göktolga et al. (2017).

In the DNS calculations, in house developed code (Bastiaans et al., 2001; Groot, 2003; Van Oijen et al., 2007) was used. In the code, fully compressible Navier-Stokes equations are

solved together with the transport equations for control variables, which read:

$$\frac{\partial \rho}{\partial t} + \frac{\partial (\rho u_i)}{\partial x_i} = 0 \tag{1}$$

$$\rho \frac{\partial u_j}{\partial t} + \rho u_i \frac{\partial u_j}{\partial x_i} = -\frac{\partial p}{\partial x_j} + \frac{\partial \sigma_{ij}}{\partial x_i} \tag{2}$$

$$\rho \frac{\partial Z_t}{\partial t} + \rho u_i \frac{\partial Z_t}{\partial x_i} = \frac{\partial}{\partial x_i}\left(\frac{\lambda}{c_p}\frac{\partial Z_t}{\partial x_i}\right), \tag{3}$$

$$\rho \frac{\partial \mathcal{Y}}{\partial t} + \rho u_i \frac{\partial \mathcal{Y}}{\partial x_i} = \frac{\partial}{\partial x_i}\left(\frac{\lambda}{Le_{\mathcal{Y}} c_p}\frac{\partial \mathcal{Y}}{\partial x_i}\right) + \omega_{\mathcal{Y}}, \tag{4}$$

$$\rho c_v \frac{\partial T}{\partial t} + \rho c_v u_i \frac{\partial T}{\partial x_i} = \frac{\partial}{\partial x_i}\left(\lambda \frac{\partial T}{\partial x_i}\right) - p\frac{\partial u_i}{\partial x_i} + \sigma_{ij}\frac{\partial u_i}{\partial x_j} + q \tag{5}$$

where the variables solved for are density $\rho$, velocity $u_j$, transported mixture fraction $Z_t$, progress variable $\mathcal{Y}$, and temperature $T$. $c_v$ and $c_p$ are specific heats at constant volume and pressure, $\lambda$ is thermal conductivity, $\sigma$ is the stress tensor, $Le_{\mathcal{Y}}$ and $\omega_{\mathcal{Y}}$ are Lewis number and chemical source term of the progress variable, $q$ is the heat release rate in W/m$^3$. Variables like $c_v$, $q$, $\lambda$, as well as the viscosity used in stress term calculation are looked up from the MuSt-FGM tables. For numerical discretization, an implicit 6th order compact finite difference (FD) scheme (Lele, 1992) for diffusive terms, and a 5th order FD scheme with upwinding (de Lange, 2007) for the convective terms are employed. The tri-diagonal system originating from the implicit derivatives is solved using the Thomas algorithm. A 3rd order explicit Runge-Kutta scheme is utilized to perform the time integration. To avoid numerical instabilities at the boundaries, Navier-Stokes characteristic boundary conditions (NSCBC) (Poinsot and Lelef, 1992) are implemented.

As mentioned, in this study the JHC experiments from the University of Dally et al. (2002) are used as the baseline. The reason for selecting this case was that it mimics MILD combustion conditions properly and has extensive experimental data. From the three compositions studied in Dally et al. (2002), the HM1 case was selected because it contains the least amount of oxygen and thus represents MILD conditions the best.

In an industrial combustor, MILD conditions are often obtained via internal recirculation of flue gases. In the Adelaide JHC experimental setup, to mimic those conditions, a diluted oxidizer stream is created using a secondary burner and mixing hot combustion products from this secondary burner with fresh air at varying levels to control the oxygen levels. A cold fuel jet is issued into the diluted hot oxidizer, the two streams mix, and MILD combustion occurs in the primary burner. There is also a cold air tunnel around the hot oxidizer stream, which does not affect the combustion in the primary burner until 100 mm downstream from the fuel jet exit. This air stream is ignored in this study.

Experimentally intended constant temperature and species boundary conditions for the HM1 case are given in **Table 1**. However, due to experimental imperfections, in reality these variables are not constant in space and deviate from the intended conditions. Especially the temperature profile of the diluted oxidizer shows large variations due to the effect of cooling around the fuel pipe. Radial profiles of species and temperature were measured in the experiments at different axial locations. The measurements at $z = 4$ mm are assumed as the actual boundary conditions. In this work, simulations with only the real experimental conditions are performed, and they are referred to as "actual" profile cases. Profiles of temperature and oxidizer for the actual profile case as applied in the simulations are shown in **Figure 1**.

**TABLE 1 |** Intended boundary conditions for the HM1 case of the JHC experiments.

| Fuel | Oxidizer |
|---|---|
| T = 305 K | T = 1300 K |
| $Y_{H_2} = 0.11$ | $Y_{O_2} = 0.03$ |
| $Y_{CH_4} = 0.89$ | $Y_{N_2} = 0.85$ |
| | $Y_{H_2O} = 0.065$ |
| | $Y_{CO_2} = 0.055$ |

DNS computations were performed in the form of igniting mixing layers. A schematic of the computational domain is shown in **Figure 2**. In the experiments the inner diameter of the fuel jet is 4.25 mm, whereas in the DNS the equivalent height of the fuel slab in y-direction is kept as $w = 2$ mm to decrease the computational costs. In the DNS calculations, the fuel and oxidizer parts are simply extended in the third (z) direction so that the configuration is more like a slot burner. The reason for this is to make the calculation of the statistics easier. Periodic boundary conditions in the streamwise (x) and spanwise (z) directions, and non-reflecting outlet boundary conditions in the transverse (y) direction are used. An initial relative velocity of 67 m/s is given between the oxidizer and fuel layers in the streamwise direction, resulting in a Reynolds number of $Re = \Delta U w \rho/\mu = 67 \times 2 \times 10^{-3} \times 0.36/(1.17 \times 10^{-5}) = 4120$, which is in the order of the experimental value of 9482. Initial homogeneous and isotropic turbulent fluctuations with an intensity of 5% ($u'/\Delta U$) are imposed to the fuel, which helps the shear layer between the fuel and oxidizer to develop faster and accelerate the mixing. It is realistic to impose turbulent fluctuations to the fuel because in the experiments the fuel jet has a high velocity and comes through a long pipe before entering the primary burner, and thus has developed turbulence before mixing with the oxidizer. The magnitude of these fluctuations was not measured in the experiments, therefore the intensity of 5% is estimated.

The number of mesh points for the domain size shown in **Figure 2** is $253 \times 505 \times 127$, in x, y, and z-directions, which results in a uniform mesh size of ~0.040 mm. During DNS calculations, Kolmogorov length scale was monitored and a minimum value of 0.024 mm was observed. Since this value is in the order of magnitude of the grid spacing, the spatial resolution can be regarded as sufficient (Moin and Mahesh, 1998). Because the code is fully compressible, acoustic waves need to be resolved, which requires very small time step. In all the DNS calculations, the time step is taken as $1 \times 10^{-8}$ s, and the validity of this choice is controlled by checking the CFL number for acoustic waves.

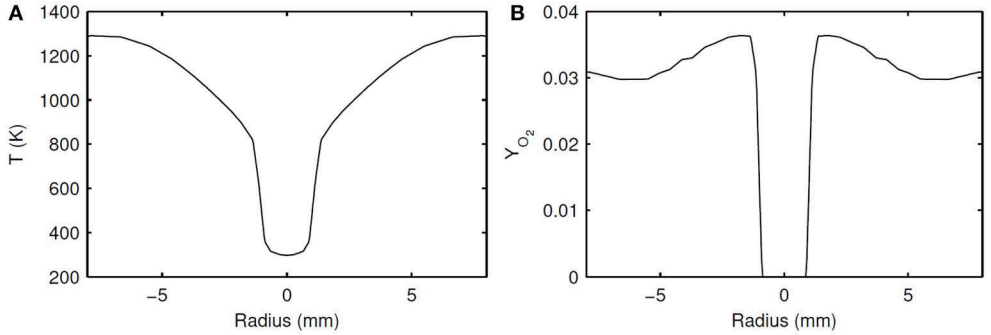


**FIGURE 1 |** Inlet radial profiles of temperature **(A)** and $Y_{O_2}$ **(B)**, scaled from the measured experimental values.

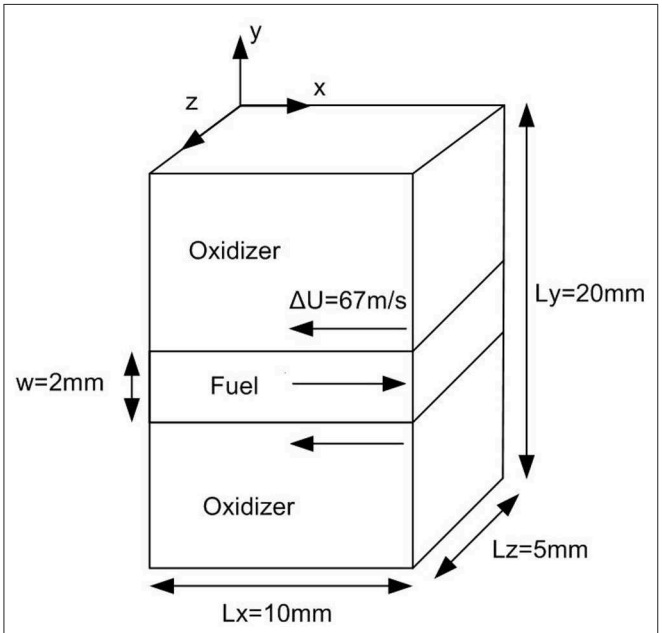


**FIGURE 2 |** Not-to-scale sketch of the simulation domain in 3D DNS.

Since the main goal of this study is to model the effects of temperature and species change in the oxidizer stream, the first issue to address is how to determine the control variable which can take these profile changes into account. Note that only the temperature and $O_2$ content changes are considered and other species' (namely $H_2O$ and $CO_2$) profiles in the oxidizer are assumed to be constant because their variations are marginal and the effects on chemistry are negligible, as observed in 1D flame analyses (not shown here). Depending on the $O_2$ content, the mass fraction of $N_2$ is adjusted so that $\sum Y_i = 1$.

As seen in **Figure 1**, the temperature values in the oxidizer are unique for this range, which makes it a good candidate as a control variable. However, because temperature changes with chemical progress, it is not independent of the progress variables. To solve this problem, a normalized and passive version of temperature is defined, i.e., it varies between 0 and 1, and has no source term. It is therefore similar to a mixture fraction which is defined specially for the oxidizer region, and it was coined as "$Z_O$". The diffusivity of $Z_O$ was chosen the same as the diffusivity of temperature, i.e., thermal conductivity, and thus $Le_{Z_O} = 1$. The profiles of $Z_O$ in composition and physical space for the Adelaide JHC case are shown in **Figure 3**, where $Z_t$ is the transported mixture fraction. Mathematical description and transport equations solved for $Z_O$ are shown in Equations (6)–(8), where $T_0$ represents the initial temperature.

$$Z_O = \frac{T_0 - T_{0,min}}{T_{0,max} - T_{0,min}} \tag{6}$$

$$\rho \frac{\partial (Z_O)}{\partial t} + \rho u_i \frac{\partial (Z_O)}{\partial x_i} = \frac{\partial}{\partial x_i} \left( \frac{\lambda}{Le_{Z_O} c_p} \frac{\partial (Z_O)}{\partial x_i} \right) \tag{7}$$

$$Le_{Z_O} = 1 \tag{8}$$

With the introduction of $Z_O$, the species mass fractions and temperature can be represented as $Y_i = Y_i(Z_t, Z_O, \mathcal{Y}_1, \mathcal{Y}_2), T = T(Z_t, Z_O, \mathcal{Y}_1, \mathcal{Y}_2)$, where $\mathcal{Y}_1$ is the first progress variable representing the pre-ignition chemistry, and $\mathcal{Y}_2$ is the second progress variable representing the oxidation chemistry in the MuSt-FGM context.

The definition and selection of $Z_O$ as the control variable representing the oxidizer is similar to what Ihme et al. have used, where they defined an oxidizer split, which would model the effects of the outermost air shroud as well (Ihme and Pitsch, 2008). However, unlike in their study, in this work $Z_O$ was varied within the coflow during the flamelet generation process, and the outermost air shroud part was ignored. The $Z_O$ definition used here is also very similar to the second mixture fraction from the work of Sarras et al. (2014), which is defined as a scaled oxygen mass fraction. However, they further included enthalpy deficit as an extra control variable, and thus represented the species mass fractions as $Y_i = Y_i(Z_1, Z_2, \mathcal{Y}, \Delta h)$. In their case, the temperature variation in the coflow cannot uniquely represent the oxygen variation, and thus the addition of enthalpy deficit as an extra control variable is reasonable.

In order to create the required flamelets, $Z_O$ values corresponding to experimental data points were selected, and 1D autoigniting flame calculations were performed using the

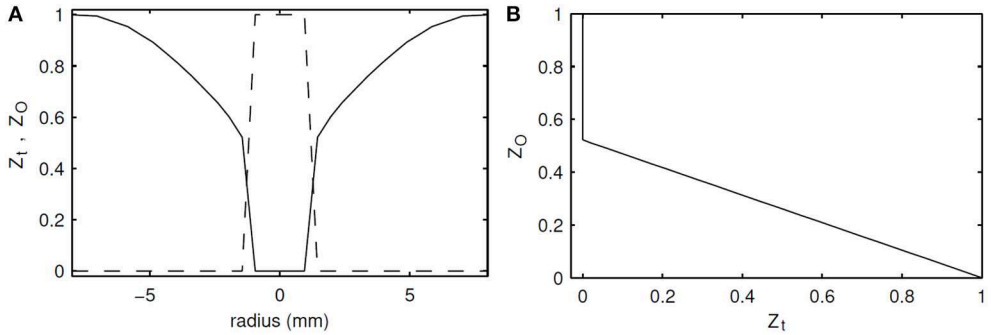


**FIGURE 3 |** Initial profiles of $Z_O$ (solid) and $Z_t$ (dashed) in radial direction **(A)**, and against each other **(B)**.

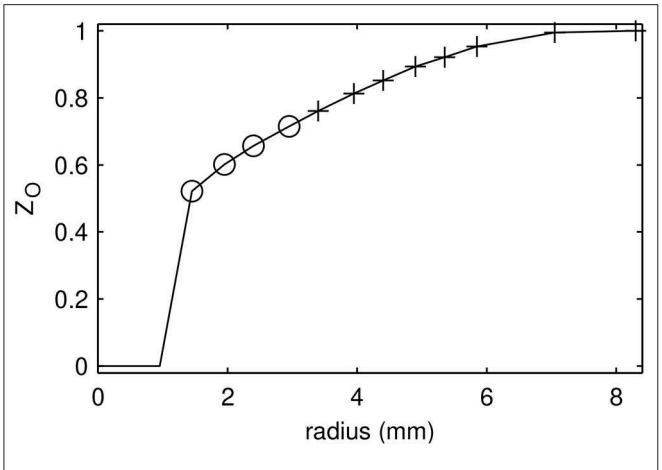


**FIGURE 4 |** Selected $Z_O$ values with autoignition occurring (plus) and not occurring (circle).

composition and temperature data corresponding to each $Z_O$ value as the boundary condition for the oxidizer side. The composition at the fuel side was kept constant as 50% hydrogen and 50% methane by volume. It was observed that at some lower $Z_O$ values, autoignition does not happen because the oxidizer temperature is too low. In **Figure 4**, the selected $Z_O$ values for which autoignition occurs are shown. The smallest $Z_O$ value which autoignites is 0.710, which corresponds to the oxidizer temperature of 1009 K; and the largest $Z_O$ value which does not autoignite is 0.664, which corresponds to the oxidizer temperature of 962 K. Having non-autoigniting $Z_O$ values poses two problems: the first one is that the MuSt-FGM tables for the second stage (oxidation) at those $Z_O$ values simply cannot be generated, due to the lack of autoignition. The second issue is that even though compositions corresponding to low $Z_O$ values cannot autoignite by themselves, when the ignition occurs at higher $Z_O$ values, heat and species would diffuse into the lower $Z_O$ regions and could trigger ignition. To be able to model such an ignition triggering, and to be able to create tables at lower $Z_O$ values, additional measures have to be taken.

To solve this problem, Ma and Roekaerts used a smaller strain rate than what they used by default, and later switched to the extinguishing flamelet approach (Ma and Roekaerts, 2016). In the current case, however, even for strain rates as low as 1 $s^{-1}$, autoignition could not be obtained for the lower $Z_O$ values. Furthermore, since this case is an autoigniting one overall, utilizing extinguishing flamelets for every composition is not representative of the system. Using extinguishing flamelets for the non-igniting compositions and autoigniting flamelets for the igniting compositions would cause discontinuity in the tables.

In this work, several methods are proposed to tackle this problem. They are outlined one-by-one in the following subsections.

## 2.1. Method 1–2D Flamelets

A possible solution to non-igniting oxidizer points problem is to use 2D flamelets like in Hasse and Peters' work (Hasse and Peters, 2005), where they applied it to model one oxidizer and two fuel streams in Diesel engine combustion. In the current study, instead of solving the case in flamelet coordinates, a simulation was performed in 2D physical space, and converted into flamelet coordinates subsequently ($x$, $y$, $t \rightarrow Z_t$, $Z_O$ and PVs). The temperature, $Z_O$ and $Z_t$ profiles of this simulation are given in **Figure 5**, where the top part is the oxidizer with temperature gradient, and the bottom part is the fuel. Open outflow boundary conditions were given on all boundaries, and zero initial velocity was defined in the domain. The transient evolution of species and temperature was calculated. As can be seen in **Figure 5**, $Z_t$ is varied in y-coordinate, $Z_O$ is varied in x-coordinate, and changes in the progress variables are represented by the time coordinate. While the temperature rises with time due to chemical progress, $Z_t$ and $Z_O$ only diffuse. By using 2D flamelets, the diffusion of heat and species from higher $Z_O$ regions to lower $Z_O$ regions is also included, which means that the ignition of lower $Z_O$ values triggered by higher $Z_O$ values can be modeled, and lower $Z_O$ points pose no problem for the table generation.

## 2.2. Method 2–Forced Ignition

A different approach to solving the problem of non-autoigniting flamelets would be to ignite them artificially. This can be achieved by mixing the initial composition of the non-autoigniting cases with the steady burning composition of the same case by an appropriate ratio, and then letting this artificial mixture to ignite. Note that even though these low $Z_O$ compositions cannot autoignite, when initialized using an already burning solution,

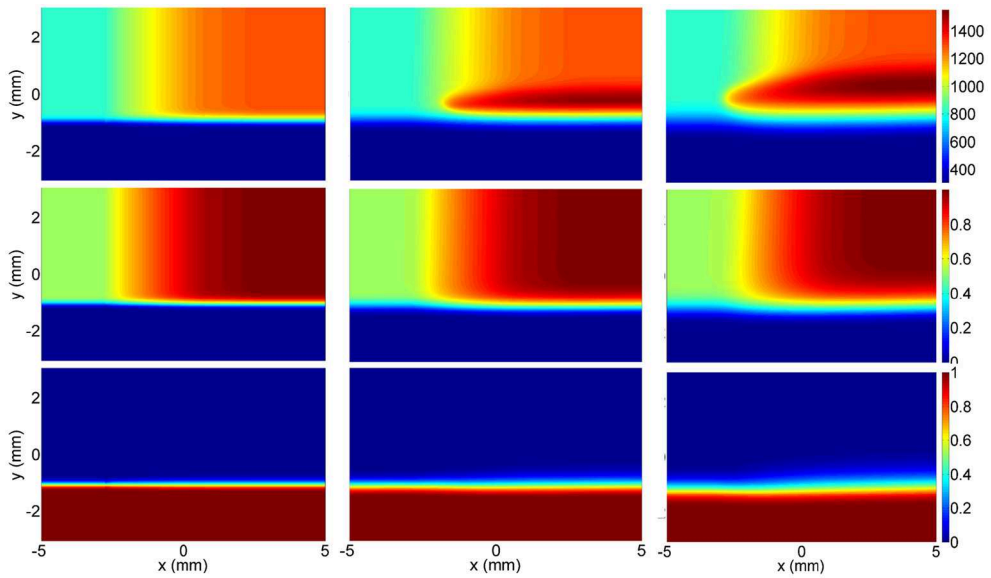


**FIGURE 5 |** Temperature **(Top)**, $Z_O$ **(Middle)**, and $Z_t$ **(Bottom)** fields for the 2D flamelet generation simulation at $t = 0.0, 1.0, 3.0$ ms from left to right.

steady burning solutions can be obtained. The initial composition is obtained by purely mixing the fuel and oxidizer, and it constitutes the first flamelet of the MuSt-FGM table for that $Z_O$ value. The artificial mixture becomes the second flamelet, and the transient solution from the artificial mixture toward steady solution constitute the rest of the flamelets. To describe the process step by step:

- By initializing the solution with an already burning case, obtain a steady burning solution of a non-autoigniting $Z_O$ point.
- By mixing the steady burning solution of that non-autoigniting $Z_O$ point with its initial state, obtain an artificial mixture that can autoignite by itself. This step is shown in Equations (9) and (10), where $Y_{new}$, $Y_{st}$ and $Y_{in}$ represent the species mass fraction of the artificial mixture, steady solution and initial mixture, respectively, and $h$ represents the enthalpy with the same notation of the subscripts.
- By trial and error, find the minimum weight $m$ in Equations (9) and (10), which can provide a mixture that can autoignite.
- Using the initial mixing state, artificially created mixture, and the time evolution of the autoigniting case from the artificial mixture until the steady burning solution; create MuSt-FGM tables.

$$Y_{new} = m \cdot Y_{st} + (1 - m) \cdot Y_{in} \quad (9)$$

$$h_{new} = m \cdot h_{st} + (1 - m) \cdot h_{in} \quad (10)$$

This approach is called as "Forced Ignition" in the remaining of the text. The idea behind this approach is to find the minimum weight $m$ where the originally non-autoigniting composition can take off by itself in terms of ignition, and tabulate this autoignition region. Any flamelet which has lower precursor values than the threshold flamelet will quench and not lead to ignition. During an FGM run, if the diffusion of precursor species and heat from an autoigniting $Z_O$ value are high enough to reach this threshold, then the composition at non-autoigniting $Z_O$ will be able to sustain ignition. If the diffusion levels are lower and not continuous, then they will not be sufficient to cause an ignition.

To explain the flamelet creation process in the forced ignition approach more clearly, flamelets from an originally non-autoigniting $Z_O$ value are given in **Figure 6**. The blue curve represents the initial mixing line, which does not autoignite by itself. By initializing the field from an already burning solution, a steady burning solution for this $Z_O$ value can be obtained, and it is represented with the black curve. Later, the solutions represented by the blue and black curves were mixed by different ratios and then it was checked whether this new solution could autoignite by itself. The mixture that could autoignite with a minimum contribution from the initial mixture solution (min blue/black ratio, so to say) is shown with the red curve in the figure. The red curve, which was also called as artificial mixture so far, will be referred to as "forcing flamelet" from here on. The autoigniting flamelets obtained from the forcing flamelet were stored to create the MuSt-FGM tables, and they are represented with the gray curves in **Figure 6**. While creating MuSt-FGM tables, the source terms at the forcing flamelet were set to the same source terms as the initial mixing line (blue curve), because otherwise any increase in progress variable would result in a significant source term during MuSt-FGM run. This is caused by the large gap between the blue and red curves, the linear interpolation used in the lookup procedure, and the non-linear relation between progress variables and their source terms.

## 2.3. Method 3–Default Method

The third approach to the non-autoigniting $Z_O$ points issue is to perform no additional treatment, and leave the non-autoigniting

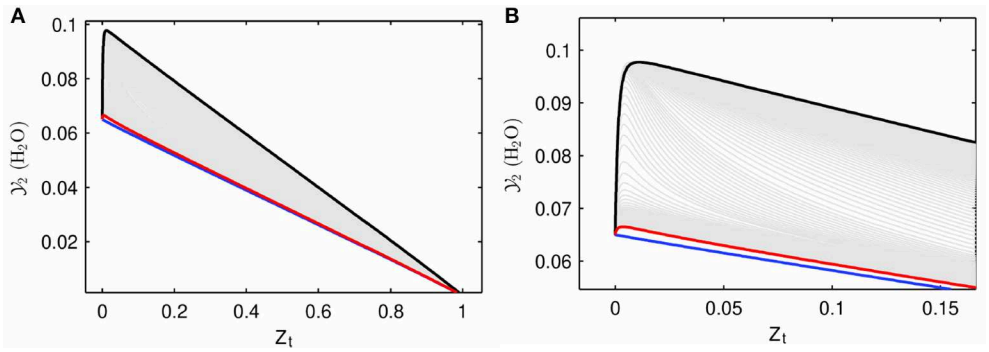


**FIGURE 6 |** Flamelets created with forced ignition approach. Blue line is the initial mixture, black line is the steady burning solution, and the red line is the mixture of the two which then autoignites and generates flamelets represented with gray lines. This case is for $Z_O = 0.664$, with a weight $m = 0.05$. **(A,B)** Show different $Z_t$ ranges of the same figure.

flamelets as they are. Since each progress variable represent a different stage in the MuSt-FGM approach, even though the mixture would not ignite, some pre-ignition chemistry happens regardless and thus can be parameterized by $\mathcal{Y}_1$. As a result, the first lookup table would be non-empty, and the lookup would proceed using only the first table. The implementation of this approach is straightforward, but it misses the conditions where the diffused heat and species from the autoignited compositions would ignite the non-autoigniting compositions. This approach is referred to as "Default Method" in the rest of the text.

**Figure 7** shows two sample MuSt-FGM tables for the first (pre-ignition) stage. **Figure 7A** is from an autoigniting $Z_O$ value, and it is seen that the maximum value for $\mathcal{Y}_1$ and its source term reach $\sim 3 \times 10^{-5}$ and 0.035, respectively. Whereas it is seen from **Figure 7B**, which is from a non-autoigniting $Z_O$ value, that both the source term and maximum value for $\mathcal{Y}_1$ are orders of magnitude lower. This is expected because of the lack of autoignition. However, the table shown in **Figure 7B** is still usable in a MuSt-FGM calculation as the source terms are very small but non-zero.

## 2.4. Method 4–Extrapolation

The final approach for the problem of non-autoigniting $Z_O$ values is to remove those flamelets from the MuSt-FGM table generation all together, and to perform an extrapolation for those compositions during the MuSt-FGM simulations using the autoigniting compositions. For all the variables that are looked up from the tables, linear extrapolation is adapted.

# 3. RESULTS

## 3.1. 1D Results

As a first validation step, comparing the results of different modeling approaches with the detailed chemistry case in 1D is reasonable, because the capability of the models to represent the chemistry and diffusion in the absence of turbulence can be verified. In 1D simulations, the initial profiles of $Z_O$ and $Z_t$ as seen in **Figure 3** are provided as initial conditions, no velocity is induced, and transient interaction of thermal/molecular diffusion and chemistry is calculated. Therefore this calculation is not a counter-flow flamelet simulation. In the detailed chemistry case and in the flamelet generation, DRM19 reaction mechanism (Kazakov and Frenklach, 1994), which includes 21 species and 84 reactions, was used.

The extrapolation approach failed to give any results as the computations diverged after only a few time steps. This is because the lowest $Z_O$ value ($Z_O = 0.514$) is the one closest to the fuel, and therefore the whole region between the fuel and oxidizer is being extrapolated (see **Figure 3**). In addition, the extrapolation step is very large, from $Z_O = 0.710$ to $Z_O = 0.514$, while the range of $Z_O$ values for which the MuSt-FGM tables exist is from $Z_O = 0.710$ to $Z_O = 1.0$. This introduces a large error in the lookup procedure of many crucial variables, which leads to a quick divergence in the computations.

From the 1D calculation results, spatially averaged heat release rate and the maximum $\mathcal{Y}_2 = Y_{H_2O}$ in the whole computational domain are shown in **Figure 8**. These two variables give a good indication of when the ignition happens, and how fast and intense the oxidation reactions take place. The ignition delay times are also given in **Table 2** for all the simulated cases. As seen in **Figure 8** and **Table 2**, the forced ignition and default table cases predict the ignition delay fairly well, with an error of about 4% for both cases compared to the detailed chemistry case. The accuracy of the same cases in predicting the peak of the average heat release rate is less, with an error of about 20%. On the other hand, the 2D flamelet table case completely misses the ignition delay, and performs worse in terms of the peak average heat release rate. It is worth investigating why the 2D flamelet table performs so poorly.

When the progress variable source terms for the first flamelets were checked for the 2D flamelet case at non-autoigniting $Z_O$ values, it was seen that they were at sufficient levels to autoignite by themselves, as shown in **Figure 9**. It is seen that even though the source term for $\mathcal{Y}_2$ at the first flamelet of $Z_O = 0.664$ case is not as high as in $Z_O = 0.710$ case, it is still much larger than its counterpart created with the default table option. This level of source term is sufficient to lead to autoignition. The reason for this high source term can be explained as follows: During the 2D flamelet simulation, higher $Z_O$ values ignite and

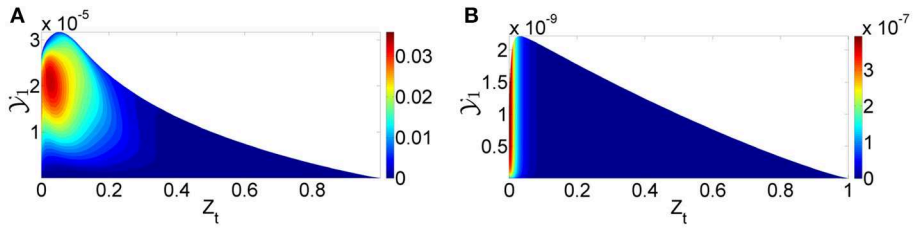


**FIGURE 7 |** MuSt-FGM first stage table samples for the default method. **(A)** Is an example of an autoigniting $Z_O$ value ($Z_O = 0.710$), and **(B)** is an example of a non-autoigniting $Z_O$ value ($Z_O = 0.664$). Contour values represent the source term of $\mathcal{Y}_1$. Note the difference in the range of $\mathcal{Y}_1$ values and source terms.

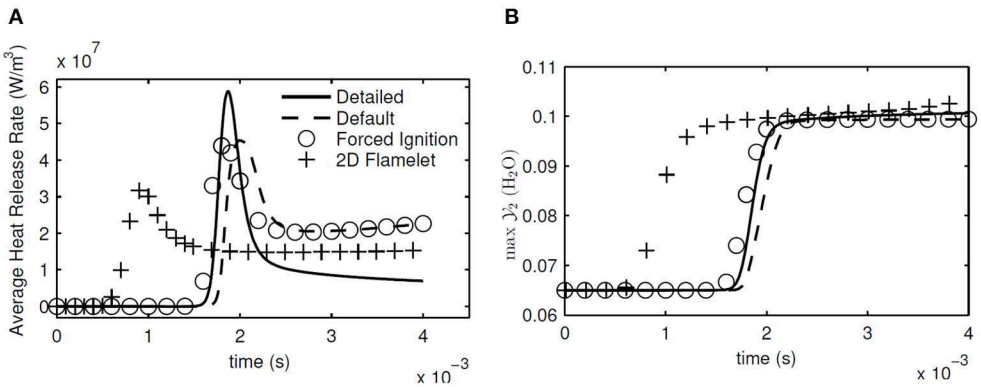


**FIGURE 8 |** Evolution of average heat release rate **(A)** and maximum $\mathcal{Y}_2$ in the whole domain **(B)** in 1D calculations with detailed chemistry, default table, forced ignition table, and 2D flamelet table.

**TABLE 2 |** Ignition delay times for different cases.

| Simulation coordinates | Simulation type | Ignition delay |
|---|---|---|
| 1D | Detailed chemistry | 1.76 ms |
| 1D | MuSt-FGM default table | 1.68 ms |
| 1D | MuSt-FGM forced ignition table | 1.83 ms |
| 1D | MuSt-FGM 2D-flamelet table | 0.71 ms |
| 1D | MuSt-FGM extrapolation | No result |
| 3D | Detailed chemistry | 1.04 ms |
| 3D | MuSt-FGM default table | 0.76 ms |
| 3D | MuSt-FGM forced ignition Table | 0.91 ms |
| 3D | MuSt-FGM 2D-flamelet table | No result |
| 3D | MuSt-FGM extrapolation | No result |

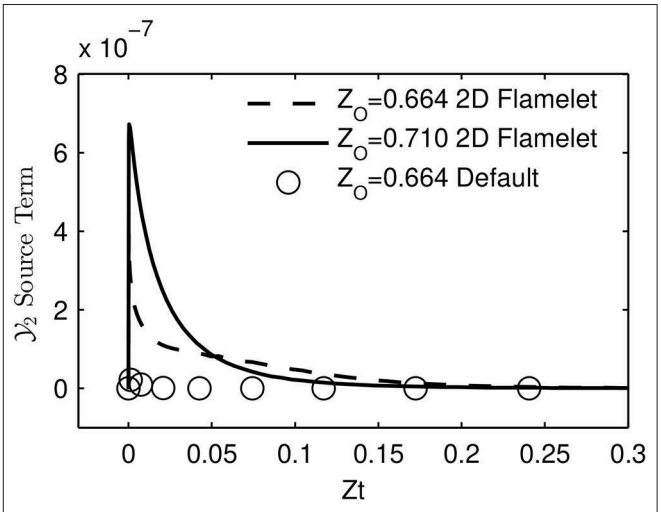


**FIGURE 9 |** Source term of $\mathcal{Y}_2$ at the first flamelet for different cases.

$\mathcal{Y}_1$ values increase orders of magnitude, and then $\mathcal{Y}_1$ diffuses into lower (non-autoigniting) $Z_O$ values. This creates source terms at lower $Z_O$ values and triggers ignition, as intended with the 2D flamelet approach. However, these source terms are also tabulated at lower progress variable values, i.e., close to the initial mixing line, and cause lower $Z_O$ values to autoignite during an FGM simulation. This is an unintended consequence, because the goal is not to cause lower $Z_O$ compositions to autoignite, but to let them sustain the ignition triggered by diffusion. Since lower $Z_O$ values are closest to the fuel in physical space, this error causes the 2D flamelet case to fail in terms of ignition delay prediction.

The default case can predict the ignition delay well because no extra treatment is performed and thus no artificial source term is induced, and in the forced ignition case the artificial source term is removed by setting the source terms at the forcing flamelet same as in the initial mixing line. However, it should be mentioned that part of the reason why extra treatment is performed for non-autoigniting compositions is to be able to

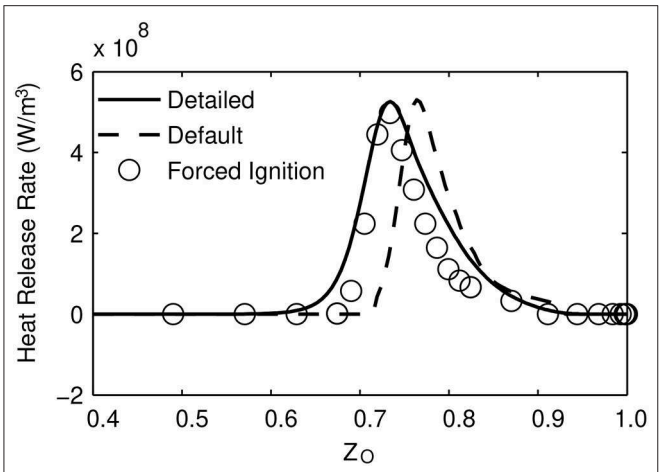


**FIGURE 10 |** Heat release rate at different $Z_O$ values. The values are taken from the time when the peak average heat release rate occurs for each case.

capture the effects of triggered ignition at those compositions with the help of diffusion from autoigniting regions. These effects are more visible in the turbulent cases, because the turbulence helps the entrainment of hot parts of the oxidizer with fuel. It is also worth mentioning that judging by the success of ignition delay prediction, it can be concluded that $Z_O$ represents the variation in the oxidizer temperature and resulting chemistry changes well.

To check why peak average heat release rate is lower in the MuSt-FGM cases, the distribution of the heat release rate in the $Z_O$ coordinate is investigated. In **Figure 10**, this distribution for each case when the peak average heat release rate happens is given. It can be seen that location and distribution of the heat release rate in $Z_O$ space is well captured in the forced ignition case compared to the detailed chemistry case, whereas the default case predicts a heat release at higher $Z_O$ values. This is reasonable because the default case does not have any second stage table (and thus considerable heat release) at lower $Z_O$ values. It is also seen that both MuSt-FGM cases predict the maximum heat release rate correctly, but the heat release rate remains high for a wider range of $Z_O$ values in the detailed chemistry case, which explains the difference in the peak average heat release rates. This might be because the tables are generated using a constant strain rate of 200 $s^{-1}$, which does not represent the situation for this 1D simulation, where there is only diffusion transport. Nevertheless, the actual goal is to simulate the 3D cases properly, and because it is necessary to entrain the hot parts of the oxidizer and bring them into contact with the fuel to get ignition in the 3D case, flamelets generated with a strain rate is a better option.

## 3.2. 3D Results

As in 1D simulations, average heat release rate and maximum $\mathcal{Y}_2$ are calculated and shown in **Figure 11** to make a first comparison between the detailed chemistry and MuSt-FGM. Again the ignition delay times are given in **Table 2** as well. Note that since the 2D flamelet case performs poorly for the 1D case, it was not used further in the 3D simulations. The forced ignition case predicts the ignition delay with an error of 12% compared to the detailed chemistry case, which is a decent prediction given the complex structure of the case with preferential diffusion, temperature variations and turbulence. The default case does not perform that well, with the error increasing to 30%. Both MuSt-FGM cases over-predict the maximum increase of $\mathcal{Y}_2$ by about 25%, which is a considerable error. It is also noteworthy that the ignition delay drops by a factor of two compared to the 1D simulations due to the turbulent entrainment, and this effect can be captured with MuSt-FGM cases without any extra treatment.

Looking at the average heat release rates, it is seen that both MuSt-FGM cases over-predict the peak values compared to the detailed chemistry case. For the forced ignition case, the error for the prediction of the peak average heat release rate is 68%, whereas for the default case it is 43%. Especially for the forced ignition case, the error is at unacceptable levels. In addition to the peak values, also the end value of the average heat release rate is over-estimated by both MuSt-FGM cases. However, it should also be mentioned that the initial increasing slope and the final decreasing slope in time for the average heat release rate are captured rather well with the forced ignition case. As for the maximum $\mathcal{Y}_2$ prediction, the peak value throughout the simulation is over-predicted by 10% by both cases.

When the reasons for early ignition and high heat release rates for the MuSt-FGM cases are investigated, it is seen that the preferential diffusion-curvature interactions are playing a role. This interaction can be summarized as follows: flame curvature enhances or lessens the effects of preferential diffusion (Pitz et al., 2014), this causes a scatter of species in the composition space, this scatter is interpreted as progress in the FGM context, and as a result higher than actual heat release rates are retrieved from the FGM tables. To demonstrate how this interaction affects the distribution in the composition space, the scatter of $\mathcal{Y}_2$ before the ignition (at $t = 0.9$ ms) is shown in **Figure 12**. In the MuSt-FGM context, this effect is even more intensified, because the scatter in $\mathcal{Y}_2$ would cause a premature lookup from the second stage table, which would cause even higher heat release rates retrieved.

In order to demonstrate how the error due to the scatter of species reflects in the actual MuSt-FGM run, contour plots of heat release rate from the detailed chemistry and forced ignition case are shown in **Figure 13**. The time chosen for each case is when the peak average heat release rate occurs, and the slice in z-direction is chosen as where the maximum heat release rate happens. It is seen that the detailed chemistry case has a more spotty ignition only at the bottom side, whereas the MuSt-FGM case with forced ignition table has a distributed ignition region both at the top and bottom sides. It should also be pointed out that while the average heat release rate differs in two cases by 68%, the difference in maximum heat release rate is 25%, which further supports that the over-prediction of the average heat release rate is because the MuSt-FGM cases lack the variations caused by the scatter of the species.

# 4. CONCLUSIONS

In this study, temperature and oxygen variations in the oxidizer of the Adelaide JHC burner were modeled in the MuSt-FGM context. A new passive variable was defined based on the

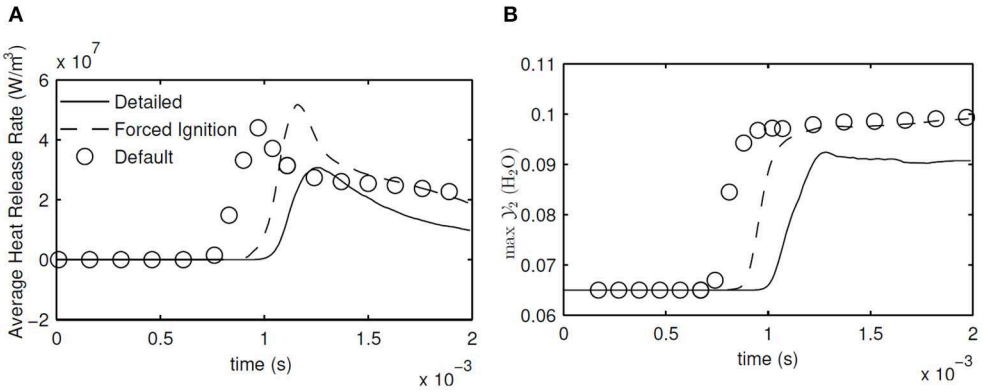


**FIGURE 11 |** Evolution of average heat release rate **(A)** and maximum $\mathcal{Y}_2$ in the whole domain **(B)** in 3D DNS calculations with detailed chemistry and 3D MuSt-FGM with default and forced ignition tables.

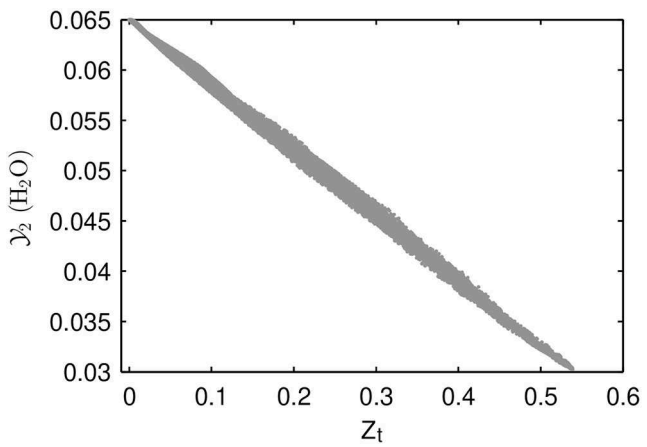


**FIGURE 12 |** Distribution of $\mathcal{Y}_2$ for the 3D detailed chemistry case at $t = 0.9$ ms. Note the wide scatter despite almost unity Lewis number of $\mathcal{Y}_2$ ($Le_{\mathcal{Y}_2} = 0.98$).

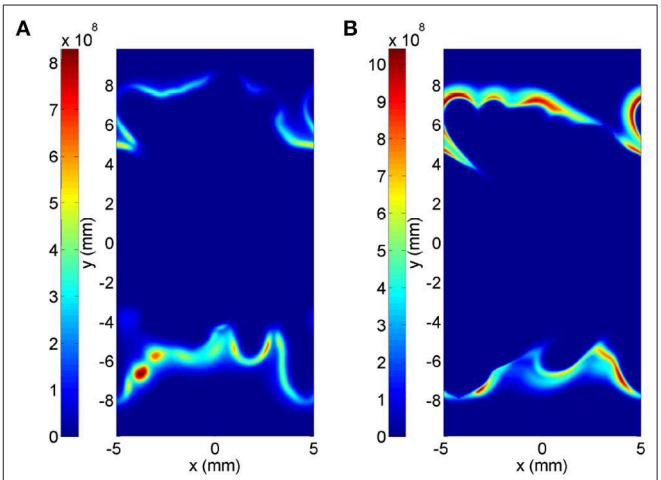


**FIGURE 13 |** Heat release rate contours (in W/m$^3$) for the detailed chemistry case **(A)** and the MuSt-FGM forced ignition table case **(B)**, at the time when the peak average heat release rate occurs ($t = 1.25$ ms and $t = 1.16$ ms, respectively), and at the z-coordinate where the maximum heat release rate occurs. Please note the difference in color scales.

normalized temperature values, coined as $Z_O$, and used as the extra control variable. Unsteady counter-flow simulations were performed for each $Z_O$ point to create the necessary flamelets for MuSt-FGM table generation. However, it was realized that not all the compositions in the oxidizer can autoignite. To solve this problem, four approaches were proposed; (1) 2D flamelet creation, (2) helping the non-autoigniting compositions to ignite by mixing with the steady burning solution, (3) simply performing nothing extra and using only the first table (pre-ignition chemistry) of the non-autoigniting regions, (4) not using the non-autoigniting $Z_O$ points in the table generation and applying an extrapolation for those regions. The following conclusions can be drawn from the results and analyses:

- Judging from 1D simulation results, $Z_O$ is a good control variable definition to model the variations in the oxidizer.
- For the current case, creating flamelets from a physical 2D flame simulation did not work well, due to the highly diffusive precursors creating source terms at mixing lines of non-autoigniting $Z_O$ points.
- Extrapolation toward non-autoigniting $Z_O$ values caused the simulations to quickly diverge.
- Although 3D MuSt-FGM with the default table performed well in the 1D simulation, the prediction of the ignition delay as well as the heat release rate deteriorated considerably in the 3D DNS computations.
- 3D MuSt-FGM with the forced ignition case performed better for the ignition delay prediction. However, investigation of the results made it clear that the curvature-preferential diffusion interactions are important for this case.

Although there are open points for improvement such as the inclusion of the curvature-preferential diffusion interactions; considering the difficulty of the investigated

MILD combustion case with preferential diffusion, turbulence and the temperature variations; the overall modeling performance for the MuSt-FGM approach can be regarded as successful. Compared to the detailed chemistry case, the ignition delay and the general trend of the average heat release rate are captured fairly well, although the peak value of the average heat release rate is considerably over-predicted.

## DATA AVAILABILITY STATEMENT

The datasets generated for this study are available on request to the corresponding author.

## AUTHOR CONTRIBUTIONS

MG has performed the simulations and written the article. As the Ph.D. supervisors, JO and PG have guided the research and provided feedback on the manuscript. JO has conceived and directed the research.

## FUNDING

The Ph.D. project, out of which this study was conducted, had been funded by Dutch Technology Foundation (STW, now part of NWO), under the project name Clean Combustion of Future Fuels and project number 10766.

## ACKNOWLEDGMENTS

Authors wish to thank Prof. Bassam Dally for generously providing the experimental data from the JHC experiments performed in his lab. This study is the result of a project funded by Dutch Technology Foundation (STW, now part of NWO). Computational power provided at the Dutch National Supercomputer, Cartesius, is greatly acknowledged.

## REFERENCES

Abtahizadeh, E., Sepman, A., Hernández-Pérez, F., van Oijen, J., Mokhov, A., de Goey, P., et al. (2013). Numerical and experimental investigations on the influence of preheating and dilution on transition of laminar coflow diffusion flames to mild combustion regime. *Combust. Flame* 160, 2359–2374. doi: 10.1016/j.combustflame.2013.05.020

Afarin, Y., and Tabejamaat, S. (2013). The effect of fuel inlet turbulence intensity on h2/ch4 flame structure of mild combustion using the les method. *Combust. Theory Model.* 17, 383–410. doi: 10.1080/13647830.2012.742570

Albin, T., da Franca, A. A., Varea, E., Kruse, S., Pitsch, H., Abel, D. (2015). "Potential and challenges of MILD combustion control for gas turbine applications," in *Active Flow and Combustion Control 2014*. Notes on Numerical Fluid Mechanics and Multidisciplinary Design. Vol. 127. ed. R. King (Cham: Springer).

Barlow, R., Frank, J., Karpetis, A., and Chen, J.-Y. (2005). Piloted methane/air jet flames: transport effects and aspects of scalar structure. *Combust. Flame* 143, 433–449. doi: 10.1016/j.combustflame.2005.08.017

Bastiaans, R., Somers, L., and de Lange, H. (2001). "Dns of non-premixed combustion in a compressible mixing layer, using simple chemistry," in *Modern Simulation Strategies for Turbulent Flow*, ed B. Geurts (Philadelphia, PA: RT Edwards), 247–261.

Cabra, R., Myhrvold, T., Chen, J., Dibble, R., Karpetis, A., and Barlow, R. (2002). Simultaneous laser raman-rayleigh-lif measurements and numerical modeling results of a lifted turbulent h2/n2 jet flame in a vitiated coflow. *Proc. Combust. Inst.* 29, 1881–1888. doi: 10.1016/S1540-7489(02)80228-0

Cavaliere, A., and de Joannon, M. (2004). Mild combustion. *Prog. Energy and Combust. Sci.* 30, 329–366. doi: 10.1016/j.pecs.2004.02.003

Chen, Z., Reddy, V., Ruan, S., Doan, N., Roberts, W., and Swaminathan, N. (2017). Simulation of mild combustion using perfectly stirred reactor model. *Proc. Combust. Inst.* 36, 4279–4286. doi: 10.1016/j.proci.2016.06.007

Christo, F., and Dally, B. B. (2005). Modeling turbulent reacting jets issuing into a hot and diluted coflow. *Combust. Flame* 142, 117–129. doi: 10.1016/j.combustflame.2005.03.002

Dally, B., Masri, A., Barlow, R., and Fiechtner, G. (1998). Instantaneous and mean compositional structure of bluff-body stabilized nonpremixed flames. *Combust. Flame* 114, 119–148.

Dally, B. B., Karpetis, A., and Barlow, R. S. (2002). Structure of turbulent non-premixed jet flames in a diluted hot coflow. *Proc. Combust. Inst.* 29, 1147–1154. doi: 10.1016/S1540-7489(02)80145-6

De Joannon, M., Sorrentino, G., and Cavaliere, A. (2012). MILD combustion in diffusion-controlled regimes of hot diluted fuel. *Combust. Flame* 159, 1832–1839. doi: 10.1016/j.combustflame.2012.01.013

de Lange, H. (2007). Acoustic upwinding for sub-and super-sonic turbulent channel flow at low Reynolds number. *Int. J. Numer. Meth. Fl.* 55, 205–223. doi: 10.1002/fld.1446

De, A., Oldenhof, E., Sathiah, P., and Roekaerts, D. (2011). Numerical simulation of Delft-jet-in-hot-coflow (DJHC) flames using the eddy dissipation concept model for turbulence–chemistry interaction. *Flow Turbul. Combust.* 87, 537–567. doi: 10.1007/s10494-011-9337-0

Derudi, M., and Rota, R. (2011). Experimental study of the mild combustion of liquid hydrocarbons. *Proc. Combust. Inst.* 33, 3325–3332. doi: 10.1016/j.proci.2010.06.120

Doan, N. A. K., Swaminathan, N., and Minamoto, Y. (2018). Dns of mild combustion with mixture fraction variations. *Combust. Flame* 189, 173–189. doi: 10.1016/j.combustflame.2017.10.030

Donini, A., Martin, S., Bastiaans, R., van Oijen, J., and de Goey, L. (2013). "Numerical simulations of a premixed turbulent confined jet flame using the flamelet generated manifold approach with heat loss inclusion," in *Proceedings of the ASME Turbo Expo 2013: Turbine Technical Conference and Exposition* (San Antonio, TX). doi: 10.1115/GT2013-94363

Duwig, C., Li, B., Li, Z., and Aldén, M. (2012). High resolution imaging of flameless and distributed turbulent combustion. *Combust. Flame* 159, 306–316. doi: 10.1016/j.combustflame.2011.06.018

Duwig, C., Stankovic, D., Fuchs, L., Li, G., and Gutmark, E. (2007). Experimental and numerical study of flameless combustion in a model gas turbine combustor. *Combust. Sci. Technol.* 180, 279–295. doi: 10.1080/00102200701739164

Evans, M., Medwell, P., Wu, H., Stagni, A., and Ihme, M. (2017). Classification and lift-off height prediction of non-premixed mild and autoignitive flames. *Proc. Combust. Inst.* 36, 4297–4304. doi: 10.1016/j.proci.2016.06.013

Fiorina, B., Baron, R., Gicquel, O., Thevenin, D., Carpentier, S., and Darabiha, N. (2003). Modelling non-adiabatic partially premixed flames using flame-prolongation of ildm. *Combust. Theory Model.* 7, 449–470. doi: 10.1088/1364-7830/7/3/301

Gicquel, O., Darabiha, N., and Thévenin, D. (2000). Liminar premixed hydrogen/air counterflow flame simulations using flame prolongation of ildm with differential diffusion. *Proc. Combust. Inst.* 28, 1901–1908. doi: 10.1016/S0082-0784(00)80594-9

Göktolga, M. U., van Oijen, J. A., and de Goey, L. P. H. (2015). 3D DNS of MILD combustion: a detailed analysis of heat loss effects, preferential diffusion, and flame formation mechanisms. *Fuel* 159, 784–795. doi: 10.1016/j.fuel.2015.07.049

Göktolga, M. U., van Oijen, J. A., and de Goey, L. P. H. (2017). Modeling MILD combustion using a novel multistage FGM method. *Proc. Combust. Inst.* 36, 4269–4277. doi: 10.1016/j.proci.2016.06.004

Groot, G. R. A. (2003). *Modelling of Propagating Spherical and Cylindrical Premixed Flames*. Ph.D. thesis, Technische Universiteit Eindhoven, Eindhoven.

Hasse, C., and Peters, N. (2005). A two mixture fraction flamelet model applied to split injections in a di diesel engine. *Proc. Combust. Inst.* 30, 2755–2762. doi: 10.1016/j.proci.2004.08.166

Ihme, M., and Pitsch, H. (2008). Modeling of radiation and nitric oxide formation in turbulent nonpremixed flames using a flamelet/progress variable formulation. *Phys. Fluids* 20:055110. doi: 10.1063/1.2911047

Ihme, M., and See, Y. C. (2011). Les flamelet modeling of a three-stream mild combustor: analysis of flame sensitivity to scalar inflow conditions. *Proc. Combust. Inst.* 33, 1309–1317. doi: 10.1016/j.proci.2010.05.019

Ihme, M., Zhang, J., He, G., and Dally, B. (2012). Large-eddy simulation of a jet-in-hot-coflow burner operating in the oxygen-diluted combustion regime. *Flow Turbul. Combust.* 89, 449–464. doi: 10.1007/s10494-012-9399-7

Kazakov, A., and Frenklach, M. (1994). *DRM19 Reaction Mechanism*. Available online at: http://www.me.berkeley.edu/drm/ (accessed August 06, 2015).

Kruse, S., Kerschgens, B., Berger, L., Varea, E., and Pitsch, H. (2015). Experimental and numerical study of mild combustion for gas turbine applications. *Appl. Energy* 148, 456–465. doi: 10.1016/j.apenergy.2015.03.054

Kulkarni, R. M., and Polifke, W. (2013). LES of Delft-jet-in-hot-coflow (DJHC) with tabulated chemistry and stochastic fields combustion model. *Fuel Process. Technol.* 107, 138–146. doi: 10.1016/j.fuproc.2012.06.015

Lammel, O., Stohr, M., Kutne, P., Dem, C., Meier, W., and Aigner, M. (2012). Experimental analysis of confined jet flames by laser measurement techniques. *Jour. Eng. Gas Turbines Power* 134, 041506–041515. doi: 10.1115/1.4004733

Lele, S. K. (1992). Compact finite difference schemes with spectral-like resolution. *J. Comput. Phys.* 103, 16–42.

Li, P., Mi, J., Dally, B., Wang, F., Wang, L., Liu, Z., et al. (2011). Progress and recent trend in mild combustion. *Sci. China Technol. Sci.* 54, 255–269. doi: 10.1007/s11431-010-4257-0

Ma, L., and Roekaerts, D. (2016). Modeling of spray jet flame under mild condition with non-adiabatic fgm and a new conditional droplet injection model. *Combust. Flame* 165, 402–423. doi: 10.1016/j.combustflame.2015.12.025

Mendez, L. A., Tummers, M., van Veen, E., and Roekaerts, D. (2015). Effect of hydrogen addition on the structure of natural-gas jet-in-hot-coflow flames. *Proc. Combust. Inst.* 35, 3557–3564. doi: 10.1016/j.proci.2014.06.146

Minamoto, Y., Dunstan, T., Swaminathan, N., and Cant, R. (2013). DNS of EGR-type turbulent flame in mild condition. *Proc. Combust. Inst.* 34, 3231–3238. doi: 10.1016/j.proci.2012.06.041

Minamoto, Y., Swaminathan, N., Cant, S. R., and Leung, T. (2014). Morphological and statistical features of reaction zones in MILD and premixed combustion. *Combust. Flame* 161, 2801–2814. doi: 10.1016/j.combustflame.2014.04.018

Moin, P., and Mahesh, K. (1998). Direct numerical simulation: a tool in turbulence research. *Annu. Rev. Fluid Mech.* 30, 539–578.

Oldenhof, E., Tummers, M., Van Veen, E., and Roekaerts, D. (2011). Role of entrainment in the stabilisation of jet-in-hot-coflow flames. *Combust. Flame* 158, 1553–1563.

Perpignan, A. A., Rao, A. G., and Roekaerts, D. J. (2018). Flameless combustion and its potential towards gas turbines. *Prog. Energy Combust. Sci.* 69, 28–62. doi: 10.1016/j.apenergy.2017.02.010

Peters, N. (1984). Laminar diffusion flamelet models in non-premixed turbulent combustion. *Prog. Energy and Combust. Sci.* 10, 319–339. doi: 10.1016/0360-1285(84)90114-X

Pierce, C. D., and Moin, P. (2004). Progress-variable approach for large-eddy simulation of non-premixed turbulent combustion. *J, Fluid Mechan.* 504, 73–97. doi: 10.1017/S0022112004008213

Pitz, R. W., Hu, S., and Wang, P. (2014). Tubular premixed and diffusion flames: effect of stretch and curvature. *Prog. Energy Combust. Sci.* 42, 1–34. doi: 10.1016/j.pecs.2014.01.003

Poinsot, T. J., and Lelef, S. (1992). Boundary conditions for direct simulations of compressible viscous flows. *J. Comput. Phys.* 101, 104–129.

Sarras, G., Mahmoudi, Y., Arteaga Mendez, L., van Veen, E., Tummers, M., and Roekaerts, D. (2014). Modeling of turbulent natural gas and biogas flames of the delft jet-in-hot-coflow burner: Effects of coflow temperature, fuel temperature and fuel composition on the flame lift-off height. *Flow Turbul. Combust.* 93, 607–635. doi: 10.1007/s10494-014-9555-3

Sepman, A. V., Abtahizadeh, S. E., Mokhov, A. V., van Oijen, J. A., Levinsky, H. B., and de Goey, L. P. H. (2013b). Numerical and experimental studies of the NO formation in laminar coflow diffusion flames on their transition to MILD combustion regime. *Combust. Flame* 160, 1364–1372. doi: 10.1016/j.combustflame.2013.02.027

Sepman, A. V., Mokhov, A., and Levinsky, H. (2013a). Spatial structure and NO formation of a laminar methane-nitrogen jet in hot coflow under MILD conditions: a spontaneous raman and LIF study. *Fuel* 103, 705–710. doi: 10.1016/j.fuel.2012.10.010

Somers, L. M. T. (1994). *The simulation of flat flames with detailed and reduced chemical models*. Ph.D. thesis, Technische Universiteit Eindhoven, Eindhoven.

Swaminathan, N. (2019). Physical insights on mild combustion from dns. *Front. Mechan. Eng.* 5:59. doi: 10.3389/fmech.2019.00059

Tang, Z., Ma, P., Li, Y.-L., Tang, C., Xing, X., and Lin, Q. (2010). Design and experiment research of a novel pulverized coal gasifier based on flameless oxidation technology. *Proc. CSEE* 30, 50–55.

van Oijen, J. (2013). Direct numerical simulation of autoigniting mixing layers in MILD combustion. *Proc. Combust. Inst.* 34, 1163–1171. doi: 10.1016/j.proci.2012.05.070

Van Oijen, J., Bastiaans, R., and De Goey, L. (2007). Low-dimensional manifolds in direct numerical simulations of premixed turbulent flames. *Proc. Combust. Inst.* 31, 1377–1384. doi: 10.1016/j.proci.2006.07.076

van Oijen, J., and de Goey, L. (2000). Modelling of premixed laminar flames using flamelet-generated manifolds. *Combust. Sci. Technol.* 161, 113–137. doi: 10.1080/00102200008935814

Vasavan, A., de Goey, P., and van Oijen, J. (2018). Numerical study on the autoignition of biogas in moderate or intense low oxygen dilution nonpremixed combustion systems. *Energy Fuels* 32, 8768–8780. doi: 10.1021/acs.energyfuels.8b01388

Wünning, J., and Wünning, J. (1997). Flameless oxidation to reduce thermal NO-formation. *Prog. Energy Combust. Sci.* 23, 81–94.

**Conflict of Interest:** The authors declare that the research was conducted in the absence of any commercial or financial relationships that could be construed as a potential conflict of interest.

frontiers in Mechanical Engineering

ORIGINAL RESEARCH
published: 04 March 2020
doi: 10.3389/fmech.2020.00005

# Heat Release Rate Markers for the Adelaide Jet in Hot Coflow Flame

*Marco Ferrarotti[1,2], Ruggero Amaduzzi[1], Davide Bascherini[3], Chiara Galletti[3]* and Alessandro Parente[1]**

[1] Aero-Thermo-Mechanics Laboratory, Ecole Polytechnique de Bruxelles, Université Libre de Bruxelles, Brussels, Belgium, [2] Service de Thermique et de Combustion, Université de Mons, Mons, Belgium, [3] Civil and Industrial Engineering Department, University of Pisa, Pisa, Italy

In the present work, the correlation between the Heat Releaser Rate (HRR) and species mole fractions and net reaction rates is studied. The PaSR closure model is employed in a RANS framework to implement a detailed kinetic scheme, including the excited species OH*, used as a HRR marker. The effect of oxygen dilution on the combustion regime is investigated, as it can lead to Moderate or Intense Low-Oxygen Dilution (MILD) conditions. Two cases with different levels of oxygen concentration are analyzed. The results suggest the possibility of combining chemical species to construct an appropriate scalar to achieve better correlation with the HRR. It is found that typical markers such as radicals O, OH, OH* correlate fairly well with the HRR but improved correlations can be achieved with appropriate species mole fractions combinations, particularly for the MILD region of the flame.

**Keywords: heat release rate, heat release rate markers, OH*, laser induced fluorescence, jet in hot coflow, Moderate or Intense Low-Oxygen Dilution**

OPEN ACCESS

***Edited by:***
*Timothy S. Fisher, University of California, Los Angeles, United States*

***Reviewed by:***
*Tanvir I. Farouk, University of South Carolina, United States*
*Khanh Duc Cung, Southwest Research Institute, United States*
*Jamie Mi, Peking University, China*

***Correspondence:**
*Chiara Galletti*
*chiara.galletti@unipi.it*
*Alessandro Parente*
*Alessandro.Parente@ulb.be*

***Specialty section:***
*This article was submitted to Thermal and Mass Transport, a section of the journal Frontiers in Mechanical Engineering*

***Received:*** *07 June 2019*
***Accepted:*** *22 January 2020*
***Published:*** *04 March 2020*

***Citation:***
*Ferrarotti M, Amaduzzi R, Bascherini D, Galletti C and Parente A (2020) Heat Release Rate Markers for the Adelaide Jet in Hot Coflow Flame. Front. Mech. Eng. 6:5. doi: 10.3389/fmech.2020.00005*

## 1. INTRODUCTION

The Heat Release Rate (HRR) is a key physical quantity in combustion processes. It represents the amount of heat released per unit of time and space due to chemical reactions. Its spatial distribution directly influences important physical phenomena such as flame-turbulence interactions, sound generation and its interaction with flames. This latter may results in combustion instabilities, thus affecting the behavior of practical devices, such as gas turbines (Nikolaou and Swaminathan, 2014).

The mathematical expression of HRR is:

$$HRR = \sum_{\alpha=1}^{N} \dot{\omega}_\alpha h^0_{f,\alpha} \tag{1}$$

where $N$ is the number of species, $\dot{\omega}_\alpha$ is the reaction rate of the $\alpha$-th chemical species, and $h^0_{f,\alpha}$ is its standard enthalpy of formation. Clearly, a direct measurement of the HRR would involve the accurate determination of a significant number of scalars simultaneously (Nikolaou and Swaminathan, 2014). Due to such a high complexity, it is more practical to measure a quantity that presents some correlation with this rate over the relevant range of flame and flow parameters (Najm et al., 1998b), to qualitatively estimate the local HRR.

Generally, chemiluminescence of natural excited species, e.g., OH*, CH*, (where *denotes an electronically excited state) and Laser-Induced Fluorescence (LIF) techniques

(Najm et al., 1998a,b; Paul and Najm, 1998; Röder et al., 2013; Sidey and Mastorakos, 2015) are used to identify the reaction zone and its topology. However, the choice of the scalars able to identify the reaction region can be influenced by the specific chemical-physical behavior of the combustion process, determined in turn both by operative conditions and fuel mixture (Najm et al., 1998a,b; Nikolaou and Swaminathan, 2014). For instance, Vagelopoulos and Frank (2005) showed that the CH marker provides a reasonable correlation with the HRR only for undiluted reactant mixtures with equivalence ratios, $\phi$, of 0.8–1.2, whereas Najm et al. (1998a,b) and Paul and Najm (1998) showed that the formyl radical, HCO, is a good HRR-marker for stoichiometric or slightly rich ($\phi = 1.2$) methane and dimethyl ether-air laminar flames. Moreover, the flame stretch effects coming from flame-vortex interaction do not significantly influence this correlation (Najm et al., 1998b). According to the authors, the robust correlation between HRR and HCO concentration may be attributed to three main reasons: (1) HCO is a major intermediate species in oxydation of $CH_4$ to $CO_2$; (2) its concentration is directly dependent on its production rate; (3) HCO production is directly dependent on the concentration of $CH_2O$, that in turn directly depends on the reaction $CH_3 + O <=> CH_2O + H$, which shows the largest fractional influence on heat release rate (Paul and Najm, 1998). Nevertheless, Minamoto and Swaminathan (2014), Mulla et al. (2016), and Nikolaou and Swaminathan (2014) highlighted the difficulty of accurately measuring HCO concentration due to its low signal to noise ratio, thus suggesting to use the more reliable product of OH and $CH_2O$ local signals. Indeed, such species are involved as reactants in HCO formation from formaldehyde through the reaction $OH + CH_2O <=> HCO + H_2O$. This reconstructed LIF-signal was demonstrated to be a clear HRR-marker for the investigated conditions. Up to now, a wide number of different analysis (Fayoux et al., 2005; Richter et al., 2005; Li et al., 2018) on flame topology has relied on this assumption. Sidey and Mastorakos (2015) compared the presence of OH and OH* with the flame primary heat release region under MILD conditions, suggesting that the sole OH may not be a comprehensive HRR marker for MILD regime.

In more recent studies, Nikolaou and Swaminathan (2014) and Mulla et al. (2016) re-examined the validity of this reaction rate as flame marker for a certain number of combustion conditions. In particular, using Direct Numerical Simulations (DNS) data, they investigated undiluted and diluted methane-air flames, and multicomponent fuel mixtures under both laminar and turbulent conditions. The diluted case operated in Moderate or Intense Low oxygen Dilution (MILD) conditions (Minamoto and Swaminathan, 2014). Remarkable findings shown were: (1) a large fractional contribution of a reaction to the HRR does not automatically imply that this will have a good correlation with the HRR (Nikolaou and Swaminathan, 2014); thus, the rate of the aforementioned reaction, $CH_3 + O <=> CH_2O + H$, which often shows a high fractional influence on HRR, is not necessarily well correlated with the HRR. (2) HRR correlation is strongly dependent on the equivalence ratio. As a consequence, alternative markers were proposed. The product of H and $CH_2O$ concentrations, corresponding to reaction $H + CH_2O <=> HCO + H_2$, instead of OH and $CH_2O$ ones was suggested for turbulent MILD and conventional premixed methane-air flames. The viability of H-$CH_2O$ product LIF signal was demonstrated in Mulla et al. (2016).

The aim of this study is to add further understanding on the adequacy of the various HRR markers under diluted condition of a methane/hydrogen-air mixture for both MILD and not-MILD conditions. To this purpose, the widely studied Adelaide Jet in Hot Coflow (JHC) burner (Dally et al., 2002; Medwell et al., 2007; Wang et al., 2011) is modeled following Christo and Dally (2005), Aminian et al. (2012), Parente et al. (2016), Ferrarotti et al. (2019). Firstly, spatial correlations of chemical species and reaction rates with the local HRR are studied. Thence, appropriate combinations of species mole fractions are also taken into consideration and compared with conventional markers.

# 2. METHODOLOGY

## 2.1. Adelaide Jet in Hot Coflow Burner

The Adelaide JHC (Dally et al., 2002) has been extensively studied and modeled in literature because of its ability to emulate the MILD combustion regime as well as the large number of available experimental data. Hence, it represents a reference test case to validate computational models. For sake of clarity, a sketch of the burner is shown in **Figure 1**, together with numerical predictions of the OH radical for the two configurations investigated in this work. Inlet conditions are reported in **Table 1**. A central fuel jet made up of $CH_4$ and $H_2$ (50/50 by vol.) issues in a hot coflow (temperature of 1300K), made up of combustion products of fixed $CO_2$ and $H_2O$ (mass fractions $Y_{CO_2}$ = 6.5%, $Y_{H_2O}$ = 5.5%) and variable $O_2$ and $N_2$, coming from a secondary burner mounted upstream. The JHC burner is placed in a wind tunnel which feeds room temperature air at the same velocity of the coflow. In the configurations of interest for this study, namely HM1 and HM3 of Dally et al. (2002), coflow oxygen concentrations of 3% and 9% by mass, respectively, are considered. The same terminology of Dally et al. (2002) will be used in this paper for these two flames. The strong dilution kept in the HM1 configuration allows to emulate MILD combustion conditions in the first 100 mm of the flame (Medwell et al., 2007). After that, the entrained air from the surroundings changes the flame structure, which becomes closer to a standard diffusion flame, as shown in **Figure 1B**.

## 2.2. Numerical Model

Unsteady Favre-Averaged Numerical Simulations (uFANS) were performed using ANSYS Fluent R19.5. A two-dimensional axisymmetric grid, 0.6 m along axial direction and 0.2 m wide, of about 35k quadrilateral cells was employed. Two additional meshes were considered to evaluate the Grid Convergence Index (GCI), which was lower than 3% for temperature and major species. Moreover, a large refinement was set across the reaction zone to well capture gradients of composition and temperature. The standard k-$\epsilon$ with the first constant of the dissipation rate equation $C_{\epsilon 1} = 1.6$ (hence modified for round jets as suggested by Pope, 1978; Christo and Dally, 2005) was chosen as turbulence model. Turbulence-chemistry interactions were modeled using

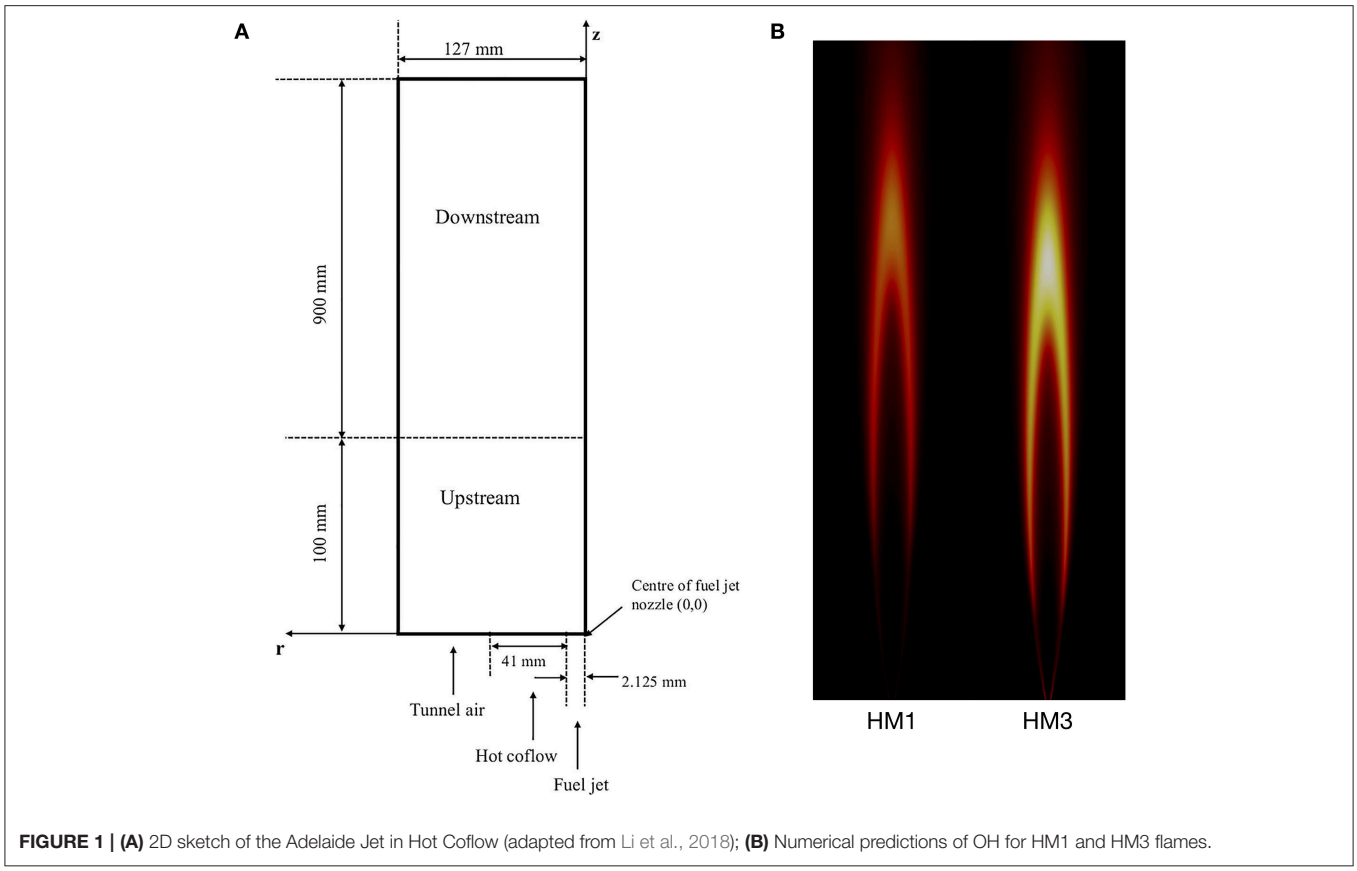


**FIGURE 1 | (A)** 2D sketch of the Adelaide Jet in Hot Coflow (adapted from Li et al., 2018); **(B)** Numerical predictions of OH for HM1 and HM3 flames.

**TABLE 1 |** JHC inlet velocities and temperatures.

| Profiles | Fuel jet | Coflow | Tunnel |
|---|---|---|---|
| Velocity [m/s] | 58.74 | 3.2 | 3.2 |
| Temperature [K] | 305 | 1300 | 294 |

the Partially Stirred Reactor (PaSR) model (Chomiak, 1990; Golovitchev and Chomiak, 2001). As with other reactor based models, the computational cell is split into two zones, one reactive and one in which only mixing occurs. The reactive zone mass fraction is estimated considering both the characteristic chemical and mixing time-scales $\tau_c$ and $\tau_{mix}$:

$$\kappa = \frac{\tau_c}{\tau_c + \tau_{mix}}. \tag{2}$$

The approach suggested by Ferrarotti et al. (2019) was used to express $\tau_{mix}$: the mixing time-scale is proportional to the integral time-scale $\frac{\kappa}{\epsilon}$:

$$\tau_{mix} = C_{mix}\frac{\kappa}{\epsilon}. \tag{3}$$

Based on previous studies (Ferrarotti et al., 2019), a constant $C_{mix}$ of 0.5 was considered. A dynamic approach (Sanders and Gökalp, 1998; Raman and Pitsch, 2007; Ye, 2011; Li et al., 2018; Ferrarotti et al., 2019) was then followed: the mixing time-scale $\tau_{mix}$ is defined based on local properties of the flow field, as it is estimated as the ratio of the mixture fraction variance $Z''^2$ to the mixture fraction dissipation rate $\chi$:

$$\tau_{mix} = \frac{\tilde{Z''^2}}{\tilde{\chi}}. \tag{4}$$

Transport equations for the Favre average of the two variables can be written as:

$$\frac{D\bar{\rho}\widetilde{Z''^2}}{Dt} = \frac{\partial}{\partial x_j}(\rho(D_m + D_t)\frac{\partial\widetilde{Z''^2}}{\partial x_j}) + 2\rho D_t(\frac{\partial\tilde{Z}}{\partial x_j})^2 - \rho\tilde{\chi}, \tag{5}$$

$$\begin{aligned}\frac{D\rho\tilde{\chi}}{Dt} &= \frac{\partial}{\partial x_j}(\rho(D_m + D_t)\frac{\partial\tilde{\chi}}{\partial x_j}) - C_{D_1}\bar{\rho}\frac{\tilde{\chi}^2}{\widetilde{Z''^2}} - C_{D_2}\bar{\rho}\frac{\tilde{\chi}\tilde{\epsilon}}{\tilde{\kappa}} \\ &\quad + C_{P_1}\frac{\tilde{\chi}}{\widetilde{Z''^2}}P_f + C_{P_2}\frac{\tilde{\chi}}{\tilde{\kappa}}P_k.\end{aligned} \tag{6}$$

where $Z$ is the mixture fraction, $D_t$ is the turbulent diffusivity, $P_f = -2\bar{\rho}\widetilde{u_k''Z''}(\frac{\partial\tilde{Z}}{\partial x_k})$ is the production of scalar fluctuation and $P_k = -\bar{\rho}\widetilde{u_k''u_i''}(\frac{\partial\tilde{U}_i}{\partial x_k})$ is the production of turbulent kinetic energy. The set of coefficients $C_{P_1}$, $C_{P_2}$, $C_{D_1}$, $C_{D_2}$ used is the one proposed by Ye (2011). The discrete ordinate (DO) method was used to solve the radiative transfer equation, estimating

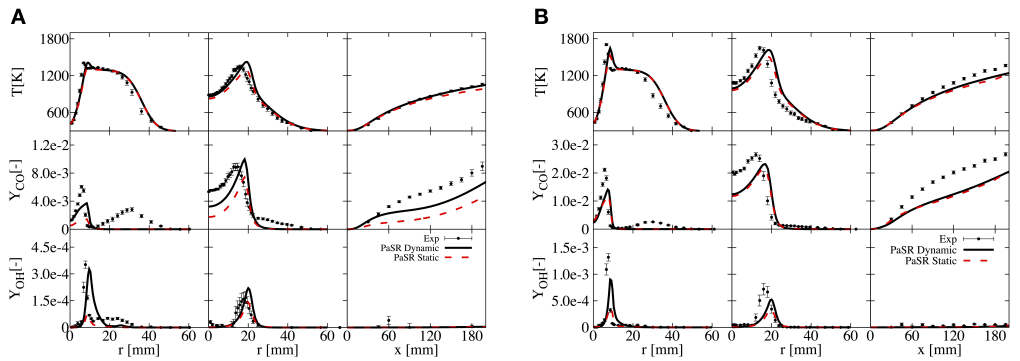


**FIGURE 2 |** Comparison of *T*, *OH*, and *CO* for static and dynamic PaSR with experimental data at axial locations of 30 and 120 mm and along the axis for HM1 **(A)** and HM3 **(B)** configurations.

spectral properties of the gaseous medium with the Weighted Sum of Gray Gases Model (WSGGM). Detailed chemistry was taken into account using the GRI2.11 mechanism (Bowman et al., 2020), excluding nitrogen-containing species. A sub-mechanism assembled by Kathrotia et al. (2012) and used also by Doan et al. (2018) was added to the main mechanism, to account for the conventional HRR-marker OH ($A^2\Sigma^+$), namely OH*. OH* is generally accepted as a marker for the flame-front structure and heat release rate, therefore its inclusion in the mechanism should enhance the description of the phenomena. This sub-mechanism consists of twelve reactions, whose Arrhenius terms are taken from Kathrotia et al. (2010), Tamura et al. (1998), and Smith et al. (2002). The resulting mechanism contains 32 chemical species and 187 reactions. To reduce the computational time associated to detailed chemistry, the *In situ* Adaptive Tabulation (ISAT) method by Pope (1997) was adopted with an ISAT tolerance of $10^{-5}$.

## 2.3. Analysis

HRR, chemical species mole fraction ($X_\alpha$, where $\alpha$ is the species index) and net reaction rate ($\dot{\omega}_r$, where $r$ is the reaction index) values were sampled along the radial direction at various axial distances from the burner nozzle. Each sampled profile is 50 mm long starting from the burner axis. Obtained data were used to estimate the metric $Z(\nu)$ at each axial location as proposed by Nikolaou and Swaminathan (2014), to appreciate how much a scalar $\nu$ is representative of the HRR. In particular, $Z(\nu)$ for the radial segment $s$ is defined as:

$$Z_s(\nu) = \sum_{n=1}^{Np} \left(\frac{|HRR_{n,s}|}{max_s(|HRR|)} - \frac{|\nu_{n,s}|}{max_s(|\nu|)}\right)^2. \quad (7)$$

In the equation above, $Np$ indicates the number of points of the radial segment, $max_s(|HRR|)$ and $max_s(\nu)$ are the maximum HRR and $\nu$ of that segment, respectively, while $\nu$ can be any scalar of interest. For the current case, it is either the mole fraction of the $\alpha$ chemical species $X_\alpha$, or the reaction rate $\dot{\omega}_r$. $Z_s(\nu)$ was normalized as $Z_s^+ = 100 \cdot Z_s/max(Z_s)$, as explained by Nikolaou and Swaminathan (2014). The Z-metric gives an idea on how well a normalized scalar reproduces the spatially matched normalized HRR. At each radius, the lowest values of $Z_s^+(\nu)$ identifies the scalars that best correlate with the HRR. It is worth to repeat that the fractional contribution of a reaction to the HRR is not a good way to identify the best HRR markers, whereas the $Z$-metric is a more rigorous technique, and for this reason was chosen as benchmark for comparison. If the chosen scalar is the net reaction rate, it may have positive and negative contributions to $Z$, thus giving ambiguous results. However, the top-correlating reactions have either only positive or negative contributions, without influencing the adequacy of the above definition. The results obtained in terms of mole fractions and reactions are presented in Sections 3.1 and 3.2. In Section 3.3, the analysis is also performed substituting to $\nu$ appropriate combinations of mole fractions to verify if there are products of species concentrations that may be more suitable for HRR identification.

# 3. RESULTS AND DISCUSSION

## 3.1. HM1 Case

The simulation results are first confronted with the experimental data from Dally et al. (2002), considering both static and dynamic approaches. Profiles of temperature, OH and CO at the axial locations of 30 and 120 mm, and along the axis are shown in **Figure 2** for HM1 (A) and HM3 (B). It can be appreciated how the simulation well reproduce the experimental measurements, as reported in Ferrarotti et al. (2019). Only results from the dynamic approach are presented from here onwards.

**Figure 3** show $Z_s^+(X_\alpha)$ values for the HM1 case (coflow $Y_{O_2} =$ 3%), calculated according to Equation (7) when $\nu = X_\alpha$, namely for all the 32 species of the employed mechanism. Furthermore, the product mole fractions of OH and $CH_2O$ proposed by Paul and Najm (1998), and of H and $CH_2O$ suggested by Nikolaou and Swaminathan (2014) are also taken into consideration. Six graphics, one for the respective axial location, $x$, collect only the first twelve values of $Z_s^+(X_\alpha)$ in ascending order. According to Equation (7), the lowest values are representative of best correlations with HRR. At this point, it is worth to remember that MILD combustion is achieved in the first 100 mm downstream of the burner exit for the HM1 case. After that, the entrained

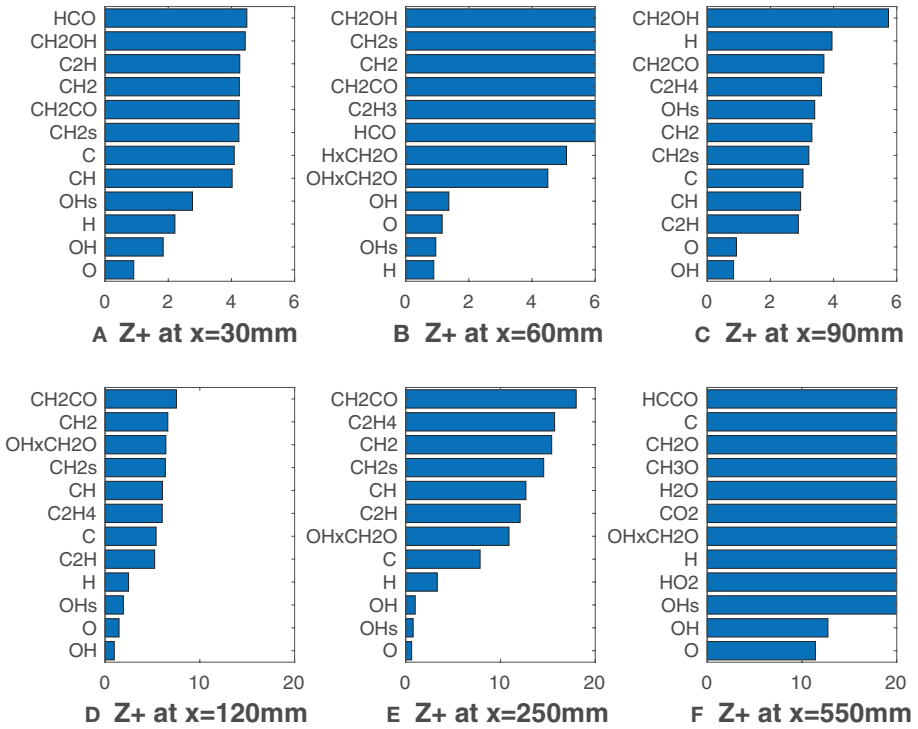


**FIGURE 3 |** HM1 case: best correlated species at various axial locations. Lower $Z_s^{\pm}(X_\alpha)$ values mean better correlation.

oxygen from the surrounding changes the combustion behavior. As shown in **Figure 3A**, for $x = 30$ mm all the species exhibit rather low values of $Z_s^+(X_\alpha)$, as $Z^+$ never exceeds 5. O, H, and the conventional HRR-markers OH and OH* provide the lowest values. At this axial location the flame brush is quite thin and the low $Z_s^+(X_\alpha)$ for most of the scalars can be attributed to this reason. **Figures 3B,C** show a different species ranking for $x = 60$ mm and $x = 90$ mm: for the former H and OH* provide lower values of $Z^+$, while O and OH are better correlated in the latter. However, at these locations, a clear selection of the best potential HRR markers cannot be made. Besides, $Z_s^+(X_\alpha)$ is generally low (under 10) for all the listed species suggesting that different scalars could be used to detect the reaction zone. Nevertheless, this behavior changes moving further from the jet nozzle: at $x = 120$ mm (**Figure 3D**) the gap between the four radicals, O, OH, OH*, H and the others becomes higher while the values of $Z_s^+(X_\alpha)$ grow. This difference is clear in **Figure 3E** where O, OH, OH* are unambiguously the top-three markers, while H usually presents a slightly lower matching with the HRR. At $x = 550$ mm (**Figure 3F**) and higher distances (not reported here) HRR decreases and all the correlations are lost rapidly. It is interesting to note that the formyl radical, HCO, conventionally used as marker with LIF techniques, displays higher values among the correlated species Moreover, contrary to what proposed by Najm et al. (1998b), the product of OH and $CH_2O$ mole fractions does not seem to be a good HRR marker, since its $Z_s^+$ is not within the top-five species. This finding may be due to the different chemical pathway followed when methane is diluted with hydrogen and is consistent with results from Kathrotia et al. (2012).

**Figure 4** adds further insights in this behavior, showing the normalized $Z$-metric obtained in terms of reactions rates instead of species concentrations. Hence, in Equation (7) the scalar $\nu$ is substituted with the kinetic reaction rate, $\dot{\omega}_r$ (where the subscript $r$ indicates the reaction). What stands out is that several reactions from the added OH($A^2\Sigma^+$) sub-mechanism appear among the top correlated reactions at many axial locations, while the reactions $O + CH_3 <=> H + CH_2O, OH + CH_2O <=> HCO + H_2O$ suggested by Najm et al. (1998b) and Paul and Najm (1998) and the reaction $H + CH_2O <=> HCO + H_2$ proposed by Nikolaou and Swaminathan (2014) are not present among the ones reported. This may be due to the fuel enrichment with hydrogen, since the cited literature refers to methane-only configurations. This is in line with the previous observations on mole fractions, which do not identify formaldehyde and formyl radical among the markers. Third-body reactions are present in the top ranking positions throughout the flame. The excitation reaction $H + O + M <=> M + OH^*$ (Kathrotia et al., 2012), together with $CH + O_2 <=> OH^* + CO$, is responsible for the formation of the common HRR marker (Sidey and Mastorakos, 2015; Doan et al., 2018). At $x = 60$ mm and $x = 90$ mm (**Figures 4B,C**) the third-body reaction of oxygen, $2O + M <=> O_2 + M$, shows the lowest values of $Z_s^{(+)}(\omega_r)$ and remains in the top-seven markers till the last sample. A conspicuous number of reactions involving the hydrogen peroxide, $H_2O_2$, and the hydroperoxyl radical, $HO_2$, replace the previous ones in the last

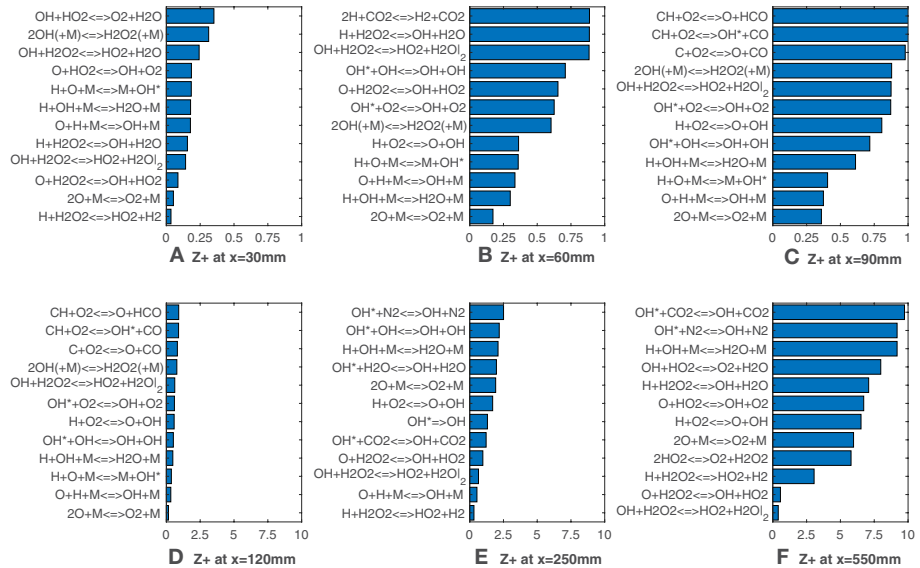


**FIGURE 4 |** HM1 case: best correlated net reaction rates at various axial locations. Lower $Z_s^+(\dot{\omega}_r)$ values mean better correlation.

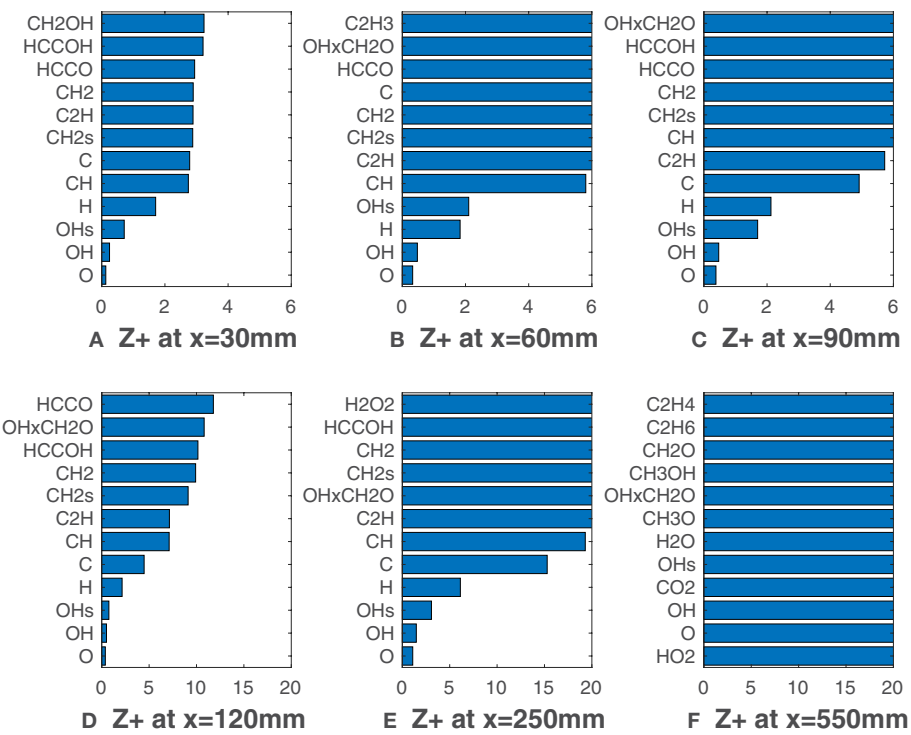


**FIGURE 5 |** HM3 case: best correlated species at various axial locations. Lower $Z_s^+(X_\alpha)$ values mean better correlation.

sampled segment at $x = 550$ mm (**Figure 4F**). Moreover, at this axial location, the reactions $H + HO_2 <=> 2OH$ and $H + HO_2 <=> O + H_2O$ do not appear, even though their reaction rates were found to be good HRR indicators by Nikolaou and Swaminathan (2014) for lean to near-stoichiometric methane-air mixtures and especially at low value of HRR.

## 3.2. Comparison With HM3 Case

**Figure 5** reports $Z_s^+(X_\alpha)$ relative to the coflow oxygen concentration of 9%, i.e., HM3 flame. With this configuration the flame is visible since its beginning (**Figure 1B**), and MILD conditions are not reached. Unlike **Figures 3A–D**, O, OH, OH* radicals show unambiguously greater correlation with

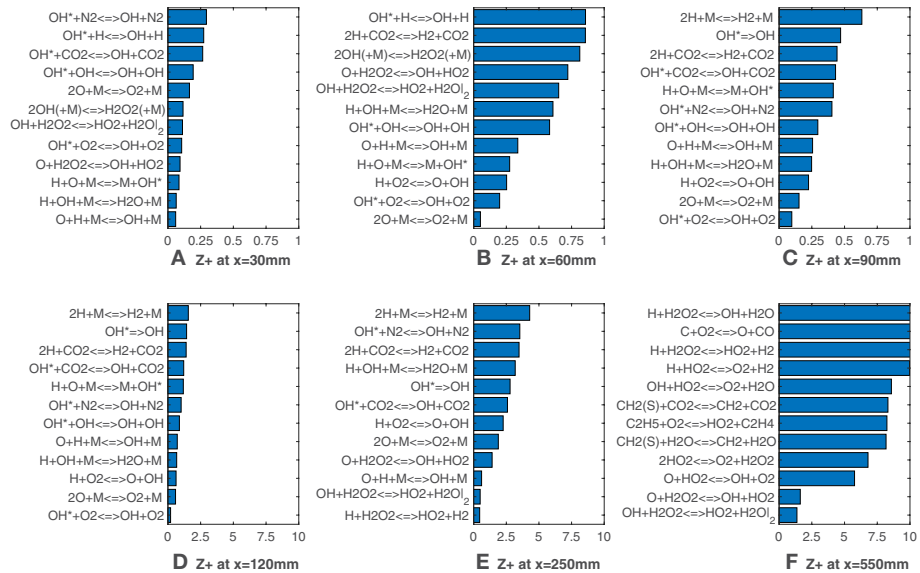


**FIGURE 6 |** HM3 case: best correlated net reaction rates at various axial locations. Lower $Z_s^+(\dot{\omega}_r)$ values mean better correlation.

HRR if compared to the other species. O and OH present slightly higher $Z_s^+(X_\alpha)$-values throughout the entire domain. As previously underlined, at long distances HRR decades and $Z_s^+(X_\alpha)$ increases fast for all the species. It is interesting to note that this last phenomena emerges a bit before if compared to the HM1 case. Indeed, in the HM1 configuration combustion is somewhat slowed down due to MILD conditions. This leads to a slightly longer flame for $Y_{O_2} = 3\%$, explaining why the correlations drop down later with respect to the HM3 case. The product of OH and $CH_2O$ mole fractions appears as well in **Figure 5**, always having a higher $Z_s^+(X_\alpha)$ value. It is clear that the influence of oxygen concentration plays a significant role in determining the best HRR-markers. For the HM3 case the distinction between the top three markers O, OH, OH* and the others is noticeable from the beginning of the combustion process, whereas, for the 3% coflow case, this distinction becomes clearer only downstream of 100 mm of flame, due to the higher level of entrained oxygen from surroundings.

Looking now at **Figure 6**, it is interesting to note that values of $Z_s^+(\dot{\omega}_r)$ are generally lower up to 90 mm if compared with the HM1 case. The OH* formation reaction appears again as a good indicator of heat release as several reactions from the sub-mechanism are listed. Also in this case, for $x = 250$ mm and $x = 550$ mm (**Figures 6E,F**), reactions involving hydroperoxyl radical show a very good agreement with the HRR. In the latter, $OH+H2O2 <=> HO2+H2O$ and $O+H2O2 <=> OH+HO2$ cover the first positions, suggesting that their rates could be good HRR markers at this location with the 9% coflow oxygen concentration.

## 3.3. Combinations of Mole Fractions

**Figures 7**, **8** report $Z_s^+(\nu)$ calculated substituting species mole fractions $X_\alpha$ and their combinations to $\nu$. It is noteworthy that several combinations present values lower than the lowest ones recorded in **Figures 3**, **5**. The product of O and OH shows a very good agreement with the HRR and is the solution of choice till $x = 120$ mm (**Figure 7**). This notable results may suggest that for MILD combustion under the conditions of interest, an appropriate combination of species can identify the reaction zone more precisely than a single species, thus with less uncertainty on the choice of the right scalar. Just above the combination OxOH (here x is the product symbol), combinations of H, O, OH and OH* show also a very good correlation metric. At higher distances, combinations of these 3 radicals with the major species $H_2O$ and $CO_2$ are ranked first. As expected, this change occurs first for the HM3 configuration (**Figure 8**).

The distributions of HRR, mole fraction and combinations are reported and compared in **Figure 9**. The 6 graphics correspond to 3 positions of the 2 cases studied, i.e., $x = 60$ mm, $x = 120$ mm and $x = 550$ mm, respectively. Only radial profiles of the top-two species and the top-two combinations are drawn together with the HRR. All these scalars are normalized with respect to their own maximum. It is worth noting that both species mole fractions and combinations capture the HRR peak very well in **Figures 9A,B,D,E**. The main difference is associated to the tails of the curves, for low values of HRR. In particular, using the mole fraction products allows to have a higher correlation in these branches and capture the near-zero HRR behavior. This might also suggest a good detection of local extinction. Different considerations should be done for **Figures 9C,F**. At $x = 550$ mm, the HRR curve is wider and, as stated previously, the sole species are not a very good HRR marker, especially for the HM3 case.

Looking to the contour plots (**Figure 10**) reported as a qualitative example, it is possible to identify the 3 zones previously underlined. Two black dotted lines divide this zones

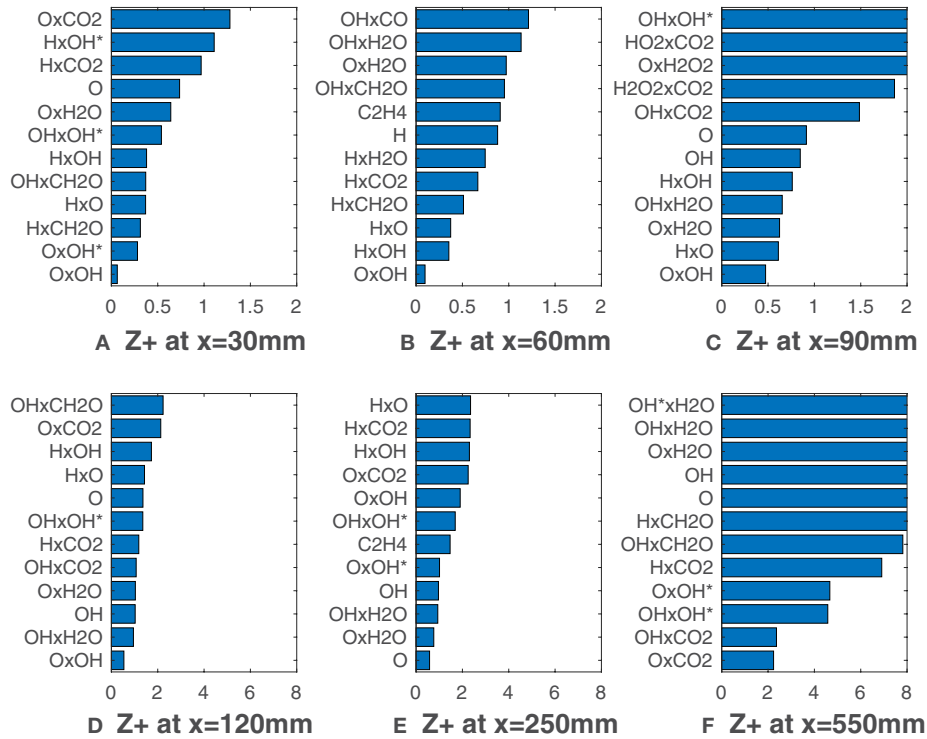


**FIGURE 7 |** HM1 case: best correlated markers at various axial locations. Lower $Z_s^+(\nu)$ values mean better correlation. Here $\nu$ comprehends both $X_\alpha$ and their combinations.

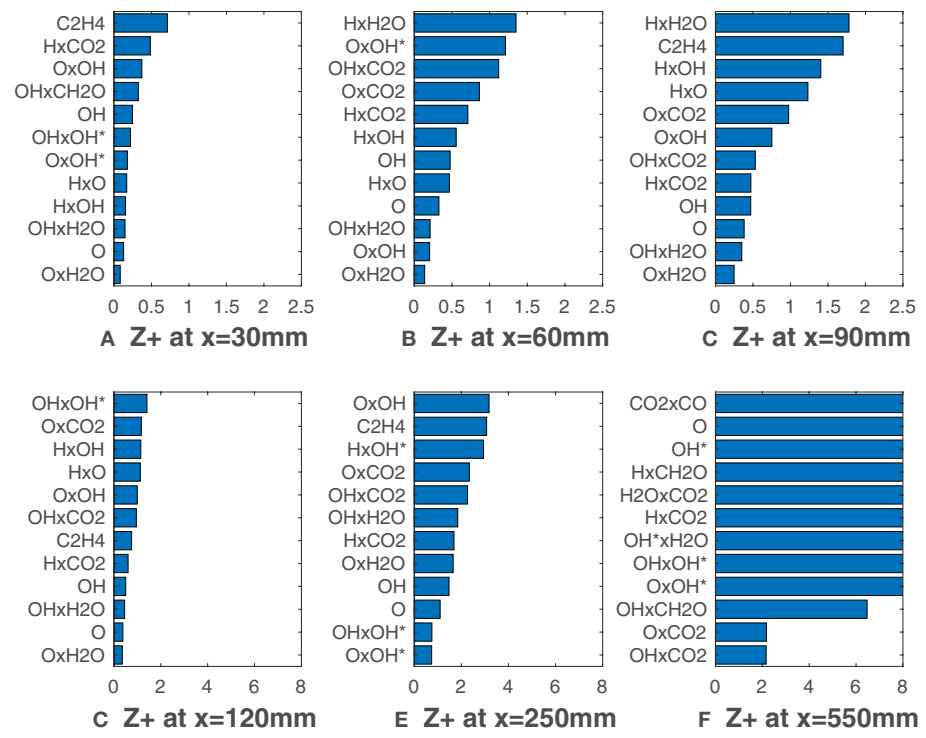


**FIGURE 8 |** HM3 case: best correlated markers at various axial locations. Lower $Z_s^+(\nu)$ values mean better correlation. Here $\nu$ comprehends both $X_\alpha$ and their combinations.

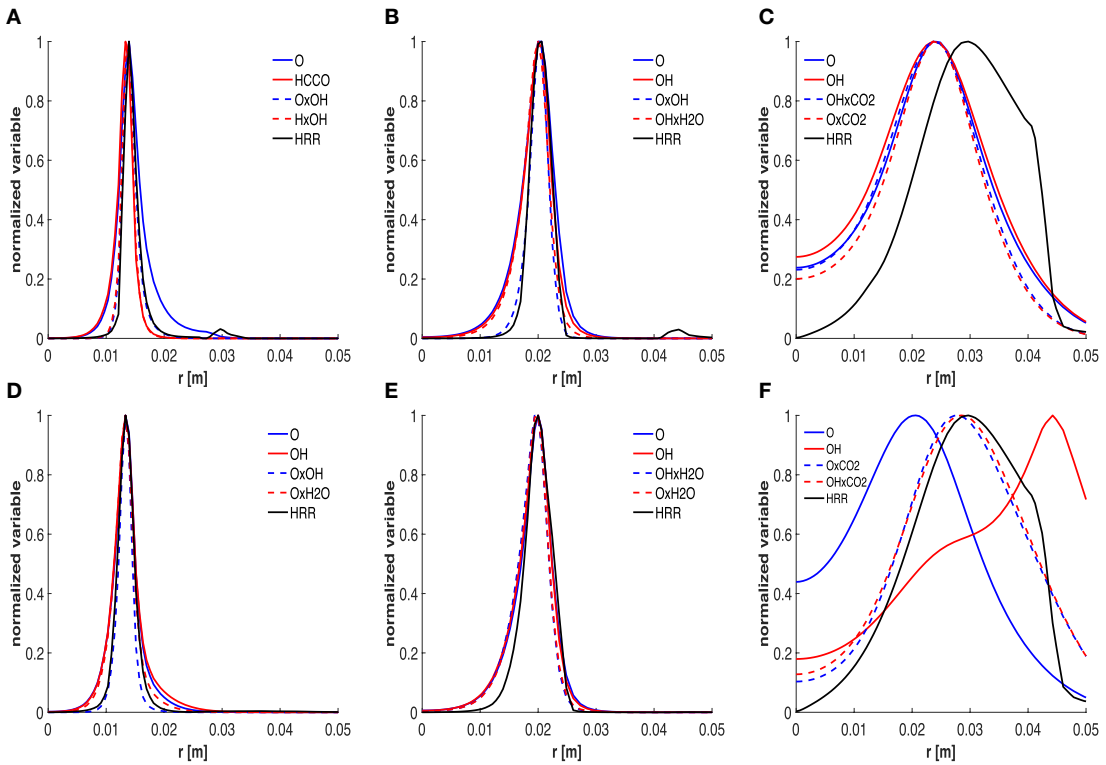


**FIGURE 9 |** Trends of normalized HRR, top-two mole fractions and combinations at 60 **(A,D)**, 120 **(B,E)** and 550 **(C,F)** mm, respectively. First and second row refer to the HM1 and HM3 cases, respectively.

at $x = 150$ mm and $x = 450$ mm. For each part, the best HRR marker combination is reported.

## 4. CONCLUSION

The choice of the right HRR marker is fuel-mixture specific and depends also on operative conditions. Therefore, the applicability of conventional HRR markers is not universal and should be tested for different flame configurations. To further investigate the applicability of the different available markers, numerical simulations of the Adelaide JHC were carried out with detailed chemistry, including the excited species OH*. The interesting feature of the JHC is the possibility to module oxygen dilution and the change in combustion behavior observed when the entrained oxygen from surroundings changes the flame from invisible to visible. Hence, correlations between HRR and both species mole fractions and reaction rates were investigated at various axial locations along the radial direction for two level of coflow oxygen mass fractions, 3% and 9%.

In summary, in a clear distinction among $Z_s^+(X_\alpha)$ values cannot be made for the HM1 case in the first 120 mm of flame. In this range the radical OH is always one of the four top markers (**Figure 3**). Further downstream from the burner, the top-three markers are O, OH, OH* radicals. The reaction rates that better correlate with the HRR are shown to belong mostly to reactions of the OH* sub-mechanism and involve primarily these radicals together with other species such as H, $O_2$, $HO_2$, $H_2O_2$, $H_2O$, CO, $CO_2$. Some of these appearing only at high axial locations. For the HM3 configuration, a very good agreement between the top-three radicals O, OH, OH* and the HRR was found right from the first axial location (**Figure 5**), suggesting that a higher oxygen level allows better correlation with the HRR. This is in line with the change in the results of the HM1 case, since beyond $x = 100$ mm, the entrained air increase the available oxygen for the flame (Dally et al., 2002; Medwell et al., 2007). With regard to the most correlated reaction rates, their relative reactions involve again the aforementioned 10 species.

Even though conventional HRR markers such as OH and OH* perform well along most of the flame, a better detection of the reaction zone may be achieved using appropriate combinations of species. Considering the change of the combustion behavior due to the entrained oxygen from the air stream, different parts of the flame should be detected by different markers. For the HM1 case, the combination of O and OH mole fractions seems to be the right choice for the MILD region while beyond $x = 150$ mm, the HRR is well captured by the product $OxCO_2$, for both the configurations. Finally, only in the region far from the nozzle, i.e.,

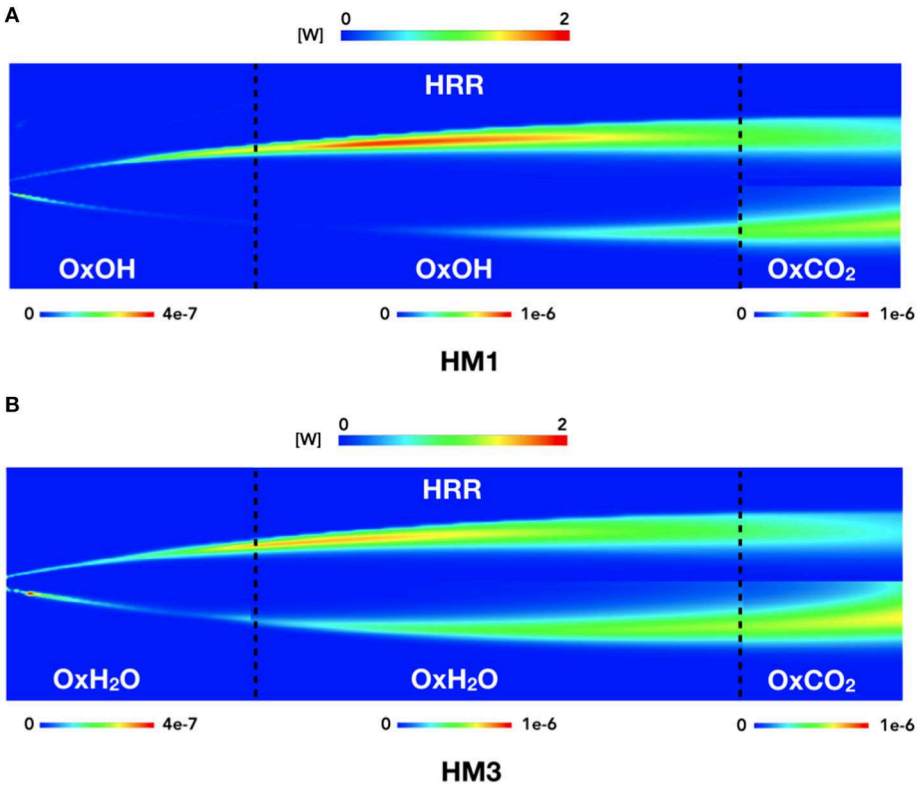


**FIGURE 10 |** HM1 and HM3 contour plots of HRR compared to species products contours. The three zones are split as follows: from 0 to 150 mm, from 150 to 450 mm, and from 450 to 550 mm.

the last 150 mm of the studied domain, the low and wide values of HRR are better captured by combinations of O and OH with carbon dioxide.

The applicability of these markers for other conditions and fuel mixtures will be subject of future studies.

## DATA AVAILABILITY STATEMENT

All datasets generated for this study are included in the article.

## AUTHOR CONTRIBUTIONS

MF carried out the numerical simulations and the post-processing, and lead the manuscript writing. RA and DB contributed to the CFD simulations and paper writing. CG and AP supervised the work, critically discussed the results, and contributed to the writing.

## FUNDING

This project has received funding from the European Research Council (ERC) under the European Union's Horizon 2020 research and innovation programme under grant agreement no. 714605. MF wishes to thank the Fonds de la Recherche Scientifique FNRS Belgium for financing his research.

## ACKNOWLEDGMENTS

The authors thank B. B. Dally at University of Adelaide for granting access to the experimental data.

## REFERENCES

Aminian, J., Galletti, C., Shahhosseini, S., and Tognotti, L. (2012). Numerical investigation of a mild combustion burner: analysis of mixing field, chemical kinetics and turbulence-chemistry interaction. *Flow Turbul. Combust.* 88, 597–623. doi: 10.1007/s10494-012-9386-z

Bowman, C. T., Hanson, R. K., Davidson, D. F., Gardiner, W. C. Jr., Lissianski, V., Smith, G. P., et al. (2020). Gri 2.11 Mechanism. Available online at: http://www.me.berkeley.edu/gri_mech/

Chomiak, J. (1990). *Combustion: A Study in Theory, Fact and Application.* New York, NY: Abacus Press; Gorden and Breach Science Publishers.

Christo, F., and Dally, B. (2005). Modeling turbulent reacting jets issuing into a hot and diluted coflow. *Combust. Flame* 142, 117–129. doi: 10.1016/j.combustflame.2005.03.002

Dally, B., Karpetis, A., and Barlow, R. (2002). Structure of turbulent non-premixed jet flames in a diluted hot coflow. *Proc. Combust. Inst.* 29, 1147–1154. doi: 10.1016/S1540-7489(02)80145-6

Doan, N., Swaminathan, N., and Minamoto, Y. (2018). Dns of mild combustion with mixture fraction variations. *Combust. Flame* 189, 173–189. doi: 10.1016/j.combustflame.2017.10.030

Fayoux, A., Zähringer, K., Gicquel, O., and Rolon, J. (2005). Experimental and numerical determination of heat release in counterflow premixed laminar flames. *Proc. Combust. Inst.* 30, 251–257. doi: 10.1016/j.proci.2004.08.210

Ferrarotti, M., Li, Z., and Parente, A. (2019). On the role of mixing models in the simulation of mild combustion using finite-rate chemistry combustion models. *Proc. Combust. Inst.* 37, 4531–4538. doi: 10.1016/j.proci.2018.07.043

Golovitchev, V., and Chomiak, J. (2001). "Numerical modeling of high temperature air flameless combustion," in *Proceedings of the 4th International Symposium on High Temperature Air Combustion and Gasification (HiTACG)* (Rome), 27–30.

Kathrotia, T., Fikri, M., Bozkurt, M., Hartmann, M., Riedel, U., and Schulz, C. (2010). Study of the h+o+m reaction forming OH*: Kinetics of OH* chemiluminescence in hydrogen combustion systems. *Combust. Flame* 157, 1261–1273. doi: 10.1016/j.combustflame.2010.04.003

Kathrotia, T., Riedel, U., Seipel, A., Moshammer, K., and Brockhinke, A. (2012). Experimental and numerical study of chemiluminescent species in low-pressure flames. *Appl. Phys. B* 107, 571–584. doi: 10.1007/s00340-012-5002-0

Li, Z., Ferrarotti, M., Cuoci, A., and Parente, A. (2018). Finite-rate chemistry modelling of non-conventional combustion regimes using a partially-stirred reactor closure: combustion model formulation and implementation details. *Appl. Energy* 225, 637–655. doi: 10.1016/j.apenergy.2018.04.085

Medwell, P. R., Kalt, P., and Dally, B. (2007). Simultaneous imaging of oh, formaldehyde, and temperature of turbulent nonpremixed jet flames in a heated and diluted coflow. *Combust. Flame* 148, 48–61. doi: 10.1016/j.combustflame.2006.10.002

Minamoto, Y., and Swaminathan, N. (2014). Scalar gradient behaviour in mild combustion. *Combust. Flame* 161, 1063–1075. doi: 10.1016/j.combustflame.2013.10.005

Mulla, I., Dowlut, A., Hussain, T., Nikolaou, Z., Chakravarthy, S., Swaminathan, N., et al. (2016). Heat release rate estimation in laminar premixed flames using laser-induced fluorescence of ch2o and h-atom. *Combust. Flame* 165, 373–383. doi: 10.1016/j.combustflame.2015.12.023

Najm, H., Knio, O., Paul, P., and Wyckoff, P. (1998a). A study of flame observables in premixed methane - air flames. *Combust. Sci. Technol.* 140, 369–403. doi: 10.1080/00102209808915779

Najm, H., Paul, P., Mueller, C., and Wyckoff, P. (1998b). On the adequacy of certain experimental observables as measurements of flame burning rate. *Combust. Flame* 113, 312–332. doi: 10.1016/S0010-2180(97)00209-5

Nikolaou, Z., and Swaminathan, N. (2014). Heat release rate markers for premixed combustion. *Combust. Flame* 161, 3073–3084. doi: 10.1016/j.combustflame.2014.05.019

Parente, A., Malik, M., Contino, F., Cuoci, A., and Dally, B. (2016). Extension of the eddy dissipation concept for turbulence/chemistry interactions to mild combustion. *Fuel* 163, 98–111. doi: 10.1016/j.fuel.2015.09.020

Paul, P., and Najm, H. (1998). Planar laser-induced fluorescence imaging of flame heat release rate. *Symp. (Int.) Combust.* 27, 43–50. doi: 10.1016/S0082-0784(98)80388-3

Pope, S. (1978). An explanation of the turbulent round-jet/plane-jet anomaly. *AIAA J.* 16, 279–281. doi: 10.2514/3.7521

Pope, S. (1997). Computationally efficient implementation of combustion chemistry using *in situ* adaptive tabulation. *Combust. Theory Model.* 1, 41–63. doi: 10.1080/713665229

Raman, V., and Pitsch, H. (2007). A consistent LES/filtered-density function formulation for the simulation of turbulent flames with detailed chemistry. *Proc. Combust. Inst.* 31, 1711–1719. doi: 10.1016/j.proci.2006.07.152

Richter, M., Collinm, R., Nygren, J., Aldeacute, M., Hildingsson, N., and Johansson, B. (2005). Studies of the combustion process with simultaneous formaldehyde and OH PLIF in a direct-injected hcci engine. *JSME Int. J. Ser. B Fluids Ther. Eng.* 48, 701–707. doi: 10.1299/jsmeb.48.701

Röder, M., Dreier, T., and Schulz, C. (2013). Simultaneous measurement of localized heat-release with OH/CH2O-LIF imaging and spatially integrated OH* chemiluminescence in turbulent swirl flames. *Proc. Combust. Inst.* 34, 3549–3556. doi: 10.1016/j.proci.2012.06.102

Sanders, J., and Gökalp, I. (1998). Scalar dissipation rate modelling in variable density turbulent axisymmetric jets and diffusion flames. *Phys. Fluids* 10, 938–948. doi: 10.1063/1.869616

Sidey, J., and Mastorakos, E. (2015). Visualization of mild combustion from jets in cross-flow. *Proc. Combust. Inst.* 35, 3537–3545. doi: 10.1016/j.proci.2014.07.028

Smith, G., Luque, J., Park, C., Jeffries, J., and Crosley, D. (2002). Low pressure flame determinations of rate constants for OH(A) and CH(A) chemiluminescence. *Combust. Flame* 131, 59–69. doi: 10.1016/S0010-2180(02)00399-1

Tamura, M., Berg, P., Harrington, J., Luque, J., Jeffries, J., Smith, G., et al. (1998). Collisional quenching of CH(A), OH(A), and NO(A) in low pressure hydrocarbon flames. *Combust. Flame* 114, 502–514. doi: 10.1016/S0010-2180(97)00324-6

Vagelopoulos, C., and Frank, J. (2005). An experimental and numerical study on the adequacy of CH as a flame marker in premixed methane flames. *Proc. Combust. Inst.* 30, 241–249. doi: 10.1016/j.proci.2004.08.243

Wang, F., Mi, J., Li, P., and Zheng, C. (2011). Diffusion flame of a CH4/H2 jet in hot low-oxygen coflow. *Int. J. Hyd. Energy* 36, 9267–9277. doi: 10.1016/j.ijhydene.2011.04.180

Ye, I. (2011). *Investigation of the scalar variance and scalar dissipation rate in URANS and LES (Ph.D. thesis),* University of Waterloo, Waterloo, ON, Canada.

**Conflict of Interest:** The authors declare that the research was conducted in the absence of any commercial or financial relationships that could be construed as a potential conflict of interest.

frontiers in Mechanical Engineering

MINI REVIEW
published: 06 March 2020
doi: 10.3389/fmech.2020.00007

# Critical Issues of Chemical Kinetics in MILD Combustion

*Pino Sabia* and Mara de Joannon*

*Istituto di Ricerche Sulla Combustione, Consiglio Nazionale delle Ricerche, Naples, Italy*

Mild combustion processes occur with mixtures highly diluted and preheated by a strong recirculation of hot exhausted gases (thus mass and sensible enthalpy) within the combustion chamber. This strategy configures a process based on autoignition kernels outside or close to flammability limits transported by convection in the combustion chamber, thus defining a process with unique physical and chemical features drastically different from traditional deflagrative-diffusive flames. The article aims at analyzing the recent issues relative to kinetic aspects involved in moderate or intense low-oxygen dilution (MILD) combustion processes. First, the article comes through the identification of peculiar experimental features of simple hydrocarbons oxidation process induced by highly preheated and diluted conditions in model reactors typical of chemical engineering. Second, the effects of steam and carbon dioxides on fuel oxidation process, whose presence within the combustion chamber is imposed by high levels of hot gas recirculation, are addressed. Third, the article comes through a thorough analysis of recent scientific contributions on kinetic aspects of MILD combustion processes to identify the critical points in modeling activities.

**Keywords: jet stirred flow reactor, tubular flow reactor, combustion regimes, temperature oscillations, NTC behavior, $H_2O$ and $CO_2$ chemical effects, chemistry modeling queries**

OPEN ACCESS

***Edited by:***
*Nesrin Ozalp,*
*University of Minnesota Duluth,*
*United States*

***Reviewed by:***
*Tanvir I. Farouk,*
*University of South Carolina,*
*United States*
*Shiyou Yang,*
*Ford Motor Company, United States*

****Correspondence:***
*Pino Sabia*
*sabia@irc.cnr.it*

***Specialty section:***
*This article was submitted to Thermal and Mass Transport, a section of the journal Frontiers in Mechanical Engineering*

***Received:*** *18 October 2019*
***Accepted:*** *28 January 2020*
***Published:*** *06 March 2020*

***Citation:***
*Sabia P and de Joannon M (2020) Critical Issues of Chemical Kinetics in MILD Combustion. Front. Mech. Eng. 6:7. doi: 10.3389/fmech.2020.00007*

## INTRODUCTION

The attention of the scientific and industrial community involved in the identification and development of energy production systems has been devoted to new technologies under the keywords of high efficiency and reduced emissions. Given this background, clean combustion processes still can play an important role, but they are required to be flexible with respect to thermal loads, to respond to the fluctuation of energy produced (Luo et al., 2015) by renewable sources in virtue of their intrinsic intermittence (Lund and Kempton, 2008; Keyhani et al., 2010; Østergaard, 2012; Abdmouleh et al., 2015) and to be flexible with respect to fuel nature itself, given the high variability of fuels composition and smart "energy carriers" (Spliethoff et al., 1996; McKendry, 2002; Demirbas, 2004; Hosseini and Wahid, 2016; Van Vuuren et al., 2017; SMARTCATs COST[1]). Such a further requirement embitters the difficulties to develop advanced combustion technologies, because new processes [i.e., staged combustion, lean premixed, etc. (Zabetta et al., 2005; Huang and Yang, 2009; Dunn-Rankin, 2011; Cozzi and Coghe, 2012)] may work properly in restricted ranges of system parameters.

Among new combustion concepts, one promising candidate to simultaneously meet thermal efficiency needs and pollutant emission restrictions, while responding to fuel and thermal load flexibility, appears to be the moderate or intense low-oxygen dilution (MILD) combustion

[1]SMARTCATs COST *Action CM1404*, http://www.smartcats.eu/.

(Wünning and Wünning, 1977; Weber et al., 2000, 2005; Cavaliere and de Joannon, 2004; Dally et al., 2004; Milani and Wünning, 2007). This combustion is also renewed as flameless oxidation (or FLOX) (Wünning and Wünning, 1977; Milani and Wünning, 2007), high-temperature air combustion (Katsuki and Hasegawa, 1998; Tsuji et al., 2003), and low-temperature combustion for engine applications (Saxena and Bedoya, 2013).

The MILD combustion has been successfully employed in furnaces and boilers, and it could be potentially used into many other applications, such as gas turbines, biogas burners, burners for hydrogen reformers, or for combined heat and power (CHP) units and engines (Levy et al., 2004; Riccius et al., 2005; Lückerath et al., 2008; Khalil and Gupta, 2011; Li et al., 2011; Reddy et al., 2015; Ho et al., 2016). In addition, MILD-oxyfuel combustion for coal combustions represents a subcategory of MILD processes with high potentiality to overcome problems relative to oxycombustion systems (Li et al., 2011, 2013).

MILD combustion relies on a strong recirculation of mass and sensible enthalpy by recycling the exhausted gases to dilute and simultaneously preheat fresh reactants (Wünning and Wünning, 1977; Katsuki and Hasegawa, 1998; Weber et al., 2000, 2005; Tsuji et al., 2003; Cavaliere and de Joannon, 2004; Dally et al., 2004; Milani and Wünning, 2007; Khalil and Gupta, 2011; Saxena and Bedoya, 2013; Reddy et al., 2015). The intrinsic nature of the process is based on autoignition/fuel-ultra-lean kernels that increase in size while being transported by convection (Van Oijen, 2013; Minamoto and Swaminathan, 2015), imposed by high-turbulence exhausted gas recirculation fluid-dynamics patterns, thus defining a process with homogenous intensive parameters within the combustion chamber (Özdemir and Peters, 2001; Noor et al., 2013a; Sidey et al., 2014; Sidey and Mastorakos, 2015).

Characteristic working temperatures are modest ($T <$ 1,500 K) and below critical values for the production of pollutants (i.e., $NO_x$, particulate matter; Wünning and Wünning, 1977; Weber et al., 2000; Cavaliere and de Joannon, 2004; Milani and Wünning, 2007), while complete fuel conversion, high thermal efficiencies, and process stability are ensured by the high recirculated sensible enthalpy. Because the stability of the oxidation process does not rely on heat feedback mechanisms from the flame front, as in conventional diffusion/deflagrative flames, but on the recycled sensible heat, the process is intrinsically highly flexible with respect to fuels chemical/physical properties and quality (Weber et al., 2005; Colorado et al., 2010; Derudi and Rota, 2011; Hosseini and Wahid, 2013; Noor et al., 2013a), given that the mixture temperature after the mixing process between fresh reactants and recirculated gas is higher than mixtures autoignition one.

MILD combustion processes present unique physical/chemical features, drastically different from traditional combustion systems, which should be discussed at basic levels for the fine comprehension of the process itself. The structure of the reactive region (Özdemir and Peters, 2001; de Joannon et al., 2012a,b; Van Oijen, 2013; Minamoto et al., 2014; Minamoto and Swaminathan, 2015; Sorrentino et al., 2019), the chemistry (de Joannon et al., 2005; Zhukov et al., 2005; Li et al., 2014; Sabia et al., 2014; Lubrano Lavadera et al., 2018b), and the interaction between chemistry–turbulence (Dally et al., 2004; Parente et al., 2008, 2016; Isaac et al., 2013; Noor et al., 2013b) represent key points to address, with strong implications also on modeling activities (Dally et al., 2004; Parente et al., 2008, 2016; Isaac et al., 2013; Noor et al., 2013b).

Among the issues to consider, the chemical aspect of the oxidation process represents a fundamental one. In fact, the high levels of dilution coupled with moderate working temperatures imply a drastic change of the kinetics involved during the fuel oxidation process with respect to flame chemistry, with relatively lower chemical characteristic times and heat release rates (Dally et al., 2004; de Joannon et al., 2005; Zhukov et al., 2005; Parente et al., 2008, 2016; Isaac et al., 2013; Noor et al., 2013b; Li et al., 2014; Sabia et al., 2014; Lubrano Lavadera et al., 2018b). Furthermore, it occurs in presence of great amounts of non-inert species, such as carbon dioxide and steam, which can alter the kinetic routes by means of several effects, here reported:

1) Thermal: higher heat capacities with respect to $N_2$, thus lower adiabatic flame temperature;
2) Kinetic: they participate directly in bimolecular reactions and enhance the role of third-molecular reactions because of higher third-body efficiencies with respect to $N_2$. For these effects, a huge literature has been produced in the last decade, as reported in the next paragraphs (Fedyaeva et al., 2018; Lubrano Lavadera et al., 2018a).

In addition, these species can modify the structure of the reactive region because of the variation of the transport properties of the mixture (Dally et al., 2004; Mardani et al., 2010, 2013) and lowering local temperatures by enhancing heat radiation transfer (Dally et al., 2004; Mardani et al., 2013; Sorrentino et al., 2018; Zhang et al., 2019) mechanisms, because of their high radiative properties.

In this article, the chemical issues of MILD combustion processes are discussed. They will be analyzed throughout the implication on simple hydrocarbons oxidation chemistry, but the discussion could be extended to higher pressures (Gurentsov et al., 2002; Zhukov et al., 2005; Sjöberg et al., 2007; Le Cong and Dagaut, 2008, 2009a,b; Anderlohr et al., 2010; Xie et al., 2014b; Donohoe et al., 2015), to $H_2$ and syngas (Mueller et al., 1999; Park et al., 2003; Wang et al., 2003; Zabetta et al., 2005; Le Cong and Dagaut, 2008; Lee et al., 2012; Xie et al., 2014a), or to high-molecular-weight paraffins at elevated pressures (Sjöberg et al., 2007; Anderlohr et al., 2010).

## OXIDATION PROCESS OF SIMPLE HYDROCARBONS UNDER DILUTED CONDITION

MILD oxidation configures as a chemically controlled process with characteristic kinetic times relatively longer than the ones involved in traditional flames. Within this slow oxidation regime, system exchange phenomena can drastically endorse the establishment of instabilities if coupled with complex heat reaction release rates, given the high non-linearity of exothermic/endothermic reactions. The direct experimental

evidence is the insurgence of peculiar oxidation phenomena, as reported in the following.

**Figure 1** is relative to the experimental combustion regimes detected for methane/oxygen mixtures diluted in nitrogen at $d =$ 90% at environmental pressure in a jet stirred flow reactor (JSFR) (de Joannon et al., 2005) and in a tubular flow reactor (TFR) (Sabia et al., 2014).

**Figures 1A,B** are relative to the JSFR. The mixture averaged residence time ($\tau$) is 0.5 s. The characteristic combustion regimes were summarized in a carbon/oxygen feed ratio/mixture inlet temperature (C/O-$T_{in}$) map. Steady combustion and dynamic behaviors were identified. The widest region corresponds to steady stationary combustion conditions. For C/O < 0.55 and for 1,150 < $T_{in}$ < 1,200 K, the system shows more complex behaviors with the establishment of temperature oscillations in time. As it can be seen from **Figure 1A**, this area is divided into several zones on the basis of different temperature waveforms (**Figure 1B**). This range of behavior reflects the richness of oxidation kinetics promoted under MILD conditions.

Numerical investigations devoted to the delineation of the controlling kinetics of these phenomenologies revealed that methane oxidation at low temperatures (<1,000 K) is sustained by this set of reactions $H + O_2 + M = HO_2 + M$, $HO_2 + HO_2 = H_2O_2 + O_2$, and $H_2O_2 + M = OH + OH + M$ coupled with $HCO + O_2 = CO + HO_2$ for $HO_2$ production, whereas methane converts to CO through the following chemical

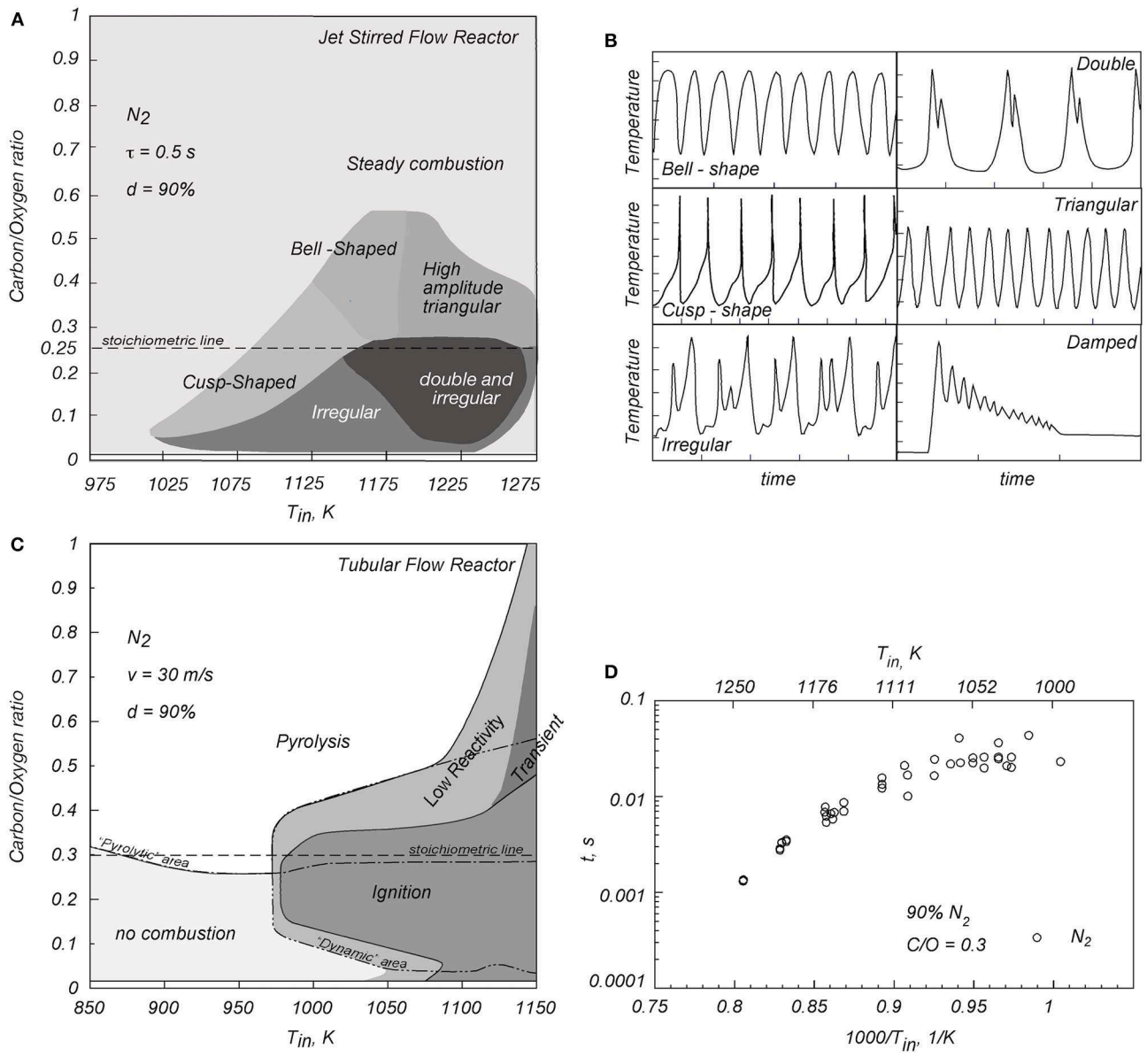


**FIGURE 1 | (A,B)** Dynamic behaviors and temperature oscillation shapes for a methane/oxygen mixture in a JSFR, from de Joannon et al. (2005). **(C,D)** Combustion regimes, and NTC-like behavior of autoignition delay times for propane/oxygen mixtures in a TFR, from Sabia et al. (2014).

route $CH_3 + HO_2 \rightarrow CH_3O \rightarrow CH_2O \rightarrow HCO \rightarrow CO$) (de Joannon et al., 2005; Glarborg and Bentzen, 2007; Le Cong and Dagaut, 2008, 2009a,b; Mendiara and Glarborg, 2009; Wang et al., 2013; Sabia et al., 2014, 2015; Xie et al., 2014a; Song et al., 2015; Lubrano Lavadera et al., 2016, 2018a). For the conditions where temperature oscillations were detected, methyl radicals are directly oxidized to $CH_2O$ ($CH_3 + OH \rightarrow CH_2O + H_2$) by OH radicals produced by the high-temperature branching mechanism of the subsystem $H_2/O_2$. At the same time, methyl radicals recombine to ethane ($CH_3 + CH_3 + M = C_2H_6 + M$), followed by $C_2$ dehydrogenation/pyrolytic routes. The competition between oxidation/recombination–pyrolytic routes, coupled with system heat exchange phenomena, promotes instabilities (de Joannon et al., 2005; Sabia et al., 2014; Lubrano Lavadera et al., 2018b). The enhanced role of the methyl recombination routes for these temperatures is emphasized also in other works (Zhukov et al., 2005; Li et al., 2014).

For higher $T_{in}$ (>1,250 K), the activation of further oxidative routes ($CH_3 + OH + M \rightarrow CH_3OH \rightarrow CH_2OH \rightarrow CH_2O$) followed by $CH_2O \rightarrow HCO \rightarrow CO \rightarrow CO_2$, or $CH_3 + OH \rightarrow CH_2(s) \rightarrow CH_2 \rightarrow CH \rightarrow CO$, relieves the system from the inhibiting effect of methyl radicals conversion to ethane; thus, the system reaches a steady stationary state (Lubrano Lavadera et al., 2018b).

**Figures 1C,D** are relative to experimental tests in a TFR (Sabia et al., 2014). It is equipped with thermocouples equi-displaced along the axial coordinate of the system, to detect ignition/oxidation states. Following the same methodology used for the JSFR data, the characteristic combustion regimes were summarized in a C/O-$T_{in}$ map.

For low $T_{in}$ (850–975 K), no combustion was detected for C/O <0.3 (stoichiometric condition), whereas for rich mixtures, a pyrolytic behavior was identified (temperature values lower than the isothermal inlet profiles). As $T_{in}$ is increased, for C/O = 0.3, the operative conditions lead to ignition, defined as a temperature increase of 10 K (Mardani et al., 2010, 2013) with respect to the inlet axial one ($T_{in}$). When $T_{in}$ is increased up to 1,080 K, the ignition region extends to fuel leaner conditions, while remaining almost constant for the fuel-rich side. For $T_{in}$ >1,120 K, the ignition region extends up to C/O = 0.5. Between the ignition and the pyrolysis–no combustion regions, a low reactivity behavior occurs with a temperature increase lower than 10 K with respect to $T_{in}$, thus not satisfying the ignition criterion (de Joannon et al., 2002; Evans et al., 2017).

Conditions included within the dynamic line show oscillatory behaviors, for which two temperature profiles are recorded, downstream of a steady ignition point, periodically switching from one to the other in time. The last region, indicated as transient (enclosed by the dotted line), identifies conditions where mixtures temporarily ignite, leading to a temporarily first steady state, followed by a second final one.

**Figure 1D** reports the autoignition delay times ($t$) with respect to mixture inlet temperature ($T_{in}$) for the stoichiometric condition in the Arrhenius plot diagram. The autoignition delay time is defined as the ratio between the axial positions where the temperature increase is equal to 10 K and the flow mean velocity (Sabia et al., 2014). The autoignition delay time curve shows two different slopes with respect to $T_{in}$: for $T_{in}$ lower than about 1,100 K, $t$ is almost independent from $T_{in}$, whereas for $1{,}000/T_{in}$ <0.9, $t$ linearly diminishes with temperature. Such a trend was identified for 0.15 < C/O < 0.3. Congruently with the methane dynamic behavior in the JSFR, the negative temperature coefficient (NTC)-like phenomenology and the oscillatory regimes detected in the TFR emerge from the competing methyl radicals oxidative/recombination–pyrolytic routes at intermediate temperatures (1,000 < $T$ < 1,100 K), whereas the $H_2/O_2$ system is passing from the low- to the high-temperature branching mechanism.

In similar operative conditions, NTC-like and oscillatory behaviors were detected in other systems for simple hydrocarbons (Cadman et al., 2000; Penyazkov et al., 2005; Zhukov et al., 2005; Gallagher et al., 2008; Sabia et al., 2013; Lubrano Lavadera et al., 2016, 2018a; Hashemi et al., 2017).

As evident, the nature of such behaviors is very different from conventional "cool" flame or "NTC" phenomena observed for low-molecular-weight paraffins at high pressures (Herzler et al., 2004; Gallagher et al., 2008; Hashemi et al., 2016, 2017, 2019) or high-molecular-weight paraffins (Sokolov et al., 1996; Basevich and Frolov, 2007; Ju et al., 2019; Wang et al., 2019), where the oxidation chemistry of alkyl-peroxide radicals is fundamental. In particular, for high-molecular-weight paraffins, a double $O_2$ addition to alkyl-radicals and internal isomerization to ketohydroperoxy radicals, ruled by equilibrium reactions, determine temperature oscillations in time or the NTC behavior (if referred to ignition delay times), coupled with heat exchange mechanisms.

## OXIDATION PROCESS OF SIMPLE HYDROCARBONS UNDER DILUTED CONDITION IN PRESENCE OF $H_2O$ AND $CO_2$

As examples of the chemical effects of $H_2O$ and $CO_2$ on combustion processes, **Figure 2** reports some recent experimental data, adapted from Sabia et al. (2015), Lubrano Lavadera et al. (2016, 2018a). In **Figure 2**, round symbols are relative to the $N_2$- diluted mixtures, triangles to the $CO_2$-diluted mixtures, and squares to the $H_2O$–partially diluted one. **Figure 2A** shows the experimental $\Delta T = (T_{reactor} - T_{inlet})$ obtained for the stoichiometric condition obtained in a JSFR (de Joannon et al., 2005; Sabia et al., 2014) for these three cases. The residence time ($\tau$) is equal to 0.5 s, and the overall mixture dilution level ($d$) is 90%.

For the $N_2$-diluted mixture, the oxidation onset occurs for $T_{in}$ = 880 K. The system temperature increases monotonously up to $T_{in}$ = 940 K, and then the oxidation occurs throughout temperature oscillatory regimes, likewise the methane (**Figures 1A,B**). For this oxidation regime, the maximum and minimum values detected during the oscillatory behavior (full symbols) are reported. Afterward, for $T_{in}$ = 1,100 K, a stationary steady condition is identified.

The experimental $\Delta T$ for the $CO_2$-diluted mixture and the system partially diluted in $H_2O$ (45% $H_2O$−55% $N_2$) are similar to the ones relative to the $N_2$-diluted one. Nonetheless, the

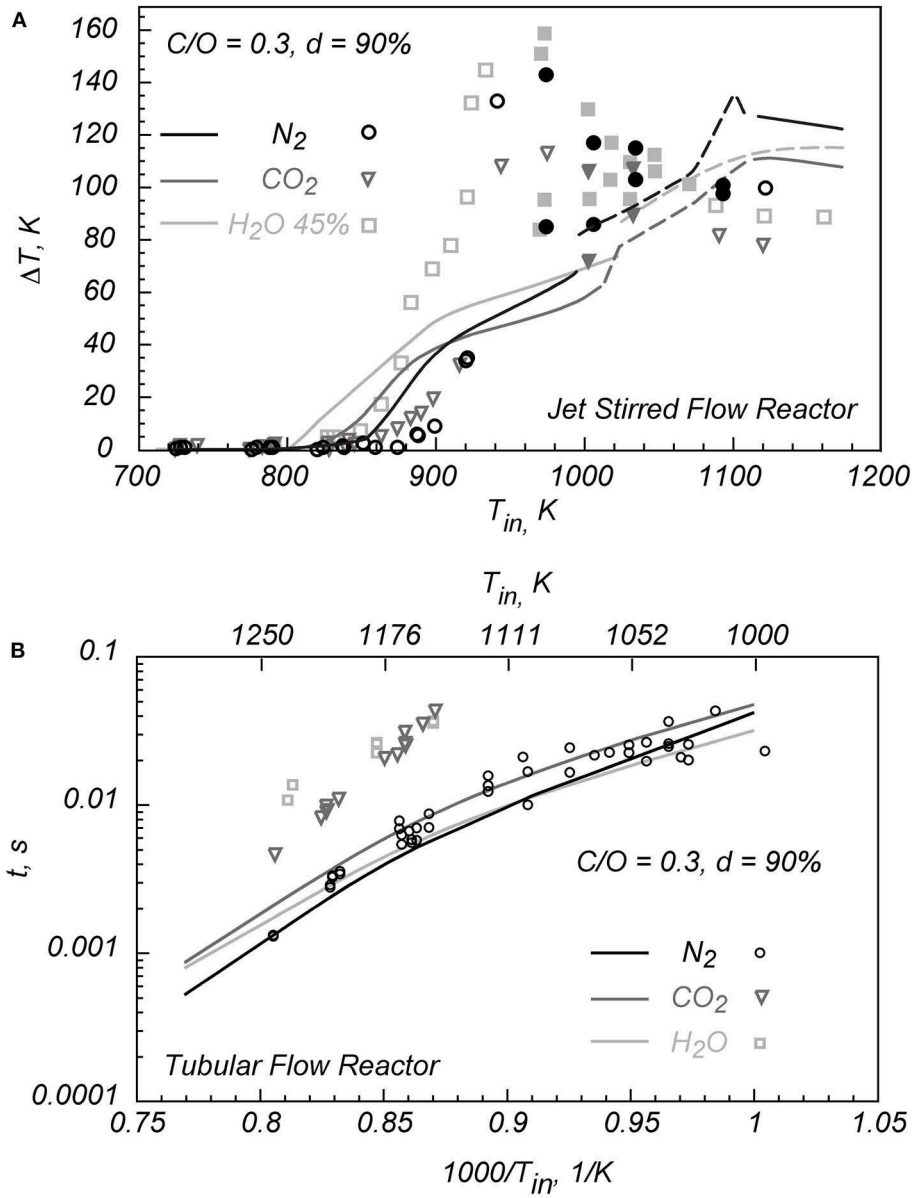


**FIGURE 2 |** Effects of $H_2O$ and $CO_2$ on the oxidation process of stoichiometric $C_3H_8/O_2$ mixtures in a JSFR **(A)**, adapted from Lubrano Lavadera et al. (2018a) and Lubrano Lavadera et al. (2016), and the autoignition delay times of stoichiometric $C_3H_8/O_2$ mixtures in a TFR **(B)**, adapted from Sabia et al. (2015).

oxidation onset occurs, respectively, for $T_{in} = 820$ K and for $T_{in} = 850$ K, thus slightly anticipating the reactivity with respect to the reference system. For $CO_2$, oscillation occurs for 1,030 K $< T_{in} <$ 1,100 K, whereas for the system diluted in $H_2O$ for 980 K $< T_{in} <$ 1,100 K. Afterward, a stationary steady state regime is detected for both the mixtures. At high temperatures, the system diluted in $N_2$ shows a higher temperature increment.

Along with the experimental data, **Figure 2A** reports the numerical simulations obtained with a detailed kinetic model PoliMi (Cadman et al., 2000; Faravelli et al., 2003; Frassoldati et al., 2003), as reported in Lubrano Lavadera et al. (2018a) and Lubrano Lavadera et al. (2016). In general, it well-predicts both the anticipating effect of $CO_2$ and $H_2O$ at low temperatures and the temperature oscillatory behaviors (dashed lines), even though overestimates system reactivities at low temperatures, considering $\Delta T$ as the reference parameter.

**Figure 2B** shows the experimental autoignition delay times ($t$) for a stoichiometric propane/oxygen mixture diluted at $d = 90\%$ in $N_2$, $CO_2$, and $H_2O$ along with numerical predictions (lines) (Sabia et al., 2015).

For the system diluted in $CO_2$ and $H_2O$, the experimental autoignition delay times ($t$) are longer of almost one order of magnitude with respect to the ones obtained for the $N_2$-diluted mixture.

The autoignition delay times obtained for $N_2$ are predicted with a good approximation, but this consistency fails for the other two diluents. Because MILD combustion configures as a continuous autoignition states, the fine comprehension of the chemical effect of $CO_2$ and $H_2O$ is mandatory.

## DISCUSSION AND CONCLUSION

There are different main aspects that should be considered in the development of detailed oxidation chemistry for MILD combustion processes.

The first point concerns the complexity of the oxidation process at low ($T < 1{,}000$ K) to intermediate ($1{,}000$ K $< T <$ $1{,}200$ K) temperatures. In fact, under these operative conditions, the numbers of species and consequently of elementary reactions are meaningfully larger with respect to the ones necessary to describe the high-temperature flame oxidation processes. This implies high computational cost for computational fluid dynamics (CFD) calculations, because detailed chemistries are required. As previously shown, the light hydrocarbons chemistry under these operating conditions is governed by a delicate balance between slow oxidation and recombination/pyrolytic channels. Uncertainties of the Arrhenius parameters (Konnov, 2008; Varga et al., 2015) of elementary reactions and of thermodynamic data have a stronger impact on the predictive performance of kinetic models with respect to conventional flame conditions. In fact, at high temperatures, the performance of kinetic schemes relies on the proper description of the high-temperature branching reactions of the subsystem $H_2/O_2$. The fast chemistry promoted by such reactions may hide the elementary reaction constants uncertainties of slow reactions, reducing the impact of their relative weight in the prediction of combustion features.

The presence of $H_2O$ and $CO_2$ *ab initio* poses several problems. First, their interaction on fuel oxidation kinetics process is an aspect not contemplated for traditional systems, where $H_2O$ and $CO_2$ are present as combustion products in the postoxidation phase, thus acting only on a subset of kinetic reactions that involve few species close to equilibrium conditions. On the contrary, $CO_2$ and $H_2O$ can drastically alter the ignition process in dependence of operating conditions with a twofold interaction. They increase system reactivity at low temperatures (Sabia et al., 2007, 2015; Sjöberg et al., 2007; Anderlohr et al., 2010; Lubrano Lavadera et al., 2016), but delay it at intermediate–high temperatures (Mueller et al., 1999; Cadman et al., 2000; de Joannon et al., 2002; Park et al., 2003; Wang et al., 2003, 2013; Herzler et al., 2004; Penyazkov et al., 2005; Zabetta et al., 2005; Basevich and Frolov, 2007; Glarborg and Bentzen, 2007; Sjöberg et al., 2007; Gallagher et al., 2008; Le Cong and Dagaut, 2009a,b; Mendiara and Glarborg, 2009; Mardani et al., 2010, 2013; Lee et al., 2012; Sabia et al., 2013, 2015; Chen and Ghoniem, 2014; Xie et al., 2014a; Song et al., 2015; Zou et al., 2015; Hashemi et al., 2016, 2017, 2019; Lubrano Lavadera et al., 2016, 2018a; Evans et al., 2017; He et al., 2017; Fedyaeva et al., 2018; Sorrentino et al., 2018; Zhang et al., 2019).

These effects mainly depend on the interaction that such species have on the branching mechanisms, related to the $H_2/O_2$ subsystem. At low temperatures, the ignition–oxidation chemistry is sustained by hydrogen peroxides molecule formation and decomposition to OH radicals, namely, $H + O_2 + M = HO_2 + M$, $HO_2 + HO_2 = H_2O_2 + O_2$, and $H_2O_2 + M = OH + OH + M$. At intermediate–high temperatures, the branching mechanism relies on the following set of reaction $H + O_2 = OH + O$, $O + H_2 = OH + H$, and $OH + H_2 = H_2O + H$.

Literature works, relative to $H_2O$ and $CO_2$ effects on $H_2$ oxidation (Mueller et al., 1999; Park et al., 2003; Wang et al., 2003; Lee et al., 2012; Xie et al., 2014b), suggest that they act on the low-temperature mechanism due to their high third-body collisional efficiencies, enhancing the reaction $H + O_2 + M = HO_2 + M$ to the detriment of $H + O_2 = OH + O_2$ at low temperatures. At high temperatures, $H_2O$ delays reaction $H_2 + OH = H_2O + H$, by shifting its equilibrium state, and $O + H_2 = OH + H$ as O radicals is consumed by reaction $O + H_2O = OH + OH$. In general, $H_2O$ leads to a change of radicals distribution, decreasing H and O while promoting OH concentration. At high temperatures, $CO_2$ further inhibits reaction $H + O_2 = OH + O$ by consuming H radicals throughout decomposition reactions ($CO_2 + H = CO + OH$) (Glarborg and Bentzen, 2007; Le Cong and Dagaut, 2008, 2009a,b; Mendiara and Glarborg, 2009; Song et al., 2015).

Fuel oxidation chemistry in presence of $H_2O$ and $CO_2$ is further complicated by their possibility to interact with the $C_1$-$C_2$ reactions directly in bimolecular reactions or indirectly as third-body species in third-molecular reactions.

Such species can sensibly alter the intermediate temperature consumption of $CH_3$ rates by promoting methyl recombination routes to $C_2$ species, as high collisional efficiency third-body species. Steam can partially reconvert methyl radicals back to methane ($CH_3 + H_2O = CH_4 + OH$), thus inhibiting system reactivity (Sabia et al., 2015). At the same time, $CO_2$ can strongly interact in the $C_1$ high-temperature chemistry through the reaction $CH_2(S)/CH_2 + CO_2 = CH_2O + CO$ (Glarborg and Bentzen, 2007; Le Cong and Dagaut, 2009a,b; Mendiara and Glarborg, 2009; Sabia et al., 2015; He et al., 2017). Recently, He et al. (He et al., 2017) have introduced a new methyl radical conversion channel ($CH_3 \rightarrow CH_3OCO \rightarrow CH_2O$ and $CH_3 \rightarrow CH_3OCO \rightarrow CO$) exclusive in $O_2/CO_2$ atmospheres for methane oxidation chemistry at high temperatures.

As it has emerged within this brief description, kinetic mechanisms involve a set of third-molecular reactions whose role is emphasized by third-molecular species with high collisional efficiencies (such $CO_2$ and $H_2O$). In this context, the reaction $H + O_2 + M = HO_2 + M$ plays a crucial role for $HO_2$ radical production. In this regard, it is worth mentioning that big uncertainties on kinetic parameters still remain (Konnov, 2008; Varga et al., 2015). All these works highlight that for such a reaction there are considerable scattered data especially for the low-pressure limit with big uncertainties for third-bodies collisional efficiencies. Some recent efforts to calculate these values were made by Jasper et al. (2015) for monoatomic and biatomic species, whereas Shao et al. (2019) have recently proposed new values for $H_2O$ and $CO_2$.

The problem relative to third-body collisional efficiency uncertainties is even more relevant if it is considered that they may exhibit temperature dependence. For instance, Baulch et al. (1988) suggested a temperature dependence $k(H_2O)/k(N_2) = 1.36T^{0.4}$ for water in the reaction $H + O_2 + M = HO_2 + M$, whereas Davis et al. (2005) suggested a temperature dependence $k(H_2O)/k(MN_2) = 60T^{0.25}$ for water in the elementary reaction $H + H + M = H_2 + M$. Also, for the reaction $CH_4 + H = CH_3 + H_2$, Jasper et al. (2013) suggested $(H_2O)/k(Ar_r)$ should be 3 at 300 K and 7 at 2,000 K.

The definition itself of third-body species with third-molecular efficiencies different from 1 is ambiguous. Several authors have proposed third-body collisional efficiencies also for $H_2O_2$ and $HO_2$, with collisional efficiencies similar to the ones declared for steam (Gerasimov and Shatalov, 2013).

In addition, the basic chemistry of the $H_2/O_2$ mechanism would require a right description of $H + HO_2$ reactions (i.e., $H + HO_2 = OH + OH$, $H + HO_2 = H_2 + O_2$, and $HO_2 + OH = H_2O + O_2$, $H + HO_2 = H_2O + O$) (Conaire et al., 2004; Mousavipour and Saheb, 2007; Burke et al., 2010, 2012; Shimizu et al., 2011), whereas for high-pressure conditions, the inclusion of reaction $H + OH + M = H_2O + M$ would be fundamental for the description of laminar flame speeds (Conaire et al., 2004; Konnov, 2008; Burke et al., 2012). Konnov (2008) also suggested the inclusion of the termolecular reaction $HO_2 + HO_2 + M = H_2O_2 + O_2 + M$ for laminar flame speed prediction.

Burke et al. (2010) have recently suggested that the pressure dependence description should be described separately for different bath gases, with center broadening factors from 0.5 to 0.7 for Ar, 0.5 to 0.7 for $N_2$, and 0.6 to 0.8 for $H_2O$. Burke et al. (2010) have also discussed the necessity to include "non-linear mixing rules" for the reaction $H + O_2 + M = HO_2 + M$ in presence of multicomponent bath gases, in agreement with Li et al. (2004).

In this perspective, at low–intermediate temperatures and in presence of conspicuous amount of non-inert species, the chemical kinetic validation procedure suffers the lack of experimental results in simple and controlled facilities.

## AUTHOR CONTRIBUTIONS

MJ and PS have synergistically contributed to the research concept and design and equally contributed to the manuscript through fruitful discussions and data analyses. The work represents a summary of their joint research activities. PS has assembled the data and written the first release of the manuscript. MJ has critically revised the paper up to the final version.

## REFERENCES


Abdmouleh, Z., Alammari, R. A., and Gastli, A. (2015). Review of policies encouraging renewable energy integration & best practices. *Renew. Sustain. Energy Rev.* 45, 249–262. doi: 10.1016/j.rser.2015.01.035

Anderlohr, J. M., Pires da Cruz, A., Bounaceur, R., and Battin-Leclerc, F. (2010). Thermal and kinetic impact of CO, $CO_2$, and $H_2O$ on the postoxidation of IC-engine exhaust gases. *Combust. Sci. Technol.* 182, 39–59. doi: 10.1080/00102200903190844

Basevich, V. Y., and Frolov, S. M. (2007). Kinetics of blue flames in the gas-phase oxidation and combustion of hydrocarbons and their derivatives. *Russian Chem. Rev.* 76, 867–884. doi: 10.1070/RC2007v076n09ABEH003703

Baulch, D. L., Griffiths, J. F., Pappin, A. J., and Sykes, A. F. (1988). Third-body interactions in the oscillatory oxidation of hydrogen in a well stirred flow reactor. *J. Chem. Soc. Faraday Trans.* 84, 1575–1586. doi: 10.1039/f19888401575

Burke, M. P., Chaos, M., Dryer, F. L., and Ju, Y. (2010). Negative pressure dependence of mass burning rates of $H_2/CO/O_2$/diluent flames at low flame temperatures. *Combust. Flame* 157, 618–631. doi: 10.1016/j.combustflame.2009.08.009

Burke, M. P., Chaos, M., Ju, Y., Dryer, F. L., and Klippenstein, S. J. (2012). Comprehensive $H_2/O_2$ kinetic model for high-pressure combustion. *Int. J. Chem. Kinet.* 44, 444–474. doi: 10.1002/kin.20603

Cadman, P., Thomas, G. O., and Butler, P. (2000). The auto-ignition of propane at intermediate temperatures and high pressures. *Phys. Chem. Chem. Phys.* 2, 5411–5419. doi: 10.1039/b003665j

Cavaliere, A., and de Joannon, M. (2004). Mild combustion. *Prog. Energy Combust. Sci.* 30 329–366. doi: 10.1016/j.pecs.2004.02.003

Chen, L., and Ghoniem, A. F. (2014). Modeling CO2 chemical effects on CO formation in oxy-fuel diffusion flames using detailed, quasi-global, and global reaction mechanisms. *Combust. Sci. Technol.* 186, 829–848. doi: 10.1080/00102202.2014.883384

Colorado, A. F., Herrera, B. A., and Amell, A. A. (2010). Performance of a flameless combustion furnace using biogas and natural gas. *Bioresour. Technol.* 101, 2443–2449. doi: 10.1016/j.biortech.2009.11.003

Conaire, Ó. M., Curran, H. J., Simmie, J. M., Pitz, W. J., and Westbrook, C. K. (2004). A comprehensive modeling study of hydrogen oxidation. *Int. J. Chem. Kinet.* 36, 603–622. doi: 10.1002/kin.20036

Cozzi, F., and Coghe, A. (2012). Effect of air staging on a coaxial swirled natural gas flame. *Exp. Thermal Fluid Sci.* 43, 32–39. doi: 10.1016/j.expthermflusci.2012.04.002

Dally, B. B., Riesmeier, E., and Peters, N. (2004). Effect of fuel mixture on moderate and intense low oxygen dilution combustion. *Combust. Flame* 137, 418–431. doi: 10.1016/j.combustflame.2004.02.011

Davis, S. G., Joshi, A. V., Wang, H., and Egolfopoulos, F. (2005). An optimized kinetic model of $H_2/CO$ combustion. *Proc. Combust. Inst.* 30, 1283–1292. doi: 10.1016/j.proci.2004.08.252

de Joannon, M., Cavaliere, A., Donnarumma, R., and Ragucci, R. (2002). Dependence of autoignition delay on oxygen concentration in mild combustion of high molecular weight paraffin. *Proc. Combust. Inst.* 29, 1139–1146. doi: 10.1016/S1540-7489(02)80144-4

de Joannon, M., Cavaliere, A., Faravelli, T., Ranzi, E., Sabia, P., and Tregrossi, A. (2005). Analysis of process parameters for steady operations in methane mild combustion technology. *Proc. Combust. Inst.* 30, 2605–2612. doi: 10.1016/j.proci.2004.08.190

de Joannon, M., Sabia, P., Cozzolino, G., Sorrentino, G., and Cavaliere, A. (2012b). Pyrolitic and oxidative structures in hot oxidant diluted oxidant (HODO) MILD combustion. *Combust. Sci. Technol.* 184, 1207–1218. doi: 10.1080/00102202.2012.664012

de Joannon, M., Sorrentino, G., and Cavaliere, A. (2012a). MILD combustion in diffusion-controlled regimes of hot diluted fuel. *Combust. Flame* 159, 1832–1839. doi: 10.1016/j.combustflame.2012.01.013

Demirbas, A. (2004). Combustion characteristics of different biomass fuels. *Prog Energy Combust. Sci.* 30, 219–230. doi: 10.1016/j.pecs.2003.10.004

Derudi, M., and Rota, R. (2011). Experimental study of the mild combustion of liquid hydrocarbons. *Proc. Combust. Inst.* 33, 3325–3332. doi: 10.1016/j.proci.2010.06.120

Donohoe, N., Heufer, K. A., Aul, C. J., Petersen, E. L., Bourque, G., Gordon, R., et al. (2015). Influence of steam dilution on the ignition of hydrogen, syngas

and natural gas blends at elevated pressures. *Combust. Flame* 162, 1126–1135. doi: 10.1016/j.combustflame.2014.10.005

Dunn-Rankin, D. (Ed.). (2011). *Lean Combustion: Technology and Control*. San Diego, CA: Academic Press.

Evans, M. J., Chinnici, A., Medwell, P. R., and Ye, J. (2017). Ignition features of methane and ethylene fuel-blends in hot and diluted coflows. *Fuel* 203, 279–289. doi: 10.1016/j.fuel.2017.04.113

Faravelli, T., Frassoldati, A., and Ranzi, E. (2003). Kinetic modeling of the interactions between NO and hydrocarbons in the oxidation of hydrocarbons at low temperatures. *Combust. Flame* 132, 188–207. doi: 10.1016/S0010-2180(02)00437-6

Fedyaeva, O. N., Artamonov, D. O., and Vostrikov, A. A. (2018). Features of propene oxidation in argon, carbon dioxide and water vapor media at a high density of reagents. *J. Eng. Thermophys.* 27, 405–414. doi: 10.1134/S1810232818040045

Frassoldati, A., Faravelli, T., and Ranzi, E. (2003). Kinetic modeling of the interactions between NO and hydrocarbons at high temperature. *Combust. Flame* 135, 97–112. doi: 10.1016/S0010-2180(03)00152-4

Gallagher, S. M., Curran, H. J., Metcalfe, W. K., Healy, D., Simmie, J. M., and Bourque, G. (2008). A rapid compression machine study of the oxidation of propane in the Negative Temperature Coefficient regime. *Combust. Flame* 153, 316–333. doi: 10.1016/j.combustflame.2007.09.004

Gerasimov, G. Y., and Shatalov, O. P. (2013). Kinetic mechanism of combustion of hydrogen–oxygen mixtures. *J. Eng. Phys. Thermophys.* 86, 987–995. doi: 10.1007/s10891-013-0919-7

Glarborg, P., and Bentzen, L. L. (2007). Chemical effects of a high $CO_2$ concentration in oxy-fuel combustion of methane. *Energy Fuels* 22, 291–296. doi: 10.1021/ef7005854

Gurentsov, E. V. E., Divakov, O. G. E., and Eremin, A. V. (2002). Ignition of multicomponent hydrocarbon/air mixtures behind shock waves. *High Temp.* 40, 379–386. doi: 10.1023/A:1016012007493

Hashemi, H., Christensen, J. M., Gersen, S., Levinsky, H., Klippenstein, S. J., and Glarborg, P. (2016). High-pressure oxidation of methane. *Combust. Flame* 172, 349–364. doi: 10.1016/j.combustflame.2016.07.016

Hashemi, H., Christensen, J. M., Harding, L. B., Klippenstein, S. J., and Glarborg, P. (2019). High-pressure oxidation of propane. *Proc. Combust. Inst.* 37, 461–468. doi: 10.1016/j.proci.2018.07.009

Hashemi, H., Jacobsen, J. G., Rasmussen, C. T., Christensen, J. M., Glarborg, P., Gersen, S., et al. (2017). High-pressure oxidation of ethane. *Combust. Flame* 182, 150–166. doi: 10.1016/j.combustflame.2017.03.028

He, Y., Zou, C., Song, Y., Luo, J., Jia, H., Chen, W., et al. (2017). Comparison of the characteristics and mechanism of CO formation in $O_2/N_2$, $O_2/CO_2$ and $O_2/H_2O$ atmospheres. *Energy* 141, 1429–1438. doi: 10.1016/j.energy.2017.11.043

Herzler, J., Jerig, L., and Roth, P. (2004). Shock-tube study of the ignition of propane at intermediate temperatures and high pressures. *Combust. Sci. Technol.* 176, 1627–1637. doi: 10.1080/00102200490487201

Ho, R. J., Kumaran, P., and Yusoff, M. Z. (2016). "Development of high efficiency and low emission low temperature combustion diesel engine with direct egr injection", in *IOP Conference Series: Earth and Environmental Science 32 012016. IOP Conference Series: Earth and Environmental Science, Volume 32, International Conference on Advances in Renewable Energy and Technologies (ICARET 2016)*, Putrajaya.

Hosseini, S. E., and Wahid, M. A. (2013). Biogas utilization: experimental investigation on biogas flameless combustion in lab-scale furnace. *Energy Conver. Manage.* 74, 426–432. doi: 10.1016/j.enconman.2013.06.026

Hosseini, S. E., and Wahid, M. A. (2016). Hydrogen production from renewable and sustainable energy resources: promising green energy carrier for clean development. *Renew. Sustain. Energy Rev.* 57, 850–866. doi: 10.1016/j.rser.2015.12.112

Huang, Y., and Yang, V. (2009). Dynamics and stability of lean-premixed swirl-stabilized combustion. *Prog. Energy Combust. Sci.* 35, 293–364. doi: 10.1016/j.pecs.2009.01.002

Isaac, B. J., Parente, A., Galletti, C., Thornock, J. N., Smith, P. J., and Tognotti, L. (2013). A novel methodology for chemical time scale evaluation with detailed chemical reaction kinetics. *Energy Fuels* 27, 2255–2265. doi: 10.1021/ef301961x

Jasper, A. W., Miller, J. A., and Klippenstein, S. J. (2013). Collision efficiency of water in the unimolecular reaction $CH_4$ $(+H_2O)$ $\leftrightarrows$ $CH_3+(+H_2O)$: One-dimensional and two-dimensional solutions of the low-pressure-limit master equation. *J. Phys. Chem. A* 117, 12243–12255. doi: 10.1021/jp409086w

Jasper, A. W., Oana, C. M., and Miller, J. A. (2015). "Third-body" collision efficiencies for combustion modeling: hydrocarbons in atomic and diatomic baths. *Proc. Combust. Inst.* 35, 197–204. doi: 10.1016/j.proci.2014.05.105

Ju, Y., Reuter, C. B., Yehia, O. R., Farouk, T. I., and Won, S. H. (2019). Dynamics of cool flames. *Prog. Energy Combust. Sci.* 75:100787. doi: 10.1016/j.pecs.2019.100787

Katsuki, M., and Hasegawa, T. (1998). The science and technology of combustion in highly preheated air. *Proc. Combust. Inst.* 27, 3135–3146. doi: 10.1016/S0082-0784(98)80176-8

Keyhani, A., Marwali, M. N., and Dai, M. (2010). *Integration of Green and Renewable Energy in Electric Power Systems,* Vol. 20. Hoboken, NJ: Wiley.

Khalil, A. E. E., and Gupta, A. K. (2011). Distributed swirl combustion for gas turbine application. *Appl. Energy* 88, 4898–4907. doi: 10.2514/6.2011-64

Konnov, A. A. (2008). Remaining uncertainties in the kinetic mechanism of hydrogen combustion. *Combust. Flame* 152, 507–528. doi: 10.1016/j.combustflame.2007.10.024

Le Cong, T., and Dagaut, P. (2008). Experimental and detailed kinetic modeling of the oxidation of methane and methane/syngas mixtures and effect of carbon dioxide addition. *Combust. Sci. Technol.* 180, 2046–2091. doi: 10.1080/00102200802265929

Le Cong, T., and Dagaut, P. (2009a). Oxidation of $H_2/CO_2$ mixtures and effect of hydrogen initial concentration on the combustion of $CH_4$ and $CH_4/CO_2$ mixtures: experiments and modeling. *Proc. Combust. Inst.* 32, 427–435. doi: 10.1016/j.proci.2008.05.079

Le Cong, T., and Dagaut, P. (2009b). Experimental and detailed modeling study of the effect of water vapor on the kinetics of combustion of hydrogen and natural gas, impact on NOx. *Energy Fuels* 23, 725–734. doi: 10.1021/ef800832q

Lee, M. C., Seo, S. B., Yoon, J., Kim, M., and Yoon, Y. (2012). Experimental study on the effect of $N_2$, $CO_2$, and steam dilution on the combustion performance of H2 and CO synthetic gas in an industrial gas turbine. *Fuel* 102, 431–438. doi: 10.1016/j.fuel.2012.05.028

Levy, Y., Sherbaum, V., and Arfi, P. (2004). Basic thermodynamics of floxcom, the low-nox gas turbines adiabatic combustor. *Appl. Thermal Eng.* 24, 1593–1605. doi: 10.1016/j.applthermaleng.2003.11.022

Li, J., Zhao, Z., Kazakov, A., and Dryer, F. L. (2004). An updated comprehensive kinetic model of hydrogen *combustion.Int. J. Chem. Kinet.* 36, 566–575. doi: 10.1002/kin.20026

Li, P., Dally, B. B., Mi, J., and Wang, F. (2013). MILD oxy-combustion of gaseous fuels in a laboratory-scale furnace. *Combust. Flame* 160, 933–946. doi: 10.1016/j.combustflame.2013.01.024

Li, P., Mi, J., Dally, B. B., Wang, F., Wang, L., Liu, Z., et al. (2011). Progress and recent trend in MILD combustion. *Sci. China Technol. Sci.* 54, 255–269. doi: 10.1007/s11431-010-4257-0

Li, P., Wang, F., Mi, J., Dally, B. B., and Mei, Z. (2014). MILD combustion under different premixing patterns and characteristics of the reaction regime. *Energy Fuels* 28, 2211–2226. doi: 10.1021/ef402357t

Lubrano Lavadera, M., Sabia, P., de Joannon, M., Cavaliere, A., and Ragucci, R. (2018a). Propane oxidation in a jet stirred flow reactor. the effect of $H_2O$ as diluent species. *Exp. Thermal Fluid Sci.* 95, 35–43. doi: 10.1016/j.expthermflusci.2018.01.008

Lubrano Lavadera, M., Song, Y., Sabia, P., Herbinet, O., Pelucchi, M., Stagni, A., et al. (2018b). Oscillatory behavior in methane combustion: influence of the operating parameters. *Energy Fuels* 32, 10088–10099. doi: 10.1021/acs.energyfuels.8b00967

Lubrano Lavadera, M. L., Sabia, P., Sorrentino, G., Ragucci, R., and de Joannon, M. (2016). Experimental study of the effect of $CO_2$ on propane oxidation in a jet stirred flow reactor. *Fuel* 184, 876–888. doi: 10.1016/j.fuel.2016.06.046

Lückerath, R., Meier, W., and Aigner, M. (2008). FLOX® combustion at high pressure with different fuel compositions. *J. Eng. Gas Turb. Power* 130:011505. doi: 10.1115/1.2749280

Lund, H., and Kempton, W. (2008). Integration of renewable energy into the transport and electricity sectors through V2G. *Energy Pol.* 36, 3578–3587. doi: 10.1016/j.enpol.2008.06.007

Luo,X., Wang, J., Dooner, M., and Clarke, J. (2015). Overview of current development in electrical energy storage technologies and the application potential in power system operation. *Appl. Energy* 137, 511–536. doi: 10.1016/j.apenergy.2014.09.081

Mardani, A., Tabejamaat, S., and Ghamari, M. (2010). Numerical study of influence of molecular diffusion in the mild combustion regime. *Combust. Theory Model.* 14, 747–774. doi: 10.1080/13647830.2010.512959

Mardani, A., Tabejamaat, S., and Hassanpour, S. (2013). Numerical study of CO and $CO_2$ formation in $CH_4/H_2$ blended flame under MILD condition. *Combust. Flame* 160, 1636–1649. doi: 10.1016/j.combustflame.2013.04.003

McKendry, P. (2002). Energy production from biomass (part 2): conversion technologies. *Bioresour. Technol.* 83, 47–54. doi: 10.1016/S0960-8524(01)00119-5

Mendiara, T., and Glarborg, P. (2009). Reburn chemistry in oxy-fuel combustion of methane. *Energy Fuels* 23, 3565–3572. doi: 10.1021/ef9001956

Milani, A., and Wünning, J. G. (2007). Flameless oxidation technology, advanced combustion and aero thermal technologies. *Environ. Protect. Pollut. Reduct.* 6, 343–352. doi: 10.1007/978-1-4020-6515-6_26

Minamoto, Y., and Swaminathan, N. (2015). Subgrid scale modelling for MILD combustion. *Proc. Combust. Inst.* 35, 3529–3536. doi: 10.1016/j.proci.2014.07.025

Minamoto, Y., Swaminathan, N., Cant, S. R., and Leung, T. (2014). Morphological and statistical features of reaction zones in MILD and premixed combustion. *Combust. Flame* 161, 2801–2814. doi: 10.1016/j.combustflame.2014.04.018

Mousavipour, S. H., and Saheb, V. (2007). Theoretical study on the kinetic and mechanism of H+ $HO_2$ reaction. *Bull. Chem. Soc. Japan* 80, 1901–1913. doi: 10.1246/bcsj.80.1901

Mueller, M. A., Yetter, R. A., and Dryer, F. L. (1999). Flow reactor studies and kinetic modeling of the $H_2/O_2$/NOx and CO/$H_2O/O_2$/NOx reactions. *Int. J. Chem. Kinet.* 31, 705–724. doi: 10.1002/(SICI)1097-4601(1999)31:10>705::AID-JCK4<3.0.CO;2-#

Noor, M. M., Wandel, A. P., and Yusaf, T. (2013a). Analysis of recirculation zone and ignition position of non-premixed bluff-body for biogas mild combustion. *Int. J. Automot. Mech. Eng.* 8, 1176–1186. doi: 10.15282/ijame.8.2013.8.0096

Noor, M. M., Wandel, A. P., and Yusaf, T. (2013b). Design and development of mild combustion burner. *J. Mech. Eng. Sci.* 5, 662–676. doi: 10.15282/jmes.5.2013.13.0064

Østergaard, P. A. (2012). Comparing electricity, heat and biogas storages' impacts on renewable energy integration. *Energy* 37, 255–262. doi: 10.1016/j.energy.2011.11.039

Özdemir, I. B., and Peters, N. (2001). Characteristics of the reaction zone in a combustor operating at mild combustion. *Exp. Fluids* 30, 683–695. doi: 10.1007/s003480000248

Parente, A., Galletti, C., and Tognotti, L. (2008). Effect of the combustion model and kinetic mechanism on the MILD combustion in an industrial burner fed with hydrogen enriched fuels. *Int. J. Hydrog. Energy* 33, 7553–7564. doi: 10.1016/j.ijhydene.2008.09.058

Parente, A., Malik, M. R., Contino, F., Cuoci, A., and Dally, B. B. (2016). Extension of the eddy dissipation concept for turbulence/chemistry interactions to MILD combustion. *Fuel* 163, 98–111. doi: 10.1016/j.fuel.2015.09.020

Park, J., Hwang, D. J., Choi, J. G., Lee, K. M., Keel, S. I., and Shim, S. H. (2003). Chemical effects of $CO_2$ addition to oxidizer and fuel streams on flame structure in H2–O2 counterflow diffusion flames. *Int. J. Energy Res.* 27, 1205–1220. doi: 10.1002/er.946

Penyazkov, O. G., Ragotner, K. A., Dean, A. J., and Varatharajan, B. (2005). Autoignition of propane–air mixtures behind reflected shock waves. *Proc. Combust. Inst.* 30, 1941–1947. doi: 10.1016/j.proci.2004.08.122

Reddy, V. M., Katoch, A., Roberts, W. L., and Kumar, S. (2015). Experimental and numerical analysis for high intensity swirl based ultra-low emission flameless combustor operating with liquid fuels. *Proc. Combust. Inst.* 35, 3581–3589. doi: 10.1016/j.proci.2014.05.070

Riccius, O., Smith, R., Güthe, F., and Flohr, P. (2005). "The GT24/26 combustion technology and high hydrocarbon ("c2+") fuels", in *ASME Turbo Expo 2005: Power for Land, Sea, and Air; American Society of Mechanical Engineers* (Reno, NV: ASME Turbo Expo), 595–602.

Sabia, P., de Joannon, M., Lubrano Lavadera, M., Giudicianni, P., and Ragucci, R. (2014). Autoignition delay times of propane mixtures under MILD conditions at atmospheric pressure. *Combust. Flame* 161, 3022–3030. doi: 10.1016/j.combustflame.2014.06.006

Sabia, P., de Joannon, M., Picarelli, A., and Ragucci, R. (2013). Methane auto-ignition delay times and oxidation regimes in MILD combustion at atmospheric pressure. *Combust. Flame* 160, 47–55. doi: 10.1016/j.combustflame.2012.09.015

Sabia, P., Lubrano Lavadera, M., Giudicianni, P., Sorrentino, G., Ragucci, R., and de Joannon, M. (2015). CO2 and H2O effect on propane auto-ignition delay times under mild combustion operative conditions. *Combust. Flame* 162, 533–543. doi: 10.1016/j.combustflame.2014.08.009

Sabia, P., Romeo, F., de Joannon, M., and Cavaliere, A. (2007). VOC destruction by water diluted hydrogen mild combustion. *Chemosphere* 68, 330–337. doi: 10.1016/j.chemosphere.2006.12.061

Saxena, S., and Bedoya, I. D. (2013). Fundamental phenomena affecting low temperature combustion and HCCI engines, high load limits and strategies for extending these limits. *Prog Energy Combust. Sci.* 39, 457–488. doi: 10.1016/j.pecs.2013.05.002

Shao, J., Choudhary, R., Susa, A., Davidson, D. F., and Hanson, R. K. (2019). Shock tube study of the rate constants for H+O2+M→ HO2+M (M=Ar, H2O, CO2, N2) at elevated pressures. *Proc. Combust. Inst.* 37, 145–152. doi: 10.1016/j.proci.2018.05.077

Shimizu, K., Hibi, A., Koshi, M., Morii, Y., and Tsuboi, N. (2011). Updated kinetic mechanism for high-pressure hydrogen combustion. *J. Propuls. Power* 27, 383–395. doi: 10.2514/1.48553

Sidey, J., and Mastorakos, E. (2015). Visualization of MILD combustion from jets in cross-flow. *Proc. Combust. Inst.* 35, 3537–3545. doi: 10.1016/j.proci.2014.07.028

Sidey, J., Mastorakos, E., and Gordon, R. L. (2014). Simulations of autoignition and laminar premixed flames in methane/air mixtures diluted with hot products. *Combust. Sci. Technol.* 186, 453–465. doi: 10.1080/00102202.2014.883217

Sjöberg, M., Dec, J. E., and Hwang, W. (2007). "Thermodynamic and chemical effects of EGR and its constituents on HCCI autoignition," in *SAE Transactions*. 271–289. doi: 10.4271/2007-01-0207

Sokolov, O. V., Parfenov, Y. V., Arutyunov, V. S., Basevich, V. V., and Vedeneev, V. L. (1996). Study of cool-dame phenomena during self-ignition of methane-oxygen mixtures. *Russian Chem. Bull.* 45, 2316–2320. doi: 10.1007/BF01435374

Song, Y., Zou, C., He, Y., and Zheng, C. (2015). The chemical mechanism of the effect of $CO_2$ on the temperature in methane oxy-fuel combustion. *Int. J. Heat Mass Transf.* 86, 622–628. doi: 10.1016/j.ijheatmasstransfer.2015.03.008

Sorrentino, G., Ceriello, G., De Joannon, M., Sabia, P., Ragucci, R., Van Oijen, J., et al. (2018). Numerical investigation of moderate or intense low-oxygen dilution combustion in a cyclonic burner using a flamelet-generated manifold approach. *Energy Fuels* 32, 10242–10255. doi: 10.1021/acs.energyfuels.8b01099

Sorrentino, G., Sabia, P., Bozza, P., Ragucci, R., and de Joannon, M. (2019). Low-$NO_x$ conversion of pure ammonia in a cyclonic burner under locally diluted and preheated conditions. *Appl. Energy* 254:113676. doi: 10.1016/j.apenergy.2019.113676

Spliethoff, H., Greul, U., Rüdiger, H., and Hein, K. R. (1996). Basic effects on $NO_x$ emissions in air staging and reburning at a bench-scale test facility. *Fuel* 75, 560–564. doi: 10.1016/0016-2361(95)00281-2

Tsuji, H., Gupta, A., Hasegawa, T., Katsuki, M., Kishimoto, K., and Morita, M. (2003). *High Temperature Air Combustion, From Energy Conservation to Pollution Reduction.* Boca Raton, FL: CRC Press.

Van Oijen, J. A. (2013). Direct numerical simulation of autoigniting mixing layers in MILD combustion. *Proc. Combust. Inst.* 34, 1163–1171. doi: 10.1016/j.proci.2012.05.070

Van Vuuren, D. P., Stehfest, E., Gernaat, D. E., Doelman, J. C., Van den Berg, M., Harmsen, M., et al. (2017). Energy, land-use and greenhouse gas emissions trajectories under a green growth paradigm. *Glob. Environ. Change* 42, 237–250. doi: 10.1016/j.gloenvcha.2016.05.008

Varga, T., Nagy, T., Olm, C., Zsély, I. G., Pálvölgyi, R., Valkó, É., et al. (2015). Optimization of a hydrogen combustion mechanism using both direct and indirect measurements. *Proc. Combust. Inst.* 35, 589–596. doi: 10.1016/j.proci.2014.06.071

Wang, B. L., Olivier, H., and Grönig, H. (2003). Ignition of shock-heated $H_2$-air-steam mixtures. *Combust. Flame* 133, 93–106. doi: 10.1016/S0010-2180(02)00552-7

Wang, L., Liu, Z., Chen, S., Zheng, C., and Li, J. (2013). Physical and chemical effects of $CO_2$ and $H_2O$ additives on counterflow diffusion flame burning methane. *Energy Fuels* 27, 7602–7611. doi: 10.1021/ef401559r

Wang, Z., Herbinet, O., Hansen, N., and Battin-Leclerc, F. (2019). Exploring hydroperoxides in combustion: history, recent advances and perspectives. *Prog. Energy Combust. Sci.*73, 132–181. doi: 10.1016/j.pecs.2019.02.003

Weber, R., Orsino, S., Lallemant, N., and Verlaan, A. (2000). Combustion of natural gas with high temperature air and large quantities of flue gas. *Proc. Combust. Inst*. 28, 1315–1321. doi: 10.1016/S0082-0784(00)80345-8

Weber, R., Smart, J. P., and vd Kamp, W. (2005). On the (MILD) combustion of gaseous, liquid, and solid fuels in high temperature preheated air. *Proc. Combust. Inst.* 30, 2623–2629. doi: 10.1016/j.proci.2004.08.101

Wünning, J. A., and Wünning, J. G. (1977). Flameless oxidation to reduce thermal no-formation. *Prog. Energy Combust. Sci.* 23, 81–94. doi: 10.1016/S0360-1285(97)00006-3

Xie, Y., Wang, J., Xu, N., Yu, S., and Huang, Z. (2014b). Comparative study on the effect of $CO_2$ and $H_2O$ dilution on laminar burning characteristics of $CO/H_2$/air mixtures. *Int. J. Hydrog. Energy* 39, 3450–3458. doi: 10.1016/j.ijhydene.2013.12.037

Xie, Y., Wang, J., Xu, N., Yu, S., Zhang, M., and Huang, Z. (2014a). Thermal and chemical effects of water addition on laminar burning velocity of syngas. *Energy Fuels* 28, 3391–3398. doi: 10.1021/ef4020586

Zabetta, E. C., Hupa, M., and Saviharju, K. (2005). Reducing NOx emissions using fuel staging, air staging, and selective noncatalytic reduction in synergy. *Ind. Eng. Chem. Res.* 44, 4552–4561. doi: 10.1021/ie050051a

Zhang, Z., Li, X., Zhang, L., Luo, C., Lu, B., Xu, Y., et al. (2019). Effect of $H_2O/CO_2$ mixture on heat transfer characteristics of pulverized coal MILD-oxy combustion. *Fuel Process. Technol.* 184:27. doi: 10.1016/j.fuproc.2018.11.011

Zhukov, V. P., Sechenov, V. A., and Starikovskii, A. Y. (2005). Autoignition of a lean propane-air mixture at high pressures. *Kinet Catal.* 46, 319–327. doi: 10.1007/s10975-005-0079-7

Zou, C., He, Y., Song, Y., Han, Q., Liu, Y., Guo, F., et al. (2015). The characteristics and mechanism of the NO formation during oxy-steam combustion. *Fuel* 158, 874–883. doi: 10.1016/j.fuel.2015.06.034

**Conflict of Interest:** The authors declare that the research was conducted in the absence of any commercial or financial relationships that could be construed as a potential conflict of interest.

frontiers in Mechanical Engineering

MINI REVIEW
published: 20 March 2020
doi: 10.3389/fmech.2020.00013

# $NO_x$ Formation in MILD Combustion: Potential and Limitations of Existing Approaches in CFD

*Salvatore Iavarone*[1]* *and Alessandro Parente*[2]

[1] Department of Engineering, University of Cambridge, Cambridge, United Kingdom, [2] Aero-Thermo-Mechanics Department, Université Libre de Bruxelles, Brussels, Belgium

Emissions of nitrogen oxides ($NO_X$) from combustion systems remain a lingering environmental issue, being these species either greenhouse gases or acid rain precursors. Moderate or Intense Low-oxygen Dilution (MILD) combustion can reduce the emissions of $NO_X$ thanks to its characteristic features (i.e., homogeneous reaction zones, reduced temperature peaks, diluted mixtures of reactants) that influence and change the main chemical pathways of $NO_X$ formation. A summary of the relevant routes of formation and destruction of $NO_X$ in MILD combustion is presented in this review, along with the identification of the sources of uncertainty that prevent reaching an overall consensus in the literature about the dominant $NO_X$ chemical pathway in MILD regime. Computational Fluid Dynamics (CFD) approaches are essential tools for investigating the critical phenomena occurring in MILD combustion and the design of pollutant-free turbulent combustion systems. This paper provides an outline of the modeling approaches employed in CFD simulations of turbulent combustion systems to predict $NO_X$ emissions in MILD conditions. An assessment of the performances of selected models in estimating $NO_X$ formation in a lab-scale MILD combustion burner is then presented, followed by a discussion about relevant modeling issues, perspectives and opportunities for future research.

**Keywords: MILD combustion, $NO_x$ formation, $NO_x$ chemistry, $NO_x$ post processing, chemical reactor network, detailed chemistry, reactor-based combustion models**

OPEN ACCESS

***Edited by:***
*Dipankar Chatterjee, Central Mechanical Engineering Research Institute (CSIR), India*

***Reviewed by:***
*Khanh Duc Cung, Southwest Research Institute (SwRI), United States*
*Md Nurun Nabi, Central Queensland University, Australia*

***Correspondence:**
*Salvatore Iavarone*
*si339@cam.ac.uk*

***Specialty section:***
*This article was submitted to Thermal and Mass Transport, a section of the journal Frontiers in Mechanical Engineering*

***Received:*** *23 November 2019*
***Accepted:*** *28 February 2020*
***Published:*** *20 March 2020*

***Citation:***
*Iavarone S and Parente A (2020) $NO_x$ Formation in MILD Combustion: Potential and Limitations of Existing Approaches in CFD. Front. Mech. Eng. 6:13. doi: 10.3389/fmech.2020.00013*

## 1. INTRODUCTION

Moderate and Intense Low-Oxygen Dilution (MILD) combustion (Cavaliere and de Joannon, 2004) technologies have become of vigorous industrial interest since they are able to reduce the environmental concerns linked to the use of both conventional and alternative fuels. MILD combustion, otherwise indicated as Flameless (Wünning and Wünning, 1997) or High-Temperature Air Combustion (HiTAC) (Gupta, 2004), can limit the emissions of pollutants like carbon monoxide (CO), nitrogen oxides ($NO_x$) and soot (Dally et al., 2004; Li et al., 2006; Szegö et al., 2008) and provide elevated combustion efficiency and fuel flexibility (Sabia et al., 2007; Medwell and Dally, 2012). The abatement of pollutants is achieved through a strong recirculation of exhaust gases in the reaction zone: the fresh gases are hence diluted and heated up above their self-ignition temperature, and the combustion process is homogeneously distributed across a broad domain rather than confined to a flame front (de Joannon et al., 2012). For industrial processes whose primary aspects are energy efficiency and homogeneous distribution of high temperatures inside

the combustion chamber (e.g., steel, glass, and ceramic industry), MILD combustion is a suitable and favorable technology.

MILD combustion can significantly reduce NO$_x$ formation via diminished temperature peaks, which inhibit the NO$_x$ thermal route (Zeldovich, 1946). However, considerable NO$_x$ emissions can still be observed (Mancini et al., 2002; Parente et al., 2011; Li et al., 2013). Other NO$_x$ formation routes, namely prompt (Fenimore, 1971), N$_2$O-intermediate (Malte and Pratt, 1975), and NNH-intermediate (Bozzelli and Dean, 1995), are held accountable for the not negligible emissions of NO$_x$ in MILD regime. This review provides a summary of the current knowledge about the NO$_x$ formation routes in homogeneous combustion systems working in MILD conditions.

The overall mechanism leading to NO$_x$ formation is one of the peculiar features that make MILD combustion substantially different from conventional combustion processes. Computational Fluid Dynamics (CFD) approaches have been successfully used to investigate these features and gain insights that are aiding the design of pollutant-free MILD combustion systems. Correct predictions of NO$_x$ emissions require an accurate description of the temperature field, along with main and radical species concentrations. Hence, reliable numerical models of the intertwined phenomena occurring in combustion, namely turbulence, chemistry, and heat transfer, are necessary. An overview of the different modeling approaches for NO$_x$ formation in CFD simulations of MILD combustion systems is presented, along with a discussion about their potential and limitations.

## 2. CHEMISTRY OF NO$_X$ FORMATION IN MILD COMBUSTION

The routes leading to the formation of NO$_x$ in combustion systems mostly involve the insertion of radicals such as O, CH$_x$, and H, into the triple bond of molecular nitrogen present in combustion air (Miller and Bowman, 1989). This mechanism forms reactive nitrogen intermediates (cyanides, N$_2$O, NNH, etc.) that are subsequently oxidized to produce NO$_x$. Alternatively, NO$_x$ are produced through oxidation reactions of organic nitrogen chemically bound in the fuel. The thermal route and fuel-N route, when nitrogen is present in the fuel, are the relevant pathways of NO$_x$ formation in conventional combustion regimes, whereas in non-conventional regimes, such as MILD, the prompt, the N$_2$O-intermediate, and the NNH-intermediate pathways must be considered. A graphical overview of the above-mentioned pathways leading to the formation of NO from molecular nitrogen is presented in **Figure 1**.

The kinetic mechanism of the thermal route is quite well established in the literature (Glarborg et al., 2018). Thermal NO$_x$ emissions are prevalent in lean systems characterized by temperatures above 1800 K and high residence times. The prompt pathway has been revised in fairly recent studies that identified the formation of the NCN species as the most important initial step of the prompt route (Cui et al., 1999; Moskaleva and Lin, 2000). The kinetic parameters of the reaction of NCN formation, $CH + N_2 \rightleftharpoons NCN + H$, have been established within a factor of two by several experimental and modeling investigations (Vasudevan et al., 2007; Harding et al., 2008; Sutton et al., 2012; Klippenstein et al., 2018) and included in novel mechanisms (Lamoureux et al., 2016; Glarborg et al., 2018; Song et al., 2019). Since the CH species is produced by the oxidation of hydrocarbons and forms the NCN species by insertion into the triple bond of molecular nitrogen, the predictions of NO$_x$ emissions via the prompt route is also affected by the accuracy of the kinetic mechanisms of hydrocarbon oxidation (Santner et al., 2016). The prompt route is typical of fuel-rich systems and is dominant at temperatures below 1800 K. Li et al. (2014) showed that the prompt mechanism is the main source of NO in fuel-rich conditions in a laboratory-scale MILD combustion furnace. Prompt was also found to be the prevalent pathway in a numerical/experimental study in laminar co-flow diffusion flames on their transition to MILD combustion regime (Sepman et al., 2013). Preheating, dilution, and recirculation of burned gases are crucial for establishing MILD combustion and seem to favor the prompt mechanism over the other routes while reducing the overall emissions of NO$_x$. Lee and Choi (2009) reported that the prompt route is predominant in high-temperature diluted-air combustion at low oxygen concentration in a coaxial jet flame. A numerical study (Abtahizadeh et al., 2012) investigating the effects of dilution and internal recirculation of burned gases on NO$_x$ formation also revealed that the prompt mechanism is the dominant reaction pathway. In the same study, it was further shown that the NO emissions are decreased by increasing the dilution ratio, as confirmed by other investigations performed in a lab-scale MILD combustion furnace (Szegö et al., 2008; Li et al., 2013).

The N$_2$O-intermediate pathway plays an essential role in fuel-lean systems with temperatures below 1800 K and high pressures, and its mechanism is fairly well established (Glarborg et al., 2018). The NNH pathway is relevant when hydrogen-enriched fuel mixtures are oxidized, since H$_2$ reacts with N$_2$ to form the NNH intermediate species. The kinetics of this route is still under investigation: the uncertainty in the heat of formation of NNH may alter the NO predictions by a factor of two (Klippenstein et al., 2011), and the rate constants for the limiting reaction $NNH + O \rightleftharpoons NH + NO$ reported in the literature (Bozzelli and Dean, 1995; Hayhurst and Hutchinson, 1998; Konnov et al., 2001; Haworth et al., 2003; Klippenstein et al., 2011) vary by more than an order of magnitude. However, recent kinetic models (Zhang et al., 2017; Glarborg et al., 2018; Song et al., 2019) have been updated with thermo-chemical and kinetic quantities estimated via ab initio transition state calculations (Klippenstein et al., 2011). The inclusion of the N$_2$O and NNH routes has been crucial in obtaining accurate predictions of NO emissions for several lab-scale burners (Galletti et al., 2009; Mardani and Tabejamaat, 2012; Wang et al., 2015) and semi-industrial furnaces (Parente et al., 2011; Li et al., 2013) operating in MILD conditions. Li et al. (2014) showed that the N$_2$O route dominates NO formation in lean conditions (equivalence ratio $\phi < 0.8$) in a lab-scale MILD furnace, whereas the NNH pathway is predominant in the presence of H$_2$-enriched mixtures, in accordance with other studies

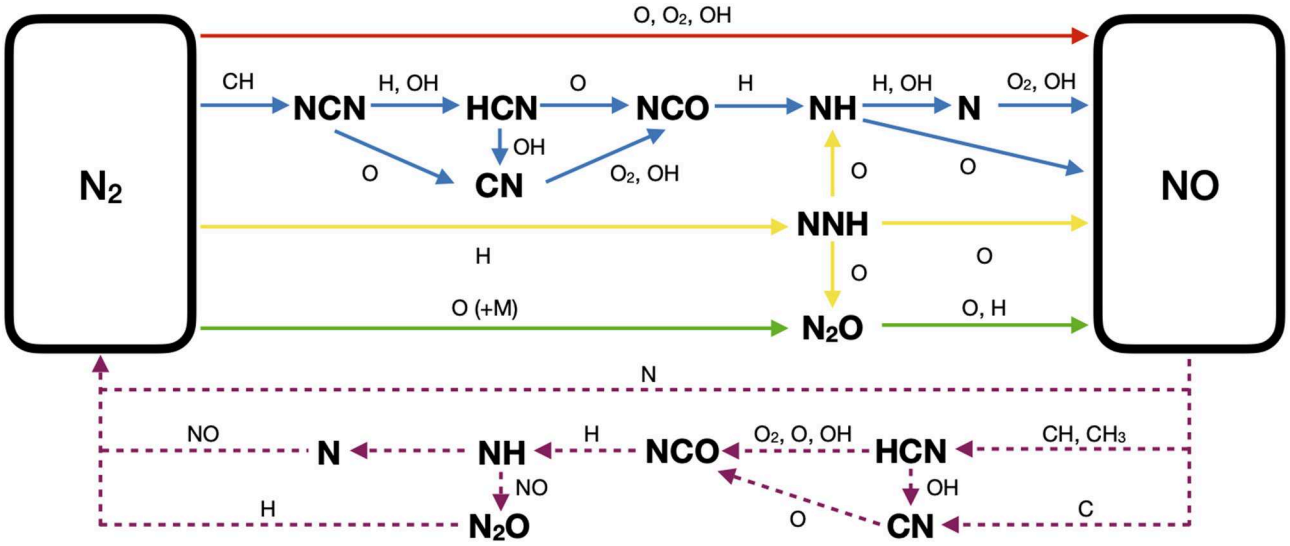


**FIGURE 1 |** Simplified scheme of formation and destruction pathways of the NO species: thermal (red solid arrow), prompt (blue solid arrows), $N_2O$-intermediate (green solid arrows), NNH-intermediate (yellow solid arrows), and reburning (purple dashed arrows).

(Skottene and Rian, 2007; Parente et al., 2011; Wang et al., 2015). Although Cho and Chung (2009) showed that $N_2O$-intermediate is negligible at lean conditions ($\phi < 0.8$) in $CH_4$/air counterflow premixed flames, Guo et al. (2005) found that the $N_2O$ and NNH routes are the main responsible of NO formation for ultra-lean ($\phi < 0.7$) counterflow $CH_4$-$H_2$/air premixed flames. It was shown that the addition of hydrogen increased the emission of NO due to the enhancement in the rate of the NNH and $N_2O$ routes.

A reduced formation of $NO_x$ in MILD combustion is also attributed to the increasing relevance of the reburning route with respect to conventional combustion (Wünning and Wünning, 1997; Nicolle and Dagaut, 2006). In reburning, $NO_x$ are removed from the combustion products by reactions with hydrocarbon radicals. Reburning was found to be favored by the decrease in oxygen content and temperature of the coflow in the Adelaide Jet in Hot Coflow (JHC) flame (Wang et al., 2015), a jet that emulates MILD conditions via the injection of a heated and vitiated coflow (Dally et al., 2002). However, uncertainty still persists regarding the reactions that should be included in the reburning route to achieve accurate $NO_x$ predictions (Perpignan et al., 2018a). A simplified scheme of the reburning pathway is included in **Figure 1**.

As illustrated in this section, a significant number of studies have investigated the relative impact of the different pathways of $NO_x$ formation in MILD regime. Although qualitative formation trends can be identified, no agreement has been reached regarding an overall dominant source of $NO_x$ in MILD combustion. The influence of the burner operating conditions, such as temperature, composition of the reactants, and dilution levels, on the contribution of a certain route to the $NO_x$ emissions remains considerable. Moreover, uncertainty remains in the kinetics of prompt and NNH routes and in the methods of isolating the contribution of a single route with respect to the others, given their interdependence. Further research is desirable to quantify and reduce these sources of uncertainty.

## 3. CFD MODELING OF $NO_X$ EMISSIONS IN MILD CONDITIONS

In conventional combustion, it is recognized that the flame structure is dominated by the fast fuel-oxidizer reactions, other than the nitrogen pollutant chemistry. Thus, $NO_x$ formation models are often decoupled from the CFD main calculation and executed after the flame structure has developed. Poor effect of $NO_x$ chemistry on the overall temperature and flow fields have prompted the development of post-processing tools of CFD results. Most of these tools take the flow and temperature fields from the CFD simulation and carry out a calculation on a Chemical Reactor Network (CRN) built from the CFD grid using criteria based on the similarities of local temperature and species concentration.

The simplest post-processing tool considers a limited number of transport equations for pollutant species, such as NO, and intermediates, such as $N_2O$, and global reacting steps for each $NO_x$ formation pathway. Equilibrium or quasi-steady-state assumptions are taken for the radical and intermediate species that are not transported but are involved in the $NO_x$ chemistry. The Arrhenius equation for the kinetic rates is integrated over a beta Probability Density Function ($\beta$-PDF) for the temperature (Peters, 2001), to account for the effect of temperature fluctuations on the mean reaction rates. This cost-effective approach has been used in several MILD combustion studies to model $NO_x$ emissions (Mancini et al., 2002; Galletti et al., 2009; Parente et al., 2011; Li et al., 2013).

A more sophisticated method consists in using rate of production analysis (ROPA) and sensitivity analysis to recognize

the main reaction paths and develop reduced multi-step kinetic mechanisms of $NO_x$ formation. Two reduced-order mechanisms were developed specifically for MILD combustion (Galletti et al., 2015) starting from two detailed schemes (Ranzi et al., 1994; Glarborg et al., 1998). The most important reactions were identified via sensitivity analysis performed on a Perfectly Stirred Reactor (PSR) at wide ranges of temperatures and residence times typical of MILD combustion conditions. The quasi-steady-state assumption was made for some of the species involved in those reactions and a reduced expression for the NO formation rate including thermal, $N_2O$, and NNH routes was obtained. The prompt NO route was accounted for via a global reaction rate (De Soete, 1975). The chemical source term in the post-processing transport equation for NO was obtained from the reduced mechanisms, and the predictions of NO showed adequate agreement with the experimental data of the Adelaide JHC flame (Dally et al., 2002). Hence, the reduced mechanisms performed reasonably well for the conditions on which they were tailored. However, errors may be introduced when extrapolating to different conditions than those used for fitting: as for the simplest post-processing tool mentioned above, the mechanism reduction relies on the assumptions of partial equilibrium and quasi-steady state that can fail under certain conditions and affect the predictivity of the reduced chemical schemes.

A CRN approach that employs a detailed mechanism with relatively low computational costs was presented by Frassoldati et al. (Frassoldati et al., 2010): the network was built on the CFD grid and a detailed kinetic mechanism was adopted to estimate the $NO_x$ emissions, whereas a simple chemical scheme was employed for the CFD simulation itself. The numerical algorithm of the CRN approach was refined (Cuoci et al., 2013) to allow the resolution of networks with a significant number of PSRs ($\sim 10^5$), which are required in the presence of complex fluid dynamics. The formation of $NO_x$ was quite successfully modeled in laboratory flames (Bergmann et al., 1998; Barlow et al., 2000) and in a small-scale MILD combustor (Veríssimo et al., 2011). The joint CFD-CRN method was also employed to predict $NO_x$ emissions in a interturbine flameless combustor for gas turbines: the flamelet generate manifolds (FGM) method was used to model the combustion process in the CFD simulation, whereas a detailed mechanism was considered in the resolution of the network of PSRs (Perpignan et al., 2018b). Although the CRN approach can be used to evaluate the variation of $NO_x$ emissions under different operating conditions in a cost-effective way, the reliability of the CRN predictions is strongly dependent on the accuracy of the underlying CFD simulation. Moreover, network parameters such as number and type of reactors, mass flow rates and residence times, have to be tuned on the combustion conditions and a general effective method for the optimization of these parameters has not been validated yet.

Detailed kinetic mechanisms that include both hydrocarbons oxidation and $NO_x$ chemistry are necessary to improve predictivity and comprehensiveness of CFD simulations of turbulent MILD combustion systems. They include mutual NO-hydrocarbons interactions that are incorporated in the $NO_x$ chemistry, especially in prompt and reburning routes. The effects of turbulence-related fluctuations on the mean reaction rates become more prominent when detailed kinetic mechanisms are considered for $NO_x$ formation. Turbulent combustion models have been developed over the years following two main assumptions: infinitely fast chemistry (compared to the scale of turbulence) and finite-rate chemistry. The recognizing feature of MILD combustion is relatively low Damköhler numbers (Parente et al., 2008). Hence, models that account for the effects of turbulence interactions on finite-rate chemical reactions should be considered (Minamoto and Swaminathan, 2015). The Eddy Dissipation Concept (EDC) (Granm and Magnussen, 1996) is a finite-rate chemistry combustion model and has found wide application for the simulation of MILD combustion systems thanks to affordable, although not negligible, computational costs when compared to more sophisticated models such as the Transported Probability Density Function (TPDF) methods. Several numerical investigations (Mardani and Tabejamaat, 2012; Gao et al., 2013; Wang et al., 2015; Jiang et al., 2018; Shu et al., 2018) have analyzed the relative importance of $NO_x$ formation routes in the Adelaide JHC burner using EDC with detailed kinetic mechanisms, showing that an overall good agreement can be reached. Chomiak (1990) proposed the Partially Stirred Reactor (PaSR) model to represent a PSR with imperfect mixing. PaSR and EDC are conceptually similar since they both model combustion as a sequence of reaction and mixing steps in locally uniform regions. In EDC, the features of these regions are defined by two parameters, $C_\tau$ and $C_\gamma$, which are either supposed constant or calculated based on local turbulence parameters, as proposed in recent studies (Parente et al., 2016; Evans et al., 2019). In PaSR, a reacting region volume fraction $\kappa$ is defined based on local estimations of chemical and mixing time scales. Better results in terms of predicted temperatures and main species concentrations in the Adelaide JHC burner have been achieved by both Reynolds Averaged Navier Stokes (RANS) and Large Eddy Simulation (LES) studies employing the PaSR model (Li et al., 2018; Ferrarotti et al., 2019; Iavarone et al., 2019) with respect to EDC. However, estimating the formation of $NO_x$ may require the resolution of chemical source terms with different characteristic time scales, since the reactions forming NO occur in a wider range of time scales compared to those of the main combustion process. Thus, a PaSR formulation that relates the source terms of the $NO_x$ species to their formation time scales, resulting in different values of $\kappa$ for the $NO_x$ species, was presented (Iavarone et al., 2019).

**Figure 2** provides a comparison of the capabilities of some of the CFD modeling approaches mentioned above to replicate the emission of $NO_x$ measured in the Adelaide JHC burner. The burner has been the target of numerous numerical studies in the context of $NO_x$ formation modeling. It consists of an insulated and cooled central fuel jet supplying an equimolar mixture of $CH_4$ and $H_2$. The fuel jet is surrounded coaxially by an annulus containing the hot co-flow flue gases produced by a secondary burner mounted upstream. The hot combustion products are further mixed with air and nitrogen to control the oxygen levels. The burner is placed inside a tunnel. Details of the geometry can be found in Dally et al. (2002). **Figure 2** reports the radial profiles of mass fraction of the NO species measured at the axial locations $z = 60/120/200$ mm for

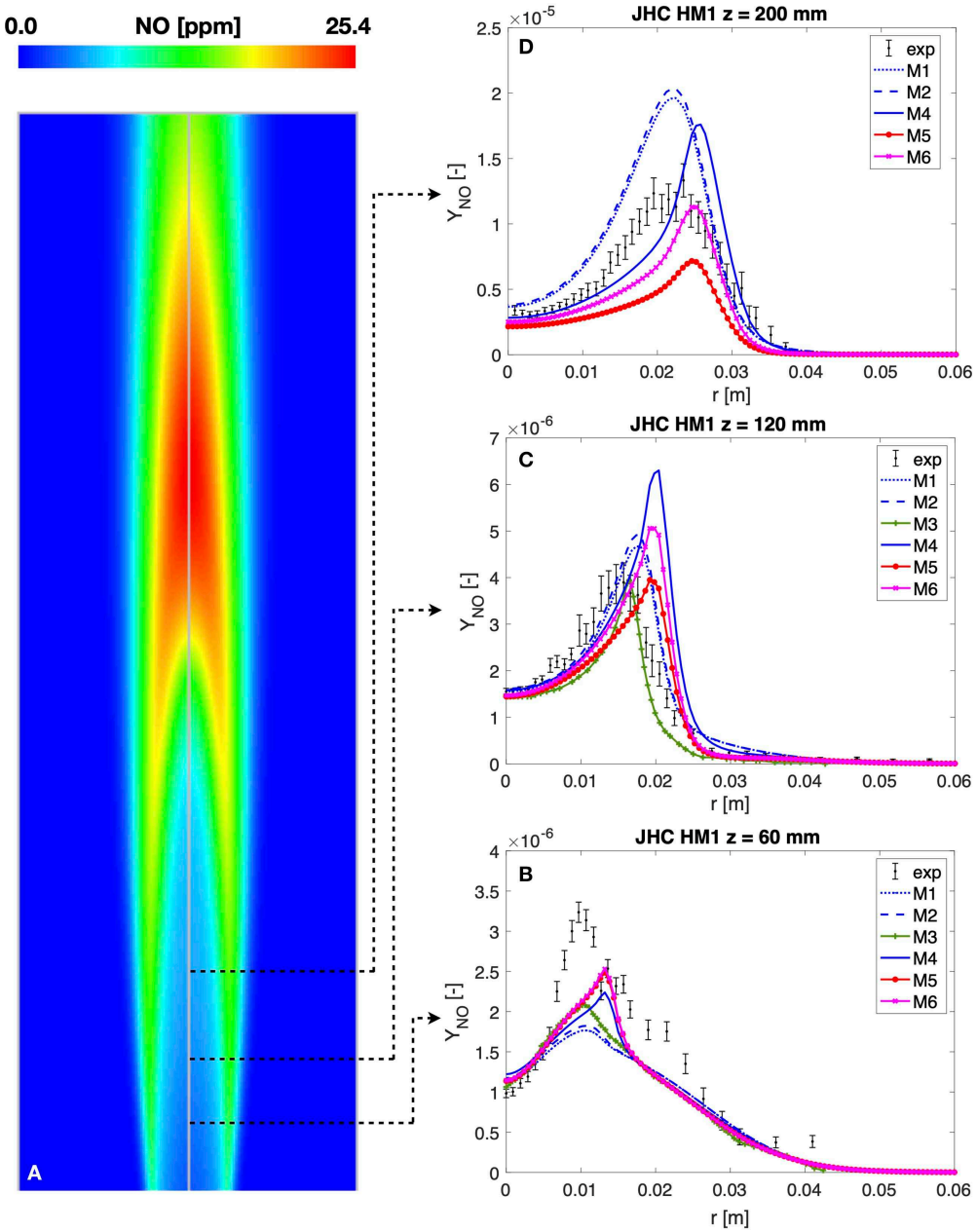


| Simulation | Combustion model | Kinetic scheme | $NO_x$ modeling |
|---|---|---|---|
| **M1** | EDC with $C_\tau$=1.5 | KEE | Post-processing |
| **M2** | EDC with $C_\tau$=1.5 | KEE | Post-processing |
| **M3** | EDC with $C_\tau$=0.82 | GRI2.11 | Detailed chemistry |
| **M4** | EDC with $C_\tau$=1.5 | GRI2.11 | Detailed chemistry |
| **M5** | PaSR with single κ | GRI2.11 | Detailed chemistry |
| **M6** | PaSR with multi κ | GRI2.11 | Detailed chemistry |

**FIGURE 2 | (A)** Contour plot of NO mass fraction in the Adelaide Jet in Hot Coflow (JHC) burner for the experimental case HM1 (jet Reynolds number Re = 10 k, coflow inlet temperature $T_{cof}$ = 1300 K, and $Y_{O_2}$ = 0.03 in the coflow) (Dally et al., 2002). **(B–D)** Experimental and numerical radial profiles of NO mass fraction at axial locations $z$ = 60/120/200 mm in the Adelaide JHC burner. The experimental profiles include both the mean values and the error bar with 99.5% confidence interval associated with a Student's distribution for the true mean value. The relevant settings of the numerical simulations are reported in the explanatory table at the bottom.

the experimental case HM1 (Dally et al., 2002). Case HM1 is characterized by 3% oxygen content (as mass fraction) in the co-flow, inlet temperature of the co-flow $T_{cof} = 1300$ K, and fuel-jet Reynolds number Re = 10k. Measurements of NO were taken via the single-point Raman-Rayleigh-laser-induced fluorescence technique. The selected numerical results are provided by RANS studies that differs from one another in terms of employed chemical mechanism [either KEE, (Bilger et al., 1990) or GRI2.11, (Bowman et al., 1996)] and combustion model (either EDC or PaSR). The use of the KEE mechanism implies the use of a post-processing tool for the estimation of NO, whereas in the GRI2.11 scheme the $NO_x$ chemistry is included. Models M1 and M2 make use of the EDC model and the KEE mechanism. Model M1 employs global schemes for thermal, prompt, $N_2O$ and NNH formation routes. In contrast, model M2 considers the same global scheme for prompt formation as model M1 and multi-step mechanisms for the other routes. These mechanisms were reduced by ROPA for the Adelaide JHC flame conditions based on the POLIMI kinetic scheme (Galletti et al., 2009). Models M3 and M4 consider EDC with different values for the $C_\tau$ constant, i.e., $C_\tau = 0.82$ (Shu et al., 2018) and $C_\tau = 1.5$, respectively, and the GRI2.11 mechanism. Models M5 and M6 employ the PaSR model and the GRI2.11 scheme. Model M5 consider a single value of $\kappa$ in the PaSR formulation for all the species, whereas model M6 uses additional specific values of $\kappa$ for the $NO_x$ species, as put forth by Iavarone et al. (2019).

It can be noticed that model M6 provides improved predictions of NO at axial locations $z = 60$ mm and $z = 200$ mm. A slight overestimation persists at $z = 120$ mm, along with a displacement of the NO profile. The latter is due to the shift of the predicted profiles of relevant quantities for $NO_x$ formation, such as temperature and OH concentration, reported in Iavarone et al. (2019). The cause may be attributed not only to the kinetic mechanism and the combustion model employed, but also to the choice of the turbulence model, which must be able the replicate the spreading of the jet flame. At axial location $z = 120$ mm, the use of the post-processing tool (models M1 and M2) leads to better predictions than the ones from a detailed mechanism (model M4), given the same combustion model, namely EDC with constant $C_\tau = 1.5$. The results of models M1 and M2 are also comparable with those of model M6 at $z = 120$ mm. However, these models provide an underestimation of NO emissions at $z = 60$ mm and a significant overestimation at $z = 200$ mm. This overestimation is likely due to the absence of the reburning route and the assumption of a global scheme for the prompt route, which was found to be the main contributor to NO formation in the corresponding study (Galletti et al., 2015). For models M5-M6, Iavarone et al. (2019) found that the contribution of each pathway to the peak of NO formation at $z = 200$ mm is as follows (in decreasing order): NNH>thermal>prompt>$N_2O$. The analysis has been extended to the other two axial locations: at $z = 60$ mm the rank is prompt>NNH>$N_2O$>thermal, whereas at $z = 120$ mm the NNH contribution overcomes the prompt one and the rank is thus NNH>prompt>$N_2O$>thermal. Same results have been obtained for simulation M4, showing that the contribution rank is not affected by using a different combustion model. These trends can be related to the structure of the JHC flame. Three subregions can be identified: a fuel-rich region located inside the jet, a reaction region inside the shear layer, and a fuel-lean region. The results show that the NO emissions are produced through the prompt route in the fuel-rich region before $z = 120$ mm and through the NNH route further downstream, where the temperature increases in the reactive region and less fuel-rich conditions occur. Hence, the NNH route is proven to be a relevant mechanism of $NO_x$ formation in $H_2$-enriched turbulent diffusion flames under MILD conditions. The thermal route is suppressed under the low temperature conditions, and the $N_2O$ mechanism is not important. This is in agreement with the results of Gao et al. (2013). Finally, it can also be noticed from **Figure 2** that biases in the combustion closure can be as important as the level of the accuracy of the chemical scheme employed.

## 4. DISCUSSION AND CONCLUSION

MILD combustion represents a promising technology to comply with restrictive policies on pollutant emissions prompted by growing environmental issues. MILD combustion can provide low emissions of $NO_x$ thanks to the alteration of the corresponding chemistry. This alteration is caused by the peculiar features of MILD regime, namely homogeneous reaction zones, reduced temperature peaks, and changes in the composition of reactants and subsequent radical species pool. As a consequence, prompt, $N_2O$-intermediate, NNH-intermediate, and reburning routes, which may be typically neglected in conventional combustion systems, end up playing a crucial role in the formation (and destruction) of $NO_x$ in MILD regime. Although several studies have analyzed the relative impact of the $NO_x$ chemical pathways on the emissions of $NO_x$ in MILD combustion, a dominant source has not been identified. The lack of consensus is given by several factors: (a) variability of the operating conditions at which the MILD regime is established; (b) considerable uncertainty still present in the kinetics of NNH and prompt routes; (c) strong interconnection between the hydrocarbon chemistry and the $NO_x$ chemistry, via prompt and reburning routes in particular; (d) ambiguity in the methods of isolating the contribution of a single route with respect to the others, given their interdependence; (e) role of closure sub-models, such as hydrocarbon oxidation kinetics and turbulence-chemistry interactions.

CFD tools remain crucial to aid the investigation and the design of turbulent MILD combustion systems. A summary of $NO_x$ formation modeling approaches employed in CFD simulations has been presented in this review. The approaches span from the estimation of the $NO_x$ emissions through CFD post-processing with simple kinetic mechanisms to the modeling of $NO_x$ formation with detailed kinetic schemes incorporated in turbulence-chemistry interaction models. Even though fairly good predictions of $NO_x$ emissions may be obtained by post-processing techniques, their use can be negatively affected by: (a) lack of necessary detail when simple kinetic mechanisms are used; (b) lack of generality, with risks when extrapolating,

since important parameters must be adjusted on the combustion conditions and are thus case-dependent; (c) strong dependence on the accuracy of the underlying CFD simulation. On the other hand, the use of detailed mechanisms with reactor-based combustion models, desirable in terms of improved predictivity at still affordable computational costs, can be affected by the challenge of accounting for the gap of chemical time scales between nitrogen chemistry and fuel-oxidizer reactions. Therefore, models that bridge these different scales are necessary, since it has been shown that biases in the combustion closure are as important as the level of the accuracy of the chemical scheme employed.

To reduce the uncertainty related to the use of combustion models, one could leverage Direct Numerical Simulations (DNS), which solve the entire range of spatial and temporal scales of the turbulence avoiding the need for a combustion closure. DNS has been recently used to provide useful insights on the physics of MILD combustion and validate combustion models under this regime (Swaminathan, 2019). Indeed, a DNS study confirmed the flaws of the flamelet approaches in MILD combustion due to the presence of microscopic flame interactions that result into distributed reaction zones at the macroscopic level (Minamoto and Swaminathan, 2015). A-priori assessments of combustion models can be beneficial also for the prediction of $NO_x$ emission with detailed kinetic mechanisms incorporated in finite-rate chemistry combustion models. Moreover, DNS of igniting mixing layers have been performed at conditions similar to those of the Adelaide JHC experiments to study autoignition in MILD combustion (Göktolga et al., 2015), whereas the effect of turbulence intensity and level of premixing on $NO_x$ formation were studied via DNS in Karimkashi et al. (2016) and Luca et al. (2017), respectively. Thus, employing DNS data can be beneficial for $NO_x$ formation modeling in MILD combustion. So far, affordable DNS solvers can accommodate reduced kinetic schemes. However, in the next few years, the increasing computational resources can facilitate the inclusion of more detailed schemes, with the possibility to explore the range of time scales involved in the $NO_x$ chemistry and shed light on the importance of specific $NO_x$ pathways in MILD combustion. More validation studies of newly available kinetic mechanisms and combustion models are to be accomplished using data coming from either experiments or DNS of turbulent MILD burners to reach clear conclusions about the role and the modeling of $NO_x$ formation routes, fuel oxidation chemistry, and turbulence-chemistry interactions in the predictions of $NO_x$ emissions in MILD combustion.

## AUTHOR CONTRIBUTIONS

SI and AP have contributed to the research concept and design. They equally contributed to the manuscript through literature review and useful discussions. The work contains parts of their joint research activities. SI has assembled the data and written the first release of the manuscript. AP has critically revised the paper up to the final version.

## FUNDING

This work has been financially supported by the Wiener Anspach Foundation and has received funding from the European Research Council (ERC) under the European Union's Horizon 2020 research and innovation programme under grant agreement No. 714605.

## REFERENCES

Abtahizadeh, E., van Oijen, J., and de Goey, P. (2012). Numerical study of mild combustion with entrainment of burned gas into oxidizer and/or fuel streams. *Combust. Flame* 159, 2155–2165. doi: 10.1016/j.combustflame.2012.02.004

Barlow, R., Fiechtner, G., Carter, C., and Chen, J.-Y. (2000). Experiments on the scalar structure of turbulent CO/H2/N2 jet flames. *Combust. Flame* 120, 549–569. doi: 10.1016/S0010-2180(99)00126-1

Bergmann, V., Meier, W., Wolff, D., and Stricker, W. (1998). Application of spontaneous raman and rayleigh scattering and 2D lif for the characterization of a turbulent CH4/H2/N2 jet diffusion flame. *Appl. Phys. B* 66, 489–502. doi: 10.1007/s003400050424

Bilger, R., Stårner, S., and Kee, R. (1990). On reduced mechanisms for methane/air combustion in nonpremixed flames. *Combust. Flame* 80, 135–149. doi: 10.1016/0010-2180(90)90122-8

Bowman, C., Hanson, R., Davidson, D. Jr., Gardiner, W., Lissianski, V., Smith, G., et al. (1996). *Gri-mech 2.11*. Available online at: http://www.me.berkeley.edu/gri-mech

Bozzelli, J. W., and Dean, A. M. (1995). O + NNH: a possible new route for nox formation in flames. *Int. J. Chem. Kinet.* 27, 1097–1109. doi: 10.1002/kin.550271107

Cavaliere, A., and de Joannon, M. (2004). Mild combustion. *Prog. Energy Combust. Sci.* 30, 329–366. doi: 10.1016/j.pecs.2004.02.003

Cho, E.-S., and Chung, S. H. (2009). Numerical evaluation of $NO_x$ mechanisms in methane-air counterflow premixed flames. *J. Mech. Sci. Technol.* 23, 659–666. doi: 10.1007/s12206-008-1222-y

Chomiak, J. (1990). *Combustion: A Study in Theory, Fact and Application*. Abacus Press/Gorden and Breach Science Publishers.

Cui, Q., Morokuma, K., Bowman, J. M., and Klippenstein, S. J. (1999). The spin-forbidden reaction CH+N2 = HCN+N revisited. II. nonadiabatic transition state theory and application. *J. Chem. Phys.* 110, 9469–9482. doi: 10.1063/1.478949

Cuoci, A., Frassoldati, A., Stagni, A., Faravelli, T., Ranzi, E., and Buzzi-Ferraris, G. (2013). Numerical modeling of nox formation in turbulent flames using a kinetic post-processing technique. *Energy Fuels* 27, 1104–1122. doi: 10.1021/ef3016987

Dally, B., Karpetis, A., and Barlow, R. (2002). Structure of turbulent non-premixed jet flames in a diluted hot coflow. *Proc. Combust. Inst.* 29, 1147–1154. doi: 10.1016/S1540-7489(02)80145-6

Dally, B., Riesmeier, E., and Peters, N. (2004). Effect of fuel mixture on moderate and intense low oxygen dilution combustion. *Combust. Flame* 137, 418–431. doi: 10.1016/j.combustflame.2004.02.011

de Joannon, M., Sorrentino, G., and Cavaliere, A. (2012). Mild combustion in diffusion-controlled regimes of hot diluted fuel. *Combust. Flame* 159, 1832–1839. doi: 10.1016/j.combustflame.2012.01.013

De Soete, G. G. (1975). Overall reaction rates of no and N2 formation from fuel nitrogen. *Symp. (Int.) Combust.* 15, 1093–1102. doi: 10.1016/S0082-0784(75)80374-2

Evans, M., Petre, C., Medwell, P., and Parente, A. (2019). Generalisation of the eddy-dissipation concept for jet flames with low turbulence and low damköhler number. *Proc. Combust. Inst.* 37, 4497–4505. doi: 10.1016/j.proci.2018.06.017

Fenimore, C. (1971). Formation of nitric oxide in premixed hydrocarbon flames. *Symp. (Int.) Combust.* 13, 373–380. doi: 10.1016/S0082-0784(71)80040-1

Ferrarotti, M., Li, Z., and Parente, A. (2019). On the role of mixing models in the simulation of mild combustion using finite-rate chemistry combustion models. *Proc. Combust. Inst* 37, 4531–4538. doi: 10.1016/j.proci.2018.07.043

Frassoldati, A., Sharma, P., Cuoci, A., Faravelli, T., and Ranzi, E. (2010). Kinetic and fluid dynamics modeling of methane/hydrogen jet flames in diluted coflow. *Appl. Ther. Eng.* 30, 376–383. doi: 10.1016/j.applthermaleng.2009.10.001

Galletti, C., Ferrarotti, M., Parente, A., and Tognotti, L. (2015). Reduced no formation models for CFD simulations of mild combustion. *Int. J. Hyd. Energy* 40, 4884–4897. doi: 10.1016/j.ijhydene.2015.01.172

Galletti, C., Parente, A., Derudi, M., Rota, R., and Tognotti, L. (2009). Numerical and experimental analysis of no emissions from a lab-scale burner fed with hydrogen-enriched fuels and operating in mild combustion. *Int. J. Hyd. Energy* 34, 8339–8351. doi: 10.1016/j.ijhydene.2009.07.095

Gao, X., Duan, F., Lim, S. C., and Yip, M. S. (2013). Nox formation in hydrogen–methane turbulent diffusion flame under the moderate or intense low-oxygen dilution conditions. *Energy* 59, 559–569. doi: 10.1016/j.energy.2013.07.022

Glarborg, P., Alzueta, M. U., Dam-Johansen, K., and Miller, J. A. (1998). Kinetic modeling of hydrocarbon/nitric oxide interactions in a flow reactor. *Combust. Flame* 115, 1–27. doi: 10.1016/S0010-2180(97)00359-3

Glarborg, P., Miller, J. A., Ruscic, B., and Klippenstein, S. J. (2018). Modeling nitrogen chemistry in combustion. *Prog. Energy Combust. Sci.* 67, 31–68. doi: 10.1016/j.pecs.2018.01.002

Göktolga, M. U., van Oijen, J. A., and de Goey, L. P. H. (2015). 3D DNS of mild combustion: a detailed analysis of heat loss effects, preferential diffusion, and flame formation mechanisms. *Fuel* 159, 784–795. doi: 10.1016/j.fuel.2015.07.049

Granm, I., and Magnussen, B. (1996). A numerical study of a bluff-body stabilized diffusion flame. Part 2. Influence of combustion modeling and finite-rate chemistry. *Combust. Sci. Technol.* 119, 191–217.

Guo, H., Smallwood, G. J., Liu, F., Ju, Y., and Gülder, Ö. L. (2005). The effect of hydrogen addition on flammability limit and nox emission in ultra-lean counterflow CH4/air premixed flames. *Proc. Combust. Inst.* 30, 303–311. doi: 10.1080/00102209608951999

Gupta, A. K. (2004). Thermal characteristics of gaseous fuel flames using high temperature air. *J. Eng. Gas Turb. Power* 126, 9–19. doi: 10.1115/1.1610009

Harding, L. B., Klippenstein, S. J., and Miller, J. A. (2008). Kinetics of CH + N2 revisited with multireference methods. *J. Phys. Chem. A* 112, 522–532. doi: 10.1021/jp077526r

Haworth, N. L., Mackie, J. C., and Bacskay, G. B. (2003). An ab initio quantum chemical and kinetic study of the NNH + O reaction potential energy surface. How important is this route to no in combustion? *J. Phys. Chem. A* 107, 6792–6803. doi: 10.1021/jp034421p

Hayhurst, A., and Hutchinson, E. (1998). Evidence for a new way of producing no via nnh in fuel-rich flames at atmospheric pressure. *Combust. Flame* 114, 274–279. doi: 10.1016/S0010-2180(97)00328-3

Iavarone, S., Cafiero, M., Ferrarotti, M., Contino, F., and Parente, A. (2019). A multiscale combustion model formulation for nox predictions in hydrogen enriched jet flames. *Int. J. Hyd. Energy* 44, 23436–23457. doi: 10.1016/j.ijhydene.2019.07.019

Jiang, X., Li, P., Guo, J., Hu, F., Wang, F., Mi, J., et al. (2018). Detailed investigation of no mechanism in non-premixed oxy-fuel jet flames with CH4/H2 fuel blends. *Int. J. Hyd. Energy* 43, 8534–8557. doi: 10.1016/j.ijhydene.2018.03.100

Karimkashi, S., Bolla, M., Wang, H., and Hawkes, E. R. (2016). "A direct numerical simulation study of turbulence intensity effects on nox formation in freely propagating premixed flames," in *20th Australasian Fluid Mechanics Conference* (Perth, WA).

Klippenstein, S. J., Harding, L. B., Glarborg, P., and Miller, J. A. (2011). The role of nnh in no formation and control. *Combust. Flame* 158, 774–789. doi: 10.1016/j.combustflame.2010.12.013

Klippenstein, S. J., Pfeifle, M., Jasper, A. W., and Glarborg, P. (2018). Theory and modeling of relevance to prompt-no formation at high pressure. *Combust. Flame* 195, 3–17. doi: 10.1016/j.combustflame.2018.04.029

Konnov, A., Colson, G., and Ruyck, J. D. (2001). No formation rates for hydrogen combustion in stirred reactors. *Fuel* 80, 49–65. doi: 10.1016/S0016-2361(00)00060-0

Lamoureux, N., Merhubi, H. E., Pillier, L., de Persis, S., and Desgroux, P. (2016). Modeling of no formation in low pressure premixed flames. *Combust. Flame* 163, 557–575. doi: 10.1016/j.combustflame.2015.11.007

Lee, K., and Choi, D. (2009). Analysis of no formation in high temperature diluted air combustion in a coaxial jet flame using an unsteady flamelet model. *Int. J. Heat Mass Transf.* 52, 1412–1420. doi: 10.1016/j.ijheatmasstransfer.2008.08.015

Li, G., Stankovic, D., Overman, N., Cornwell, M., Gutmark, E., and Fuchs, L. (2006). "Experimental study of flameless combustion in gas turbine combustors," in *44th AIAA Aerospace Sciences Meeting and Exhibit* (Reno, NV). doi: 10.2514/6.2006-546

Li, P., Dally, B. B., Mi, J., and Wang, F. (2013). Mild oxy-combustion of gaseous fuels in a laboratory-scale furnace. *Combust. Flame* 160, 933–946. doi: 10.1016/j.combustflame.2013.01.024

Li, P., Wang, F., Mi, J., Dally, B., Mei, Z., Zhang, J., et al. (2014). Mechanisms of no formation in mild combustion of CH4/H2 fuel blends. *Int. J. Hyd. Energy* 39, 19187–19203. doi: 10.1016/j.ijhydene.2014.09.050

Li, Z., Ferrarotti, M., Cuoci, A., and Parente, A. (2018). Finite-rate chemistry modelling of non-conventional combustion regimes using a partially-stirred reactor closure: combustion model formulation and implementation details. *Appl. Energy* 225, 637–655. doi: 10.1016/j.apenergy.2018.04.085

Luca, S., Attili, A., and Bisetti, F. (2017). "Direct numerical simulations of $NO_x$ formation in spatially developing turbulent premixed bunsen flames with mixture inhomogeneity," in *55th AIAA Aerospace Sciences Meeting* (Grapevine, TX). doi: 10.2514/6.2017-0603

Malte, P., and Pratt, D. (1975). Measurement of atomic oxygen and nitrogen oxides in jet-stirred combustion. *Symp. (Int.) Combust.* 15, 1061–1070. doi: 10.1016/S0082-0784(75)80371-7

Mancini, M., Weber, R., and Bollettini, U. (2002). Predicting nox emissions of a burner operated in flameless oxidation mode. *Proc. Combust. Inst.* 29, 1155–1163. doi: 10.1016/S1540-7489(02)80146-8

Mardani, A., and Tabejamaat, S. (2012). Nox formation in H2-CH4 blended flame under mild conditions. *Combust. Sci. Technol.* 184, 995–1010. doi: 10.1080/00102202.2012.663991

Medwell, P. R., and Dally, B. B. (2012). Effect of fuel composition on jet flames in a heated and diluted oxidant stream. *Combust. Flame* 159, 3138–3145. doi: 10.1016/j.combustflame.2012.04.012

Miller, J. A., and Bowman, C. T. (1989). Mechanism and modeling of nitrogen chemistry in combustion. *Prog. Energy Combust. Sci.* 15, 287–338. doi: 10.1016/0360-1285(89)90017-8

Minamoto, Y., and Swaminathan, N. (2015). Subgrid scale modelling for mild combustion. *Proc. Combust. Inst.* 35, 3529–3536. doi: 10.1016/j.proci.2014.07.025

Moskaleva, L., and Lin, M. (2000). The spin-conserved reaction ch + n2 = h + ncn: a major pathway to prompt no studied by quantum/statistical theory calculations and kinetic modeling of rate constant. *Proc. Combust. Inst.* 28, 2393–2401. doi: 10.1016/S0082-0784(00)80652-9

Nicolle, A., and Dagaut, P. (2006). Occurrence of no-reburning in mild combustion evidenced via chemical kinetic modeling. *Fuel* 85, 2469–2478. doi: 10.1016/j.fuel.2006.05.021

Parente, A., Galletti, C., and Tognotti, L. (2008). Effect of the combustion model and kinetic mechanism on the mild combustion in an industrial burner fed with hydrogen enriched fuels. *Int. J. Hyd. Energy* 33, 7553–7564. doi: 10.1016/j.ijhydene.2008.09.058

Parente, A., Galletti, C., and Tognotti, L. (2011). A simplified approach for predicting no formation in mild combustion of CH4–H2 mixtures. *Proc. Combust. Inst.* 33, 3343–3350. doi: 10.1016/j.proci.2010.06.141

Parente, A., Malik, M. R., Contino, F., Cuoci, A., and Dally, B. B. (2016). Extension of the eddy dissipation concept for turbulence/chemistry interactions to mild combustion. *Fuel* 163, 98–111. doi: 10.1016/j.fuel.2015.09.020

Perpignan, A. A., Rao, A. G., and Roekaerts, D. J. (2018a). Flameless combustion and its potential towards gas turbines. *Prog. Energy Combust. Sci.* 69, 28–62. doi: 10.1016/j.pecs.2018.06.002

Perpignan, A. A. V., Talboom, M. G., Levy, Y., and Rao, A. G. (2018b). Emission modeling of an interturbine burner based on flameless combustion. *Energy Fuels* 32, 822–838. doi: 10.1021/acs.energyfuels.7b02473

Peters, N. (2001). *Turbulent Combustion*. Cambridge, UK: Cambridge University Press.

Ranzi, E., Sogaro, A., Gaffuri, P., Pennati, G., and Faravelli, T. (1994). A wide range modeling study of methane oxidation. *Combust. Sci. Technol.* 96, 279–325. doi: 10.1080/00102209408935359

Sabia, P., de Joannon, M., Fierro, S., Tregrossi, A., and Cavaliere, A. (2007). Hydrogen-enriched methane mild combustion in a well stirred reactor. *Exp. Therm. Fluid Sci.* 31, 469–475. doi: 10.1016/j.expthermflusci.2006.04.016

Santner, J., Ahmed, S. F., Farouk, T., and Dryer, F. L. (2016). Computational study of nox formation at conditions relevant to gas turbine operation: part 1. *Energy Fuels* 30, 6745–6755. doi: 10.1021/acs.energyfuels.6b00420

Sepman, A., Abtahizadeh, S., Mokhov, A., van Oijen, J., Levinsky, H., and de Goey, L. (2013). Numerical and experimental studies of the no formation in laminar coflow diffusion flames on their transition to mild combustion regime. *Combust. Flame* 160, 1364–1372. doi: 10.1016/j.combustflame.2013.02.027

Shu, Z., Dai, C., Li, P., and Mi, J. (2018). Nitric oxide of mild combustion of a methane jet flame in hot oxidizer coflow: its formations and emissions under h2o, co2 and n2 dilutions. *Fuel* 234, 567–580. doi: 10.1016/j.fuel.2018.07.057

Skottene, M., and Rian, K. E. (2007). A study of nox formation in hydrogen flames. *Int. J. Hyd. Energy* 32, 3572–3585. doi: 10.1016/j.ijhydene.2007.02.038

Song, Y., Marrodán, L., Vin, N., Herbinet, O., Assaf, E., Fittschen, C., et al. (2019). The sensitizing effects of NO2 and no on methane low temperature oxidation in a jet stirred reactor. *Proc. Combust. Inst.* 37, 667–675. doi: 10.1016/j.proci.2018.06.115

Sutton, J. A., Williams, B. A., and Fleming, J. W. (2012). Investigation of ncn and prompt-no formation in low-pressure C1–C4 alkane flames. *Combust. Flame* 159, 562–576. doi: 10.1016/j.combustflame.2011.08.023

Swaminathan, N. (2019). Physical insights on mild combustion from DNS. *Front. Mech. Eng.* 5:59. doi: 10.3389/fmech.2019.00059

Szegö, G., Dally, B., and Nathan, G. (2008). Scaling of nox emissions from a laboratory-scale mild combustion furnace. *Combust. Flame* 154, 281–295. doi: 10.1016/j.combustflame.2008.02.001

Vasudevan, V., Hanson, R. K., Bowman, C. T., Golden, D. M., and Davidson, D. F. (2007). Shock tube study of the reaction of CH with N2: overall rate and branching ratio. *J. Phys. Chem. A* 111, 11818–11830. doi: 10.1021/jp075638c

Veríssimo, A. S., Rocha, A. M. A., and Costa, M. (2011). Operational, combustion, and emission characteristics of a small-scale combustor. *Energy Fuels* 25, 2469–2480. doi: 10.1021/ef200258t

Wang, F., Li, P., Zhang, J., Mei, Z., Mi, J., and Wang, J. (2015). Routes of formation and destruction of nitrogen oxides in CH4/H2 jet flames in a hot coflow. *Int. J. Hyd. Energy* 40, 6228–6242. doi: 10.1016/j.ijhydene.2015.03.047

Wünning, J., and Wünning, J. (1997). Flameless oxidation to reduce thermal no-formation. *Prog. Energy Combust. Sci.* 23, 81–94. doi: 10.1016/S0360-1285(97)00006-3

Zeldovich, Y. (1946). The oxidation of nitrogen in combustion explosions. *Acta Physicochim. URSS* 21, 577–628.

Zhang, Y., Mathieu, O., Petersen, E. L., Bourque, G., and Curran, H. J. (2017). Assessing the predictions of a nox kinetic mechanism on recent hydrogen and syngas experimental data. *Combust. Flame* 182, 122–141. doi: 10.1016/j.combustflame.2017.03.019

**Conflict of Interest:** The authors declare that the research was conducted in the absence of any commercial or financial relationships that could be construed as a potential conflict of interest.

frontiers in Mechanical Engineering

MINI REVIEW
published: 24 March 2020
doi: 10.3389/fmech.2020.00010

# Diffusion Ignition Processes in MILD Combustion: A Mini-Review

*Giancarlo Sorrentino*[1]*, *Antonio Cavaliere*[1], *Pino Sabia*[2], *Raffaele Ragucci*[2] and *Mara de Joannon*[2]

[1] Dipartimento di Ingegneria Chimica, dei Materiali e della Produzione Industriale, Università degli studi di Naples "Federico II", Naples, Italy, [2] Istituto di Ricerche sulla Combustione (IRC), Consiglio Nazionale delle Ricerche (CNR), Naples, Italy

MILD combustion processes belong to new combustion technologies developed to achieve efficient and clean fuel conversion. The basic concept behind its implementation is the use of high levels of hot exhausted gas recirculation within the combustion chamber. They simultaneously dilute fresh reactants, to control system temperatures and pollutants emission, while promoting fuel complete oxidation. The combination of low maximum system working temperatures and high diluted mixtures with intense pre-heating delineates an oxidation process with unique chemical and physical features, such as uniformity of scalars at macroscale related to distributed reacting regions at microscale, extremely different from conventional flames. In turn, this requires the definition and characterization of new elementary processes, not ascribable to traditional deflagration or diffusive flame structures, which, in literature have been identified as "diffusion ignition." The present mini-review reports on several literature characterizations of such reactive structures under steady and unsteady conditions combining evidences from numerical, experimental, and/or theoretical studies. Both premixed and non-premixed configurations were analyzed in terms of system temperature, heat release, and species distributions as key parameters to describe the intrinsic nature of such new elementary processes. Analyses were realized changing the main system external parameters (mixture pre-heating temperature, dilution level in several feeding configurations) moving from traditional to MILD conditions. Results highlighted the "distributed ignition" nature of igni-diffusive structures, with implication on the thickness of the oxidation structures in the mixture fraction space, the presence/absence of a pyrolysis region, and the correlation of the maximum heat release with the mixture stoichiometric.

**Keywords: MILD combustion, distributed ignition, igni-diffusion, dilution level, heat release**

OPEN ACCESS

***Edited by:***
*Nesrin Ozalp,*
*University of Minnesota Duluth,*
*United States*

***Reviewed by:***
*Jinhua Wang,*
*Xi'an Jiaotong University, China*
*Christine Mounaïm-Rousselle,*
*University of Orléans, France*

***Correspondence:**
*Giancarlo Sorrentino*
*g.sorrentino@unina.it*

***Specialty section:***
*This article was submitted to Thermal and Mass Transport, a section of the journal Frontiers in Mechanical Engineering*

***Received:*** *25 October 2019*
***Accepted:*** *20 February 2020*
***Published:*** *24 March 2020*

***Citation:***
*Sorrentino G, Cavaliere A, Sabia P, Ragucci R and de Joannon M (2020) Diffusion Ignition Processes in MILD Combustion: A Mini-Review. Front. Mech. Eng. 6:10. doi: 10.3389/fmech.2020.00010*

## INTRODUCTION

Elementary structures in combustion such as laminar diffusion layers have been characterized in the literature (Tsuji, 1982; Chao et al., 1991; Darabiha, 1992; Chen et al., 2012). Dilution and preheating of reactants pointed out some peculiarities that were examined through numerical, experimental, and theoretical studies in the last decades (de Joannon et al., 2009; Abtahizadeh et al., 2012; Sepman A. et al., 2013; Sorrentino et al., 2013). Diffusive ignition process under MILD combustion was deeply investigated (Cavaliere and de Joannon, 2004).

The relevance of such processes concerns several fields of application such as low heating value fuel oxidation (Maruta et al., 2007), destruction of VOC, or combustion in flows with internal recirculation.

Diffusion ignition can be described in 1-D spatial conditions, but usually they are very difficult to mimic in simple experiments due to such low dimensionality. 2-D experiments where fuel jets are injected in co-flowing or cross-flowing oxidizer streams are easier to realize for diluted and preheated conditions.

Jet in hot flows configuration was used to reproduce diffusion ignition processes (Adelaide or Delft jet in hot coflow) in both the laminar (LJHC) and turbulent (JHC) cases when inlet reactant temperatures are higher than ignition ones (Medwell et al., 2007, 2009; Choi et al., 2009; Oldenhof et al., 2011; Sepman A. V. et al., 2013). In particular, methane and $CH_4/H_2$ blends were analyzed by Medwell et al. (2007) and Al-Noman et al. (2016), whereas Oldenhof et al. (2010) analyzed the stabilization region of natural gas mixtures burning in a hot/diluted coflow by recording the flame luminescence with an intensified high-speed camera. The spatial distributions of the hydroxyl radical (OH), formaldehyde ($H_2CO$), and temperature imaged by laser diagnostic techniques were obtained for ethylene flames by Medwell et al. (2008) whereas Choi and Chung (2010) investigated the autoignition characteristics of laminar lifted ethylene flames in coflow air with elevated temperature over 800 K. Arndt et al. (2019) studied the autoignition of propane jet-in-hot coflow with high-speed OH* chemiluminescence imaging and high-speed Rayleigh scattering for mixture fraction, temperature, and scalar dissipation rate measurements. Liquid fuels, such as ethanol (Correia Rodrigues et al., 2015; Ye et al., 2016), have been also studied in some preliminary works.

The reactive structure features that were recognized in these studies can be summarized in such points:

1. Combustion Mode Type:
   - Diffusion–ignition
   - Standard deflagration or diffusion flame
   - Mixed-mode regimes (partially premixed).
2. Diffusion Ignition is Strongly Sensitive to Boundary Conditions More Than Standard 1-D Deflagrative/Diffusion Flame Processes.

The same type of analysis has been also performed in Jet in Hot Cross Flow configuration (Sidey and Mastorakos, 2015; Wagner et al., 2017) where fuel was injected into hot and vitiated air crossflow. Results suggested that autoignition is the dominant stabilization mechanism.

A wide numerical/theoretical characterization of igni-diffusive steady structures under MILD conditions was reported in the literature with 1-D counterflow configurations. Reactive structures were analyzed as a function of feeding configurations from several groups (de Joannon et al., 2012a,b; Zou et al., 2014; He et al., 2016).

In the following sections, the peculiarity of diffusion ignition processes will be analyzed for steady or unsteady conditions.

## STEADY DIFFUSION IGNITION: HDDI AND HCDI

Distributed combustion regime occurs in technologies where dilution and preheating of reactants are used for efficient and clean energy conversion (Li et al., 2011; Khalil and Gupta, 2017; Perpignan et al., 2018). In practical systems, gas recirculation is adopted (Sorrentino et al., 2018a; Sabia et al., 2019). Low combustion temperatures and high dilution/pre-heating alter the fuel conversion with respect to traditional flames (Maruta et al., 2000; Minamoto et al., 2014; Minamoto and Swaminathan, 2015).

Elementary processes that undergo MILD combustion influence the controlling parameters (Cavaliere et al., 2016). In particular, the reactivity under stoichiometric conditions is comparable with the one related to fuel-lean or fuel-rich conditions (de Joannon et al., 2010). It follows that reactions are homogeneously distributed (Plessing et al., 1998; Özdemir and Peters, 2001).

In particular, the characterization of diffusion-controlled combustion processes developing in a steady 1-D layer was reported in the literature with several numerical studies by means of the opposed jets configuration (de Joannon et al., 2007; Cheong et al., 2017; Mameri et al., 2018).

This section takes into account numerical characterization of steady mixing layers with diluted and/or preheating streams with different feeding configurations as a function of main parameters.

In this review article, a sub-classification of steady diffusion ignition process will be used as reported in the following:

1. Reactants with homogenous mixture composition and preheating of inert flow as main controlling parameters [homogeneous charge diffusion ignition (HCDI)]
2. Non-premixed flows with reactants dilution and preheating as main controlling parameters [hot diluted diffusion ignition (HDDI)].

In the HCDI mode (de Joannon et al., 2007; Mastorakos, 2009; Goh et al., 2013), a homogeneous reactant charge interacts with inert (such as nitrogen or carbon dioxide) at high temperature (i.e., combustion products) and this yields a counter-diffusion layer. On the other hand, the HDDI is realizable for non-premixed streams with a certain level of dilution and/or preheating (de Joannon et al., 2009; Chen and Zheng, 2011; Ye et al., 2017). The initial conditions of HCDI processes are fixed on one side of spatial coordinate homogeneous reactants in a fixed composition and the species on the other side are inert (for instance combustion products) at high temperature, as reported in the sketch of the insert in **Figure 1A**. As is well-known, a premixed fuel/air mixture outside the flammability limit cannot support a deflagration process. Several experimental studies have reported the occurrence of this process when the heat source is a heated wall or a high-temperature inert flow in a laminar (Darabiha et al., 1988; Smooke et al., 1991; Zheng et al., 2002) or turbulent (Blouch et al., 1998) counterflow. In particular, Mastorakos et al. (1995) investigated the effects of simultaneous dilution and preheat of reactants by mixing with hot combustion products in turbulent counterflow flames formed near the impinging region of two opposed jets. Examples of this reactive structure are also obtained in a counterflow configuration as shown in the sketch of **Figure 1A** for a methane/oxygen stream that impinges toward high-temperature flows. The bulk flow velocities define the system strain rate. The sketch in **Figure 1A** shows the location of the reactive region (orange area) when the mixture is outside the flammability limits

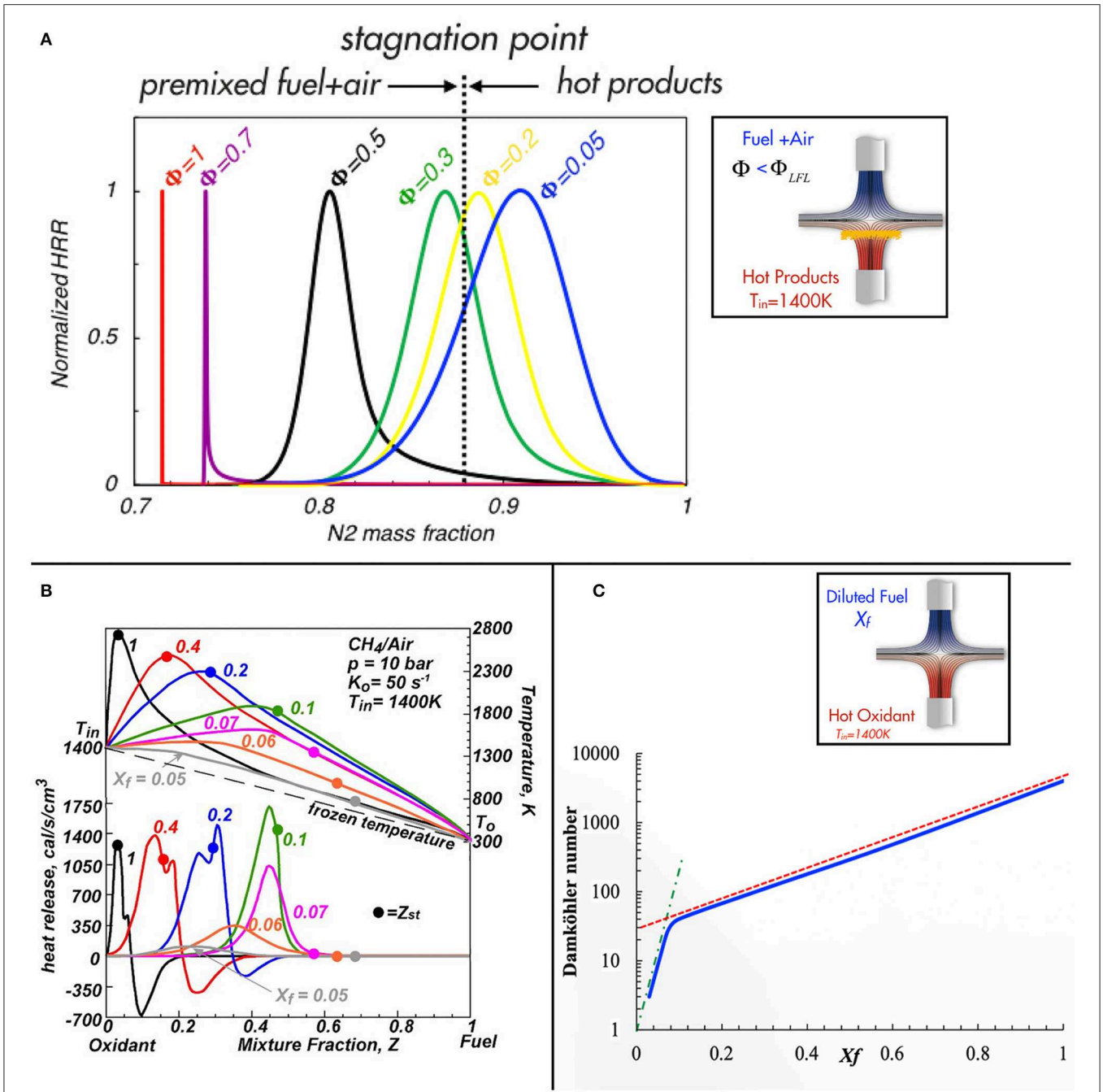


**FIGURE 1 |** Normalized heat release rate as a function of $N_2$ mass fraction in HCDI configuration **(A)**. **(B)** Reports temperature and heat release rate in a HDDI (HODF) configuration [adapted from de Joannon et al. (2009) with permission from Elsevier] and Damköhler number in **(C)**.

($\Phi < \Phi_{LFL}$). Such counterflow allows for the characterization of several HCDI or deflagration structures (de Joannon et al., 2007). In particular, the results shown in **Figure 1A** (Cavaliere et al., 2016) reports a homogeneous fuel/air charge continuously heated by a hot inert flow of $N_2$ (mimicking combustion products). A premixed $CH_4$-air flow, characterized by an inlet temperature ($T_0$) and velocity ($V_0$), is fed toward an opposed flow of nitrogen at high temperatures ($T_{in}$). The distance $D$ between the jets is 2 cm. Numerical analysis was carried out by means of Oppdif application for counterflow configurations of ChemKin 3.7 package by using the GRI 3.0 mechanism as kinetics model. The enthalpy production reported in **Figure 1A** with a red curve at $T_{in} = 1{,}400$ K for $k = 50\ s^{-1}$ is positioned on the premixed fuel/air side for $\Phi = 1$ with a very thin reactive region. By decreasing the inlet equivalence ratio, these heat release curves are different from those at $\Phi = 1$ as they

are broadened, and are shifted closer to the stagnation point. Notably, the reactive zone location passes the stagnation point for $\Phi < 0.2$ when the mixture is outside the flammability limits. In this case, the oxidative structures are located on the hot products side.

In summary, the figure demonstrates that a great variety of oxidation structures may be stabilized in HCDI processes and the features of the oxidation process are related to the diffusion between the hot products and the air/fuel charge. Such behavior can be ascribed to MILD combustion and it has features that partially explain the distributed and noiseless characteristic reported for some flameless applications (Wünning and Wünning, 1997; Khidr et al., 2017; Zhou et al., 2017). In fact, the reactive process is distributed on a wide mixture fraction region and the transition from HCDI to deflagration is gradual (Sidey et al., 2014).

Combustion processes in which the reactants are separated yield diffusion flames and they can be obtained in a counter-diffusion reactor when it is fed with oxidant and fuel in opposite directions along the same axis. In MILD combustion, such streams can be diluted with inert species (such as combustion products) and can be heated to such high temperatures that the frozen temperature is higher than the ignition one (de Joannon et al., 2010; Sidey and Mastorakos, 2016).

In this case, the non-premixed configuration, as reported in the sketch of **Figure 1C**, is characterized by fuel at ambient temperature and molar fraction $X_f$ that is fed vs. an opposed airflow at a fixed preheating temperature ($T_{in}$). The flow rates are kept constant to fix the bulk strain rates $K_0 = V_0/D$. In **Figure 1B**, the structure of the reactive zone was depicted for HODF where temperature and heat release rate profiles as a function of the mixture fraction ($Z$) were reported for several $X_f$ values. The plots of **Figure 1B** (adapted by de Joannon et al., 2009) were obtained at $P = 10$ bar for a $CH_4$/Air system. They refer to diluted methane at ambient temperature diffusing in hot air at $T_{in} = 1{,}400$ K, i.e., a HODF (Hot Oxidant Diluted Fuel) feeding in a SICF (Steady Igniting Counter-Flow). Numerical tools and kinetics mechanisms are the same used for HCDI cases reported before. Methane content was varied from $X_f = 1$ to 0.05 by means of $N_2$ dilution. The stoichiometric mixture fraction location is indicated on the profiles with dots. The heat release profile (lower part of **Figure 1B**) reported with the black curve is related to an undiluted case and it exhibits a maximum in correspondence of $Z_{st}$ whereas pyrolytic regions with negative heat release occur for fuel-rich region. A similar behavior was obtained for $T$ (upper part) that reaches a maximum value of about 2,800 K. The fuel dilution strongly alters the oxidative structure as a function of its magnitude and it emphasizes the difference with respect to conventional conditions. For $X_f = 0.5$, the $T_{max}$ values are shifted toward higher $Z$ and the oxidation region in the heat release profile shifts and widens. The pyrolytic region is enlarged toward higher $Z$ with strong reduction of the minimum heat release rate. This behavior becomes more clear by decreasing $X_f$, causing the vanishing of the pyrolytic region for dilution level higher than 85%. In fact, when the dilution level reaches 90% ($X_f = 0.1$), heat release profiles exhibit only a single maximum that diminishes its intensity with $X_f$. Moreover, the most important effect of the dilution is a shift of the oxidative region backward toward lower $Z$, in opposite direction with the stoichiometry (as reported by the colored dots that indicate the $Z_{st}$ location).

Therefore, by summarizing, several peculiar characteristics have been pointed out as discriminative for the occurrence of different combustion regimes. They have been related to reactive region thickness, absence of a pyrolysis region, and the correlation of the maximum heat release with the $Z_{st}$. Following such criteria, the features of the reaction zone suggested a different name for the elementary process with respect to standard diffusion ones, and thus, HDDI was chosen for such non-premixed case.

The results above reported revealed that both the HDDI and HCDI modes support a "distributed ignition" behavior. Moreover, a strong extinction resilience was also reported in several literature papers as another important feature of such MILD processes (Sidey et al., 2016; Evans et al., 2017; Sidey and Mastorakos, 2018). All these features are linked to each other.

Another important synthetic representation of MILD features is reported with the blue curve in **Figure 1C** where Damköhler number is reported vs. the fuel mole fraction. Its evaluation is based on the ratio between a characteristic convective time (based on the strain rate) and a kinetic one. More specifically, it diminishes from about 7,000 to 50 by decreasing the $X_f$ value from 1 to 0.1. Also, in this case, the most relevant variation is shown at 90% fuel dilution where Da undergoes a significant change. This is correlated to a "gradual" behavior of the reactive process that entails a continuous increase of chemical kinetics times with respect to a reference fluid-dynamic one. It is of interest that the Damköhler number change is three orders of magnitude with respect to undiluted cases. In particular, two asymptotic behaviors can be identified with the dashed red line for $0.15 < X_f < 1$ and with the dashed-dotted green one for $X_f < 0.1$. Such paradigm shift in the reactive structures at a fixed dilution level was also identified in several literature papers for diluted conditions in SICF (Fotache et al., 1997, 1998; Abtahizadeh et al., 2012) and confirmed also for low-heating value fuels (Kwiatkowski and Mastorakos, 2016).

## UNSTEADY DIFFUSION IGNITION

Igni-diffusive structure characterizations are possible in 1-D configurations by following the temporal evolution of diffusion layer ignition/oxidation for diluted and preheated conditions in wide parameter ranges. In this case, unsteady elementary processes strongly depend on the boundary conditions and fluid-dynamics pattern. In particular, literature evidenced two main possibilities for transient diffusion-controlled combustion processes in 1-D configurations: IML (Igniting Mixing Layer) and ICF (Igniting Counter-Flow).

IML can be defined as a "universal" or "zero-order" configuration because it represents the natural evolution of diffusive-reactive process (Abtahizadeh et al., 2015). Therefore, it is of interest as reference case because the temporal evolution refers to an initial unmixed mixture where the initial mixture fraction gradient is not prescribed by a fixed strain rate

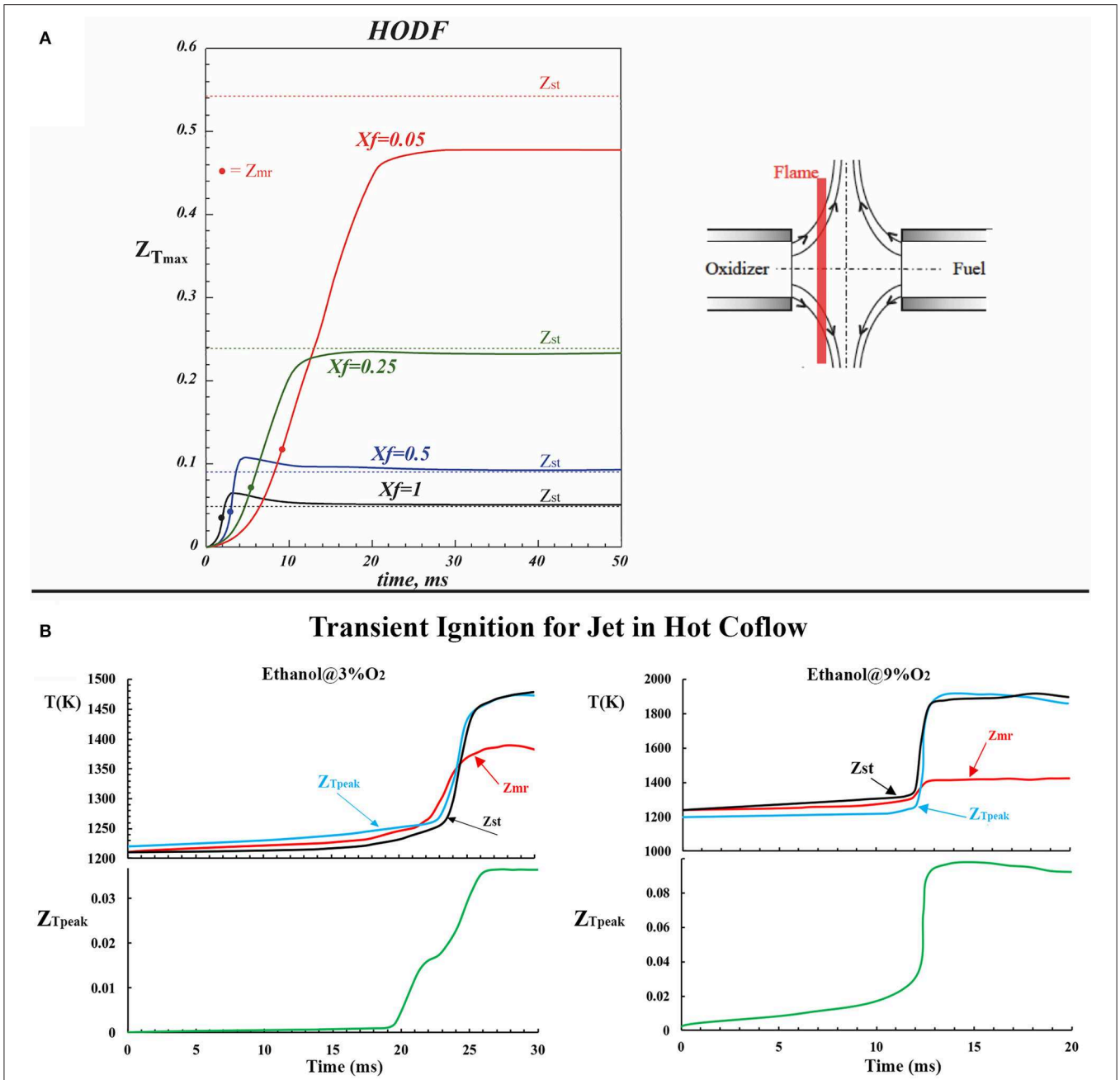


**FIGURE 2 |** Temporal evolution of mixture fraction where the peak temperature occurs for HODF conditions **(A)** adapted from Sorrentino et al. (2013) with permission from Elsevier. **(B)** Reports transient numerical computations for ethanol in JHC flames with the boundary conditions obtained from the experiments by Ye et al. (2018). Temperature and $Z_{Tpeak}$ as a function of time were reported for two oxygen levels.

but is controlled by molecular diffusion. It is a key process also for inferring tabulated chemistry information for complex systems (Sorrentino et al., 2018b). IML was reported in the literature to evaluate ignition characteristics (most reactive mixture fraction) of diluted fuels in comparison with Auto-Ignition and Homogeneous Ignition (Mastorakos et al., 1997; Im et al., 1998; Sreedhara and Lakshmisha, 2000; Hilbert and Thévenin, 2002; van Oijen, 2013).

ICF in steady strain flow field is the configuration in which the transient diffusion ignition process evolves in a developed mixing layer originated by a mixture fraction in two opposed laminar jets, where the initial mixture fraction is distributed according to frozen mixing due to applied strain. This kind of process was one of the most characterized in the literature because it can be obtained through coflow configurations for both the undiluted and diluted cases, as already underlined in the *Introduction*

section (Cabra et al., 2002; Dally et al., 2002; Chung, 2007). In this case, several regimes such as autoignition, flame propagation, and diffusion ignition can occur (Medwell et al., 2016; Schulz et al., 2017).

Unsteady 1-D reactive diffusive layer evolution has been depicted for HODF conditions in **Figure 2A** by reporting the numerical results obtained in ICF configuration and adapted by the results of Sorrentino et al. (2013).

The profiles in **Figure 2A** show the temporal evolution of the maximum temperature location in the mixture fraction space. The solid dots depict the location of the most reactive mixture fraction ($Z_{mr}$) whereas the dashed lines are related to the position of $Z_{st}$. It is worthwhile to note that, for undiluted or slightly diluted conditions ($0.2 < X_f < 1$), the location of $Z_{mr}$ and $Z_{st}$ is very close to each other. It means that ignition and stabilization phenomena occur in the same mixture fraction and time intervals (Im et al., 2000). Therefore, in such cases, the diffusive structure growth in time is limited to a narrow mixture fraction space. For $X_f < 0.1$, the main effect of MILD combustion (because the reactant dilution slows down the oxidative chemical kinetics) is to increase the distance between the "most reactive" mixture fraction and the "stoichiometric" one. In each case, the most reactive mixture fraction is always placed on the high-temperature side (preheated oxidizer in **Figure 2A**) and the location is not affected by dilution (Viggiano and Magi, 2004; Yoo et al., 2011).

The aforementioned behaviors were confirmed for ethanol-diluted flames in JHC configuration, as reported in the numerical results of **Figure 2B**, where boundary conditions were obtained from Ye et al. (2018). Unsteady flamelet equations were solved in time and mixture fraction space using the FlameMaster program (Pitsch, 1998). It shows the peak temperature as a function of time for ethanol at 3 and 9% of $O_2$. The mixture fraction where the peak temperature occurs is denoted as $Z_{Tpeak}$. As the oxygen level reduces from 9 to 3%, the ignition process becomes prolonged with a reduced temperature increase. Thus, flames in the 3% $O_2$ case are close to diffusion ignition cases, being distributed with a low temperature increase.

Recent DNS studies (Doan et al., 2018) confirmed the importance of dilution and $Z_{mr}$ location on the stabilization but they also depicted that non-premixed turbulent MILD combustion is a complex process with spatial and temporal ignition fronts, non-premixed, and propagating flames that are strongly convoluted and interacting. In particular, multiple igniting mixing layers can interact between themselves and the annihilation of peripheral isolines may strongly influence the reactive structures (Sorrentino et al., 2017).

## CONCLUSIVE REMARKS

The analyses reported so far have emphasized that the occurrence of MILD combustion in diffusion-controlled conditions strongly differs from deflagration and diffusion flames. These characteristics are of interest in comparison to the conventional flame structure where the mixture fraction range in which the reaction takes place is quite narrow and changes slightly with dissipation rate. In contrast, the oxidation structure of MILD combustion shifts along the mixture fraction space according to different boundary conditions (temperature and dilution). The features of diffusion ignition are related to several peculiarities such as distributed ignition, flameless oxidation, and heat release not correlated with stoichiometric mixture fraction, differently from flame structured processes.

Strong extinction resilience and gradual ignition are also distinctive characteristics of such reactive structures that were highlighted by analyzing the unsteady evolution of the diffusive reactive layer under preheated and diluted conditions.

## AUTHOR CONTRIBUTIONS

GS and PS were involved in the bibliographic research to include in the manuscript the most important literature contributions on the diffusion ignition process in MILD combustion. They have also strongly contributed in writing several parts of the article. AC and MJ gave their support in the theoretical background regarding categorization and classification of MILD combustion processes. RR gave important insights and hints in the physical description of diffusion ignition and its connection with dimensionless numbers. He also strongly revised the English language in the manuscript.

## FUNDING

This work was financially supported with funding of the MSE-CNR project 2013–2014 Miglioramento dell'efficienza energetica dei sistemi di conversione locale di energia.

## ACKNOWLEDGMENTS

This article is based upon work from COST Action SMARTCATs (CM1404), supported by COST (European Cooperation in Science and Technology, http://www.cost.eu).

## REFERENCES

Abtahizadeh, E., de Goey, P., and van Oijen, J. (2015). Development of a novel flamelet-based model to include preferential diffusion effects in autoignition of $CH_4/H_2$ flames. *Combust. Flame* 162, 4358–4369. doi: 10.1016/j.combustflame.2015.06.015

Abtahizadeh, E., van Oijen, J., and de Goey, P. (2012). Numerical study of Mild combustion with entrainment of burned gas into oxidizer and/or fuel streams. *Combust. Flame* 159, 2155–2165. doi: 10.1016/j.combustflame.2012.02.004

Al-Noman, S., Choi, S. K., and Chung, S. H. (2016). Numerical study of laminar nonpremixed methane flames in coflow jets: autoignited lifted flames with tribrachial edges and MILD combustion at elevated temperatures. *Combust. Flame* 171, 119–132. doi: 10.1016/j.combustflame.2016.06.021

Arndt, C. M., Papageorge, M. J., Fuest, F., Sutton, J. A., and Meier, W. (2019). Experimental investigation of the auto-ignition of a transient propane Jet-in-Hot-Coflow. *Proc. Combust. Inst.* 37, 2117–2124. doi: 10.1016/j.proci.2018.06.195

Blouch, J. D., Sung, C. J., Fotache, C. G., and Law, C. K. (1998). Turbulent ignition of non-premixed hydrogen by heated counterflowing atmospheric air. *Symposium on Combust.* 27, 1221–1228. doi: 10.1016/S0082-0784(98)80526-2

Cabra, R., Myhrvold, T., Chen, J. Y., Dibble, R. W., Karpetis, A. N., and Barlow, R. S. (2002). Simultaneous laser raman-rayleigh-lif measurements and numerical modeling results of a lifted turbulent $H_2/N_2$ jet flame in a vitiated coflow. *Proc. Combust. Inst.* 29, 1881–1888. doi: 10.1016/S1540-7489(02)80228-0

Cavaliere, A., and de Joannon, M. (2004). Mild combustion. *Prog. Energy Combust. Sci.* 30, 329–366. doi: 10.1016/j.pecs.2004.02.003

Cavaliere, A., de Joannon, M., Sabia, P., Sorrentino, G., and Ragucci, R. (2016). "Highly preheated lean combustion," in *Lean Combustion: Technology and Control, 2nd Edn,* Vol. 3, eds D. Dunn-Rankin and P. Therkelsen (London: Imprint by Academic Press), 63–105. doi: 10.1016/B978-0-12-804557-2.00003-1

Chao, B. H., Law, C. K., and T'ien, J. S. (1991). Structure and extinction of diffusion flames with flame radiation. *Symp. Combust.* 23, 523–531. doi: 10.1016/S0082-0784(06)80299-7

Chen, S., Mi, J., Liu, H., and Zheng, C. (2012). First and second thermodynamic-law analyses of hydrogen-air counter-flow diffusion combustion in various combustion modes. *Int. J. Hydrogen Energy* 37, 5234–5245. doi: 10.1016/j.ijhydene.2011.12.039

Chen, S., and Zheng, C. (2011). Counterflow diffusion flame of hydrogen-enriched biogas under MILD oxy-fuel condition. *Int. J. Hydr. Energy* 36, 15403–15413. doi: 10.1016/j.ijhydene.2011.09.002

Cheong, K. P., Li, P., Wang, F., and Mi, J. (2017). Emissions of NO and CO from counterflow combustion of CH4 under MILD and oxyfuel conditions. *Energy* 124, 652–664. doi: 10.1016/j.energy.2017.02.083

Choi, B. C., and Chung, S. H. (2010). Autoignited laminar lifted flames of methane, ethylene, ethane, and n-butane jets in coflow air with elevated temperature. *Combust. Flame* 157, 2348–2356, doi: 10.1016/j.combustflame.2010.06.011

Choi, B. C., Kim, K. N., and Chung, S. H. (2009). Autoignited laminar lifted flames of propane in coflow jets with tribrachial edge and mild combustion. *Combustion Flame* 156, 396–404, doi: 10.1016/j.combustflame.2008.10.020

Chung, S. H. (2007). Stabilization, propagation and instability of tribrachial triple flames. *Proc. Combustion Inst.* 31, 877–892. doi: 10.1016/j.proci.2006.08.117

Correia Rodrigues, H., Tummers, M. J., van Veen, E. H., and Roekaerts, D. J. E. M. (2015). Effects of coflow temperature and composition on ethanol spray flames in hot-diluted coflow. *Int. J. Heat Fluid Flow* 51, 309–323. doi: 10.1016/j.ijheatfluidflow.2014.10.006

Dally, B. B., Karpetis, A. N., and Barlow, R. S. (2002). Structure of turbulent non-premixed jet flames in a diluted hot coflow. *Proc. Combustion Inst.* 29, 1147–1154. doi: 10.1016/S1540-7489(02)80145-6

Darabiha, N. (1992). Transient behaviour of laminar counterflow hydrogen-air diffusion flames with complex chemistry. *Combust. Sci. Technol.* 86, 163–181. doi: 10.1080/00102209208947193

Darabiha, N., Candel, S. M., Giovangigli, V., and Smooke, M. D. (1988). Extinction of strained premixed propane-air flames with complex chemistry. *Combust. Sci. Tech.* 60, 267–285. doi: 10.1080/00102208808923988

de Joannon, M., Matarazzo, A., Sabia, P., and Cavaliere, A. (2007). Mild combustion in homogeneous charge diffusion ignition (HCDI) regime. *Proc. Combust. Inst.* 31, 3409–3416. doi: 10.1016/j.proci.2006.07.039

de Joannon, M., Sabia, P., and Cavaliere, A. (2010). "Mild Combustion" in *Handbook of Combustion, Vol. 5, New Technologies*, eds M. Lackner, F. Winter, A. K. Agarwal (Weinheim: Wiley-VCH Verlag), 237–255. doi: 10.1002/9783527628148.hoc081

de Joannon, M., Sabia, P., Cozzolino, G., Sorrentino, G., and Cavaliere, A. (2012a). Pyrolitic and oxidative structures in hot oxidant diluted oxidant (HODO) MILD combustion. *Combust. Sci. Tech.* 184, 1207–1218. doi: 10.1080/00102202.2012.664012

de Joannon, M., Sabia, P., Sorrentino, G., and Cavaliere, A. (2009). Numerical study of mild combustion in hot diluted diffusion ignition (HDDI) regime. *Proc. Combust. Inst.* 32, 3147–3154. doi: 10.1016/j.proci.2008.09.003

de Joannon, M., Sorrentino, G., and Cavaliere, A. (2012b). MILD combustion in diffusion-controlled regimes of Hot Diluted Fuel. *Combust. Flame* 159, 1832–1839. doi: 10.1016/j.combustflame.2012.01.013

Doan, N. A. K., Swaminathan, N., and Minamoto, Y. (2018). DNS of MILD combustion with mixture fraction variations. *Combust. Flame* 189, 173–189. doi: 10.1016/j.combustflame.2017.10.030

Evans, M. J., Chinnici, A., Medwell, P. R., and Ye, J. (2017). Ignition features of methane and ethylene fuel-blends in hot and diluted coflows. *Fuel* 203, 279–289. doi: 10.1016/j.fuel.2017.04.113

Fotache, C. G., Kreutz, T. G., and Law, C. K. (1997). Ignition of counterflowing methane versus heated air under reduced and elevated pressures. *Combust. Flame* 108, 442–470. doi: 10.1016/S0010-2180(97)81404-6

Fotache, C. G., Sung, C. J., Sun, C. J., and Law, C. K. (1998). Mild oxidation regimes and multiple criticality in nonpremixed hydrogen-air counterflow. *Combust. Flame* 112, 457–471. doi: 10.1016/S0010-2180(97)00132-6

Goh, K. H. H., Geipel, P., Hampp, F., and Lindstedt, R. P. (2013). Regime transition from premixed to flameless oxidation in turbulent JP-10 flames. *Proc. Combust. Inst.* 34, 3311–3318. doi: 10.1016/j.proci.2012.06.173

He, Y., Zou, C., Song, Y., Liu, Y., and Zheng, C. (2016). Numerical study of characteristics on NO formation in methane MILD combustion with simultaneously hot and diluted oxidant and fuel (HDO/HDF). *Energy* 112, 1024–1035. doi: 10.1016/j.energy.2016.07.020

Hilbert, R., and Thévenin, D. (2002). Autoignition of turbulent non-premixed flames investigated using direct numerical simulations. *Combust. Flame* 128, 22–37. doi: 10.1016/S0010-2180(01)00330-3

Im, H. G., Chen, J. H., and Law, C. K. (1998). Ignition of hydrogen-air mixing layer in turbulent flows. *Symp. Combust.* 27, 1047–1056. doi: 10.1016/S0082-0784(98)80505-5

Im, H. G., Raja, L. L., Kee, R. J., and Petzold, L. R. (2000). A numerical study of transient ignition in a counterflow nonpremixed methane-air flame using adaptive time integration. *Combust. Sci. Tech.* 158, 341–363. doi: 10.1080/00102200008947340

Khalil, A. E. E., and Gupta, A. K. (2017). Towards colorless distributed combustion regime. *Fuel* 195, 113–122. doi: 10.1016/j.fuel.2016.12.093

Khidr, K. I., Eldrainy, Y. A., and Kassaby, E. L. (2017). Towards lower gas turbine emissions: flameless distributed combustion. *Renew. Sustain. Energy Rev.* 67, 1237–1266. doi: 10.1016/j.rser.2016.09.032

Kwiatkowski, K., and Mastorakos, E. (2016). Regimes of nonpremixed combustion of hot low-calorific-value gases derived from biomass gasification. *Energy Fuels* 30, 4386–4397. doi: 10.1021/acs.energyfuels.5b02580

Li, P. F., Mi, J. C., Dally, B. B., Wang, F. F., Wang, L., Liu, Z. H., et al. (2011). Progress and recent trend in MILD combustion. *Sci. China Technol. Sci.* 54, 255–269. doi: 10.1007/s11431-010-4257-0

Mameri, A., Tabet, F., and Hadef, A. (2018). MILD combustion of hydrogenated biogas under several operating conditions in an opposed jet configuration. *Int. J. Hydrogen Energy* 43, 3566–3576. doi: 10.1016/j.ijhydene.2017.04.273

Maruta, K., Abe, K., Hasegawa, S., Maruyama, S., and Sato, J. N. I. (2007). Extinction characteristics of CH 4 /CO 2 versus O 2 /CO 2 counterflow non-premixed flames at elevated pressures up to 0.7 MPa. *Proc. Combust. Inst.* 31, 1223–1230. doi: 10.1016/j.proci.2006.08.013

Maruta, K., Muso, K., Takeda, K., and Niioka, T. (2000). Reaction zone structure in flameless combustion. *Proc. Combust. Inst.* 28, 2117–2123. doi: 10.1016/S0082-0784(00)80621-9

Mastorakos, E. (2009). Ignition of turbulent non-premixed flames. *Prog. Energy Combust. Sci.* 35, 57–97. doi: 10.1016/j.pecs.2008.07.002

Mastorakos, E., Baritaud, T. A., and Poinsot, T. J. (1997). Numerical simulations of autoignition in turbulent mixing flows. *Combust. Flame* 109, 198–223. doi: 10.1016/S0010-2180(96)00149-6

Mastorakos, E., Taylor, A. M. K. P., and Whitelaw, J. H. (1995). Extinction of turbulent counterflow flames with reactants diluted by hot products. *Combust. Flame* 102, 101–114. doi: 10.1016/0010-2180(94)00252-N

Medwell, P. R., Evans, M. J., Chan, Q. N., and Katta, V. R. (2016). Laminar flame calculations for analyzing trends in autoignitive jet flames in a hot and vitiated coflow. *Energy Fuels* 30, 8680–8690. doi: 10.1021/acs.energyfuels.6b01264

Medwell, P. R., Kalt, P. A. M., and Dally, B. B. (2007). Simultaneous imaging of OH, formaldehyde, and temperature of turbulent nonpremixed jet flames in a heated and diluted coflow. *Combust. Flame* 148, 48–61. doi: 10.1016/j.combustflame.2006.10.002

Medwell, P. R., Kalt, P. A. M., and Dally, B. B. (2008). Imaging of diluted turbulent ethylene flames stabilized on a Jet in Hot Coflow (JHC) burner. *Combust. Flame* 152, 100–113. doi: 10.1016/j.combustflame.2007.09.003

Medwell, P. R., Kalt, P. A. M., and Dally, B. B. (2009). Reaction zone weakening effects under hot and diluted oxidant stream conditions. *Combust. Sci. Tech.* 181, 937–953. doi: 10.1080/00102200902904138

Minamoto, Y., and Swaminathan, N. (2015). Subgrid scale modelling for MILD combustion. *Proc. Combust. Inst.* 35, 3529–3536. doi: 10.1016/j.proci.2014.07.025

Minamoto, Y., Swaminathan, N., Cant, R. S., and Leung, T. (2014). Reaction zones and their structure in MILD combustion. *Combust. Sci. Tech.* 186, 1075–1096. doi: 10.1080/00102202.2014.902814

Oldenhof, E., Tummers, M. J., van Veen, E. H., and Roekaerts, D. J. E. M. (2010). Ignition kernel formation and lift-off behaviour of jet-in-hot-coflow flames. *Combust. Flame* 157, 1167–1178. doi: 10.1016/j.combustflame.2010.01.002

Oldenhof, E., Tummers, M. J., van Veen, E. H., and Roekaerts, D. J. E. M. (2011). Role of entrainment in the stabilisation of jet-in-hot-coflow flames. *Combust. Flame* 158, 1553–1563. doi: 10.1016/j.combustflame.2010.12.018

Özdemir, I. B., and Peters, N. (2001). Characteristics of the reaction zone in a combustor operating at mild combustion. *Exper. Fluids* 30, 683–695. doi: 10.1007/s003480000248

Perpignan, A. A. V., Gangoli Rao, A., and Roekaerts, D. J. E. M. (2018). Flameless combustion and its potential towards gas turbines. *Progr. Energy Combust. Sci.* 69, 28–62. doi: 10.1016/j.pecs.2018.06.002

Pitsch, H. (1998). *A C++ Computer Program for 0-D and 1-D Laminar Flame Calculations*. Aachen: RWTH.

Plessing, T., Peters, N., and Wünning, J. G. (1998). Laseroptical investigation of highly preheated combustion with strong exhaust gas recirculation. in *Symposium (International) on Combustion.* Vol. 27, No. 2, pp. 3197–3204, Elsevier. doi: 10.1016/S0082-0784(98)80183-5

Sabia, P., Sorrentino, G., Bozza, P., Ceriello, G., Ragucci, R., and de Joannon, M. (2019). Fuel and thermal load flexibility of a MILD burner. *Proc. Combust. Inst.* 37, 4547–4554. doi: 10.1016/j.proci.2018.09.003

Schulz, O., Jaravel, T., Poinsot, T., Cuenot, B., and Noiray, N. (2017). A criterion to distinguish autoignition and propagation applied to a lifted methane-air jet flame. *Proc. Combust. Inst.* 36, 1637–1644. doi: 10.1016/j.proci.2016.08.022

Sepman, A., Abtahizadeh, E., Mokhov, A., van Oijen, J., Levinsky, H., and de Goey, P. (2013). Experimental and numerical studies of the effects of hydrogen addition on the structure of a laminar methane-nitrogen jet in hot coflow under MILD conditions. *Int. J. Hydrogen Energy* 38, 13802–13811. doi: 10.1016/j.ijhydene.2013.08.015

Sepman, A. V., Mokhov, A. V., and Levinsky, H. B. (2013). Spatial structure and NO formation of a laminar methane-nitrogen jet in hot coflow under MILD conditions: a spontaneous Raman and LIF study. *Fuel* 103, 705–710. doi: 10.1016/j.fuel.2012.10.010

Sidey, J., and Mastorakos, E. (2015). Visualization of MILD combustion from jets in cross-flow. *Proc. Combust. Inst.* 35, 3537–3545. doi: 10.1016/j.proci.2014.07.028

Sidey, J., Mastorakos, E., and Gordon, R. L. (2014). Simulations of autoignition and laminar premixed flames in methane/air mixtures diluted with hot products. *Combust. Sci. Tech.* 186, 453–465. doi: 10.1080/00102202.2014.883217

Sidey, J. A. M., Giusti, A., and Mastorakos, E. (2016). Simulations of laminar non-premixed flames of kerosene with hot combustion products as oxidiser. *Combust. Theory Model.* 20, 958–973. doi: 10.1080/13647830.2016.1201146

Sidey, J. A. M., and Mastorakos, E. (2016). Simulations of laminar non-premixed flames of methane with hot combustion products as oxidiser. *Combust. Flame* 163, 1–11. doi: 10.1016/j.combustflame.2015.07.034

Sidey, J. A. M., and Mastorakos, E. (2018). Pre-chamber ignition mechanism: simulations of transient autoignition in a mixing layer between reactants and partially-burnt products. *Flow Turbulence Combust.* 101, 1093–1102. doi: 10.1007/s10494-018-9960-0

Smooke, M. D., Crump, J., Seshadri, K., and Giovangigli, V. (1991). Comparison between experimental measurements and numerical calculations of the structure of counterflow, diluted, methane-air, premixed flames. *Symp. Combust.* 23, 463–470. doi: 10.1016/S0082-0784(06)80292-4

Sorrentino, G., Ceriello, G., de Joannon, M., Sabia, P., Ragucci, R., van Oijen, J., et al. (2018b). Numerical investigation of moderate or intense low-oxygen dilution combustion in a cyclonic burner using a flamelet-generated manifold approach. *Energy Fuels* 32, 10242–10255. doi: 10.1021/acs.energyfuels.8b01099

Sorrentino, G., de Joannon, M., Sabia, P., Ragucci, R., and Cavaliere, A. (2017). Numerical investigation of the ignition and annihilation of CH4/N2/O2 mixtures under MILD operative conditions with detailed chemistry. *Combust. Theory Model.* 21, 120–136. doi: 10.1080/13647830.2016.1220624

Sorrentino, G., Sabia, P., de Joannon, M., Bozza, P., and Ragucci, R. (2018a). Influence of preheating and thermal power on cyclonic burner characteristics under mild combustion. *Fuel* 233, 207–214. doi: 10.1016/j.fuel.2018.06.049

Sorrentino, G., Scarpa, D., and Cavaliere, A. (2013). Transient inception of MILD combustion in hot diluted diffusion ignition (HDDI) regime: a numerical study. *Proc. Combust. Inst.* 34, 3239–3247. doi: 10.1016/j.proci.2012.08.002

Sreedhara, S., and Lakshmisha, K. N. (2000). Direct numerical simulation of autoignition in a non-premixed, turbulent medium. *Proc. Combust. Inst.* 28, 25–33. doi: 10.1016/S0082-0784(00)80191-5

Tsuji, H. (1982). Counterflow diffusion flames. *Prog. Energy Combust. Sci.* 8, 93–119. doi: 10.1016/0360-1285(82)90015-6

van Oijen, J. A. (2013). Direct numerical simulation of autoigniting mixing layers in MILD combustion. *Proc. Combust. Inst.* 34, 1163–1171. doi: 10.1016/j.proci.2012.05.070

Viggiano, A., and Magi, V. (2004). A 2-D investigation of n-heptane autoignition by means of direct numerical simulation. *Combust. Flame* 137, 432–443. doi: 10.1016/j.combustflame.2004.03.003

Wagner, J. A., Grib, S. W., Dayton, J. W., Renfro, M. W., and Cetegen, B. M. (2017). Flame stabilization analysis of a premixed reacting jet in vitiated crossflow. *Proc. Combust. Inst.* 36, 3763–3771. doi: 10.1016/j.proci.2016.07.020

Wünning, J. A., and Wünning, J. G. (1997). Flameless oxidation to reduce thermal no-formation. *Prog. Energy Combust. Sci.* 23, 81–94. doi: 10.1016/S0360-1285(97)00006-3

Ye, J., Medwell, P. R., Dally, B. B., and Evans, M. J. (2016). The transition of ethanol flames from conventional to MILD combustion. *Combust. Flame* 171, 173–184. doi: 10.1016/j.combustflame.2016.05.020

Ye, J., Medwell, P. R., Evans, M. J., and Dally, B. B. (2017). Characteristics of turbulent n-heptane jet flames in a hot and diluted coflow. *Combust. Flame* 183, 330–342. doi: 10.1016/j.combustflame.2017.05.027

Ye, J., Medwell, P. R., Kleinheinz, K., Evans, M. J., Dally, B. B., and Pitsch, H. G. (2018). Structural differences of ethanol and DME jet flames in a hot diluted coflow. *Combust. Flame* 192, 473–494. doi: 10.1016/j.combustflame.2018.02.025

Yoo, C. S., Richardson, E. S., Sankaran, R., and Chen, J. H. (2011). A DNS study on the stabilization mechanism of a turbulent lifted ethylene jet flame in highly-heated coflow. *Proc. Combust. Inst.* 33, 1619–1627. doi: 10.1016/j.proci.2010.06.147

Zheng, X. L., Blouch, J. D., Zhu, D. L., Kreutz, T. G., and Law, C. K. (2002). Ignition of premixed hydrogen/air by heated counterflow. *Proc. Combust. Inst.* 29, 1637–1643. doi: 10.1016/S1540-7489(02)80201-2

Zhou, B., Costa, M., Li, Z., Aldén, M., and Bai, X. S. (2017). Characterization of the reaction zone structures in a laboratory combustor using optical diagnostics: from flame to flameless combustion. *Proc. Combust. Inst.* 36, 4305–4312. doi: 10.1016/j.proci.2016.06.182

Zou, C., Cao, S., Song, Y., He, Y., Guo, F., and Zheng, C. (2014). Characteristics and mechanistic analysis of CO formation in MILD regime with simultaneously diluted and preheated oxidant and fuel. *Fuel* 130, 10–18. doi: 10.1016/j.fuel.2014.04.004

**Conflict of Interest:** The authors declare that the research was conducted in the absence of any commercial or financial relationships that could be construed as a potential conflict of interest.

frontiers in Mechanical Engineering

ORIGINAL RESEARCH
published: 04 June 2020
doi: 10.3389/fmech.2020.00020

# Evaluation of Modeling Approaches for MILD Combustion Systems With Internal Recirculation

*Ruggero Amaduzzi*[1,2]*, *Giuseppe Ceriello*[3], *Marco Ferrarotti*[1,2], *Giancarlo Sorrentino*[3] and *Alessandro Parente*[1,2]

[1] Aero-Thermo-Mechanics Department, Université Libre de Bruxelles, Brussels, Belgium, [2] Combustion and Robust Optimization Group (BURN), Université Libre de Bruxelles and Vrije Universiteit Brussel, Brussels, Belgium, [3] Dipartimento di Ingegneria Chimica, dei Materiali e della Produzione Industriale, Università degli Studi di Napoli "Federico II," Naples, Italy

Numerical simulations employing two different modeling approaches are performed and validated against experimental results from a moderate or intense low-oxygen dilution (MILD) system with internal recirculation. The flamelet-generated manifold (FGM) and partially stirred reactor (PaSR) closures are employed in a Reynolds-averaged Navier–Stokes (RANS) framework to carry out the numerical simulations. The results show that the FGM model strongly overpredicts temperature profiles in the reactive region, while yielding better results along the central thermocouple. The PaSR closures based on a prescribed mixing time constant, $C_{mix}$, of 0.01, 0.1, and 0.5 are compared, showing that a $C_{mix}$ value of 0.5 is the most appropriate choice for the cases under investigation. A PaSR formulation allowing local estimation of the $C_{mix}$ value is found to provide improved results for both the lateral and central thermocouples. A flame index analysis, used to assess the ability of FGM and PaSR to capture intense mixing of the cyclonic burner, indicates how the FGM model predicts a typical non-premixed region after the injection zone, contrary to the experimental observation.

**Keywords: MILD combustion, cyclonic burner, tabulated chemistry, PaSR, detailed chemistry**

OPEN ACCESS

***Edited by:***
*David B. Go,*
*University of Notre Dame,*
*United States*

***Reviewed by:***
*Khanh Duc Cung,*
*Southwest Research Institute (SwRI),*
*United States*
*Georgios Mavropoulos,*
*National Technical University of Athens, Greece*
*Feifei Wang,*
*Huazhong University of Science and Technology, China*

***Correspondence:**
*Ruggero Amaduzzi*
*ruggero.amaduzzi@ulb.ac.be*

***Specialty section:***
*This article was submitted to Thermal and Mass Transport, a section of the journal Frontiers in Mechanical Engineering*

***Received:*** *29 November 2019*
***Accepted:*** *08 April 2020*
***Published:*** *04 June 2020*

***Citation:***
*Amaduzzi R, Ceriello G, Ferrarotti M, Sorrentino G and Parente A (2020) Evaluation of Modeling Approaches for MILD Combustion Systems With Internal Recirculation. Front. Mech. Eng. 6:20. doi: 10.3389/fmech.2020.00020*

## INTRODUCTION

The simultaneous requirements of thermal efficiency, fuel flexibility, and low pollutant emission are the main drivers for the development of innovative combustion-based systems. Several concepts were developed in the last decades, to achieve lower temperatures of the oxidation region and avoid the formation of several classes of pollutants. In particular, a number of combustion concepts based on the internal or external dilution and/or preheating of main reactants were proposed. They include flameless oxidation (Wünning and Wünning, 1997), colorless combustion (Khalil and Gupta, 2017), high-temperature air combustion (HiTAC) (Rafidi and Blasiak, 2006), and moderate or intense low-oxygen dilution (MILD). Examples of implementation of these technologies include furnaces, boilers, and gas turbines.

MILD combustion plays today a crucial role in the development of flexible, efficient, and nonpolluting technologies. Notably, its feeding conditions allow the establishment of a distributed reaction zone, with almost uniform temperatures in the combustion chamber, absence of a visible flame, very low levels of noise and fluctuations, absence of soot particles, and negligible $NO_x$ and CO emissions (Cavaliere and de Joannon, 2004). In the last decades, strong attention was given to the turbulent combustion modeling of such processes. In fact, the unique thermochemical features related to the turbulence–chemistry interaction have led to the development of new

modeling paradigms or to the adaptation of the ones already used for conventional conditions (De and Dongre, 2015). In such systems, the flue gases' recirculation decreases the oxygen level of the reactant mixture, thus slowing down the kinetic rates in such a way that the characteristic chemical timescales approach the mixing timescales; that is, the Damköhler number is close to unity (Özdemir and Peters, 2001). Due to such modifications of the reaction zone, appropriate turbulence/chemistry interaction models need to be developed (Frassoldati et al., 2010). In particular, detailed kinetic mechanisms should be considered to correctly capture the thermochemical variable distributions (temperature and main species fields) and pollutant emissions in particular.

The complexity of MILD reaction structures has pushed the development of a number of approaches for Reynolds-averaged Navier–Stokes (RANS) (Galletti et al., 2007) and large-eddy simulations (LES) (Duwig et al., 2007), which can be divided into flamelet-like and finite-rate approaches, depending on the assumptions made with respect to the accessible reaction state space (Pope, 2013).

Flamelet-based models allow us to include detailed chemistry effects at an affordable computational cost, as the chemical state space is calculated in a preprocessing step, and it is then accessed during the actual simulation via a number of scalars (typically the mixture fraction and a progress variable) that parameterize the chemical state space (Pierce and Moin, 2001, 2004). In this context, tabulated chemistry techniques such as the flamelet-generated manifold (FGM) (Van Oijen and De Goey, 2000) and flamelet progress variable (FPV) (Pierce and Moin, 2001, 2004) techniques have acquired a key role in the combustion community, and their effectiveness has been demonstrated for a number of problems and configurations. Recently, Abtahizadeh et al. (2015) showed that the canonical structure used for tabulation strongly influences the representation of MILD combustion in jet in hot coflow (JHC) configurations. Such results were confirmed by Sorrentino et al. (2018a), for a cyclonic flow burner. A relevant challenge in FGM/FPV approaches is to include the effects of exhaust gas recirculation in the lookup tables, to properly represent the dilution and heat loss effects (Lamouroux et al., 2014). The inclusion of additional variables in the tabulation procedure is a very demanding task and can lead to expensive computational fluid dynamics (CFD) simulations due to the increased manifold dimensionality (from 3D or 4D to 6D).

Reaction rate-based approaches have been also proposed in the literature and applied to MILD conditions. Among them, it is worth mentioning the eddy dissipation concept (EDC) (Magnussen, 2005) and the partially stirred reactor (PaSR) model, originally proposed by Chomiak (1990). Both models divide each grid cell into two regions: the reacting structures, modeled as ideal reactors, and the surrounding fluid mixture. The main difference between the two approaches lies in the estimation of the reacting structures' volume fraction. In EDC, the latter is solely based on the turbulence properties of the flow, obtained by means of an energy cascade model (Magnussen, 2005). In PaSR, the reacting fraction explicitly depends on both the mixing and chemical timescales. Recently, the PaSR model was used to simulate the Adelaide JHC, using both RANS (Ferrarotti et al., 2019) and LES (Ihme and See, 2011), with very satisfactory results. Despite the encouraging progress in the use of reactor-based models for MILD combustion, there are still open questions related to the general applicability of the concept to different configurations. To this end, the availability of experimental data in MILD conditions is key.

Both the Adelaide and Delft JHC configurations (Dally et al., 2002; Oldenhof et al., 2011) mimic MILD conditions by feeding diluted and hot streams to the coflow, impacting directly the system characteristic chemical timescale. This simplified configuration makes it possible to perform optical diagnostics and deliver high-fidelity experimental data that are crucial for model development. However, in industrial MILD configurations, the distributed conditions are a consequence of the internal aerodynamic recirculation and the modification of the local mixing timescales. Closed furnaces operating in MILD conditions allow, in principle, challenging of the ability of turbulent combustion models to appropriately capture turbulence/chemistry interactions. For instance, Ferrarotti et al. (2018) applied the PaSR model for a quasi-industrial burner fed with natural gas, showing the relevance of both mixing and chemical timescales as well as of the comprehensiveness of the chemical mechanism.

The availability of experimental data in furnace configurations is generally limited due to the presence of an enclosure. In addition, available data in MILD conditions are limited to narrow operative conditions. Based on such considerations, the present study reports the investigation of a novel cyclonic burner (Sorrentino et al., 2018b). A methane-fired small-scale burner was employed, and detailed internal temperature measurements were used to characterize the local thermal field. Experimental temperature measurements were used to validate two different modeling paradigms, a tabulated chemistry approach, FGM, and a reactor-based model, PaSR. The comparison was carried out for two experimental configurations, involving standard air and diluted air as the oxidizer stream. The main aim of the paper is to identify current potential and limitations of turbulent combustion closures for the investigation of more complex MILD combustion configurations.

## EXPERIMENTAL TEST CASE

The geometrical features and characteristics of the cyclonic burner used in this article to mimic MILD combustion conditions have been reported in previous works (de Joannon et al., 2017; Ferrarotti et al., 2019; Sabia et al., 2019; Sorrentino et al., 2019). In the following, the key features of the device are discussed.

It consists of a lab-scale combustor ($20 * 20$ cm$^2$ of square section and a height of 5 cm) where a cyclonic and toroidal flow field is established through two couples of coaxial oxidant/fuel inlet jets located in an antisymmetric configuration. In **Figure 1**, a sketch of the burner midplane, the feeding configuration, and the position of the thermocouples are shown. Oxidizer and fuel injection pipes are placed 2 and 4.5 cm from the lateral walls, respectively. The flue gas exit is placed at the top-central side.

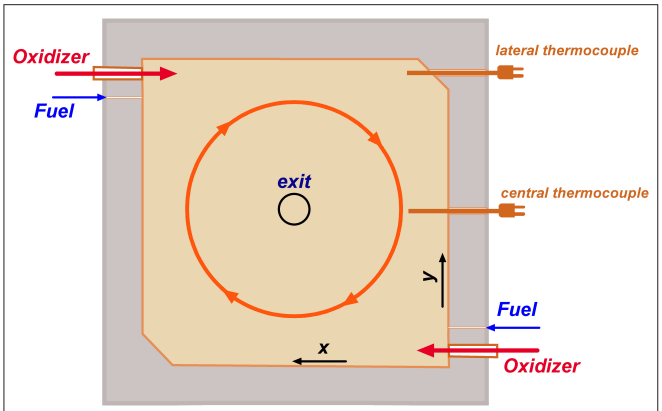


**FIGURE 1 |** Sketch of the midplane of the combustion chamber.

In the present manuscript, methane was used as a fuel and air as oxidizer.

MILD conditions are ensured thanks to the strong internal recirculation of burned products that stabilizes locally a distributed ignition. Such a microscopic feature of MILD combustion corresponds macroscopically to reduced temperature gradients (high levels of temperature uniformity) with very low pollutant emissions.

Two shielded N-type thermocouples can be moved along the $y$-direction. The lateral one is placed 0.02 m from the wall, whereas the central thermocouple is located 0.01 m from the confinement.

External ceramic preheating ovens were used to fix the boundary conditions in terms of external temperature, thus controlling the heat flux through the surroundings. The burner was built with a three-layer structure of alumina, a thick layer of heat-insulating material, and an outer shell of stainless steel 310s. The oxidant flow passes through heaters, to keep fixed the inlet temperature to the desired values ($T_{\text{in}}$).

In the present work, the two experimental configurations illustrated in **Table 1** were investigated. In the first case, the fuel (pure methane) was injected at the environmental temperature (300 K) with a jet velocity of 15.8 m/s, while the oxidizer (preheated air) was fed at a fixed preheating level of 1,000 K ($T_{\text{in}}$) and with a jet velocity of 17.8 m/s. The inlet equivalence ratio was kept constant at the stoichiometric value. Moreover, a mean overall heat loss flux at walls ($Q_{\text{W}}$) was estimated by means of thermocouples placed on outer and inner surfaces of the walls to be equal to 13 kW/m$^2$, for the investigated conditions. In the second case, the air stream was diluted with 90% $N_2$ by volume. The equivalence ratio was kept to stoichiometric value, and the inlet temperatures were as in case 1; the fuel jet velocity was 15.8 m/s, while the oxidizer jet was 54.17 m/s.

**TABLE 1 |** List of the conditions investigated in this study.

| Case | Fuel | Oxidizer | $V_{\text{ox}}$ (m/s) | $V_{\text{F}}$ (m/s) | $T_{\text{Ox}}$ (K) | $T_{\text{F}}$ (K) |
|---|---|---|---|---|---|---|
| 1 | $CH_4$ | $O_2$ 21%, $N_2$ 79% | 17.8 | 15.8 | 1,000 | 300 |
| 2 | $CH_4$ | $O_2$ 6.9%, $N_2$ 93.1% | 54.17 | 15.8 | 1,000 | 300 |

## MODELING TOOLS

Numerical simulations were carried out using RANS, with the commercial code Ansys Fluent 19.3. The grid was generated with the software Ansys Workbench. A grid independence study was performed using a polyhedral grid with a number of cells ranging from 100 to 400 k. The selected grid consisted of 450 k polyhedral elements. Reynolds stresses were solved using the RNG $k$–$\varepsilon$ turbulence model with swirl-dominated flow corrections to take into account the high swirl level in the combustor. The discrete ordinate (DO) radiation model was used, while the radiation properties of the reacting mixture are accounted for with the weighted-sum-of-gray-gases (WSGG) model, using the coefficients proposed by Smith et al. (1982).

For the turbulence–chemistry interaction, PaSR and FGM models were adopted. As with other reactor-based models, the computational cell in PaSR is split into two zones, the reaction structures and the surrounding fluid. The overall reaction progress is determined by the exchange between the two regions. The mass fraction of the reaction zone is estimated, considering both the characteristic chemical and mixing timescales:

$$\kappa = \frac{\tau_c}{\tau_c + \tau_{mix}} \tag{1}$$

$$\overline{\dot{\omega}} = \kappa \frac{\rho\left(Y_i^* - Y^0\right)}{\tau^*} \tag{2}$$

A first set of simulations was performed to determine the influence of the kinetic mechanism on the results. The detailed mechanisms GRI2.11 (Bilger et al., 1990; Bowman et al., 1996) and GRI3.0 (Smith et al., 2011), along with the reduced mechanism KEE (Bilger et al., 1990), were used. Then, a sensitivity to the PaSR model parameters was carried out, with special emphasis on the determination of the mixing scale. First, $\tau_{mix}$ was estimated as in Ferrarotti et al. (2018), considering a fraction of the integral timescale $\kappa/\epsilon$ by means of a constant $C_{mix}$:

$$\tau_{mix,s} = C_{mix}\frac{\kappa}{\epsilon} \tag{3}$$

Values of $C_{mix}$ ranging 0.01, 0.1, and 0.5 were considered. Then, a dynamic approach was used, as proposed in Ferrarotti et al. (2019), based on local properties of the flow field. $\tau_{mix,d}$ is estimated with the ratio of the mixture fraction variance, $Z''^2$, to the mixture fraction dissipation rate, $\chi$:

$$\tau_{mix,\ d} = \frac{\widetilde{Z''^2}}{\tilde{\chi}} \tag{4}$$

The determination of $\tau_{mix,d}$ requires the solution of transport equations for $\widetilde{Z''^2}$ and $\tilde{\chi}$, expressed as

$$\frac{D\rho\widetilde{Z''^2}}{Dt} = \frac{\partial}{\partial x_j}\left(\rho\left(D_m + D_t\right)\frac{\partial\widetilde{Z''^2}}{\partial x_j}\right) + 2\rho D_t\left(\frac{\partial\tilde{Z}}{\partial x_j}\right)^2 - \rho\tilde{\chi} \tag{5}$$

$$\frac{D\rho\tilde{\chi}}{Dt} = \frac{\partial}{\partial x_j}\left(\rho\left(D_m + D_t\right)\frac{\partial\tilde{\chi}}{\partial x_j}\right) - C_{D_1}\bar{\rho}\frac{\widetilde{\chi^2}}{\widetilde{Z''^2}} - C_{D_2}\bar{\rho}\frac{\tilde{\chi}\tilde{\epsilon}}{\tilde{\kappa}} + C_{P_1}\frac{\tilde{\chi}}{\widetilde{Z''^2}}P_f + C_{P_2}\frac{\tilde{\chi}}{\tilde{\kappa}}P_\kappa \tag{6}$$

where $Z$ is the mixture fraction, $D_t$ is the turbulent diffusivity, $P_f = -2\widetilde{\bar{\rho}u_k''Z''}(\frac{\partial\tilde{Z}}{\partial x_k})$ is the production of scalar fluctuation, and $P_k = -\widetilde{\bar{\rho}u_k''u_i''}(\frac{\partial\tilde{U}_i}{\partial x_k})$ is the production of turbulent kinetic energy. The set of coefficients $C_{P_1}$, $C_{P_2}$, $C_{D_1}$, $C_{D_2}$ used is the one proposed in Keehan Ye (2011). The resulting system is solved using an unsteady RANS (URANS) approach.

The PaSR model was benchmarked to the FGM model (Van Oijen and De Goey, 2000). In FGM, 1D flame configurations were employed by means of igniting mixing layer (IML) (Abtahizadeh et al., 2015) and premixed flamelet equations (Van Oijen et al., 2016). The thermochemical quantities were tabulated as functions of the mixture fraction and progress variable. At the CFD runtime, only the transport equations for the mean values and the variances of the controlling variables (in addition to continuity, momentum, and energy) were solved, and all the required parameters were retrieved. Specifically, the main assumptions behind the FGM method are that a turbulent flame can be represented by an ensemble of laminar flames, and the $n$-dimensional composition space can be replaced by a lower-dimensional manifold (Chen et al., 2018; Sorrentino et al., 2018a). The flamelet equations were computed through the specialized solver Chem1D, developed at the University of Technology of Eindhoven (TU/e) (Somers, 1994). A unity Lewis number assumption was chosen, whereas the GRI3.0 chemical mechanism was used.

Two controlling variables were chosen, a progress variable $Y$ and a mixture fraction $Z$, to represent the mixing between fuel and oxidizer. Usually, under traditional combustion conditions, the standard FGM model adopts combustion products, such as $CO_2$ and $H_2O$, to define the progress variable. Nevertheless, in this work, $HO_2$ was also included. Indeed, Medwell et al. (2008) stressed the role of precursor species like $HO_2$ in MILD combustion. Therefore, a combination of $H_2O$, $CO_2$, and $HO_2$ was selected as progress variable to include the effects of both preignition and oxidation chemistry. The general form of the progress variable is

$$Y = \sum_{i=1}^{N_{sp}} \alpha_i X_i \tag{7}$$

where $X_i$ is the molar fractions and $\alpha_i$ the weight factors of the generic species $i$, which were optimized to yield a smooth mapping between the state space and the transported variables. In this work, the coefficients $\alpha$ were chosen as $\alpha_{H_2O} = 100/W_{H_2O}$, $\alpha_{CO_2} = 100/W_{CO_2}$, $\alpha_{HO_2} = 1{,}000/W_{HO_2}$, where $W_i$ denotes the molar mass of species $i$. $\alpha_i = 0$ for all other species. Moreover, the progress variable was scaled between 0 and 1, to make it independent of the mixture fraction. The controlling variables and the lookup tables were defined by means of Matlab R2019a (The Mathworks Inc., 2019) scripts. Thus, all the thermochemical parameters calculated from flamelet equations were tabulated as a function of $Y$ and $Z$.

Once defined, the laminar and adiabatic 2D tables were imported on Fluent using the FGM dedicated routine. The effect of the turbulence was considered incrementing the manifold dimension from 2 to 4, using a presumed $\beta$ – PDF approach (Fiorina et al., 2005). In this way, both the mean values (100 table points) and the variances (11 table points) of $Y$ and $Z$ are considered as controlling variables.

During a simulation, the turbulent transport equations for the mean and variance of the mixture fraction ($\tilde{Z}$ and $\widetilde{Z_\upsilon}$, respectively) and for the mean and variance of the progress variable ($\tilde{Y}$ and $\widetilde{Y_\upsilon}$, respectively) are solved in addition to the Favre-averaged mass, momentum, and enthalpy conservation equations. The four steady-state transport equations read as follows:

$$\frac{\partial\bar{\rho}\tilde{u}_j\tilde{Z}}{\partial x_j} = \frac{\partial}{\partial x_j}\left[\left(\bar{\rho}D + \frac{\mu_t}{Sc_t}\right)\frac{\partial\tilde{Z}}{\partial x_j}\right] \tag{8}$$

$$\frac{\partial\bar{\rho}\tilde{u}_j\tilde{Y}}{\partial x_j} = \frac{\partial}{\partial x_j}\left[\left(\bar{\rho}D + \frac{\mu_t}{Sc_t}\right)\frac{\partial\tilde{Y}}{\partial x_j}\right] + \overline{\omega_Y} \tag{9}$$

$$\frac{\partial\bar{\rho}\tilde{u}_j\widetilde{Z_\upsilon}}{\partial x_j} = \frac{\partial}{\partial x_j}\left[\left(\bar{\rho}D + \frac{\mu_t}{Sc_t}\right)\frac{\partial\widetilde{Z_\upsilon}}{\partial x_j}\right] + C_1\frac{\mu_t}{Sc_t}\frac{\partial\tilde{Z}}{\partial x_i}\frac{\partial\tilde{Z}}{\partial x_i} - C_2\bar{\rho}\frac{\tilde{\varepsilon}}{\tilde{k}}\widetilde{Z_\upsilon} \tag{10}$$

$$\frac{\partial\bar{\rho}\tilde{u}_j\widetilde{Y_\upsilon}}{\partial x_j} = \frac{\partial}{\partial x_j}\left[\left(\bar{\rho}D + \frac{\mu_t}{Sc_t}\right)\frac{\partial\widetilde{Y_\upsilon}}{\partial x_j}\right] + 2\frac{\mu_t}{Sc_t}\frac{\partial\tilde{Y}}{\partial x_i}\frac{\partial\tilde{Y}}{\partial x_i} - C_2\bar{\rho}\frac{\tilde{\varepsilon}}{\tilde{k}}\widetilde{Y_\upsilon} + \overline{2Y''\omega_Y} \tag{11}$$

In the equations above, $\bar{\rho}$ is the mean density, $\tilde{u}_j$ is the mean velocity vector, $D$ is the molecular diffusion coefficient, $\mu_t$ is the turbulent viscosity, $Sc_t$ is the turbulent Schmidt number, $\overline{\omega_Y}$ is the mean chemical source term of the progress variable, $C_1$ and $C_2$ are the modeling constants, $\tilde{k}$ is the mean turbulent kinetic energy, and $\tilde{\varepsilon}$ is the mean dissipation rate.

Since the lookup tables were created from adiabatic flamelets, heat losses were not included in the manifold and, therefore, only considered in the CFD simulations. The accuracy of this approach is then related to the accuracy associated with the inclusion of the enthalpy in Fluent once the adiabatic tables are imported. In particular, the software includes enthalpy by freezing the species in the adiabatic flamelets and recalculating the temperatures and the progress variable source terms with the enthalpy.

## RESULTS AND DISCUSSION

Case 1 (described in **Table 1**) is first considered. **Figure 2** shows the temperature profiles along the lateral thermocouple

obtained with the PaSR model in combination with three chemical mechanisms, the GRI3.0, GRI2.11, and KEE, using a $C_{mix}$ of 0.1. It can be observed that the temperature profiles are almost superimposed, with differences never exceeding 4%. Based on this observation, it was decided to keep the KEE mechanism for the subsequent simulations, to reduce the associated computational time.

In **Figures 3A,B**, the numerical predictions were compared to the experiments in terms of temperature profiles along the central and lateral thermocouples. It can be observed how the FGM method shows a good agreement with the experiments for the central thermocouple (**Figure 3A**). In particular, the temperature profile predicted by FGM is quite homogeneous, and it well captures the temperature peaks in the near-wall regions, only slightly overestimating it by about 50 K. However, when looking at the lateral position, FGM strongly overpredicts the experimental trend of about 200°, with a very localized peak close to the inlet zone ($x < 0.06$ m). Such a strong difference between the central and lateral positions suggests that the model predicts a very early ignition after injection, contrary to the experimental observations suggesting distributed reaction conditions. The fact that the reaction and heat release region predicted by FGM are very localized also explains why FGM well captures the central thermal field, the progress variable being unitary in this area and heat transfer dominating the flow features. The inability of FGM to capture the initiation and extension of the reaction region can be related to the absence of a controlling variable, taking into account the internal dilution by the combustion products, in the construction of the lookup table.

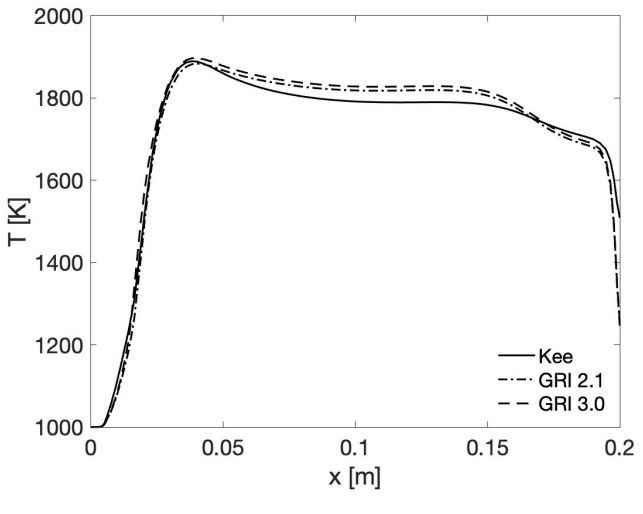


**FIGURE 2 |** Case 1 PaSR results along the lateral thermocouple. Comparison of KEE, GRI2.11, and GRI3.0 mechanisms for $C_{mix} = 0.1$.

**Figures 3A,B** also show the PaSR predictions for different values of the $C_{mix}$ constant. As a remainder, increasing $C_{mix}$ increases the mixing timescale value. The temperature profiles obtained with $C_{mix}$ values of 0.01, 0.1, and 0.5 clearly show the strong sensitivity of the model to the estimation of the mixing scale. In particular, decreasing $C_{mix}$ impacts the mean reaction rate in two ways, via the reacting structure fraction $\kappa$ and the residence time in the reacting structures (taken equal to the mixing time). When $C_{mix}$ is reduced, representative of a condition of intense mixing, the reacting fraction $\kappa$ (Equation 1) is increased, indicating that the whole computational cells evolve toward a perfectly stirred reactor. At the same time, the denominator in Equation (2) decreases, thus impacting directly the mean reaction rate, which is increased. A close observation of **Figures 3A,B** suggests that a $C_{mix}$ value of 0.5 is the most appropriate choice for the case under investigation, in agreement with previous results (Ferrarotti et al., 2018, 2019). Nevertheless, when looking at the centerline thermocouple (**Figure 3A**), all PaSR simulations underpredict the temperature near the outlet zone ($0.06 < x < 0.14$ m), while overestimating the temperature

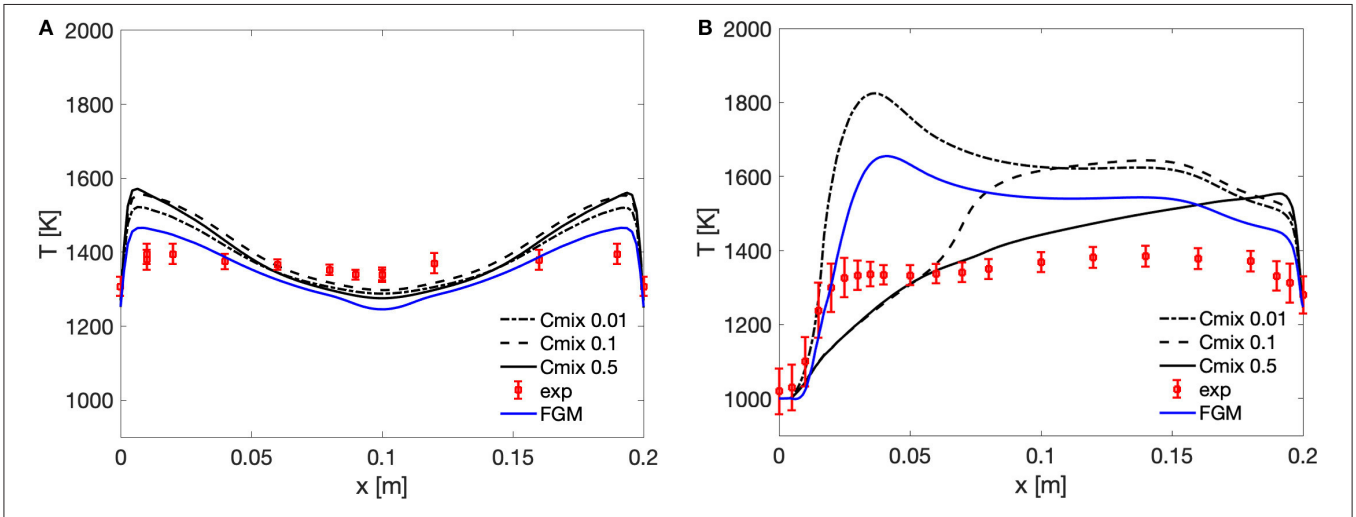


**FIGURE 3 |** Case 1 comparison between FGM and PaSR with $C_{mix}$ of 0.01, 0.1, and 0.5 and experimental values along the central and lateral thermocouples. **(A)** Central thermocouple profiles. **(B)** Lateral thermocouple profiles.

level on the sides. The shapes of the PaSR temperature profile clearly indicate that the model can capture the existence of a distributed reaction region, but not to the extent suggested by the experimental measurements, showing a very uniform profile. This is further confirmed by the analysis of **Figure 3B**, which shows how the PaSR results show a delayed ignition with respect to the experimental data, as the temperature peak reduces and moves downstream of the fuel injection. Increasing $C_{mix}$ helps to reduce the temperature overpredictions along the thermocouples, although the central thermocouple profile is still not quite well represented, as the maximum temperature is about 150 K higher than the experimental values. Opposed to experimental data, the PaSR simulation still retains two defined reaction zones, which are the cause of the temperature spikes along the central thermocouple profile (**Figure 3A**).

Interestingly, as $C_{mix}$ is decreased, FGM and PaSR become more similar. This is explained by the direct impact that the mixing timescale has on the mean reaction rate (Equation 2). As discussed above, a reduction in $\tau_{mix}$ directly impacts $\bar{\dot{\omega}}$ and increases it. This is further confirmed by the analysis of the Damköhler number maps presented in **Figure 4**, showing how the Damköhler in the domain decreases by one order of magnitude as $C_{mix}$ is decreased from 0.5 to 0.01. As $D\alpha$ decreases, the reactive zone mass fraction $\kappa$ (Equation 1) increases, thus increasing the mean reaction rate as well. The combined effects of reducing $\tau^*$ and increasing $\kappa$ in **Equation 2** results in the above-mentioned temperature spikes in the $C_{mix} = 0.01$ case.

One tool that can be helpful to understand the differences between the two models results is the so-called normalized flame index, introduced by Yamashita et al. (1996) and defined by Bray et al. (2005), Domingo et al. (2002), and Knudsen and Pitsch (2009, 2012) as

$$\xi = \frac{\nabla Y_F \cdot \nabla Y_O}{|\nabla Y_F \cdot \nabla Y_O|} \tag{12}$$

By definition, the index takes the value of $\xi = +1$ in premixed flames and $\xi = -1$ in non-premixed ones. It can be then useful to assess the ability of the model to capture the premixed nature

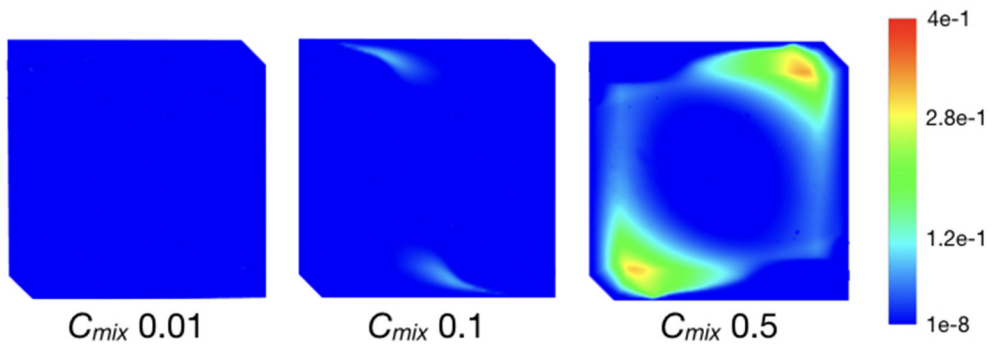


**FIGURE 4 |** Case 1 Damköhler contours for PaSR static simulations with $C_{mix}$ of 0.01, 0.1, and 0.5.

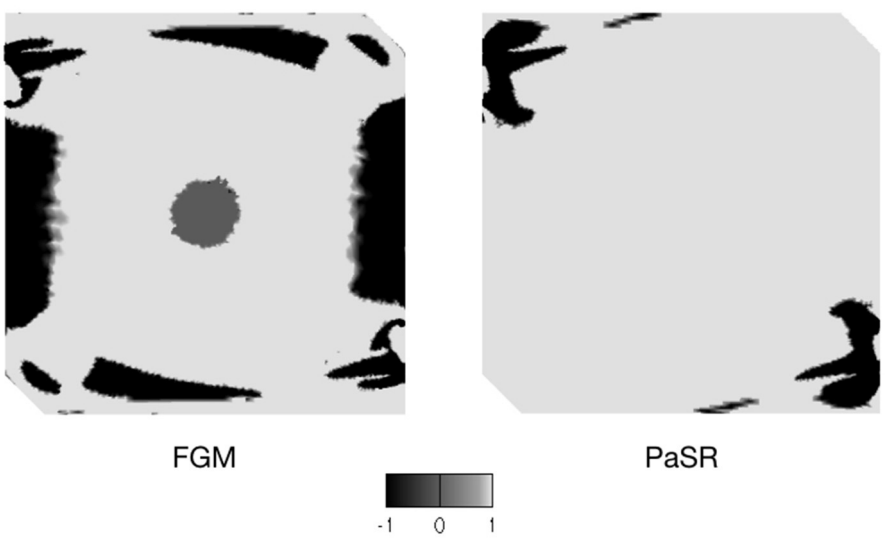


**FIGURE 5 |** Case 1 flame index contours for FGM and PaSR static simulations.

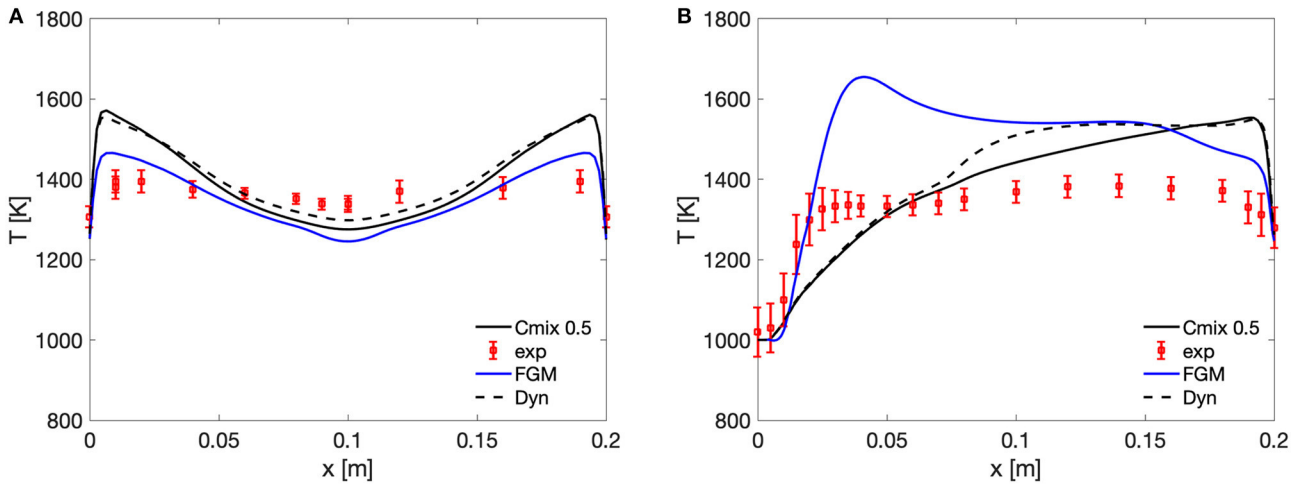


**FIGURE 6 |** Case 1 static and dynamic PaSR results compared to experimental values along the central and lateral thermocouples. **(A)** Central thermocouple profiles. **(B)** Lateral thermocouple profiles.

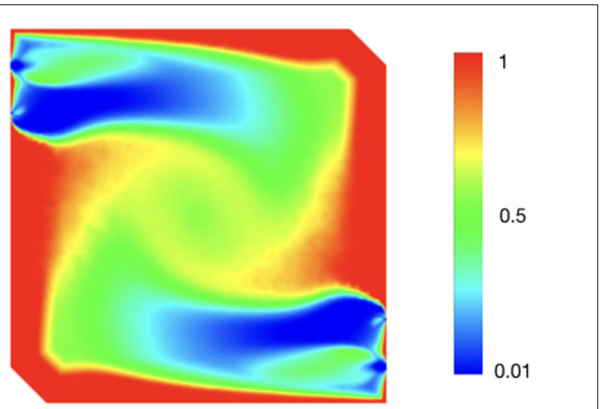


**FIGURE 7 |** Case 1 $C_{mix_{eq}}$ contour for the PaSR dynamic model.

of the combustion process under MILD conditions. **Figure 5** shows the contours of the flame index obtained using both the PaSR model, using $C_{mix} = 0.5$, and FGM. It can be observed that the two models yield quite different results. With the PaSR case, the non-premixed region is almost exclusively restricted to the injection zone, between $x = 0$ m and $x = 0.05$ m; in the rest of the chamber mixing, it occurs effectively before reaction, and the flame index is $+1$, indicating a premixed region. The same cannot be said about FGM: beside the injection zone, the flame index contour presents four additional regions close to the chamber walls, where the flame index value is $-1$, thus indicating a non-premixed flame structure. This can be ascribed to the very assumptions of the FGM formulation used in the present work and specifically to the lack of a dilution parameter to describe the mixing between fresh reactants and combustion products before reaction, thus resulting in the temperature overprediction shown in **Figure 3B**.

The PaSR results presented above clearly show that the model can potentially capture the distributed features of MILD combustion. At the same time, the estimation of the mixing timescale has a key role in the structure of the reaction zone and the temperature levels. In particular, it is clear that the use of a simple approach for $\tau_{mix}$, based on a fraction of the integral mixing scale, is not appropriate to describe the complexity of turbulence–chemistry interactions in the system under investigation. Therefore, the dynamic model (Equations 5, 6) was used for the same configuration, to assess whether the scalar time of a (non)reactive scalar could represent an appropriate choice. It should be stressed here that a large uncertainty is associated to the determination of this scalar dissipation rate via Equation 6 (Knudsen and Pitsch, 2009): the coefficients used in such an equation are the result of a calibration on simple-flow configurations (Ferrarotti et al., 2019) and might be inadequate for the complex flow under investigation. The results of the dynamic model using the coefficient by Keehan Ye (2011) show results very close to the $C_{mix} = 0.5$ case. As shown in **Figures 6A,B**, the temperature profiles along the lateral thermocouple are almost identical, with the exception of the zone between $x = 0.07$ m and $x = 0.15$ m, where the dynamic model yields slightly higher temperatures and a flatter profile. The dynamic model yields slightly lower maximum temperatures in the reaction zone along the central thermocouple and lower temperatures around $x = 0.1$ m. **Figure 7** shows the contour of the equivalent $C_{mix_{eq}}$ for the dynamic case. The equivalent $C_{mix_{eq}}$ is calculated as follows (Ferrarotti et al., 2019):

$$C_{mix_{eq}} = \frac{\tau_{mix,d}}{k/\varepsilon} \tag{13}$$

where $\tau_{mix,d}$ is the mixing timescale for the dynamic approach defined in section Modeling Tools. It is possible to see in **Figure 7** how the average value of $C_{mix_{eq}}$ in the reaction zone is close to 0.5, thus explaining the agreement of the static and dynamic

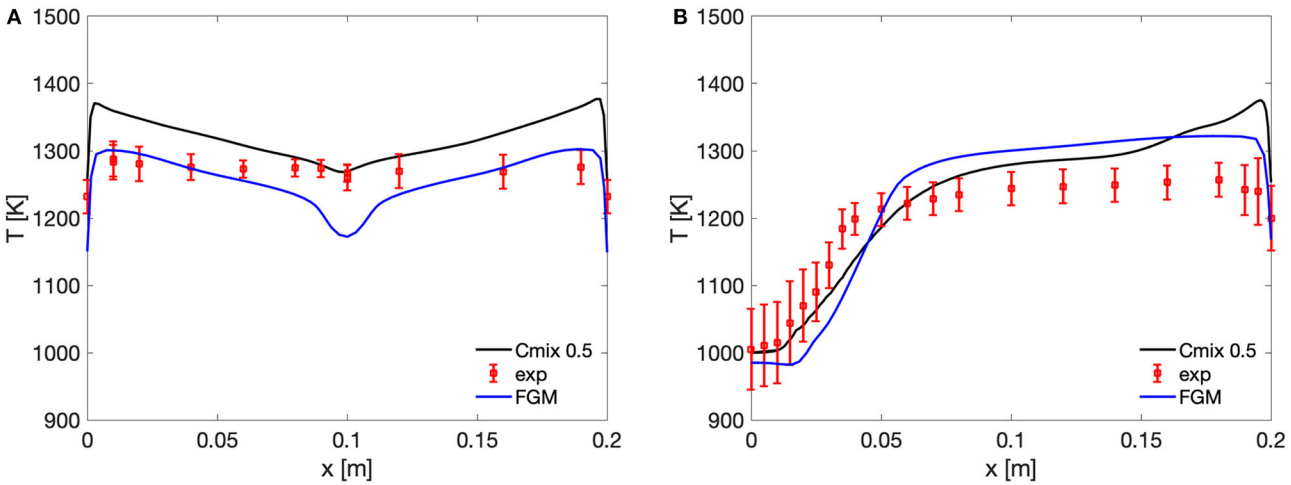


**FIGURE 8 |** Case 2 FGM and static PaSR with $C_{mix} = 0.5$ results compared to experimental values along the central and lateral thermocouples. **(A)** Central thermocouple profiles. **(B)** Lateral thermocouple.

cases. However, the dynamic model still cannot capture the initial ignition of the system. The reason for such deficiency can be explored by means of sophisticated models for turbulent mixing, using for instance detached eddy simulation (DES) and LES.

The FGM and static PaSR with $C_{mix} = 0.5$ were then tested for the experimental conditions of case 2 (**Table 1**). With respect to case 1, both FGM and PaSR better capture the experimental trends. This is probably due to the dilution of the oxidizer stream, which causes the smoothing of the reaction process, resulting in a homogeneous temperature distribution. **Figure 8** shows that, while FGM better predicts the temperature peak along the central thermocouple, the PaSR model enhances the temperature predictions in the ignition region along the lateral thermocouple, although it overpredicts the peak temperature by about 100 K. With respect to the central thermocouple, the PaSR model slightly overpredicts the peak temperature, while FGM underpredicts the observed values in the central region, that is, close to the outlet.

## CONCLUSIONS

Numerical simulations of a lab-scale MILD cyclonic burner were carried out with two different turbulence–chemistry interaction closures, FGM and PaSR, in a RANS framework. The numerical results were compared to the available experimental temperature measurements, in the ignition zone and in the burner midplane.

The main findings can be summarized as follows:

- The thermocouple profiles overall are better represented by the PaSR model results; while the FGM model yields slightly better results along the central thermocouple, the PaSR model better captures the typical slow ignition of MILD systems in both operative conditions.
- A $C_{mix}$ of 0.5 seems to be the better fit for these combinations of fuel and operative conditions. The *a posteriori* analysis of the dynamic PaSR model equivalent $C_{mix_{eq}}$ shows that for the static model, $C_{mix} = 0.5$ is the optimal value for the present cases.
- The analysis of the flame index reveals that the two models determine quite different mixing behaviors: FGM results show that the reaction regions all exhibit non-premixed behavior, while on the other hand the PaSR model determines mostly a premixed environment. As can be expected, the two different behaviors reflect on the temperature profiles, as the different ways mixing is handled between the two models strongly affect the computation of the reaction rates. Further experimental investigations of the cyclonic burner could then be key to determining which of the two numerical approaches would be the better option.
- With the increase of the dilution level in case 2, the differences in the predictive capabilities of the two models lower; the dilution slows down the reaction process, yielding a more homogeneous temperature field, thus explaining the lack of a strong temperature overprediction in the reactive regions by the FGM model as in case 1.

Even though PaSR results are overall better than those of FGM, both closures display some limitations which can be ascribed to the turbulent mixing models employed in RANS computations. For this reason, LES analysis of the same burner will be carried out, to explore the effect of turbulent mixing modeling accuracy on the results.

## DATA AVAILABILITY STATEMENT

The datasets generated for this study are available on request to the corresponding author.

## AUTHOR CONTRIBUTIONS

GC and GS provided experimental results and FGM results. RA and MF provided PaSR results and wrote first draft of the manuscript. GC wrote sections of the manuscript. All authors

contributed to manuscript revision and approved the submitted version and contributed conception and design of the study.

## ACKNOWLEDGMENTS

This project has received funding from the European Research Council (ERC) under the European Union's Horizon 2020 research and innovation program under grant agreement no. 714605. The first and third authors wish to thank the Fonds de la Recherche Scientifique (FNRS) Belgium for financing their research. This article is based upon work from COST Action SMARTCATs (CM1404), supported by COST (European Cooperation in Science and Technology, http://www.cost.eu).

## REFERENCES

Abtahizadeh, E., de Goey, P., and van Oijen, J. (2015). Development of a novel flamelet-based model to include preferential diffusion effects in autoignition of CH4/H2 flames. *Combust. Flame* 162, 4358–4369. doi: 10.1016/j.combustflame.2015.06.015

Bilger, R. W., Stårner, S. H., and Kee, R. J. (1990). On reduced mechanisms for methane/air combustion in nonpremixed flames. *Combus. Flame* 80, 135–149. doi: 10.1016/0010-2180(90)90122-8

Bowman, C. T., Hanson, R. K., Davidson, D. F., Gardiner W. C. Jr., Lissianski, V., Smith, G. P., et al. (1996). Available online at: http://combustion.berkeley.edu/gri-mech/releases.html

Bray, K., Domingo, P., and Vervisch, L. (2005). Role of the progress variable in models for partially premixed turbulent combustion. *Combust. Flame* 141, 431–437. doi: 10.1016/j.combustflame.2005.01.017

Cavaliere, A., and de Joannon, M. (2004). Mild combustion. *Progr. Energy Combust. Sci*. 30, 329–366. doi: 10.1016/j.pecs.2004.02.003

Chen, Z. X., Doan, N. A. K., Lv, X. J., Swaminathan, N., Ceriello, G., Sorrentino, G., et al. (2018). Numerical study of a cycloinic combustor under Moderate or Intense Low-Oxygen Dilution conditions using non-adiabatic tabulated chemistry. *Energy Fuels* 32, 10256–10265. doi: 10.1021/acs.energyfuels.8b01103

Chomiak, J. (1990). *Combustion: A Study in Theory, Fact and Application*. Abacus Press/Gorden and Breach Science Publishers.

Dally, B. B., Karpetis, A. N., and Barlow, R. S. (2002). Structure of turbulent non-premixed jet flames in a diluted hot coflow. *Proc. Combust. Inst*. 29, 1147–1154. doi: 10.1016/S1540-7489(02)80145-6

de Joannon, M., Sabia, P., Sorrentino, G., Bozza, P., and Ragucci, R. (2017). Small size burner combustion stabilization by means of strong cyclonic recirculation. *Proc. Combust. Inst*. 36, 3361–3369. doi: 10.1016/j.proci.2016.06.070

de Joannon, M., Sorrentino, G., and Cavaliere, A. (2012). MILD combustion in diffusion-controlled regimes of hot diluted fuel. *Combust. Flame* 159, 1832–1839. doi: 10.1016/j.combustflame.2012.01.013

De, A., and Dongre, A. (2015). Assessment of turbulence-chemistry interaction models in MILD combustion regime. *Flow Turbul. Combust*. 94, 439–478. doi: 10.1007/s10494-014-9587-8

Domingo, P., Vervisch, L., and Bray, K. (2002). Partially premixed flamelets in LES of non-premixed turbulent combustion. *Combust. Theory Model*. 6, 529–551. doi: 10.1088/1364-7830/6/4/301

Duwig, C., Stankovic, D., Fuchs, L., Li, G., and Gutmark, E. (2007). Experimental and numerical study of flameless combustion in a model gas turbine combustor. *Combust. Sci. Technol*. 180, 279–295. doi: 10.1080/00102200701739164

Ferrarotti, M., Fürst, M., Cresci E., de Paepe, W., and Parente, A. (2018). Key modeling aspects in the simulation of a quasi-industrial 20 kW moderate or intense low-oxygen dilution combustion chamber. *Energy Fuels* 32, 10228-10241. doi: 10.1021/acs.energyfuels.8b01064

Ferrarotti, M., Li, Z., and Parente, A. (2019). On the role of mixing models in the simulation of MILD combustion using finite-rate chemistry combustion models. *Proc. Combust. Inst*. 37, 4531–4538. doi: 10.1016/j.proci.2018.07.043

Fiorina, B., Gicquel, O., Vervisch, L., Carpentier, S., and Darabiha, N. (2005). Premixed turbulent combustion modleing using tabulated chemistry and PDF. *Proc. Combust. Inst*. 30, 867–874. doi: 10.1016/j.proci.2004.08.062

Frassoldati, A., Sharma, P., Cuoci, A., Faravelli, T., and Ranzi, E. (2010). Kinetic and fluid dynamics modeling of methane/hydrogen jet flames in diluted coflow. *Appl. Thermal Eng*. 30, 376–383. doi: 10.1016/j.applthermaleng.2009.10.001

Galletti, C., Parente, A., and Tognotti, L. (2007). Numerical and experimental investigation of a MILD combustion burner. *Combust. Flame* 151, 649–664. doi: 10.1016/j.combustflame.2007.07.016

Ihme, M., and See, Y. C. (2011). LES flamelet modeling of a three-stream MILD combustor: analysis to sensitivity to scalar inflow conditions. *Proc. Combust. Inst*. 33, 1309–1317. doi: 10.1016/j.proci.2010.05.019

Keehan Ye, I. (2011). *Investigation of the Scalar Variance and Scalar Dissipation Rate in URANS and LES*. PhD thesis, University of Waterloo, Waterloo, Ontario, Canada.

Khalil, A. E., and Gupta, A. K. (2017). Towards colorless distributed combustion regime. *Fuel* 195, 113–122. doi: 10.1016/j.fuel.2016.12.093

Knudsen, E., and Pitsch, H. (2009). A general flamelet transformation useful for distinguishing between premixed and non-premixed modes of combustion. *Combust. Flame* 153, 678–696. doi: 10.1016/j.combustflame.2008.10.021

Knudsen, E., and Pitsch, H. (2012). Capabilities and limitations of multi-regime flamelet combustion models. *Combust. Flame* 159, 242–264. doi: 10.1016/j.combustflame.2011.05.025

Lamouroux, J., Ihme, M., Fiorina, B., and Gicquel, O. (2014). Tabulated chemistry approach for diluted combustion regimes with internal recirculation and heat losses. *Combust. Flame* 161, 2120–2136. doi: 10.1016/j.combustflame.2014.01.015

Magnussen, B. F. (2005). "The eddy dissipation concept, a bridge between science and technology," in *ECCOMAS Thematic Conference on Computational Combustion* (Lisbon).

Medwell, P. R., Kalt, P. A. M., and Dally, B. B. (2008). Imaging of diluted turbulent ethylene flames stabilized on a Jet in Hot Coflow (JHC) burner. *Combust. Flame* 152, 100–113. doi: 10.1016/j.combustflame.2007.09.003

Oldenhof, E., Tummers, M. J., Van Veen, E. H., and Roekaerts, D. J. E. M. (2011). Role of entrainment in the stabilisation of jet-in-hot-coflow flames. *Combust. Flame* 158, 1553–1563. doi: 10.1016/j.combustflame.2010.12.018

Özdemir, I. B., and Peters, N. (2001). Characteristics of the reaction zone in a combustor operating at MILD combustion. *Exp. Fluids* 30, 683–695. doi: 10.1007/s003480000248

Pierce, C., and Moin, P. (2001). *Progress-Variable Approach for Large-Eddy Simulation Of Turbulent Combustion*. Ph.D. Thesis, Mechanical Engineering Dept., Stanford University, Stanford.

Pierce, C., and Moin, P. (2004). Progress-variable approach for large-eddy simulation of non-premixed turbulent combustion. *J. Fluid Mech*. 504, 73–97. doi: 10.1017/S0022112004008213

Pope, S. (2013). Small scales, many species and the manifold challenges of turbulent combustion. *Proc. Combust. Inst*. 34:1–31. doi: 10.1016/j.proci.2012.09.009

Rafidi, N., and Blasiak, E. (2006). Heat transfer characteristics of HiTAC heating furnace using regenerative burners. *Appl. Thermal Eng*. 26, 2027–2034. doi: 10.1016/j.applthermaleng.2005.12.016

Sabia, P., Sorrentino, G., Bozza, P., Ceriello, G., Ragucci, R., and de Joannon, M. (2019). Fuel and thermal load flexibility of a MILD burner. *Proc. Combust. Inst*. 37, 4547–4554. doi: 10.1016/j.proci.2018.09.003

Smith, G. P., Golden, D. M., Frenklach, M., Moriarty, N. W., Eiteneer, B., Goldenberg, M., et al. (2011). *GRI-Mech 3.0*. Available online at: http://combustion.berkeley.edu/gri-mech/releases.html (accessed May 20, 2020).

Smith, T. F., Shen, Z. F., and Friedman, J. N. (1982). Evaluation of coefficients for the weighted sum of gray gases model. *J. Heat Transf*. 104, 602–608. doi: 10.1115/1.3245174

Somers, L. M. T. (1994). *The Simulation of Flat Flames With Detailed and Reduced Chemical Models* (PhD thesis).

Sorrentino, G., Ceriello, G., De Joannon, M., Sabia, P., Ragucci, R., Van Oijen, J., et al. (2018a). Numerical investigation of moderate or intense low-oxygen dilution combustion in a cyclonic burner using a flamelet-generated manifold approach. *Energy Fuels* 32, 10242–10255. doi: 10.1021/acs.energyfuels.8b01099

Sorrentino, G., Sabia, P., Bozza, P., Ragucci, R., and de Joannon, M. (2019). Low-NOx conversion of pure ammonia in a cyclonic burner under locally diluted and preheated conditions. *Appl. Energy* 254:113676. doi: 10.1016/j.apenergy.2019.113676

Sorrentino, G., Sabia, P., de Joannon, M., Bozza, P., and Ragucci, R. (2018b). Influence of preheating and thermal power on cyclonic burner characteristics under MILD combustion. *Fuel* 233, 207–214. doi: 10.1016/j.fuel.2018.06.049

The Mathworks Inc. (2019). *MATLAB Version* 9.6.

Van Oijen, J. A., and De Goey, L. P. H. (2000). Modelling of premixed laminar flames using flamelet-generated manifolds. *Combust. Sci. Technol*. 161, 113–137. doi: 10.1080/00102200008935814

Van Oijen, J. A., Donini, A., Bastiaans, R. J. M., ten Thije Boonkkamp, J. H. M., and de Goey, L. P. H. (2016). State-of-the-art in premixed combustion modeling using flamelet generated manifolds. *Progr. Energy Combust. Sci*. 57, 30–74. doi: 10.1016/j.pecs.2016.07.001

Wünning, J. A., and Wünning, J. G. (1997). Flameless oxidation to reduce thermal NO formation. *Progr. Energy Combust. Sci*. 23, 81–94. doi: 10.1016/S0360-1285(97)00006-3

Yamashita, H., Shimada, M., and Takeno, T. (1996). A numerical study on flame stability at the transition point of jet diffusion flames. *Proc. Combust. Inst*. 26, 27–34. doi: 10.1016/S0082-0784(96)80196-2

**Conflict of Interest:** The authors declare that the research was conducted in the absence of any commercial or financial relationships that could be construed as a potential conflict of interest.

frontiers in Mechanical Engineering

MINI REVIEW
published: 16 November 2020
doi: 10.3389/fmech.2020.512501

# A Review of the Numerical Investigations of Jet-In-Hot-Coflow Burner With Reactor-Based Models

*Zhiyi Li*[1,2]* *and Alessandro Parente*[1,2]*

[1]*Université Libre de Bruxelles, Ecole polytechnique de Bruxelles, Aero-Thermo-Mechanics Laboratory, Bruxelles, Belgium,* [2]*Université Libre de Bruxelles and Vrije Universiteit Brussel, Combustion and Robust Optimization Group (BURN), Brussels, Belgium*

Moderate or Intense Low-oxygen Dilution (MILD) combustion is considered as one of the most promising novel combustion technologies, as it ensures high efficiency and very low emissions ($NO_x$ and CO). Because of the high level of dilution, the system reactivity is reduced and the chemical time scale is increased compared to conventional flames. Therefore, combustion models accounting for finite-rate chemistry are needed to study the characteristics of such flames. Reactor based models, such as the Partially Stirred Reactor and the Eddy Dissipation Concept models have been successfully used to model MILD combustion. This article describes recent progress and developments in the application of reactor based models for the simulation of the jet-in-hot-coflow burners that emulate MILD combustion. The main objective is to provide an overview about the current state of the art of reactor based models for turbulence-chemistry interactions in MILD regime and outline future prospects for the further development of such models. The literature acknowledges both Reynolds Averaged Navier Stokes and Large Eddy Simulations studies, with various operating conditions as well as different fuels. The results indicate that it is necessary to include both the mixing and chemical time scales explicitly in the combustion model formulation. Because of the distributed reaction area, according to recent investigations, Large Eddy Simulation grid can be sufficient to resolve the MILD combustion reacting structures. The present review underlines the importance of finite rate chemistry in MILD combustion simulations, as well as of providing reliable estimation of the characteristic time scales.

**Keywords: jet-in-hot-coflow burner, reactor-based models, MILD combustion, turbulence-chemistry interaction, finite rate chemistry**

OPEN ACCESS

***Edited by:***
*Timothy S. Fisher,*
*University of California, Los Angeles,*
*United States*

***Reviewed by:***
*Kan Zha,*
*Sandia National Laboratories (SNL),*
*United States*
*Amir Mardani,*
*Sharif University of Technology, Iran*

***Correspondence:**
*Zhiyi Li*
*zhiyi.li@ulb.ac.be*
*Alessandro Parente*
*alessandro.parente@ulb.ac.be*

***Specialty section:***
*This article was submitted to Thermal and Mass Transport, a section of the journal Frontiers in Mechanical Engineering*

***Received:*** *15 November 2019*
***Accepted:*** *05 October 2020*
***Published:*** *16 November 2020*

***Citation:***
*Li Z and Parente A (2020) A Review of the Numerical Investigations of Jet-In-Hot-Coflow Burner With Reactor-Based Models. Front. Mech. Eng. 6:512501. doi: 10.3389/fmech.2020.512501*

## INTRODUCTION

Facing the current challenges of air pollution and energy shortage, it is urgent to develop fuel flexible, efficient and environmentally friendly combustion technologies. Novel combustion technologies with low emissions, high efficiency and fuel flexibility have become essential under these challenges (Li, 2019). In this context, one promising technology in energy production and manufacturing is Moderate or Intense Low oxygen Dilution (MILD) combustion (Wünning and Wünning, 1997; Cavaliere and de Joannon, 2004; de Joannon et al., 2012).

MILD combustion is established by diluting the fresh reactants with the combustion products and preheating the charge above the self-ignition temperature of the fuel (de Joannon et al., 2012). The

high dilution is responsible for the widening of the reaction zone, while the mixing with hot exhaust gases ensures that reaction takes place also outside of the flammability limits. In terms of characteristic scales, the dilution lowers the oxygen concentration and smooths the temperature peaks. As a result, the chemical time scale increases and the strong interaction between chemistry reaction and mixing makes the investigation of such flames more challenging than conventional combustion regimes. The availability of validation data is then crucial to advance the current understanding of MILD combustion and further push its implementation in industrial applications. To decrease the influence of geometric complexity encountered in practical devices, simplified lab-scale axis-symmetric jet burners are generally used to emulate MILD conditions—for example, the jet-in-hot-coflow (JHC) burner (Dally et al., 2002; Oldenhof et al., 2010).

The JHC burner features a central jet and a secondary burner providing hot exhaust products as a coflow, reproducing the flue gas recirculation. The oxygen level in the coflow is highly diluted by adding nitrogen and it is generally controlled below 10% by mass or volume (Dally et al., 2002; Medwell et al., 2007; Oldenhof et al., 2010; Medwell and Dally, 2012; Ye et al., 2015a; Ye et al., 2017). The literature acknowledges a large number of studies on JHC burners, both experimental and numerical (Dally et al., 2002; Oldenhof et al., 2010; De et al., 2011; Medwell and Dally, 2012; Evans et al., 2015; Parente et al., 2015; Li et al., 2017). Both gaseous (Dally et al., 2002; Medwell et al., 2007; Oldenhof et al., 2010; Medwell and Dally, 2012; Mardani and Karimi Motaalegh Mahalegi, 2019), simple hydrocarbon fuels and liquid (Ye et al., 2015a; Ma et al., 2016; Ye et al., 2017;Ye et al., 2018; Mahalegi and Mardani, 2019), oxygenated or long-chain alkane fuels have been used as fuel. The liquid, long-chain alkane fuels show different characteristics (Ye et al., 2015a; Ye et al., 2017) under MILD conditions, compared to gaseous fuels.

Numerical investigations on the JHC burners were carried out mainly using Reynolds Averaged Navier-Stokes (RANS) (Christo and Dally, 2005; Frassoldati et al., 2009; Mardani et al., 2010; Shabanian et al., 2012; Parente et al., 2015; Evans et al., 2015; Aminian et al., 2016; Mardani, 2017; Evans et al., 2017; Chen et al., 2017; Li et al., 2017; Li et al., 2018b) simulation and Large Eddy Simulation (LES) (Afarin et al., 2011; Ihme and See, 2011; Ihme et al., 2012; Li et al., 2019). LES can capture more faithfully the flow features while RANS is still important for preliminary investigations, because of its reduced computational cost. However, despite high computational efficiency of RANS simulation, non-equilibrium phenomena are not well captured by steady-state assumptions. To this end, Large Eddy Simulation (LES) can provide superior results with respect to RANS.

Due to the presence of the coflow and the intense low-oxygen dilution, combustion in JHC burner is characterised by a relatively low Damköhler number ($Da = \tau_m/\tau_c$, *the ratio of the mixing to chemical time scale*). The interactions between the chemical reaction and fluid dynamics has therefore become more important. Finite-rate chemistry models with detailed chemical mechanisms are necessary. On one hand, combustion models for conventional flames usually rely on the assumption of time-scale separation (i.e., steady flamelets and related models). These models are computationally efficient, while the thermo-chemical space accessible in the numerical simulations is constrained. Furthermore, huge effort could be spent on the pre-processing steps, especially when dilution level in MILD regime and heat losses are considered (Lamouroux et al., 2014; Locci et al., 2014). On the other hand, the use of transported PDF methods (Haworth and Pope, 2010) appears still computationally prohibitive, especially for practical combustion systems. Reactor based models, including the Partially Stirred Reactor (PaSR) (Chomiak, 1990; Golovitchev and Chomiak, 2001) approach and the Eddy Dissipation Concept (EDC) (Magnussen, 1981; Gran and Magnussen, 1996; Magnussen, 2005) model, have been extensively used in the past years because of their affordable treatment of detailed chemistry, showing promise for modelling MILD combustion.

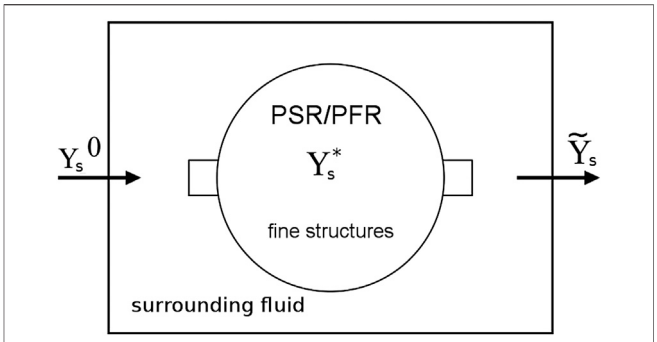


**Figure 1 |** Conceptual drawing of the reactor based models.

## REACTOR BASED MODELS

Both the Partially Stirred Reactor (PaSR) approach and the Eddy Dissipation Concept (EDC) model are based on the assumption that each computational cell can be separated into two zones. Th reacting zone is generally referred to as "fine structures" (Magnussen, 1981; Chomiak, 1990; Gran and Magnussen, 1996; Golovitchev and Chomiak, 2001; Magnussen, 2005) while the non-reacting one is the "surrounding fluid". Combustion takes place in the fine structures in contact with a surrounding fluid. The average reaction rate in a cell is then the results of an exchange between the fine structure and surrounding fluid. The fine structures are modelled as Perfectly Stirred Reactors (PSR) or Plug Flow Reactors (PFR). A conceptual drawing of the PaSR and EDC model is presented in **Figure 1**.

### Eddy Dissipation Concept Model

The EDC model is based on a cascade model (Gran and Magnussen, 1996) providing the mass fraction of the fine structures, $\gamma_\lambda$, and the mean residence time of the fluid within the fine structures $\tau^*$, as a function of the flow characteristic scales:

$$\gamma_\lambda = C_\gamma \left(\frac{\nu\tilde{\epsilon}}{\tilde{k}^2}\right)^{\frac{1}{4}}, \quad (1)$$

$$\tau^* = C_\tau \left(\frac{\nu}{\tilde{\epsilon}}\right)^{\frac{1}{2}}. \quad (2)$$

In **Eq. 1** and **Eq. 2**, ν is the kinematic viscosity, $C_\gamma = 2.1377$ and $C_\tau = 0.4083$ are model constants (Gran and Magnussen, 1996). The mean reaction rate (source term in the species transport equation) is expressed as (Gran and Magnussen, 1996):

$$\overline{\dot{\omega}}_s = -\frac{\bar{\rho}\gamma_\lambda^M \chi}{\tau^*\left(1-\gamma_\lambda^N \chi\right)}\left(\tilde{Y}_s - Y_s^*\right). \quad (3)$$

The term $\tilde{Y}_s$ in **Eq. 3** denotes the mean mass fraction of the species *s* between the fine structures and the surrounding fluid and $Y_s^*$ is the mass fraction of species *s* in the fine structures. The reacting fraction of fine structures is denoted with χ and it is often set to unity (Lewandowski and Ertesvåg, 2018; Lewandowski et al., 2020b). In **Eq 3**, M = 2 and N = 3. In the other two version of the EDC model (Magnussen, 1981, 2005), the combinations M = 3/N = 3 and M = 2/N = 2 have been used.

## Partially Stirred Reactor Model

In the PaSR model (Chomiak, 1990; Golovitchev and Chomiak, 2001), the parameter κ is used to represent the mass fraction of the reaction zone (fine structures) in the computational cell. It can be estimated as (Chomiak, 1990; Golovitchev and Chomiak, 2001; Kärrholm, 2008):

$$\kappa = \frac{\tau_c}{\tau_c + \tau_{mix}}, \quad (4)$$

where $\tau_c$ and $\tau_{mix}$ are the characteristic chemical and mixing time scales in each cell, respectively. The mean source term provided to the species transport equation can be expressed as:

$$\overline{\dot{\omega}}_s = \kappa \frac{\tilde{\rho}\left(Y_s^* - \tilde{Y}_s\right)}{\tau^*}, \quad (5)$$

where $\tau^*$ represents the residence time in the reactive structure. In order to get $Y_s^*$, a system of ODE is solved for the reacting structures.

## Finite-Rate Chemistry Effects

In both models, the mean mass fraction $\tilde{Y}_s$ is obtained by solving transport equations for the reactive scalars induced in the kinetic mechanism. The mass fraction of each species inside the fine structures $Y_s^*$ is estimated assuming that the latter are Perfectly Stirred Reactors (PSR), which allows to use detailed chemical mechanisms (Gran and Magnussen, 1996):

$$\frac{\dot{\omega}_s^*}{\rho^*} = \frac{1}{\tau^*}\left(Y_s^* - Y_0\right), \quad (6)$$

where $\dot{\omega}_s^*$ is the formation rate of species s and $Y_0$ is the species mass fraction in the surrounding fluid (Gran and Magnussen, 1996). Alternatively, the fine structures can be modelled as Plug Flow Reactors (PFR), evolving over a characteristic time equal to $\tau^*$:

$$\frac{Y_s^*}{dt} = \frac{\dot{\omega}_s}{\rho}. \quad (7)$$

# DISCUSSION

Successful predictions of JHC flames are reported in the literature. In the context of RANS simulation using EDC model, over-predictions of temperature were observed using standard EDC constants of $C_\gamma = 2.1377$ and $C_\tau = 0.4083$, as reported by different authors (De et al., 2011; Aminian et al., 2012; Shabanian et al., 2012; Evans et al., 2015; Li et al., 2017; Mardani, 2017; Li et al., 2018b). Aminian et al. (Aminian et al., 2012) performed RANS simulation on the JHC burner with $CH_4/H_2$ as fuel. In the experiments, the co-flow oxygen level was adjusted to 3%, 6% and 9% with the addition of $N_2$. The fuel jet Reynolds number was 10,000. They found out that the standard EDC over-predicts the peak temperature downstream of the burner (120 mm from the burner exit). They concluded that residence time in the fine structures should be increased, to decrease the average reaction rate. To this end, the value of $C_\tau$ was increased to 1.5 and 3.0. It was finally concluded that $C_\tau = 1.5$ was the best option for both co-flow oxygen levels, i.e., 3% and 9%.

De et al. (2011) studied Delft JHC with Dutch natural gas as a fuel, numerically. Under-prediction of the flame lift-off height was observed with the EDC model, while the flame temperature were generally over-estimated. The authors proposed to change not only the time scale constant $C_\tau$, as done by Aminian et al. (2012), but also $C_\gamma$, to directly impact the mass fraction of reacting structures. Based on a sensitivity analysis, the authors finally selected $C_\tau = 3.0$ or $C_\gamma = 1.0$ ($C_\tau$ and $C_\gamma$ are not changed at the same time).

The modified $C_\tau$ constant value used by De et al. was adopted by Shabanian et al., (2012), when simulating the JHC burner fed with ethylene. The modified k-ϵ model reported by Aminian et al. (2012) was used. They compared three different combustion models in their research work: the steady flamelet model, EDC and transported PDF. Results obtained with the adjusted EDC coefficients and transported PDF showed superior performances compared to the standard steady flamelet model. Christo et al. (Christo and Dally, 2005) also compared three combustion models: ξ/PDF, flamelet model and EDC model in RANS, leading to the conclusion that conserved-scalar based models like ξ/PDF and flamelet models are inadequate for the JHC configuration. Chitgarha et al. (Chitgarha and Mardani, 2018) investigated the potential of flamelet modelling for JHC flames with RANS as well. Results with lower accuracy than the EDC model are obtained, though lower computational cost is required by the flamelet model. Chen et al. explored the tabulation of a Perfectly Stirred Reactor (PSR) covering the entire flammability range to model the JHC case. Good agreement is observed except for the CO prediction Chen et al. (2017). Furthermore, Kim et al. (Kim et al., 2005) explored the application of conditional moment closure (CMC) model on the JHC configuration, showing attractive predictions.

Evans et al. (Evans et al., 2015) carried out a systematic study and found out that adjusting the EDC parameters to $C_\gamma = 1.0$ and $C_\tau = 3.0$ resulted in significantly improved predictions under different fuel compositions ($C_2H_4$, $H_2$, $N_2$). Later in 2016, Tu et al. (Tu et al., 2016) adopted $C_\gamma = 1.0$ and $C_\tau = 3.0$ to investigate the physical and chemical effects of $CO_2$ addition to $CH_4/H_2$ JHC Flames. The same was done by Li et al. (Li et al., 2018b), when evaluating the on the fly chemistry reduction and tabulation methods with detailed kinetic mechanisms. Additionally, the combination of $C_\gamma = 1.0$ and $C_\tau = 1.47$ was also tested, showing satisfactory predictions of the Dutch natural gas and biogas JHC flames.

The studies discussed above focused on the modification of $C_\tau$ or $C_\gamma$, based on available experimental data. Different from the previous authors, Mardani et al. (Mardani, 2017) proposed a modification of the energy cascade parameters $C_{D1}$ and $C_{D2}$, eventually affecting the values of $C_\tau$ and $C_\gamma$. In their work, the constant $C_{D2}$ was changed from 0.0239 to 27 while $C_{D1}$ was kept to its original value of 0.134. By this variation, the $C_\tau$ and $C_\gamma$ coefficients in EDC model were varied between 0.0893–3.0 and 1.0–5.795, respectively. By these changes, the model was able to capture the flame lift-off of the reaction zone location and features.

Several sensitivity analyses have been carried out on the JHC burner using EDC model (De et al., 2011; Aminian et al., 2012; Shabanian et al., 2012; Tu et al., 2016; Mardani, 2017; Li et al., 2018a; Li et al., 2018b), to investigate the effect of different modelling choices, focusing on turbulent and combustion model parameters, as well as on the fuel and co-flow compositions. A comprehensive sensitivity study of the JHC burner was carried out by Li et al. (2017), using RANS. Their investigation includes the effect of turbulent combustion model formulations, boundary conditions, differential diffusion, turbulence model parameters and kinetic mechanisms on the results. Results showed that the reactors chosen, namely as Perfectly Stirred Reactors (PSR) or Plug Flow Reactors (PFR), to model the reaction fine structures, do not have a major impact on the results. Moreover, increased kinetic mechanism complexity does not lead to major improvements on the numerical predictions, suggesting that low-temperature oxidation mechanism are not relevant to the fuels and conditions investigated. While the inclusion of differential (molecular) diffusion and the appropriate choice of turbulent non-dimensional values such as Schmidt and Prandtl numbers helped to improve the prediction accuracy. The effect of molecular diffusion was also investigated by Salavati-Zadeh et al. (2018) with the conclusion that the inclusion of the molecular diffusion with proper Schmidt numbers for each species improves the prediction accuracy. The importance of differential diffusion was recognized by Christo and Dally, (2005) and Mardani et al. (2010) as well. In the work of Li et al. (2017), three different Eddy Dissipation Concept (EDC) model formulations were compared as well, showing their interaction with the choice of the $C_{1\epsilon}$ constant in the $k-\epsilon$ turbulence model. Christo and Dally, (2005) also studied the interactions between combustion model and turbulence model under RANS framework, concluding that the variations of k-ϵ model like the renormalization group and the relizable k-ϵ models perform worse than the standard k-ϵ with the modified constant of $C_{\epsilon 1} = 1.6$.

All EDC modifications presented above were based on a fitting procedure aimed at alleviating the temperature over-estimation observed with the standard EDC formulation. Parente et al. (2015) proposed a modification of EDC based on the revision of the energy cascade, taking into account the microscopically distributed features of MILD combustion. In particular, it was assumed that the reacting structures propagated with a turbulent flame speed expressed using the Damköhler formulation for high-intensity turbulence. With this assumption, the energy cascade coefficients $C_{D1}$ and $C_{D2}$ could be expressed as a function of the local turbulent Reynolds and Damköhler number of the flow. The estimation of the chemical time scale required in the Damköhler number was first based on a global reaction mechanism, and later extended to detailed chemistry by Evans et al. (2019). Beside the model constants $C_{D1}$ and $C_{D2}$, Lewandowski and Ertesvåg (2018) proposed a modification on the reacting fraction $\chi$ of fine structures, which is often set to unity in other studies. They observed better agreement with experimental measurement when the reacting fraction is reduced below unity, with an improvement of both temperature and lift-off height predictions.

With the exception of the EDC formulation proposed by Parente et al. (2015) and Evans et al. (2019), the mass fraction of the fine structures and the residence time are solely determined by flow properties in EDC. However, MILD combustion is driven by the strong overlap of fluid dynamic and chemical scales. This suggests that the characteristic chemical time scale shall be included in the definition of the reacting structure features. This has pushed the investigation of PaSR approach for modelling MILD combustion. As indicated in **Section 2.2**, both chemical time scale and mixing time scale are used for the determination of $\kappa$, which is the factor accounting for non-perfect mixing (turbulence-chemistry interaction). Li et al. (2017) compared the EDC model with standard model constants to the standard PaSR model, for the simulation of JHC burner with $C_2H_4$, $H_2$, $H_2O$ as fuel. The prediction of mean temperate and species mass fraction (including $H_2O$ and NO) improved significantly using PaSR, indicating its potential for MILD combustion. There are several ways to estimate the characteristic time scales required by the model (Li et al., 2018a; Ferrarotti et al., 2019). It was showed that appropriate choices of mixing and chemical time scales are crucial to ensure the prediction accuracy. Li and Ferrarotti et al. (Li et al., 2018a; Ferrarotti et al., 2019) reported that a dynamic evaluation for mixing time scale show superior performance for the configuration. The dynamic evaluation adopts mixing time scale as the ratio between the variance of mixture fraction and its dissipation rate, rather than global estimations based on Kolmogorov or integral mixing scales. Different approaches to evaluate chemical time scale were also compared, based on the species formation rates, the reaction rates and the eigenvalues of the formation rate Jacobian matrix (Li et al., 2018a). Various co-flow oxygen dilution levels and Reynolds numbers over a wide range of operating conditions (with $C_2H_4$, $H_2$, $H_2O$ as fuel) were included in the validation work.

The JHC configuration was also investigated using LES, to improve the prediction of intermediate and minor species, as well as to capture the intermittency observed in some configurations when increasing the fuel jet Reynolds number (Parente et al., 2015). LES using a three-stream Flamelet Progress Variable

**TABLE 1 |** Comparison of combustion models

| Models | Details | Findings | References |
|---|---|---|---|
| Standard EDC (RANS) | — | Over-predicted temperature at axial location = 120 mm | De et al. (2011); Aminian et al. (2012); Shabanian et al. (2012); Evans et al. (2015); Li et al. (2017); Mardani (2017); Li et al. (2018b) |
| Modified EDC (RANS) | Increased $C_\tau$ and/or decreased $C_\gamma$ | Alleviated temperature over-prediction at axial location = 120 mm | De et al. (2011); Aminian et al. (2012); Shabanian et al. (2012); Evans et al. (2015); Tu et al. (2016); Li et al. (2018b) |
| | Modified $C_{D1}$ and $C_{D2}$ | - $C_\tau$ and $C_\gamma$ changed accordingly<br>- Capture the flame lift-off well | Mardani (2017); Parente et al. (2015) |
| Dynamic EDC (RANS) | Model constants determined locally and reacting fraction in fine structures $\chi$ = 1.0 | Satisfactory prediction at various axial locations and generalized models | Parente et al. (2015); Evans et al. (2019) |
| — | local model constants with reacting fraction $\chi$ variation | Improved prediction compared to unifom $\chi$ = 1.0 | Lewandowski and Ertesvåg (2018); Lewandowski et al. (2020b, a) |
| PaSR model (RANS) | Mixing and chemical time scales included explictly | Prediction at axial location $\geqslant$ 60 mm improved significantly compared to standard EDC | Li et al. (2017) |
| Dynamic PaSR model (RANS) | Dynamic mixing time scale | Improved prediction compared to standard PaSR, especially the high turbulence case | Li et al. (2018a); Ferrarotti et al. (2019) |
| Flamelet model (RANS) | — | - Computationaly efficient<br>- Inadequate for JHC configuration | Shabanian et al. (2012); Christo and Dally (2005); Chitgarha and Mardani (2018) |
| Tabulated PSR model (RANS) | — | - Computationaly efficient<br>- CO modelling is not satisfactory | Chen et al. (2017) |
| Transported PDF (RANS) | — | - Provide superior results<br>- Computationally inefficient | Shabanian et al. (2012) |
| Conditional moment closure (RANS) | — | Conditional fluctuations of reactive scalars should be small enough for first-order closure | Kim et al. (2005) |
| Flamelet progress variable (LES) | — | - High workload for pre-processing<br>- Largely increased table size with high dilution and heat losses<br>- Less CPU hour needed | Ihme and See (2011); Ihme et al. (2012); Lamouroux et al. (2014); Locci et al. (2014) |
| PaSR (LES) | $\kappa$ evaluated with mixing and chemical time scale | - No effort needed for pre-processing<br>- Over-all good agreement<br>- Compromise efficiency between tabulation based models and transported PDF model | Li et al. (2019) |
| Implicit models (LES) | $\kappa$ = 1 | - Similar performance as PaSR model<br>- No need to estimate time scales | Li et al. (2019) |

**TABLE 2 |** Absolute errors for temperature predictions (%) reported in literature with various combustion models

| Models | Description | 30 mm | 60 mm | 120 mm | Case | References |
|---|---|---|---|---|---|---|
| Standard EDC (RANS) | Standard constants | 0.8 | 4.8 | 27.4 | HM1 | Aminian et al. (2012) |
| | | 8.2 | 10.6 | 25.7 | HM2 | |
| | | 5.8 | 8.2 | 20.2 | HM3 | |
| Modified EDC (RANS) | $C_\tau$ = 1.5 | 3.0 | 0.7 | 13.3 | HM1 | Aminian et al. (2012) |
| | | 1.3 | 2.9 | 13.1 | HM2 | |
| | | 2.0 | 0.5 | 9.5 | HM3 | |
| | $C_\tau$ = 3.0 | 7.9 | 6.0 | 0.4 | HM3 | Aminian et al. (2012) |
| | $C_\tau$ = 1.47, $C_\gamma$ = 1.90 | 3.8 | 3.6 | 5.6 | HM1 | Parente et al. (2015) |
| | $C_{D2}$ = 0.02 | 2.1 | 1.8 | 8.8 | HM1 | Mardani (2017) |
| | $C_{D2}$ = 0.25 | 0.7 | 0.2 | 15.6 | HM1 | |
| | $C_{D2}$ = 1.0 | 2.0 | 1.7 | 13.2 | HM1 | |
| | $C_{D2}$ = 27 | 5.8 | 5.4 | 1.7 | HM1 | |
| | $C_{D2}$ = 0.02 | 0.5 | 0.5 | 8.5 | HM3 | |
| | $C_{D2}$ = 0.25 | 1.3 | 2.8 | 14.0 | HM3 | |
| | $C_{D2}$ = 1.0 | 2.3 | 0.4 | 13.2 | HM3 | |
| | $C_{D2}$ = 27 | 14.5 | 11.7 | 1.6 | HM3 | |
| Dynamic EDC (RANS) | | 3.48 | 1.75 | 9.35 | HM1 | Parente et al. (2015) |
| | | 1.84 | 4.37 | 2.27 | HM2 | |
| | | 8.56 | 10.49 | 3.08 | HM3 | |
| Flamelet model (RANS) | | 5.46 | 3.76 | — | HM1 | Chitgarha and Mardani (2018) |
| | | 13.7 | 8.03 | — | HM3 | |

(FPV) formulation (tabulated based model) was employed by Ihme et al. (Ihme and See, 2011; Ihme et al., 2012) to model the JHC flame. Satisfactory agreement with the experimental data were obtained for mean temperature and major species mass fractions. While the use of FPV-based approaches in MILD combustion is promising, the highly diluted feature of MILD combustion often leads to high dimensional tables (Lamouroux et al., 2014; Locci et al., 2014), whose generation can be challenging and time consuming. Afarin et al. (2011) used PaSR to investigate the reaction zone structure and the distribution of temperature and minor species mass fractions, showing satisfactory accuracy. Li et al. (2019) presented a detailed comparison between the conventional PaSR model and two implicit combustion models, in which the filtered source term comes directly from the chemical term, without inclusion of turbulence effects. Results indicated that all three models could accurately predict the combustion of $CH_4/H_2$ in the JHC configuration, indicating that the sub-grid closure parameter $\kappa$ played a minor role for the case under investigation. This suggested that, for low Damköhler number systems, the reacting structures can be potentially resolved on the LES grid.

A detailed comparison of different models applied on the JHC configuration is presented in **Table 1** and the prediction errors on several axial locations is summarized in **Table 2**. The errors reported in **Table 2** focus on the JHC burner with $CH_4/H_2$ 50%/50% as fuel and with 3% (HM1)/6% (HM2)/9% (HM3) oxygen levels in the coflow. It is worth mentioning that at around 100 mm downstream of the jet outlet, entertainment from the surroundings tunnel air starts to have an effect on the flame (Dally et al., 2002).

## CONCLUSION

The present paper reports a short review on the application of reactor based models to the simulation of a canonical MILD combustion system, the jet in hot coflow (JHC) burner. Successful predictions of JHC burner with finite-rate models were reported, with both Reynolds Average Navier-Stokes (RANS) simulation and Large Eddy Simulation (LES). The main conclusions drawn can be summarized as follows:

- The Eddy Dissipation Concept (EDC) model and its modified versions (with modified model constants) were first considered by most authors (De et al., 2011; Aminian et al., 2012; Shabanian et al., 2012; Tu et al., 2016; Mardani, 2017; Li et al., 2018a; Li et al., 2018b) for the prediction of a jet-in-hot-coflow (JHC) burner with RANS simulation. However, there is a lack of generality.
- The estimation of local EDC parameters based on the local turbulent Reynolds number and Damköhler numbers (Parente et al., 2015) could significantly improve the predictions in the context of MILD combustion, making the inclusion of chemical time scale (needed to estimate Damköhler number) important.
- In PaSR, the turbulence-chemistry interaction factor is based on a more general definition which requires the estimation of both chemical and mixing time scales. The choice of such scales has a crucial impact on the model prediction (Li et al., 2018a).
- A dynamic evaluation of mixing time scale in PaSR RANS formulation was proposed, presenting superior performance

than the other globally defined mixing models under a wide range of JHC flame operating conditions (Li et al., 2018a; Ferrarotti et al., 2019).
- The LES formulation of PaSR model along with other implicit combustion models show superior advantage for the prediction on the JHC flames (Li et al., 2019).
- Future studies shall focus on the generalisation and unification of reactor-based approaches, using available DNS data in MILD combustion (Minamoto and Swaminathan, 2015; Doan and Swaminathan, 2019) together with machine learning and optimization algorithms.
- Future studies should also target more complex fuels, such as oxygenated hydrocarbons and long-chain alkanes under MILD conditions. Because they have shown different characteristics, such as the appearance of visible flames and increased pollutant emissions, as indicated by (Weber et al., 2005; Saha et al., 2014; Ye et al., 2015b).

## AUTHOR CONTRIBUTIONS

ZL wrote this paper. AP contributed to the paper conception and writing.

## FUNDING

This project has received funding from the European Research Council, Starting Grant No. 714605, and the European Union's Horizon 2020 research and innovation program under the Marie Skłodowska-Curie grant agreement No. 643134.

## ACKNOWLEDGMENTS

Some sentences in the article were rephrased from the PhD thesis (Li et al., 2019) of the first author ZL.

## REFERENCES

Afarin, Y., Tabejamaat, S., and Mardani, A. (2011). "Large eddy simulation study of H2/CH4 flame structure at MILD condition." In Seventh mediterranean combustion symposium, Naples, Italy, September 11–September 15

Aminian, J., Galletti, C., Shahhosseini, S., and Tognotti, L. (2012). Numerical investigation of a MILD combustion burner: analysis of mixing field, chemical kinetics and turbulence-chemistry interaction. *Flow, Turbul. Combust.* 88, 597–623. doi:10.1007/s10494-012-9386-z

Aminian, J., Galletti, C., and Tognotti, L. (2016). Extended EDC local extinction model accounting finite-rate chemistry for MILD combustion. *Fuel* 165, 123–133. doi:10.1016/j.fuel.2015.10.041

Cavaliere, A., and de Joannon, M. (2004). MILD combustion. *Prog. Energy Combust. Sci.* 30, 329–366. doi:10.1016/j.pecs.2004.02.003

Chen, Z., Reddy, V., Ruan, S., Doan, N., Roberts, W., and Swaminathan, N. (2017). Simulation of mild combustion using perfectly stirred reactor model. *Proc. Combust. Inst.* 36, 4279–4286. doi:10.1016/j.proci.2016.06.007

Chitgarha, F., and Mardani, A. (2018). Assessment of steady and unsteady flamelet models for mild combustion modeling. *Int. J. Hydrogen Energy* 43, 15551–15563. doi:10.1016/j.ijhydene.2018.06.071

Chomiak, J. (1990). *Combustion: a study in theory, fact and application*. New York, NY: Abacus Press/Gorden and Breach Science Publishers

Christo, F. C., and Dally, B. B. (2005). Modelling turbulent reacting jets issuing into a hot and diluted coflow. *Combust. Flame* 142, 117–129. doi:10.1016/j.combustflame.2005.03.002

Dally, B. B., Karpetis, A. N., and Barlow, R. S. (2002). Structure of turbulent non-premixed jet flames in a diluted hot coflow. *Proc. Combust. Inst.* 29, 1147–1154. doi:10.1016/s1540-7489(02)80145-6

De, A., Oldenhof, E., Sathiah, P., and Roekaerts, D. (2011). Numerical simulation of Delft-Jet-in-Hot-Coflow (DJHC) flames using the Eddy Dissipation Concept model for turbulence-chemistry interaction. *Flow, Turbul. Combust.* 87, 537–567. doi:10.1007/s10494-011-9337-0

de Joannon, M., Sorrentino, G., and Cavaliere, A. (2012). MILD combustion in diffusion-controlled regimes of hot diluted fuel. *Combust. Flame* 159, 1832–1839. doi:10.1016/j.combustflame.2012.01.013

Doan, N. A. K., and Swaminathan, N. (2019). Autoignition and flame propagation in non-premixed MILD combustion. *Combust. Flame* 201, 234–243. doi:10.1016/j.combustflame.2018.12.025

Evans, M., Chinnici, A., Medwell, P., and Ye, J. (2017). Ignition features of methane and ethylene fuel-blends in hot and diluted coflows. *Fuel* 203, 279–289. doi:10.1016/j.combustflame.2018.12.025

Evans, M. J., Medwell, P. R., and Tian, Z. F. (2015). Modelling lifted jet flames in a heated coflow using an optimised eddy dissipation concept model. *Combust. Sci. Technol.* 187, 1093–1109. doi:10.1016/j.fuel.2017.04.113

Evans, M., Petre, C., Medwell, P., and Parente, A. (2019). Generalisation of the eddy-dissipation concept for jet flames with low turbulence and low damköhler number. *Proc. Combust. Inst.* 37, 4497–4505. doi:10.1080/00102202.2014.1002836

Ferrarotti, M., Li, Z., and Parente, A. (2019). On the role of mixing models in the simulation of MILD combustion using finite-rate chemistry combustion models. *Proc. Combust. Inst.* 37, 4531–4538. doi:10.1016/j.proci.2018.06.017

Frassoldati, A., Sharma, P., Cuoci, A., Faravelli, T., and Ranzi, E. (2009). Kinetic and fluid dynamics modeling of methane/hydrogen jet flames in diluted coflow. *Appl. Therm. Eng.* 30, 376–383. doi:10.1016/j.applthermaleng.2009.10.001

Golovitchev, V., and Chomiak, J. (2001). Numerical modeling of high temperature air flameless combustion. In The 4th international symposium on high temperature air combustion and gasification

Gran, I., and Magnussen, B. F. (1996). A numerical study of a bluff-body stabilized diffusion flame, part 2: influence of combustion modelling and finite-rate chemistry. *Combust. Sci. Technol.* 119, 191–217. doi:10.1080/00102209608951999

Haworth, D., and Pope, S. (2010). *Transported probability density function methods for Reynolds-averaged and large-eddy simulations*. New York, NY:(Springer)

Ihme, M., and See, Y. C. (2011). LES flamelet modeling of a three-stream MILD combustor: analysis of flame sensitivity to scalar inflow conditions. *Proc. Combust. Inst.* 33, 1309–1317. doi:10.1016/j.proci.2010.05.019

Ihme, M., Zhang, J., He, G., and Dally, B. (2012). Large Eddy Simulation of a Jet-in-Hot-Coflow burner operating in the oxygen-diluted combustion regime. *Flow, Turbul. Combust.* 89, 449–464 doi:10.1007/s10494-012-9399-7

Kärrholm, F. P. (2008). Numerical Modelling of diesel spray injection, turbulence Interaction and combustion. *Phd thesis*, Chalmers University of Technology, Chalmers, Sweden

Kim, S. H., Huh, K. Y., and Dally, B. (2005). Conditional moment closure modeling of turbulent nonpremixed combustion in diluted hot coflow. *Proc. Combust. Inst.* 30, 751–757. doi:10.1016/j.proci.2004.08.161

Lamouroux, J., Ihme, M., Fiorina, B., and Gicquel, O. (2014). Tabulated chemistry approach for diluted combustion regimes with internal recirculation and heat losses. *Combust. Flame* 161, 2120–2136. doi:10.1016/j.combustflame.2014.01.015

Lewandowski, M. T., and Ertesvåg, I. S. (2018). Analysis of the eddy dissipation concept formulation for mild combustion modeling. *Fuel* 224, 687–700. doi:10.1016/j.fuel.2018.03.110

Lewandowski, M. T., Li, Z., Parente, A., and Pozorski, J. (2020a). Generalised eddy dissipation concept for mild combustion regime at low local Reynolds and damköhler numbers. part 2: validation of the model. *Fuel* 278, 117773 doi:https://doi.org/10.1016/j.fuel.2020.117773

Lewandowski, M. T., Parente, A., and Pozorski, J. (2020b). Generalised eddy dissipation concept for mild combustion regime at low local Reynolds and damköhler numbers. part 1: model framework development. *Fuel* 278, 117743, doi:10.1016/j.fuel.2020.117743

Li, Z., Cuoci, A., and Parente, A. (2019). Large eddy simulation of mild combustion using finite rate chemistry: effect of combustion sub-grid closure. *Proc. Combust. Inst.* 37, 4519–4529. doi:10.1016/j.proci.2018.09.033

Li, Z., Cuoci, A., Sadiki, A., and Parente, A. (2017). Comprehensive numerical study of the Adelaide Jet in Hot-Coflow burner by means of RANS and detailed chemistry. *Energy* 139, 555–570. doi:10.1016/j.energy.2017.07.132

Li, Z., Ferrarotti, M., Cuoci, A., and Parente, A. (2018a). Finite-rate chemistry modelling of non-conventional combustion regimes using a partially-stirred reactor closure: combustion model formulation and implementation details. *Appl. Energy* 225, 637–655. doi:10.1016/j.apenergy.2018.04.085

Li, Z., Lewandowski, M. T., Contino, F., and Parente, A. (2018b). Assessment of on-the-fly chemistry reduction and tabulation approaches for the simulation of moderate or intense low-oxygen dilution combustion. *Energy and Fuels* 32, 10121–10131. doi:10.1021/acs.energyfuels.8b01001

Li, Z. (2019). Sub-grid models for Large Eddy Simulation of non-conventional combustion regimes. Ph.D. thesis. Darmstadt(Germany): Université libre de Bruxelles and Technische Universitæt Darmstadt

Locci, C., Colin, O., and Michel, J. B. (2014). Large Eddy simulations of a small-scale flameless combustor by means of diluted homogeneous reactors. *Flow, Turbul. Combust.* 93, 305–347. doi:10.1007/s10494-014-9548-2

Ma, L., Naud, B., and Roekaerts, D. (2016). Transported pdf modeling of ethanol spray in hot-diluted coflow flame. *Flow, Turbul. Combust.* 96, 469–502. doi:10.1007/s10494-015-9623-3

Magnussen, B. F. (1981). "On the structure of turbulence and a generalized Eddy Dissipation Concept for chemical reaction in turbulent flow." In 19$^{th}$AIAA aerospace science meeting, St. Louis, Missouri

Magnussen, B. F. (2005). "The Eddy Dissipation Concept a bridge between science and technology." In ECCOMAS thematic conference on computational combustion, Lisbon, Portugal

Mahalegi, H. K. M., and Mardani, A. (2019). Ethanol spray combustion under a mild condition: a chemical kinetic study. *Energy & Fuels* 33, 11861–11886. doi:10.1021/acs.energyfuels.9b02665

Mardani, A., and Karimi Motaalegh Mahalegi, H. (2019). Hydrogen enrichment of methane and syngas for mild combustion. *Int. J. Hydrogen Energy* 44, 9423–9437. doi:10.1016/j.ijhydene.2019.02.072

Mardani, A. (2017). Optimization of the Eddy Dissipation Concept (EDC) model for turbulence-chemistry interactions under hot diluted combustion of ch4/h2. *Fuel* 191, 114–129. doi:10.1016/j.fuel.2016.11.056

Mardani, A., Tabejamaat, S., and Ghamari, M. (2010). Numerical study of influence of molecular diffusion in the MILD combustion regime. *Combust. Theor. Model.* 14, 747–774. doi:10.1080/13647830.2010.512959

Medwell, P. R., and Dally, B. B. (2012). Effect of fuel composition on jet flames in a heated and diluted oxidant stream. *Combust. Flame* 159, 3138–3145. doi:10.1016/j.combustflame.2012.04.012

Medwell, P. R., Kalt, P. A., and Dally, B. B. (2007). Imaging of diluted turbulent ethylene flames stabilized on a Jet in Hot Coflow (JHC) burner. *Combust. Flame* 152, 100–113. doi:10.1016/j.combustflame.2007.09.003

Minamoto, Y., and Swaminathan, N. (2015). Subgrid scale modelling for MILD combustion. *Proc. Combust. Inst.* 35, 3529–3536. doi:10.1016/j.proci.2014.07.025

Oldenhof, E., Tummers, M. J., van Veen, E., and Roekaerts, D. (2010). Ignition kernel formation and lift-off behaviour of Jet-in-Hot-Coflow flames. *Combust. Flame* 157, 1167–1178. doi:10.1016/j.combustflame.2010.01.002

Parente, A., Malik, M. R., Contino, F., Cuoci, A., and Dally, B. B. (2015). Extension of the Eddy Dissipation Concept for turbulence/chemistry interactions to MILD combustion. *Fuel* 163, 98–111. doi:10.1016/j.fuel.2015.09.020

Saha, M., Dally, B. B., Medwell, P. R., and Cleary, E. M. (2014). Moderate or Intense Low oxygen Dilution (MILD) combustion characteristics of pulverized coal in a self-recuperative furnace. *Energy & Fuels* 28, 6046–6057. doi:10.1021/ef5006836

Salavati-Zadeh, A., Esfahanian, V., Najafi], S. B. N., Saeed, H., and Mohammadi, M. (2018). Kinetic simulation of flameless burners with methane/hydrogen blended fuel: effects of molecular diffusion and schmidt number. *Int. J. Hydrogen Energy* 43, 5972–5983. doi:10.1016/j.ijhydene.2017.11.149

Shabanian, S. R., Medwell, P. R., Rahimi, M., Frassoldati, A., and Cuoci, A. (2012). Kinetic and fluid dynamic modeling of ethylene jet flames in diluted and heated oxidant stream combustion conditions. *Appl. Therm. Eng.* 52, 538–554. doi:10.1016/j.applthermaleng.2012.12.024

Tu, Y., Su, K., Liu, H., Chen, S., Liu, Z., and Zheng, C. (2016). Physical and chemical effects of $CO_2$ addition on $CH_4$/$H_2$ flames on a Jet-in-Hot-Coflow (JHC) burner. *Energy and Fuels* 30, 1390–1399. doi:10.1021/acs.energyfuels.5b02499

Wünning, J. A., and Wünning, J. G. (1997). Flameless oxidation to reduce thermal NO-formation. *Prog. Energy Combust. Sci.* 23, 81–94. doi:10.1016/s0360-1285(97)00006-3

Weber, R., Smart, J. P., and vd Kamp, W. (2005). On the (MILD) combustion of gaseous, liquid, and solid fuels in high temperature preheated air. *Proc. Combust. Inst.* 30, 2623–2629. doi:10.1016/j.proci.2004.08.101

Ye, J., Medwell, P. R., Evans, M. J., and Dally, B. B. (2017). Characteristics of turbulent n-heptane jet flames in a hot and diluted coflow. *Combust. Flame* 183, 330–342. doi:10.1016/j.combustflame.2017.05.027

Ye, J., Medwell, P. R., Kleinheinz, K., Evans, M. J., Dally, B. B., and Pitsch, H. G. (2018). Structural differences of ethanol and dme jet flames in a hot diluted coflow. *Combust. Flame* 192, 473 – 494. doi:10.1016/j.combustflame.2018.02.025

Ye, J., Medwell, P. R., Varea, E., Kruse, S., Dally, B. B., and Pitsch, H. G. (2015a). An experimental study on mild combustion of prevaporised liquid fuels. *Appl. Energy* 151, 93–101. doi:10.1016/j.apenergy.2015.04.019

Ye, J., Medwell, P. R., Varea, E., Kruse, S., Dally, B. B., and Pitsch, H. G. (2015b). An experimental study on MILD combustion of prevaporised liquid fuels. *Appl. Energy* 151, 93–101. doi:10.1016/j.apenergy.2015.04.019

**Conflict of Interest:** The authors declare that the research was conducted in the absence of any commercial or financial relationships that could be construed as a potential conflict of interest.

frontiers in Mechanical Engineering

MINI REVIEW
published: 05 May 2021
doi: 10.3389/fmech.2021.505923

# Mini-Review: Heat Transfer Mechanisms in MILD Combustion Systems

*Giuseppe Ceriello*[1], *Giancarlo Sorrentino*[1]*, *Antonio Cavaliere*[1], *Mara de Joannon*[2] and *Raffaele Ragucci*[2]

[1] Dipartimento di Ingegneria Chimica, dei Materiali e della Produzione Industriale, Università degli studi di Napoli "Federico II", Naples, Italy, [2] Istituto di Scienze e Tecnologie per l'Energia e la Mobilità Sostenibili (STEMS), Consiglio Nazionale delle Ricerche (CNR), Naples, Italy

MILD combustion has a wide potential in enhancing thermal efficiency with nearly zero emissions. It has no visible flame since the radiation from the reacting zones is attenuated due to both the intermediate species at reduced temperatures, induced by intensely burned gas recirculation, and the absence of particulate emitters. Beyond these main features, there are other characteristics such as temperature uniformity and distributed ignition that have to be addressed and analyzed looking at the peculiar role of the heat transfer for such reactors. First, the category of combustion systems object of the study is described. Afterwards an analysis on the heat transfer mechanisms under MILD combustion of gaseous fuels is carried out. Therefore, in this Mini-Review, several literature findings highlighting the role of the heat transfer on the combustion peculiarities of MILD reactors (i.e., temperature uniformity, distributed ignition, low pollutant emissions) are reported and discussed. Heat exchange modes, in fact, contribute to providing MILD macroscopic characteristics by means of the strong interplay between wall and gas heat transfer, instead of the reactive structure. In particular, the thermal behavior of these systems is analyzed in order to stress the distinctive role of the heat loss and the relative contributions of the convective and radiative terms. Heat transfer mechanisms between gas and walls and their interactions, in fact, favor the wide temperature distribution within the chamber. In order to better understand the different effects of the heat transfer under MILD regime, the mechanisms regarding walls and recirculating gas are separately investigated.

**Keywords: MILD combustion, heat transfer, radiation, WSGG model, blackbody**

OPEN ACCESS

***Edited by:***
*Dipankar Chatterjee, Central Mechanical Engineering Research Institute (CSIR), India*

***Reviewed by:***
*Dirk J. E. M. Roekaerts, Delft University of Technology, Netherlands*
*Ronan Vicquelin, CentraleSupélec, France*

***Correspondence:**
*Giancarlo Sorrentino*
*g.sorrentino@unina.it*

***Specialty section:***
*This article was submitted to Thermal and Mass Transport, a section of the journal Frontiers in Mechanical Engineering*

***Received:*** *18 October 2019*
***Accepted:*** *26 March 2021*
***Published:*** *05 May 2021*

***Citation:***
*Ceriello G, Sorrentino G, Cavaliere A, de Joannon M and Ragucci R (2021) Mini-Review: Heat Transfer Mechanisms in MILD Combustion Systems. Front. Mech. Eng. 7:505923. doi: 10.3389/fmech.2021.505923*

## INTRODUCTIVE CONCEPTS: MILD COMBUSTION REACTOR FEATURES

Moderate or Intense Low-oxygen Dilution (MILD) Combustion (Cavaliere and de Joannon, 2004) is characterized by low-oxygen concentrations and high inlet temperatures. Important characteristics of this oxidation process are homogeneous temperatures, distributed ignition (Khalil and Gupta, 2017), absence of visible flames (Karyeyen et al., 2019) and low CO, $NO_x$ and soot emissions (de Joannon et al., 2012). It is a very good candidate for low-calorific-value (Huang et al., 2014; Sabia et al., 2019), hydrogen, nitrogen-based (Sabia et al., 2019) fuels and industrial ones (Parente et al., 2008). The process occurs under conditions different from conventional ones because of the strong interplay between mixing, chemistry and heat transfer (Lamouroux et al., 2014; Chen et al., 2018).

Several facilities such as the Jet-in-Hot-Coflows (Medwell et al., 2008; Oldenhof et al., 2010), and the Cabra flame (Cabra et al., 2005), are used to reproduce highly diluted and preheated conditions, on the basis of kinetic time-scales modifications. In all these cases the combustion process is unconfined and occurs far from the walls, under adiabatic conditions (Kim et al., 2005; De and Dongre, 2015).

MILD is realized by using exhaust gas recirculation (Cavigiolo et al., 2003; Minamoto et al., 2013). The internal EGR is obtained through proper chamber designs (Veríssimo et al., 2013), by realizing long residence times (Li et al., 2014) due to convoluted and confined flow-fields (Sorrentino et al., 2018). Gas entrainment (de Joannon et al., 2017) lead to chemical time-scales comparable to mixing ones (Özdemir and Peters, 2001) and reflect the importance of impinging wall-jets (de Joannon et al., 2017) or cavity flows (Chinnici et al., 2017).

These systems, identified hereafter as "MILD reactors," are classified with respect to nominal MILD requisites. Specifically, the inlet-feeding temperature ($T_{in}$), should be higher than the spontaneous-ignition one ($T_{ign}$), and the differential temperature increase between products and reactants ($\Delta T_{product}$), should be lower than $T_{ign}$. In the current literature, three main configurations of MILD reactors can be identified with respect to the strategy they use to fulfill the above-mentioned conditions (Perpignan et al., 2018). In the following, a review of these configurations is given.

The first configuration regards reactors where $T_{in} > T_{ign}$ and $\Delta T_{product} < T_{ign}$ are satisfied through external feeding. This is the case of post-combustion systems. Fuel-rich (Giménez-López et al., 2011) or fuel-lean re-burning processes (Miller et al., 1998; Kim et al., 2012) are examples of in-furnace and/or post-furnace $NO_x$ abatement systems. Fuel is injected in exhaust/oxygen mixtures for jet-engine systems (Fureby, 2000) or waste incineration (Parr et al., 1996).

Another group of MILD reactors refers to the case $T_{in} > T_{ign}$, obtained by external feeding while $\Delta T_{product} < T_{ign}$, through intra-reactor phenomena. Such a condition is typically obtained in recuperative/regenerative furnace systems (Wünning and Wünning, 1997; Katsuki and Hasegawa, 1998; Özdemir and Peters, 2001; Rafidi and Blasiak, 2006; Li et al., 2014) in which part of the combustion heat is subtracted by walls through exhausts reverse flow (Nemitallah et al., 2018).

The third MILD reactors category involves those systems where both requirements are fulfilled by internal recirculation and heat exchange strategies. Also, in this case, many different fluid-dynamic arrangements can be used. In particular, parallel jets (Abtahizadeh et al., 2012; Huang et al., 2014; Cheong et al., 2019) and cyclonic flow configurations (de Joannon et al., 2017). The former has also been used for burners in regenerative conditions (Wünning and Wünning, 1997; Katsuki and Hasegawa, 1998; Rafidi and Blasiak, 2006; Li et al., 2014). Regarding the cyclonic systems, LUCY burner (Sorrentino et al., 2016) is a valuable example of MILD reactor with a tailored flow-field (Sorrentino et al., 2017).

In the second and third categories, the condition $\Delta T_{product} < T_{ign}$, is influenced by heat exchange at walls, and the residence time poses severe design restrictions (Kruse et al., 2015). Indeed, heat loss plays a key role in reducing the reacting mixture temperature (Szegö et al., 2009). On the other hand, a sufficiently high temperature must be guaranteed inside the reactor itself. In other words, the walls are responsible for both the heat loss by products and the heat gain by reactants (Danon et al., 2011).

Energy equation includes contributions of the three heat transfer modes: conduction, convection and thermal radiation, where the latter is included through the radiative flux divergence (Özışık, 1973; Viskanta, 2005; Dombrovsky and Baillis, 2010; Modest, 2013). In the following sections, the contributions of each heat transfer mechanism under MILD conditions are analyzed and discussed.

The overall heat transfer is conceptually divided into three phenomena: gas-to-gas, gas-to-wall and wall-to-wall.

## GAS TO GAS HEAT TRANSFER

EGR is essential in MILD to mix fresh reactants with exhausts in order to lower the reaction-rate and sustain the oxidation for diluted conditions (Tu et al., 2015). Thus, the reactor design (Liu et al., 2015) must ensure the required convection and radiation levels. High concentrations of absorbing and emitting $H_2O/CO_2$ mixtures inside the combustion chamber (Dorigon et al., 2013) lead to enhanced radiative re-absorptions. This effect is not negligible and contributes to the system thermal homogeneity, as highlighted in several literature papers (Zhang et al., 2019; Ceriello et al., 2020).

The specific aerodynamic requirements of MILD Combustion (enhanced jet mixing through high inlet jets momentum and large scale recirculation of flue gases) influence the contribution of convective heat transfer mode. In particular the share of convective heat transfer in the MILD mode is enhanced by the higher velocity and momentum of air at the inlet when compared to the conventional combustion mode (Riahi et al., 2013). On the other hand the increased internal recirculation enhances the convective heat transfer process and this effect is more marked in MILD oxyfuel combustion processes (Chen et al., 2012).

In **Figure 1**, emissivity of $CO_2$ and $H_2O$ as functions of the temperature at different products between total pressure and length of the enclosure (Hottel and Cohen, 1958), and modified by Alberti et al. (2015), are reported. Those trends show that, for both species, when the temperature of the mixture gets lower, the emissivity increases. For MILD systems, operating in the range $1{,}000 < T < 1{,}400$ K, the standard gas emissivity of burned products results higher with respect to conventional combustion (where $T > 1{,}800$ K). This is due to both the effect of lower system temperatures and $CO_2/H_2O$ higher partial pressures. Therefore, the effect of the re-absorption is noticeable in MILD, even for a small-scale apparatus (Sorrentino et al., 2018; Zhang et al., 2019).

To model radiative re-absorption, the spectral dependence of the radiative properties of the exhausts must be known. The most accurate method to calculate the radiative properties of the combustion products is the line-by-line integration (Chu et al., 2011; Zeng et al., 2020) which uses spectroscopic databases

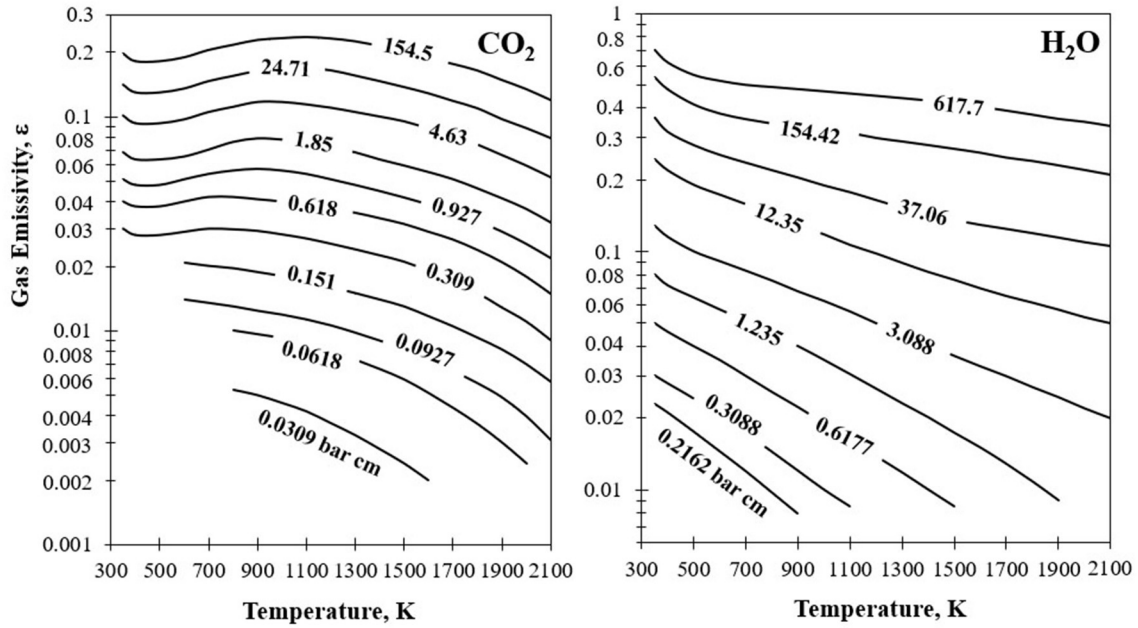


**FIGURE 1 |** Total emissivity of pure carbon dioxide (left) and pure water vapor (right) as a function of temperature (Hottel and Cohen, 1958) and modified by Alberti et al. (2015).

(Rothman et al., 2010; Gordon et al., 2017; Pannier and Laux, 2019). However, LBL calculation is not feasible for the CFD of complex combustion systems. Very few works showed LBL with Monte Carlo methods coupled to CFD for combustion applications (Zhao et al., 2013; Ren et al., 2018).

Intermediate between LBL and global models, narrow band models such as the correlated-k approach has also been retained in some works by solving the radiative transfer equation in the CFD using a Monte-Carlo based on the emission-reciprocity method (ERM) (Koren et al., 2018; Rodrigues et al., 2019).

Global models such as the full spectrum correlated-K method (FSK) and the spectral line based weighted sum of gray gas method (SLW) have received a lot of attention because of their accuracy and low computational costs. Despite that, their implementation is not straightforward since the correlation of FSK and SLW are usually offered for single gas species.

A simple solution that is commonly used in commercial CFD codes, due to its computational efficiency, relies on the resolution of only one radiative transfer equation to obtain the total radiation intensity field by replacing the spectral absorption coefficient with the mean gray absorption coefficient (Galletti et al., 2007; Pallarés et al., 2007; Yang et al., 2007). In such cases simplified radiation models optimized for combustion systems can be developed by using the detailed information given by the spectral databases (Paul et al., 2019).

Usually, in numerical modeling of MILD/Flameless systems the Weighted-Sum-of-Gray-Gases Model, WSGGM (Modest, 1991), is adopted to model the spectrally dependent properties of the combustion gases, making use of updated spectral databases. A possible choice is to use the coefficient proposed by Smith et al. (1982). Modified WSGG (Bordbar et al., 2014; Cassol et al., 2014) were recently developed. In particular, the coefficients proposed in this models were used to account for various temperature and different concentrations of $H_2O/CO_2$ in each computational cell. According to this radiative database, both the absorption coefficients and the black body weights of the gray gases depend on molar ratio, while only the weights depend on temperature. Modified WSGG models were applied for simulating MILD condition in several works (Galletti et al., 2007; Sorrentino et al., 2018).

An interesting modification of the WSGG model is represented by the SLW (Webb et al., 2018) where detailed gas spectroscopic data are captured by a designed distribution function (Denison and Webb, 1993). It gives some improvements with respect to WSGG (Krishnamoorthy et al., 2010; Webb et al., 2018). However, since the MILD does not have strong gradients of temperature and concentration, the improvements of SLW with respect to WSGG do not justify the increase of computational costs. Therefore, the flameless nature of the MILD process supports the use of a modified WSGG to obtain reliable results for such systems.

Regarding the solution method of the radiative-transfer-equation (RTE), considering the intermediate optical thickness of MILD, the Discrete Ordinate (DO) radiation model (Chui and Raithby, 1993) seems an appropriate choice. DO approximation converts the RTE into a series of differential equations along directions (Modest, 2013).

On the other hand, some studies showed that P1 model gave worse prediction than DO for MILD (Frassoldati et al., 2010). Moreover very few works used Monte Carlo methods in MILD

burners and results differed by <5% with respect to DO, but the latter model was preferred because of its lower computational cost (Galletti et al., 2007).

## GAS TO WALL HEAT TRANSFER

Some literature works reported the relative importance of convective and radiative modes in MILD combustion. In particular, heat transfer characteristics from the furnace walls for $H_2O/CO_2$ mixtures (Zhang et al., 2019) were analyzed and they showed that the $H_2O$ increase enhanced the share of heat radiation. When $H_2O$ is substitute for $CO_2$, the influence of heat capacity progressively declines and the effect of heat capacity on strengthening convective heat transfer or weakening radiative heat transfer gradually decreases. Moreover, thermal performance analysis of hybrid solar receiver MILD combustor showed that the ratio of radiative to convective heat transfer rate is found to be dependent on the fuel type (Chinnici et al., 2019).

In this context, engineering global assessments on the importance of radiative heat transfer with respect to convective one can be obtained for MILD systems without solving RTE if average values of fluid and wall temperatures are available and by adopting several approximations.

In a combustion system, the overall heat transfer flux between gas and walls, $Q$, in $W/m^2$, can be expressed as the sum of a convective, $Q_c$, and a radiative term, $Q_r$ (Baukal, 2000), as follows:

$$\mathbf{Q = Q_c + Q_r}, \tag{1}$$

with

$$\mathbf{Q_c} = \bar{\mathbf{h}}_\mathbf{c}\,(\mathbf{T_f - T_w}) \tag{2}$$

$$\mathbf{Q_r} = \varepsilon_\mathbf{g}\sigma\left(\mathbf{T_g^4 - T_w^4}\right) \tag{3}$$

In such relations, $\bar{h}_c$ is the average convection heat transfer coefficient over the heat transfer area, in $W/m^2\ K$, $T_w$ the wall surface temperature, $T_f$ the fluid temperature, $T_g$ and $\varepsilon_g$ are the exhaust ($H_2O/CO_2$ mixture) mean temperature and emissivity, respectively (Kreith et al., 2011). In the expression of the radiative heat flux, $Q_r$, the view factors are considered to have value 1. This assumption for the flux leaving gas and reaching walls is supported by the black body cavity behavior of MILD systems. Moreover, since the combustion process extends to the whole volume under MILD conditions, the view factor can be assumed to be 1 as well.

In the expression of Equation (3), both the black walls and gas are assumed to emits and absorbs heat at all wavelengths. A more accurate expression can be found in the book by Lefebvre and Ballal (2010) where the gas emits only a few narrow bands of wavelengths and absorbs only those wavelengths included in its emission bands.

For a MILD reactor, as reported in several works (Chinnici et al., 2017; Sorrentino et al., 2018; Zhang et al., 2019), the fluid temperature, $T_f$, can be approximated to the mean gas temperature inside the combustion chamber, $T_g$, because of the absence of steep gradients and peaks:

$$\mathbf{T_f = T_g} \tag{4}$$

This approximation is commonly adopted for industrial furnaces and denoted as Well-Stirred model (Hewitt et al., 1994). Therefore, the ratio between radiative and convective term reads

$$\frac{\mathbf{Q_r}}{\mathbf{Q_c}} = \frac{\varepsilon_\mathbf{g}\sigma\mathbf{T_w^3}}{\bar{\mathbf{h}}_\mathbf{c}}\left(\left(\frac{\mathbf{T_g}}{\mathbf{T_w}}\right)^2 + \mathbf{1}\right)\left(\frac{\mathbf{T_g}}{\mathbf{T_w}} + \mathbf{1}\right) \tag{5}$$

In **Figure 2** this dimensionless parameter is showed for both $CO_2$ and $H_2O$ as a function of the gas temperature, $T_g$, at different wall temperatures, $T_w$ (solid black lines). The values of the gas emissivity as a function of their temperature, $\varepsilon_g(T_g)$, were read from Hottel's diagrams (**Figure 1**).

In order to approximate the MILD operating conditions of the cyclonic burner LUCY, reported in Sorrentino et al. (2018), the product of pressure and length and the convective coefficient $h_f$ were set to 10 bar cm and 35 $\frac{W}{m^2}K$, respectively.

According to Sorrentino et al. (2018), MILD conditions are located in the red regions, where the radiative heat transfer between gases and walls is around 1.5 times the convective one, for both the gases (**Figure 2**). This outcome supports one of the main results of the referred work: radiative heat transfer modeling is essential in a cyclonic MILD burner for computations (Sorrentino et al., 2018).

The heat transfer analysis was here reported for a specific configuration (cyclonic burner with $h_f = 35$ W/m$^2$/K) for illustrative purposes. In such a case both the presence of cavity flows in the chamber and wall jets near the inlet region influenced the wall convective heat transfer. Clearly, such analysis can be replicated for different MILD/Flameless systems on the basis of the aerodynamics characteristics of the system. It is here worthwhile to note that the design choices for MILD systems related to flow pattern features and/or inlet jets configurations strongly influence the convective heat transfer rate.

Moreover, in **Figure 2**, the role of the temperature of the walls appears to be fundamental to move from a convective-based to a radiative-based heat transfer mode. The latter favors the stabilization of MILD conditions, as well proved by Chinnici et al. (2017) though a proper control of the heat flux distribution at walls.

The analysis carried out for the cyclonic burner in **Figure 2** could be easily replicated for different MILD/Flameless systems with a large amount of internally recirculating combustion products (Rafidi and Blasiak, 2006; Noor et al., 2013; Huang et al., 2017; Zhang et al., 2019).

## WALL TO WALL HEAT TRANSFER

In black enclosures, radiative transfer depends on view factors and surface temperatures. For diffuse-gray enclosures, thermal radiation is also a function of the surface's emissivity (Modest, 2013). Considering gray and nearly opaque surfaces, part of the "gas-to-walls" radiative heat transfer can be seen as a "gas-to wall-to gas" contribution, which means that a portion of the radiation emitted by the mixture to the walls is reflected and absorbed from the gas itself, result in making the thermal field more uniform. This effect is enhanced by the "wall-to-wall" contribution of the

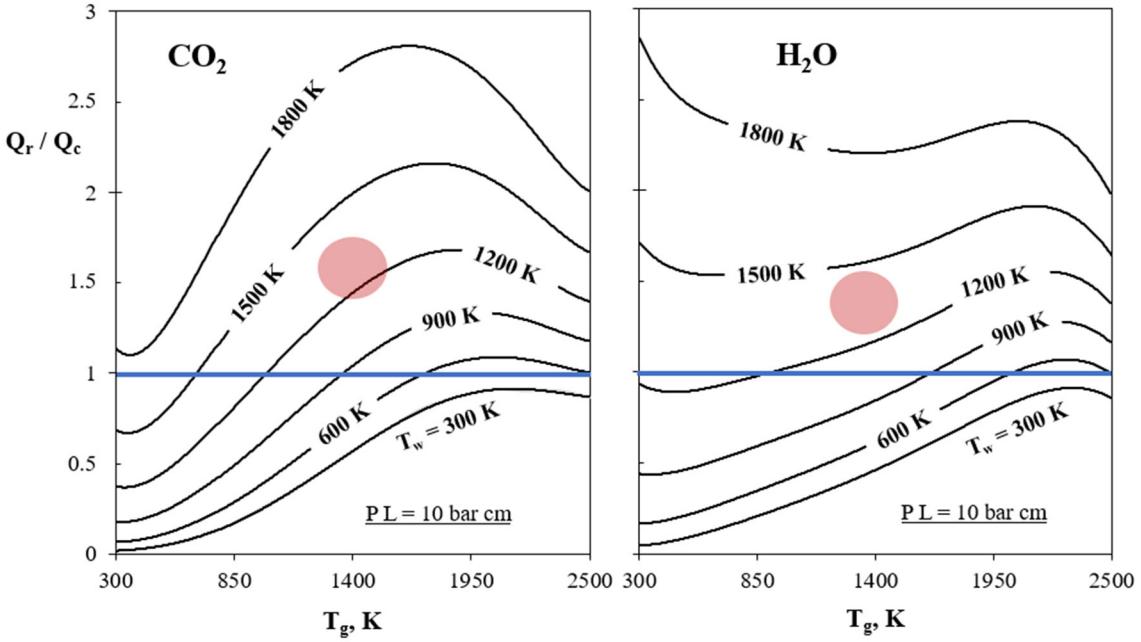


**FIGURE 2 |** Trends of the ratio between radiation and convection for $CO_2$ (left) and $H_2O$ (right) as a function of the mean gas temperature and at different wall temperatures, for a small-scale cyclonic reactor (Sorrentino et al., 2018).

apparatus and, therefore, by the tendency of the system to behave as a blackbody cavity.

In order to express this characteristic, the Gebhart factor (Gebhart, 1961) can be used. In fact, the radiative heat exchanged in an enclosure composed of surfaces with piecewise constant temperature and emissivity can be calculated in terms of Gebhart factors (Gebhart, 1961; Dahlquist and Björck, 2008), $G_{ij}$, which are defined as a fraction of energy leaving surface $i$ which reaches surface $j$ and is absorbed. The Gebhart factors $G_{ij}$ equals the view factors, $F_{ij}$, for black surface. The net radiative heat exchange $Q_k^{rad}$ between any surface $k$ and all the others $N$ surfaces of the enclosure can be expressed in terms of the Gebhart factors as

$$\mathbf{Q_k^{rad}} = \mathbf{A_k}\varepsilon_\mathbf{k}\sigma\theta_\mathbf{k}^\mathbf{4} - \sum_{\mathbf{j=1}}^{\mathbf{N}} \mathbf{A_j}\varepsilon_\mathbf{j}\sigma\mathbf{G_{ij}}\theta_\mathbf{j}^\mathbf{4} \tag{6}$$

where $A_j$, $\varepsilon_j$, $\theta_j$, $A_k$, $\varepsilon_k$ and $\theta_k$ are area, emissivity, and temperature of surface $j$ and area, emissivity, and temperature of surface $k$, respectively (Atherton et al., 1987). The proposed wall-to-wall heat transfer treatment is based on the assumption of temperature uniformity at the walls and transparent medium between the walls. This peculiar feature is well-reported for MILD reactors (Chinnici et al., 2017; Sorrentino et al., 2018) and it is emphasized for high values of the Surface/Volume ratio where the participating medium is distributed to the whole reactor volume.

MILD reactors with confinement, exhibit Gebhart factors (related to the outlet section) that are usually lower than 0.1 (Chinnici et al., 2017; Sorrentino et al., 2018; Zhang et al., 2019), when evaluated on the basis of reactor information.

MILD combustion is usually employed in furnaces or boilers where inner walls are built with refractory materials with emissivity that is usually higher than 0.7.

Therefore, these systems tend to behave as a cavity maximizing the "gas-to-wall-to-gas re-absorption." This mechanism ensures uniform walls temperature inside the chamber. On the other hand, the radiation that cannot leave the system contributes to wall temperatures homogeneity with higher radiation-to-convection ratio, as reported in **Figure 2**.

## CONCLUDING REMARKS

The mini-review highlighted the role of the heat transfer for systems where MILD combustion is achieved by means of EGR. The investigation of the different transport mechanisms pointed out the key role of heat exchange mechanisms in realizing the performances and features of the MILD regime.

The "gas to gas" heat transfer mechanism is crucial both for convection and radiation. The convective term is due to the high velocities, required to ensure elevated EGR, and the confinement of the flows by the walls. Moreover, the recirculating combustion products ($H_2O/CO_2$ mixture) are involved in the radiative re-absorption.

Appropriate models are needed for gases radiative properties. Among them, WSGG model based on radiative databases created *ad-hoc* for mixtures of combustion products at high temperatures is a reasoning solution.

Regarding the "gas to wall" interaction, a quantitative analysis on a MILD reactor (Sorrentino et al., 2018) was carried out

and it was demonstrated that the radiation is the dominant heat transfer mechanism between reactive mixture and walls. Such a result is known for traditional large-scale furnaces, but it represents an interesting finding for a small-scale Flameless system.

Finally, the "wall to wall" heat exchange was analyzed, pointing out that MILD systems behave as black body cavity due to their confined enclosures. Therefore, the walls at high temperature strongly exchange heat by irradiation contributing to the system homogeneity.

Convective and radiative heat transfer modes have remarkable effects also on design and simulation of MILD systems, especially concerning the temperature uniformity.

## AUTHOR CONTRIBUTIONS

GS and GC were involved in the bibliographic research to include in the manuscript the most important literature contributions on the effect of heat transfer on MILD systems. They have also strongly contributed in writing several parts of the article. AC and MdJ gave their support in the theoretical background regarding identification and classification of MILD Combustion processes. RR gave important insights and hints in the physical description of convective and radiative heat transfer phenomena involved in combustion technologies. He also strongly revised the English language in the manuscript. All authors contributed to the article and approved the submitted version.

## REFERENCES


Abtahizadeh, E., van Oijen, J., and De Goey, P. (2012). Numerical study of mild combustion with entrainment of burned gas into oxidizer and/or fuel streams. *Combust. Flame* 159, 2155–2165. doi: 10.1016/j.combustflame.2012.02.004

Alberti, M., Weber, R., and Mancini, M. (2015). Re-creating Hottel's emissivity charts for carbon dioxide and extending them to 40 bar pressure using HITEMP-2010 data base. *Combust. Flame* 162, 597–612. doi: 10.1016/j.combustflame.2014.09.005

Atherton, L. J., Derby, J. J., and Brown, R. A. (1987). Radiative heat exchange in Czochralski crystal growth. *J. Cryst. Growth* 84, 57–78. doi: 10.1016/0022-0248(87)90114-X

Baukal, C. E. (2000). *Heat Transfer in Industrial Combustion.* Boca Raton, NY: CRC Press.

Bordbar, M. H., Wecel, G., and Hyppänen, T. (2014). A line by line based weighted sum of gray gases model for inhomogeneous $CO_2$-$H_2O$ mixture in oxy-fired combustion. *Comb. Flame* 161, 2435–2445. doi: 10.1016/j.combustflame.2014.03.013

Cabra, R., Chen, J. Y., Dibble, R. W., Karpetis, A. N., and Barlow, R. S. (2005). Lifted methane-air jet flames in a vitiated coflow. *Combust. Flame* 143, 491–506. doi: 10.1016/j.combustflame.2005.08.019

Cassol, F., Brittes, R., França, F. H., and Ezekoye, O. A. (2014). Application of the weighted-sum-of-gray-gases model for media composed of arbitrary concentrations of $H_2O$, $CO_2$ and soot. *Int. J. Heat Mass Transf.* 79, 796–806. doi: 10.1016/j.ijheatmasstransfer.2014.08.032

Cavaliere, A., and de Joannon, M. (2004). Mild combustion. *Progr. Energ. Comb. Sci.* 30, 329–366. doi: 10.1016/j.pecs.2004.02.003

Cavigiolo, A., Galbiati, M. A., Effuggi, A., Gelosa, D., and Rota, R. (2003). Mild combustion in a laboratory-scale apparatus. *Combust. Sci. Technol.* 175, 1347–1367. doi: 10.1080/00102200302356

Ceriello, G., Sorrentino, G., Cavaliere, A., Sabia, P., de Joannon, M., and Ragucci, R. (2020). The role of dilution level and canonical configuration in the modeling of MILD combustion systems with internal recirculation. *Fuel* 264:116840. doi: 10.1016/j.fuel.2019.116840

Chen, L., Yong, S. Z., and Ghoniem, A. F. (2012). Oxy-fuel combustion of pulverized coal: characterization, fundamentals, stabilization and CFD modeling. *Progr. Energ. Comb. Sci.* 38, 156–214. doi: 10.1016/j.pecs.2011.09.003

Chen, Z. X., Doan, N. A. K., Lv, X. J., Swaminathan, N., Ceriello, G., Sorrentino, G., et al. (2018). A numerical study of a cyclonic combustor under MILD conditions using non-adiabatic tabulated chemistry. *Energy Fuels* 32, 10256–10265. doi: 10.1021/acs.energyfuels.8b01103

Cheong, K. P., Wang, G., Wang, B., Zhu, R., Ren, W., and Mi, J. (2019). Stability and emission characteristics of nonpremixed MILD combustion from a parallel-jet burner in a cylindrical furnace. *Energy* 170, 1181–1190. doi: 10.1016/j.energy.2018.12.146

Chinnici, A., Tian, Z. F., Lim, J. H., Nathan, G. J., and Dally, B. B. (2017). Comparison of system performance in a hybrid solar receiver combustor operating with MILD and conventional combustion. Part II: effect of the combustion mode. *Sol. Energy* 147, 479–488. doi: 10.1016/j.solener.2017.02.054

Chinnici, A., Tian, Z. F., Lim, J. H., Nathan, G. J., and Dally, B. B. (2019). Thermal performance analysis of a syngas-fuelled hybrid solar receiver combustor operated in the MILD combustion regime. *Comb. Sci. Tech.* 191, 2–17. doi: 10.1080/00102202.2018.1452381

Chu, H., Liu, F., and Zhou, H. (2011). Calculations of gas thermal radiation transfer in one-dimensional planar enclosure using LBL and SNB models. *Int. J. Heat Mass Transf.* 54, 4736–4745. doi: 10.1016/j.ijheatmasstransfer.2011.06.002

Chui, E. H., and Raithby, G. D. (1993). Computation of radiant heat transfer on a nonorthogonal mesh using the finite–volume method. *Numer. Heat Transf. Part B Fundam.* 23, 269–288. *doi: 10.1080/10407799308914901*

Dahlquist, G., and Björck, Å. (2008). *Numerical Methods in Scientific Computing, Volume I*. Philadelphia, PA: Society for Industrial and Applied Mathematics.

Danon, B., Cho, E. S., De Jong, W., and Roekaerts, D. J. E. M. (2011). Numerical investigation of burner positioning effects in a multi-burner flameless combustion furnace. *Appl. Thermal Eng.* 31, 3885–3896. doi: 10.1016/j.applthermaleng.2011.07.036

de Joannon, M., Sabia, P., Sorrentino, G., Bozza, P., and Ragucci, R. (2017). Small size burner combustion stabilization by means of strong cyclonic recirculation. *Proc. Combust. Inst.* 36, 3361–3369. doi: 10.1016/j.proci.2016.06.070

de Joannon, M., Sorrentino, G., and Cavaliere, A. (2012). MILD combustion in diffusion-controlled regimes of hot diluted fuel. *Combust. Flame* 159, 1832–1839. doi: 10.1016/j.combustflame.2012.01.013

De, A., and Dongre, A. (2015). Assessment of turbulence-chemistry interaction models in MILD combustion regime. *Flow Turbul. Combust.* 94, 439–478. doi: 10.1007/s10494-014-9587-8

Denison, M. K., and Webb, B. W. (1993). An absorption-line blackbody distribution function for efficient calculation of total gas radiative transfer. *J. Quant. Spectrosc. Radiat. Transf.* 50, 499–510. doi: 10.1016/0022-4073(93)90043-H

Dombrovsky, L. A., and Baillis, D. (2010). *Thermal Radiation in Disperse Systems: An Engineering Approach*. Redding, CT: Begell House.

Dorigon, L. J., Duciak, G., Brittes, R., Cassol, F., Galarça, M., and França, F. H. R. (2013). WSGG correlations based on HITEMP2010 for computation of thermal radiation in non-isothermal, non-homogeneous $H_2O/CO_2$ mixtures. *Int. J. Heat Mass Transf.* 64, 863–873. doi: 10.1016/j.ijheatmasstransfer.2013.05.010

Frassoldati, A., Sharma, P., Cuoci, A., Faravelli, T., and Ranzi, E. (2010). Kinetic and fluid dynamics modeling of methane/hydrogen jet flames in diluted coflow. *Appl. Thermal Eng.* 30, 376–383. doi: 10.1016/j.applthermaleng.2009.10.001

Fureby, C. (2000). Large Eddy simulation of combustion instabilities in a jet engine afterburner model. *Combust. Sci. Technol.* 161, 213–243. doi: 10.1080/00102200008935818

Galletti, C., Parente, A., and Tognotti, L. (2007). Numerical and experimental investigation of a mild combustion burner. *Combust. Flame* 151, 649–664. doi: 10.1016/j.combustflame.2007.07.016

Gebhart, B. (1961). Surface temperature calculations in radiant surroundings of arbitrary complexity-for gray, diffuse radiation. *Int. J. Heat Mass Transf.* 3, 341–346. doi: 10.1016/0017-9310(61)90048-5

Giménez-López, J., Aranda, V., Millera, A., Bilbao, R., and Alzueta, M. U. (2011). An experimental parametric study of gas reburning under conditions

of interest for oxy-fuel combustion. *Fuel Process. Technol.* 92, 582–589. doi: 10.1016/j.fuproc.2010.11.014

Gordon, I. E., Rothman, L. S., Hill, C., Kochanov, R. V., Tan, Y., Bernath, P. F., et al. (2017). The HITRAN2016 molecular spectroscopic database. *J. Quant. Spectrosc. Radiative Transf.* 203, 3–69. doi: 10.1016/j.jqsrt.2017.06.038

Hewitt, G. F., Shires, G. L., and Bott, T. R. (1994). *Process Heat Transfer*. Boca Raton, FL: CRC Press.

Hottel, H. C., and Cohen, E. S. (1958). Radiant heat exchange in a gas-filled enclosure: allowance for nonuniformity of gas temperature. *AIChE J.* 4, 3–14. doi: 10.1002/aic.690040103

Huang, M., Zhang, Z., Shao, W., Xiong, Y., Liu, Y., Lei, F., et al. (2014). Effect of air preheat temperature on the MILD combustion of syngas. *Energy Convers. Manag.* 86, 356–364. doi: 10.1016/j.enconman.2014.05.038

Huang, X., Tummers, M. J., and Roekaerts, D. J. E. M. (2017). Experimental and numerical study of MILD combustion in a lab-scale furnace. *Energy Procedia* 120, 395–402. doi: 10.1016/j.egypro.2017.07.231

Karyeyen, S., Feser, J. S., and Gupta, A. K. (2019). Hydrogen concentration effects on swirl-stabilized oxy-colorless distributed combustion. *Fuel* 253, 772–780. doi: 10.1016/j.fuel.2019.05.008

Katsuki, M., and Hasegawa, T. (1998). "The science and technology of combustion in highly preheated air," in *Symposium (International) on Combustion*, Vol. 27 (Pittsburgh, PA), 3135–3146. doi: 10.1016/S0082-0784(98)80176-8

Khalil, A. E. E., and Gupta, A. K. (2017). Towards colorless distributed combustion regime. *Fuel* 195, 113–122. doi: 10.1016/j.fuel.2016.12.093

Kim, H. Y., Baek, S. W., and Kim, S. W. (2012). Investigation of fuel lean reburning process in a 1.5 MW boiler. *Appl. Energy* 89, 183–192. doi: 10.1016/j.apenergy.2011.05.027

Kim, S. H., Huh, K. Y., and Dally, B. (2005). Conditional moment closure modeling of turbulent nonpremixed combustion in diluted hot coflow. *Proc. Combust. Inst.* 30, 751–757. doi: 10.1016/j.proci.2004.08.161

Koren, C., Vicquelin, R., and Gicquel, O. (2018). Multiphysics simulation combining large-eddy simulation, wall heat conduction and radiative energy transfer to predict wall temperature induced by a confined premixed swirling flame. *Flow Turb. Comb.* 101, 77–102. doi: 10.1007/s10494-018-9895-5

Kreith, F., Manglik, R., and Bohn, M. (2011). *Principles of Heat Transfer, 7th Edn*. Stamford, CT: Cengage Learning.

Krishnamoorthy, G., Sami, M., Orsino, S., Perera, A., Shahnam, M., and Huckaby, E. D. (2010). Radiation modelling in oxy-fuel combustion scenarios. *Int. J. Comput. Fluid Dyn.* 24, 69–82. doi: 10.1080/10618562.2010.485567

Kruse, S., Kerschgens, B., Berger, L., Varea, E., and Pitsch, H. (2015). Experimental and numerical study of MILD combustion for gas turbine applications. *Appl. Energy* 148, 456–465. doi: 10.1016/j.apenergy.2015.03.054

Lamouroux, J., Ihme, M., Fiorina, B., and Gicquel, O. (2014). Tabulated chemistry approach for diluted combustion regimes with internal recirculation and heat losses. *Combust. Flame* 161, 2120–2136. doi: 10.1016/j.combustflame.2014.01.015

Lefebvre, A. H., and Ballal, D. R. (2010). *Gas Turbine Combustion: Alternative Fuels and Emissions, 3rd Edn.* Boca Raton, FL: CRC Press.

Li, P., Wang, F., Mi, J., Dally, B. B., and Mei, Z. (2014). MILD combustion under different premixing patterns and characteristics of the reaction regime. *Energy Fuels* 28, 2211–2226. doi: 10.1021/ef402357t

Liu, B., Wang, Y. H., and Xu, H. (2015). Mild combustion in forward flow furnace of refinery-off gas for low-emissions by deflector. *Appl. Therm. Eng.* 91, 1048–1058. doi: 10.1016/j.applthermaleng.2015.08.078

Medwell, P. R., Kalt, P. A. M., and Dally, B. B. (2008). Imaging of diluted turbulent ethylene flames stabilized on a Jet in Hot Coflow (JHC) burner. *Combust. Flame* 152, 100–113. doi: 10.1016/j.combustflame.2007.09.003

Miller, C. A., Touati, A. D., Becker, J., and Wendt, J. O. L. (1998). "NOx abatement by fuel-lean reburning: laboratory combustor and pilot-scale package boiler results," in *Symposium (International) on Combustion*, Vol. 27, (Pittsburgh, PA), 3189–3195. doi: 10.1016/S0082-0784(98)80182-3

Minamoto, Y., Dunstan, T. D., Swaminathan, N., and Cant, R. S. (2013). DNS of EGR-type turbulent flame in MILD condition. *Proc. Combust. Inst.* 34, 3231–3238 doi: 10.1016/j.proci.2012.06.041

Modest, M. F. (1991). The weighted-sum-of-gray-gases model for arbitrary solution methods in radiative transfer. *ASME J. Heat Transfer*. 113, 650–656. doi: 10.1115/1.2910614

Modest, M. F. (2013). *Radiative Heat Transfer*. San Diego, CA: Academic Press. doi: 10.1016/B978-0-12-386944-9.50023-6

Nemitallah, M. A., Rashwan, S. S., Mansir, I. B., Abdelhafez, A. A., and Habib, M. A. (2018). Review of novel combustion techniques for clean power production in gas turbines. *Energy Fuels* 32, 979–1004. doi: 10.1021/acs.energyfuels.7b03607

Noor, M. M., Wandel, A. P., and Yusaf, T. (2013). Design and development of MILD combustion burner. *J. Mech. Eng. Sci.* 5, 662–676. doi: 10.15282/jmes.5.2013.13.0064

Oldenhof, E., Tummers, M. J., van Veen, E. H., and Roekaerts, D. J. E. M. (2010). Ignition kernel formation and lift-off behaviour of jet-in-hot-coflow flames. *Combust. Flame* 157, 1167–1178. doi: 10.1016/j.combustflame.2010.01.002

Özdemir, I. B., and Peters, N. (2001). Characteristics of the reaction zone in a combustor operating at mild combustion. *Exp. Fluids* 30, 683–695. doi: 10.1007/s003480000248

Özışık, M. N. (1973). *Radiative Transfer and Interactions With Conduction and Convection*. New York, NY: Werbel & Peck.

Pallarés, J., Arauzo, I., and Williams, A. (2007). Integration of CFD codes and advanced combustion models for quantitative burnout determination. *Fuel* 86, 2283–2290. doi: 10.1016/j.fuel.2007.01.036

Pannier, E., and Laux, C. O. (2019). RADIS: a nonequilibrium line-by-line radiative code for $CO_2$ and HITRAN-like database species. *J. Quant. Spectrosc. Radiative Transf.* 222, 12–25. doi: 10.1016/j.jqsrt.2018.09.027

Parente, A., Galletti, C., and Tognotti, L. (2008). Effect of the combustion model and kinetic mechanism on the MILD combustion in an industrial burner fed with hydrogen enriched fuels. *Int. J. Hydrogen Energy* 33, 7553–7564. doi: 10.1016/j.ijhydene.2008.09.058

Parr, T. P., Gutmark, E., Wilson, K., Hanson-Parr, D. M., Yu, K., Smith, R. A., et al. (1996). Compact incinerator afterburner concept based on vortex combustion. *Symp. Combust.* 26, 2471–2477. doi: 10.1016/S0082-0784(96)80078-6

Paul, C., Haworth, D. C., and Modest, M. F. (2019). A simplified CFD model for spectral radiative heat transfer in high-pressure hydrocarbon–air combustion systems. *Proc. Comb. Inst.* 37, 4617–4624. doi: 10.1016/j.proci.2018.08.024

Perpignan, A. A. V., Gangoli Rao, A., and Roekaerts, D. J. E. M. (2018). Flameless combustion and its potential towards gas turbines. *Prog. Energy Combust. Sci.* 69, 28–62. doi: 10.1016/j.pecs.2018.06.002

Rafidi, N., and Blasiak, W. (2006). Heat transfer characteristics of HiTAC heating furnace using regenerative burners. *Appl. Therm. Eng.* 26, 2027–2034. doi: 10.1016/j.applthermaleng.2005.12.016

Ren, T., Modest, M. F., and Roy, S. (2018). Monte Carlo simulation for radiative transfer in a high-pressure industrial gas turbine combustion chamber. *J. Eng. Gas Turb. Power* 140:051503. doi: 10.1115/1.4038153

Riahi, S., Roekaerts, D. J. E. M., and Lupant, D. (2013). "Numerical comparative study of heat transfer in flameless and conventional combustion in a 30-kW furnace," in *Proceedings of the European Combustion Meeting* (Lund).

Rodrigues, P., Gicquel, O., Franzelli, B., Darabiha, N., and Vicquelin, R. (2019). Analysis of radiative transfer in a turbulent sooting jet flame using a Monte Carlo method coupled to large eddy simulation. *J. Quant. Spectrosc. Radiative Transf.* 235, 187–203. doi: 10.1016/j.jqsrt.2019.07.003

Rothman, L. S., Gordon, I. E., Barber, R. J., Dothe, H., Gamache, R. R., Goldman, A., et al. (2010). HITEMP, the high-temperature molecular spectroscopic database. *J. Quant. Spectrosc. Radiat. Transf.* 111, 2139–2150. doi: 10.1016/j.jqsrt.2010.05.001

Sabia, P., Sorrentino, G., Bozza, P., Ceriello, G., Ragucci, R., and de Joannon, M. (2019). Fuel and thermal load flexibility of a MILD burner. *Proc. Combust. Inst.* 37, 4547–4554. doi: 10.1016/j.proci.2018.09.003

Smith, T. F., Shen, Z. F., and Friedman, J. N. (1982). Evaluation of coefficients for the weighted sum of gray gases model. *J. Heat Transf.* 104, 602–608. doi: 10.1115/1.3245174

Sorrentino, G., Ceriello, G., de Joannon, M., Sabia, P., Ragucci, R., Van Oijen, J., et al. (2018). Numerical investigation of moderate or intense low-oxygen dilution combustion in a cyclonic burner using a flamelet-generated manifold approach. *Energy Fuels* 32, 10656–10667. doi: 10.1021/acs.energyfuels.8b01099

Sorrentino, G., Göktolga, U., De Joannon, M., Van Oijen, J., Cavaliere, A., and De Goey, P. (2017). An experimental and numerical study of MILD combustion in a cyclonic burner. *Energy Procedia* 120, 649–656. doi: 10.1016/j.egypro.2017.07.173

Sorrentino, G., Sabia, P., De Joannon, M., Cavaliere, A., and Ragucci, R. (2016). The effect of diluent on the sustainability of MILD combustion in a cyclonic burner. *Flow Turbul. Combust.* 96, 449–468. doi: 10.1007/s10494-015-9668-3

Szegö, G. G., Dally, B. B., and Nathan, G. J. (2009). Operational characteristics of a parallel jet MILD combustion burner system. *Combust. Flame* 156, 429–438. doi: 10.1016/j.combustflame.2008.08.009

Tu, Y., Liu, H., Chen, S., Liu, Z., Zhao, H., and Zheng, C. (2015). Effects of furnace chamber shape on the MILD combustion of natural gas. *Appl. Therm. Eng.* 76, 64–75. doi: 10.1016/j.applthermaleng.2014.11.007

Veríssimo, A. S., Rocha, A. M. A., and Costa, M. (2013). Importance of the inlet air velocity on the establishment of flameless combustion in a laboratory combustor. *Exp. Therm. Fluid Sci.* 44, 75–81. doi: 10.1016/j.expthermflusci.2012.05.015

Viskanta, R. (2005). *Radiative Transfer in Combustion Systems: Fundamentals and Applications.* West Lafayette, IN: Purdue University.

Webb, B. W., Ma, J., Pearson, J. T., and Solovjov, V. P. (2018). SLW modeling of radiation transfer in comprehensive combustion predictions. *Combust. Sci. Technol.* 190, 1392–1408. doi: 10.1080/00102202.2018.1452123

Wünning, J. A., and Wünning, J. G. (1997). Flameless oxidation to reduce thermal NO-formation. *Prog. Energy Combust. Sci.* 23, 81–94. doi: 10.1016/S0360-1285(97)00006-3

Yang, Y. B., Newman, R., Sharifi, V., Swithenbank, J., and Ariss, J. (2007). Mathematical modelling of straw combustion in a 38 MWe power plant furnace and effect of operating conditions. *Fuel* 86, 129–142. doi: 10.1016/j.fuel.2006.06.023

Zeng, X., Liang, C., Duan, L., Chen, X., Liu, D., and Ma, J. (2020). A GPU-based line-by-line method for thermal radiation transfer of $H_2O$, $CO_2$, and $H_2O/CO_2$ mixture. *Appl. Thermal Eng.* 167:114799. doi: 10.1016/j.applthermaleng.2019.114799

Zhang, Z., Li, X., Zhang, L., Luo, C., Lu, B., Xu, Y., et al. (2019). Effect of $H_2O/CO_2$ mixture on heat transfer characteristics of pulverized coal MILD-oxy combustion. *Fuel Process. Technol.* 184, 27–35. doi: 10.1016/j.fuproc.2018.11.011

Zhao, X. Y., Haworth, D. C., Ren, T., and Modest, M. F. (2013). A transported probability density function/photon Monte Carlo method for high-temperature oxy–natural gas combustion with spectral gas and wall radiation. *Combust. Theory Model.* 17, 354–381. doi: 10.1080/13647830.2013.766365

**Conflict of Interest:** The authors declare that the research was conducted in the absence of any commercial or financial relationships that could be construed as a potential conflict of interest.

# Advantages of publishing in Frontiers

**OPEN ACCESS**
Articles are free to read for greatest visibility and readership

**FAST PUBLICATION**
Around 90 days from submission to decision

**HIGH QUALITY PEER-REVIEW**
Rigorous, collaborative, and constructive peer-review

**TRANSPARENT PEER-REVIEW**
Editors and reviewers acknowledged by name on published articles

**Frontiers**
Avenue du Tribunal-Fédéral 34
1005 Lausanne | Switzerland

**Visit us:** www.frontiersin.org
**Contact us:** frontiersin.org/about/contact

**REPRODUCIBILITY OF RESEARCH**
Support open data and methods to enhance research reproducibility

**DIGITAL PUBLISHING**
Articles designed for optimal readership across devices

**FOLLOW US**
@frontiersin

**IMPACT METRICS**
Advanced article metrics track visibility across digital media

**EXTENSIVE PROMOTION**
Marketing and promotion of impactful research

**LOOP RESEARCH NETWORK**
Our network increases your article's readership